

# **The Design of Sulfur Dioxide-Releasing Linkers for Siderophore-Based Trojan Horse Conjugates**

Conor M. Black

Doctor of Philosophy

University of York

Chemistry

September 2021

## Abstract

A rise in the number of bacterial strains resistant to both front-line treatment and “last resort” antibiotics means there is an urgent need for the development of new antimicrobial agents, or the modification of old antibiotic classes to extend their lifespans. The Trojan Horse approach offers a potential means of achieving both of these objectives by exploiting bacterial nutrient transport for antibiotic delivery.

The primary aim of this research was the development of new biolabile linkers that can undergo cleavage inside the cytoplasm of bacteria, releasing an active antimicrobial species. A series of conjugates containing electron-deficient aromatic sulfonamide linkers were designed for this purpose; these can undergo release of sulfur dioxide (SO<sub>2</sub>) on reaction with biological thiols, and can be modified to undergo concurrent release of an antimicrobial unit.

A conjugate bearing an SO<sub>2</sub>-releasing 2,4-dinitrobenzenesulfonamide group, and containing monocatecholate siderophore aminochelin was synthesised and characterised to determine whether siderophore units could potentiate the antimicrobial activity of SO<sub>2</sub>. While rapid release of SO<sub>2</sub> is observed on reaction with thiols, the conjugate displayed poor antimicrobial activity against a range of bacteria, likely a combination of poor bacterial uptake, and SO<sub>2</sub> release alone being insufficient for good antimicrobial activity.

Two conjugates containing ciprofloxacin as an antimicrobial component were synthesised and characterised. Conjugates based on a 4-carboxyl-2-nitrobenzenesulfonamide linker displayed slow SO<sub>2</sub> release on reaction with glutathione. Screening of a desferrioxamine conjugate of this type vs. a panel of bacteria showed reduced activity compared to the parent ciprofloxacin, with the slow release of ciprofloxacin potentially a limiting factor. In contrast, rapid SO<sub>2</sub> release was observed for conjugates containing a novel pyrazine-sulfonamide linker, although these display instability in MHII broth, a common bacterial growth medium. An azotochelin conjugate containing this linker also displayed reduced activity compared to ciprofloxacin in bacterial assays.

## Table of Contents

Abstract.....	2
Table of Contents.....	3
Table of Figures, Schemes and Tables .....	6
Accompanying Material.....	26
Acknowledgements .....	27
Declaration .....	29
<b>Chapter 1 :.....</b>	<b>30</b>
<b>1.1 Antimicrobial Agents – Development and Resistance .....</b>	<b>31</b>
1.1.1 The Discovery of Antibiotics .....	31
1.1.2 The Modern Antibiotic Catalogue.....	34
1.1.3 The Rise of Antibiotic Resistance.....	41
<b>1.2 Iron and Siderophores.....</b>	<b>44</b>
1.2.1 Iron – Vital for Life .....	44
1.2.2 Bacterial Iron Acquisition and Siderophores .....	45
1.2.3 Bacterial Siderophore Uptake Systems .....	50
<b>1.3 Trojan Horse Strategies .....</b>	<b>53</b>
1.3.1 Natural Siderophore Trojan Horses – Sideromycins.....	54
1.3.2 Synthetic Siderophore-Based Trojan Horse Conjugates .....	59
1.3.3 Siderophore Conjugates with Covalent Linkers.....	60
1.3.3.1 Conjugates with Periplasmic Targets – $\beta$ -lactams .....	60
1.3.3.2 Conjugates with Periplasmic Targets – Other .....	64
1.3.3.3 Conjugates with Cytoplasmic Targets .....	66
<b>1.4 Biolabile Linkers.....</b>	<b>70</b>
1.4.1 Self-Immolative Linkers .....	71
1.4.1.1 Hydrolytically-Labile Linkers .....	73
1.4.1.2 Acid/Base-Labile Linkers .....	74
1.4.1.3 Thiol-Reactive Linkers .....	75
1.4.1.4 Enzyme-Cleavable Linkers.....	79
1.4.1.5 External Stimuli .....	82
1.4.2 Biolabile Linkers in Synthetic Siderophore Trojan Horses .....	83
<b>1.5 Gas-Releasing Antimicrobial Prodrugs.....</b>	<b>93</b>
1.5.1 Nitric Oxide-Releasing Antimicrobials .....	94
1.5.2 Carbon Monoxide-Releasing Antimicrobials.....	96
1.5.3 Sulfur Dioxide-Releasing Antimicrobials.....	97
<b>1.6 Summary and Conclusions .....</b>	<b>101</b>
<b>1.7 Research Aims.....</b>	<b>101</b>
<b>Chapter 2 :.....</b>	<b>103</b>
<b>2.1 Introduction.....</b>	<b>104</b>
2.1.1 2,4-Dinitrobenzenesulfonamides .....	104
2.1.2 The Partitioning of Biological Thiols .....	105
2.1.3 2,4-Dinitrobenzenesulfonamide-Based Anticancer Prodrugs.....	106
2.1.4 2,4-Dinitrobenzenesulfonamide-Based Antimicrobial Prodrugs .....	109
<b>2.2 Conjugate Design and Experimental Considerations .....</b>	<b>113</b>
<b>2.3 Synthetic Plan .....</b>	<b>118</b>
<b>2.4 Conjugate Syntheses .....</b>	<b>121</b>

<b>2.5 Iron Complexation Studies .....</b>	<b>130</b>
<b>2.6 SO<sub>2</sub> Release Studies.....</b>	<b>137</b>
<b>2.7 Biological Studies .....</b>	<b>147</b>
2.7.1 Assays vs. <i>Staphylococcus aureus</i> .....	148
2.7.1.1 <i>S. aureus</i> and Siderophore Utilisation.....	148
2.7.1.2 Biological Screening and Results.....	149
2.7.2 Assays vs. <i>Bacillus subtilis</i> .....	153
2.7.2.1 <i>B. subtilis</i> and Siderophore Utilisation .....	153
2.7.2.2 Biological Screening and Results.....	154
2.7.3 Assays vs. Wild-Type <i>Escherichia coli</i> .....	156
2.7.3.1 <i>E. coli</i> and Siderophore Utilisation .....	156
2.7.3.2 Biological Screening and Results.....	158
2.7.4 Assays vs. <i>entA</i> -deficient <i>Escherichia coli</i> .....	160
2.7.5 Discussion of Biological Results .....	164
<b>2.8 Summary and Conclusions .....</b>	<b>165</b>
<b>2.9 Future Work.....</b>	<b>166</b>
<b>Chapter 3 : .....</b>	<b>169</b>
<b>3.1 Introduction .....</b>	<b>170</b>
3.1.1 Structure of SO <sub>2</sub> -Releasing Linker .....	170
3.1.1.1 4-Carboxyl-2-nitrobenzenesulfonamide Linkers in Biology .....	173
3.1.2 Antimicrobial Component .....	175
3.1.3 Siderophore Component .....	176
<b>3.2 Conjugate Design and Synthetic Plan.....</b>	<b>178</b>
3.2.1 Synthetic Considerations for Sulfonyl Chlorides.....	179
3.2.2 Protecting Groups and Planned Synthetic Route to 3-14 .....	181
3.2.3 Synthetic Routes to Control Compounds .....	184
<b>3.3 Conjugate Syntheses .....</b>	<b>186</b>
3.3.1 Sulfonyl Chloride Component.....	186
3.3.2 Ciprofloxacin Component and Linker Coupling .....	189
3.3.3 Revised Synthetic Route to 3-14.....	193
3.3.4 Final Methyl Ester Deprotection and Attempted Purification.....	199
3.3.5 Synthesis of Microbiological Control Compounds.....	205
<b>3.4 Aqueous Solubility of Compounds.....</b>	<b>210</b>
<b>3.5 Iron Complexation Studies via Native ESI Mass Spectrometry .....</b>	<b>212</b>
<b>3.6 SO<sub>2</sub> Release Studies.....</b>	<b>213</b>
<b>3.7 Biological Studies .....</b>	<b>217</b>
3.7.1 Screening on Agar Plates .....	219
3.7.2 MIC/MBC Screening.....	221
<b>3.8 Summary and Conclusions .....</b>	<b>223</b>
<b>3.9 Future Work.....</b>	<b>226</b>
<b>Chapter 4 : .....</b>	<b>229</b>
<b>4.1 Introduction .....</b>	<b>230</b>
4.1.1 The Potential of Heterocyclic Sulfonamides .....	230
4.1.2 Existing Heterocyclic Sulfonamides and Reactivity with Thiols .....	232
4.1.2.1 6-Membered Heterocycles Sulfonamides.....	232
4.1.2.2 5-Membered Heterocyclic Sulfonamides.....	233
4.1.2.3 5/6-Membered Heterocyclic Sulfones .....	234
4.1.3 Synthesis of Heterocyclic Sulfonamides .....	237
4.1.4 Selection of Heterocyclic Sulfonamide Target.....	241
4.1.5 Selection of Siderophore Component .....	242
<b>4.2 Conjugate Design and Synthetic Plan.....</b>	<b>244</b>

4.2.1 Planned Synthetic Route to Sulfonyl Chloride .....	245
4.2.2 Proposed Synthetic Route to Sulfonamide 4-43 .....	247
4.2.3 Proposed Installation of Azotochelin and Final Deprotection .....	248
4.2.4 Proposed Synthetic Routes to Control Compounds .....	250
<b>4.3 Synthesis.....</b>	<b>252</b>
4.3.1 Synthesis of Ciprofloxacin Component .....	252
4.3.2 Synthesis of Pyrazine Sulfonamide .....	253
4.3.3 Instability of Pyrazine-Sulfonamide 4-42 to Hydrogenation.....	257
4.3.4 Revised Synthetic Route to 4-32.....	258
4.3.5 Synthesis of New Azotochelin Component.....	261
4.3.6 Synthesis of New Pyrazine-Sulfonamide Component.....	262
4.3.7 Coupling of 4-55 and 4-61 and Final Deprotection.....	264
4.3.8 Synthesis of Control Compounds.....	267
<b>4.4 SO<sub>2</sub> Release Studies.....</b>	<b>271</b>
<b>4.5 Conjugate Solubility and Stability.....</b>	<b>274</b>
<b>4.6 Biological Studies .....</b>	<b>279</b>
4.6.1 Initial Screening on Agar Plates .....	281
<b>4.7 Summary and Conclusions .....</b>	<b>282</b>
<b>4.8 Future Work.....</b>	<b>285</b>
<b>Chapter 5 : .....</b>	<b>288</b>
<b>5.1 General Considerations .....</b>	<b>289</b>
5.1.1 Materials.....	289
5.1.2 Instrumentation.....	289
5.1.3 HPLC/LCMS Analysis and Purification .....	290
5.1.4 Specific Glassware Setups.....	292
<b>5.2 Synthesis.....</b>	<b>293</b>
<b>5.3 UV-Visible Experiments.....</b>	<b>382</b>
5.3.1 Job Plot Method .....	382
5.3.2 UV-Based SO <sub>2</sub> Release Studies.....	383
5.3.3 Solubility Testing.....	384
<b>5.4 HPLC-Based Methods .....</b>	<b>385</b>
5.4.1 SO <sub>2</sub> Release by HPLC.....	385
5.4.2 HPLC Stability Tests.....	387
<b>5.5 Native ESI Mass Spectrometry.....</b>	<b>390</b>
<b>5.6 Biological Studies .....</b>	<b>391</b>
5.6.1 Chapter 2 .....	391
5.6.1.1 Media .....	391
5.6.1.2 Growth of Cultures .....	392
5.6.1.3 Bacterial Growth Assays .....	392
5.6.2 Chapter 3 and 4 .....	393
5.6.2.1 Disc Diffusion Assays.....	393
5.6.2.2 Forced Adaptation Assays.....	393
5.6.2.3 MIC/MBC Assays .....	394
Abbreviations.....	396
References .....	400

## Table of Figures, Schemes and Tables

Figure 1.1 Structure of streptomycin, the first known antibiotic to treat TB. .....	31
Figure 1.2 Sample of bone displaying typical golden tetracycline fluorescence under visible light (458 nm). Reprinted with permission from Pautke <i>et al.</i> , <i>J. Anat.</i> , 2010, 217, 1, 76-82. <sup>11</sup> Copyright 2010, John Wiley and Sons.....	32
Figure 1.3 Structure of pyocyanin, the active ingredient in Emmerich and Löw's bacterial extracts. ....	33
Figure 1.4 Structures of arsphenamine. Initially thought to be a dimer, a study in 2005 showed that the structure is a mix of the trimer and the pentamer. <sup>16</sup> .....	33
Figure 1.5 Structures of penicillin G (benzylpenicillin) and protosil, the first of the sulfonamide antibiotics. ....	34
Figure 1.6 Generic structures of the penicillin antibiotics, and related subgroups. ....	35
Figure 1.7 Structure of erythromycin, the first commercial macrolide antibiotic.....	35
Figure 1.8 Structures of nalidixic acid, the first fluoroquinolone antibiotic, and the generic structure of second to fourth generation fluoroquinolones. .....	36
Figure 1.9 Structure of the first two commercial tetracycline antibiotics. .	37
Figure 1.10 Structure of sulfonamide antibiotic sulfamethoxazole and trimethoprim, plus <i>p</i> -aminobenzoic acid and dihydrofolic acid, the two substrates of the folic acid synthesis pathway they mimic. ....	37
Figure 1.11 Structure of the aminoglycoside antibiotic kanamycin, with central 2-deoxystreptamine core highlighted in red. ....	38
Figure 1.12 Structure of vancomycin, the first glycopeptide antibiotic.....	39
Figure 1.13 Structure of the oxazolidinone antibiotic linezolid. ....	39
Figure 1.14 Antibiotics from new classes approved since 2003. ....	40
Figure 1.15 Infographic created by the Pew Charitable Trusts to show the spread of the NDM-1 enzyme. <sup>64</sup> .....	41
Figure 1.16 Common iron-binding ligands and their appearance in a wide variety of siderophore structures. Iron-binding groups are highlighted in	

coloured circles: red = catechol, blue = hydroxamate, green = $\alpha$ -hydroxycarboxylate, yellow = other. ....	46
Figure 1.17 Equilibria for determination of formation constants of hexadentate and bidentate catechol siderophores.....	47
Figure 1.18 Comparison of some hexadentate siderophores and their pFe values at pH 7.40. ....	48
Figure 1.19 Structure of mixed hydroxamate-carboxylate siderophore aerobactin, and pFe of enterobactin (solid line), desferrioxamine B (dotted line) and aerobactin (dashed line) as a function of pH. Reprinted from <i>Int. J. Med. Microbiol.</i> , Vol. 296, Valdebenito <i>et al.</i> , <i>Environmental factors influence the production of enterobactin, salmochelin, aerobactin and yersiniabactin in Escherichia coli strain Nissle 1917</i> , 513-520, Copyright 2006, with permission from Elsevier. ....	49
Figure 1.20 Diagram of typical bacterial siderophore uptake mechanism in Gram-negative bacteria. ....	51
Figure 1.21 Diagram of typical bacterial siderophore uptake mechanism in Gram-positive bacteria. ....	52
Figure 1.22 Cartoon representation of Trojan Horse strategy.....	53
Figure 1.23 Structure of cefiderocol, the first Trojan Horse antibiotic approved for human usage (antibiotic unit highlighted in red).....	54
Figure 1.24 Chemical structures of the albomycins. The stereochemistry here is that reported in a total synthesis published in 2018, <sup>141</sup> which matches the antibiotic stereochemistry reported in 2000. <sup>137</sup> ....	56
Figure 1.25 Structures of the salmycins, and proposed mechanism of antibiotic release post iron removal. ....	57
Figure 1.26 Chemical structure of ferrimycin A <sub>1</sub> . Antibiotic unit highlighted in red.....	58
Figure 1.27 General structure of siderophore-antibiotic conjugates. ....	59
Figure 1.28 Ferricrocin and desferrioxamine conjugates synthesised by Zähler <i>et al.</i> The siderophore components are highlighted in black, and the antibiotic in red. <sup>166</sup> ....	60
Figure 1.29 Structures of two early siderophore- $\beta$ -lactam conjugates. The antimicrobial component is highlighted in red. <sup>168,169</sup> ....	61

Figure 1.30 $\beta$ -lactam conjugate with synthetic hexadentate siderophore synthesised by Ji <i>et al.</i> The antimicrobial unit is highlighted in red, and the linker unit in blue. <sup>170</sup> .....	62
Figure 1.31 $\beta$ -lactam-enterobactin conjugates synthesised by Zheng and Nolan. <sup>171</sup> .....	63
Figure 1.32 Structure of cefiderocol. ....	64
Figure 1.33 Structure of vancomycin-siderophore conjugate <b>1-9</b> . <sup>183</sup> .....	65
Figure 1.34 Structures of daptomycin-siderophore conjugate <b>1-10</b> and phenothiazine-siderophore conjugate <b>1-11</b> . <sup>118,185</sup> .....	66
Figure 1.35 Structures of siderophore conjugates of antibiotics with cytoplasmic targets. Any linkers present between siderophores and antibiotics are highlighted in blue. <sup>186-189</sup> .....	67
Figure 1.36 Previous fluoroquinolone-siderophore conjugates synthesised by the Duhme-Klair and Routledge groups. <sup>190-192</sup> .....	68
Figure 1.37 Structures of the <i>apo</i> and gallium-bound forms of a ferrichrome-ciprofloxacin conjugate. <sup>193</sup> .....	69
Figure 1.38 Hydrolytic stability of some (acyloxy)alkyl linkers studied by Zheng and Nolan (HEPES buffer, pH 7.5, 30 °C). <sup>210</sup> .....	74
Figure 1.39 General structures of antibody-drug conjugates containing methoxybenzylacetal and hydrazone linkers.....	75
Figure 1.40 Examples of anticancer and antibacterial conjugates containing self-immolative disulfide linkers. <sup>223</sup> The self-immolative trigger is highlighted in a green box, the rest of the self-immolative system is green, and any other linker components are blue. ....	77
Figure 1.41 Structure of <b>ICT 2588</b> , an enzymatically cleaved anticancer conjugate. <sup>237,238</sup> .....	80
Figure 1.42 Design and structure of the Val-Cit linker. <sup>239</sup> .....	81
Figure 1.43 Structure of hydrolysable pyoverdin conjugates with methylenedioxy linker highlighted in green, and remainder of linker highlighted in blue. <sup>194</sup> .....	84
Figure 1.44 Pyochelin-fluoroquinolone conjugates containing a labile methylenedioxy linker. <sup>261,262</sup> .....	85
Figure 1.45 Structure of an enterobactin conjugate ( <b>1-34</b> ) containing a methylenedioxy linker. <sup>210</sup> .....	86



Figure 1.46 Structure of oxazolidinone conjugate <b>1-35</b> containing a methylene bridge synthesised by Paulen <i>et al.</i> , and the related non-biolabile conjugate <b>1-14</b> . The methylene bridge is highlighted in green, and other linker components highlighted in blue. <sup>187</sup> .....	87
Figure 1.47 Structures of desferridanoxamine conjugates <b>1-36</b> and <b>1-37</b> synthesised by Wencewicz <i>et al.</i> The hydroxamate group responsible for the potential cyclisation mechanism is highlighted in green. <sup>143</sup> .....	88
Figure 1.48 Mechanism for trimethyl lock cyclisation (with steric clash indicated) and structures of desferrioxamine conjugates <b>1-38</b> to <b>1-40</b> based on this self-immolative linker. The different trigger groups for the self-immolative reaction are highlighted in green boxes. <sup>189,263</sup> .....	89
Figure 1.49 Structure of enterobactin-based Trojan Horse conjugates synthesised by Neumann <i>et al.</i> <sup>264,265</sup> .....	90
Figure 1.50 Structure of siderophore-cephalosporin-oxazolidinone conjugate <b>1-43</b> . The cephalosporin is highlighted in green, and the oxazolidinone in red. <sup>267</sup> .....	91
Figure 1.51 Structure of protease-cleaved siderophore conjugates developed by Boyce <i>et al.</i> The cleaved protein sequence is highlighted in green, and the antimicrobials in red. <sup>268</sup> .....	92
Figure 1.52 Some examples of NO delivery agents, including cysteine-nitrosothiol ( <b>1-46</b> ), nitroglycerine ( <b>1-47</b> ), sodium nitroprusside ( <b>1-48</b> ), diethylamine diazeniumdiolate ( <b>1-49</b> ), and a cephalosporin-NO conjugate ( <b>1-50</b> , NO release is triggered by cephalosporin hydrolysis). <sup>277</sup> .....	94
Figure 1.53 Structures of delamanid and pretomanid.....	96
Figure 1.54 Structures of a range of CORMs. For the organic CORM <b>1-55</b> , the site of CO release is highlighted in green.....	97
Figure 1.55 Structures of various SO <sub>2</sub> -releasing systems, including Kodama <i>et al.</i> 's UV-activated compound <b>1-58</b> . .....	99
Figure 1.56 Phototriggered SO <sub>2</sub> -releasing conjugates <b>1-59</b> and <b>1-60</b> . <sup>314</sup> ....	99
Figure 2.1 Structure of <b>DNS-DOX</b> , a 2,4-dinitrobenzenesulfonamide prodrug of doxorubicin. Drug highlighted in red. <sup>305</sup> .....	106
Figure 2.2 Structure of <b>DNS-SN-38</b> , a 2,4-dinitrobenzenesulfonate ester prodrug of anticancer drug SN-38. Drug highlighted in red. <sup>306</sup> .....	107

Figure 2.3 Structures of 2,4-dinitrobenzene-containing prodrugs that utilise self-immolative linkers. Drug highlighted in red, self-immolative linker highlighted in green, dye highlighted in purple. <sup>334,335</sup> .....	108
Figure 2.4 Prodrugs developed by Malla <i>et al.</i> for the formation of ion channels in cell membranes. 2-Hydroxyisophthalamide section highlighted in red. <sup>308</sup> .....	108
Figure 2.5 Structure of SO <sub>2</sub> -releasing polymer <b>2-4</b> developed by Shen <i>et al.</i> <sup>336</sup> .....	109
Figure 2.6 Structure of <b>1-56</b> , the most effective of the 2,4-dinitrobenzenesulfonamides developed by Chakrapani <i>et al.</i> vs. <i>M. tuberculosis</i> . <sup>301,303</sup> .....	110
Figure 2.7 A graph to demonstrate the correlation of SO <sub>2</sub> release rate to antimycobacterial activity (reproduced using data from reference 303).	110
Figure 2.8 Two of the 2,4-dinitrobenzenesulfonamide antimicrobials developed by Phetsang <i>et al.</i> <sup>337</sup> .....	112
Figure 2.9 Structure of potential SO <sub>2</sub> -releasing prodrug <b>2-9</b> based on monocatechol siderophore aminochelin. 2,4-Dinitrobenzenesulfonamide component highlighted in red. ....	113
Figure 2.10 Diagram of the “knowns and unknowns” of uptake routes involving monocatechol siderophores in Gram-negative bacteria. ....	114
Figure 2.11 Structure of monocatechol siderophore aminochelin. ....	114
Figure 2.12 Structure of the monocatechol siderophore vanchrobactin and the norfloxacin-aminochelin conjugate <b>2-10</b> . ....	115
Figure 2.13 Structure of oxazolidinone-aminochelin conjugate <b>1-14</b> synthesised by Paulen <i>et al.</i> .....	116
Figure 2.14 Structures of various compounds used to detect SO <sub>2</sub> release. ....	117
Figure 2.15 Structure of proposed aminochelin conjugate <b>2-9</b> . ....	118
Figure 2.16 Aromatic region of <sup>1</sup> H NMR spectra for the product mix formed post-sulfonamide formation when DIPEA used as a base. Position of key 2,4-dinitrobenzenesulfonamide protons indicated. ....	123
Figure 2.17 Potential equilibrium between Fe(III)-catechol complexes in solution. S = solvent. For the bis(catechol) other isomers are possible. ..	131

Figure 2.18 Structure of <i>N</i> -ethyl-2,3-dihydroxybenzamide <b>2-29</b> employed for Job plot analysis.....	132
Figure 2.19 Colours of solutions obtained from continuous variance method from high ligand concentration (left) to high iron concentration (right). Image acquired by James Southwell.....	133
Figure 2.20 UV-vis spectra for selected ligand:metal ratios in Tris buffer.	134
Figure 2.21 UV-vis spectra for selected ligand:metal ratios in M9 medium. ....	135
Figure 2.22 Job plot for absorbance at maxima observed in Tris buffer. .	136
Figure 2.23 Job plot for absorbance at maxima observed in M9 media...	137
Figure 2.24 Structure of SO <sub>2</sub> -detecting dye <b>2-11</b> . ....	137
Figure 2.25 UV-Visible spectrum for the reaction of <b>1-56</b> with cysteine in the presence of dye <b>2-11</b> over 30 mins, and photos of the solution before and after the reaction.....	139
Figure 2.26 UV-Vis spectrum of sulfonamide conjugate <b>2-9</b> on reaction with cysteine (10 equivalents) over 7 hours in 10% MeCN:HEPES buffer (pH 7.4). The shift in the absorbance maxima over time is indicated. ....	140
Figure 2.27 UV-vis spectrum of <b>1-56</b> on reaction with glutathione (10 equivalents) over 12 hours in 10% MeCN:HEPES buffer (pH 7.4). Times shown are in minutes. ....	141
Figure 2.28 Plot of absorbance at 340 nm vs. time for sulfonamides <b>1-56</b> , <b>2-9</b> , <b>2-15</b> and <b>2-19</b> on reaction with glutathione (10 eq.) in HEPES buffer (pH 7.4). All experiments are a mean average of 3 experiments, apart from <b>2-15</b> , which is a mean average of 2 experiments. Error bars are calculated as the standard deviation of the mean. ....	142
Figure 2.29 Plot of absorbance at 340 nm vs. time for first two hours of reaction between sulfonamides <b>1-56</b> , <b>2-9</b> , <b>2-15</b> and <b>2-19</b> with glutathione. ....	143
Figure 2.30 UV-Vis spectrum of <b>2-9</b> in the presence of 0.33 eq. Fe(III), and photo of corresponding cuvette. ....	144
Figure 2.31 Colour difference between Fe(NTA)-containing solutions of <b>2-15</b> before (left) and after (right) reaction with glutathione. ....	144

Figure 2.32 Plots of absorbance at 340 nm vs. time for conjugates <b>2-9</b> and <b>2-15</b> on reaction with glutathione (10 eq.) in the presence and absence of 0.33 eq. Fe(NTA). .....	146
Figure 2.33 Structures of compounds that underwent biological screening. ....	147
Figure 2.34 Siderophores produced by <i>S. aureus</i> . ....	149
Figure 2.35 Growth curves for selected concentrations of <b>2-9</b> , <b>2-22</b> and <b>2-23</b> vs. <i>S. aureus</i> in Tryptic Soy Broth. Experiments for <b>2-9</b> and <b>2-22</b> are a mean average of 3 wells, <b>2-23</b> is a mean average of two wells. Error bars are calculated as the standard error of the mean. ....	151
Figure 2.36 Growth curves for intermediate concentrations between 500 and 50 $\mu$ M of <b>2-9</b> vs. <i>S. aureus</i> . Curves are a mean average of three wells. Error bars are calculated as the standard error of the mean. ....	152
Figure 2.37 Photo of 500 $\mu$ M and 250 $\mu$ M wells plated onto agar at end of assay. Growth of golden <i>S. aureus</i> cultures can be observed.....	152
Figure 2.38 Structures of bacillibactin and <i>N</i> -2,3-dihydroxybenzoylglycine, native siderophores of <i>B. subtilis</i> .....	154
Figure 2.39 Growth curves for selected concentrations of <b>2-9</b> , <b>2-22</b> and <b>2-23</b> vs. <i>B. subtilis</i> in LB media. Experiments are an average of two wells. Error bars are calculated as the standard error of the mean. ....	155
Figure 2.40 Native siderophores that can be biosynthesised by various <i>E. coli</i> strains. Production of siderophores is strain-dependent (i.e. Not all strains will be able to make all of these siderophores). ....	157
Figure 2.41 Growth curves for selected concentrations of <b>2-9</b> , <b>2-22</b> and <b>2-23</b> vs. <i>E. coli</i> in both LB media (blue, squares) and M9 media (red, circles). Experiments are an average of two wells. Error bars are calculated as the standard error of the mean. ....	159
Figure 2.42 Growth curves for concentrations of <b>2-9</b> vs. <i>E. coli entA</i> mutant in plain M9 media (confluent overnight growth). Experiments are an average of two wells. Error bars are calculated as the standard error of the mean. ....	161
Figure 2.43 Photo of overnight cultures for wild-type (1 and 3) and <i>entA</i> mutant (2 and 4) in Chelex-treated M9 (left) and Chelex-treated M9 + 10 $\mu$ M Fe(NTA) (right). ....	162

Figure 2.44 Growth curves for selected concentrations of <b>2-23</b> vs. <i>entA</i> mutant cultured overnight in Chelex M9 plus 10 $\mu$ M Fe(NTA). Experiments are an average of two wells. Error bars are calculated as the standard error of the mean. ....	163
Figure 2.45 Structures of synthesised 2,4-dinitrobenzenesulfonamide conjugates <b>2-9</b> , <b>2-15</b> and <b>2-19</b> , and microbiological "SO <sub>2</sub> -free" control <b>2-23</b> . ....	165
Figure 2.46 Structure of hydroxamate siderophore desferrioxamine B, and potential structure of a future SO <sub>2</sub> -releasing prodrug <b>2-35</b> based on desferrioxamine B.....	168
Figure 3.1 Schematic to demonstrate generic structure of target siderophore-sulfonamide-antimicrobial conjugate. ....	171
Figure 3.2 Exchange of nitro group for carboxylic acid group in biolabile linker design.....	172
Figure 3.3 General structure of "reporter resins" containing anthracene.	173
Figure 3.4 Two examples of solid-phase synthesis products achieved via strategies involving the 4-carboxyl-2-nitrobenzenesulfonamide group as a cleavable linker. <sup>424-426</sup> .....	173
Figure 3.5 General structure of probes developed by Yokoshima <i>et al.</i> <sup>427</sup>	173
Figure 3.6 Fluorescent/ <sup>19</sup> F-active ( <b>3-8</b> ) and bioluminogenic ( <b>3-9</b> ) probes synthesised by Ito <i>et al.</i> , and probe for detecting reactive cysteine residues in proteins developed by Lee <i>et al.</i> ( <b>3-10</b> ). <sup>428,431</sup> .....	174
Figure 3.7 Structures of anticancer prodrugs containing etoposide ( <b>3-11</b> ) and doxorubicin ( <b>3-12</b> ), and 2,4-dinitrobenzenesulfonamide prodrug <b>DNS-DOX</b> . Drug moieties highlighted in red. <sup>432</sup> .....	175
Figure 3.8 Structure of second-generation fluoroquinolone ciprofloxacin. ....	176
Figure 3.9 Structures of hexadentate hydroxamate siderophore desferrioxamine, and three examples of catecholate siderophores of varying denticity, plus associated pFe(III) values at pH 7.40. Groups involved in iron coordination are highlighted in red. ....	177
Figure 3.10 Structure of proposed ciprofloxacin-desferrioxamine conjugate <b>3-14</b> . ....	178

Figure 3.11 Aromatic region of the <sup>1</sup> H NMR spectrum of <b>3-25</b> , demonstrating the characteristic multiplet pattern observed for the aromatic protons of 4-carboxyl-2-nitrobenzene rings with substituents at the 1-position.....	187
Figure 3.12 Identified byproducts from synthesis of sulfonyl chloride <b>3-27</b> . .....	189
Figure 3.13 Overlaid HPLC traces for compounds <b>3-48</b> , <b>3-50</b> and <b>3-49</b> . Recorded on an Agilent HPLC, Eclipse XDB-C18 column, 30-70% MeCN:H <sub>2</sub> O, 220 nm wavelength. ....	199
Figure 3.14 Overlaid HPLC traces for deprotected DFO conjugate <b>3-14</b> and dicarboxylic acid <b>3-41</b> . Recorded on a Shimadzu HPLC at 254 nm detection on an Eclipse XDB-C18 column, 25-70% MeCN:H <sub>2</sub> O.....	201
Figure 3.15 Observed peaks in LCMS analysis of second overlapping HPLC peak at 7.34 min, and structure of iron conjugate <b>3-51</b> consistent with observed mass (data obtained by Reach Separations). ....	202
Figure 3.16 Observed peaks in LCMS analysis of first overlapping HPLC peak at 7.15 min, and structure of aluminium/silicon conjugates consistent with observed mass (data obtained by Reach Separations). ....	203
Figure 3.17 Structure of complex <b>3-59</b> observed by native ESI mass spectrometry. ....	213
Figure 3.18 UV-visible spectra for the reaction of <b>3-36</b> with glutathione in the presence of dye <b>2-11</b> , recorded over 24 hours. The spectra displayed are at intervals of 50 minutes. ....	214
Figure 3.19 Change in concentration of <b>3-36</b> over 74 hours on reaction with glutathione in HEPES buffer as determined by HPLC.....	216
Figure 3.20 Structures of conjugate <b>3-14</b> and microbiological controls assessed in antimicrobial assays.....	217
Figure 3.21 Structures of DFO conjugate <b>3-14</b> , and microbiological controls <b>3-31</b> , <b>3-34</b> and <b>3-36</b> .....	224
Figure 3.22 Potential alternative SO <sub>2</sub> -releasing linkers. ....	227
Figure 3.23 Structure of potential replacements for optimisation of the fluoroquinolone and siderophore units. For <b>3-61</b> , the inserted ethers are highlighted in red.....	228
Figure 4.1 Structure of 6-uracilsulfonamide ( <b>4-1</b> ). <sup>546</sup> .....	232

Figure 4.2 Structures of heterocyclic sulfones that can act as anticancer/anti-apoptosis agents, and undergo reaction with biological thiols. For structure <b>4-20</b> , Ad = adamantane.....	237
Figure 4.3 Structure of initial 5-pyrazinecarboxylic acid group for design of a first heterocyclic sulfonamide biolabile linker ( <b>4-29</b> ), and desired 5-chloropyrazine-2-carboxylic acid starting material.....	242
Figure 4.4 Structure of tetradentate catecholate siderophore azotochelin. ....	243
Figure 4.5 Structures of previous azotochelin conjugates synthesised by McKee <i>et al.</i> <sup>606</sup> .....	243
Figure 4.6 Structure of previous phenothiazine-azotochelin conjugate synthesised by Tarapdar <i>et al.</i> <sup>185</sup> .....	244
Figure 4.7 Structure of initial synthetic target <b>4-32</b> .....	244
Figure 4.8 Protecting group strategies for carboxylic acid of pyrazine.....	246
Figure 4.9 Overlaid <sup>1</sup> H NMR spectra for variable temperature experiments for <b>4-37</b> in DMSO-d <sub>6</sub> to show coalescing of potential rotameric carbamate resonances.....	254
Figure 4.10 Sulfoxide intermediate <b>4-54</b> observed in some oxidative chlorination reactions of benzyl thioether <b>4-38</b> . ....	256
Figure 4.11 Structure of proposed intermediates in HCl-mediated deprotection of <b>4-63</b> .....	267
Figure 4.12 Plot of absorbance vs. time for pyrazine-sulfonamide <b>4-49</b> and 2,4-dinitrobenzenesulfonamide <b>1-56</b> at their respective absorbance maximum (329 and 340 nm) on reaction with glutathione (10 eq.) at pH 7.40. ....	273
Figure 4.13 Stability and solubility of <b>4-52</b> in Mueller-Hinton II media over 23 hours at 37 °C as determined by HPLC analysis. ....	276
Figure 4.14 Solubility of ciprofloxacin in Mueller-Hinton II media over 23 hours at 37 °C as determined by HPLC analysis. ....	276
Figure 4.15 Stability and solubility of <b>4-32</b> in Mueller-Hinton II media over 27 hours at 37 °C as determined by HPLC analysis. ....	277
Figure 4.16 Stability of <b>4-49</b> in aqueous HEPES buffer (pH 7.4) over 24 hours at 37 °C as determined by HPLC analysis. ....	278

Figure 4.17 Stability of <b>4-52</b> in aqueous HEPES buffer (pH 7.4) over 22 hours at 37 °C as determined by HPLC analysis. ....	278
Figure 4.18 Structure of Trojan Horse conjugate <b>4-32</b> and related microbiological controls, plus TFA salt <b>4-49</b> . ....	283
Figure 4.19 Structure of coumarin sulfonate ester <b>4-70</b> . ....	286
Figure 5.1 Glassware setup for reactions carried out with BBr <sub>3</sub> . ....	292
Figure 5.2 Photo of hotplate setup for HPLC reactions. ....	385
Figure 5.3 Calibration curve for determining the concentration of <b>3-36</b> relative to caffeine in SO <sub>2</sub> release experiments. ....	386
Figure 5.4 Calibration curve for determining the concentration of <b>4-32</b> relative to caffeine in stability experiments in MHII media. ....	388
Figure 5.5 Calibration curve for determining the concentration of <b>4-52</b> relative to caffeine in stability experiments in MHII media. ....	388
Figure 5.6 Calibration curve for determining the concentration of ciprofloxacin relative to caffeine in stability experiments in MHII media. ....	389
Figure 5.7 Calibration curve for determining the concentration of <b>4-49</b> relative to caffeine in stability experiments in HEPES buffer. ....	389
Figure 5.8 Calibration curve for determining the concentration of <b>4-52</b> relative to caffeine in stability experiments in HEPES buffer. ....	390
Scheme 1.1 Activation of the first self-immolative prodrug system, developed by Carl <i>et al.</i> <sup>207</sup> The trigger (the enzymatically cleaved <i>N</i> -Boc lysine) is highlighted in a green box, the self-immolative unit is green, and the released <i>p</i> -nitroaniline is red. ....	71
Scheme 1.2 Two examples of common elimination and cyclisation mechanisms for self-immolative linkers. <b>X = NH, O, S</b> . The location of the self-immolation trigger is shown in green. ....	72
Scheme 1.3 An example of the multiple functionalities that can be incorporated into a linker. ....	72
Scheme 1.4 Self-immolative chains developed by de Groot <i>et al.</i> , <sup>208</sup> and an example of multi-drug release from a single aromatic ring (adapted from Srinivasarao and Low). <sup>199</sup> ....	73
Scheme 1.5 Base-mediated cleavage of a self-immolative triazole linker ( <b>1-24</b> ). Base-labile pivaloyl ester highlighted in green box. <sup>218</sup> ....	75



Scheme 1.6 Self-immolation mechanisms of some disulfide systems. <sup>200,223,225</sup> .....	76
Scheme 1.7 Equilibria of maleimides that can undergo retro-Michael reaction. The released thiol is highlighted in green.....	78
Scheme 1.8 Pyridazinediones studied by the Chudasama group, mechanisms of release, and an example of pyridazinedione difunctionalisation. The displaced thiol groups are highlighted in green. <sup>235,236</sup> .....	79
Scheme 1.9 Click components used by Rossin <i>et al.</i> for their ADC, and the mechanism of activation. <sup>259,260</sup> .....	83
Scheme 1.10 Examples of some mechanisms of NO action within bacterial cells. Adapted from Carpenter and Schoenfisch. <sup>278</sup> .....	95
Scheme 1.11 Structure of thiol-activated SO <sub>2</sub> prodrugs synthesised by Chakrapani group, plus mechanism of activation. <sup>301,303,304</sup> .....	98
Scheme 1.12 Nitroreductase-activated SO <sub>2</sub> -coumarin-ciprofloxacin conjugate <b>1-61</b> synthesised by Pardeshi <i>et al.</i> <sup>315</sup> Coumarin component indicated in purple. <sup>315</sup> .....	100
Scheme 2.1 Alkylation of 2,4-dinitrobenzenesulfonamides demonstrated by Fukuyama <i>et al.</i> , and deprotection conditions for removal of nosyl and 2,4-DNS groups. <sup>319</sup> .....	105
Scheme 2.2 Difference in reactivity for 2,4-dinitrobenzenesulfonamides compared to 2- and 4-nitrobenzenesulfonamides. ....	111
Scheme 2.3 Reaction mechanism proposed for SO <sub>2</sub> release from 2,4-dinitrobenzenesulfonamides, including key protonated sulfonamide intermediate (highlighted in red). ....	112
Scheme 2.4 Proposed mechanism for reaction of sulfite with coumarin-based dye <b>2-11</b> . <sup>345</sup> .....	118
Scheme 2.5 Planned synthetic route to catechol-sulfonamide <b>2-9</b> . ....	119
Scheme 2.6 Proposed synthetic route to two-carbon linker catechol-sulfonamide <b>2-15</b> . ....	120
Scheme 2.7 Planned synthetic route to catechol-free sulfonamide <b>2-19</b> . ....	121
Scheme 2.8 Synthesis of benzyl-protected aminochelin ( <b>2-13</b> ). a) 1) BnCl, K <sub>2</sub> CO <sub>3</sub> , EtOH, reflux, 24 h; 2) Sodium chlorite, sulfamic acid, acetone:H <sub>2</sub> O (5:4), 2 h, 67% over two steps; b) 1,4-diaminobutane, CDI, THF, 22 h, 38%. .....	121

Scheme 2.9 Products obtained from sulfonamide formation when DIPEA used as a base. a) 2,4-Dinitrobenzenesulfonyl chloride, DIPEA, DCM (anhydrous), 0 °C to rt, 46 h.....	122
Scheme 2.10 Proposed mechanism of Smiles rearrangement. Acidic sulfonamide proton highlighted in red. ....	123
Scheme 2.11 Synthesis of sulfonamide <b>2-14</b> . a) 2,4-Dinitrobenzenesulfonyl chloride, lutidine, DCM (anhydrous), 0 °C to rt, 28 h, 98%.....	124
Scheme 2.12 Synthesis of conjugate <b>2-9</b> via BBr <sub>3</sub> -mediated deprotection of hydroxyl groups. a) BBr <sub>3</sub> , DCM (anhydrous), rt, 7 h, then preparative HPLC purification, 40%.....	125
Scheme 2.13 Synthesis of TFA salt <b>2-17</b> . a) <i>N</i> -Boc ethylenediamine, EDC.HCl, HOBT, DCM, 24 h, 88%; b) TFA (10% v/v), DCM, 4 h, 77%. ....	126
Scheme 2.14 Synthesis of <b>2-18</b> . a) 1 M NaOH (aq.), then 2,4-dinitrobenzenesulfonyl chloride, lutidine, DCM (anhydrous), 20 h, 86%. 126	126
Scheme 2.15 Synthesis of two-carbon conjugate <b>2-15</b> . a) BBr <sub>3</sub> , DCM, N <sub>2</sub> , 24 h; then preparative LCMS purification, 55%.....	127
Scheme 2.16 Synthesis of catechol-free conjugate <b>2-19</b> . a) Phenol, NaOH (10% w/v aq.), 2 h, 35%; b) 1,4-Diaminobutane, H <sub>2</sub> O, N <sub>2</sub> , 50 °C, 24 h, 60%; c) 2,4-dinitrobenzenesulfonyl chloride, lutidine, DCM, 0 °C to rt, 96 h, 48%. ....	127
Scheme 2.17 Synthesis of Chakrapani compounds <b>1-56</b> and <b>2-22</b> . a) Benzylamine, pyridine, DCM (anhydrous), 0 °C to rt, 24 h, 65%; b) propargyl bromide, K <sub>2</sub> CO <sub>3</sub> , DMF, rt, 24 h, 68%. ....	128
Scheme 2.18 Synthesis of SO <sub>2</sub> -free control <b>2-23</b> . a) 1-Chloro-2,4-dinitrobenzene, Et <sub>3</sub> N, DCM (anhydrous), 18 h, 71%; b) BBr <sub>3</sub> , DCM, N <sub>2</sub> , 22 h; then preparative HPLC purification, 22%.....	129
Scheme 2.19 Synthesis of SO <sub>2</sub> -detecting dye <b>2-11</b> . a) 1) Diethyl malonate, piperidine, EtOH, reflux, 24 h; 2) conc. HCl, AcOH, reflux, 24 h, 52%; b) POCl <sub>3</sub> , DMF, N <sub>2</sub> , 70 °C, 23 h, 68%; c) MeI, MeCN, N <sub>2</sub> , 75 °C, 24 h, 53%; d) <b>2-28</b> , EtOH, reflux, 18 h, 90%. ....	130
Scheme 2.20 Synthesis of model monocatecholamine <b>2-29</b> . a) Ethylamine (2 M in THF), Et <sub>3</sub> N, THF, 72 h, 94%; b) H <sub>2</sub> , 10% Pd-C, EtOH, 96 h, 86%. ....	133
Scheme 2.21 Reaction of <b>1-56</b> with cysteine. a) Cysteine (10 eq.), <b>2-11</b> (0.1 eq.), 10% MeCN:HEPES, pH 7.4, rt, 30 mins. ....	138

Scheme 2.22 Equilibrium between S-adduct <b>2-32</b> and N-adduct <b>2-33</b> in cysteine-dinitrobenzene conjugates, and structure of alternative thiol glutathione (GSH). .....	140
Scheme 2.23 Outcome of reaction between <b>1-56</b> and glutathione. a) GSH (10 eq.), 10% MeCN:HEPES, pH 7.4, rt, 12 h. ....	141
Scheme 2.24 Pathway for biosynthesis of 2,3-dihydroxybenzoic acid from chorismate. <sup>412</sup> .....	160
Scheme 3.1 Esterification and subsequent decomposition of 3,5-dinitro-4-chlorobenzoic acid. ....	171
Scheme 3.2 Structure of solid-phase linker employed by Kay <i>et al.</i> , and method of cleavage to generate free amine. <sup>417</sup> .....	172
Scheme 3.3 Key reaction sequence in proposed synthesis of DFO conjugate <b>3-14</b> . ....	179
Scheme 3.4 Retrosynthetic analysis of sulfonyl chlorides. ....	180
Scheme 3.5 Proposed synthetic route to sulfonyl chloride <b>3-16</b> . ....	180
Scheme 3.6 Structure of oxidative chlorination agent 1,3-dichloro-5,5'-dimethylhydantoin (DCDMH) and the potential mechanism for oxidative chlorination of benzyl thioethers proposed by Pu <i>et al.</i> <sup>459</sup> .....	181
Scheme 3.7 Proposed synthetic route to TMSE-protected ciprofloxacin <b>3-24</b> . ....	182
Scheme 3.8 Proposed synthetic route to methyl ester-protected sulfonyl chloride component <b>3-27</b> . ....	183
Scheme 3.9 Proposed synthetic route from sulfonyl chloride <b>3-27</b> to DFO conjugate <b>3-14</b> . ....	184
Scheme 3.10 Planned synthetic route to morpholine-containing DFO +, Cipro – control <b>3-31</b> . ....	185
Scheme 3.11 Planned synthetic route to Cipro +, DFO – control <b>3-34</b> . ....	186
Scheme 3.12 Proposed synthetic route to Cipro –, DFO – control <b>3-36</b> . ..	186
Scheme 3.13 Methyl ester protection of 4-chloro-3-nitrobenzoic acid. a) H <sub>2</sub> SO <sub>4</sub> , MeOH, reflux, 18 h, 96%. ....	187
Scheme 3.14 Synthesis of benzyl thioether <b>3-26</b> and sulfonyl chloride <b>3-27</b> . a) BnSH, DIPEA, MeOH (anhydrous), 0 °C to rt, 22 h, 91%; b) DCDMH, MeCN:AcOH:H <sub>2</sub> O (40:1.5:1), 0 °C, 3 h. ....	188

Scheme 3.15 Synthesis of TMSE-protected Boc-ciprofloxacin <b>3-23</b> . a) Trimethylsilylethanol, HBTU, DMAP, DIPEA, DCM (anhydrous), 24 h, 78%. .....	189
Scheme 3.16 Synthesis of deprotected TMSE-ciprofloxacin <b>3-24</b> , and formation of ciprofloxacin hydrochloride <b>3-37</b> . a) 3 M HCl in MeOH, 0 °C, 1 to 3.5 h.....	190
Scheme 3.17 Synthesis of TMSE-protected ciprofloxacin <b>3-40</b> from Fmoc-protected ciprofloxacin <b>3-39</b> . a) Trimethylsilylethanol, HBTU, DMAP, DIPEA, DCM (anhydrous), 24 h, 86%; b) Piperidine, DCM, 0 °C, 90 min, 68%. .....	191
Scheme 3.18 Synthesis of TMSE-protected ciprofloxacin-sulfonamide <b>3-28</b> . a) <b>3-27</b> , lutidine, DCM (anhydrous), 0 °C to rt, 72 h, 53%.....	192
Scheme 3.19 Outcome of attempted selective hydrolysis of methyl ester of <b>3-28</b> , resulting in formation of dicarboxylic acid <b>3-41</b> . a) NaOH (aq.), 2:1 THF:MeOH, 1 h, then HCl (aq.). .....	192
Scheme 3.20 Examination of conditions resulting in the hydrolysis of TMSE ester. a) NaOH (aq.), 2:1 THF:MeOH, 1 h, quantitative. ....	193
Scheme 3.21 Revised synthetic route to sulfonyl chloride <b>3-45</b> . Key protecting group changes are highlighted in red.....	194
Scheme 3.22 Revised synthetic route to DFO conjugate <b>3-14</b> . Key protecting group changes are highlighted in red, and deprotection conditions in blue. ....	194
Scheme 3.23 Synthesis of <i>t</i> -Bu ester protected sulfonyl chloride <b>3-45</b> . a) <i>t</i> -BuOH, EDC.HCl, DMAP, DCM, 18 h, 52%; b) BnSH, DIPEA, MeOH (anhydrous), 0 °C to rt, 18 h, 71%; c) 1,3-dichloro-5,5'-dimethylhydantoin, MeCN:AcOH:H <sub>2</sub> O (40:1.5:1), 0 °C to rt, 3 h, 86%. ....	195
Scheme 3.24 Synthesis of protected ciprofloxacin-sulfonamide <b>3-47</b> . a) <b>3-45</b> , Et <sub>3</sub> N, DCM (anhydrous), 0 °C to rt, 24 h, 86%. .....	196
Scheme 3.25 Synthesis of deprotected ciprofloxacin-sulfonamide <b>3-48</b> . a) TFA (25% v/v), DCM (anhydrous), 4 h, 54%. ....	197
Scheme 3.26 Synthesis of DFO conjugate <b>3-49</b> via NHS ester <b>3-50</b> . a) NHS, EDC.HCl, DCM (anhydrous), 21 h; b) Desferrioxamine mesylate (0.95 eq.), Et <sub>3</sub> N, DMF, 50 °C, 24 h, 83% over two steps.....	198
Scheme 3.27 Test of NaOH-mediated deprotection conditions carried out on <b>3-48</b> . a) 1 M aq. NaOH (10 eq.), 3:1 MeOH:H <sub>2</sub> O, 21 h. ....	200

Scheme 3.28 NaOH-mediated methyl ester hydrolysis to yield <b>3-14</b> . a) NaOH (aq., 10 eq.), 3:1 MeOH:H <sub>2</sub> O, 24 h, c. 60%.....	201
Scheme 3.29 Attempted synthesis of <b>3-54</b> from <b>3-48</b> . a) EtNH <sub>2</sub> (2 M in THF), EDC.HCl, HOBT, Et <sub>3</sub> N, DCM, 48 h; b) 1) NHS, EDC.HCl, DCM (anhydrous), 24 h; 2) EtNH <sub>2</sub> (2 M in THF), Et <sub>3</sub> N, THF, 48 h.....	205
Scheme 3.30 Synthesis of ethyl amide <b>3-56</b> . a) NaOH, 1:1 THF:MeOH, 15 h, 81%; b) EtNH <sub>2</sub> .HCl, EDC.HCl, HOBT, Et <sub>3</sub> N, DCM (anhydrous), 20 h, 80%...	206
Scheme 3.31 Attempted synthesis of control compound <b>3-34</b> . a) 1,3-dichloro-5,5'-dimethylhydantoin, MeCN:AcOH:H <sub>2</sub> O (40:1.5:1), 0 to 20 °C, 24 h; b) <b>3-46</b> , Et <sub>3</sub> N, DCM (anhydrous), 26 h, 78% over 2 steps; c) NaOH (1 M aq., 10 eq.), MeOH:H <sub>2</sub> O (3:1), 96 h.....	207
Scheme 3.32 Synthesis of Cipro +, DFO – control <b>3-34</b> . a) Ciprofloxacin, Et <sub>3</sub> N, DCM, 22 h, 78%.....	207
Scheme 3.33 Initial synthetic route to Cipro –, DFO – control <b>3-36</b> from <b>3-57</b> . a) DCDMH, MeCN:AcOH:H <sub>2</sub> O, (40:1.5:1), 0 °C, 24 h; b) Morpholine, Et <sub>3</sub> N, DCM (anhydrous), 0 °C to rt, 23 h.....	208
Scheme 3.34 Alternative synthesis of Cipro –, DFO – control <b>3-36</b> from <b>3-26</b> . a) DCDMH, MeCN:AcOH:H <sub>2</sub> O, (40:1.5:1), 0 °C, 3 h; b) Morpholine, Et <sub>3</sub> N, DCM (anhydrous), 0 °C to rt, 18 h; c) NaOH (aq.), THF:MeOH (1:1), 24 h, 71% over 3 steps; d) EtNH <sub>2</sub> .HCl, EDC.HCl, HOBT, Et <sub>3</sub> N, DCM (anhydrous), 23 h, 52%. .....	209
Scheme 3.35 Synthesis of Cipro –, DFO + control <b>3-31</b> . a) NHS, EDC.HCl, DCM (anhydrous), 25 h; b) Desferrioxamine mesylate, Et <sub>3</sub> N, DMF, 50 °C, 24 h, 72% over 2 steps.....	210
Scheme 3.36 Reaction of <b>3-36</b> with glutathione in HEPES buffer in presence of dye <b>2-11</b> . a) GSH (10 eq.), <b>2-11</b> (0.1 eq.), 10% MeCN:HEPES, pH 7.4, rt, 24 h. ....	214
Scheme 3.37 Reaction of <b>3-36</b> with glutathione in HEPES buffer. a) GSH (10 eq.), caffeine (5 eq.), 10% MeCN:HEPES, pH 7.4, 37 °C, 74 h. ....	215
Scheme 4.1 Reactivity of selected aryl and heteroaryl chlorides with sodium methoxide, and relative S <sub>N</sub> Ar rates. Adapted from Joule and Mills. <sup>537</sup> .....	231
Scheme 4.2 Reduction pathways of nitro groups, and some mechanisms of toxicity associated with reduced species (indicated with red arrows). <sup>538,541–543</sup> Partially adapted from Nepali <i>et al.</i> <sup>538</sup> .....	231

Scheme 4.3 Varying reactivity of pyridine sulfonamides with glutathione/glutathione-S-transferase (GST). <sup>547,548</sup> .....	233
Scheme 4.4 Reaction of 2-pyrimidinesulfonamides with thioglycolic acid. <sup>549</sup> .....	233
Scheme 4.5 Reaction of 5-membered heterocyclic sulfonamides with glutathione. 0.5 mM sulfonamide, and 5/20 equivalents of glutathione were employed, and the percentage reactivity after 16-22 h was determined by HPLC after quenching with 1% H <sub>3</sub> PO <sub>4</sub> in MeCN. ....	234
Scheme 4.6 Reaction of 6-uracilmethylsulfone <b>4-8</b> with mouse liver homogenate or glutathione, with loss of methylsulfone group. <sup>546</sup> .....	235
Scheme 4.7 Reaction of 4-sulfonyl-2-pyridones with glutathione. <sup>559,560</sup> ..	236
Scheme 4.8 Reactivity of four heterocyclic methylsulfones with cysteine derivative <b>4-12</b> as studied by Toda <i>et al.</i> <sup>561</sup> .....	236
Scheme 4.9 Suggested S <sub>N</sub> i decomposition mechanism for pyrimidine-2-sulfonyl chloride (based on Kwart and Body, 1965). <sup>574</sup> .....	238
Scheme 4.10 Synthetic methodology employed by Wright and Hallström for the synthesis of heterocyclic sulfonamides. <sup>571</sup> .....	238
Scheme 4.11 Bornholdt <i>et al.</i> 's adaptation of Wright and Hallström's methodology to produce stable activated sulfonate esters. <sup>575</sup> .....	239
Scheme 4.12 Conversion of heterocyclic sulfonic acids to the corresponding sulfonyl chlorides. <sup>582,583</sup> .....	239
Scheme 4.13 Examples of other oxidative routes to heterocyclic sulfonamides. <sup>584-586</sup> .....	240
Scheme 4.14 Selected examples of organometallic coupling routes to sulfonamides/activated sulfonate esters.....	240
Scheme 4.15 Electrochemical synthesis of pyrimidine-sulfonamide <b>4-28</b> . <sup>600</sup> .....	241
Scheme 4.16 A retrosynthetic analysis of the key coupling steps to <b>4-32</b> , and identification of the three key coupling components.....	245
Scheme 4.17 Proposed synthetic route to benzyl thioether <b>4-38</b> . ....	246
Scheme 4.18 Proposed conditions for <i>in situ</i> synthesis of sulfonyl chloride <b>4-39</b> . ....	247
Scheme 4.19 Proposed synthetic route to benzyl-protected ciprofloxacin <b>4-41</b> . ....	247

Scheme 4.20 Proposed synthetic route to pyrazine-sulfonamide <b>4-43</b> ....	248
Scheme 4.21 Proposed synthesis of benzyl-protected azotochelin NHS ester <b>4-45</b> , and coupling to pyrazine-sulfonamide component <b>4-43</b> .....	249
Scheme 4.22 Proposed global debenylation to yield target conjugate <b>4-32</b> . .....	250
Scheme 4.23 Proposed synthesis of Cipro –, Azoto + control <b>4-47</b> . ....	251
Scheme 4.24 Proposed synthesis of Cipro +, Azoto – control <b>4-52</b> . ....	252
Scheme 4.25 Proposed synthesis of Cipro –, Azoto – control <b>4-53</b> . ....	252
Scheme 4.26 Synthesis of benzyl-protected ciprofloxacin <b>4-41</b> . a) Boc <sub>2</sub> O, NaHCO <sub>3</sub> , DMF (anhydrous), 18 h, then BnBr, 90 °C, 26 h, 83%; b) TFA (10% v/v), DCM, 17 h, 96%. ....	253
Scheme 4.27 Synthesis of pyrazine benzyl thioether <b>4-38</b> . a) <i>N</i> -Boc ethylenediamine, EDC.HCl, HOBt, DCM (anhydrous), 24 h, 84%; b) BnSH, Et <sub>3</sub> N, MeOH (anhydrous), 0 °C to rt, 24 h, 78%. ....	254
Scheme 4.28 Chemical equations for quenching of chloramines by sodium metabisulfite.....	255
Scheme 4.29 Synthesis of pyrazine-sulfonamide <b>4-42</b> . a) 1,3-dichloro-5,5'-dimethylhydantoin, DCM/AcOH:H <sub>2</sub> O (biphasic), 0 to 20 °C, 7.5 h; b) <b>4-41</b> , Et <sub>3</sub> N, DCM, 24 h, 61% over two steps.....	256
Scheme 4.30 Testing of hydrogenolysis conditions. a) H <sub>2</sub> , Pd(OH) <sub>2</sub> /C, THF:MeOH, 20 h. ....	258
Scheme 4.31 Proposed synthetic route to PMB-protected azotochelin <b>4-57</b> . New protecting groups highlighted in red.....	259
Scheme 4.32 Revised synthetic route to target conjugate <b>4-32</b> . Protecting group changes are highlighted in red. ....	260
Scheme 4.33 Testing of PMB deprotection conditions on pyrazine-sulfonamide <b>4-42</b> . a) HCl (129 eq.), dioxane, 0 to 20 °C, 17 h. ....	261
Scheme 4.34 Synthesis of PMB-protected azotochelin <b>4-57</b> . a) PMB-Cl, K <sub>2</sub> CO <sub>3</sub> , KI, acetone (anhydrous), reflux, 72 h, 91%; b) aq. NaOH, dioxane, 72 h, 90%; c) <i>L</i> -lysine methyl ester dihydrochloride, EDC.HCl, HOBt, DIPEA, DMF, 50 °C, 40 h, 55%; d) aq. NaOH, THF, 23 h, 71%. ....	262
Scheme 4.35 Synthesis of key pyrazine-sulfonamide <b>4-55</b> . a) 1,3-dichloro-5,5'-dimethylhydantoin, DCM/AcOH:H <sub>2</sub> O (biphasic), 0 to 20 °C, 15 h; b) ciprofloxacin, DIPEA, DCM, 0 to 20 °C, 18-24 h, 52% over two steps. ....	263

Scheme 4.36 Synthesis of TFA salt <b>4-62</b> . a) TFA (10% v/v), DCM (anhydrous), 5 h, 73%. .....	263
Scheme 4.37 Synthesis of PMB-protected azotochelin NHS ester <b>4-61</b> . a) <i>N</i> -hydroxysuccinimide, EDC.HCl, DCM, 18 h, 55%. .....	264
Scheme 4.38 Coupling of PMB-protected azotochelin NHS ester <b>4-61</b> and TFA salt <b>4-62</b> . a) <b>4-61</b> , Et <sub>3</sub> N, DCM, 24 h, 91%. .....	265
Scheme 4.39 HCl-mediated PMB removal to give target conjugate <b>4-32</b> . a) HCl, dioxane, 4.5 h, 33%. .....	266
Scheme 4.40 Synthesis of morpholine-sulfonamide TFA salt <b>4-49</b> . a) 1,3-dichloro-5,5'-dimethylhydantoin, DCM/AcOH:H <sub>2</sub> O (biphasic), 0 to 20 °C, 15 h; b) morpholine, Et <sub>3</sub> N, DCM, 0 °C to rt, 18 h, 40% over two steps; c) TFA (10% v/v), DCM, 0 °C, 5 h, 68%. .....	268
Scheme 4.41 Coupling of TFA salt <b>4-49</b> and NHS ester <b>4-61</b> . a) Et <sub>3</sub> N, DCM, 16 h, 87%. .....	269
Scheme 4.42 Synthesis of Cipro -, Azoto + control <b>4-47</b> . a) HCl, dioxane, 26 h, 36%. .....	270
Scheme 4.43 Synthesis of Cipro +, Azoto - control <b>4-52</b> . a) HCl, DCM:dioxane (3:1), 0 °C to rt, 24 h, 60%. .....	270
Scheme 4.44 Synthesis of Cipro -, Azoto - control <b>4-53</b> . a) HCl, EtOH, rt, 48 h, 61%. .....	271
Scheme 4.45 Reaction of <b>4-49</b> with glutathione in the presence of SO <sub>2</sub> -detecting dye <b>2-11</b> . a) GSH (10 eq.), <b>2-11</b> (0.1 eq.), 10% DMSO/HEPES buffer, pH 7.4, rt, 30 min. ....	272
Scheme 4.46 Reaction of <b>4-49</b> and <b>1-56</b> with glutathione in HEPES buffer. a) GSH (10 eq.), 10% DMSO/HEPES, pH 7.4, rt, 60 min; b) GSH (10 eq.), 10% MeCN/HEPES, pH 7.4, rt, 12 h. ....	273
Scheme 4.47 Synthesis of morpholine sulfonamide <b>4-68</b> and subsequent SO <sub>2</sub> release. a) 1) 1,3-dichloro-5,5'-dimethylhydantoin, DCM/AcOH:H <sub>2</sub> O (biphasic), 0 to 20 °C, 14 h; 2) morpholine, Et <sub>3</sub> N, DCM, 0 °C to rt, 5.5 h, 59% over two steps; b) GSH (10 eq.), <b>2-11</b> (0.1 eq.), 10% DMSO/HEPES, pH 7.4, rt, 2.5 h. ....	274
Scheme 4.48 Synthesis of pyridone thioether <b>4-73</b> and attempted oxidative chlorination reaction. a) CS <sub>2</sub> , <sup>t</sup> BuOK, THF, 0 °C, 1.5 h, then BnBr, 18 h, 58%; b) cyanoacetamide, <sup>t</sup> BuOK, <sup>t</sup> BuOH, 80 °C, 24 h, 52%; c) <i>N</i> -Boc-2-	



bromoethylamine, K <sub>2</sub> CO <sub>3</sub> , DMF, rt, 20 h, 50%; d) 1,3-dichloro-5,5'-dimethylhydantoin, DCM/AcOH:H <sub>2</sub> O (biphasic), 7 h, 0 °C to rt. ....	287
Table 1.1 Key enzymatically-cleaved triggers for self-immolative systems.	82
Table 3.1 Solubilities observed for <b>3-14</b> and control compounds in 2% DMSO in MHII and 50% v/v DMSO in MHII. ND = not determined. ....	212
Table 3.2 Panel of bacterial species selected for antimicrobial testing. ....	218
Table 3.3 Zones of inhibition (mm) for each compound against bacterial panel. R = ciprofloxacin-resistant, S = ciprofloxacin-sensitive, I = ciprofloxacin-susceptible with increased exposure (ie. Less sensitive, but higher doses still effective). ....	219
Table 3.4 MIC and MBC values of ciprofloxacin and <b>3-14</b> for strains of <i>S. epidermidis</i> (CN1) and <i>K. pneumoniae</i> (KL3). ND = not determined. ....	221
Table 3.5 MIC and MBC values of ciprofloxacin and <b>3-14</b> for strains of <i>S. epidermidis</i> (CN1) and <i>K. pneumoniae</i> (KL3), including strains subjected to forced adaptation assays with ciprofloxacin or <b>3-14</b> , which are indicated by *. ND = not determined. ....	222
Table 4.1 Percentage reactivity of selected 5-membered heterocyclic sulfonamides with glutathione. ....	234
Table 4.2 Solubilities observed for <b>4-32</b> , <b>4-52</b> , and <b>4-53</b> in 2% DMSO in MHII and 50% DMSO in MHII. ND = not determined. ....	275
Table 4.3 Panel of bacterial species selected for antimicrobial testing. ....	280
Table 4.4 Zones of inhibition (mm) for each compound against bacterial panel. R = ciprofloxacin-resistant, S = ciprofloxacin-sensitive, I = ciprofloxacin-susceptible with increased exposure (ie. Less sensitive, but higher doses still effective). ....	281
Table 5.1 Solvents and concentrations used for preparation of stock solutions. ....	383
Table 5.2 Stock volumes used to prepare samples for calibration curve.	386
Table 5.3 Stock solutions and volumes used for preparation of M9 media. ....	391

## **Accompanying Material**

An electronic copy of this thesis, plus data for all of the experiments presented herein, will be uploaded to an electronic repository, and will be available on request.

## Acknowledgements

*“Is your project essentially for making bacterial clickbait?” Ed Moye, 2021*

Firstly, I wish to thank my supervisors, Professor Anne Duhme-Klair and Dr Anne Routledge, for giving me the opportunity to work on this fascinating project, and for their constant support, encouragement and patience throughout this PhD. Thank you for believing in my crazy ideas, and supporting me in pursuing them, and for expanding on them with many ideas and suggestions of your own. I would also like to thank Dr Will Unsworth for acting as my IPM throughout my project, and providing a number of ideas and suggestions to improve both my research and my writing; I can only hope some of that improvement is reflected in this thesis! I would also like to thank the EPSRC for funding this research.

I also would like to say a massive thank you to all the technical staff at York, without whom I wouldn't have been able to carry out this project. To Heather and Alex, for the NMR service, to Karl, Rosaria, and Angelo, who run the mass spectrometry service, to Graeme for CHN analysis, and his accurate mass balance, to Amanda for training me on the HPLC instruments, and to Scott for keeping the service running, to our lab technician Emma, to the staff in workshops for keeping us in important bits of glassware and electronics equipment, to Dr Gavin Thomas for providing us with lab space in Biology, and to Adrian, Cerys, and Angela, for carrying out biological testing of my compounds.

Thank you to everyone in the AR and AKDK groups for your enjoyable company and consistent support throughout my PhD, for putting up with my years of rambling presentations, and for all the pub trips and board game nights. Thank you to James, my birthday twin and desk mate, for all your help with research and practical chemistry, and for the endless hours of football and FPL discussion, to Thorsten, for his excellent sense of humour and many a long Friday lunch, to Ros, for an endless supply of fantastic cakes, to Nat, for putting up with my chaos and mess in the lab, to Sophie, for her German lessons, and bringing her energy and enthusiasm to the group, and

to Ben and Lisa, for all of your help with chemistry, and generally answering my stupid questions! Thank you to all of the project students I've helped and supervised, for their hard work and willingness to try different things, and for putting up with my slightly chaotic style of mentoring. Thank you also to Dr Dan Raines, Dr Luisa Ciano and Dr Ben Coulson, who made me feel welcome when I arrived in the AKDK group, and for all their help and support, and to everyone in E014 over the last four years, including (but not limited to) Abbey, Peter, John, Luisa, Martin and Will.

Thank you to my previous supervisors at the University of Warwick, notably Dr Graham Pattison, who gave a clueless first year student his first opportunity to carry out academic research – I think it may have caught on!

Thank you to all of my friends and housemates for helping keep me sane over the course of this PhD, in particular Izaak, Charlie, Thomas, Jamie, and Ewan. Also, thank you to everyone who I've played in a brass band with at Emley, Imps and UYBB over my PhD, and everyone at UniBrass, you've been a massive source of enjoyment in these four years.

Thank you to my parents, Stephen and Julia, for their encouragement and belief, and for always being there whenever needed. Without them, I wouldn't have started down this path, and you've had faith in me every step of the way. Thank you to the rest of my family for all of their support, to my brothers, to my grandparents Pauline and Ernie, and to my other grandparents, Elsie and Cecil, you are both sadly missed, and I hope I'll get to see you again some day.

Last and definitely not least, thank you to my partner Robyn, for putting up with me even when I've been working long hours, and when I've been worrying about chemistry, for always finding some way to make me smile, for keeping me sane during the pandemic, and for being there when I've needed help and support. I can't really put into words how important your love and support has been during this entire process, and I couldn't have made it through it without you there.

## Declaration

I declare that the work presented in this thesis is my own and, to the best of my knowledge, original. This work was undertaken at the University of York under the supervision of Professor Anne-Kathrin Duhme-Klair and Dr Anne Routledge between October 2017 and September 2021. The work presented within this thesis has not been submitted for any other qualification or publication. The following work was carried out by or with the assistance of other researchers:

- All mass spectrometry experiments were performed by Mr Karl Heaton, Dr Rosaria Cercola or Mr Angelo Lopez.
- Elemental analyses were performed by Dr Graeme McAllister.
- Analytical and preparative HPLC experiments were carried out with the aid of Ms Amanda Dixon and Dr Scott Hicks.
- NMR spectra recorded on the 500 and 600 MHz spectrometers were collected by Mr Thorsten Dreher or Ms Heather Fish.
- Biological experiments in Chapter 2 were carried out by Dr Adrian Chu.
- Biological experiments in Chapter 3 and 4 were carried out by Ms Cerys Orritt and Dr Angela Oates at the Hull York Medical School.
- Syntheses of compounds **4-58**, **4-59**, **4-60** and **4-57** were shared between the author, Dr Benjamin Large, and Ms Rosalind Booth.
- Synthesis of compound **2-30** was carried out by Dr Ellis Wilde.
- Synthesis of compound **3-22** was carried out by Mr Nick Kyriacou.
- Synthesis of compound **3-38** was carried out by Ms Holly Clarke.
- Synthesis of compound **3-46** was carried out by Dr Thomas Sanderson.
- Synthesis of compound **4-69** was carried out by Mr Luke Stirland.

Conor Black

# **Chapter 1 :**

## **Introduction**

## 1.1 Antimicrobial Agents – Development and Resistance

### 1.1.1 The Discovery of Antibiotics

Antibiotics are commonly defined as medication that combats bacterial infection by inhibiting bacterial growth (bacteriostatic), or by killing the bacteria (bactericidal). The use of this term has varied over time. Selman Waksman, who discovered numerous antibiotics including streptomycin (**Figure 1.1**), one of the first known cures for tuberculosis (TB),<sup>1</sup> was the first to use the term in a medical context.<sup>2,3</sup> He defined antibiotics as “*chemical substances of microbial origin that inhibit the growth or metabolic activities of bacteria and other microorganisms.*” This definition excludes fully synthetic antibacterial classes, like sulfonamides and quinolones, but has broadened over time in popular usage to the common definition above. In a medicinal sense, the related terms antibacterial (specifically active vs. bacteria) and antimicrobial (active vs. microorganisms) may also be used.

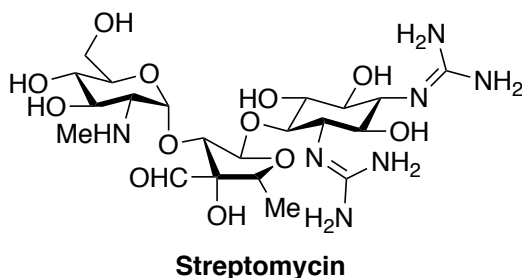


Figure 1.1 Structure of streptomycin, the first known antibiotic to treat TB.

The discovery of antibiotics was arguably one of the greatest advances of the 20<sup>th</sup> Century, allowing treatment of a wide range of conditions including tuberculosis and pneumonia, and greatly reducing bacterial infection as a cause of human death. Between 1944 and 1972, the average human life expectancy jumped by 8 years, an increase that has been largely credited to antibiotics.<sup>4</sup>

Perhaps the earliest evidence of antibiotic use in humans comes from archaeological evidence from ancient Nubia (modern day Sudan/southern Egypt).<sup>5,6</sup> Samples of bone from 350-550 AD were found to exhibit a fluorescence pattern similar to modern-day tetracycline-labelled bone<sup>7,8</sup> (tetracyclines bind to calcium in bones and teeth, yielding a complex that fluoresces under UV/visible light (**Figure 1.2**)).<sup>9-11</sup> It was later shown that the

tetracycline antibiotics were incorporated into the bone itself, rather than being present as a result of bacterial contamination.<sup>8</sup> It is suggested that, given the relatively large percentage of bone cells labelled, the source of the tetracycline must be dietary in nature. In fact, the active ingredient may have been the beer that the ancient Nubians brewed and drank!<sup>8</sup> Other early attempts at treatment of bacterial infections often employed the use of moulds, including the use of mouldy bread, with evidence from various cultures of its effectiveness.<sup>6</sup>

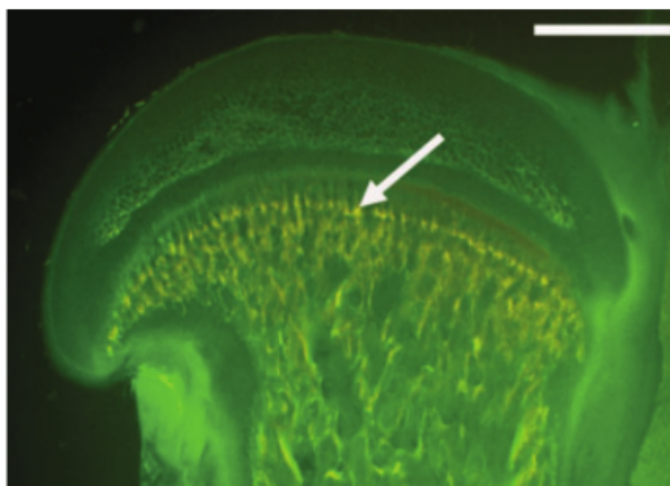
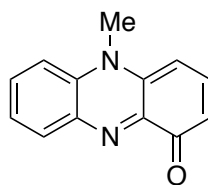


Figure 1.2 Sample of bone displaying typical golden tetracycline fluorescence under visible light (458 nm). Reprinted with permission from Pautke *et al.*, *J. Anat.*, 2010, 217, 1, 76-82.<sup>11</sup> Copyright 2010, John Wiley and Sons.

A similar strategy was employed in the 1890's by two German doctors, Rudolf Emmerich and Oscar Löw, who noted that a green bacterium causing infections in injured patients could inhibit the growth of other microbes.<sup>5,6,12</sup> They isolated samples of the bacterium, *Pseudomonas aeruginosa*, from infections in injured patients, and used extracts from the bacteria, termed pyocyanase, to try and treat infections, with mixed results (the extracts proved toxic to humans).<sup>5,6</sup> The active ingredient was later shown to be the blue pigment pyocyanin (**Figure 1.3**).<sup>13</sup>

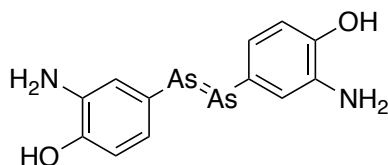




**Pyocyanin**

Figure 1.3 Structure of pyocyanin, the active ingredient in Emmerich and Löw's bacterial extracts.

The concept of a chemical that can target specific microbes inside the body was originally suggested and developed by Paul Ehrlich, who coined the phrase “magic bullet” to describe a drug that could go straight to its intended cell target.<sup>14</sup> This concept led him to develop arsphenamine, or salvarsan, which was effective in treating syphilis, and is considered the first modern chemotherapeutic drug (**Figure 1.4**).<sup>14,15</sup> Arsphenamine is an arsenic-containing compound based on arsanilic acid, which had been shown to be active against trypanosomes in 1905 (parasites responsible for sleeping sickness and Chagas disease).<sup>15</sup> This observation inspired Ehrlich, who aimed to synthesise an analogue of arsanilic acid that could be effective against syphilis, making this the first example of structure optimisation for improvement of biological activity in medicinal chemistry.<sup>14</sup>



**Arsphenamine**

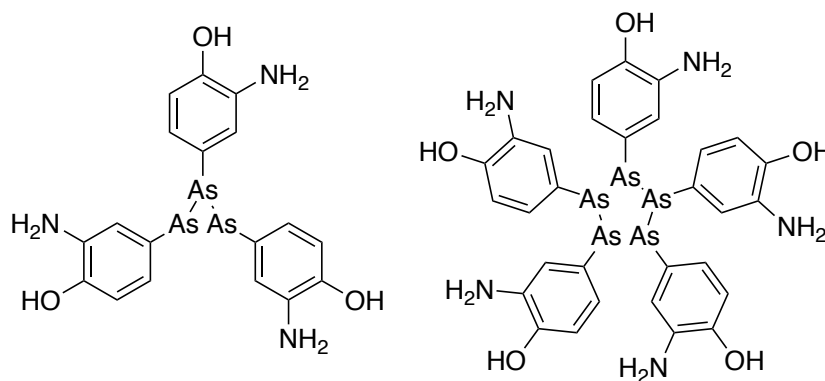


Figure 1.4 Structures of arsphenamine. Initially thought to be a dimer, a study in 2005 showed that the structure is a mix of the trimer and the pentamer.<sup>16</sup>

Further progress was made with the discovery of penicillin by Alexander Fleming in 1928, the first antimicrobial natural product to be developed into an antibiotic for use in humans,<sup>17</sup> and the development of the sulfonamide antibiotics by Gerhard Domagk at Bayer in the 1930's,<sup>18</sup> which became the first antibiotics widely used for treatment of bacterial infection (**Figure 1.5**). These discoveries, plus many more, sparked a "Golden Age" of antibiotics in the 1950's and 60's, in which almost all of the major classes of antimicrobial agents in use today were discovered.<sup>6,19</sup>

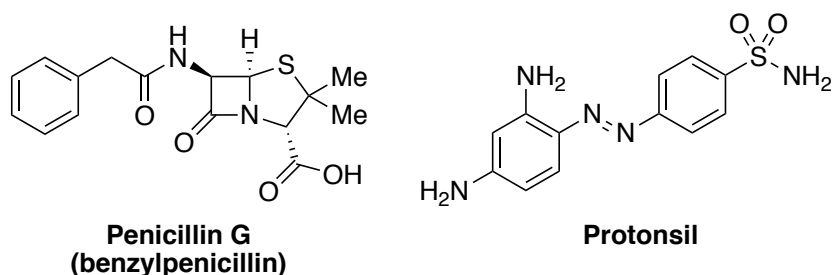


Figure 1.5 Structures of penicillin G (benzylpenicillin) and protosil, the first of the sulfonamide antibiotics.

### 1.1.2 The Modern Antibiotic Catalogue

In the modern age, a wide variety of antibiotic classes are available for treatment of bacterial infections. A 2014 study by van Boeckel *et al.* examined the volume of antibiotics sold in pharmacies across 71 countries between 2000 and 2010, providing an insight into the volumes of consumption of various antibiotics across this period.<sup>20</sup> By far the most common class in usage is the penicillins, and their related subgroup, the cephalosporins (**Figure 1.6**). These antibiotics can display activity vs. either Gram-positive or Gram-negative bacteria, and exert antimicrobial activity by covalent inhibition of penicillin binding proteins (PBPs), which catalyse the final cross-linking step in the synthesis of peptidoglycan, a key component of bacterial cell walls.<sup>21</sup> Two other major penicillin subgroups exist, the carbapenems and the monobactams, although these are less commonly prescribed.

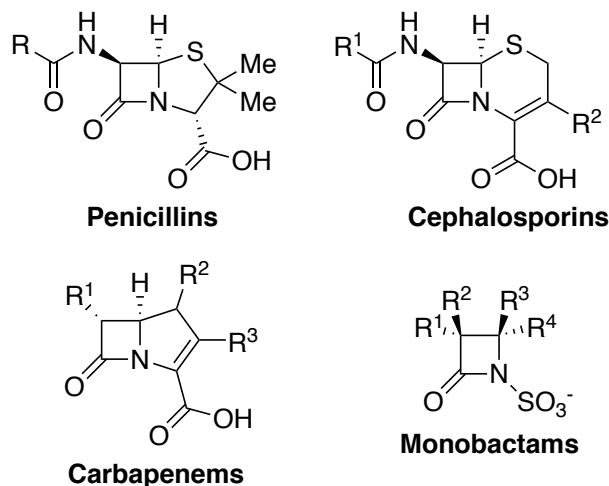


Figure 1.6 Generic structures of the penicillin antibiotics, and related subgroups.

Macrolide antibiotics were the next most common class prescribed.<sup>20</sup> These antimicrobials were originally isolated from strains of *Streptomyces* bacteria, with pikromycin the first example to be isolated and purified in 1950.<sup>22,23</sup> Erythromycin, perhaps the best-known example of this class, was discovered around the same time,<sup>24</sup> and was the first macrolide to enter clinical use in 1953 (**Figure 1.7**).<sup>25,26</sup> The common feature of this class of antibiotics is a large 12 to 16-membered macrocyclic lactone ring, which is decorated with various functional groups, often including sugar units.<sup>23</sup> Macrolides act by binding to the 50S-subunit of the prokaryotic ribosome, occupying a site within the peptide exit tunnel, which leads to premature termination of bacterial peptide synthesis.<sup>23</sup>

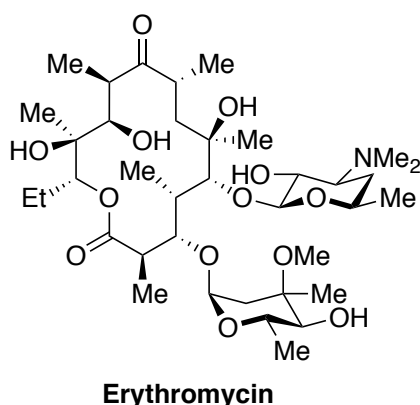


Figure 1.7 Structure of erythromycin, the first commercial macrolide antibiotic.

The fluoroquinolones also form a heavily-prescribed class of antibiotics, with four generations of derivatives available. Apart from first-generation

quinolones like nalidixic acid, this class of antibiotics typically consists of a fluorinated quinolone ring, with a wide variety of substituents (**Figure 1.8**). The presence of the fluorine atom, incorporated from the second generation onwards, resulted in greater potency and increased cell penetration.<sup>27,28</sup> Fluoroquinolones target DNA gyrase/topoisomerase IV enzymes, which are responsible for unwinding double-stranded bacterial DNA into single strands ready for transcription in DNA synthesis. This is carried out by first cleaving the tightly-coiled DNA strands.<sup>29,30</sup> The fluoroquinolones bind to the formed DNA-enzyme complex, and prevent re-ligation of the DNA, resulting in inhibition of DNA replication.<sup>31</sup> This can result in activation of the cellular SOS response, and potentially fragmentation of the chromosome, resulting in apoptosis and cell death.<sup>32</sup>

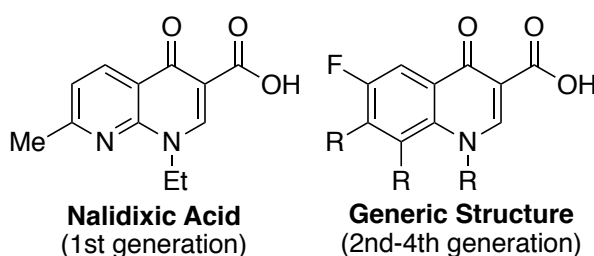


Figure 1.8 Structures of nalidixic acid, the first fluoroquinolone antibiotic, and the generic structure of second to fourth generation fluoroquinolones.

Tetracycline antibiotics are another example of a key class of antibiotics first isolated and purified from *Streptomyces* bacteria. The first example of this class, Aureomycin (chlortetracycline), was isolated from a newly-identified strain, *Streptomyces aureofaciens*, and was first approved for clinical use in 1948.<sup>33</sup> A second example, Terramycin (oxytetracycline), was discovered by researchers at Pfizer and approved for clinical use in 1950 (**Figure 1.9**).<sup>33,34</sup> Initially a bulk chemical company that had first stepped into the antibiotic market to produce penicillin during the Second World War, Terramycin was Pfizer's first independent venture into antibiotic discovery and manufacturing, and proved a massive success, so much so that Terramycin and bulk antibiotic production made up three-quarters of Pfizer's total sales in 1952.<sup>34</sup> Tetracyclines consist of a decorated naphthacene ring system consisting of four fused rings.<sup>33</sup> Tetracyclines are protein synthesis inhibitors; they are capable of binding to the 30S subunit of the bacterial ribosome, and inhibiting binding of aminoacyl tRNA to the ribosome.<sup>33</sup>

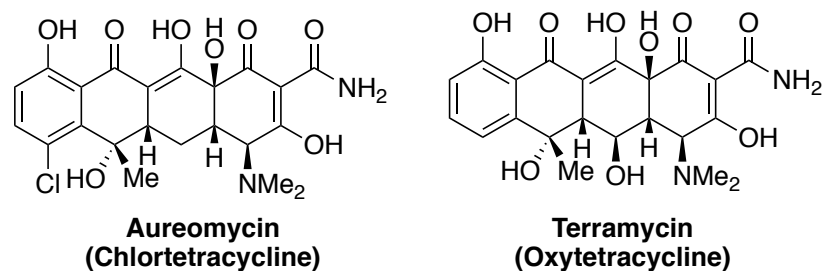


Figure 1.9 Structure of the first two commercial tetracycline antibiotics.

The final highly-prescribed (>5,000,000,000 doses) class of antibiotics is the trimethoprim class. While van Boeckel *et al.*'s original report does not specify the contents of this class, other reports of this type group sulfonamide antibiotics into the same class as trimethoprim,<sup>35,36</sup> as both antibiotics are often co-administered, due to their *in vitro* synergy.<sup>37,38</sup> Both antimicrobials act as inhibitors of folic acid synthesis. Sulfonamides act as a mimic of *p*-aminobenzoic acid (PABA), one of the substrates required for folic acid synthesis, and compete for binding to the enzyme dihydropteroate synthase (DHPS), while trimethoprim can act as a structural analogue of the pteridine part of dihydrofolic acid, and inhibit dihydrofolate reductase, another enzyme in the folic acid synthesis pathway (**Figure 1.10**).<sup>39,40</sup>

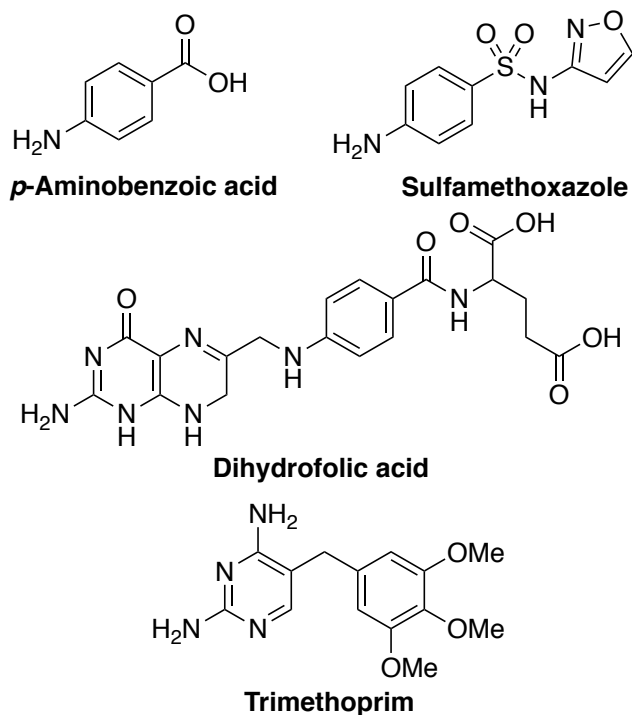
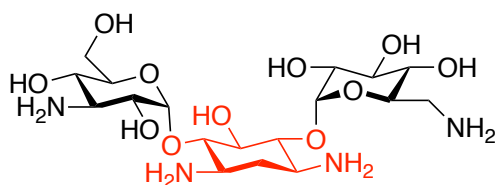


Figure 1.10 Structure of sulfonamide antibiotic sulfamethoxazole and trimethoprim, plus *p*-aminobenzoic acid and dihydrofolic acid, the two substrates of the folic acid synthesis pathway they mimic.

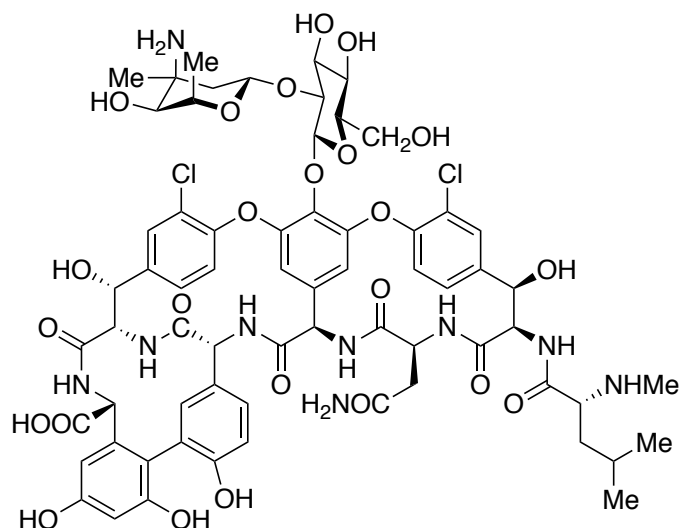
Other key classes of antibiotics do not receive the same volume of use as those described above, for a variety of reasons. Aminoglycoside antibiotics like streptomycin (**Figure 1.1**) have played a vital role in the treatment of human infections. However, their usage has declined over time, mostly due to their toxicity and side effect profile, while some of the newer antibiotic agents like carbapenems also display a broader range of activity.<sup>41,42</sup> Typically consisting of two or more amino sugars attached to a central 2-deoxystreptamine core (**Figure 1.11**), apart from in streptomycin, which contains a streptidine instead,<sup>42,43</sup> aminoglycosides bind to the 30S subunit of the bacterial ribosome, altering the conformation of the acceptor site and promoting mistranslation of proteins.<sup>42,44</sup>



**Kanamycin A**

Figure 1.11 Structure of the aminoglycoside antibiotic kanamycin, with central 2-deoxystreptamine core highlighted in red.

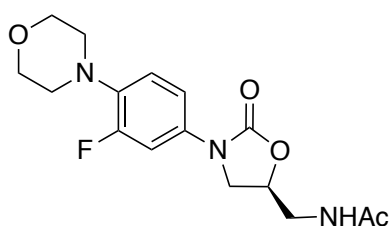
Glycopeptides are a class of antibiotic that have always seen relatively limited use due to their high toxicity and less convenient administration compared to other antibiotics developed around the same time as the first glycopeptide antibiotic, vancomycin, which came to market in 1958 (**Figure 1.12**).<sup>45</sup> Vancomycin has a short half-life in the body, and typically requires administration via an intravenous drip.<sup>45</sup> However, the increasing development of bacterial strains resistant to front-line antibiotics has forced a return to the usage of glycopeptides as last-resort antibiotics in cases of critical illness. These antibiotics function by forming a hydrogen bonding interaction with the terminal *D*-Ala-*D*-Ala residues of *N*-acetylmuramic acid and *N*-acetylglucosamine peptides before they can be cross-linked to form peptidoglycan, preventing bacterial cell wall synthesis.<sup>45,46</sup>



**Vancomycin**

Figure 1.12 Structure of vancomycin, the first glycopeptide antibiotic.

One of the newest classes of antibiotics available are the oxazolidinones. Similar to the sulfonamides and the fluoroquinolones, this class of antibiotics is fully synthetic, and not based on a natural product scaffold.<sup>47,48</sup> When the first antibiotic of this class, linezolid (**Figure 1.13**), was approved for clinical use in 2000, it became the first major new class of antibiotics to be approved since the fluoroquinolone nalidixic acid in 1963, and the topical antibiotic mupirocin in 1985.<sup>49–51</sup> The oxazolidinones contain a 3-aryl-2-oxazolidinone ring substituted at the 5-position with *S* stereochemistry.<sup>52</sup> It binds to the 50S subunit of the bacterial ribosome,<sup>53</sup> preventing the incorporation of tRNA into the acceptor site, inhibiting peptide bond formation.<sup>54</sup>



**Linezolid**

Figure 1.13 Structure of the oxazolidinone antibiotic linezolid.

Following the drought in approval of new antibiotic classes between the fluoroquinolones and oxazolidinones, a comparative torrent of antibiotics from new classes have reached the market since 2000 (**Figure 1.14**). These include daptomycin (lipopeptide, cell membrane damage), retapamulin (pleuromutilin, protein synthesis inhibitor), fidaxomicin (tiacumicin, RNA

synthesis inhibition, *C. difficile* only) and bedaquiline (diarylquinone, mycobacterial ATP synthase, TB only).<sup>50,51,55,56</sup> Other older antibiotics/antibiotic classes, like chloramphenicol, lincosamides, streptogramins and polymyxins, remain relevant,<sup>20,36</sup> and some are playing increasingly important roles in the treatment of infection, especially with the rise of bacterial resistance.<sup>57</sup>

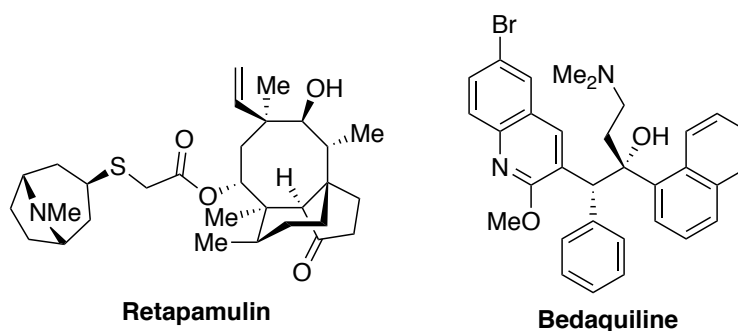
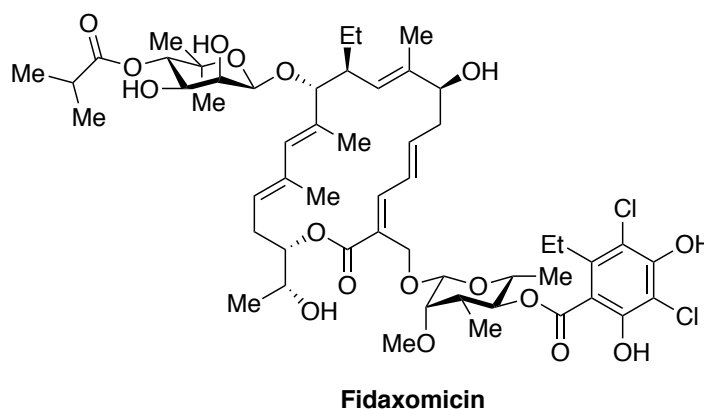
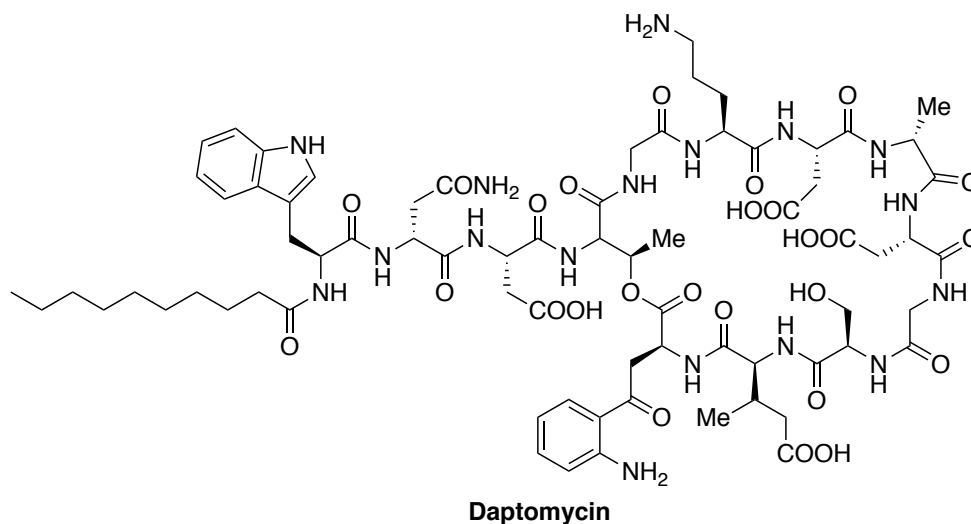


Figure 1.14 Antibiotics from new classes approved since 2003.



### 1.1.3 The Rise of Antibiotic Resistance

The systematic overuse of antibiotics, not just in medicine but also in agriculture<sup>58,59</sup> has led to the emergence of bacterial species that display resistance to the majority of front line drugs. More recently, increasing numbers of bacterial strains have been discovered to possess resistance to many of the antibiotics of “last resort”, including vancomycin,<sup>60</sup> carbapenems,<sup>61</sup> and colistin.<sup>62</sup> In the modern, highly-connected world, resistant bacterial strains have the ability to spread rapidly around the globe, a fact highlighted by the recent emergence of the enzyme NDM-1, a metallo-beta-lactamase enzyme with the ability to break down carbapenems.<sup>63</sup> Since its first discovery in 2006 in a Swedish patient, who had initially been admitted to hospital in New Delhi, India, bacteria possessing the *bla*<sub>NDM-1</sub> gene responsible for its synthesis have been detected in over 80 countries worldwide (Figure 1.15).<sup>64</sup>



Figure 1.15 Infographic created by the Pew Charitable Trusts to show the spread of the NDM-1 enzyme.<sup>64</sup>

There are a number of mechanisms by which bacteria can become resistant to antibiotics. Most are able to acquire genetic material from their environment by a process known as horizontal gene transfer, where genetic

material from other bacteria of identical or different species can be mobilised, often in the form of a plasmid, and transferred between bacterial cells.<sup>65</sup> In addition, bacteria can often produce their own antimicrobial agents to compete with other microbes in the environment; to ensure their survival, they must possess a resistance mechanism against that antimicrobial, which can then be transferred to other bacteria.<sup>65</sup> Resistance can also arise via mutations in the bacterial genome. The production of antimicrobials by bacteria creates a selection pressure in the environment, favouring the survival of resistant bacteria. As many existing antibiotics are based on these natural products used by bacteria, genes encoding resistance to them are likely to be common in the environment, This is highlighted by the 2016 discovery of a multi-drug resistant bacterium in an underground cave isolated from the surface 4 million years ago.<sup>66</sup> This bacterium (*Paenibacillus* sp. LC231) was resistant to 26 of 40 clinical antibiotics tested, and displayed five previously unknown resistance mechanisms, a case that serves to demonstrate the “reservoir” of resistance mechanisms that exist in the natural environment.<sup>66</sup>

The specific mechanisms of resistance in bacteria take four general forms:

- 1) Reduction of permeability in the bacterial cell wall/membrane
- 2) Upregulation of efflux pumps for removal of antibiotics from cytoplasm
- 3) Alterations to or degradation of the antibiotic
- 4) Alterations to the antibiotic’s target

The rise of antibiotic resistance has been exacerbated by a corresponding lack of development of new antibiotics, and especially new antibiotic classes since the “Golden Age” of antibiotic discovery.<sup>67</sup> There are a number of factors in this lack of development. Some are very human: the “Golden Age” and the rate of discovery of new antibiotics inspired a belief (and a complacency) that the problem of infection was fixed, or that development would continue at a rate sufficient to bypass any resistance that emerged. Sir Frank Macfarlane Burnet, winner of the 1960 Nobel Prize in Physiology or Medicine, remarked in 1962 that “at times one feels that to write about

infectious disease is to write of something that has passed into history”.<sup>68</sup> Many similar quotes can be found to attest to the prevalence of this viewpoint in the 1960s and 70s.<sup>69–72</sup>

The reduction in the impact of infectious diseases on everyday living has also impacted the urgency with which they are fought. Albert Schatz, one of the researchers responsible for the discovery of streptomycin in the 1940s,<sup>73</sup> had experienced the damage that TB could cause first-hand. In a 2002 interview he remembered knowing children at school and neighbours with the disease: “I saw them lose weight and waste away.” He felt an “overwhelming compulsion” to develop a new antibiotic capable of treating this deadly disease.<sup>74</sup> Nowadays, the lack of infection as a *visibly* widespread problem in the Western world could be argued to have contributed to the decline in action to combat it.

Some factors in the lack of antibiotic development are more practical, including the lack of new findings from traditional drug discovery methods like natural product screening, and the relative failure of newer approaches like genomics-based screening,<sup>19,75</sup> however the main factor is likely the economics of developing new antibiotics. Drug development is expensive; one recent estimate puts the cost of developing a new antibiotic from scratch at \$1.58 billion.<sup>76</sup> With any new antibiotics, usage will be strictly limited to slow the development of resistance, meaning the opportunity for a company to turn a profit on a new antibiotic is severely reduced. This means that large pharmaceutical companies have increasingly turned their backs on antibiotic development.<sup>75,77</sup>

This increase in the prevalence of antibiotic resistance, and the lack of progress in developing new methods to combat it, threatens to reverse the advances made by the discovery of antibiotics, potentially leading to “the end of modern medicine”.<sup>78</sup> It is clear that the development of new antibiotics or the repurposing/modification of older antibiotics to combat the spread of resistant bacteria is vital.

## 1.2 Iron and Siderophores

### 1.2.1 Iron – Vital for Life

One potential strategy towards the development of new antibiotics, or the revitalisation of older ones, is their modification towards the exploitation or targeting of bacterial nutrient uptake.<sup>79,80</sup> Bacteria must acquire a range of nutrients from their environment to enable them to survive and reproduce; among these is the first-row transition metal iron.

Indeed, iron is a vital element for almost all living organisms. It is present as a cofactor in a number of enzymes responsible for essential cellular processes, including the cytochromes in respiration,<sup>81</sup> and extends to other vital functions such as oxygen transportation in human blood, and nitrogen fixation in plants.<sup>82,83</sup> One reason for the abundance of iron in biological systems is its versatility in redox chemistry; it can change between a number of oxidation states (+2 and +3 are the most common in biological systems, with +4 also possible), and can easily undergo spin state changes depending on the surrounding ligand environment.

Despite the relative abundance of iron (it is the 4<sup>th</sup> most abundant element in the Earth's crust), it is poorly bioavailable; most iron is present in the environment as Fe(III) hydroxides, which are poorly soluble in aqueous media. At pH 7, Fe(III) is usually considered to have a solubility of  $10^{-17}$  M,<sup>84,85</sup> although more complex models place it as high as  $10^{-9}$  M.<sup>86</sup> Bacteria typically require iron concentrations between  $10^{-7}$  and  $10^{-5}$  M to achieve optimum growth, meaning they cannot rely on direct acquisition of iron from the environment to survive, and must seek a way to make it more available.<sup>85,86</sup>

A similar situation of iron restriction exists in the human body, with the vast majority of iron present complexed within haemoglobin, or stored within ferritin or haemosiderin.<sup>82,87</sup> Only a small fraction of the body's iron is present in blood plasma, and even then is mostly bound by the iron transport protein transferrin.<sup>88</sup> This compartmentalisation of iron is in part due to its toxicity; when weakly bound, it can undergo redox cycling (Fenton chemistry) between Fe(II) and Fe(III), generating harmful radical species e.g.

hydroxyl radicals.<sup>89,90</sup> The sequestration of free iron also plays a role in the immune system, preventing bacteria from acquiring the iron they need to multiply and cause infections.<sup>91,92</sup> This restriction of iron supply has been termed “nutritional immunity”.<sup>93</sup>

### 1.2.2 Bacterial Iron Acquisition and Siderophores

As iron is critical for their survival, bacteria have evolved a number of mechanisms for solubilising and scavenging iron from their environment, the most common of which is the production and release of small molecule iron chelators, known as siderophores.<sup>94</sup> These are biosynthesised and secreted in response to iron deficiency,<sup>95</sup> and form strong complexes with Fe(III).

Siderophores are selective for Fe(III) binding over Fe(II), or other divalent metal ions (Cu, Zn, Ni, Mn); this allows a selectivity for iron binding over most other metals when released in biological systems, as other biologically-relevant 3+ cations are rare.<sup>96</sup> The hard character of the Fe(III) ion, especially the high positive charge, means that hard and negatively charged donors have the highest affinity for Fe(III); in biological systems, negatively charged oxygens are used as donors.<sup>96</sup> Fe(III) also prefers a octahedral coordination sphere as it allows access to relatively stable high-spin  $d^5$  species, hence this is the most common geometry observed in iron-siderophore complexes.<sup>96</sup> Occasionally nitrogen or sulfur can be used in siderophores, although with reduced iron affinity.<sup>96</sup>

A wide variety of binding groups and denticities are observed for different siderophores. The majority of siderophores are hexadentate, allowing them to form very stable 1:1 complexes with Fe(III), however many bi-, tri-, and tetradentate examples also exist.<sup>96</sup> The individual binding units for Fe(III) tend to be bidentate, with two or three binding units combined to form the tetradentate and hexadentate structures respectively. A range of bidentate binding units are found, but the most common are catechols, hydroxamates and  $\alpha$ -hydroxycarboxylates (**Figure 1.16**).<sup>96</sup>

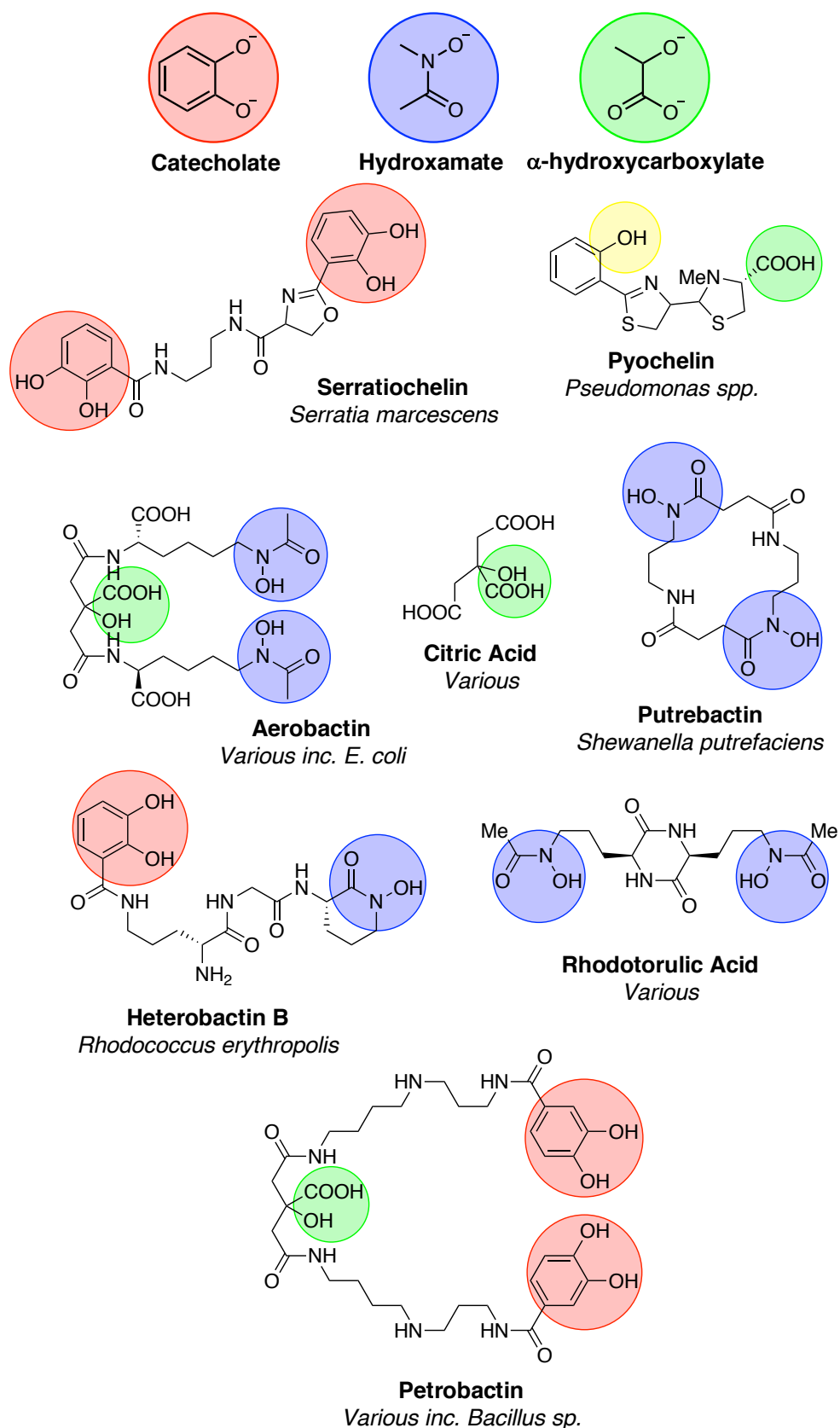
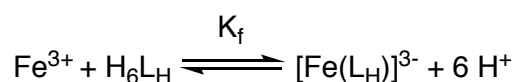


Figure 1.16 Common iron-binding ligands and their appearance in a wide variety of siderophore structures. Iron-binding groups are highlighted in coloured circles: red = catechol, blue = hydroxamate, green =  $\alpha$ -hydroxycarboxylate, yellow = other.

The strength of siderophore-iron binding was traditionally measured as the formation constant  $K_f$  for the system, usually displayed as the natural logarithm ( $\log K_f$ ).<sup>96,97</sup> For systems containing more than one siderophore,  $\log K_f$  is equal to the sum of the individual formation constants for the attachment of each ligand (**Figure 1.17**).<sup>96,97</sup> As shown in the equations below,  $\log K_f$  is representative of the iron-binding strength on complete deprotonation of the siderophore units. However, due to the varying pKa values of the iron-binding groups on siderophores (ranging from 3.5-5.0 for carboxylates to 6.5-8.0 and 11.5 for the two catechol OH groups), comparison of  $K_f$  values between siderophores, and especially siderophore classes, is difficult.<sup>96-98</sup>

For a hexadentate catecholate siderophore that loses six protons upon iron binding ( $H_6L_H$ ):



For a bidentate catecholate siderophore ( $H_2L_B$ ):

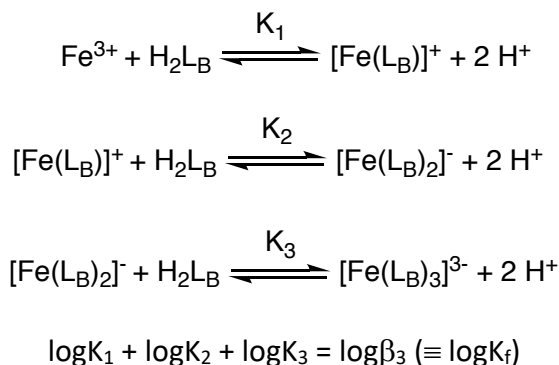


Figure 1.17 Equilibria for determination of formation constants of hexadentate and bidentate catechol siderophores.

This led to the introduction of the pFe(III) value, defined as  $-\log[Fe^{3+}]$ , where  $[Fe^{3+}]$  is the concentration of free Fe(III) in solution for a set of standard conditions ( $[Fe^{3+}_{total}] = 1 \mu M$ ,  $[Siderophore] = 10 \mu M$ ) at a set pH, usually pH 7.40. This allows comparison between siderophore binding strength in physiologically-relevant conditions.<sup>96-98</sup> A number of trends can be clearly seen by comparison of pFe(III) values at pH 7.40 (**Figure 1.18**). For example, cyclic siderophores are often stronger chelators than their linear analogues

(linear ferrioxamine B vs. cyclic ferrioxamine E), a result of the macrocyclic effect,<sup>99</sup> and catecholate siderophores are typically the strongest binders (enterobactin vs. ferrioxamine E), with catechols forming an optimal bite angle for Fe(III),<sup>100</sup> and the ionic radius of Fe(III) ideally suited to the octahedral field created by three catechol groups.<sup>96</sup>

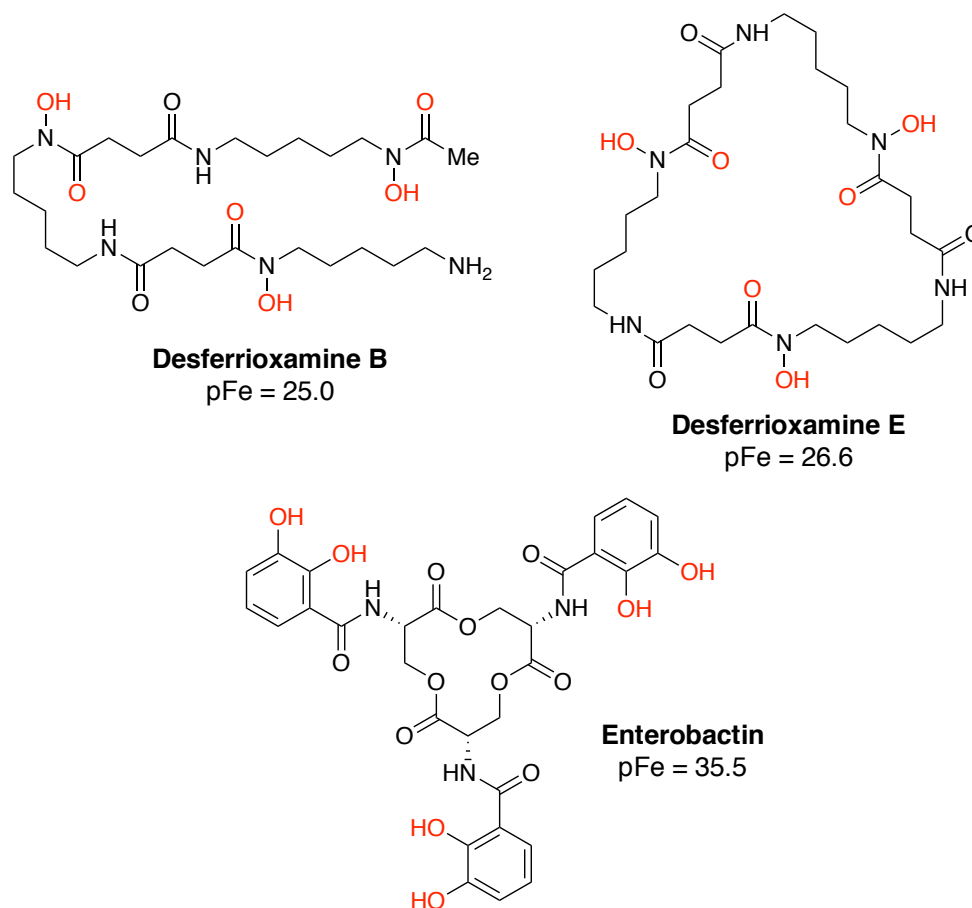


Figure 1.18 Comparison of some hexadentate siderophores and their pFe values at pH 7.40.

The pH at which pFe(III) is measured will also have an impact on the values obtained. Protons are constantly in competition with iron for binding to the siderophore donor atoms (as can be seen in the equilibria for **Figure 1.17**), so binding strength will be related to the pKa of the donor atoms. This is best exemplified by comparison of catechols and hydroxamate siderophores to carboxylates. While carboxylates such as aerobactin are weaker iron coordinators at neutral pH, the lower pKa of the carboxylic acid groups compared to hydroxamate or catechol groups makes them more suited to binding iron at low pH, where hydroxamates or catechols would be mostly



protonated, and therefore weaker chelators.<sup>97,101,102</sup> Indeed, Valdebenito *et al.* have examined the pFe of enterobactin (catecholate), desferrioxamine B (hydroxamate) and aerobactin (mixed hydroxamate-carboxylate) as a function of pH (**Figure 1.19**).<sup>102</sup> While enterobactin and desferrioxamine B clearly have a much higher pFe than aerobactin at higher pH range, below around pH 5.5 this difference is essentially neutralised, with the catecholate siderophore being mostly protonated, and therefore a weaker chelator, while the carboxylic acid of aerobactin remains mostly deprotonated, and able to bind iron more effectively.

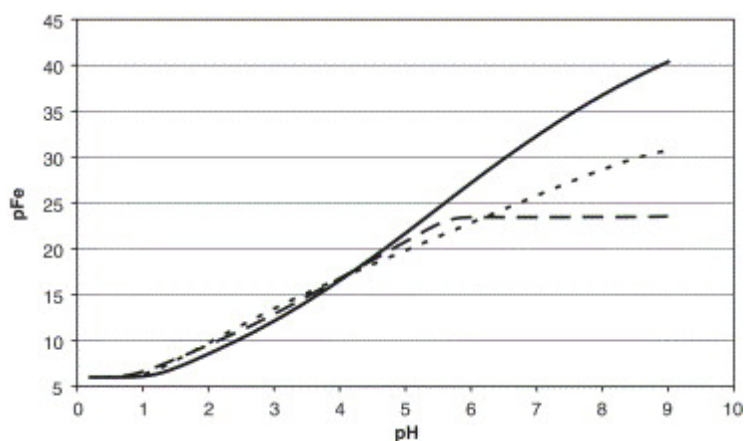
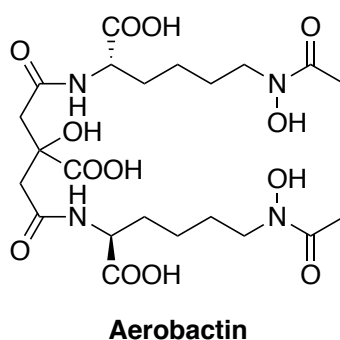


Figure 1.19 Structure of mixed hydroxamate-carboxylate siderophore aerobactin, and pFe of enterobactin (solid line), desferrioxamine B (dotted line) and aerobactin (dashed line) as a function of pH. Reprinted from *Int. J. Med. Microbiol.*, Vol. 296, Valdebenito *et al.*, *Environmental factors influence the production of enterobactin, salmochelin, aerobactin and yersiniabactin in Escherichia coli strain Nissle 1917*, 513-520, Copyright 2006, with permission from Elsevier.

### 1.2.3 Bacterial Siderophore Uptake Systems

With the large range of structural diversity that can be employed in siderophore design, it is perhaps no surprise that individual bacterial families tend to produce vastly different siderophore types, often tailored to their environments. For example, bacteria/fungi in acidic environments tend to produce carboxylate siderophores; as outlined above, these are weaker iron coordinators at neutral pH, but the lower pKa of the carboxylic acid groups compared to hydroxamate or catechol groups makes them more suited to binding iron at low pH.<sup>97,101,102</sup> While individual bacterial species will tend to biosynthesise and export one class of siderophores, they often possess the ability to scavenge siderophore classes produced by other bacterial species (termed xenosiderophores). For example, *Staphylococcus aureus* produces the carboxylate siderophores staphyloferrin A and B, but can also scavenge and utilise hydroxamate siderophores like desferrioxamine.<sup>103,104</sup>

The structural variety in siderophores, and the variations in siderophore utilisation between bacterial species, leads to key differences in iron uptake and siderophore transport systems between various bacterial species. For species such as *E. coli*, these uptake systems are well characterised.<sup>105</sup> In Gram-negative bacteria, the iron-carrying siderophores first bind to outer membrane transporter proteins and are actively transported across the outer membrane into the periplasm (**Figure 1.20**). These transporters tend to be specific for certain siderophores, or a group of structural homologs. For a bacterium to be able to scavenge xenosiderophores produced by other bacterial species, they must possess a corresponding transporter protein for recognition and uptake of that class of siderophore. The energy for the active transport is provided by interaction with a TonB complex on the inner membrane, which transmits chemical energy generated by the proton gradient across the inner membrane to the outer membrane transporter.<sup>106–</sup>

108

When in the periplasm, the siderophores bind to periplasmic binding proteins, which deliver them to a second set of active transporters in the cytoplasmic membrane. Again, the binding proteins tend to be specific for

certain siderophores, or families of siderophores, for example the binding protein FhuD in *E. coli* is specific for hydroxamate-type siderophores.<sup>109</sup> The active transporters in the cytoplasmic membrane acquire their energy from binding and hydrolysis of ATP (known as ATP-binding cassette, or ABC transporters).<sup>105</sup> Once inside the cytoplasm, there are two mechanisms of iron release depending on the siderophores used. For most, the Fe(III) ions can be reduced to Fe(II), thereby reducing the affinity of the siderophores for the Fe ions.<sup>105</sup> However, for the most powerful binders like enterobactin, enzymatic hydrolysis of the scaffold is required for iron release, as the iron remains bound strongly even in a reduced form.<sup>110</sup>

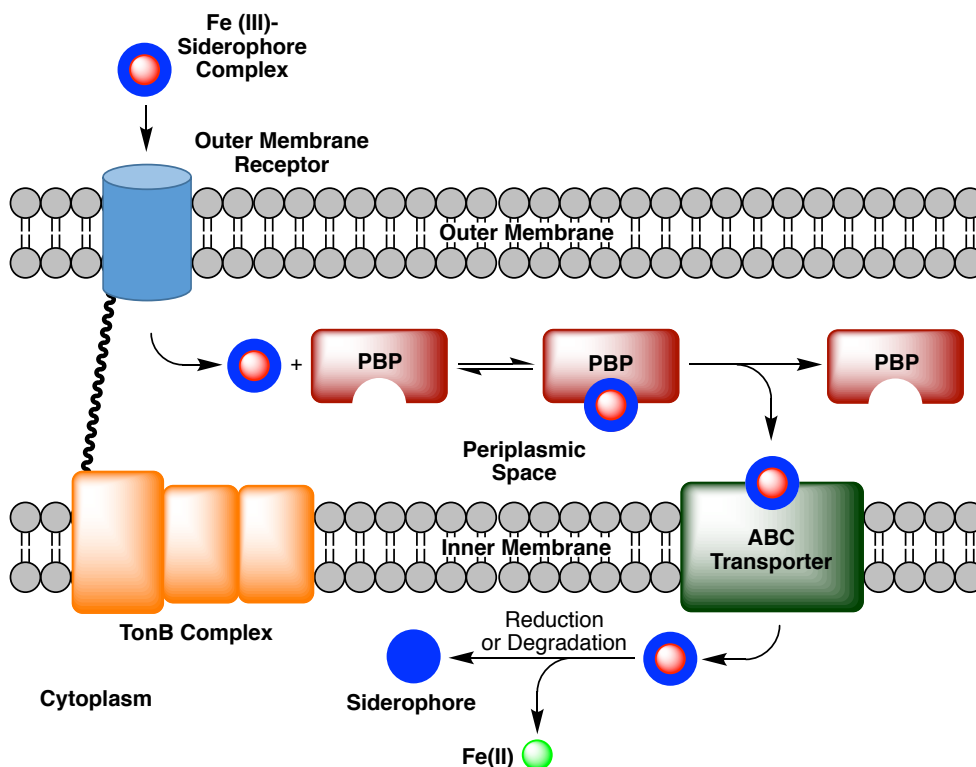


Figure 1.20 Diagram of typical bacterial siderophore uptake mechanism in Gram-negative bacteria.

While the majority of siderophore uptake in Gram-negative species follows the pathways described above, some variations exist. For example, the siderophore pyoverdine, which is produced by some *Pseudomonas* species e.g. *P. aeruginosa*, undergoes iron reduction and release in the periplasm of cells, without uptake of pyoverdine to the cytoplasm. The reduced iron can then be transported into the cytoplasm, while the siderophore component can be recycled to the extracellular medium.<sup>111,112</sup>

The process of siderophore transport remains similar for Gram-positive bacteria. As Gram-positive bacteria lack the outer membrane of Gram-negative bacteria, the iron-siderophore complexes bind directly to receptors on the cell membrane, and are transported across via ABC transporter proteins, a mode of transport analogous to that for the inner membrane of Gram-negative bacteria (**Figure 1.21**).<sup>103,113</sup>

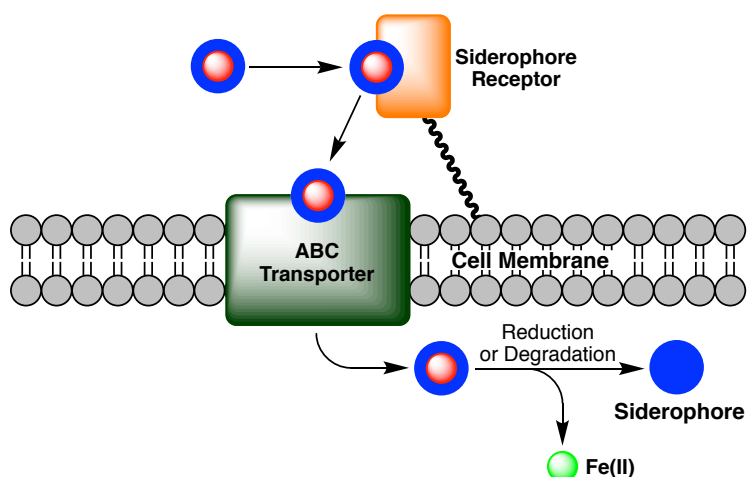


Figure 1.21 Diagram of typical bacterial siderophore uptake mechanism in Gram-positive bacteria.

In the human body, bacteria can also steal iron from iron-carrying proteins like haemoglobin and transferrin.<sup>105</sup> Bacteria can secrete proteins called haemophores to scavenge haem, or express cell surface receptors specific to haemoproteins.<sup>114</sup> In Gram-negative bacteria, the haem transport is almost identical to that for iron-siderophore complexes: it is transported across the outer membrane, picked up by periplasmic binding proteins and carried to an ABC transporter for active transport into the cytoplasm, where the haem is degraded for iron release.<sup>114</sup> In Gram-positive bacteria, the haem must first be transported via a series of proteins in the cell wall to the cell membrane before uptake and degradation can occur.<sup>103,114</sup>

Iron uptake from transferrin or lactoferrin is a key mechanism in a number of bacterial species, including the pathogenic *Neisseria* species, *N. meningitidis* and *N. gonorrhoeae*, the causative agents for meningitis and gonorrhoea respectively.<sup>115</sup> These proteins can be bound by outer membrane receptors, which can then extract the iron and transport it

through the outer membrane to a periplasmic binding protein (FbpA in *N. gonorrhoeae*).<sup>116,117</sup> This binding protein, which has a very similar iron binding site to transferrin itself,<sup>116</sup> carries iron to another transport protein complex embedded on the inner membrane, where it is transported into the cytoplasm.<sup>117</sup>

### 1.3 Trojan Horse Strategies

The well-known story of the Trojan Horse, the strategy by which the Greeks conquered the city of Troy in Greek mythology, has led to the term *Trojan Horse* becoming a byword for similar strategies in any number of fields, including a strategy for drug development that has received increasing attention in recent years, whereby an antibiotic is bound to a biologically desirable molecule that can be taken up by bacteria.<sup>80</sup> This aims to facilitate drug uptake via an alternative pathway to the regular antibiotic, therefore avoiding resistance mechanisms associated with decreased uptake (Figure 1.22).<sup>94</sup>

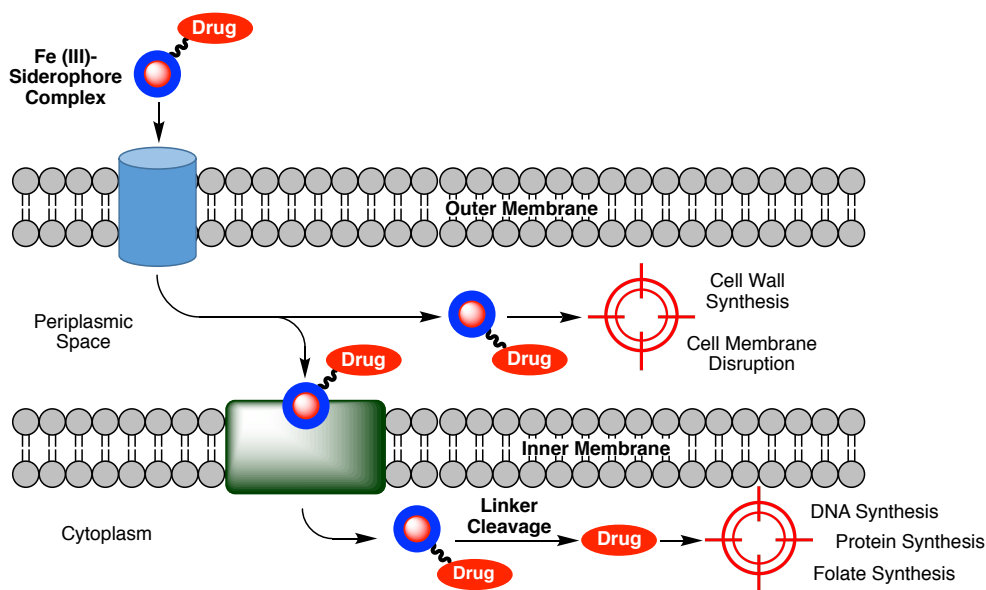
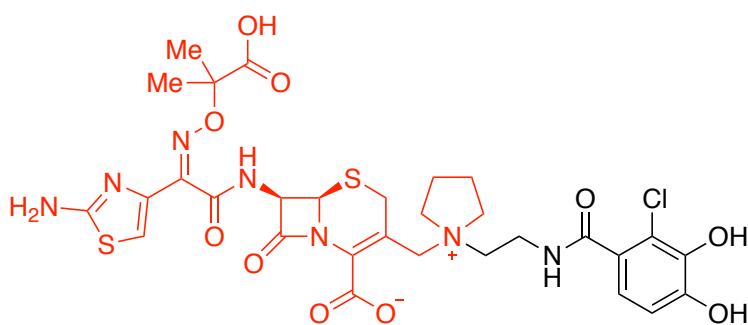


Figure 1.22 Cartoon representation of Trojan Horse strategy.

In addition, any attempt by the bacteria to counter this new threat will involve the shutting down of a nutrient uptake pathway, rendering the bacteria nutrient-deficient, and hopefully more easily targeted by the immune system. The Trojan Horse approach also offers the potential to increase the selectivity of antibiotics against bacteria cells compared to

human cells, and even activate antibiotics vs. new bacterial strains (e.g. activating Gram-positive antibiotics against Gram-negative bacteria).<sup>118</sup>

Examples of Trojan Horse vectors examined for the delivery of antibiotic conjugates include siderophores,<sup>79,119</sup> proteins,<sup>120</sup> sugars,<sup>121,122</sup> haem-like porphyrins,<sup>123,124</sup> and even Vitamin B12.<sup>125,126</sup> The antibiotic and vector in these cases can be covalently bound, or bound via a labile linker to allow release of the antibiotic from the vector within a bacterial cell.<sup>94</sup> Of these vectors, siderophores have displayed perhaps the most clinical success so far, with cefiderocol, a  $\beta$ -lactam-catecholate conjugate, being approved for use in humans by the FDA last year following success in Phase III clinical trials (Figure 1.23).<sup>127</sup>



**Cefiderocol**

Figure 1.23 Structure of cefiderocol, the first Trojan Horse antibiotic approved for human usage (antibiotic unit highlighted in red).

### 1.3.1 Natural Siderophore Trojan Horses – Sideromycins

As is often the case for ideas in medicinal chemistry, the concept of using siderophores as Trojan Horses is not a human invention. Certain species of bacteria are also capable of producing and releasing siderophore-antibiotic conjugates, which are termed sideromycins.<sup>80</sup> The first sideromycin was discovered in 1947 by Donald Reynolds and Albert Schatz, both PhD students working under Selman Waksman.<sup>128–130</sup> Isolated from a strain of the bacteria *Streptomyces griseus*, a bacterial source of many new antibiotics including streptomycin, the new antibiotic was named grisein.<sup>128–130</sup> Although the structure and mechanism of action of grisein was unknown to the original researchers, they noted an increase in grisein production when iron salts

were added to the culture medium, and that ferric salts had an inhibitory effect on the activity of the antibiotic vs. other bacteria.<sup>129</sup>

The structure was confirmed to contain bound iron in 1951 by Kuehl *et al.*, who demonstrated that it could be removed by addition of excess 8-hydroxyquinoline, yielding a compound with reduced antimicrobial activity.<sup>131</sup> At the same time, albomycin, another iron-containing antibiotic, was discovered by researchers in the USSR.<sup>132</sup> This rapidly moved into trials in animals and humans, where it proved active against infections that could not be treated with penicillin, although development of resistant strains curtailed these experiments.<sup>130,132,133</sup>

The composition of grisein and albomycin were later shown to be very similar, if not identical, by chromatographic comparisons<sup>130,134</sup> and amino acid analysis.<sup>130,135</sup> It was later discovered that the albomycin initially produced in fermentation broths (albomycin  $\delta_2$ ), can degrade to give two other biologically active products (albomycons  $\delta_1$  and  $\epsilon$ ).<sup>130</sup> Their chemical structure was not correctly determined until 1982, where the albomycons were determined to contain a linear hexadentate ferrichrome analogue (**Figure 1.24**).<sup>136</sup> The antibiotic moiety, designated SB-217452, was later discovered to act by inhibition of seryl-tRNA synthetase.<sup>137</sup> SB-217452 undergoes intracellular release following uptake, with the conjugate broken down by peptidase enzymes.<sup>138</sup> Notably, the activity of the antibiotic against *S. aureus* and *E. coli* is vastly reduced when not conjugated to the siderophore moiety (c. 30,000-fold reduction), indicating the siderophore unit is vital for good uptake.<sup>139</sup> With transporter proteins capable of ferrichrome uptake present across a range of Gram-positive and Gram-negative species, the albomycons display good broad-spectrum activity.<sup>139,140</sup>

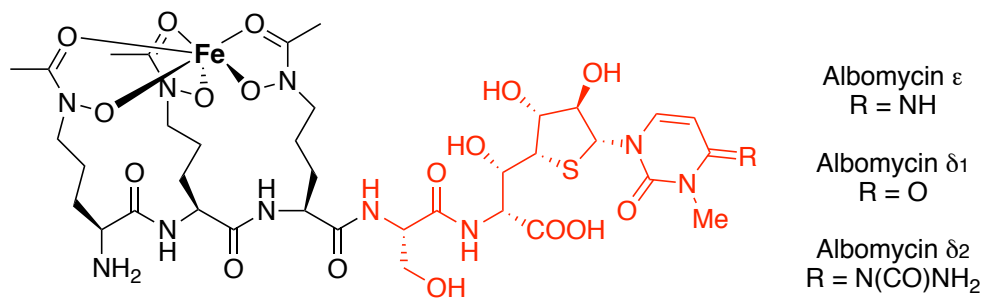


Figure 1.24 Chemical structures of the albomycins. The stereochemistry here is that reported in a total synthesis published in 2018,<sup>141</sup> which matches the antibiotic stereochemistry reported in 2000.<sup>137</sup>

A wide range of sideromycins are now known, and detailed studies of their activity and mechanism of actions have been carried out. The salmycins are a family of sideromycins that combine danoxamine (a hexadentate hydroxamate siderophore) and an aminoglycoside antibiotic; four derivatives (salmycins A-D) have been discovered (**Figure 1.25**).<sup>142</sup> The activity spectrum of the salmycins is reduced compared to the albomycins, showing low inhibitory activity vs. Gram-negative bacteria, likely caused by high specificity of the outer-membrane transporters.<sup>139</sup> A few theories exist as to the mechanism of release of the antibiotic, although the exact mechanism has not been fully confirmed. The ester link between the siderophore and the antibiotic is highly labile unless the siderophore is bound to Fe<sup>3+</sup>/Ga<sup>3+</sup>, pointing towards iron removal as a first step; a free hydroxamate group from the siderophore component is then theorised to attack the ester bond in a cyclisation reaction.<sup>133,143</sup> A similar family of sideromycins, the danomycins, have been shown to contain a danoxamine unit and an aminoglycoside sugar, but their full structure has not been confirmed.<sup>80,140,144</sup>



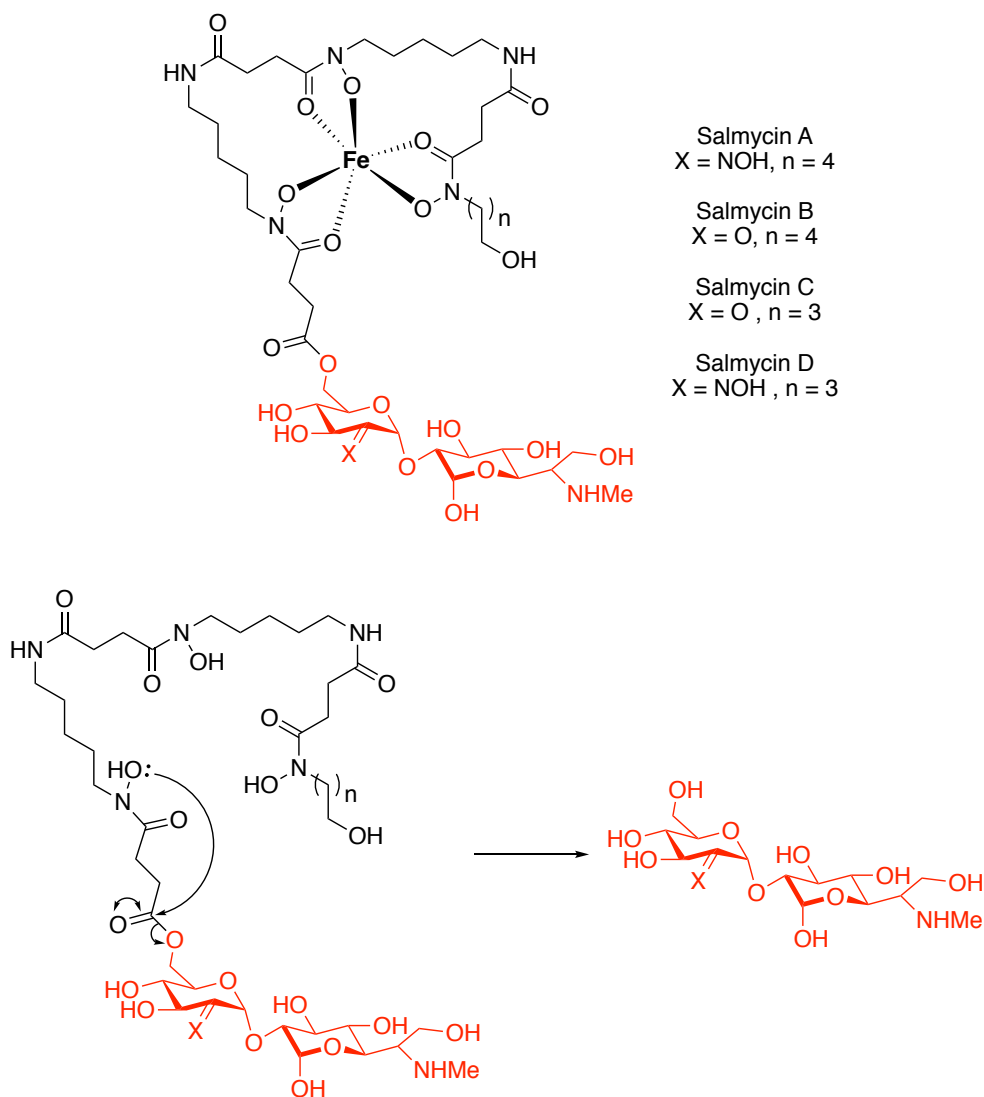


Figure 1.25 Structures of the salmycins, and proposed mechanism of antibiotic release post iron removal.

The ferrimycin family shares several similarities with the salmycins: they are also based on a hexadentate hydroxamate siderophore (this time desferrioxamine, **Figure 1.26**), and only display activity vs. Gram-positive bacteria.<sup>130,140,145,146</sup> However, the antibiotic unit differs, with the conjugate instead bearing an imino-substituted lactam, which has been shown to target protein biosynthesis, although the specific mechanism of action has not yet been determined.<sup>96,140,147</sup> The mechanism of release, although not confirmed, was postulated by Braun *et al.* as identical to that of albomycin (peptidase hydrolysis).<sup>138</sup>

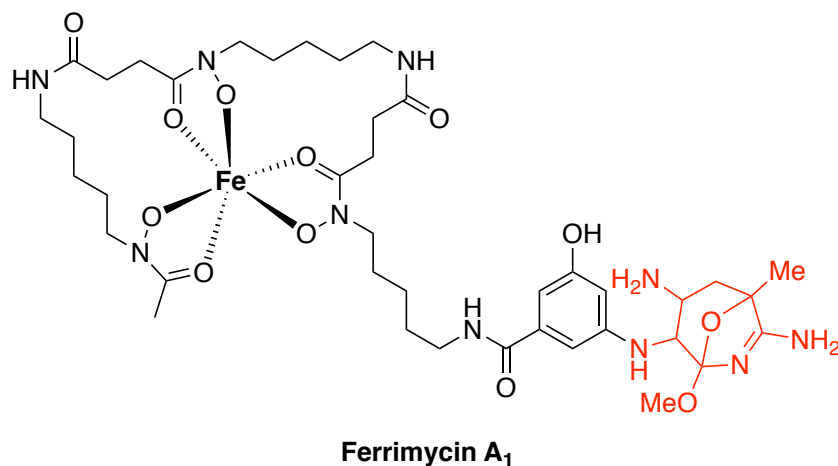


Figure 1.26 Chemical structure of ferrimycin A<sub>1</sub>. Antibiotic unit highlighted in red.

Microcins are a class of antimicrobial peptides released by certain bacterial species, capable of depolarising and forming pores in bacterial membranes.<sup>80</sup> Examples of these peptides have been found to be functionalised with salmochelin-derived siderophore units, and to exploit siderophore transport pathways, boosting activity vs. *E. coli* and *Salmonella* strains up to 10 times.<sup>80,148–150</sup> A number of other sideromycins have been identified, but not fully characterised for a variety of reasons (for example, low yield from culture or instability), including gluconimycin,<sup>151–153</sup> ASK-753,<sup>154,155</sup> and ferramidochloromycin.<sup>156</sup>

It should be noted that sideromycins often see the development of resistance when subjected to *in vitro* antibacterial assays.<sup>130,157</sup> This resistance has been suggested as a reason the sideromycins have not seen more exploration in a clinical setting.<sup>133</sup> However, it is possible that the effects of resistance to the sideromycins would be compensated by decreased iron uptake and therefore reduced fitness in the bacteria, especially if the loss of certain transport pathways is involved; this would be more relevant in a biological model, with the bacteria having to deal with the immune response as well as the treatment.<sup>133,139</sup> This has been observed by Braun *et al.* in a mouse model: *S. pneumoniae* and *Y. enterocolitica* that survived treatment with albomycin grew slower than the wild-type bacteria, with the wild-type also able to outcompete the resistant strains in competition experiments.<sup>139</sup>

### 1.3.2 Synthetic Siderophore-Based Trojan Horse Conjugates

For synthetic siderophore Trojan Horses, the general structure consists of an antibiotic bound to a siderophore unit via some linker; alternately, “hybrid” siderophore conjugates can be used, in which the siderophore is directly bound to the antibiotic (**Figure 1.27**).<sup>80</sup> There have been a plethora of reviews in this area in recent years, covering many aspects of Trojan Horse conjugates.<sup>79,80,94,96,119,133,140,143,158–165</sup>



Figure 1.27 General structure of siderophore-antibiotic conjugates.

The first siderophore-based Trojan Horse conjugates were developed by Zähler *et al.* in 1977, who attached sulfonamide antibiotics to the hydroxamate siderophores ferricrocin (**1-1**) and desferrioxamine (**1-2**, **Figure 1.28**).<sup>166</sup> Conjugate **1-1** proved to be active against *S. aureus*, but not *B. subtilis* or *E. coli* at similar concentrations to the parent drug, while conjugate **1-2** was inactive.<sup>166</sup> This study successfully demonstrated the potential utility of siderophore-based Trojan Horse conjugates, while also suggesting that simple attachment of a siderophore to a drug doesn't mean antimicrobial activity is guaranteed, and there are other factors that must be considered e.g. the selectivity of the siderophore component used, or the character of the linker between the drug and the siderophore. Some key examples of conjugates developed since this first foray into siderophore Trojan Horse conjugates are discussed below.

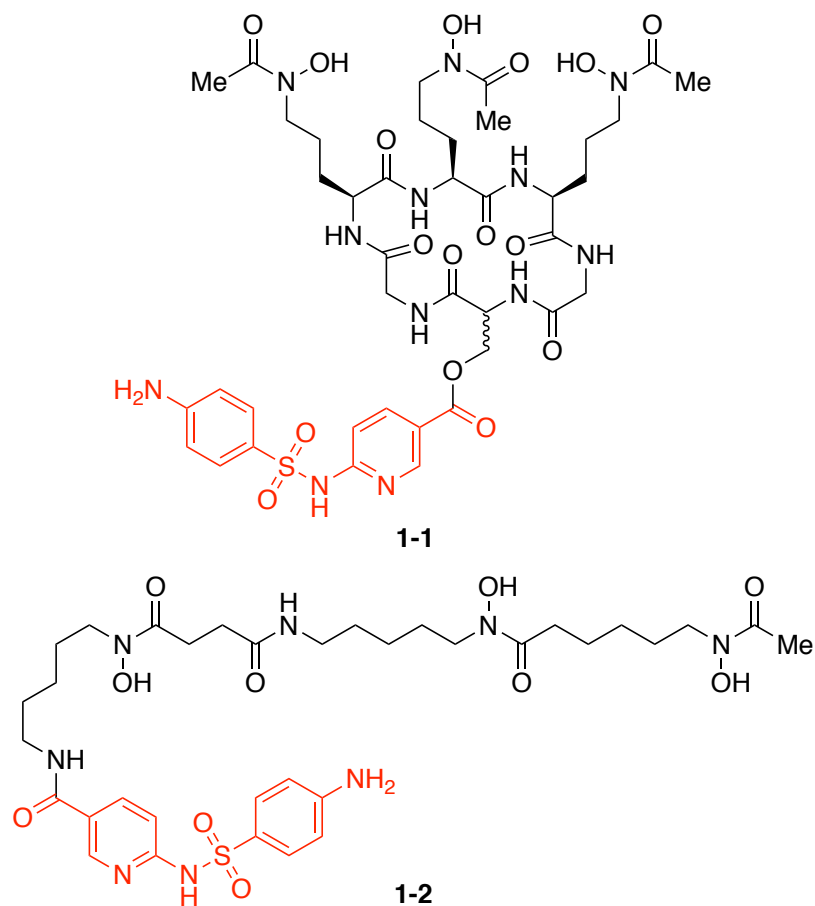


Figure 1.28 Ferricrocin and desferrioxamine conjugates synthesised by Zähler *et al.* The siderophore components are highlighted in black, and the antibiotic in red.<sup>166</sup>

### 1.3.3 Siderophore Conjugates with Covalent Linkers

#### 1.3.3.1 Conjugates with Periplasmic Targets – $\beta$ -lactams

Since this first report of a siderophore-antibiotic conjugate, many more have been synthesised and evaluated. The majority of work has been carried out with conjugates of  $\beta$ -lactam antibiotics, with very promising results.<sup>119</sup> As  $\beta$ -lactams inhibit proteins involved in cell wall synthesis, which are located in the periplasm of Gram-negative bacteria, the conjugate only needs to pass through the outer membrane to reach its target.<sup>79</sup> The target binding site on the  $\beta$ -lactams is also sufficiently separate from the siderophore unit that it shouldn't interfere with the antimicrobial activity, and no breakdown of the conjugate is required.<sup>79</sup>

An extensive review of the  $\beta$ -lactam conjugates reported up to 2000 has been carried out by Roosenberg *et al.*<sup>119</sup> The majority of conjugates

reviewed contained a simple monocatechol or hydroxypyridone unit attached to the  $\beta$ -lactam; two examples (**1-3** and **1-4**) are shown here (**Figure 1.29**). Hydroxypyridones (like that of **1-3**) are isosteres of catechols which have the ability to bind iron in an analogous fashion; they also offer greater stability than catechols, which can be methylated and deactivated from iron binding by the enzyme catechol *O*-methyltransferase (COMT).<sup>167</sup> Although they don't contain a large tetra/hexadentate siderophore unit, these conjugates often showed good activity. Conjugates that do contain larger siderophore units are still considered to offer a greater chance of recognition and uptake via the siderophore transport pathways, but this is clearly not crucial for  $\beta$ -lactam conjugates.<sup>119</sup>

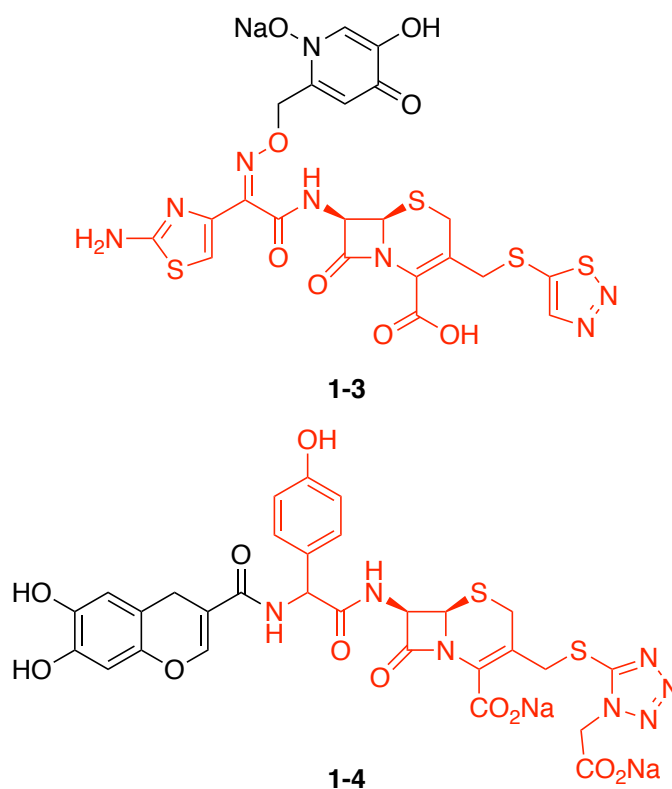


Figure 1.29 Structures of two early siderophore- $\beta$ -lactam conjugates. The antimicrobial component is highlighted in red.<sup>168,169</sup>

More recent examples of  $\beta$ -lactam conjugates include the use of a fully synthetic hexadentate catecholite by Ji *et al.*<sup>170</sup> This was intended to maintain some of the same features as enterobactin, such as the three-fold symmetry and the catecholamide binding groups, but also dispenses with the hydrolytically-labile trilactone ring, and provides a functional group for easy conjugation of antibiotics, in this case ampicillin and amoxicillin (**1-5**

and **1-6, Figure 1.30**). This conjugates also made use of acylated catechol groups, which have been shown to hydrolyse *in vitro* to give the active species and provide some protection from catechol *O*-methyltransferase enzymes.<sup>170</sup> The conjugates proved much more active than the parent antibiotics vs. a range of *P. aeruginosa* strains, especially in iron-poor conditions, where up to a 4000-fold increase in activity was observed.<sup>170</sup>

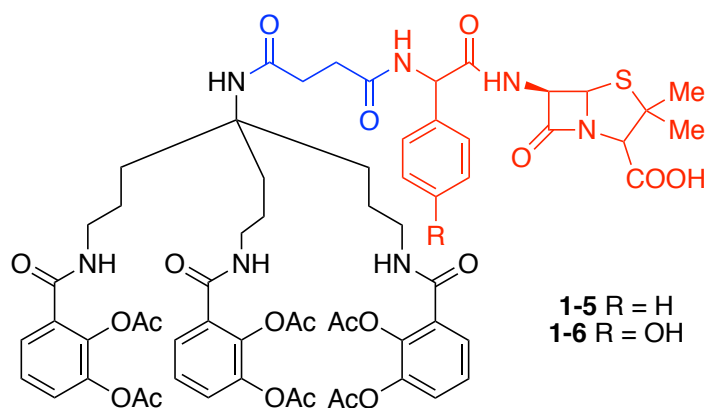


Figure 1.30  $\beta$ -lactam conjugate with synthetic hexadentate siderophore synthesised by Ji *et al.* The antimicrobial unit is highlighted in red, and the linker unit in blue.<sup>170</sup>

In contrast to this use of an enterobactin mimic, Zheng and Nolan used a modified version of native enterobactin for synthesis of a range of conjugates, with one of the catechol groups modified to incorporate a carboxyl group at the 5-position.<sup>171</sup> Two conjugates, **1-7** and **1-8** were synthesised, again using ampicillin and amoxicillin as the antibiotic components (**Figure 1.31**). **1-7** and **1-8** proved to enhance antibiotic activity up to 1000-fold vs. various *E. coli* strains, including a number of pathogenic strains. Activity relied on the presence of the FepA outer membrane transporter, with the activity enhancement removed in mutants lacking FepA; supplementation of the media with enterobactin also attenuated activity, indicating the additional enterobactin competes with the conjugate for FepA binding and uptake.<sup>171</sup>

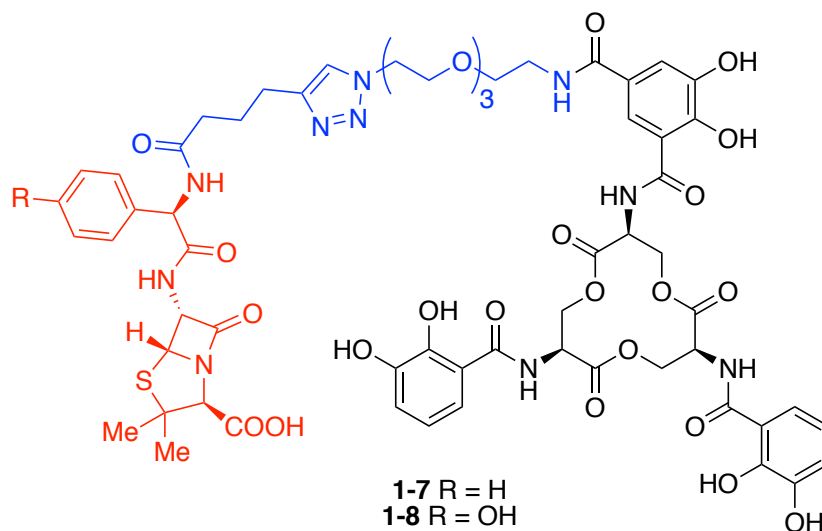
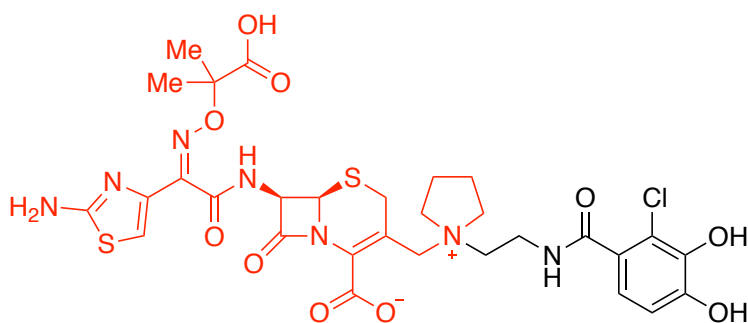


Figure 1.31  $\beta$ -lactam-enterobactin conjugates synthesised by Zheng and Nolan.<sup>171</sup>

Both of these recent examples have important implications for the design and potential applications of Trojan Horse siderophore conjugates. While Zheng and Nolan note that use of non-native siderophores often leads to poor uptake and activity,<sup>171</sup> the study by Ji *et al.* shows that carefully-designed alternatives can also be used.<sup>170</sup> With natural siderophores often offering a complex synthetic challenge, which has implications for the cost and upscaling of production, more easily synthesised artificial versions may be required if the potential of these conjugates is to be realised in a clinical setting. Both demonstrate the large increases in activity that can be obtained for conjugates over that of the parent antibiotics, including vs. bacteria not susceptible to the parent drugs, allowing older antibiotics to be repurposed to fight different types of bacteria (especially relevant for targeting Gram-negative bacteria with antibiotics that previously only worked on Gram-positive bacteria). They also indicate the great potential for creation of narrow-spectrum antimicrobials, which can select for a desired target based on the siderophore employed.

Examples of  $\beta$ -lactam antibiotic units have also demonstrated that Trojan Horse conjugates can make the successful transition to the clinic. As mentioned before, the most successful is cefiderocol (previously known as S-649266, **Figure 1.32**), which received FDA approval for use in the clinic in

2019.<sup>127</sup> This cephalosporin-based antibiotic contains an unusual 2-chloro-3,4-dihydroxybenzoic unit, chosen based on an extensive screening of various iron-chelating units.<sup>172</sup> Similar halogen-bearing catechols have been shown to be more stable to COMT enzymes, and have longer pharmacokinetic half-lives in a marmoset model.<sup>158,173</sup> A WHO report in 2017 highlighted cefiderocol and its sister drug GSK-3342830, at the time in Phase I clinical trials, as the only antibiotics currently in development that show activity against three of the WHO's four critical priority pathogens, cephalosporin-resistant *Acinetobacter baumannii*, carbapenem-resistant *Pseudomonas aeruginosa*, and carbapenem/cephalosporin-resistant *Enterobacteriaceae*.<sup>67</sup>



**Cefiderocol**

Figure 1.32 Structure of cefiderocol.

Beyond cefiderocol and GSK-3342830, a host of other  $\beta$ -lactam-based Trojan Horse antibiotics have entered clinical trials, however they have so far all failed to progress to the clinic. There are various reasons for this, ranging from susceptibility to resistance<sup>80,158,174,175</sup> to poor side effect profiles,<sup>56,176,177</sup> to loss of activity *in vivo*,<sup>178,179</sup> and finally to simple economic and chemical issues.<sup>180–182</sup> A review by André Bryskier in 2000 noted that research in catechol-containing antibiotics had often been given up due to “difficult chemistry, high cost of production, and risks of adverse effects”.<sup>180</sup>

### 1.3.3.2 Conjugates with Periplasmic Targets – Other

Other antibiotics that potentially act against targets in the Gram-negative periplasm have also been conjugated to siderophores. The Miller group has successfully synthesised conjugates of vancomycin (**1-9**)<sup>183</sup> and daptomycin (**1-10**)<sup>118</sup> with either bis(catecholate) or mixed catecholate-hydroxamate



siderophores (**Figure 1.33** and **Figure 1.34**). These antibiotics are both inactive against almost all Gram-negative bacteria, the primary factor being their large size, which makes passage of the outer membrane difficult.<sup>118,184</sup> The vancomycin conjugate, **1-9**, showed worse activity against *S. aureus* than the parent drug, but did show much improved activity against a strain of *P. aeruginosa* in iron-poor conditions.<sup>183</sup> Conjugate **1-10** showed a similarly reduced activity vs. *S. aureus*, and no activity vs. *P. aeruginosa* or *E. coli*, but proved highly active against *A. baumannii* (MIC = 0.4  $\mu$ M); this was attributed to the similarity of the siderophore component to fimsbactin, the natural siderophore produced by *A. baumannii*.<sup>118</sup> Both of these indicate that siderophore transporters can potentially uptake cargos much larger than the siderophores themselves. A further example of a conjugate with a periplasmic target comes from Tarapdar *et al.*, who synthesised a bis(catecholate) conjugate of a phenothiazine antimicrobial (**1-11**), which has previously shown activity vs. *M. tuberculosis*.<sup>185</sup> This conjugate has yet to be evaluated in a biological context.

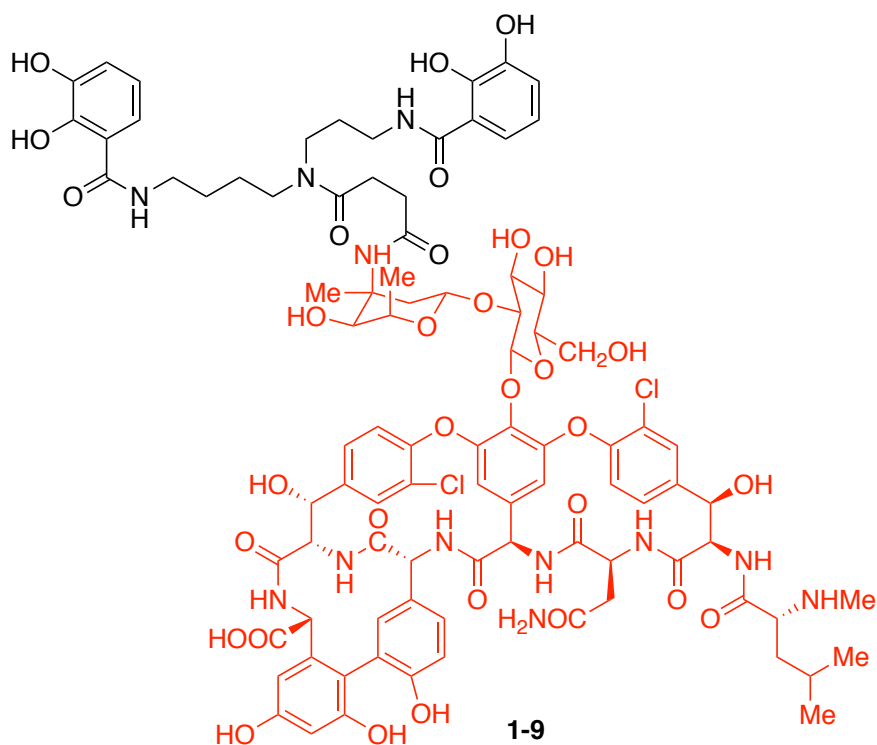


Figure 1.33 Structure of vancomycin-siderophore conjugate **1-9**.<sup>183</sup>

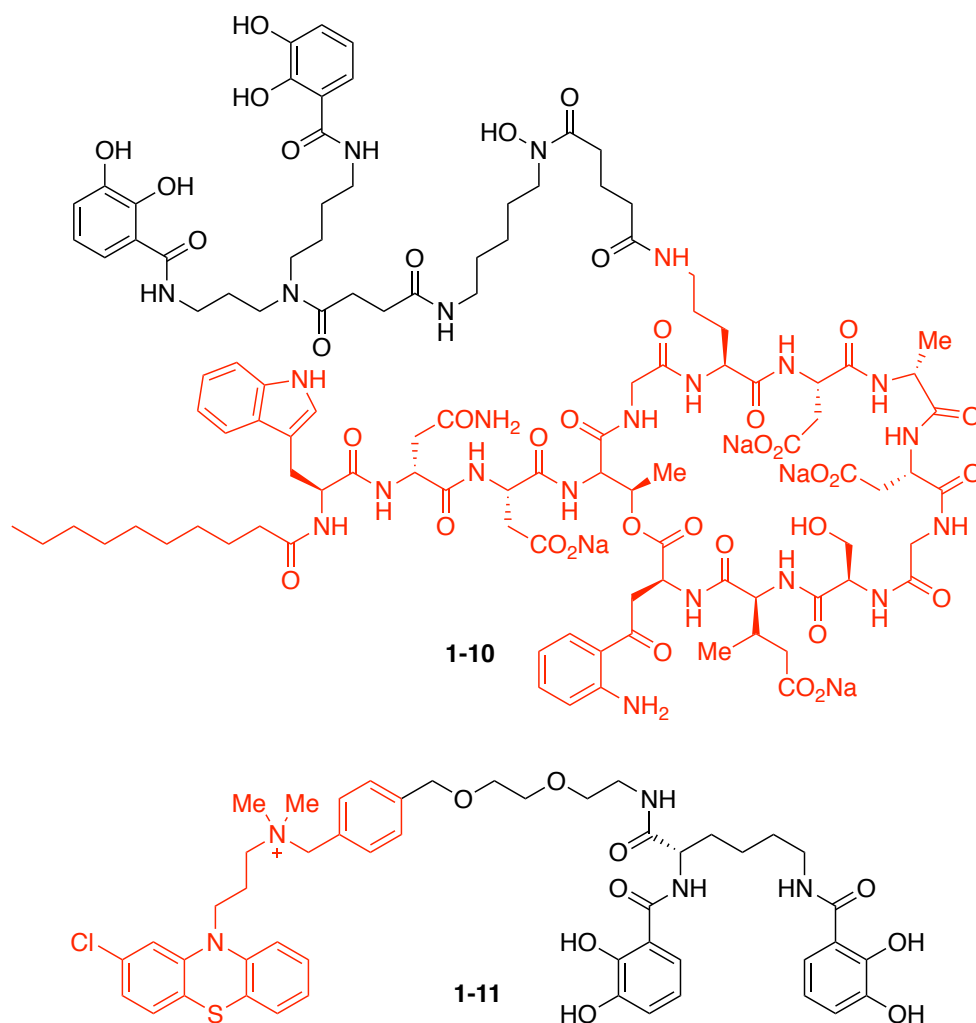


Figure 1.34 Structures of daptomycin-siderophore conjugate **1-10** and phenothiazine-siderophore conjugate **1-11**.<sup>118,185</sup>

As with the results discussed for  $\beta$ -lactam conjugates, these results highlight the great potential of Trojan Horse conjugates in activating antibiotics, and indeed other bioactive molecules, against new strains of bacteria, and the need for carefully selecting the correct siderophore component to target a specific bacterium.

### 1.3.3.3 Conjugates with Cytoplasmic Targets

A number of other conjugates have also been made for antibiotics with cytoplasmic targets. The majority of work in this area has been carried out on fluoroquinolone conjugates like **1-12**, but aminocoumarins (**1-13**)<sup>186</sup>, oxazolidinones (**1-14**)<sup>187</sup>, and macrolides (**1-15**)<sup>188</sup> have also been studied (Figure 1.35). However, they often show a reduction in activity over their parent antibiotics. One example, **1-14**, shows increased activity vs. *P.*

*aeruginosa*, however not to a sufficient level to merit further investigation (MIC increased from 1024  $\mu$ M to 128  $\mu$ M).

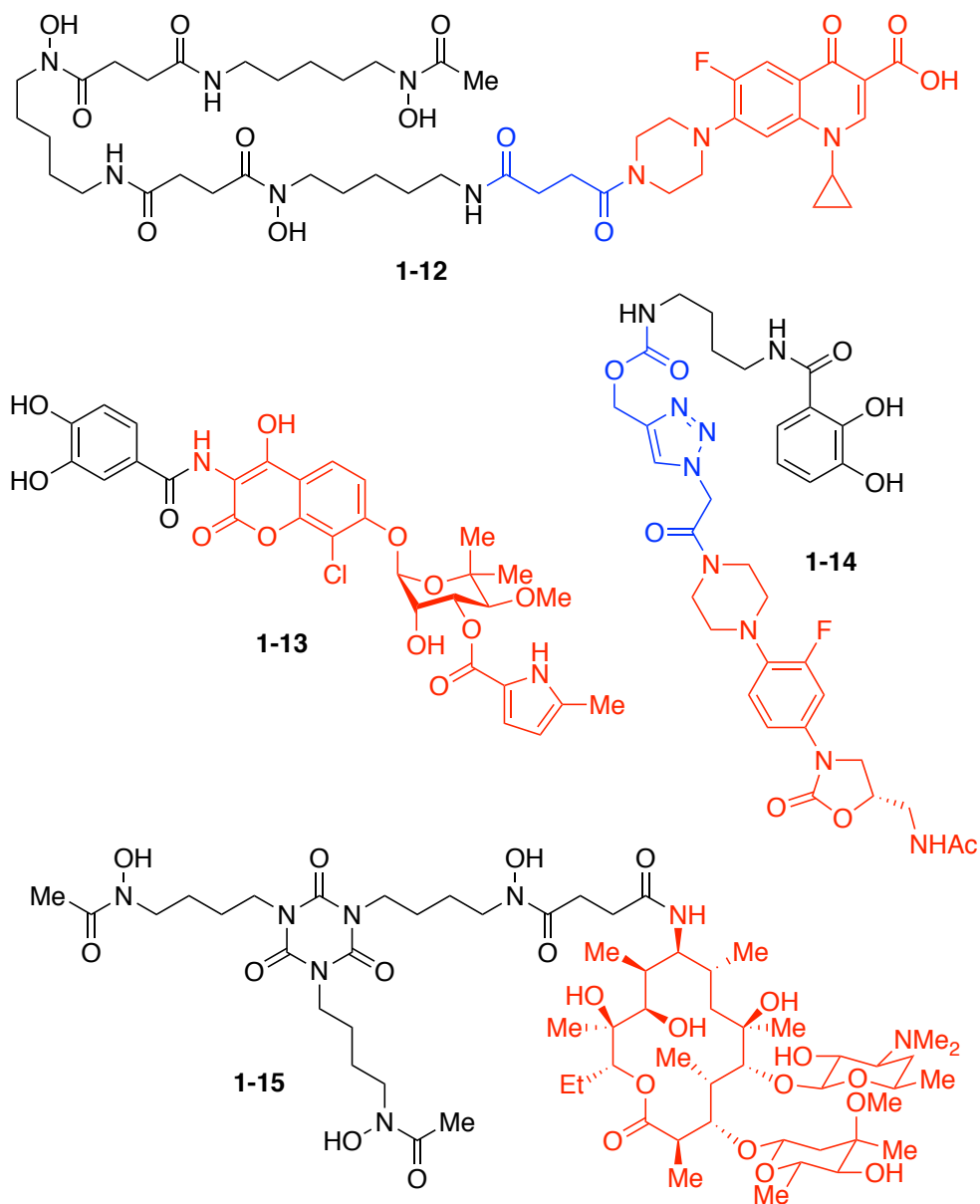


Figure 1.35 Structures of siderophore conjugates of antibiotics with cytoplasmic targets. Any linkers present between siderophores and antibiotics are highlighted in blue.<sup>186–189</sup>

This reduction in activity is very common in the case of fluoroquinolone analogues. Work from the Duhme-Klair and Routledge groups on citrate-based siderophore conjugates provides a good basis for explaining this reduction.<sup>190–192</sup> Citrate (**1-16** to **1-19**)<sup>190,192</sup> and staphyloferrin A (**1-20**)<sup>191</sup> conjugates synthesised by the groups proved less active than the parent antibiotic vs. a range of bacteria (**Figure 1.36**). A DNA gyrase assay, which measures the concentration at which the conjugate inhibits DNA gyrase (the

cytoplasmic target of ciprofloxacin) showed that higher concentrations of the conjugates were required for complete inhibition.<sup>191,192</sup> This, plus a set of molecular modelling studies,<sup>192</sup> suggested gyrase binding is inhibited by the presence of the covalently-bound linker-siderophore unit, reducing the antimicrobial activity.<sup>191,192</sup>

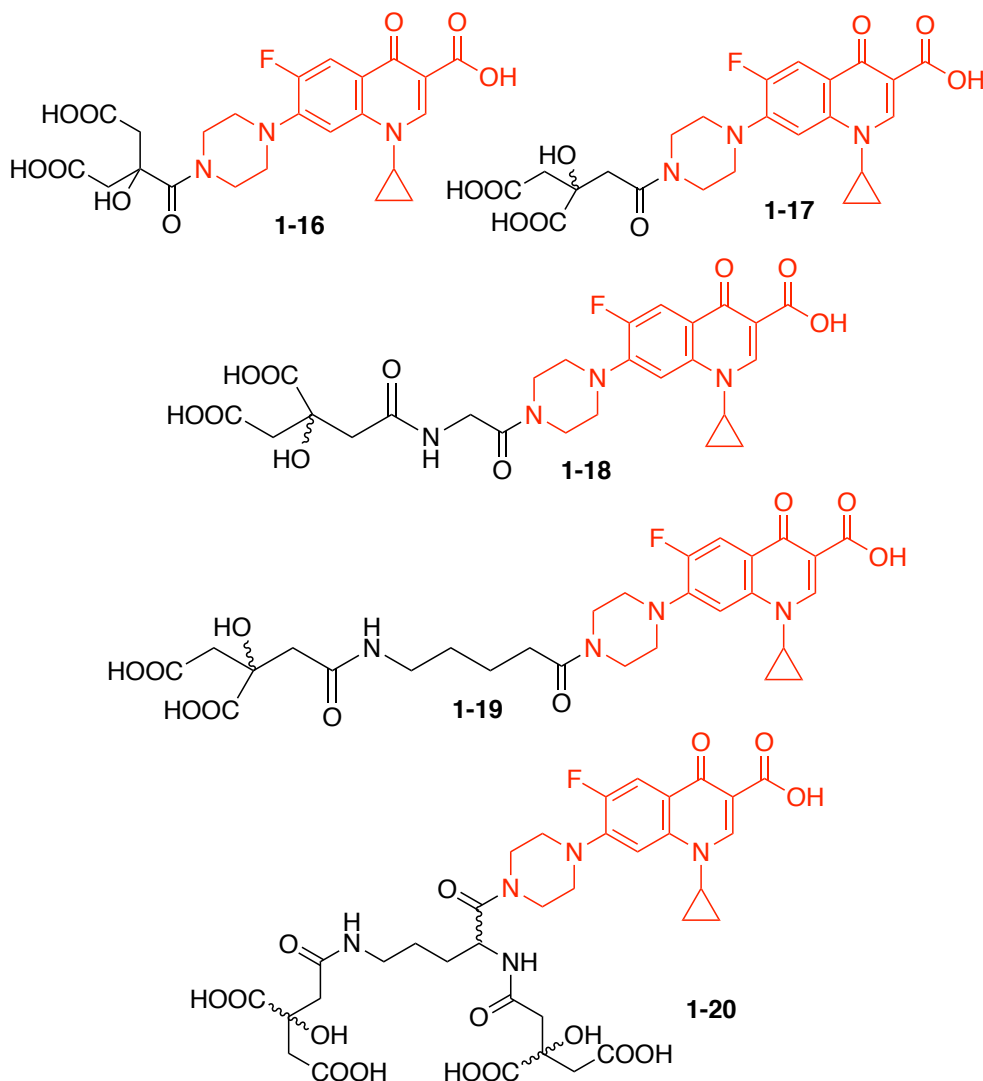


Figure 1.36 Previous fluoroquinolone-siderophore conjugates synthesised by the Duhme-Klair and Routledge groups.<sup>190–192</sup>

There is one notable exception to this general reduction in antimicrobial activity: a ferrichrome-ciprofloxacin conjugate recently designed and synthesised by Pandey *et al.*<sup>193</sup> In this example, the conjugate was examined as its unmetallated (*apo*) form (**1-21**), as well as the iron and gallium-bound conjugates (**Figure 1.37**). Ga(III) ions have a similar ionic radius to Fe(III), and therefore a similar binding affinity to siderophores; Ga-bound siderophores can also be recognised by both outer and inner-membrane

transporters.<sup>80,193</sup> Ga(III) can also have an antimicrobial effect on bacteria, with Ga(NO<sub>3</sub>)<sub>3</sub> currently in clinical trials.<sup>193</sup> Both the *apo* and the Ga(III)-bound versions of this conjugate displayed identical activity to ciprofloxacin vs. *E. coli* K-12, and the Ga(III) conjugate (**1-22**) displayed improved activity vs. *S. aureus*. No reasoning was given for this remarkable activity, which is in stark contrast to most other fluoroquinolone conjugates.<sup>80,193</sup> A DNA gyrase assay with this conjugate was not carried out; this often gives clues as to whether the linker and the siderophore interfere with target binding. It would have been interesting to see if the linker and siderophore used in this case do impede binding, as is the case with other covalently-linked systems,<sup>191,194,195</sup> and the identical activity has another possible cause.

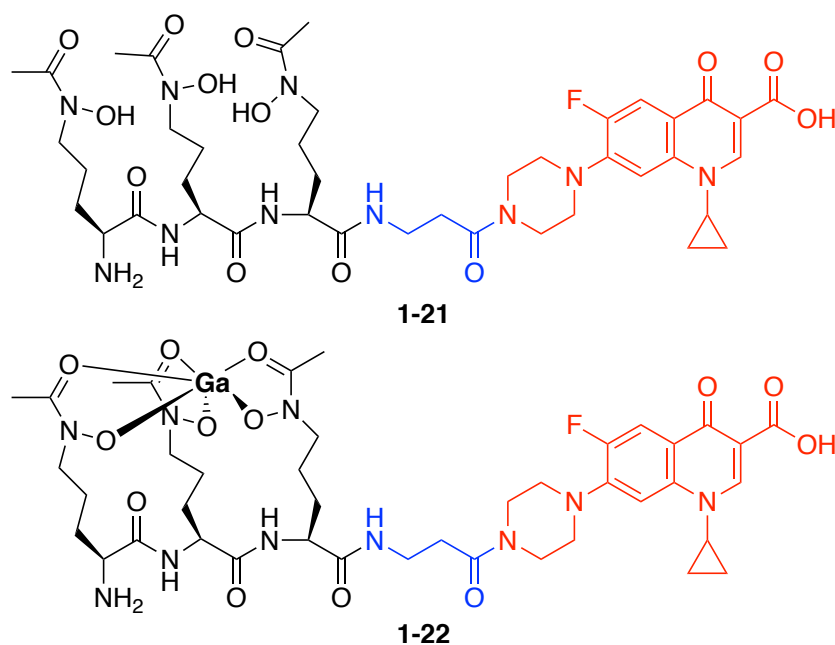


Figure 1.37 Structures of the *apo* and gallium-bound forms of a ferrichrome-ciprofloxacin conjugate.<sup>193</sup>

One of the key observations made from the study of these covalently bound conjugates is that breakdown of the conjugate in the cytoplasm is required for optimal activity.<sup>80,119,133,143,159,196</sup> Covalently-bound siderophore components seem to either hinder the bound drug from reaching its target, or interfere with its binding to the target, therefore reducing the antimicrobial activity.<sup>80,143,196</sup> This requirement for conjugate breakdown in the cytoplasm has driven a search for linkers that are hydrolysed or cleaved inside bacterial cells, termed “*biolabile linkers*” or “*biolabile bonds*”.

## 1.4 Biolabile Linkers

The concept of prodrugs, drugs that are metabolised into their active forms *in vivo*, is nothing new, having been first recognised in 1958,<sup>197</sup> however not all of the many modifications that can be used to create prodrugs are applicable to drug conjugates of any basis. Prodrug modifications tend to be made around the “edges” of molecules, with terminal groups modified to offer a simple tweak to the biological properties, and often require enzymatic cleavage for removal;<sup>197</sup> in contrast, drug conjugates tend to consist of a targeting unit attached to the desired drug via a linker, meaning they effectively require cleavage down the “centre” of the molecule, which can make enzymatic hydrolysis much harder, as the size of most drugs/targeting units may hinder an enzyme’s ability to reach and hydrolyse the bond. Especially in the case of antibiotic conjugates, the cleavage also needs to happen inside bacteria to be fully effective, otherwise the antibiotic cargo may not be able to enter the cells; many prodrug approaches do not have this requirement.

Despite these potential issues, a range of prodrug modifications have been developed to allow the release of drug components attached to a targeting unit. These cleavable linker units can be termed “*biolabile linkers*”. They often involve the inclusion of a self-immolative moiety, a linker unit that can undergo a chemical transformation in response to a biological stimulus, creating a cascade reaction leading to release of the desired drug.<sup>198</sup> Whether linker cleavage requires self-immolation or not, certain key characteristics are required for a desirable biolabile linker:

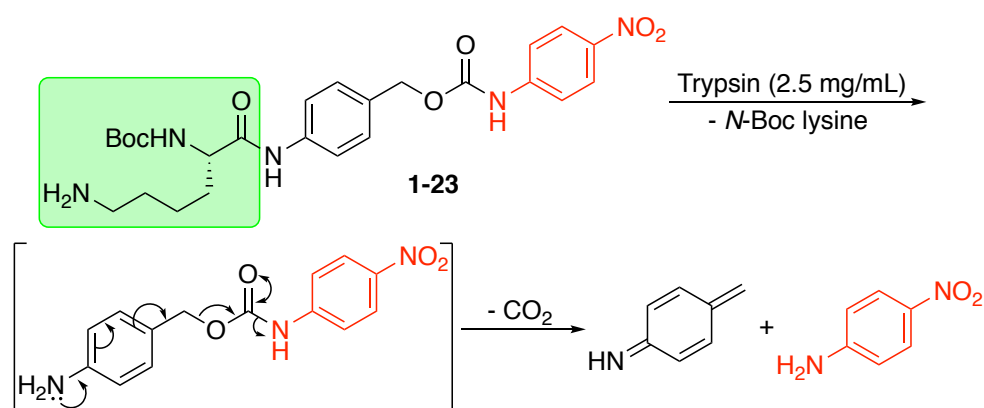
- 1) High stability while the conjugate is in circulation in the body to ensure successful delivery of conjugate to the desired target, and avoid off-target release. For most drug delivery routes, this requires the conjugate to be stable in blood plasma.<sup>199–201</sup>
- 2) No detrimental effect on pharmacokinetic properties, for example the use of hydrophobic linkers can lead to aggregation in antibody-drug conjugates, impairing their function.<sup>201</sup>
- 3) Rapid cleavage effected when trigger stimulus applied, preferably within cells.

- 4) Release of an unmodified therapeutic warhead (no additional functionalities vs. parent drug), or a modified form which retains almost identical activity.<sup>199,200</sup>
- 5) Release of drug is compatible with the drug's pharmacodynamic properties (I.e., release must be fast enough to allow the drug concentration to build up to a sufficient level to be active).
- 6) The products from any linker cleavage, and the linker itself, should be non-toxic.<sup>202</sup>

### 1.4.1 Self-Immolative Linkers

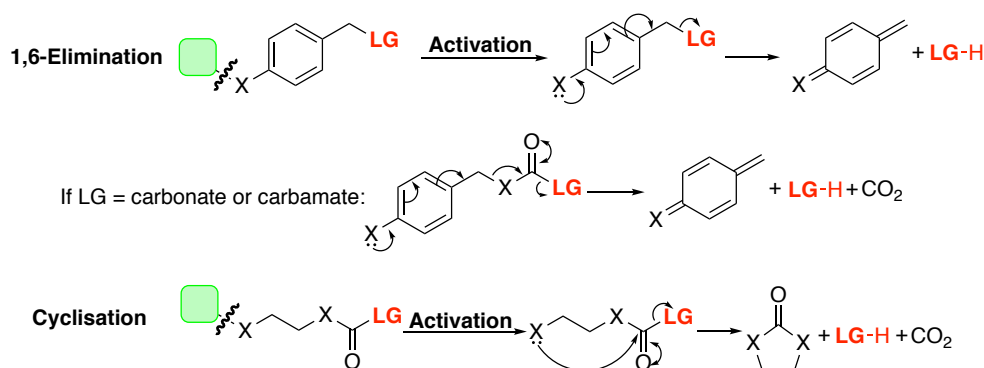
Before discussing the biological mechanisms that can be exploited to trigger the cleavage of biolabile linkers, it is worth looking at self-immolative linkers, and the mechanisms by which they function, in more detail. This field has been the subject of a number of extensive reviews in recent years.<sup>198–200,203–206</sup>

The first example of a “classic” self-immolative linker was published in 1981 by Carl *et al.*,<sup>207</sup> who reported a simple system (**1-23**) consisting of an *N*-Boc lysine unit, a *p*-aminobenzyloxycarbonyl (PABC) linker, and a *p*-nitroaniline unit (**Scheme 1.1**). On reaction with the protein hydrolase enzyme trypsin, the *N*-Boc lysine is cleaved, releasing the aniline group of the linker. This can then undergo an azaquinone methide elimination, with decomposition of the carbamate group to yield free *p*-nitroaniline.<sup>207</sup>



Scheme 1.1 Activation of the first self-immolative prodrug system, developed by Carl *et al.*<sup>207</sup> The trigger (the enzymatically cleaved *N*-Boc lysine) is highlighted in a green box, the self-immolative unit is green, and the released *p*-nitroaniline is red.

Since this first report a vast array of similar systems have been developed, with a wide variety of trigger mechanisms. There are two main mechanisms of release, self-immolation by elimination, as used in the original PABC linker, or self-immolation by cyclisation.<sup>198,203,204,206</sup> An aromatic structure is required for elimination, which most commonly happens in a 1,6-fashion (**Scheme 1.2**),<sup>198</sup> but can also occur in a 1,4-, a 1,8- or a  $\beta$ -elimination fashion.<sup>198,203,204</sup> The reactions are driven by a positive reaction entropy, and often the release of stable products e.g. CO<sub>2</sub>.<sup>198,204</sup> Cyclisation can occur with linkers based on alkyl chains, or on alkyl-substituted aromatic systems, and, similar to elimination, the reactions are driven by positive entropy and the formation of stable ring systems.<sup>198,204,206</sup> The natures of the trigger systems for these reactions are discussed in Sections 1.4.1.1 to 1.4.1.5.



**Scheme 1.2** Two examples of common elimination and cyclisation mechanisms for self-immolative linkers. **X = NH, O, S**. The location of the self-immolation trigger is shown in green.

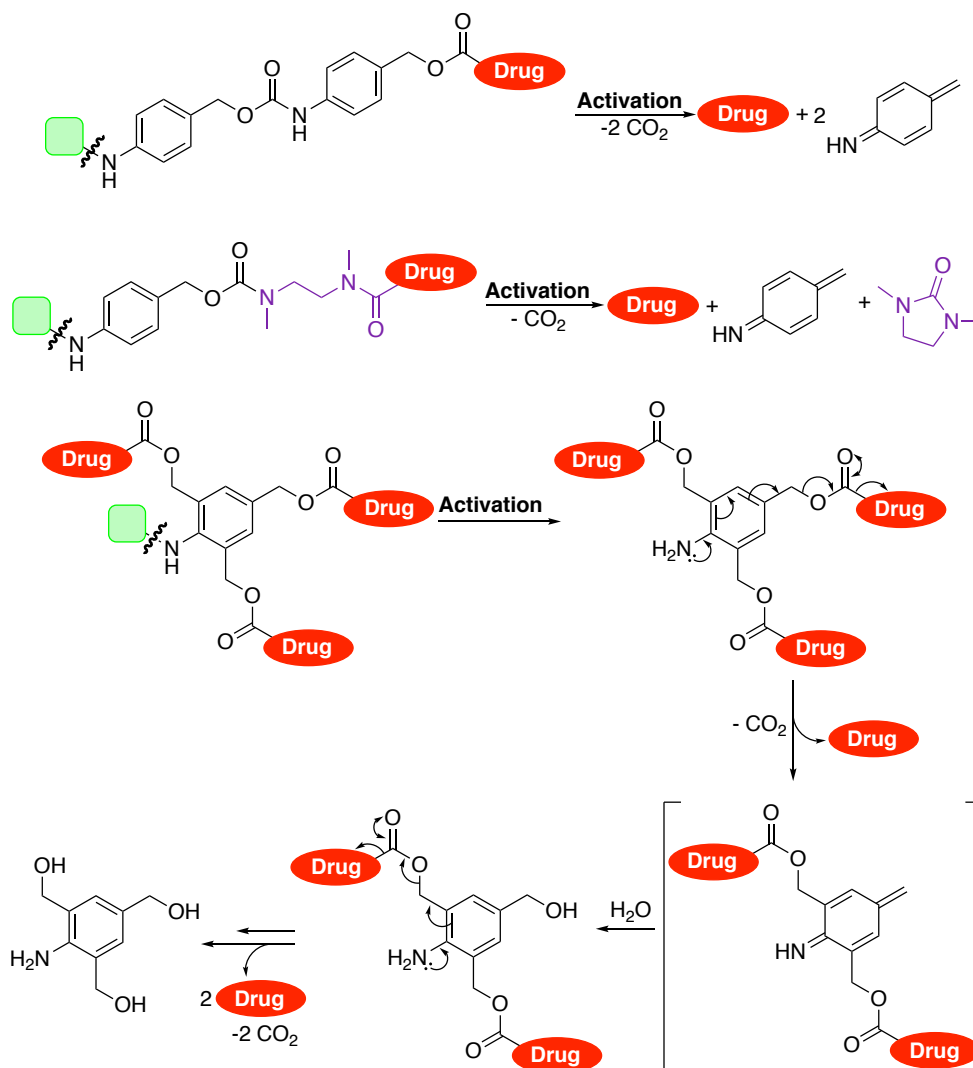
In both cases, the immolating process can also tolerate the presence of other nearby substituents, for example on the aromatic ring in an elimination process (**Scheme 1.3**).<sup>199,203</sup> This means that, as well as incorporating a releasable drug moiety and a trigger for the self-immolation process, the linker can be further functionalised with a targeting unit without affecting the release.



**Scheme 1.3** An example of the multiple functionalities that can be incorporated into a linker.



Multiple self-immolative units can be connected together to create self-immolative cascade chains, which can often increase drug release rates by placing the trigger location further from bulky drug molecules, making it more accessible for cleavage (**Scheme 1.4**).<sup>198,205,208</sup> Finally, multiple eliminations can also take place from a single aromatic ring, meaning that dendritic (branched chain) systems of self-immolative linkers can be used to facilitate release of multiple drug molecules from one central unit (termed amplified self-immolation).<sup>199,203–205</sup>



Scheme 1.4 Self-immolative chains developed by de Groot *et al.*,<sup>208</sup> and an example of multi-drug release from a single aromatic ring (adapted from Srinivasarao and Low).<sup>199</sup>

#### 1.4.1.1 Hydrolytically-Labile Linkers

A number of different mechanisms can be used to induce cleavage in biolabile linkers. The simplest of these systems are groups such as (acyloxy)alkyl esters, which can undergo hydrolysis in water at neutral pH;

the rate of hydrolysis can be tuned by changing the steric hindrance of the surrounding groups (**Figure 1.38**).<sup>209,210</sup> However, the unspecific nature of this cleavage, and the tendency for such linkers to undergo unspecific enzymatic cleavage, often renders them unsuitable for *in vivo* applications.

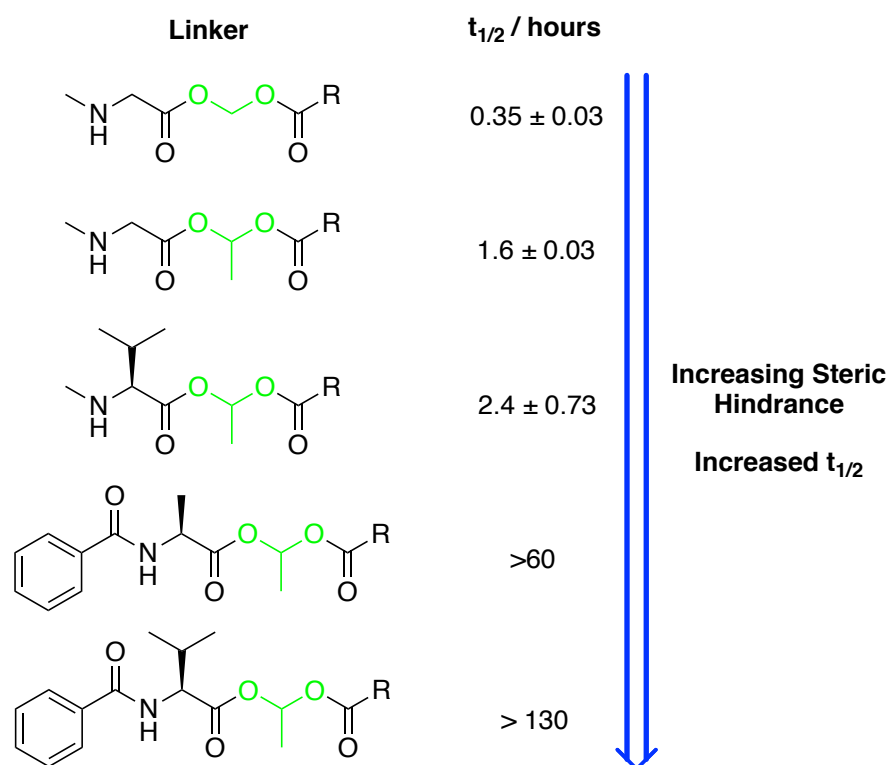


Figure 1.38 Hydrolytic stability of some (acyloxy)alkyl linkers studied by Zheng and Nolan (HEPES buffer, pH 7.5, 30 °C).<sup>210</sup>

#### 1.4.1.2 Acid/Base-Labile Linkers

A series of linkers have been shown to undergo cleavage under acidic conditions to release their payloads: these include hydrazones,<sup>199,211–213</sup> acetals,<sup>214</sup> and methoxybenzylacetals (**Figure 1.39**).<sup>199,215</sup> Of these, the hydrazone-based linkers have seen success in antibody-drug conjugates (ADCs), with two of the eight ADCs to have been approved following clinical trials utilising this linker.<sup>200,212,216</sup> However, studies on the first ADC to receive clinical approval, Mylotarg, also indicate one of the weaknesses of pH-sensitive linkers; they are often prone to instability (in this case in blood), limiting their lifetime in the body.<sup>199,217</sup> In terms of the cleavage mechanisms, methoxybenzylacetals, appear to follow a self-immolative

route, as opposed to the direct hydrolytic cleavage of hydrazones on reaction with water.<sup>199</sup>

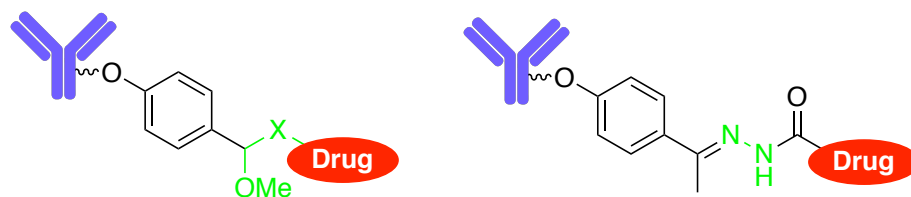
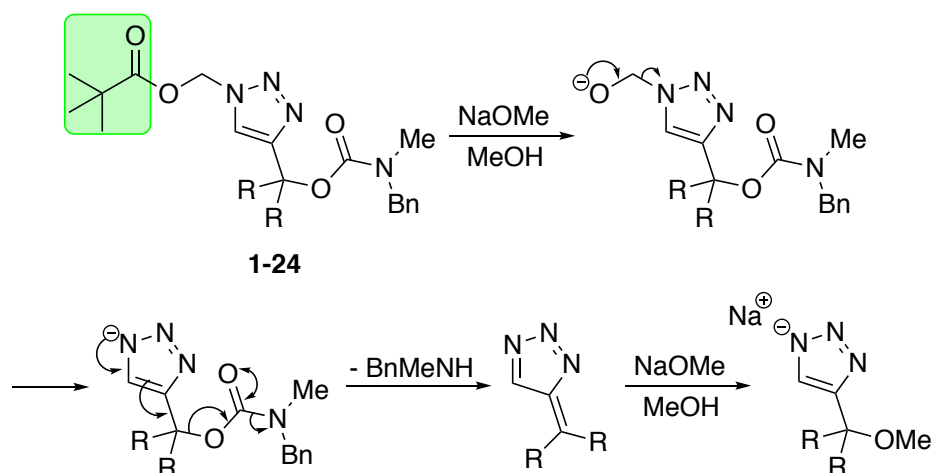


Figure 1.39 General structures of antibody-drug conjugates containing methoxybenzylacetal and hydrazone linkers.

Biolabile linkers that undergo cleavage under basic conditions can also be employed. For example, Blencowe *et al.* demonstrated base-mediated decomposition of a triazole-based self-immolative system (**1-24**) containing a base-labile pivaloyloxymethyl group on reaction with sodium methoxide in methanol (**Scheme 1.5**).<sup>218</sup> While these conditions are not applicable to biological systems, it demonstrates a potential pathway for future research to exploit.



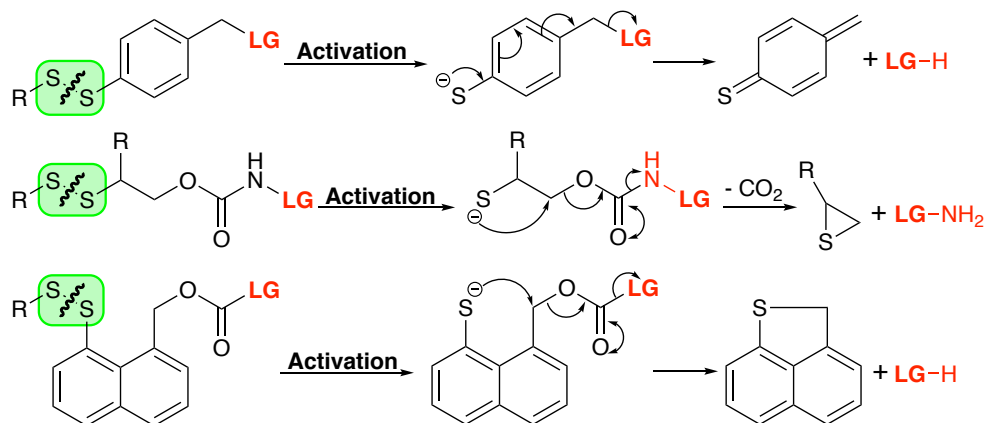
Scheme 1.5 Base-mediated cleavage of a self-immolative triazole linker (**1-24**). Base-labile pivaloyl ester highlighted in green box.<sup>218</sup>

#### 1.4.1.3 Thiol-Reactive Linkers

Disulfides are a variety of linker that can undergo both direct and self-immolative cleavage mechanisms. The direct mechanism typically involves thiol-disulfide exchange between the disulfide and glutathione in the cell cytoplasm, resulting in the release of the drug (or a glutathione-drug adduct).<sup>200</sup> The stability of the disulfides to thiol-mediated cleavage can also be tailored by increasing the steric bulk around the disulfide functionality;

this hinders the approach of biological thiols.<sup>200,219</sup> However, this cleavage mechanism requires the drug to contain a free thiol unit, which is relatively uncommon,<sup>220</sup> or undergo modification to insert one, which may have detrimental effects on its activity.<sup>221</sup>

This problem can be bypassed by creating self-immolative disulfide derivatives, for example by combination of disulfide bonds with appropriately-spaced carbonates and carbamates. On cleavage of the disulfide bond by intracellular thiols, the free thiol generated undergoes a cyclisation-elimination reaction, releasing a stable heterocycle and/or CO<sub>2</sub>, plus a free O/N-containing unit.<sup>199,222</sup> The nature of the heterocycle depends on the combination of carbonyl-containing groups present, and the linker length, with most systems tending to use linker lengths that generate 5 or 6-membered heterocycles on release,<sup>199,222,223</sup> although some cyclisation routes lead to the production of a 3-membered thiirane ring (**Scheme 1.6**).<sup>199,222,224</sup> A couple of the self-immolative mechanisms observed for disulfide-containing systems, including cyclisations to form a thiacenaphthalene unit,<sup>225</sup> and the thiirane formation, are currently unique to the disulfides. Disulfides can also act as the trigger mechanism for “classic” aromatic self-immolative systems.<sup>198,199,222,223</sup>



Scheme 1.6 Self-immolation mechanisms of some disulfide systems.<sup>200,223,225</sup>

A large number of disulfide-containing conjugates have been reported,<sup>199,223</sup> including ADCs for cancer treatment (**1-25**),<sup>226</sup> and conjugates of antibiotics to cell-penetrating peptides to target intracellular bacterial infections (**1-26**, **Figure 1.40**).<sup>227</sup> **1-25** consists of a pyrrolobenzodiazepine drug conjugated to

an antibody, and proved effective in treating cancer cells in a mouse model,<sup>226</sup> while **1-26** contains the antibiotic kanamycin attached via a disulfide to a peptide with high mammalian cell penetration, allowing clearance of intracellular *M. tuberculosis* infections in a macrophage model.<sup>227</sup> Unfortunately for their clinical potential, some disulfide-based conjugates have been reported to undergo premature drug release under *in vivo* conditions,<sup>222,228–230</sup> which would lead to off-target effects and, in the case of ADCs, potential antibody aggregation, which can in turn lead to an immune response.<sup>229,231</sup> More recent studies have focused on tuning the stability of the disulfide bonds to ensure they are sufficiently stable in blood plasma to be viable in the body, while retaining desirable intracellular release kinetics.<sup>223,230</sup>

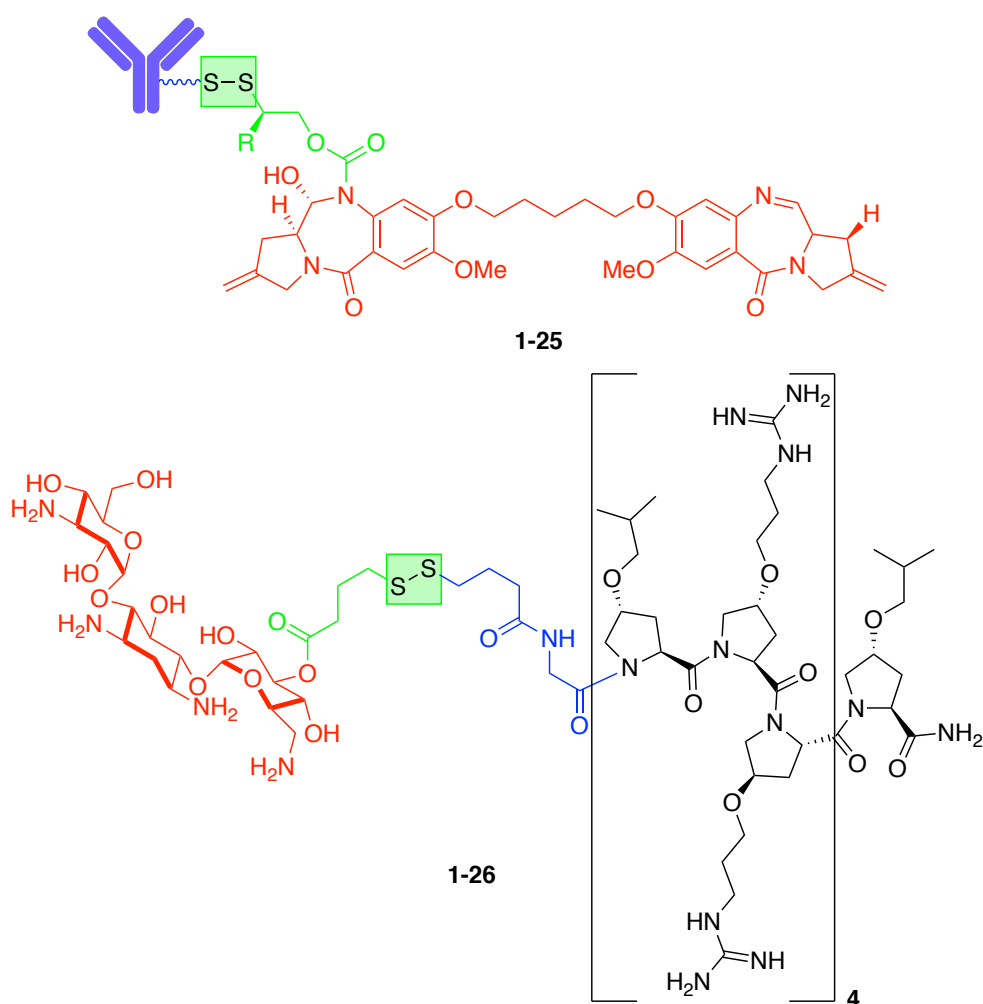
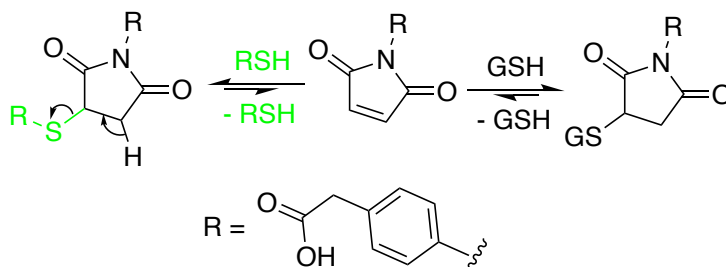


Figure 1.40 Examples of anticancer and antibacterial conjugates containing self-immolative disulfide linkers.<sup>223</sup> The self-immolative trigger is highlighted in a green box, the rest of the self-immolative system is green, and any other linker components are blue.

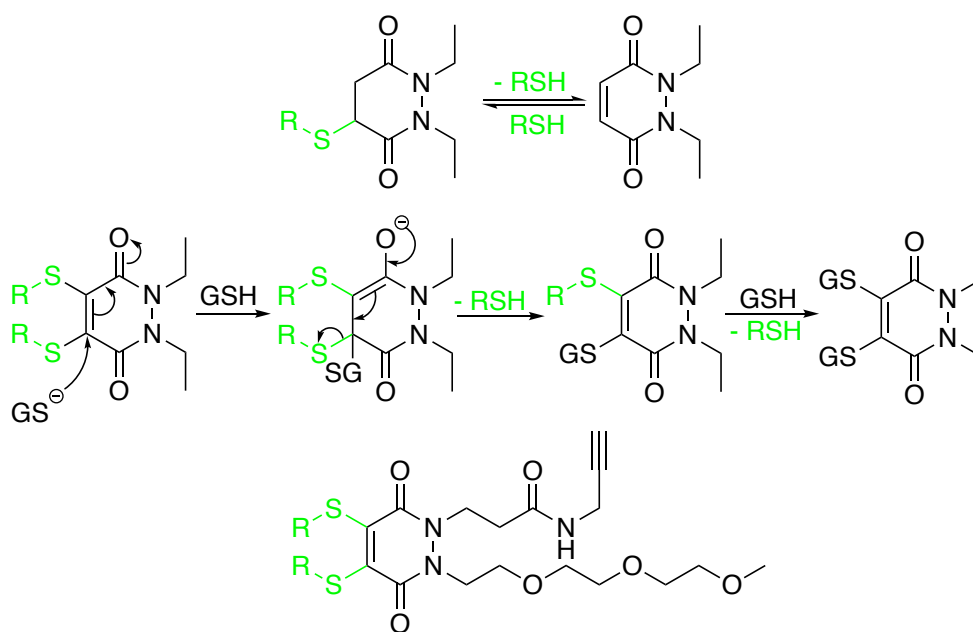
Maleimides have been extensively employed in chemical biology for covalent linkages involving thiol-containing species, including the study of cysteine-containing enzymes.<sup>232</sup> The double bond of the maleimide structure is able to undergo a fast Michael reaction with biological nucleophiles in aqueous conditions.<sup>232,233</sup> Under typical biological pH, this reaction will be specific to thiols, with amines (typically protonated) and hydroxyl groups requiring a higher pH to reach a similar nucleophilicity.<sup>232,233</sup> The soft electrophilic nature of maleimides also favours reaction with the softer thiol nucleophiles. The formed maleimide-thiol conjugates are typically very stable, but under certain conditions, they can undergo a retro-Michael reaction to reform the double bond, followed by another Michael reaction with a biological thiol like glutathione (**Scheme 1.7**).<sup>233</sup> As an equilibrium reaction, high concentrations of biological thiols favour conversion to the biological thiol adduct. The nature of the conjugated thiol in the starting conjugate also matters; the cleavage happens much faster for thiols with a lower pKa, like aryl thiols.<sup>233</sup> The cleavage is also slow compared to disulfides (c. 10-100x slower), which the authors note could aid increased stability in the blood, and prolong the period of drug delivery.<sup>233,234</sup>



Scheme 1.7 Equilibria of maleimides that can undergo retro-Michael reaction. The released thiol is highlighted in green.

In two recent papers, the Chudasama group have experimented with using pyridazinediones as cleavable linkers.<sup>235,236</sup> A saturated pyridazinedione conjugated to various thiols was shown to undergo retro-Michael addition to release the corresponding thiols, while showing no reactivity with biological thiol glutathione (even at 10x concentrations), and human serum albumin, the cysteine residue of which can often react with thiol-sensitive linkers in the blood. A similar maleimide derivative did display reaction with HSA, indicating potential problems with off-target reactivity for these

species.<sup>235</sup> Another pyridazinedione system, this time unsaturated, was able to undergo addition-elimination reactions with biological thiols. This system can be mono- or disubstituted, with a variant substituted with two aryl thiols performing best, showing complete release after 4 hours.<sup>236</sup> This scaffold can be further functionalised via the two pyridazinedione nitrogens, with synthesis of an unsymmetrical example (with different substituents on each nitrogen) demonstrated (**Scheme 1.8**).<sup>236</sup>



Scheme 1.8 Pyridazinediones studied by the Chudasama group, mechanisms of release, and an example of pyridazinedione difunctionalisation. The displaced thiol groups are highlighted in green.<sup>235,236</sup>

#### 1.4.1.4 Enzyme-Cleavable Linkers

Enzymatic hydrolysis is a common mechanism of cleavage, both for directly cleaved and self-immolative linkers. One example of direct cleavage is **ICT 2588**, a conjugate of a colchicine derivative for treatment of cancer (**Figure 1.41**).<sup>237,238</sup> This consists of an endcapped octapeptide connected to the active drug; the peptide contains a sequence recognised and cleaved by a matrix metalloproteinase; these are a series of proteases believed to play a major role in the development of cancer cells.<sup>237</sup> Following this cleavage, the remaining tetrapeptide is cleaved by nonspecific proteases to release the free drug. This example highlights one of the key problems with enzymatic cleavage as a mechanism of action – the steric bulk of the conjugate

prevents enzymes from direct hydrolysis of the bond to the drug; the initial hydrolysis has to occur away from the site of drug conjugation.

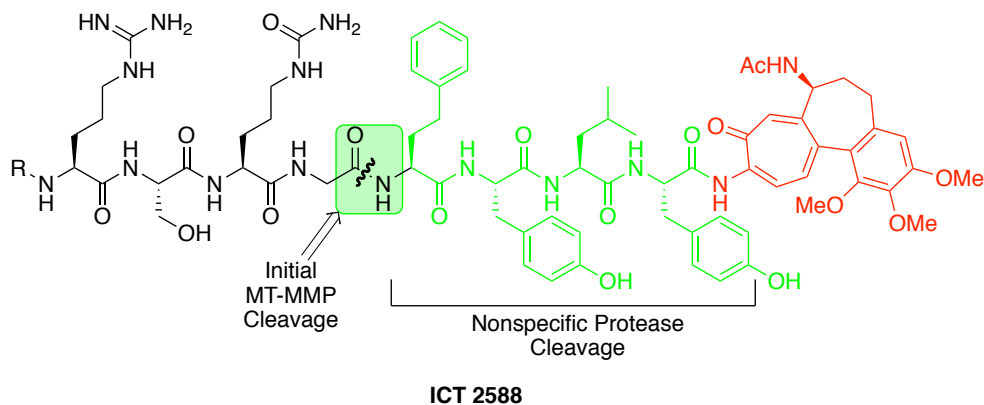


Figure 1.41 Structure of **ICT 2588**, an enzymatically cleaved anticancer conjugate.<sup>237,238</sup>

This issue can often be fixed by incorporating a self-immolative unit alongside the enzyme peptide trigger sequence. Possibly the most successful example of this is the Val-Cit linker first introduced by Dubowchik *et al.* in 2002 (**Figure 1.42**).<sup>239</sup> They experimented with a range of peptide sequences recognised by cathepsin B, a cysteine protease almost exclusively confined to lysosomes within cells, and often overexpressed in cancer cells, making it an ideal target for intracellular cleavage.<sup>200,239</sup> They discovered that conjugates of the anticancer drug doxorubicin (DOX) with both Phenylalanine-Lysine (Phe-Lys) and Valine-Citrulline (Val-Cit) linkers could be selectively and rapidly cleaved by cathepsin B. However, due to the bulky nature of the drug, efficient DOX release could not be obtained without introducing a spacer, in this case a self-immolative PABC unit, between the drug and the cathepsin-cleaved sequence.<sup>200,239</sup> The Val-Cit linker has proved the more successful of the two over time, with three of the eight market-approved antibody-drug conjugates using them to facilitate drug release.



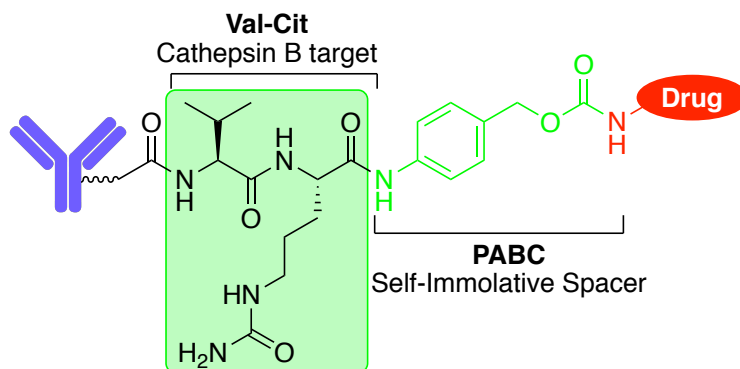


Figure 1.42 Design and structure of the Val-Cit linker.<sup>239</sup>

A number of other enzymatically cleavable triggers have been used in conjugation with self-immolative linker systems to obtain release under biological conditions, ranging from glycosylated units to nitro groups or azo bonds. Some key examples for biolabile conjugates are summarised in tabular form (**Table 1.1**). In terms of mechanism, enzymatic bond cleavage/reduction of the moieties below reveals a nucleophilic oxygen/nitrogen atom, triggering a self-immolative reaction.

Trigger	Chemical Structure	Enzyme	Ref.
Phenyl-acetamide		Penicillin-G-amidase	198,240
Asn-Pro-Val (NPV)		Neutrophil elastase	241
$\beta$ -Glucuronic Acid		$\beta$ -Glucuronidase	242,243
$\beta$ -Galactose		$\beta$ -Galactosidase	244–246

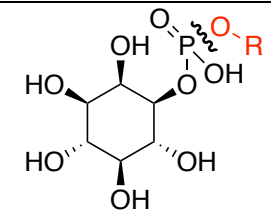
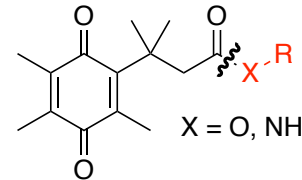
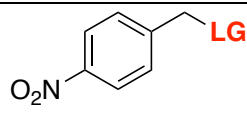
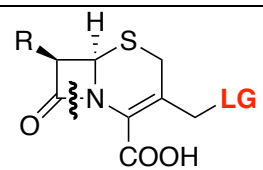
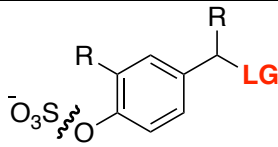
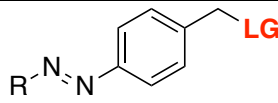
Inositol 1-phosphate		Phosphatidylinositol- specific phospholipase C ( <i>L. monocytogenes</i> )	247
Quinone		DT-diaphorase (NQO1)	248,249
Nitro		Nitroreductase	250,251
$\beta$ -Lactam		$\beta$ -Lactamase	252-254
Sulfate		Sulfatases	255
Azo		Azoreductase	256

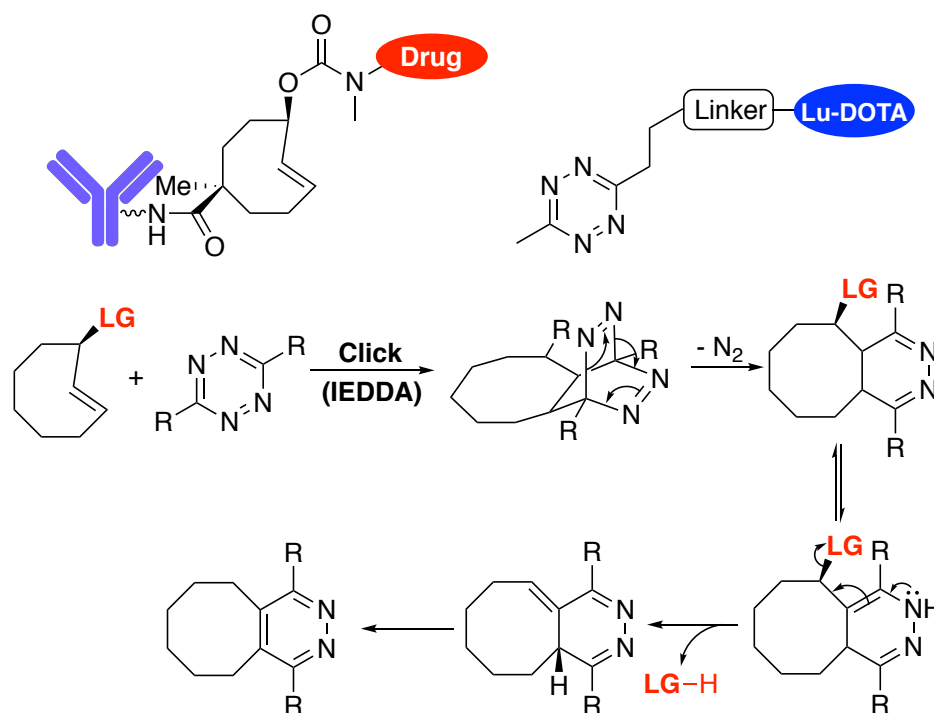
Table 1.1 Key enzymatically-cleaved triggers for self-immolative systems.

#### 1.4.1.5 External Stimuli

Self-immolative linkers can also be activated by non-biological, externally applied stimuli. This can allow an area of tissue to be selectively targeted, which is especially useful in the case of cancer treatment, as well as giving an alternative option should release strategies based on biological stimuli not provide the desired release profile. The stimuli can take the form of another chemical component added separately to the original conjugate, which can react with the conjugate to trigger drug release, or electromagnetic radiation, usually in the form of UV-Visible to Near Infrared (NIR) light.<sup>198,200,257,258</sup>

Both of these strategies come with additional complications. In the case of addition of a chemical trigger, care must be taken to flush the original conjugate from the blood so that activation can only take place in cells, avoiding off-target effects.<sup>257</sup> The trigger must also conform to the same

properties as the conjugate (e.g. low toxicity), and be able to localise in cells, which could pose a particular problem for targeting bacteria. Despite this, a number of systems, often based on click reactions, have been designed. Perhaps the most successful example to date is that of Rossin *et al.*, who examined an ADC with a click release trigger in mice, with the combination outperforming more conventional protease-triggered ADCs against the tumour model tested (**Scheme 1.9**).<sup>259</sup>



Scheme 1.9 Click components used by Rossin *et al.* for their ADC, and the mechanism of activation.<sup>259,260</sup>

#### 1.4.2 Biolabile Linkers in Synthetic Siderophore Trojan Horses

A range of siderophore Trojan Horses have been successfully synthesised containing biolabile linkers, with varying degrees of success. One of the first examples of siderophore Trojan Horse conjugates containing a biolabile linker was reported in 2001 by Hennard *et al.*<sup>194</sup> These conjugates, **1-27** and **1-28**, contained a methylenedioxy linker between the siderophore unit and two fluoroquinolones, norfloxacin and benzonaphthyridone (**Figure 1.43**). **1-27** and **1-28** both showed greater activity than identical conjugates containing stable linkers, however this activity is reduced compared to the parent norfloxacin and benzonaphthyridone. Due to the easily hydrolysable nature of the linker, it could potentially undergo extracellular hydrolysis *in vivo*, destroying the conjugate before it can reach its target.<sup>194</sup>

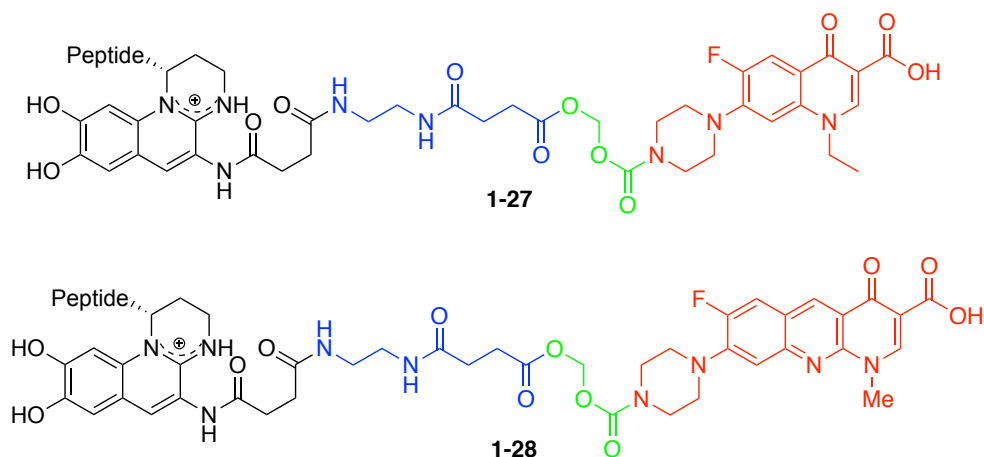


Figure 1.43 Structure of hydrolysable pyoverdins conjugates with methylenedioxy linker highlighted in green, and remainder of linker highlighted in blue.<sup>194</sup>

Rivault *et al.* and Noël *et al.* published examples of pyochelin conjugates using the same methylenedioxy linker as Hennard *et al.* in 2007 and 2011, respectively (**Figure 1.44**).<sup>261,262</sup> Rivault *et al.* were able to show two examples (**1-29** and **1-30**) containing the methylenedioxy linker that proved as active as norfloxacin against a *P. aeruginosa* strain.<sup>261</sup> However, Noël *et al.* observed only reductions in activity against three *P. aeruginosa* strains for **1-31** to **1-33** compared to the parent fluoroquinolones, although the poor solubility of the conjugates in the culture medium may have hindered the study.<sup>262</sup> Notably, two of the conjugates (**1-31** and **1-32**) proved active via a mutant strain of *P. aeruginosa* (PAD14) which lacks the TonB complex required to provide energy to the pyochelin transportation. This suggests extracellular hydrolysis of the conjugates, then uptake of the resulting free fluoroquinolones.<sup>262</sup>

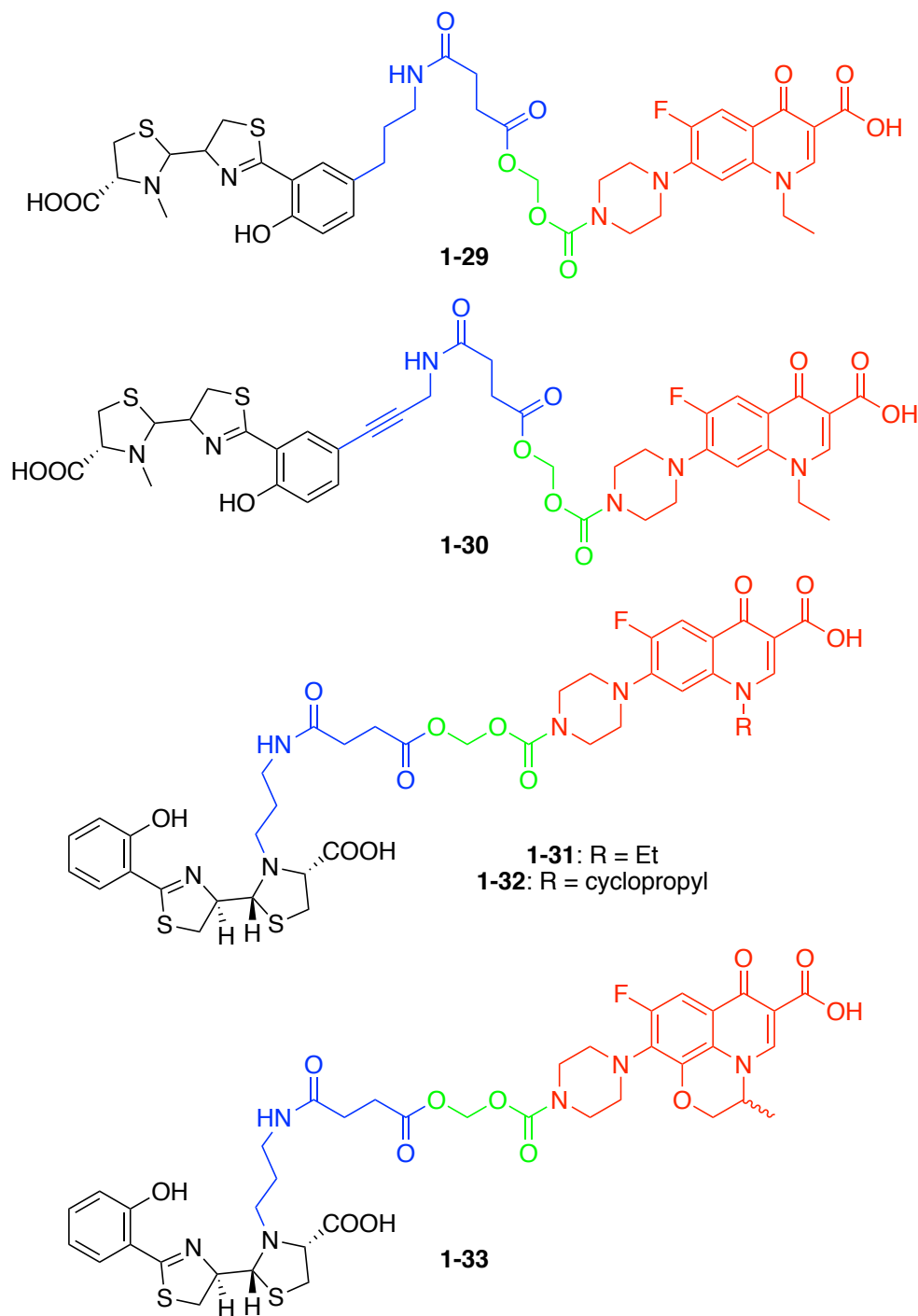


Figure 1.44 Pyochelin-fluoroquinolone conjugates containing a labile methylenedioxy linker.<sup>261,262</sup>

Zheng and Nolan also made use of substituted and unsubstituted methylenedioxy linkers for release of ciprofloxacin (the range of linkers tested is shown above in **Figure 1.38**).<sup>210</sup> By tuning the steric bulk of the groups neighbouring the linker, and introducing a methyl group to the linker, they were able to change the half-life of the linkers in solution from 21 minutes to over 130 hours (as measured by HPLC). However, these still

proved unsuccessful when applied to the synthesis of enterobactin conjugates; although a half-life of 10 hours could be achieved in the most stable conjugate (**1-34**, **Figure 1.45**), the MIC was still reduced 10x compared to the parent ciprofloxacin vs. *E. coli*. Again, this was ascribed to extracellular hydrolysis and release of ciprofloxacin.<sup>210</sup>

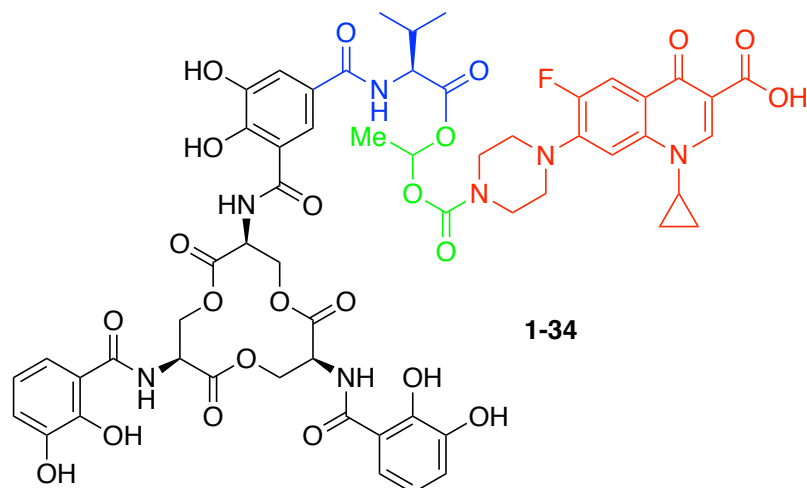


Figure 1.45 Structure of an enterobactin conjugate (**1-34**) containing a methylenedioxy linker.<sup>210</sup>

Paulen *et al.* published an example of a simple monocatechol-oxazolidinone conjugate containing a similar linker, this time a methylene bridge between an ester group and a triazole (**1-35**, **Figure 1.46**).<sup>187</sup> This linker has been shown to undergo hydrolysis under basic conditions,<sup>218</sup> however in this case failed to increase the activity beyond that of a covalently-bound version of the conjugate (**1-14**), with extracellular hydrolysis a possible cause.<sup>187</sup>

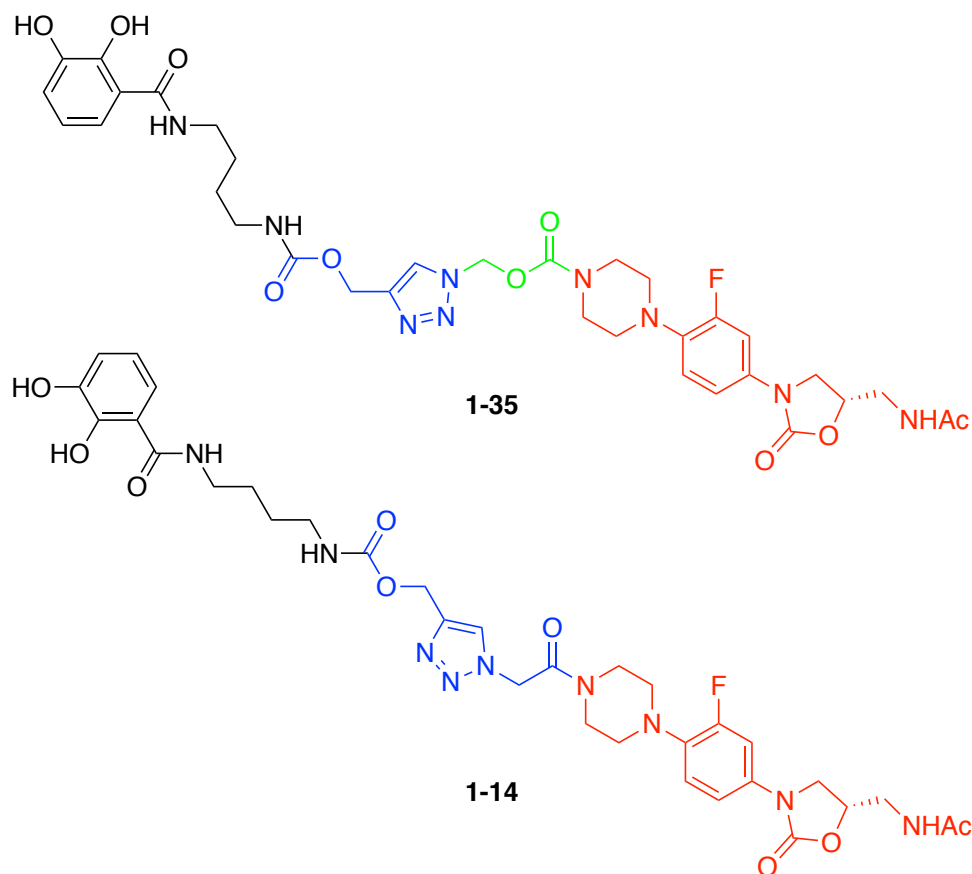


Figure 1.46 Structure of oxazolidinone conjugate **1-35** containing a methylene bridge synthesised by Paulen *et al.*, and the related non-biolabile conjugate **1-14**. The methylene bridge is highlighted in green, and other linker components highlighted in blue.<sup>187</sup>

Wencewicz *et al.* have synthesised two conjugates based on the original salmycin scaffold employed by bacteria, with a danoxamine siderophore unit bound via a succinyl linker to both ciprofloxacin (**1-36**, amide linkage) and triclosan (**1-37**, ester linkage, **Figure 1.47**).<sup>143</sup> As discussed above, the mechanism of antibiotic release from salmycin is believed to stem from attack of the ester linkage by the closest hydroxamate group in a cyclisation reaction (**Figure 1.25**). In this case, the triclosan conjugate **1-37** is observed to have comparable or improved activity to triclosan against a number of bacterial strains, but the activity of ciprofloxacin conjugate **1-36** is much reduced compared to ciprofloxacin. This suggests that if the cyclisation mechanism is indeed correct, it is much less able to hydrolyse the more stable amide linkage of **1-36** compared to the ester of **1-37**.

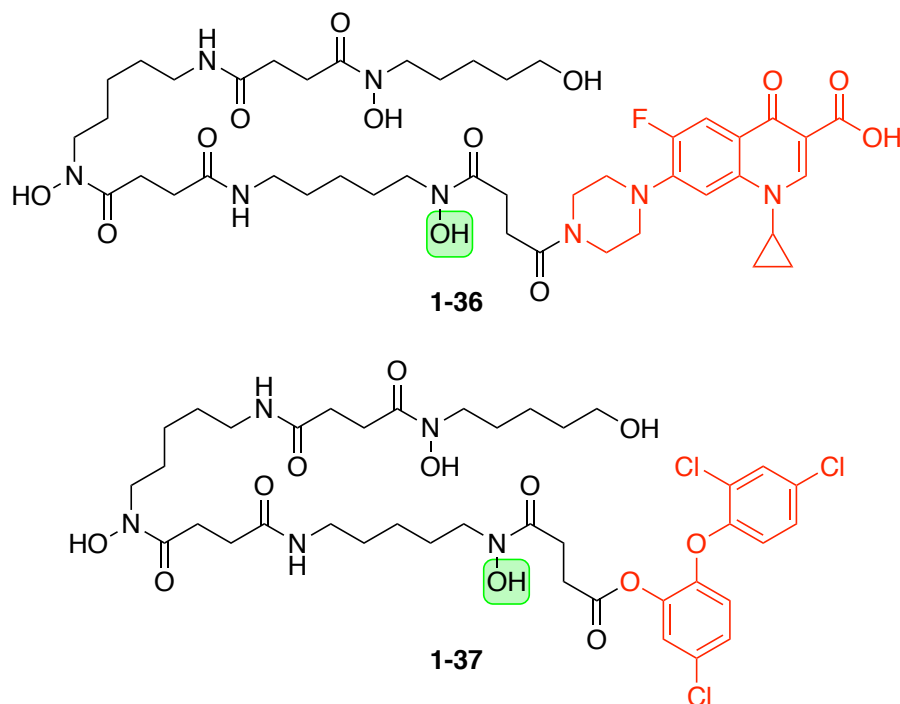


Figure 1.47 Structures of desferridanoxamine conjugates **1-36** and **1-37** synthesised by Wencewicz *et al.* The hydroxamate group responsible for the potential cyclisation mechanism is highlighted in green.<sup>143</sup>

The Miller group have synthesised three desferrioxamine conjugates and a mixed catechol-hydroxamate conjugate based on two variants of a cyclisation-based biolabile linker, the “trimethyl lock”.<sup>189,263</sup> For the original trimethyl lock design, the hydrolysis of an ester (**1-38**) or phosphate group (**1-39**) creates a free alcohol, which rapidly cyclises to form a 6-membered lactone ring, with subsequent drug release. The high rate of lactonisation is due to an unfavourable interaction between methyl groups in the structure (**Figure 1.48**).<sup>189</sup> The second variant is a reduction-triggered variant (**1-40**), which has an identical mode of release, but relies on reduction of a quinone to create the free alcohol.<sup>263</sup> This variant was inspired by the lack of substrate specificity observed for bacterial ferric reductases, meaning they might be able to reduce the quinone during/after iron reduction. Unfortunately, in all cases these conjugates displayed worse activity than their parent antibiotics vs. Gram-positive and Gram-negative bacteria.<sup>189,263</sup>



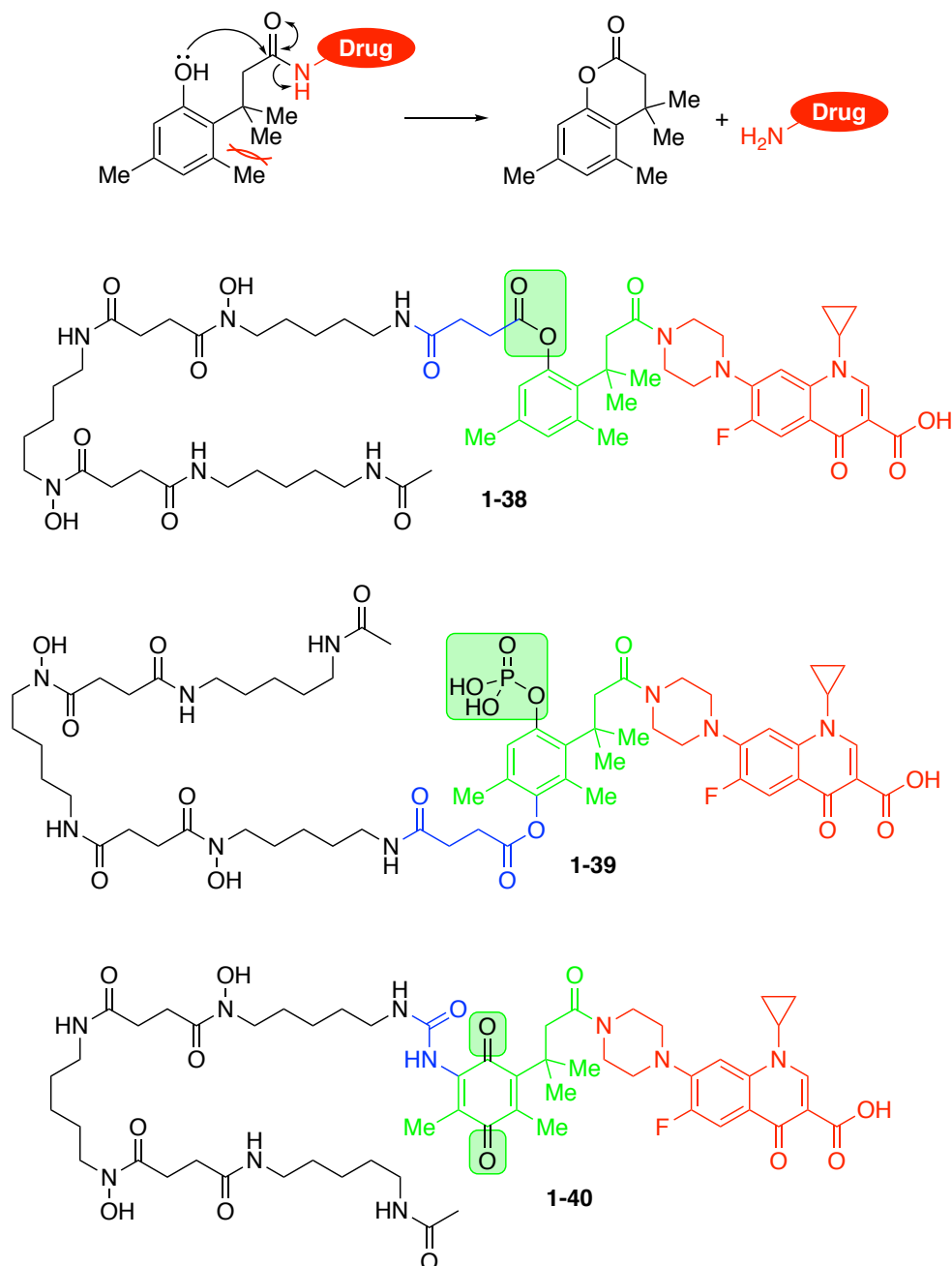


Figure 1.48 Mechanism for trimethyl lock cyclisation (with steric clash indicated) and structures of desferrioxamine conjugates **1-38** to **1-40** based on this self-immolative linker. The different trigger groups for the self-immolative reaction are highlighted in green boxes.<sup>189,263</sup>

Two papers have recently been published by Neumann *et al.* featuring two differing approaches to intracellular release from an enterobactin scaffold (**Figure 1.49**).<sup>264,265</sup> One utilises a disulfide-containing conjugate of ciprofloxacin (**1-41**) in which the disulfide bond can be cleaved on exposure to endogenous thiols like glutathione,<sup>265</sup> similar to an approach tried in the past by the Duhme-Klair and Routledge groups.<sup>266</sup> However, **1-41** displays

worse activity than the parent ciprofloxacin. The second approach involves a ciprofloxacin-enterobactin conjugate (**1-42**) that doesn't contain a true biolabile linker, but instead antibiotic activity vs. *E. coli* is granted by the hydrolysis of the enterobactin structure by IroD, an enzyme typically associated with pathogenic *E. coli* strains.<sup>264</sup> Unlike most other reported conjugates, **1-42** displays comparable activity to ciprofloxacin. The structure of the active agent is not yet known, it could be that the ciprofloxacin remains bound to the enterobactin hydrolysis products, or it could be released completely. The hydrolysis products on their own are unable to cause growth inhibition; the full enterobactin unit must be taken up to achieve activity.<sup>264</sup>

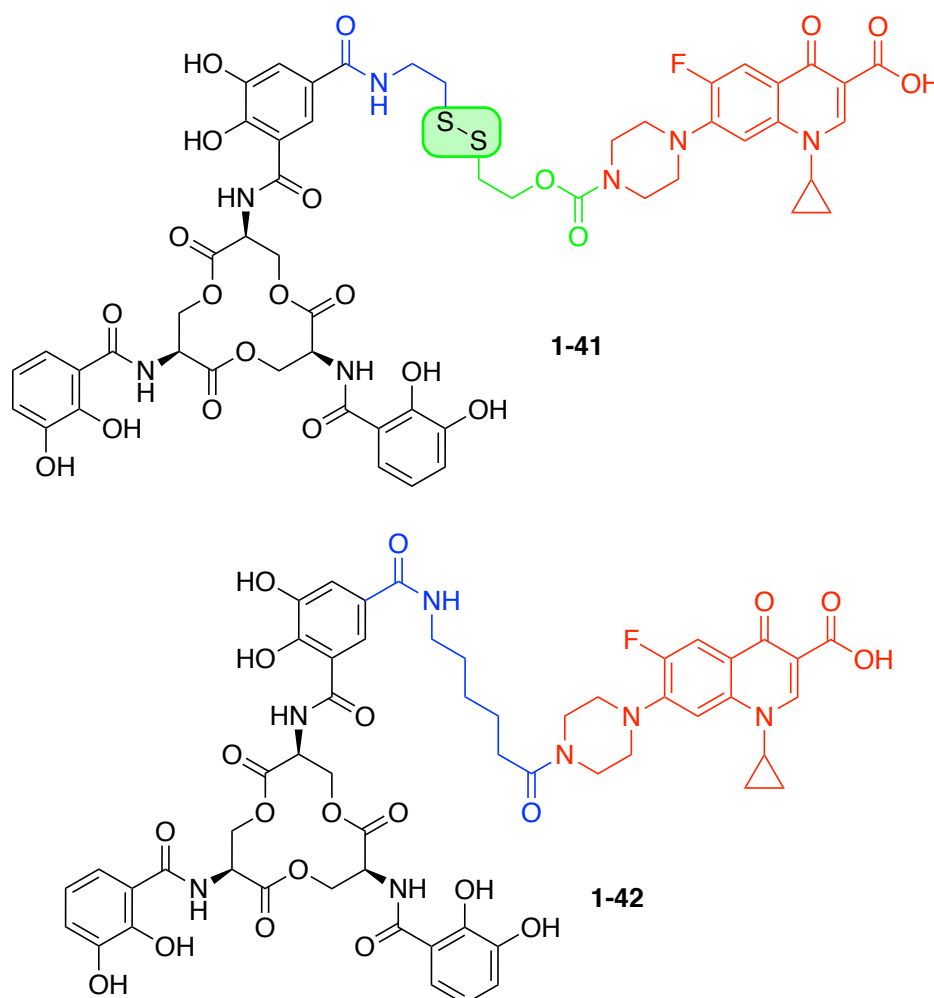


Figure 1.49 Structure of enterobactin-based Trojan Horse conjugates synthesised by Neumann *et al.*<sup>264,265</sup>

Perhaps the most successful example of a biolabile linker used in this field so far is that reported by Liu *et al.*,<sup>267</sup> who synthesised a conjugate containing an oxazolidinone antibiotic bound to a cephalosporin ( $\beta$ -lactam-containing

antibiotic), which is in turn bound to a siderophore moiety (**1-43**, **Figure 1.50**).<sup>267</sup> Oxazolidinones are typically inactive vs. Gram-negative bacteria, often due to poor permeation of the outer membrane.<sup>267</sup> However, in the case of this conjugate, the siderophore unit permits uptake through the outer membrane into the periplasm of Gram-negative bacteria. There, hydrolysis of the cephalosporin by  $\beta$ -lactamase enzymes leads to release of the oxazolidinone, which is then free to cross the cytoplasmic membrane and find its cellular target.<sup>267</sup> **1-43** displays high activity against a number of bacterial strains, including *P. aeruginosa*, and multiple *A. baumannii* strains; the activity comes in part from both the oxazolidinone and cephalosporin components, however, activity is retained for strains that show resistance to the cephalosporin component alone. Crucially, a control containing the siderophore component covalently attached to the oxazolidinone is inactive against all of the bacterial strains studied, supporting the conclusion that *in vivo* release via  $\beta$ -lactamase hydrolysis is vital for activity.<sup>267</sup>

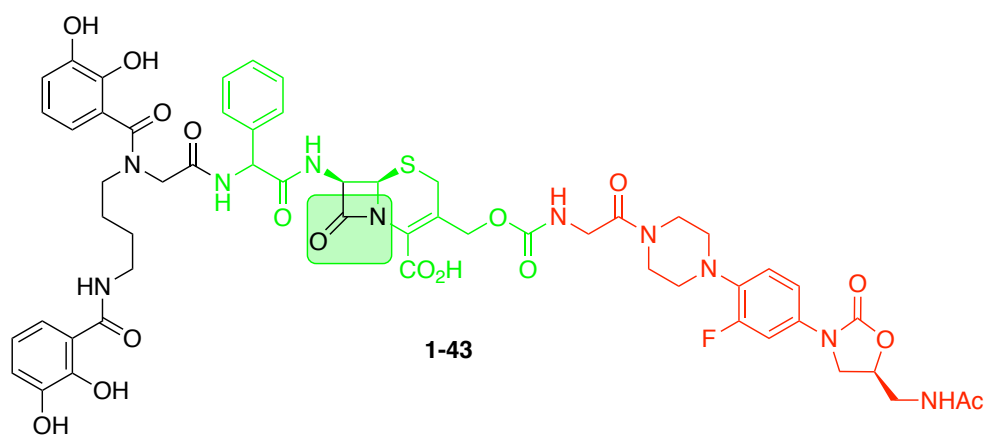


Figure 1.50 Structure of siderophore-cephalosporin-oxazolidinone conjugate **1-43**. The cephalosporin is highlighted in green, and the oxazolidinone in red.<sup>267</sup>

A novel approach to the design of protease-cleavable biolabile linkers for siderophore conjugates comes from Boyce *et al.*, who built on much of the knowledge developed through the previous work discussed above.<sup>268</sup> To simplify the requirements on the siderophore component, they aimed for cleavage of the linker in the periplasm, meaning the siderophore unit is only required to facilitate passage through the outer membrane. Instead of focusing on single protease targets, they screened a library of protein

sequences against a periplasmic extract from *E. coli* cells, allowing identification of the protein sequences that are cleaved most efficiently by protease enzymes present. The selected protein sequence (WSPKYM) was then applied to the design of siderophore conjugates containing oxazolidinone and macrolide antimicrobials (**Figure 1.51**). The resulting oxazolidinone conjugate **1-44** proved much more active against *E. coli* than the parent antimicrobial, and the macrolide conjugate **1-45** retains the activity observed for the free macrolide, indicating the conjugates can be taken up into the periplasm and undergo successful protease cleavage to release the antimicrobials, which can then cross the inner membrane as previously seen by Liu *et al.*<sup>267</sup> This platform offers great potential for the development of other enzymatically-cleaved substrates for siderophore conjugates.

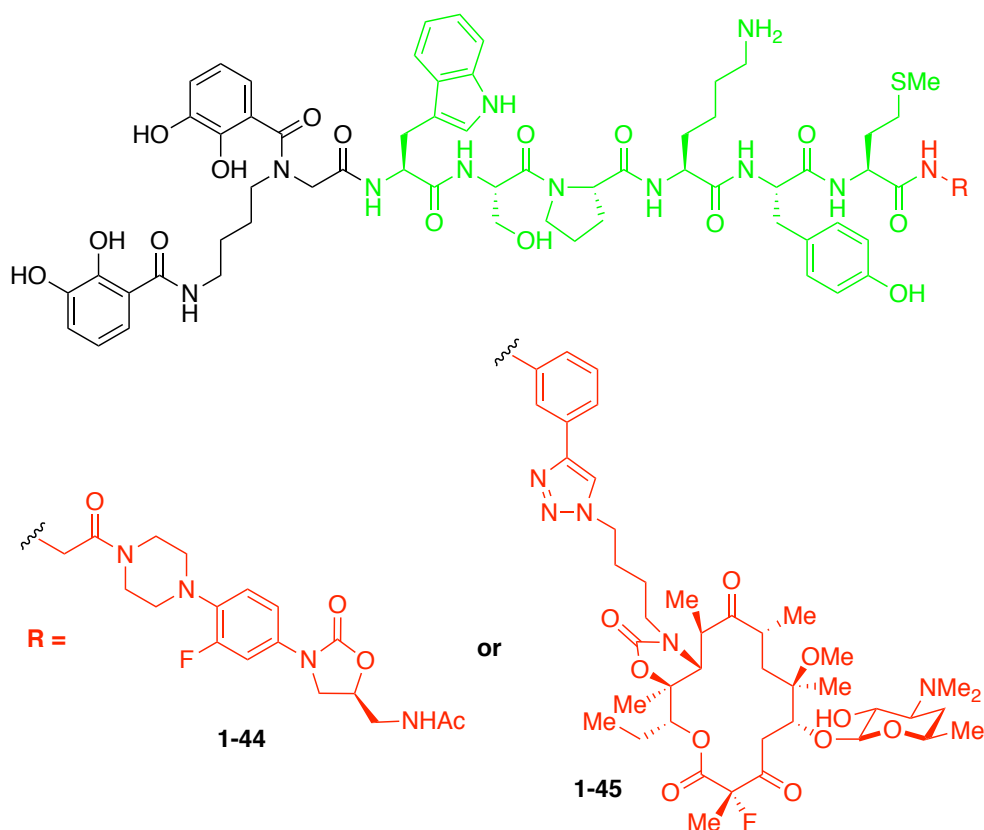


Figure 1.51 Structure of protease-cleaved siderophore conjugates developed by Boyce *et al.* The cleaved protein sequence is highlighted in green, and the antimicrobials in red.<sup>268</sup>

As some of the examples above show, there are a number of key considerations that must be taken into account for siderophore conjugates with cytoplasmic targets:

- 1) All three components of the system (the siderophore, the linker and the antibiotic) require careful optimisation.<sup>196</sup>
- 2) The antibiotic component must either be carefully modified to maintain activity, or must be released in the periplasm/cytoplasm.<sup>133,171,196,267,268</sup>
- 3) The siderophore unit must be capable of facilitating uptake into the cytoplasm (unless antibiotic release can take place in the periplasm).<sup>196,269,270</sup>
- 4) Good recognition of the siderophore unit by outer membrane receptors is required. This usually necessitates the use of native siderophores.<sup>171,270</sup>
- 5) Antibiotic conjugation should be carried out in such a way that it does not impair recognition of the siderophore unit by the transporters required for uptake.<sup>270</sup>
- 6) The siderophore should have high Fe affinity, and be able to compete with native siderophores for iron binding, otherwise uptake will be reduced.<sup>133,171,270</sup>

## 1.5 Gas-Releasing Antimicrobial Prodrugs

A number of gaseous molecules, including nitric oxide (NO) and carbon monoxide (CO) have been shown to have important biological functions. These primarily include their role as gasotransmitters involved in regulating various systemic processes, including muscle relaxation and vasodilation.<sup>271,272</sup> NO is also biosynthesised and released by macrophages as an antimicrobial.<sup>273</sup> Since the discovery of these biological functions, which demonstrate that the human body can tolerate certain levels of these otherwise toxic gases, interest in the use of gases and gas-releasing compounds as therapeutics has increased hugely.

### 1.5.1 Nitric Oxide-Releasing Antimicrobials

Antibacterial therapies involving NO have possibly attracted the most interest, almost certainly due to its existing role in the human immune system. To the best of the author's knowledge, the first report of the use of NO donors as antimicrobials comes from 1974, where cysteine-nitrosothiol (**1-46**) was shown to display antibacterial effects against a number of bacterial strains, including *Salmonella*.<sup>274</sup> Since then, a number of delivery systems have been developed, ranging from gaseous NO to organic donors like diazeniumdiolates (**Figure 1.52**).<sup>275</sup> Release mechanisms for NO are often identical to those seen for biolabile linkers, while delivery of NO to the desired target often relies on polymeric systems.<sup>276</sup>

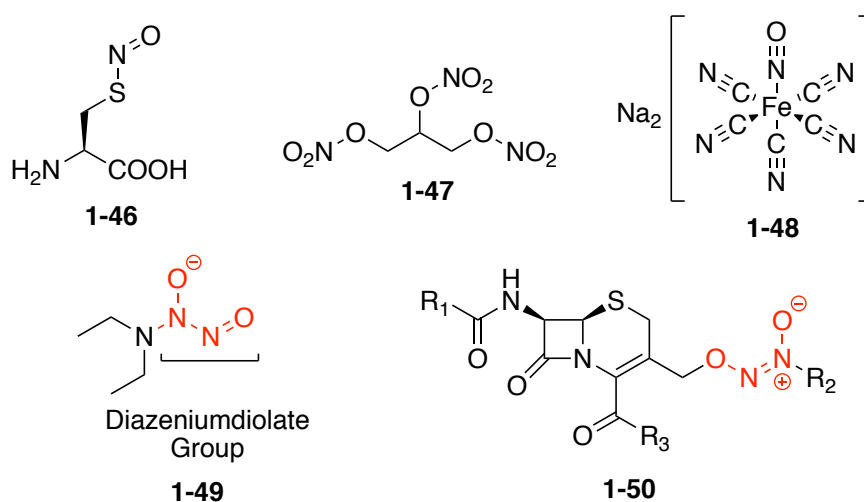
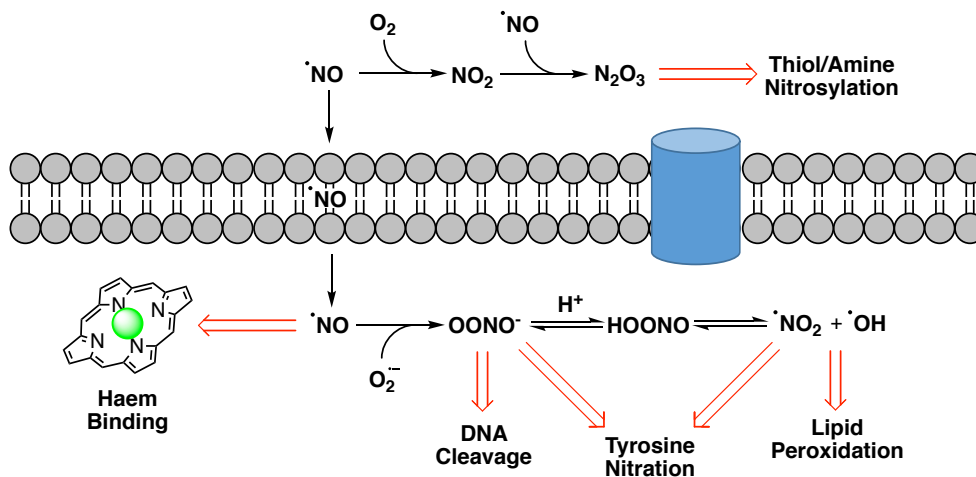


Figure 1.52 Some examples of NO delivery agents, including cysteine-nitrosothiol (**1-46**), nitroglycerine (**1-47**), sodium nitroprusside (**1-48**), diethylamine diazeniumdiolate (**1-49**), and a cephalosporin-NO conjugate (**1-50**, NO release is triggered by cephalosporin hydrolysis).<sup>277</sup>

NO can affect a variety of processes within bacterial cells. As a free radical, the NO can act on its own, or react with oxygen and reactive oxygen species (ROS) to form more reactive nitrogen oxygen species (RNOS) like peroxynitrite (OONO<sup>-</sup>).<sup>275,276,278</sup> These can induce oxidative and nitrosative stress, with damage to DNA, peroxidation of lipids, nitrosylation of thiols and binding to iron centres in enzymes (**Scheme 1.10**).<sup>275,276</sup>



Scheme 1.10 Examples of some mechanisms of NO action within bacterial cells. Adapted from Carpenter and Schoenfisch.<sup>278</sup>

It should also be noted that this antibacterial effect is highly concentration-dependent, with some species of bacteria using NO for cell signalling and regulating biofilm formation.<sup>276</sup> Nitric oxide production in *Bacillus anthracis*, the bacterium responsible for anthrax infections, has been shown to act as a virulence factor in a mouse model, with endogenous NO suppressing the Fenton reaction, and stimulating catalase enzyme activity.<sup>279</sup> This protects the cells from ROS production by the immune system; mutant strains deficient in NO production are more easily killed by the immune cells.<sup>279,280</sup> *Bacillus anthracis* can even use NO to go on the attack against the immune system, with S-nitrosylation of key proteins in the mitochondria of macrophages leading to cell death.<sup>280,281</sup>

Two NO donors, delamanid and pretomanid, have recently been approved by the EMA and the FDA respectively for use against extensively drug-resistant (XDR) tuberculosis following Phase III clinical trials (**Figure 1.53**).<sup>67,282–284</sup> These drugs have an interesting dual mechanism of action, with the ability to act as inhibitors of cell wall mycolic acid synthesis in replicating TB, and via NO release in hypoxic conditions in non-replicating TB.<sup>282</sup>

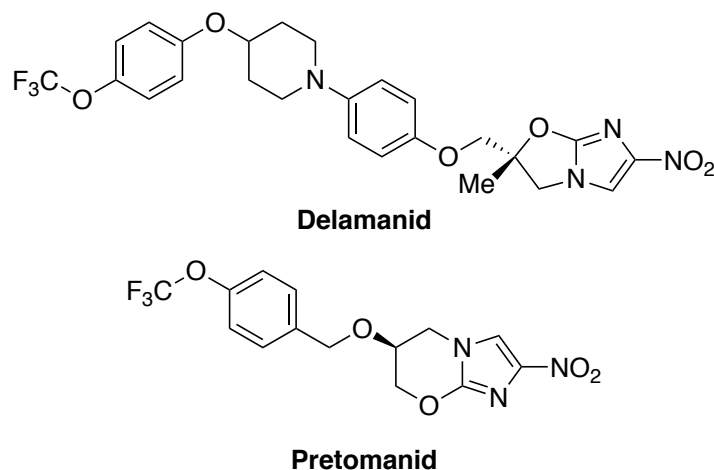


Figure 1.53 Structures of delamanid and pretomanid.

### 1.5.2 Carbon Monoxide-Releasing Antimicrobials

Carbon monoxide donors, often known as Carbon Monoxide Releasing Molecules or CORMs, have also been explored, having first been reported to have antibacterial activity in 2007.<sup>285</sup> While CO is better known as a toxic gas, it can have beneficial effects at a surprisingly high concentration; the FDA has set an upper limit of 14% haemoglobin saturation for clinical trials.<sup>286</sup> CORMs primarily take the form of metal complexes bearing CO ligands, although a number of organic examples have also been synthesised.<sup>287</sup> Various release mechanisms have been observed for CORMs, including photochemical release,<sup>288</sup> enzyme-triggered release,<sup>289</sup> and release via a “click” Diels-Alder process.<sup>290</sup> The mechanism of action is not yet clear; early work pointed to CO inducing ROS formation,<sup>291</sup> with more recent research suggesting that the metal ions in CORM complexes can play a pivotal role, and drawing questions as to what proportion of the observed activity comes from CO release.<sup>292,293</sup>

So far, metal-based CORMs have proved the most effective antibacterial agents. The first study to display antibacterial activity observed inhibition of both *S. aureus* and *E. coli* growth with Ru, Mo and Mn complexes, and demonstrated that CO release did not happen in the growth media, instead occurring inside the cells.<sup>285</sup> Further research has often focused on Mn carbonyl complexes, which can offer release via photochemical methods,<sup>288,294</sup> or in aqueous conditions.<sup>295</sup> These have shown activity against clinically relevant bacteria like *E. coli*, *P. aeruginosa* and *S.*



*pneumoniae*.<sup>288,293–296</sup> Organic CORMs have so far seen little use as antimicrobials,<sup>257</sup> although one click-triggered example (**1-55**) achieves CO release alongside release of metronidazole, with activity vs. *Helicobacter pylori*.<sup>290</sup>

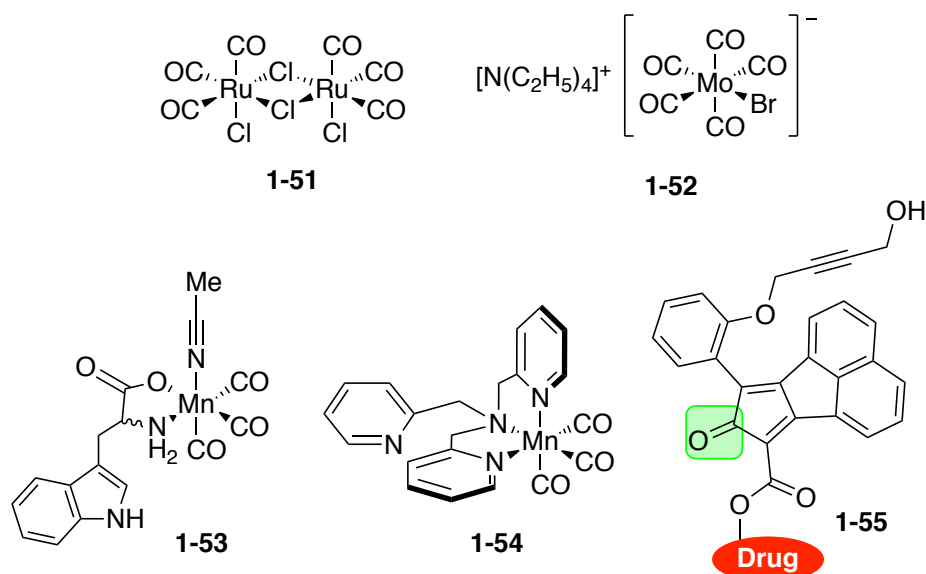


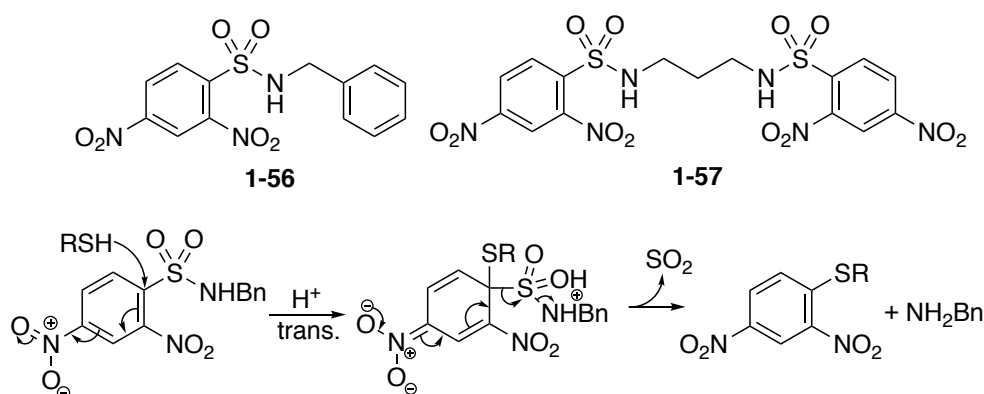
Figure 1.54 Structures of a range of CORMs. For the organic CORM **1-55**, the site of CO release is highlighted in green.

### 1.5.3 Sulfur Dioxide-Releasing Antimicrobials

In comparison to these other two gases, sulfur dioxide ( $SO_2$ ) has seen relatively little exploration of its potential use in antibacterial drugs, perhaps as its physiological role is less well known.<sup>297</sup> This is despite it having a long history of use as an antimicrobial in food technology, and especially brewing; it is claimed (although with some debate) that the Romans used burning sulfur candles to sterilise empty wine vessels, noticing that it prevented vinegary smells from occurring,<sup>298</sup> and a decree was issued in Germany in 1487 to control the amount of sulfur that could be added to wine.<sup>299</sup> Although the mechanism of  $SO_2$  toxicity to bacteria is still unclear,<sup>300</sup> it is believed to involve oxidative damage to biomolecules, and the breakdown of disulfide bridges in proteins (forming  $S-SO_3^-$  adducts).<sup>301</sup>

The first report of  $SO_2$  prodrugs as antibacterial agents was published by Chakrapani and colleagues in 2012, who synthesised a series of  $SO_2$ -releasing 2,4-dinitrobenzenesulfonamide prodrugs that undergo release on

attack by biological thiols via a nucleophilic aromatic substitution ( $S_NAr$ ) mechanism (**Scheme 1.11**).<sup>301</sup> This reactivity is enabled by the highly electron-withdrawing properties of the nitro groups and the sulfonamide group; similar compounds lacking one of the nitro groups, or with a nitro group replaced with a weaker EWG often demonstrate reduced or non-existent  $SO_2$  release.<sup>301,302</sup>



Scheme 1.11 Structure of thiol-activated  $SO_2$  prodrugs synthesised by Chakrapani group, plus mechanism of activation.<sup>301,303,304</sup>

These prodrugs were examined for their biological activity versus *M. tuberculosis*, with one compound (**1-56**) displaying a better minimum inhibitory concentration (MIC, 0.15  $\mu M$ ) than isoniazid, the front line drug of choice vs. TB (0.37  $\mu M$ ). This paper, plus a follow-up study published later that year,<sup>303</sup> showed a rough correlation between  $SO_2$  release rate and antibacterial activity. A later paper published in 2015 also demonstrated promising activity of similar compounds (including the disulfonamide **1-57**) vs. methicillin-resistant *S. aureus* and *Enterococcus faecalis*, although no antibacterial effects were observed vs. *E. coli*.<sup>304</sup> Similar 2,4-dinitrophenyl-based structures have also found use in anticancer prodrugs;<sup>305–308</sup> these will be discussed further in Chapter 2.

A number of other  $SO_2$  donors activated by photochemical, intramolecular cycloaddition or hydrolysis mechanisms have also been synthesised by the Chakrapani group and others (**Figure 1.55**).<sup>297,309–311</sup> These are often “proof-of-concept” experiments for a certain structure or release mechanism, with limited exploration of their biological activity. Of those where the biological activity has been examined, a UV-activated example (**1-58**) synthesised by

Kodama *et al.* has seen study for its potential anticancer effects.<sup>312,313</sup> The original study demonstrated that **1-58** could cause cell death on photoactivation with UV light.<sup>312</sup>

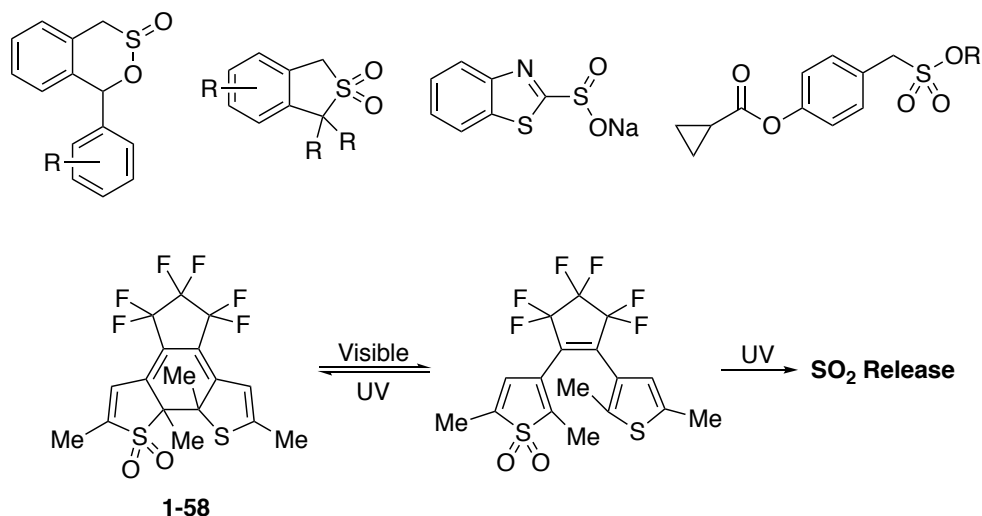


Figure 1.55 Structures of various SO<sub>2</sub>-releasing systems, including Kodama *et al.*'s UV-activated compound **1-58**.

Two examples have also been used to target bacteria; these both use SO<sub>2</sub> release in conjunction with release of an antimicrobial component.<sup>314,315</sup> The first uses an *o*-nitrobenzyl phototrigger and a slightly unusual antimicrobial component, ferulic acid ethyl ester (FAEE, **Figure 1.56**).<sup>314</sup> Ferulic acid and its derivatives are often present in plant extracts, and components of the human diet like rice and vegetables; it has previously been studied for potential antimicrobial activity, with limited success.<sup>316–318</sup> However, it does fluoresce on excitation at 330 nm, so provides a useful reporter for tracking SO<sub>2</sub> release. Incorporation of SO<sub>2</sub> release increased activity 5x vs. *E. cloacae* compared to FAEE (2.6 μM vs. 12.3 μM), with the FAEE conjugate **1-59** displaying 2x activity compared to a phenol control **1-60** (2.6 μM vs. 6.3 μM).<sup>314</sup>

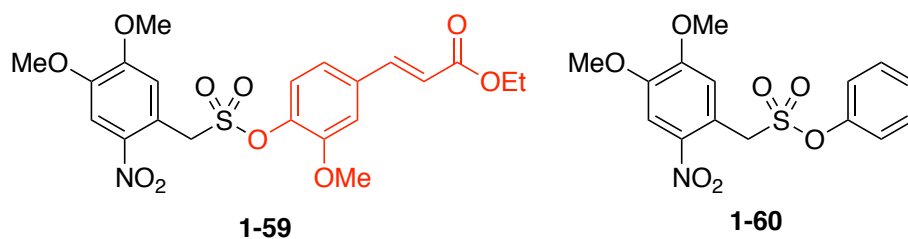
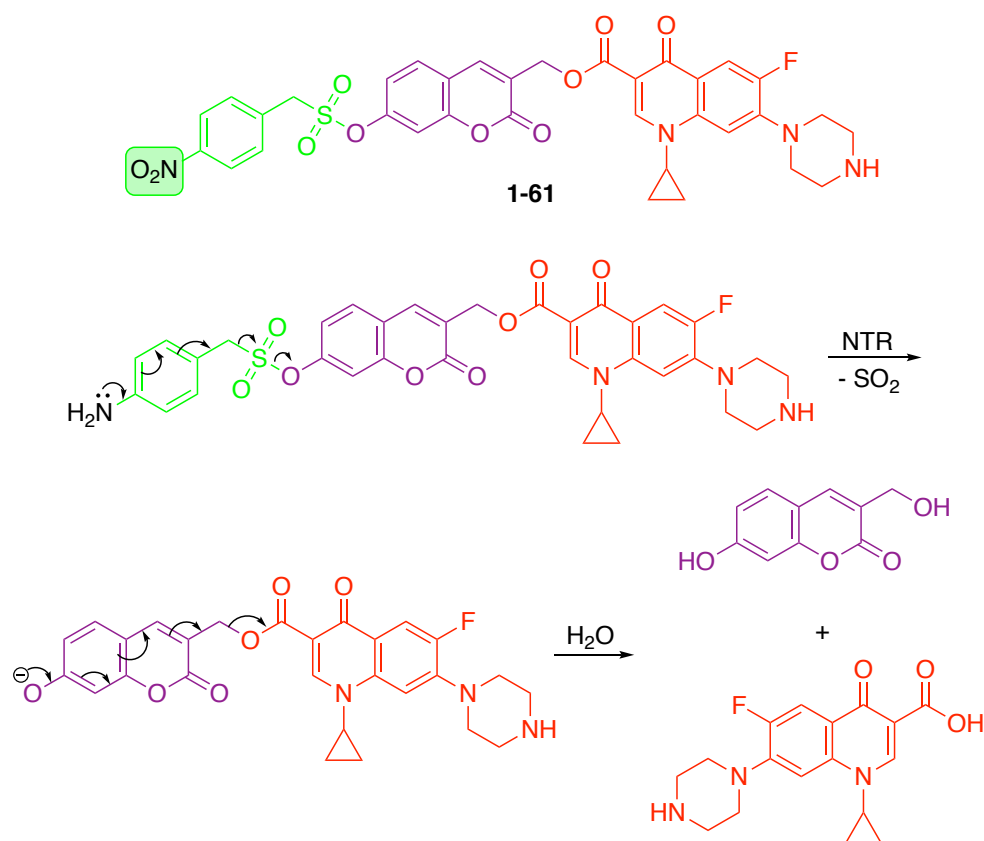


Figure 1.56 Phototriggered SO<sub>2</sub>-releasing conjugates **1-59** and **1-60**.<sup>314</sup>

The second example, another from the Chakrapani group, uses a nitroreductase trigger alongside a more conventional antibiotic, ciprofloxacin (**1-61**, **Scheme 1.12**).<sup>315</sup> This was connected to the trigger via a sulfonate group, and a further self-immolative coumarin unit, aiming to provide a fluorescent reporter. The conjugate displays sub-micromolar activity (0.043  $\mu\text{M}$  and 0.178  $\mu\text{M}$ ) against a number of *E. coli* strains, although it is less active (10-20x) than the parent ciprofloxacin. A similar pattern is observed for a number of other bacteria like *P. aeruginosa* and *S. aureus*, with micromolar activity seen, but to a lesser extent than ciprofloxacin on its own. The conjugate proves inactive vs. bacteria like *K. pneumoniae* and *M. tuberculosis*, which the authors attribute to differences in aryl nitro group reduction efficiency between the various bacteria, or differences in cell permeability and uptake of **1-61**. The conjugate also proved effective in a mouse model, with similar potency to ciprofloxacin vs. an *E. coli* strain at identical doses (10 mg/kg).<sup>315</sup>



Scheme 1.12 Nitroreductase-activated SO<sub>2</sub>-coumarin-ciprofloxacin conjugate **1-61** synthesised by Pardeshi *et al.*<sup>315</sup> Coumarin component indicated in purple.<sup>315</sup>

## 1.6 Summary and Conclusions

Trojan Horse conjugates offer great potential in the treatment of bacterial infection, with the potential to bypass membrane-associated resistance mechanisms, aid the creation of narrow spectrum antibiotics, and allow repurposing of old antibiotics like vancomycin against new bacterial strains. The incorporation of a biolabile linker into these conjugates is often crucial to their function, and their success or failure against bacteria, especially when antibiotics with a cytoplasmic target are concerned. While a wide range of biolabile linkers exist (**Section 1.4**), only a limited range have been examined in the context of Trojan Horse conjugates, with those examined primarily consisting of methylenedioxy linkers and “trimethyl lock” variants, although newer variants successfully exploit different enzymatic methods of cleavage. This has led to a requirement for the development of new biolabile linkers for Trojan Horse conjugates.

Prodrugs that release gaseous molecules like SO<sub>2</sub> or NO have also seen usage for treatment of bacterial infection, with multiple mechanisms available for triggering the release of these gases, ranging from reaction with biological thiols, to photorelease on exposure to UV light, to intramolecular cyclisation reactions. Release of these gaseous moieties can also be combined with the release of other species, for example antimicrobials like ciprofloxacin, potentially creating dual-action prodrugs.

## 1.7 Research Aims

The aim of this project was the development of new biolabile linkers, and the further examination of their usage in the context of Trojan Horse conjugates with the aim of expanding the range of linkers that can be used to offer selective and efficient cytoplasmic release. The project was also inspired by the pioneering work of Chakrapani *et al.* in the development of SO<sub>2</sub>-releasing prodrugs. With these prodrugs offering a mechanism for quick and cytoplasm-specific release of an amine component via nucleophilic attack of glutathione and subsequent SO<sub>2</sub> release, it was hypothesised that they could be adapted to the release of an antimicrobial cargo. The antimicrobial activity seen from release of SO<sub>2</sub> offered the enticing

possibility of an efficient biolabile linker that also provides another mechanism for growth inhibition beyond that of the released component, potentially creating a dual-action antibiotic.

Therefore three strands of research were pursued based on the SO<sub>2</sub> releasing systems developed by Chakrapani *et al.*:

- First, the combination of the 2,4-dinitrobenzenesulfonamides used by Chakrapani *et al.* with a simple siderophore unit was examined (Chapter 2); this aimed to examine the compatibility of SO<sub>2</sub> release with a siderophore conjugate, and also the ability of siderophore conjugation to potentiate the activity of SO<sub>2</sub> on its own.
- Second, a similar SO<sub>2</sub>-releasing system, this time containing a carboxylic acid for conjugation of a desferrioxamine siderophore moiety, and ciprofloxacin as an antimicrobial unit, was designed and synthesised (Chapter 3). This conjugate was designed to allow incorporation of an existing antimicrobial into the siderophore conjugate, with release of both the antimicrobial and SO<sub>2</sub> offering a potential route to a dual-action antimicrobial.
- Third, the use of heterocyclic sulfonamides as novel nitro-free SO<sub>2</sub>-releasing linkers was explored, and an azotochelin-sulfonamide-ciprofloxacin conjugate based on a novel heterocyclic pyrazine sulfonamide was designed and synthesised (Chapter 4).

These three strands aimed to examine the potential of these novel linkers to allow efficient antimicrobial release as biolabile linkers in a Trojan Horse conjugate.

**Chapter 2 :**  
**Can Siderophores Aid SO<sub>2</sub>**  
**Prodrugs? Synthesis and**  
**Evaluation of SO<sub>2</sub>-Releasing**  
**Aminochelin Conjugates**

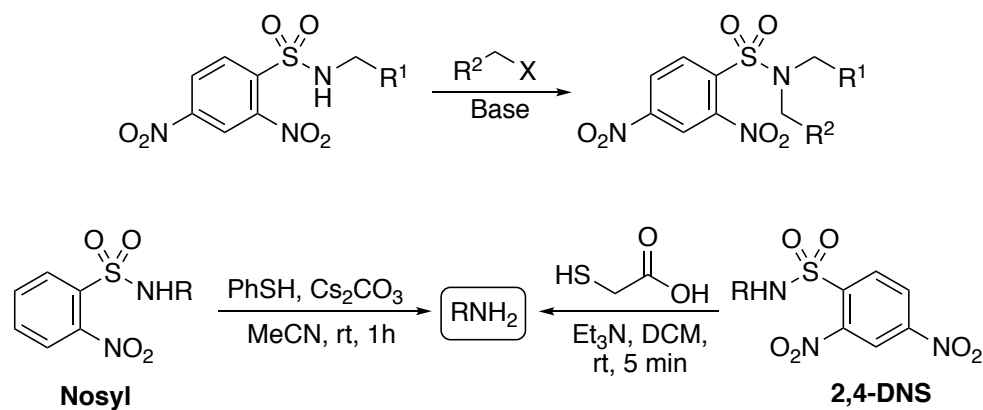
## 2.1 Introduction

### 2.1.1 2,4-Dinitrobenzenesulfonamides

As discussed in Chapter 1, the incorporation of a biolabile linker in siderophore Trojan Horse conjugates is often of vital importance to their success against bacteria, with many existing conjugates proving poorly active as a consequence of bearing either no biolabile linker, or one poorly suited to the demands of targeting bacteria.<sup>133,171,188,191,192,196</sup> A new approach to the development of new biolabile linkers was inspired by work carried out by Chakrapani *et al.* in the development of SO<sub>2</sub>-releasing prodrugs.<sup>301,303,304</sup> In this Chapter, the investigation of an SO<sub>2</sub>-releasing conjugate containing a 2,4-dinitrobenzenesulfonamide (2,4-DNS) unit (as used by Chakrapani *et al.*), conjugated to a simple bidentate siderophore, aminochelin, is discussed.

2,4-Dinitrobenzenesulfonamides offer an intriguing profile of reactivity for chemical exploitation. The two electron-withdrawing nitro groups are ideally positioned *ortho* and *para* to the sulfonamide position, allowing for maximal activation of the sulfonamide carbon towards nucleophilic aromatic substitution reactions. This reactivity has been exploited in various ways, including their use as protecting groups for amines in organic synthesis, which was first demonstrated by Fukuyama *et al.* in 1997.<sup>319</sup> They offer similar properties to the more common nosyl protecting group (2 or 4-nitrobenzenesulfonamide); in particular, both protecting groups allow alkylation of the corresponding sulfonamide, which provides a convenient route for the synthesis of secondary amines on removal of the protecting group. However, 2,4-DNS protecting groups can be removed via reaction with thiols under milder conditions (e.g. thioglycolic acid, Et<sub>3</sub>N, 5 min) than the corresponding nosyl groups (**Scheme 2.1**). indeed, 2,4-dinitrobenzenesulfonamide groups can undergo orthogonal deprotection in the presence of nosyl groups.<sup>319</sup>





Scheme 2.1 Alkylation of 2,4-dinitrobenzenesulfonamides demonstrated by Fukuyama *et al.*, and deprotection conditions for removal of nosyl and 2,4-DNS groups.<sup>319</sup>

### 2.1.2 The Partitioning of Biological Thiols

The reactivity of 2,4-dinitrobenzenesulfonamides with thiols is key to their usage as prodrugs. As described in Chapter 1, prodrugs or compounds containing biolabile linkers should remain stable while in circulation in the body until they reach their desired target, and drug release should ideally take place within cells.<sup>199–201</sup> Thiol-containing molecules, like the cofactor Coenzyme A or the antioxidant glutathione (GSH), play a key part in the biochemistry of cells. Glutathione, a tripeptide containing glycine, cysteine, and glutamic acid, is present in low mM concentrations (1-10 mM) inside many eukaryotic and prokaryotic cells.<sup>320–322</sup> It plays a vital role in maintaining redox stability within cells, reacting with reactive oxygen/nitrogen species (ROS/RNS) to prevent oxidative damage to cells.<sup>321–323</sup> This process results in the oxidation of glutathione to its corresponding disulfide (GSSG), which is readily reduced back to the free thiol by cytoplasmic enzymes e.g. thioredoxin or glutathione reductase.<sup>321,322</sup>

Under normal conditions in human cells, less than 1% of the glutathione present in the cytoplasm is in the oxidised GSSG form.<sup>320,321</sup> In contrast, extracellular glutathione concentrations are much lower (5-50  $\mu\text{M}$  in blood plasma), with the majority being present in the form of GSSG.<sup>320,324–327</sup> In addition to glutathione, human blood plasma contains a significant concentration of cysteine (up to 250  $\mu\text{M}$ ); again the vast majority is present in the oxidised form (cystine).<sup>324–327</sup>

Similar conditions can be found within bacterial cells, with the reducing conditions of the cytoplasm maintaining a high ratio of GSH to GSSG.<sup>328</sup> In Gram-negative bacteria, the periplasm is considered an oxidising environment, meaning low concentrations of free thiols are expected to be found here.<sup>329,330</sup> It should be noted that some studies have shown export of reduced glutathione from bacteria into their extracellular environment, although this has only been seen *in vitro*.<sup>331–333</sup>

### 2.1.3 2,4-Dinitrobenzenesulfonamide-Based Anticancer Prodrugs

The low concentrations of free thiols present in extracellular environments and the high concentrations present within cells provides an ideal targeting mechanism for 2,4-dinitrobenzenesulfonamide-based prodrugs, which would be expected to remain stable until they can be taken up into cells and exposed to the high intracellular concentrations of thiols. Prodrugs based on this approach have primarily been used for anticancer drugs. Johansson *et al.* synthesised a 2,4-dinitrobenzenesulfonamide prodrug of the anticancer drug doxorubicin (**DNS-DOX**, **Figure 2.1**), with the aim of increasing the lipophilicity of the prodrug, and therefore increasing its uptake into cells.<sup>305</sup> While uptake would likely be similar in normal cells and cancer cells, the researchers demonstrated overexpression of glutathione-S-transferase (GST) enzymes in cancer cells led to faster cleavage and drug release compared to normal cells.<sup>305</sup>

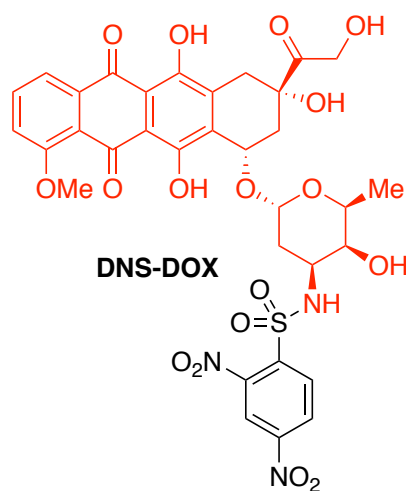


Figure 2.1 Structure of **DNS-DOX**, a 2,4-dinitrobenzenesulfonamide prodrug of doxorubicin. Drug highlighted in red.<sup>305</sup>

Whang *et al.* used a 2,4-dinitrobenzenesulfonate ester derivative of the anticancer compound SN-38 (**DNS-SN-38**, **Figure 2.2**), the active metabolite of anticancer drug irinotecan, to successfully target two ovarian cancer cell lines.<sup>306</sup> The 2,4-dinitrobenzenesulfonate ester functions in an identical manner to the corresponding sulfonamides, allowing rapid intracellular activation and release of SN-38, with the prodrug having almost identical activity to the parent drug vs. ovarian cancer cell lines.<sup>306</sup>

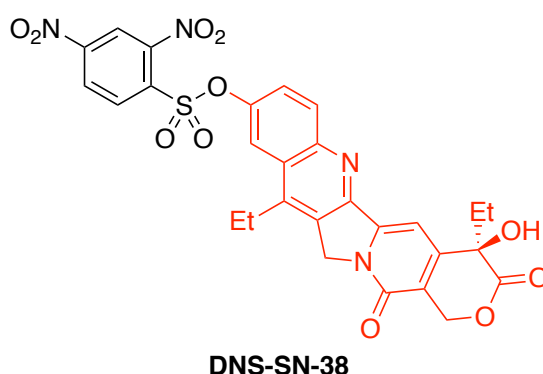


Figure 2.2 Structure of **DNS-SN-38**, a 2,4-dinitrobenzenesulfonate ester prodrug of anticancer drug SN-38. Drug highlighted in red.<sup>306</sup>

2,4-Dinitrobenzenesulfonamide or sulfonate ester units can also be used as trigger groups for self-immolative linkers. Perhaps the first example of this comes from Xu *et al.*, who utilised a 2,4-dinitrobenzenesulfonate ester in place of the sulfonamide seen before as a trigger for the release of the alkylating agent mechlorethamine (**2-1**, **Figure 2.3**).<sup>334</sup> Wang *et al.* also made use of a 2,4-dinitrobenzenesulfonate ester in their design of a bifunctional self-immolative linker **2-2**, which bears two components that can be released on activation, the anticancer drug camptothecin and a near-infrared fluorescent dye for tracking uptake in cells.<sup>335</sup>

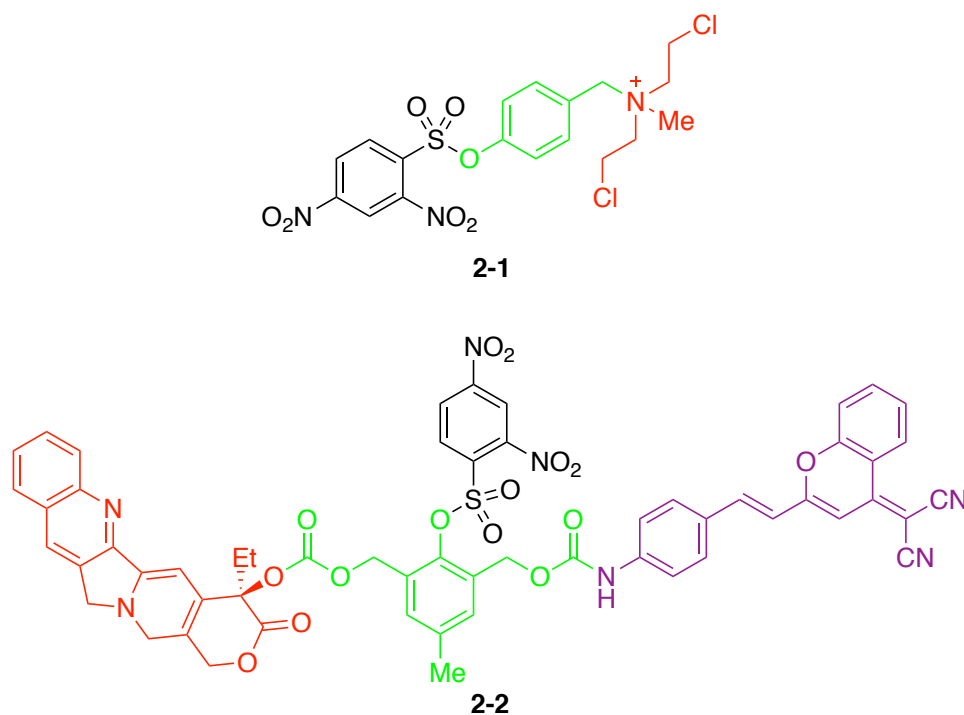


Figure 2.3 Structures of 2,4-dinitrobenzene-containing prodrugs that utilise self-immolative linkers. Drug highlighted in red, self-immolative linker highlighted in green, dye highlighted in purple.<sup>334,335</sup>

Malla *et al.* demonstrated an intriguing use of a 2,4-dinitrobenzenesulfonate ester to protect a substituted 2-hydroxyisophthalamide unit (**2-3**, **Figure 2.4**).<sup>308</sup> 2-Hydroxyisophthalamide units can self-assemble in a supramolecular fashion to form ion channels in the membrane of cells, leading to disruption and depolarisation of the membrane and triggering apoptosis. Incorporation of a bulky substituent, like the 2,4-dinitrobenzenesulfonate ester, on the 2-hydroxy group prevents this self-assembly from occurring until the substituent is successfully cleaved.<sup>308</sup>

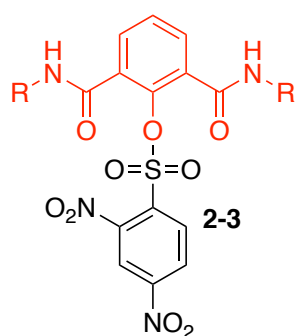


Figure 2.4 Prodrugs developed by Malla *et al.* for the formation of ion channels in cell membranes. 2-Hydroxyisophthalamide section highlighted in red.<sup>308</sup>

Finally, Shen *et al.* took a slightly different approach to those discussed above, with the incorporation of multiple 2,4-dinitrobenzenesulfonamide units within a polymer chain (**2-4**, **Figure 2.5**).<sup>336</sup> Here, SO<sub>2</sub> was demonstrated to be active on its own against cancer cells, with SO<sub>2</sub> release shown to increase the concentration of ROS in the cells. The polymer can also be loaded with the anticancer drug doxorubicin to generate doxorubicin-loaded nanoparticles; both the SO<sub>2</sub> and the doxorubicin are released on contact with intracellular thiols, and demonstrate a synergistic effect.<sup>336</sup>

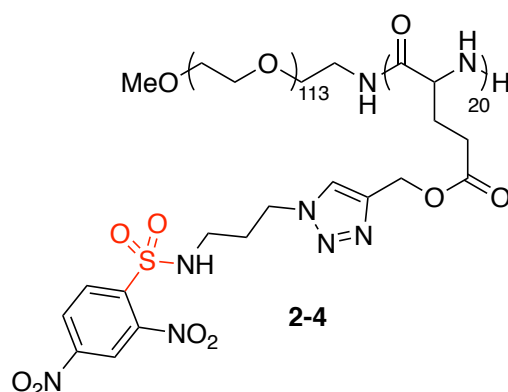


Figure 2.5 Structure of SO<sub>2</sub>-releasing polymer **2-4** developed by Shen *et al.*<sup>336</sup>

#### 2.1.4 2,4-Dinitrobenzenesulfonamide-Based Antimicrobial Prodrugs

As mentioned previously, 2,4-dinitrobenzenesulfonamide-based prodrugs have also been utilised in the design of antibacterial agents by Chakrapani and colleagues.<sup>301,303,304</sup> These prodrugs were initially screened for activity vs. *Mycobacterium tuberculosis*,<sup>301,303</sup> with later screening for activity vs. the Gram-positive bacterial species *Staphylococcus aureus* (including a methicillin-resistant strain) and *Enterococcus faecalis*, and the Gram-negative species *E. coli*.<sup>304</sup> While a number of these prodrugs proved very effective vs. *M. tuberculosis*, with benzylamine derivative **1-56** (**Figure 2.6**) displaying comparable activity to the front line TB drug isoniazid (MIC = 0.15 μM vs. 0.37 μM for isoniazid),<sup>301</sup> activity was less impressive against *S. aureus* and *E. faecalis*, with no antimicrobial activity observed vs. *E. coli*.<sup>304</sup> Alongside the antimicrobial effects of SO<sub>2</sub> release, intracellular thiol depletion via formation of a 2,4-dinitrobenzene-thiol conjugate was suggested as a mechanism of action for these compounds.

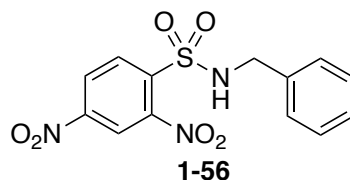


Figure 2.6 Structure of **1-56**, the most effective of the 2,4-dinitrobenzenesulfonamides developed by Chakrapani *et al.* vs. *M. tuberculosis*.<sup>301,303</sup>

A moderate correlation between SO<sub>2</sub> release rate and antimicrobial activity is observed in *M. tuberculosis*, with faster release rates associated with lower MIC values (**Figure 2.7**),<sup>301,303</sup> however a similar correlation is not observed for the other bacterial species examined.<sup>304</sup> For the non-TB strains, the authors also examined the relationship between the calculated partition coefficient (*clogP*) and MIC, with the *clogP* used as an estimate of the permeability of the compounds; no significant trend was found.<sup>304</sup> However, the MIC values for the non-TB strains did display sensitivity to the incorporation of certain functional groups, for example the propargyl group.

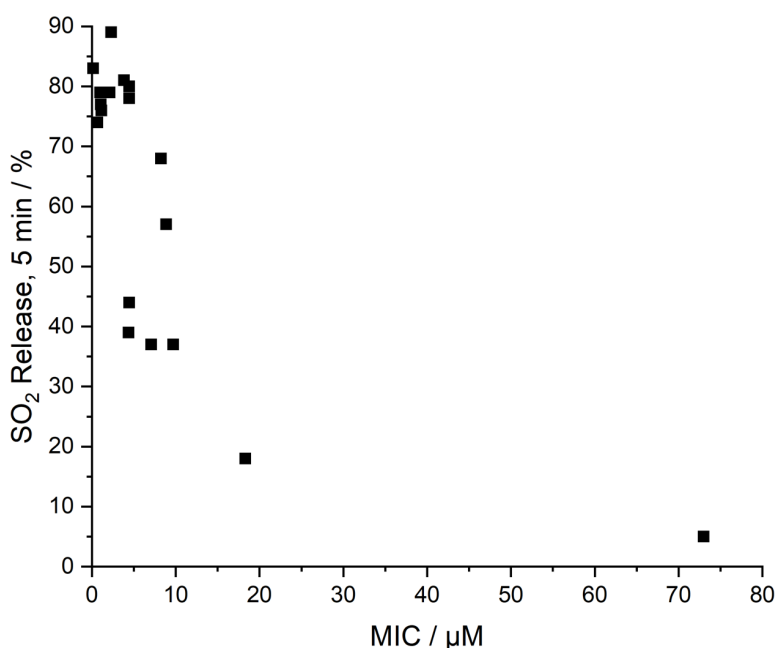
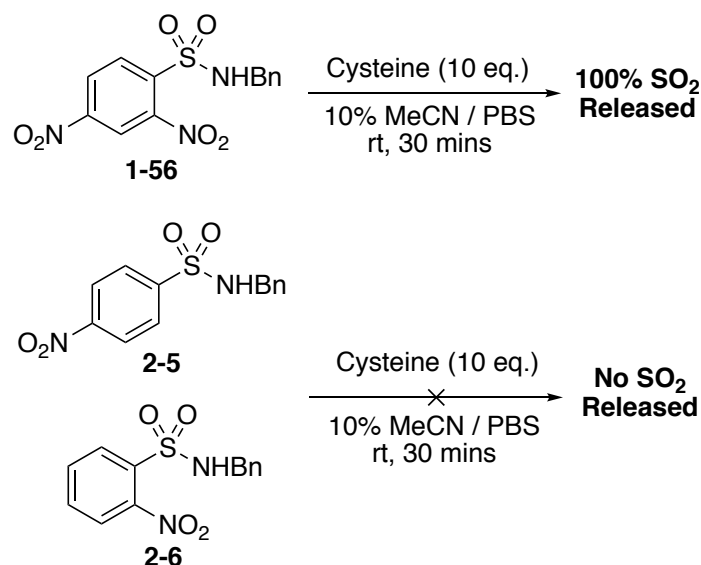


Figure 2.7 A graph to demonstrate the correlation of SO<sub>2</sub> release rate to antimycobacterial activity (reproduced using data from reference 303).

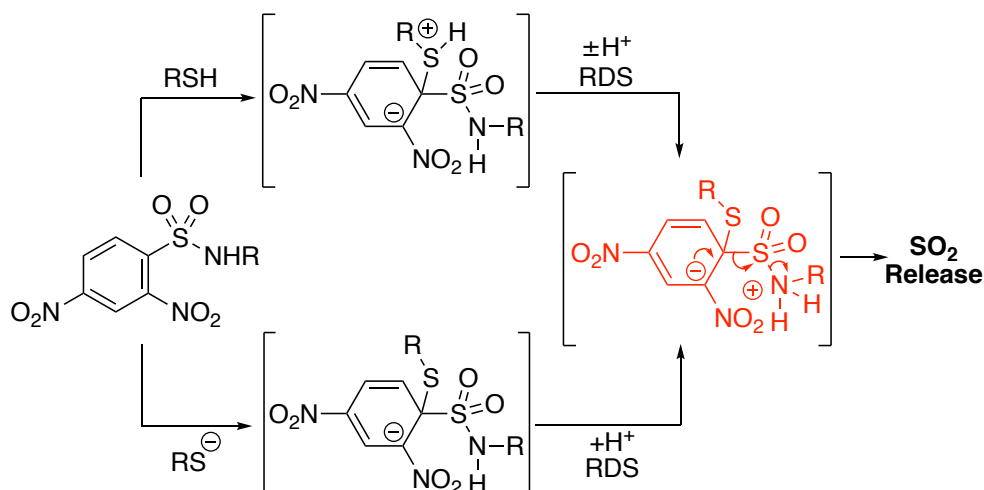
The factors affecting the rate of SO<sub>2</sub> release were also examined, with some key requirements emerging. The first of these is the requirement for two nitro groups to be present on the sulfonamide ring; while benzylamine

derivative **1-56** displayed 100% SO<sub>2</sub> release over 30 minutes at room temperature when 10 equivalents of cysteine were added (as determined by ion chromatography), mononitro derivatives **2-5** and **2-6** displayed no detected SO<sub>2</sub> release under the same conditions (**Scheme 2.2**).<sup>301</sup>



Scheme 2.2 Difference in reactivity for 2,4-dinitrobenzenesulfonamides compared to 2- and 4-nitrobenzenesulfonamides.

The rate of SO<sub>2</sub> release also displays a good correlation to the pKaH of the amine released, with a lower pKaH resulting in slower SO<sub>2</sub> release; this is rationalised via a proposed S<sub>N</sub>Ar release mechanism (**Scheme 2.3**) involving rapid nucleophilic attack of a thiol or thiolate on the sulfonamide ring, followed by protonation of the sulfonamide nitrogen in a slower, rate-determining step, before the formed Jackson-Meisenheimer intermediate collapses with loss of SO<sub>2</sub>.<sup>301,303</sup> Formation of the protonated sulfonamide intermediate is less favoured for amines with a lower pKaH, hence the slower rate of SO<sub>2</sub> release. This correlation is clearest when the amine unit involved is a substituted aniline, where the substituents can have a large impact on the pKaH.<sup>303</sup> Indeed, a Hammett relationship can be drawn between the substituent properties and the rate of SO<sub>2</sub> release.<sup>304</sup>



Scheme 2.3 Reaction mechanism proposed for SO<sub>2</sub> release from 2,4-dinitrobenzenesulfonamides, including key protonated sulfonamide intermediate (highlighted in red).

A series of sulfonamides similar to those synthesised by Chakrapani and colleagues were reported by Phetsang *et al.* in 2013.<sup>337</sup> They observed a number of compounds that were active vs. strains of *S. aureus*, including 2,4-dinitrobenzenesulfonamides **2-7** and **2-8** (Figure 2.8).

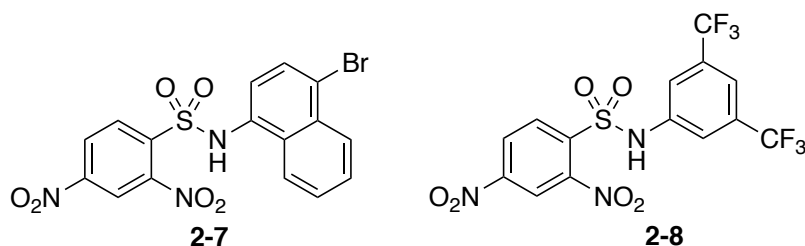


Figure 2.8 Two of the 2,4-dinitrobenzenesulfonamide antimicrobials developed by Phetsang *et al.*<sup>337</sup>

The activity of the compounds vs. *S. aureus* could not be inhibited by supplementation of the growth media with *p*-aminobenzoic acid (PABA), which has been shown to attenuate the activity of traditional sulfonamide antibiotics. This indicates the compounds must have a different mechanism of action to traditional sulfonamide antibiotics, although the authors do not explore this further. Given the similarities between these compounds and those previously discussed, this mechanism is likely to be related to SO<sub>2</sub> release, at least for those compounds containing 2,4-dinitrobenzenesulfonamides, however the authors make no reference to the two studies published by Chakrapani just a year earlier.



## 2.2 Conjugate Design and Experimental Considerations

Intrigued by the lack of activity observed vs. Gram-negative *E. coli* for the compounds developed by Chakrapani *et al.*, the development of a siderophore-containing SO<sub>2</sub>-releasing prodrug was imagined. It is possible that the lack of activity indicates that the prodrugs are unable to permeate through the two membranes of Gram-negative bacteria, which provide a significant barrier to a wide range of molecules, including many antibiotics;<sup>338</sup> the activity vs. Gram-positive bacteria, with only a single membrane to permeate, indicates that the prodrugs can function as antimicrobials if they can be successfully taken up by bacteria. The attachment of a siderophore unit to a 2,4-dinitrobenzenesulfonamide prodrug may facilitate uptake via siderophore transport pathways in Gram-negative bacteria. Initially, a simple conjugate **2-9** based on the monocatechol siderophore aminochelin was envisaged (**Figure 2.9**).

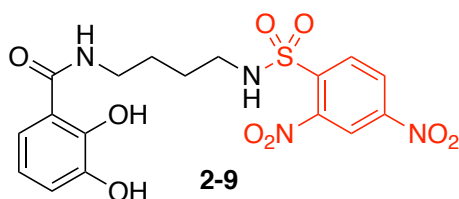


Figure 2.9 Structure of potential SO<sub>2</sub>-releasing prodrug **2-9** based on monocatechol siderophore aminochelin. 2,4-Dinitrobenzenesulfonamide component highlighted in red.

Monocatechol-based Trojan Horse conjugates have proved successful against a number of bacterial species. These successes extend to those conjugates that have progressed into clinical trials, as described in Chapter 1, with all of the conjugates entering clinical trials so far containing a single bidentate siderophore unit (either a catechol group or a hydroxypyridone group).<sup>158,339,340</sup> A number of these compounds do indeed prove active against Gram-negative bacteria, however these all contain  $\beta$ -lactam groups as the antibiotic component. The target for  $\beta$ -lactam antibiotics, the penicillin binding protein (PBP), is present in the periplasm of Gram-negative bacteria, so the activity of these compounds vs. Gram-negative bacteria indicates the monocatechol siderophores are able to mediate uptake through the outer membrane. However, it is not clear if a simple

monocatechol will be able to facilitate uptake of conjugates to the cytoplasm, where activation of the 2,4-dinitrobenzenesulfonamides and subsequent SO<sub>2</sub> release is expected to take place.

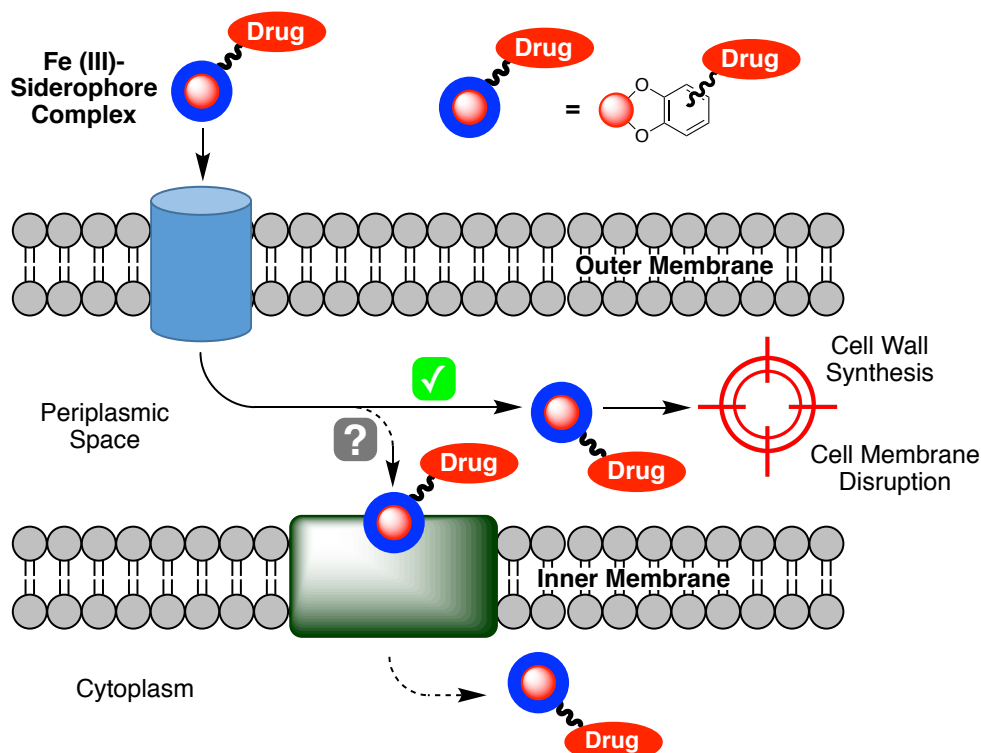
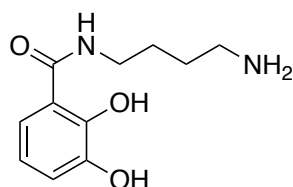


Figure 2.10 Diagram of the “knowns and unknowns” of uptake routes involving monocatechol siderophores in Gram-negative bacteria.

Aminochelin, the siderophore component chosen for this conjugate, is produced in nature by the soil bacterium *Azotobacter vinelandii* under conditions of iron limitation,<sup>341</sup> and consists of a 2,3-dihydroxybenzoic acid unit appended to 1,4-diaminobutane (**Figure 2.11**), providing a convenient amine for formation of the required 2,4-dinitrobenzenesulfonamide.



**Aminochelin**

Figure 2.11 Structure of monocatechol siderophore aminochelin.

To the best of the author’s knowledge, there are two studies detailing aminochelin-antibiotic conjugates that have appeared in the literature. The first is a conjugate of norfloxacin (**2-10**), which was synthesised by Souto *et*

*al.* as a member of an array of compounds designed to target the fish pathogen *Vibrio anguillarum*, which produces the related siderophore vanchrobactin (**Figure 2.12**).<sup>342</sup> The aminochelin conjugate proved the most active of the set, but still remained an order of magnitude less effective than norfloxacin (MIC = 0.166  $\mu$ M vs. 0.019  $\mu$ M). There is no change in the activity of **2-10** when tested against mutant strains of *V. anguillarum* unable to synthesise vanchrobactin, or transport it into cells, indicating a lack of uptake via the transport pathways used for vanchrobactin (although the authors note that aminochelin on its own is able to promote growth in the mutant strains, suggesting a different uptake pathway compared to vanchrobactin). However, the activity also remains the same in both iron-rich and iron-poor conditions; if **2-10** can be taken up via siderophore transport pathways, an increase in antimicrobial activity would be expected in the iron-poor conditions due to upregulation of iron transport pathways.<sup>163</sup>

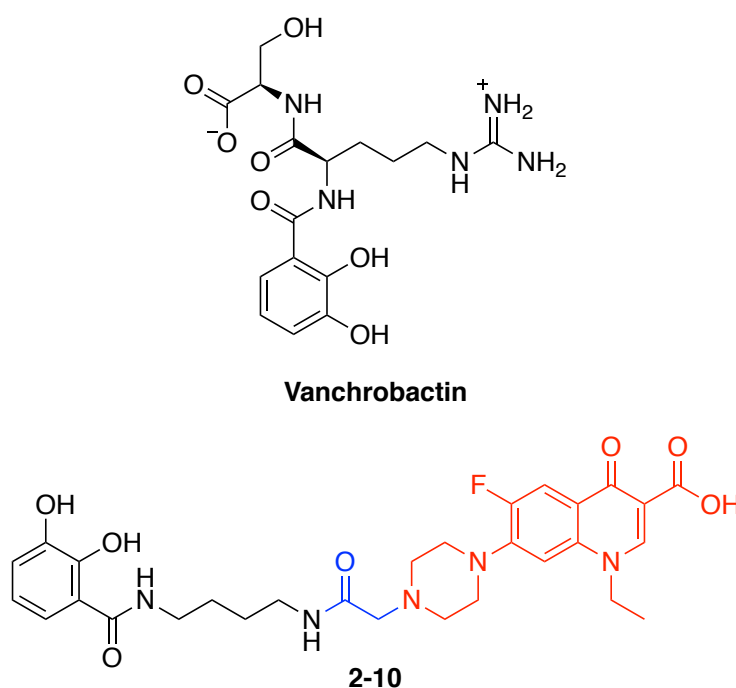


Figure 2.12 Structure of the monocatechol siderophore vanchrobactin and the norfloxacin-aminochelin conjugate **2-10**.

Another set of aminochelin conjugates was developed by Paulen *et al.*, who utilised a derivative of the oxazolidinone antibiotic linezolid for their studies.<sup>187</sup> Oxazolidinones are usually inactive against Gram-negative bacteria, likely due in part to low membrane permeability, and attaching

aminochelin was hoped to allow for better uptake via exploitation of siderophore transport pathways. The resulting conjugates were tested vs. *P. aeruginosa* (PAO1) and displayed moderately increased activity; for example, the MIC of conjugate **1-14** (Figure 2.13) is 128  $\mu\text{M}$ , compared to 1024  $\mu\text{M}$  for the parent antibiotic.

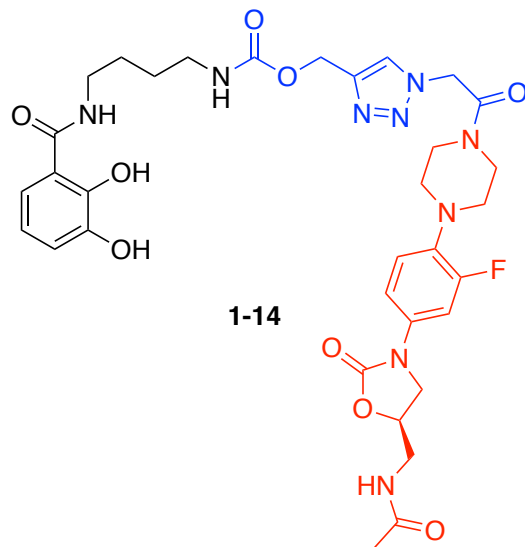


Figure 2.13 Structure of oxazolidinone-aminochelin conjugate **1-14** synthesised by Paulen *et al.*

These results possibly indicate a degree of improved uptake compared to the parent antimicrobial, although the exact transport pathway for the conjugates was not determined. The MIC remains high compared to the MICs of linezolid vs. Gram-positive bacteria, which Barbachyn and Ford reported ranges between 1 and 26  $\mu\text{M}$  depending on the strain, but often tends towards 1 to 6  $\mu\text{M}$ .<sup>52</sup> These studies indicate some possibility that the conjugation of aminochelin to 2,4-dinitrobenzenesulfonamides might allow for the development of an efficient prodrug conjugate.

One of the important considerations in the synthesis of conjugate **2-9** is the effect of incorporating a siderophore unit on the rate of  $\text{SO}_2$  release. If the rate is severely impaired, then this could have a significant impact on the efficacy of **2-9** as an antimicrobial. Therefore, the rate of release of  $\text{SO}_2$  from **2-9** needs to be examined to determine if the presence of the catechol group has a detrimental impact on  $\text{SO}_2$  release.

In previous studies, the release of SO<sub>2</sub> from prodrugs of the type studied has been monitored by both qualitative and quantitative methods. Chakrapani and colleagues used a pararosaniline assay to provide colourimetric evidence of SO<sub>2</sub> release and subsequent sulfite formation, and ion chromatography/HPLC to obtain quantitative release data.<sup>301,303,304</sup> A slight drawback of their pararosaniline assay is the requirement for HgCl<sub>2</sub> to fix sulfite as a stable disulfitomercurate(II) complex;<sup>343</sup> although only used in small volumes (50 μL), this toxic mercury compound is only available to purchase in large quantities.

Other researchers have attempted different techniques: Wang *et al.* used Ellman's reagent (5,5'-dithiobis-(2-nitrobenzoic acid)) to react with the formed sulfite ion in solution, allowing monitoring via UV-vis spectroscopy,<sup>297</sup> while Day *et al.* used Mito-Ratio-SO<sub>2</sub>, a fluorescent probe that reacts with sulfite (**Figure 2.14**).<sup>311</sup> A further paper by Chakrapani and colleagues uses a similar coumarin-based dye **2-11** to allow qualitative monitoring of SO<sub>2</sub> release via colourimetric changes, UV-vis and fluorescence imaging.<sup>344</sup>

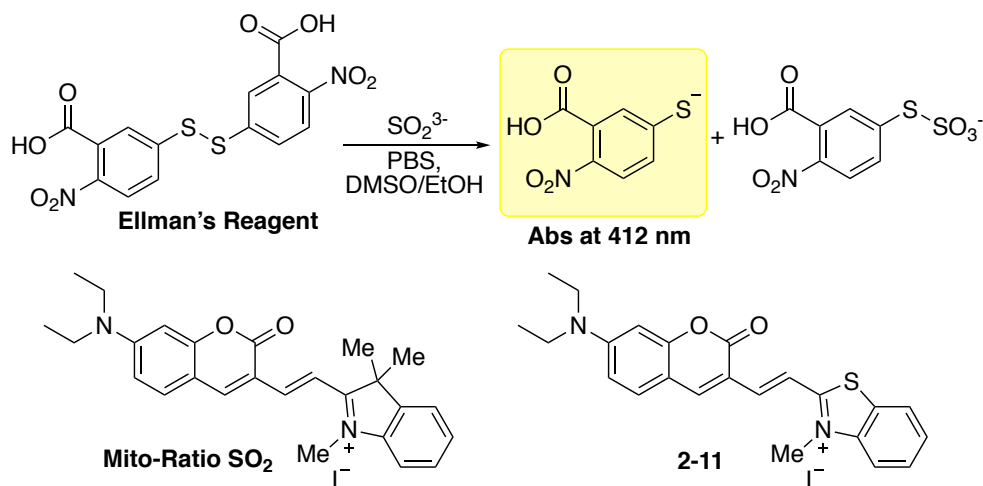
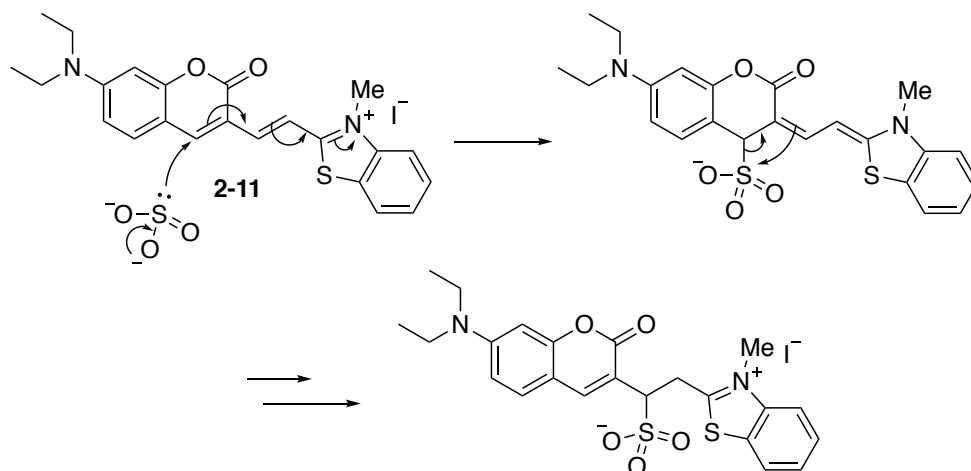


Figure 2.14 Structures of various compounds used to detect SO<sub>2</sub> release.

This particular dye, **2-11**, was developed by Sun *et al.*, who utilised SO<sub>2</sub> release from a 2,4-dinitrobenzenesulfonamide compound in the presence of cysteine to examine its suitability for SO<sub>2</sub> detection.<sup>345</sup> **2-11** can be used in either colourimetric or fluorescent assays; it fluoresces red, and forms intense pink solutions. It has a high selectivity for sulfite ions in solution, which can react with the central alkene (**Scheme 2.4**), breaking the

conjugation within the molecule, and resulting in a loss of fluorescence, and the disappearance of the pink colouring. The demonstrated usage of the dye in the presence of a 2,4-dinitrobenzenesulfonamide made it ideal for a qualitative study of SO<sub>2</sub> release from the desired compounds.



Scheme 2.4 Proposed mechanism for reaction of sulfite with coumarin-based dye **2-11**.<sup>345</sup>

In addition to these methods, the formation of a thiol conjugate of 2,4-dinitrobenzene gives a strong UV-vis absorbance band around 340 nm, meaning the reaction progress can easily be tracked by observing the increase in absorbance at this wavelength; this has previously been used to determine reaction rates in a variety of scenarios.<sup>346–348</sup>

### 2.3 Synthetic Plan

The structure of desired aminochelin conjugate **2-9** consists of aminochelin with a 2,4-dinitrobenzenesulfonyl group appended to the free amine (**Figure 2.15**). Therefore, the synthesis of **2-9** first requires the synthesis of a protected variant of aminochelin, followed by subsequent sulfonamide formation.

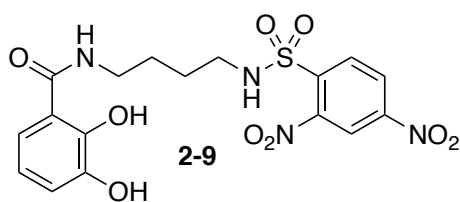
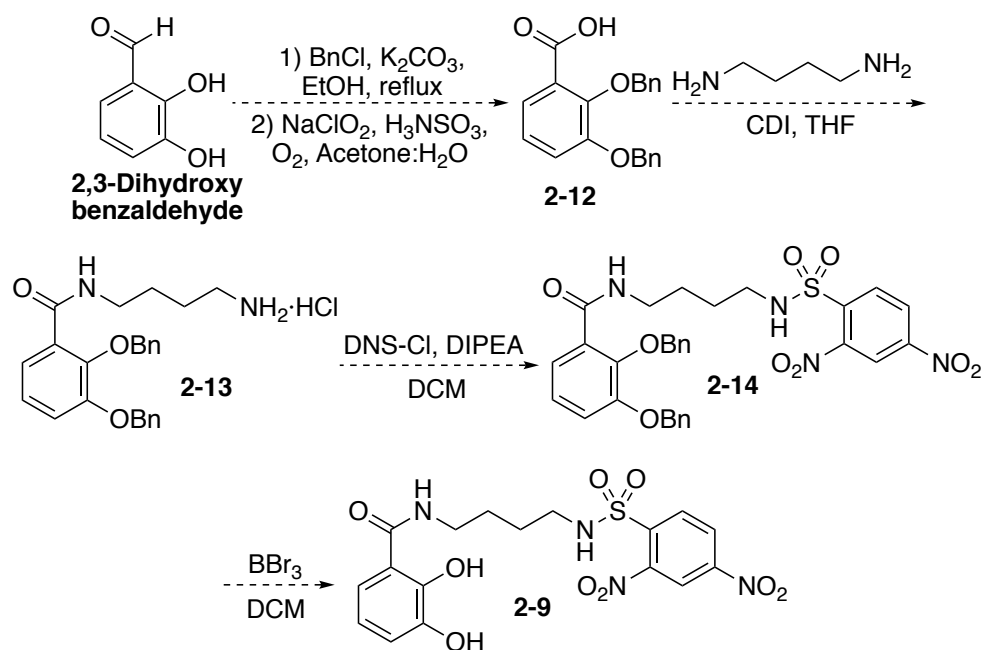


Figure 2.15 Structure of proposed aminochelin conjugate **2-9**.

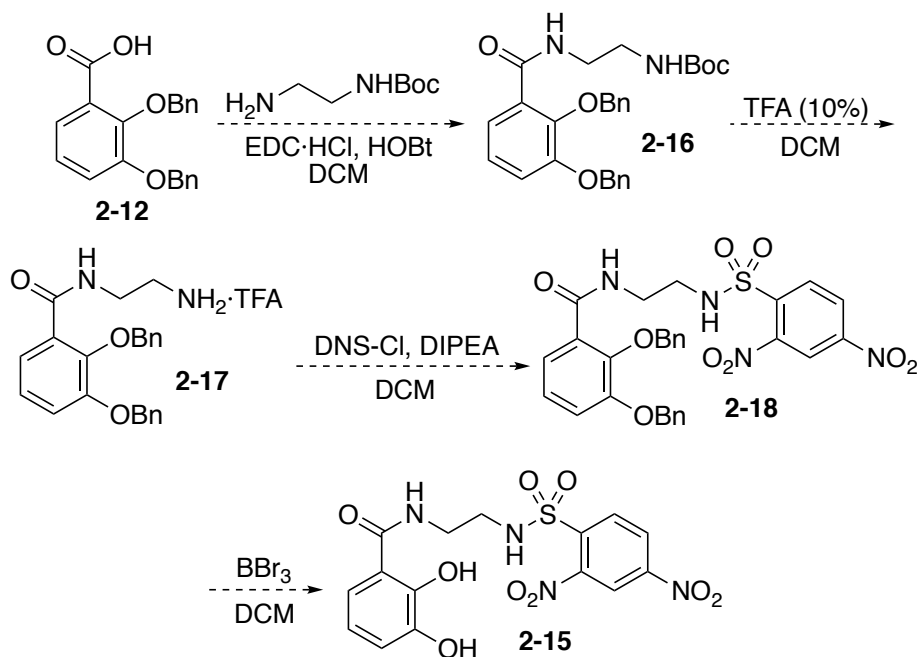
The synthesis of aminochelin is known in the literature.<sup>349,350</sup> Starting from 2,3-dihydroxybenzaldehyde, the catechol hydroxyl groups are protected to prevent oxidation and/or side reactions from occurring at later stages of the synthesis (**Scheme 2.5**);<sup>349</sup> benzyl groups are typically used,<sup>349–352</sup> although methyl and isopropyl groups have also been utilised.<sup>342,353</sup> Following oxidation of the aldehyde to give benzoic acid **2-12**, carbonyldiimidazole (CDI) coupling to 1,4-diaminobutane was proposed according to a literature method.<sup>349</sup> Sulfonamide formation was envisaged via reaction with commercially available 2,4-dinitrobenzenesulfonyl chloride (DNS-Cl) to give **2-14**, followed by removal of the benzyl groups to yield final conjugate **2-9**. While benzyl groups are typically deprotected via hydrogenation, the risk of simultaneously reducing the nitro groups on the sulfonamide led to boron tribromide (BBr<sub>3</sub>) being suggested as a deprotection reagent.



Scheme 2.5 Planned synthetic route to catechol-sulfonamide **2-9**.

Two further compounds were planned to examine different elements of conjugate **2-9** and the effect they have on either SO<sub>2</sub> release efficiency or antibacterial activity. The first is an analogue of **2-9** with a shorter two-carbon linker between the catechol group and the sulfonamide (**2-15**). While no testing for compounds with a four-carbon chain is carried out by in the studies by Chakrapani and colleagues, a two-carbon chain is employed in one example,<sup>303</sup> which **2-15** aims to mirror, with the goal of providing more information about the effects of linker length, and the presence of the

catechol group closer to the sulfonamide on SO<sub>2</sub> release. The synthesis plan for **2-15** is similar to that for **2-9** (Scheme 2.6); the key difference is the use of *N*-Boc ethylene diamine in place of 1,4-diaminobutane, and the subsequent TFA-mediated deprotection required, with both steps planned according to a literature procedure.<sup>351</sup>

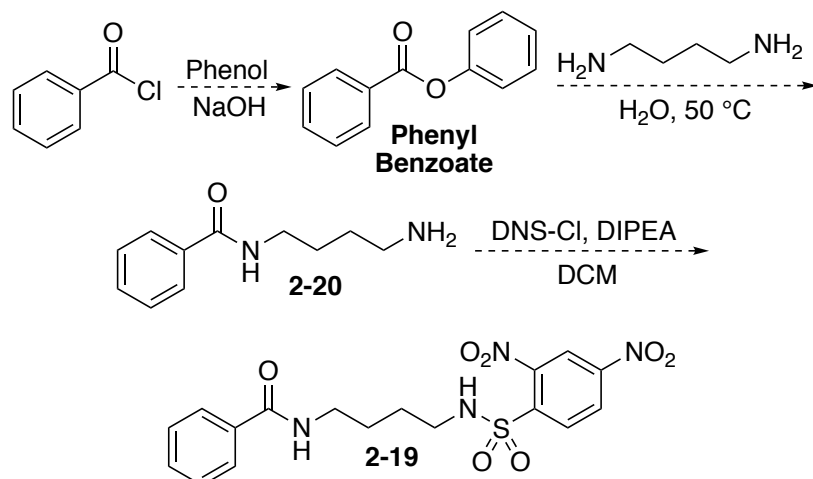


Scheme 2.6 Proposed synthetic route to two-carbon linker catechol-sulfonamide **2-15**.

The second compound, **2-19**, was an analogue of **2-9** lacking the catechol OH groups of aminochelin but retaining the four-carbon linker and benzene ring. **2-19** was intended to provide a direct comparison of the effects of the catechol group in **2-9** on SO<sub>2</sub> release, and potentially on biological activity. Here the synthetic plan deviates slightly from that of **2-9**. A literature method for the synthesis of mono-acylated amine **2-20** was selected (Scheme 2.7).<sup>354</sup> Mono-acylation of diamines is often hard to achieve with high selectivity. When acylation reactions take place in organic solvents, diamine molecules can potentially form hydrogen bonded clusters, hindering the mono-acylation reaction; the mono-acylated product is less able to form clusters and is therefore more reactive, hence the formation of large quantities of disubstituted products.<sup>355</sup> This literature method uses a minimal amount of water as a solvent, with enhanced hydrogen bonding to



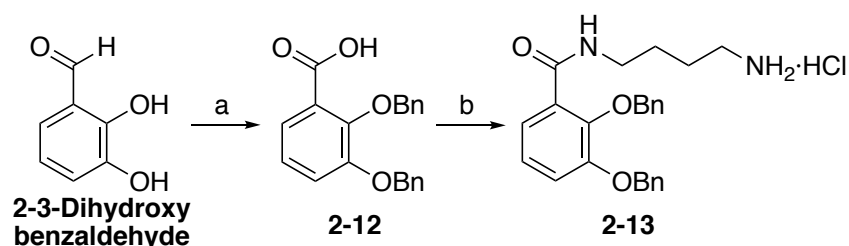
water disrupting the hydrogen bonding clusters. The subsequent sulfonamide formation is identical to that for **2-9** and **2-15**.



Scheme 2.7 Planned synthetic route to catechol-free sulfonamide **2-19**.

## 2.4 Conjugate Syntheses

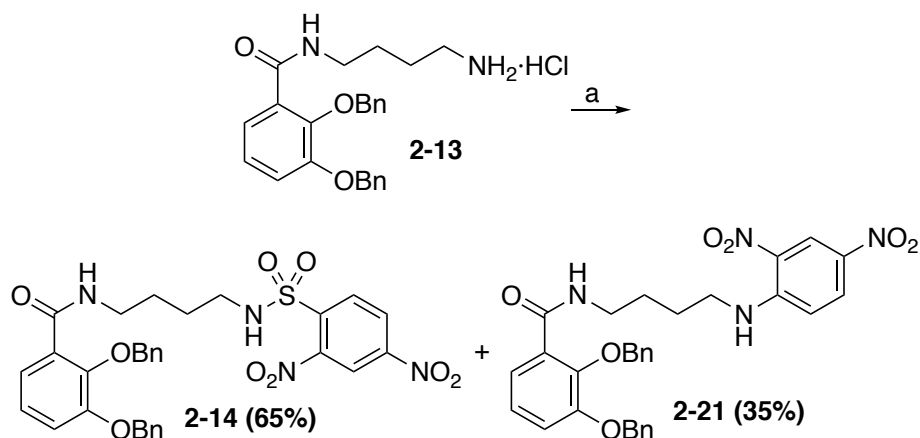
The first two steps in the synthesis of **2-9**, benzyl protection followed by oxidation, proceeded smoothly to give **2-12** in 67% isolated yield. Amide formation with CDI successfully yielded benzylated aminochelin (hydrochloride salt **2-13**, Scheme 2.8) in 38% yield. The formation of **2-13** was confirmed via the appearance of an amide proton at 8.24 ppm in the <sup>1</sup>H NMR spectrum, in addition to the CH<sub>2</sub> resonances of the coupled 1,4-diaminobutane at 3.19, 2.73, and 1.56-1.41 ppm. Further evidence was provided by ESI mass spectrometry, with peaks observed at *m/z* = 405.2180 and 427.1997 corresponding to [M+H]<sup>+</sup> and [M+Na]<sup>+</sup> molecular ions of formula C<sub>25</sub>H<sub>29</sub>N<sub>2</sub>O<sub>3</sub> and C<sub>25</sub>H<sub>28</sub>N<sub>2</sub>NaO<sub>3</sub> respectively.



Scheme 2.8 Synthesis of benzyl-protected aminochelin (**2-13**). a) 1) BnCl, K<sub>2</sub>CO<sub>3</sub>, EtOH, reflux, 24 h; 2) Sodium chlorite, sulfamic acid, acetone:H<sub>2</sub>O (5:4), 2 h, 67% over two steps; b) 1,4-diaminobutane, CDI, THF, 22 h, 38%.

With benzylated aminochelin **2-13** in hand, sulfonamide formation was initially attempted utilising DNS-Cl and DIPEA as a base (Scheme 2.9). This resulted in the formation of a mixture of products; on separation by column

chromatography, the desired sulfonamide (**2-14**) was revealed to be the major product, with formation confirmed via the presence of a peak at  $m/z = 657.1644$  in the ESI mass spectrum, corresponding to an  $[M+Na]^+$  molecular ion of formula  $C_{31}H_{30}N_4NaO_9S$ . There are also three resonances at 8.89 (d), 8.62 (dd) and 8.22 (d) ppm in the  $^1H$  NMR spectrum, corresponding to the three protons of the 2,4-dinitrobenzene ring. A significant amount of a minor side product was also obtained, which was revealed to be substituted aniline **2-21** via  $^1H$  NMR spectroscopy and mass spectrometry. One of the 2,4-dinitrobenzene protons is shifted upfield compared to its equivalent in sulfonamide **2-14** (7.17 vs. 8.22 ppm, **Figure 2.16**), indicating the presence of the adjacent electron-donating aniline nitrogen. In addition, peaks are observed at  $m/z = 571.2201$  and  $593.2016$  in the ESI mass spectrum, which can be assigned as  $[M+H]^+$  and  $[M+Na]^+$  adducts of formula  $C_{31}H_{31}N_4O_7$  and  $C_{31}H_{30}N_4NaO_7$  respectively.



Scheme 2.9 Products obtained from sulfonamide formation when DIPEA used as a base. a) 2,4-Dinitrobenzenesulfonyl chloride, DIPEA, DCM (anhydrous), 0 °C to rt, 46 h.

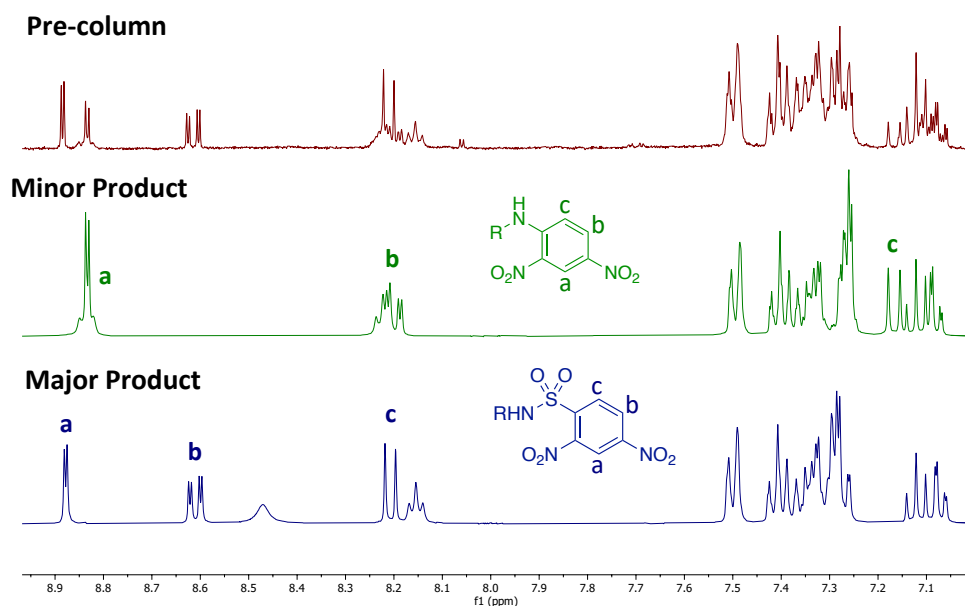
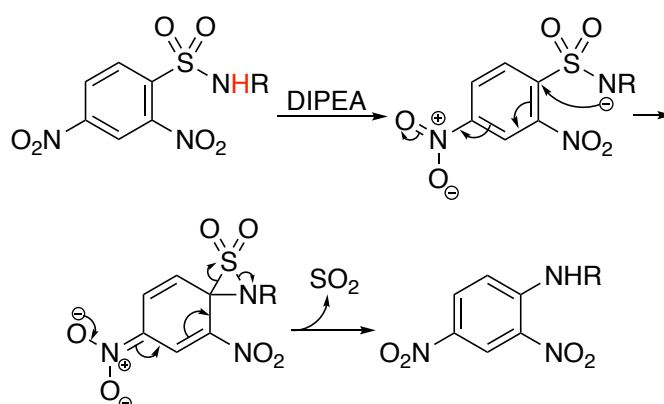


Figure 2.16 Aromatic region of  $^1\text{H}$  NMR spectra for the product mix formed post-sulfonamide formation when DIPEA used as a base. Position of key 2,4-dinitrobenzenesulfonamide protons indicated.

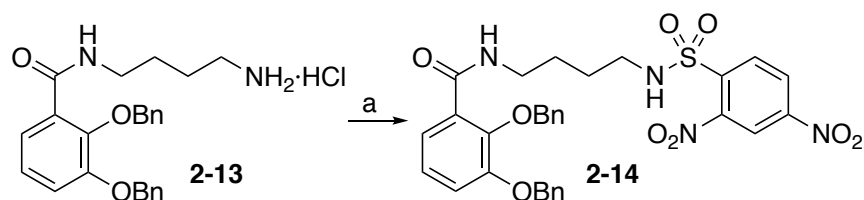
It is believed that **2-21** is formed via a Smiles rearrangement of the sulfonamide product **2-14** which is catalysed by DIPEA removing the acidic sulfonamide proton; this is predicted to have a pKa around 8 with MarvinSketch software. Similar rearrangements have been observed in the literature with electron-deficient aromatic systems; these allow facile formation of the intermediate Meisenheimer complex via nucleophilic attack on the ring (**Scheme 2.10**).<sup>319,356,357</sup>



Scheme 2.10 Proposed mechanism of Smiles rearrangement. Acidic sulfonamide proton highlighted in red.

The reaction was re-run while maintaining the temperature at 0 °C to try and minimize the Smiles rearrangement, and was followed by <sup>1</sup>H NMR spectroscopy. After 2 hours of reaction, around 60% of **2-13** is converted to products (this can be determined by comparing integrations for the benzyl CH<sub>2</sub> peaks at 5.02 for **2-13** and 4.99 for **2-14** and **2-21** in the crude <sup>1</sup>H NMR spectra of the reaction mixture). Formation of Smiles product **2-21** was not observed after 45 minutes, but it is present after 2 hours in a ratio of around 1:5 to the sulfonamide. This supports the conclusion that **2-21** comes from rearrangement of the sulfonamide via a Smiles rearrangement, rather than a direct S<sub>N</sub>Ar of the sulfonyl chloride.

As the formation of Smiles product **2-21** begins before complete consumption of starting material **2-13**, alterations to the reaction were considered to maximise the yield of **2-14**. Two alternative bases, DBU (pKaH 11.50 in H<sub>2</sub>O)<sup>358</sup> and lutidine (pKaH 6.60 in H<sub>2</sub>O)<sup>359</sup> were trialled in an attempt to prevent the Smiles rearrangement from occurring. For comparison, the pKaH of DIPEA is 10.75 in H<sub>2</sub>O.<sup>359</sup> It was hoped that the more sterically hindered nature of both DBU and lutidine might allow deprotonation of the primary amine salt of **2-13** while avoiding deprotonation of the more hindered sulfonamide. Lutidine is less basic than DIPEA, which may also help reduce deprotonation of the sulfonamide. While the reaction with DBU yielded an unidentifiable mixture of products, which were not further investigated, lutidine displayed almost full conversion to **2-14** over 25 hours, with no formation of Smiles product **2-21** observed by analysis of the <sup>1</sup>H NMR spectra of the reaction. When scaled up, **2-14** was produced in excellent yield (98%, **Scheme 2.11**).

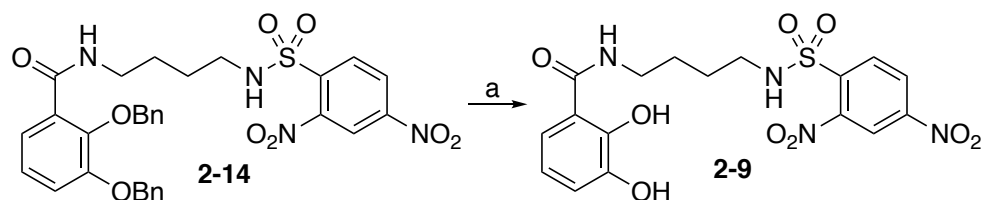


Scheme 2.11 Synthesis of sulfonamide **2-14**. a) 2,4-Dinitrobenzenesulfonyl chloride, lutidine, DCM (anhydrous), 0 °C to rt, 28 h, 98%.

The final step of the synthesis, the BBr<sub>3</sub>-mediated removal of the benzyl groups followed by quenching with wet methanol, yielded a mixture of

products, but primarily the desired catechol-sulfonamide **2-9** (**Scheme 2.12**). Successful formation of **2-9** is supported by the observed by the loss of the benzyl CH<sub>2</sub> resonances at around 5 ppm in the <sup>1</sup>H NMR spectrum, and the presence of peaks observed at *m/z* = 455.0869 and 477.0680 in the ESI mass spectrum, which can be assigned to [M+H]<sup>+</sup> and [M+Na]<sup>+</sup> adducts of molecular formulae C<sub>17</sub>H<sub>19</sub>N<sub>4</sub>O<sub>9</sub>S and C<sub>17</sub>H<sub>18</sub>N<sub>4</sub>NaO<sub>9</sub>S respectively.

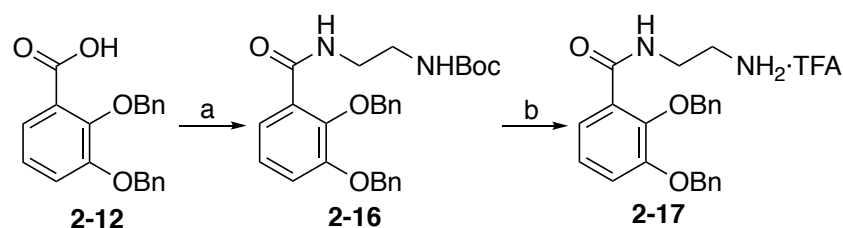
The product mixture produced by the BBr<sub>3</sub>-mediated deprotection posed a number of problems. The hydroxyl groups of deprotected catechol groups could make purification by aqueous workup or column chromatography problematic due to the increased polarity and increased aqueous solubility of **2-9** compared to its benzyl-protected derivative **2-14**. Purification by preparative HPLC was identified as the best solution. Preliminary HPLC studies were carried out to determine a suitable solvent system and run time for successful isolation of the product peak; an acetonitrile-water gradient from 40% MeCN to 70% MeCN over 15 minutes was shown to give the best separation of **2-9** from other impurities present in the HPLC. Following preparative HPLC, pure catechol-sulfonamide **2-9** was recovered in 40% yield.



Scheme 2.12 Synthesis of conjugate **2-9** via BBr<sub>3</sub>-mediated deprotection of hydroxyl groups. a) BBr<sub>3</sub>, DCM (anhydrous), rt, 7 h, then preparative HPLC purification, 40%.

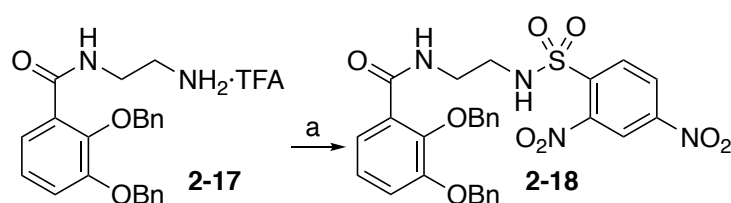
The synthesis of two-carbon analogue **2-15** proceeded in a similar fashion. EDC-mediated coupling of benzoic acid **2-12** to *N*-Boc ethylene diamine and subsequent TFA deprotection proceeds in moderate yields (68% over two steps, **Scheme 2.13**). The <sup>1</sup>H NMR spectra obtained for Boc-protected **2-16** matches that previously reported,<sup>351</sup> and the <sup>1</sup>H NMR spectrum of **2-17** displays the expected loss of the characteristic *tert*-butyl singlet at around 1.40 ppm. The formation of both can be further confirmed by ESI mass

spectrometry, with a peak observed at  $m/z = 477.2391$  in the spectrum of **2-16**, corresponding to an  $[M+H]^+$  molecular ion of formula  $C_{28}H_{33}N_2O_5$ , and another at  $m/z = 377.1863$  in the spectrum of **2-17**, corresponding to an  $[M+H]^+$  molecular ion of formula  $C_{23}H_{25}N_2O_3$ .



Scheme 2.13 Synthesis of TFA salt **2-17**. a) *N*-Boc ethylenediamine, EDC.HCl, HOBT, DCM, 24 h, 88%; b) TFA (10% v/v), DCM, 4 h, 77%.

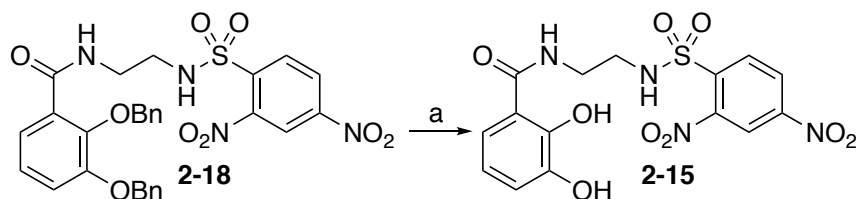
As with benzylated aminochelin **2-13**, TFA salt **2-17** was subsequently reacted with 2,4-dinitrobenzenesulfonyl chloride in the presence of lutidine (**Scheme 2.14**). The TFA salt was first stirred in aqueous sodium hydroxide (1 M),<sup>351</sup> followed by extraction with DCM and subsequent reaction with the sulfonyl chloride. The product (**2-18**) was subsequently purified by column chromatography in 86% yield. Formation of **2-18** was confirmed by observation of the characteristic d/dd/d resonances at 8.46, 8.22 and 8.11 ppm in the  $^1H$  NMR spectrum, corresponding to the 2,4-dinitrobenzene ring protons, and via the presence of a peak at  $m/z = 629.1300$  in the ESI mass spectrum consistent with an  $[M+Na]^+$  adduct of molecular formula  $C_{29}H_{26}N_4NaO_9S$ .



Scheme 2.14 Synthesis of **2-18**. a) 1 M NaOH (aq.), then 2,4-dinitrobenzenesulfonyl chloride, lutidine, DCM (anhydrous), 20 h, 86%.

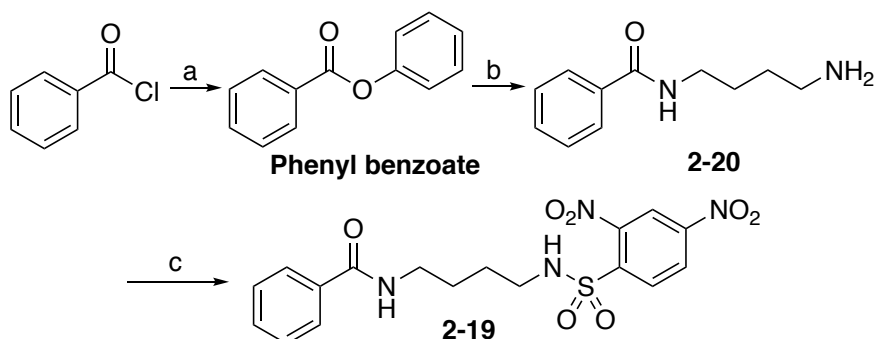
A final  $BBr_3$  deprotection of the benzyl protecting groups was followed by purification by preparative LCMS (**Scheme 2.15**). The success of the reaction and the purification can be seen from the presence of OH protons at 12.59 and 7.41 ppm in the  $^1H$  NMR spectrum (and the absence of benzyl  $CH_2$  resonances at approximately 5 ppm), and a peak observed at  $m/z = 499.0376$

in the ESI mass spectrum, corresponding to an  $[M+Na]^+$  molecular ion of formula  $C_{15}H_{14}N_4NaO_9S$ .



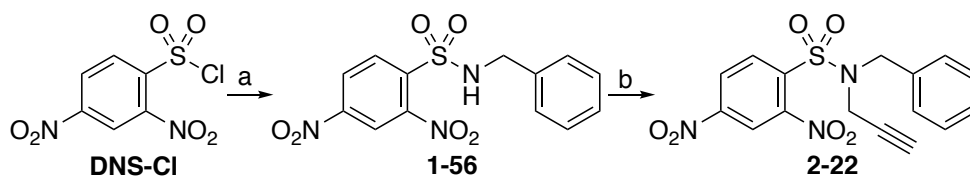
Scheme 2.15 Synthesis of two-carbon conjugate **2-15**. a)  $BBr_3$ , DCM,  $N_2$ , 24 h; then preparative LCMS purification, 55%.

The first step of the synthesis of **2-19**, the reaction of benzoyl chloride and phenol to give phenyl benzoate, was achieved in a yield of 35% following recrystallization from EtOH (**Scheme 2.16**). The next step, the monoacylation reaction, successfully yielded catechol-free amine **2-20** in 60% yield after purification by column chromatography, comparable to the literature value of 63%.<sup>354</sup> The  $^1H$  NMR spectrum of **2-20** matches that expected from the literature,<sup>360</sup> and the ESI mass spectrum displays a peak at  $m/z = 193.1335$ , consistent with an  $[M+H]^+$  molecular ion of formula  $C_{11}H_{17}N_2O$ . Sulfonamide formation to give the final catechol-free analogue **2-19** proceeded in 48% yield. As with **2-14** and **2-18**, the presence of characteristic d/dd/d resonances for the 2,4-dinitrobenzene ring at 8.68, 8.55 and 8.31 ppm in the  $^1H$  NMR spectrum suggests successful product formation, as do peaks observed at  $m/z = 423.0967$  and  $445.0784$  in the ESI mass spectrum, corresponding to  $[M+H]^+$  and  $[M+Na]^+$  adducts of molecular formulae  $C_{17}H_{19}N_4O_7S$  and  $C_{17}H_{18}N_4NaO_7S$  respectively.



Scheme 2.16 Synthesis of catechol-free conjugate **2-19**. a) Phenol, NaOH (10% w/v aq.), 2 h, 35%; b) 1,4-Diaminobutane,  $H_2O$ ,  $N_2$ , 50 °C, 24 h, 60%; c) 2,4-dinitrobenzenesulfonyl chloride, lutidine, DCM, 0 °C to rt, 96 h, 48%.

Alongside the synthesis of these three SO<sub>2</sub>-releasing conjugates, two of Chakrapani's original compounds were synthesised to allow comparison of their SO<sub>2</sub>-releasing ability and biological activity with the newly-synthesised conjugates. The first was benzylamine conjugate **1-56**; this demonstrated rapid release of SO<sub>2</sub> in Chakrapani's initial studies, and the primary amine of benzylamine also provides a close analogue to the primary amine unit in aminochelin.<sup>301</sup> This can be synthesised easily in one step from benzylamine and 2,4-dinitrobenzenesulfonyl chloride (**DNS-Cl**, **Scheme 2.17**). The second, **2-22**, a propargyl derivative of **1-56**, was chosen as it displayed good activity vs. Gram-positive MRSA and *E. faecalis*, and therefore provides a good biological control for the effects of SO<sub>2</sub> release on bacteria. It can also be synthesised by alkylation of **1-56** with propargyl bromide. Both syntheses proceed smoothly in moderate yields following purification by column chromatography, and in both cases comparison of the <sup>1</sup>H NMR spectra with reported literature spectral data supported formation of the desired products.<sup>301,304</sup>

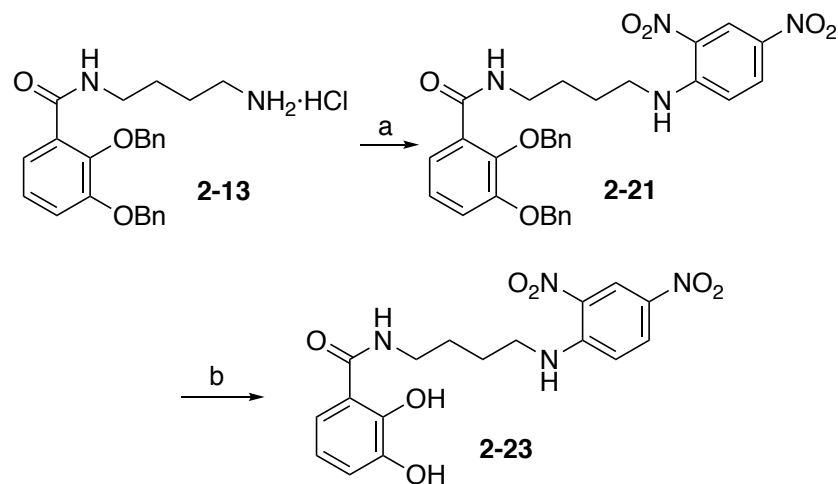


Scheme 2.17 Synthesis of Chakrapani compounds **1-56** and **2-22**. a) Benzylamine, pyridine, DCM (anhydrous), 0 °C to rt, 24 h, 65%; b) propargyl bromide, K<sub>2</sub>CO<sub>3</sub>, DMF, rt, 24 h, 68%.

A further control for the biological experiments, **2-23**, was synthesised based on **2-21**, the minor product from the Smiles rearrangement of **2-14**. This was intended to provide a close structural analogue of conjugate **2-9**, but with no ability to generate SO<sub>2</sub>. This was intended to determine whether any antimicrobial activity observed stems solely from SO<sub>2</sub> release, or whether the underlying chemical structure of the conjugate also plays a role. **2-21** was synthesised via a S<sub>N</sub>Ar method by reaction of benzylated aminochelin **2-13** with 1-chloro-2,4-dinitrobenzene (**Scheme 2.18**). BBr<sub>3</sub>-mediated deprotection and preparative LCMS purification was carried out in 22% yield, perhaps due to the poor solubility of **2-23** in the acetonitrile component of the solvent system, or low mass loading in the LCMS, which often performs

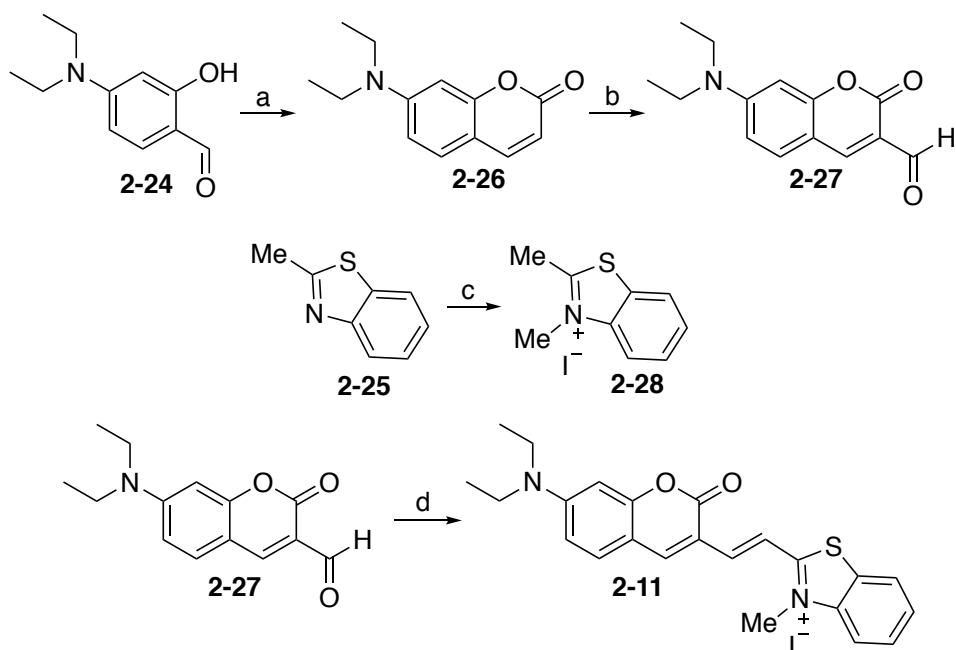


more efficiently at high mass loading. Successful synthesis of deprotected **2-23** was confirmed via the absence of benzyl CH<sub>2</sub> resonances observed at 5 ppm in the <sup>1</sup>H NMR spectrum, and the presence of a peak at *m/z* = 391.1251 in the ESI mass spectrum, corresponding to an [M+H]<sup>+</sup> molecular ion of formula C<sub>17</sub>H<sub>19</sub>N<sub>4</sub>O<sub>7</sub>.



Scheme 2.18 Synthesis of SO<sub>2</sub>-free control **2-23**. a) 1-Chloro-2,4-dinitrobenzene, Et<sub>3</sub>N, DCM (anhydrous), 18 h, 71%; b) BBr<sub>3</sub>, DCM, N<sub>2</sub>, 22 h; then preparative HPLC purification, 22%.

Finally, SO<sub>2</sub>-detecting dye **2-11** was synthesised according to two literature procedures starting from 4-diethylaminosalicylaldehyde (**2-24**) and 2-methylbenzothiazole (**2-25**).<sup>345,361</sup> A Knoevenagel condensation with diethyl malonate followed by decarboxylation gave 7-diethylaminocoumarin (**2-26**, **Scheme 2.19**), then a Vilsmeier-Haack reaction was carried out to install an aldehyde group at the 3-position (**2-27**). The <sup>1</sup>H NMR spectra of both products are consistent with literature data,<sup>361</sup> and peaks are observed at *m/z* = 240.0997 and 268.0947 in the respective ESI mass spectra corresponding to [M+Na]<sup>+</sup> molecular ions of formula C<sub>13</sub>H<sub>15</sub>NNaO<sub>2</sub> and C<sub>14</sub>H<sub>15</sub>NNaO<sub>3</sub>. Finally, a condensation reaction with 2,3-methylbenzothiazolium iodide (**2-28**, synthesised by methylation of **2-25** with MeI) gave **2-11** in high yield. Again, the <sup>1</sup>H NMR is consistent with literature data,<sup>345</sup> and the ESI mass spectrum displays a peak at *m/z* = 391.1472, consistent with an [M]<sup>+</sup> molecular ion of formula C<sub>23</sub>H<sub>23</sub>N<sub>2</sub>O<sub>2</sub>S. The overall yield starting from the salicylaldehyde was 32%.



Scheme 2.19 Synthesis of SO<sub>2</sub>-detecting dye **2-11**. a) 1) Diethyl malonate, piperidine, EtOH, reflux, 24 h; 2) conc. HCl, AcOH, reflux, 24 h, 52%; b) POCl<sub>3</sub>, DMF, N<sub>2</sub>, 70 °C, 23 h, 68%; c) MeI, MeCN, N<sub>2</sub>, 75 °C, 24 h, 53%; d) **2-28**, EtOH, reflux, 18 h, 90%.

## 2.5 Iron Complexation Studies

As part of both the SO<sub>2</sub> release studies, and potentially the biological studies of the catechol-sulfonamides, a comparison of the activity of catechol conjugates **2-9** and **2-15** in both their complexed and uncomplexed forms was envisaged. As potential siderophore mimics, **2-9** and **2-15** require iron coordination for bacterial uptake to take place via the siderophore transport pathway, with addition of iron to the catechol pre-assay the best way to ensure coordination. Indeed, a recent study by Zamora *et al.* on the uptake of catechol-type siderophores by *Campylobacter jejuni* showed that the bacteria experience better growth recovery when treated with siderophores that are pre-complexed with iron, suggesting similar biological effects could be seen if **2-9** or **2-15** were pre-loaded with iron.<sup>362</sup> However, it should also be noted that iron complexation does not always boost antimicrobial activity for Trojan Horse conjugates; there are examples of iron complexation having no effect, or even reducing activity compared to the uncomplexed conjugates.<sup>193,265</sup>

Before complexation of **2-9/2-15** for the SO<sub>2</sub> release assays or the biological assays could be carried out, the iron complexation behaviour of the monocatechol moiety needed to be investigated to determine the quantity of iron to be added. Monocatechols are capable of forming mono, bis and tris-complexes with Fe(III), with all three species in equilibrium in solution (**Figure 2.17**),<sup>363</sup> the position of the equilibrium depends on the relative concentrations of the iron and the catechol, and the pH of the solution.

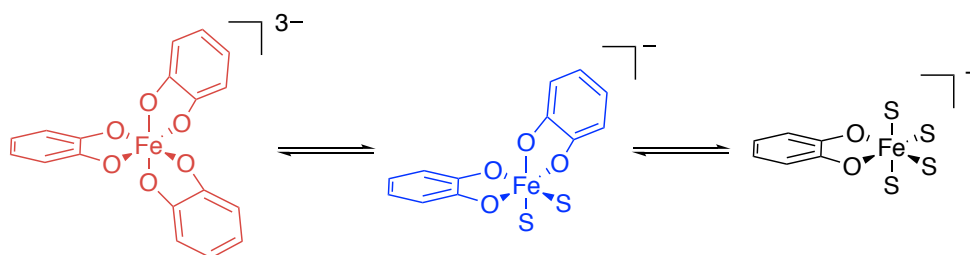


Figure 2.17 Potential equilibrium between Fe(III)-catechol complexes in solution. S = solvent. For the bis(catechol) other isomers are possible.

The iron complexation behaviour can be studied via the method of continuous variation, more commonly known as a Job plot.<sup>364</sup> This method involves the combination of a metal and a ligand in different concentrations such that the overall concentration of the two remains constant. Monitoring a property of the system, in this case the UV-Visible spectra at each concentration point, whilst keeping the pH constant, allows the determination of the ratio of iron complexes present within the equilibrium at each concentration.

By obtaining the UV-Vis spectra of each concentration, the changes in the ligand-to-metal charge transfer (LMCT) band of the Fe(III)-catechol complexes can be observed, which provides clues as to the speciation of the complexes present at each concentration when the system has reached equilibrium.<sup>363,365,366</sup> Fe(III)-catechol complexes have been extensively characterised in the literature, and the maxima of their UV-vis spectra are characteristic of the metal-ligand stoichiometry, with a  $\lambda_{\text{max}}$  of around 480-495 for the tris(catechol), 560-590 for the bis(catechol), and 680-700 nm for the monocatechol complexes.<sup>363,367-369</sup>

The Job plots to determine iron complexation behaviour were carried out based on a protocol developed by Dr Daniel Raines, who studied the complexation behaviour of monocatechols in Tris buffer by using a model catecholamine, *N*-ethyl-2,3-dihydroxybenzamide (**2-29**, **Figure 2.18**).<sup>370</sup> The amide functionality present mimics the electronics and hydrogen bonding properties of the catechol ring of the aminochelin unit in **2-9**,<sup>370</sup> and therefore provide a good insight as to the behaviour of monocatechol units in the assay medium.

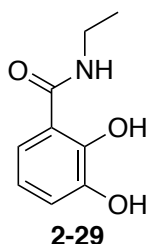
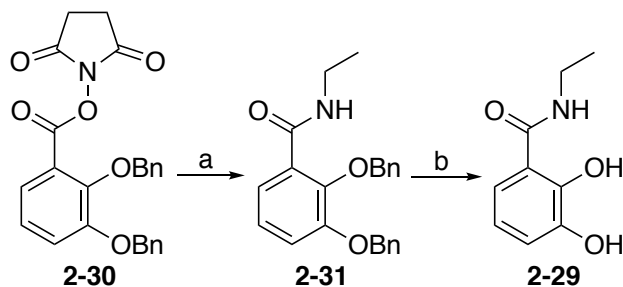


Figure 2.18 Structure of *N*-ethyl-2,3-dihydroxybenzamide **2-29** employed for Job plot analysis.

Fe(III) tends to precipitate as a variety of hydroxides in aqueous solutions at neutral pH,<sup>371</sup> which can interfere with the Job plot, as this changes the amount of iron available for complexation. To counter this, a mild chelating agent, nitrilotriacetic acid (NTA), is added to ensure the iron remains in solution. NTA mostly forms a 1:1 complex with Fe(III) with a logK value of 15.9,<sup>372</sup> while single catechols are reported to have a logK for Fe(III) of around 20 (logK for aminochelin = 19.1).<sup>350</sup> Based on this, there would be minimal competition between NTA and the monocatechol for Fe(III) binding, which is borne out in a number of studies, which show no interference of NTA with spectrophotometric measurements.<sup>373,374</sup> This was also demonstrated in the original study utilising catecholamine **2-29**, where very little difference was observed between Job plots recorded with and without NTA.<sup>370</sup>

Model catechol **2-29** was synthesised in two steps from the succinic ester of benzyl protected catechol **2-30**, which had previously been synthesised by Dr Ellis Wilde. The activated succinic ester is reacted with ethylamine according to a literature procedure,<sup>375</sup> before removal of the benzyl protecting groups via catalytic hydrogenation (**Scheme 2.20**).



Scheme 2.20 Synthesis of model monocatecholamine **2-29**. a) Ethylamine (2 M in THF), Et<sub>3</sub>N, THF, 72 h, 94%; b) H<sub>2</sub>, 10% Pd-C, EtOH, 96 h, 86%.

While the original protocol uses a stock solution of catecholamine **2-29** in DMSO, with the concentration in the final solutions maintained at 5%,<sup>370</sup> acetonitrile was used to make the initial stock solution as it had already been shown to solubilise the sulfonamide conjugates. The concentration was again kept at 5%. 10 mM stock solutions of **2-29** and Fe(NTA) were made up in MeCN and distilled water respectively. Aliquots of each solution were combined with buffer such that the total concentration of ligand plus metal remained constant at 400 μM, then left for an hour to equilibrate before recording the UV-vis spectrum of each solution. The concentrations of each component ranged from 100% ligand to 100% metal.

The first Job plot aimed to replicate the conditions used in the original protocol, with TrisHCl at pH 7.5 used as the buffer solution. The solutions obtained ranged in colour from red-pink (high ligand concentration) to dark blue (high iron concentration), with the solutions for both 100% ligand and 100% metal remaining colourless (**Figure 2.19**).



Figure 2.19 Colours of solutions obtained from continuous variance method from high ligand concentration (left) to high iron concentration (right). Image acquired by James Southwell.

The UV-vis results obtained are very similar to those obtained in the original protocol (**Figure 2.20**). A maximum at around 500 nm is observed for the highest ligand concentrations, increasing in intensity and shifting to 521 nm

when the ligand and metal are present in a 3:1 ratio, compared to 512 nm in the original protocol. The maxima of the curves continues to increase in intensity and shifts to 560 nm when the two components are present in a 2:1 ratio, indicative of the predominance of a bis(catechol) species in equilibrium.<sup>363,367</sup> This bathochromic shift continues until the maximum reaches 590 nm, which remains within the observed range of  $\lambda_{\text{max}}$  for bis(catechol) complexes.<sup>370</sup> There is no evidence for the predominance of the monocatechol complex (680-700 nm) in solution, even at the lowest possible ligand concentration. This shift in intensity and wavelength is almost identical to that observed in the original protocol, suggesting exchanging DMSO for MeCN has not affected the equilibrium between the complexes.

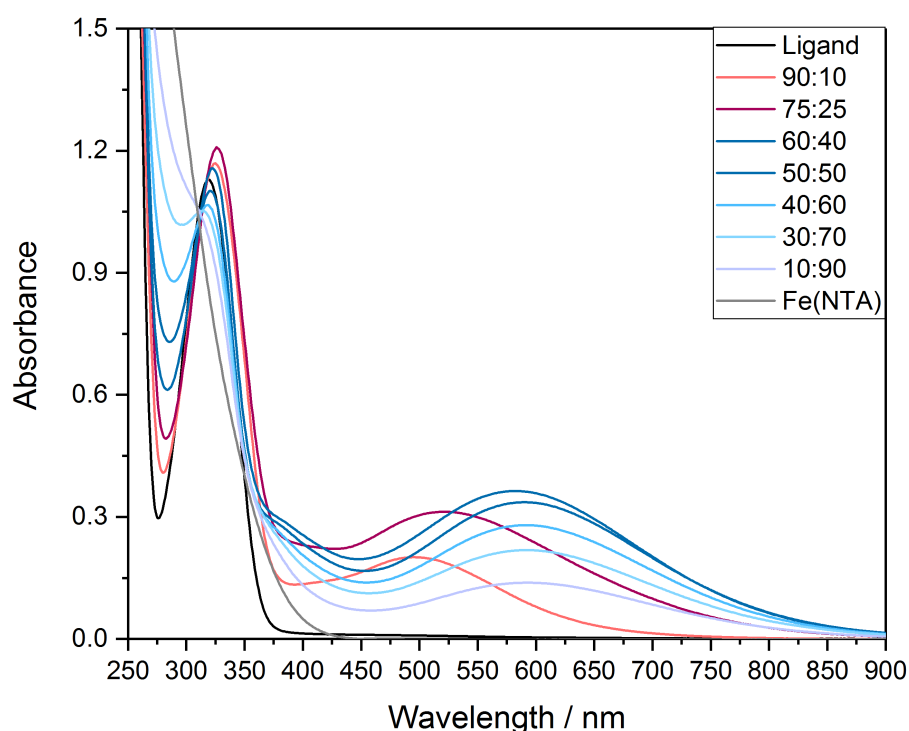


Figure 2.20 UV-vis spectra for selected ligand:metal ratios in Tris buffer.

A continuous variance experiment was then carried out in M9 minimal medium. M9 is a nutrient-poor medium used to culture *E. coli* bacteria, which was intended to be used to study the effects of the compounds on *E. coli* in low-iron conditions. It consists of a base mixture of phosphate salts,  $\text{NH}_4\text{Cl}$  and  $\text{NaCl}$  supplemented with glucose,  $\text{MgSO}_4$  and  $\text{CaCl}_2$ , with the potential to add other components as required. When the salts are combined in water, a solution with a pH of 7.0 is formed.

The results for the continuous variance in M9 are broadly similar to those for TrisHCl, with some exceptions. The initial maximum is again observed at 500 nm, but the maximum at 3:1 ligand to metal ratio is shifted higher to 530 nm. There is a minimal increase in intensity between this maximum and that of the 2:1 ratio, which is shifted lower to around 545 nm. The bathochromic shift here continues to around 577 nm (**Figure 2.21**). In general, the absorbances at the maxima are also reduced compared to the TrisHCl experiment. In addition to this, the 100% Fe(NTA) solution, which only begins absorbing at below 450 nm in TrisHCl, has a non-zero absorbance throughout the range of wavelengths scanned, the intensity of which begins to become significant below 600 nm. Finally, on leaving the solutions over the weekend, a white precipitate was observed to form in the 100% metal solution and the seven solutions with the lowest ligand concentration present, whereas no precipitate is visible in any of the TrisHCl solutions.

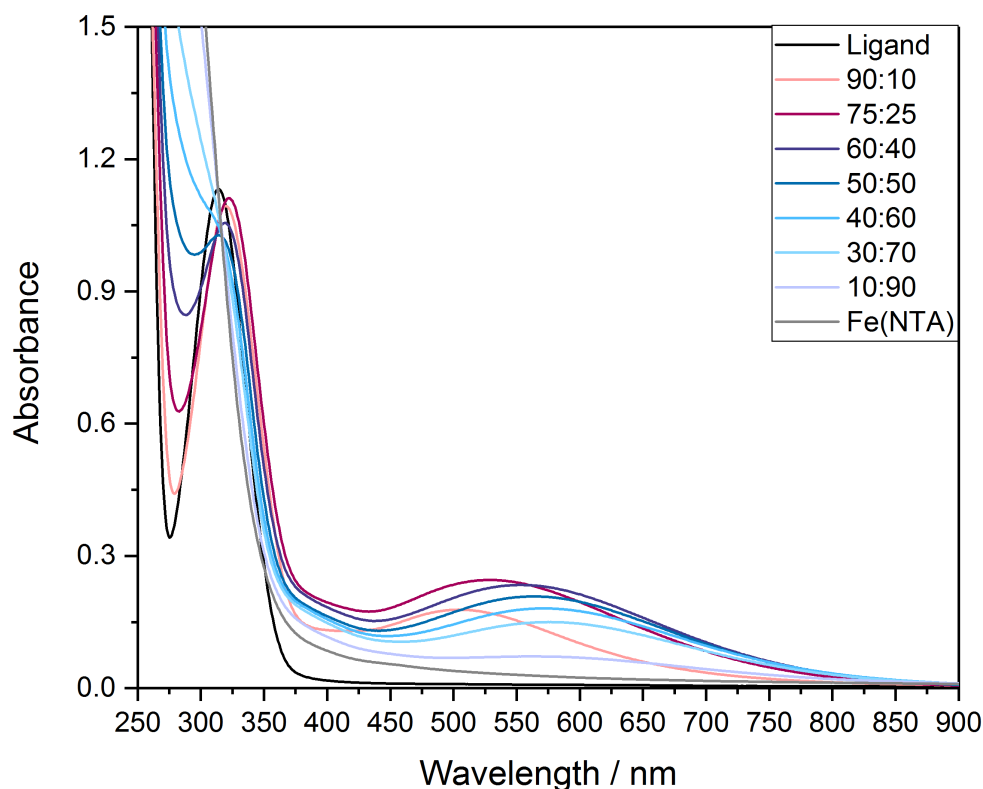


Figure 2.21 UV-vis spectra for selected ligand:metal ratios in M9 medium.

The results for the M9 experiment suggest that a component in the M9 medium is interfering with the complexation behaviour of the monocatechol, and other iron species are being formed, reducing the amount of iron available for catechol binding. The most likely candidate for

this would be the phosphate salts present, which are known to bind strongly to iron.  $\text{FePO}_4$  is also poorly soluble in aqueous solutions, and its dihydrate is known to form white precipitates.<sup>376–379</sup> The pH difference with the TrisHCl solution may also play a role; pH is known to have a strong effect on the speciation of Fe(III)-catechol complexes, with protons competing with the iron for binding the catechol oxygens.<sup>96</sup> The slightly more acidic M9 may have shifted this equilibrium towards the protons, hence the observed differences.

The maxima of both of the Job plots obtained suggests a mixture of the tris(catechol) and bis(catechol) species are present, depending on the ligand:metal ratio. Both plots show a maximum absorbance at a ligand:metal ratio of 3:1 when wavelengths consistent with the formation of the tris(catechol) species are considered, and a maximum absorbance at a ligand:metal ratio of 2:1 when wavelengths similar for wavelengths consistent with formation of the bis(catechol) species are considered (**Figure 2.22, Figure 2.23**).

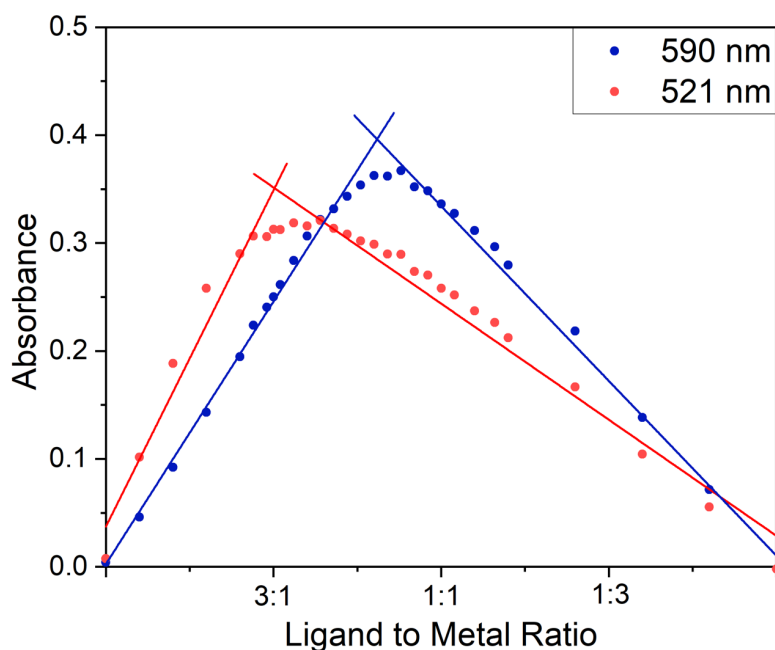


Figure 2.22 Job plot for absorbance at maxima observed in Tris buffer.



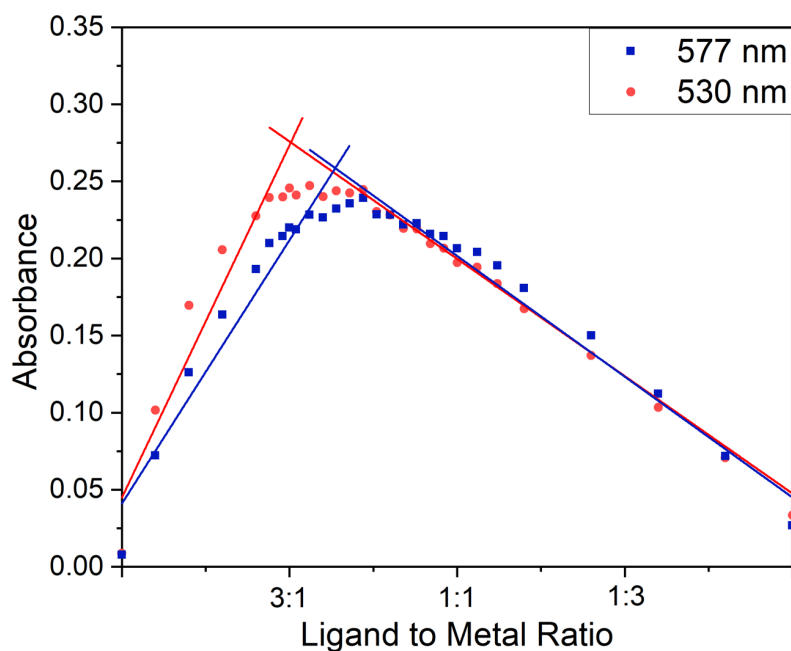


Figure 2.23 Job plot for absorbance at maxima observed in M9 media.

## 2.6 SO<sub>2</sub> Release Studies

A key part of evaluating the synthesised 2,4-dinitrobenzenesulfonamide conjugates is the examination of their ability to release SO<sub>2</sub>. With a strong correlation between SO<sub>2</sub> release rate and antimicrobial activity, at least for those conjugates tested against *M. tuberculosis*,<sup>301,303</sup> ensuring that the attachment of a siderophore component doesn't hinder the ability of the conjugates to react efficiently with thiols to release SO<sub>2</sub> is vital.

Initial qualitative studies of SO<sub>2</sub> release were carried out in the presence of synthesised dye **2-11** (Figure 2.24), with 10% MeCN in HEPES buffer used as a solvent. HEPES was selected as the buffer for its relevant pH range; it can easily be adjusted to biological pH (pH 7.4). It also lacks the ability to coordinate most metal ions, allowing the effects of adding iron to the solution to be observed without interaction with the buffer.<sup>380</sup> This can be an issue in some phosphate-based buffers, as mentioned above.

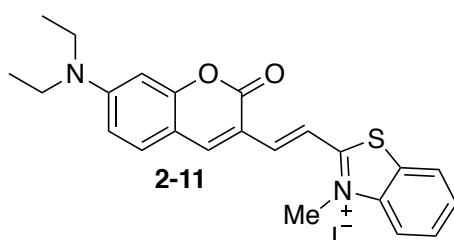
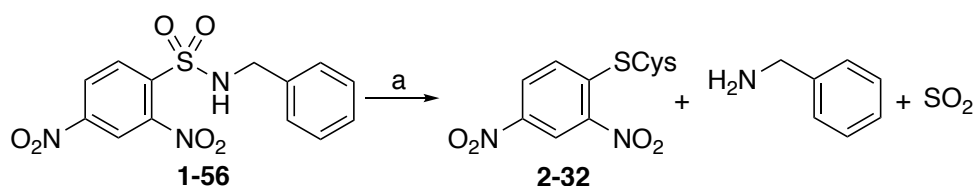


Figure 2.24 Structure of SO<sub>2</sub>-detecting dye **2-11**.

Benzylamine conjugate **1-56** was initially used to probe the experimental setup, with cysteine as the thiol component. Stock solutions of **1-56**, cysteine, and dye **2-11** were combined in a cuvette such that final concentrations of 100  $\mu\text{M}$  **1-56**, 10  $\mu\text{M}$  dye, and 1 mM cysteine were achieved, and UV-vis spectra acquired over a 30 minute time period (**Scheme 2.21**). The addition of 1 mM cysteine is intended to mimic the concentrations of biological thiols present in the cytoplasm of cells. The experimental conditions were derived from those of Sun *et al.*, who originally synthesised and evaluated dye **2-11**.<sup>345</sup>



Scheme 2.21 Reaction of **1-56** with cysteine. a) Cysteine (10 eq.), **2-11** (0.1 eq.), 10% MeCN:HEPES, pH 7.4, rt, 30 mins.

The UV-Vis spectra acquired for **1-56** in the presence of the dye and cysteine showed the rapid emergence of a new UV-vis band around 345 nm, with a shoulder at 425 nm, and the concomitant decrease in the dye absorbance band at 545 nm (**Figure 2.25**). The band at around 345 nm has been previously assigned to the cysteine-dinitrobenzene conjugate **2-32** formed upon attack of cysteine on substituted 2,4-dinitrobenzene rings, with the shoulder corresponding to the new UV-vis absorption of the dye on sulfite conjugation.<sup>345,381</sup> The progress of the reaction can also be followed by eye, with the initial pink colour of the dye becoming fainter, and a gradual change to the yellow colour of the sulfite-conjugated dye and/or the cysteine adduct being observed.

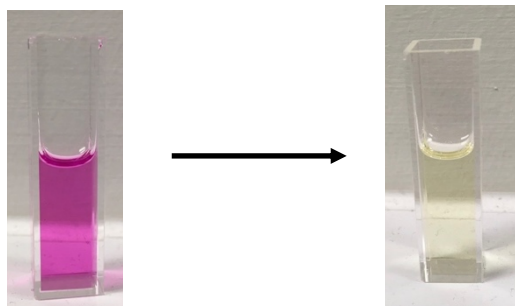
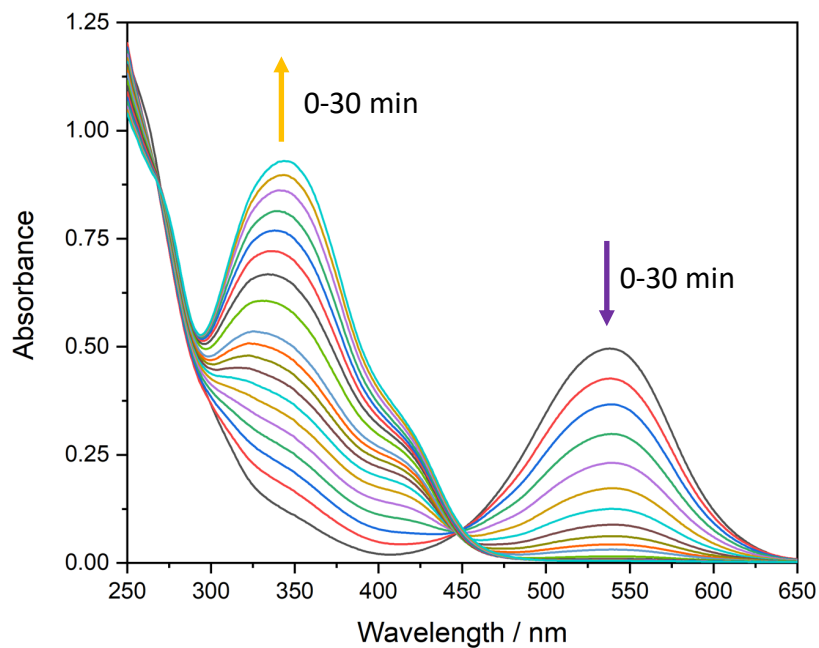


Figure 2.25 UV-Visible spectrum for the reaction of **1-56** with cysteine in the presence of dye **2-11** over 30 mins, and photos of the solution before and after the reaction.

The intensity of the band at 345 nm also allows  $\text{SO}_2$  release experiments to be carried out without the dye present. By following the increase in absorbance of this band until it plateaus, the time course of  $\text{SO}_2$  release can be clearly followed. In the dye-free experiments carried out with cysteine, a slight increase in the wavelength at which the cysteine-dinitrobenzene conjugate absorbs can be seen over time (**Figure 2.26**). This likely derives from an equilibrium between the S-adduct **2-32** and the N-adduct **2-33** in the cysteine-dinitrobenzene conjugate, which has previously been reported (**Scheme 2.22**); both adducts have been shown to have different absorbance bands (330 vs. 350 nm) and different molar absorption coefficients.<sup>381,382</sup> This shift in wavelength and molar absorption coefficient makes attempts to quantify concentrations and conversions from the adduct band difficult.

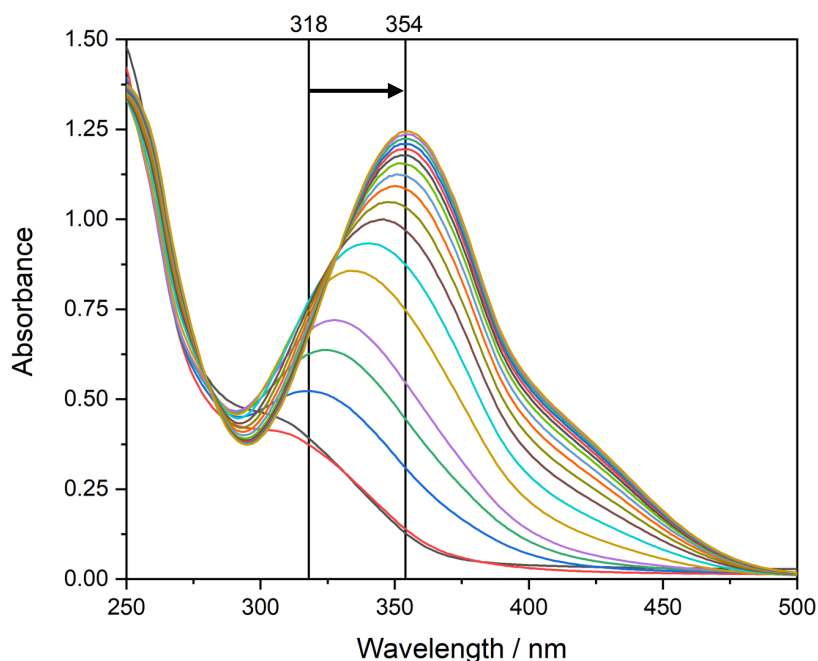
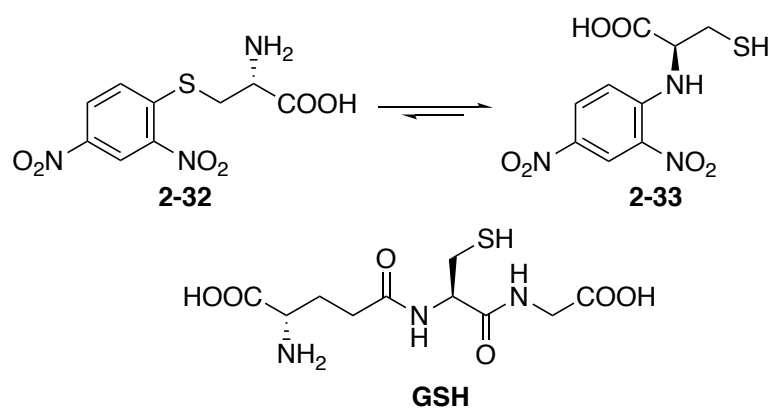


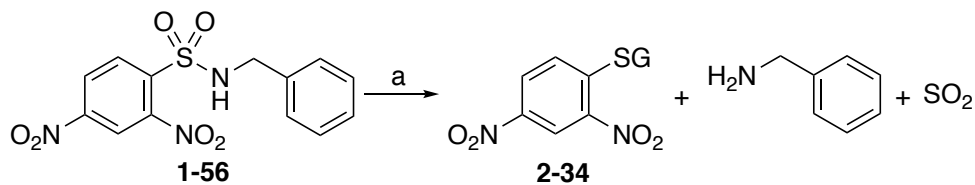
Figure 2.26 UV-Vis spectrum of sulfonamide conjugate **2-9** on reaction with cysteine (10 equivalents) over 7 hours in 10% MeCN:HEPES buffer (pH 7.4). The shift in the absorbance maxima over time is indicated.



Scheme 2.22 Equilibrium between S-adduct **2-32** and N-adduct **2-33** in cysteine-dinitrobenzene conjugates, and structure of alternative thiol glutathione (GSH).

To try and obtain more quantitative data, glutathione was used as the thiol component instead. Although the N-adduct of glutathione shows up in literature structure searches, on examination of the papers cited no evidence for its formation seems to be reported. The glutathione-dinitrobenzene adduct gives a well-defined UV-vis absorbance band at 340 nm, with a high extinction coefficient ( $10500 \text{ M}^{-1}\text{cm}^{-1}$ ).<sup>346,383</sup> Qualitative experiments with dye **2-11** and benzylamine **1-56** displayed similar results to those carried out with cysteine, as did experiments in the absence of the

dye (**Scheme 2.23**). There is no major shift in the position of the absorbance maxima over time (**Figure 2.27**).



Scheme 2.23 Outcome of reaction between **1-56** and glutathione. a) GSH (10 eq.), 10% MeCN:HEPES, pH 7.4, rt, 12 h.

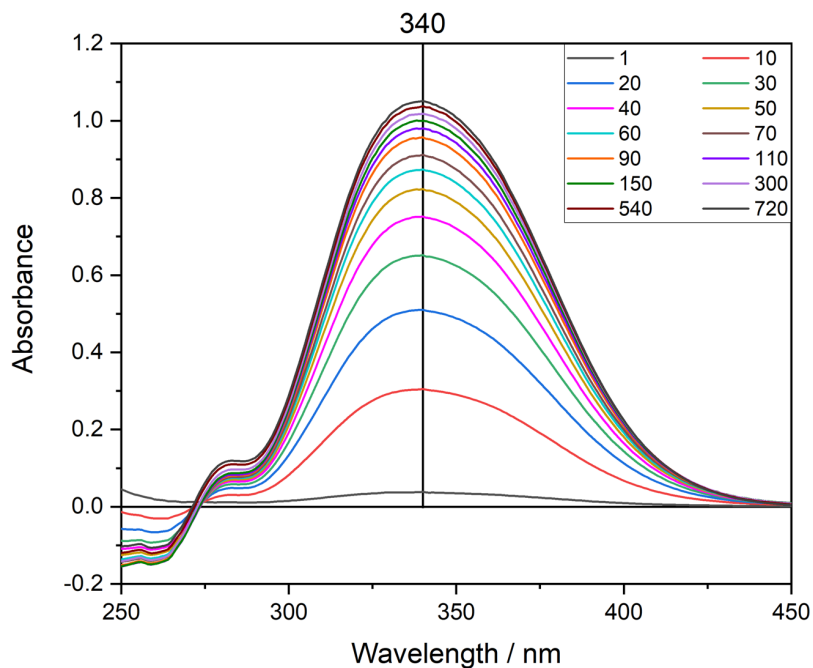


Figure 2.27 UV-vis spectrum of **1-56** on reaction with glutathione (10 equivalents) over 12 hours in 10% MeCN:HEPES buffer (pH 7.4). Times shown are in minutes.

Qualitative experiments with all of the conjugates synthesised (**2-9**, **2-15**, **2-19**) were carried out in the presence of the dye and glutathione. The conditions used are identical to those for **1-56** (10  $\mu\text{M}$  **2-11**, 100  $\mu\text{M}$  conjugate, 1 mM glutathione). Successful  $\text{SO}_2$  release was observed on each occasion, with all the conjugates demonstrating complete loss of the dye absorbance band at 545 nm within 30 minutes (with most seeing a faster decrease). These results suggest that in each case successful  $\text{SO}_2$  release can be achieved from the conjugates.

Following confirmation that all of the conjugates can undergo successful  $\text{SO}_2$  release, the relative  $\text{SO}_2$  release profiles were examined by following the

absorption peak for the glutathione adduct. As concentration is related to absorbance in a linear fashion, plotting the absorbance at the maxima over time will give a picture of the rate of increase in the concentration of the glutathione conjugate, and hence the rate of SO<sub>2</sub> release. The experiments were carried out in triplicate, with the error displayed as the standard deviation of the results. A baseline of the corresponding conjugate in 10% MeCN:HEPES buffer is used so that the spectra can clearly measure the changes in absorbance post-glutathione addition.

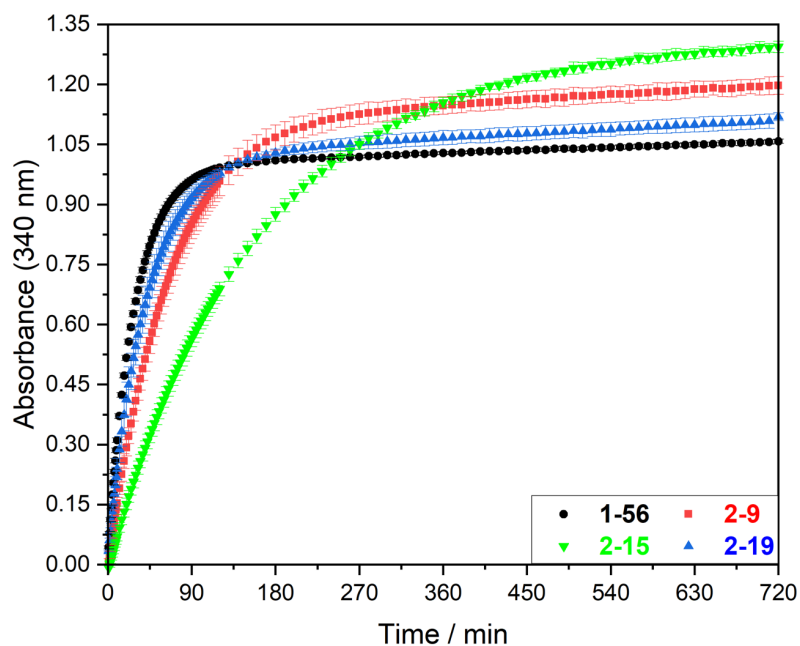


Figure 2.28 Plot of absorbance at 340 nm vs. time for sulfonamides **1-56**, **2-9**, **2-15** and **2-19** on reaction with glutathione (10 eq.) in HEPES buffer (pH 7.4). All experiments are a mean average of 3 experiments, apart from **2-15**, which is a mean average of 2 experiments. Error bars are calculated as the standard deviation of the mean.

As shown in **Figure 2.28**, **1-56**, **2-9** and **2-19** display similar kinetic profiles, with rapid increases in absorbance over the first hour of the reaction, followed by a transition to a plateau over the next two hours. The benzylamine conjugate **1-56** displays the fastest SO<sub>2</sub> release, closely followed by catechol-free control **2-19**. While **2-9** appears slower, the majority of SO<sub>2</sub> release is still taking place within the first hour, indicating limited hindrance of SO<sub>2</sub> release by the catechol groups. **2-15**, with its shorter 2-carbon linker, is noticeably slower to react than the 4-carbon

linker-based **2-9**. The differences in reactivity between the four sulfonamides can be seen more clearly in the first two hours of reaction time (Figure 2.29).

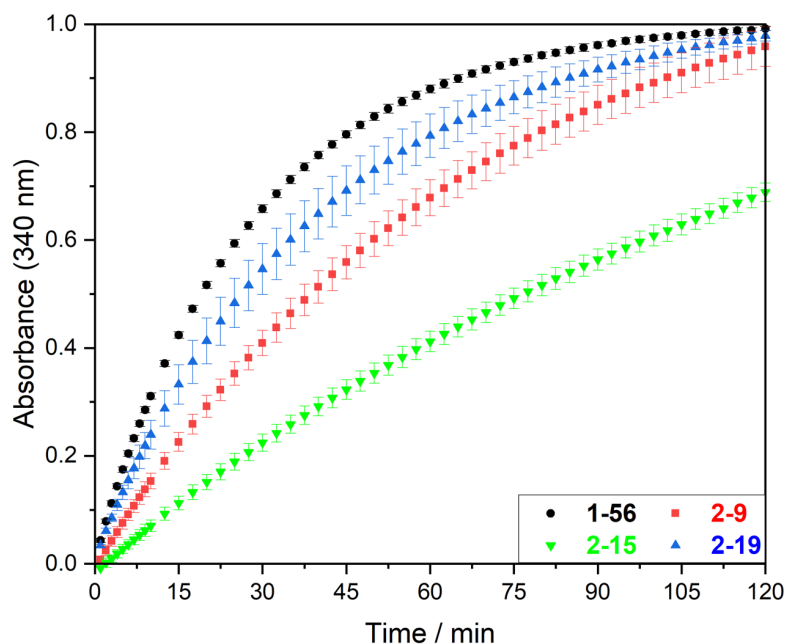


Figure 2.29 Plot of absorbance at 340 nm vs. time for first two hours of reaction between sulfonamides **1-56**, **2-9**, **2-15** and **2-19** with glutathione.

Given the shorter linker length between the catechol and the dinitrobenzene ring in **2-15**, it is possible that there is some form of intramolecular interaction between these two rings, whether in the form of pi-pi stacking, or in the form of hydrogen bonding between the substituents. This could have the effect of hindering the nucleophilic attack of glutathione on the sulfonamide. It is also notable that both **2-9** and **2-15** plateau to a higher absorbance than that expected for the glutathione conjugate at 100% conversion (c. 1.15 and 1.30 instead of the 1.05 expected given the extinction coefficient of the 2,4-dinitrobenzene-glutathione adduct **2-34**).

The release rates from **2-9** and **2-15** were also probed in the presence of Fe(III) to examine the effects of iron coordination on the rate of SO<sub>2</sub> release. 1 equivalent of Fe(III) was added for every 3 equivalents of ligand to try and achieve formation of the tris(catecholate) complex. For the release experiments, final concentrations of 100 μM donor, 1 mM thiol and 33.3 μM Fe(NTA) were used.

On addition of Fe(NTA) to a solution of **2-9** or **2-15**, a purple-blue colour forms, suggesting the formation of an iron complex (**Figure 2.30**). For **2-9**, the LMCT band of the Fe(III) complex has a maximum absorbance around 533 nm; for **2-15**, this is shifted slightly higher to around 546 nm. In both cases the absorbances are similar (c. 0.1). There is a notable colour difference before and after the reaction with GSH is carried out, with the solution changing to a pink colour (**Figure 2.31**), much more similar to the higher ligand-to-Fe ratio solutions in the Job plots carried out in Section 2.5.

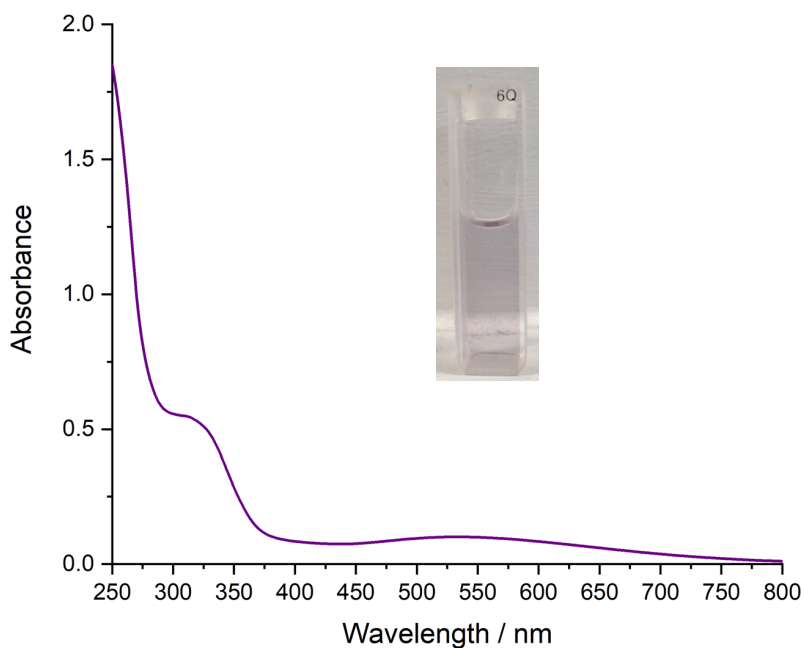


Figure 2.30 UV-Vis spectrum of **2-9** in the presence of 0.33 eq. Fe(III), and photo of corresponding cuvette.

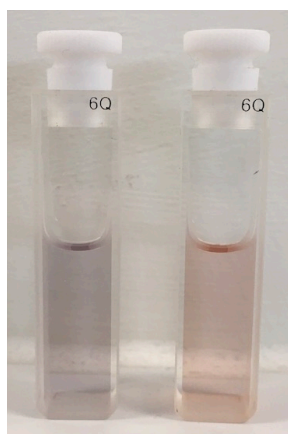


Figure 2.31 Colour difference between Fe(NTA)-containing solutions of **2-15** before (left) and after (right) reaction with glutathione.

This could indicate a slight alteration in coordination between the conjugates and the free aminochelin generated post-SO<sub>2</sub> release. Assuming



that the pH remained constant, it is possible that some of the functional groups on the 2,4-dinitrobenzenesulfonamide unit may be able to undergo intramolecular hydrogen bonding with the catechol groups on the aminochelin unit, which may hinder its ability to form an iron tris(catecholate) complex, hence the purple bis(catecholate) dominates in solution. On SO<sub>2</sub> release, this hydrogen bonding interaction would no longer be present, and the aminochelin better able to bind Fe(III) successfully, hence the colour change, which indicates predominant formation of the tris(catecholate) species. A further possibility is a change in the charge of the ligand on SO<sub>2</sub> release. Before SO<sub>2</sub> release takes place, the charge of the tris(catecholate) iron complex would be -3; such a negative charge could potentially destabilise the tris-complex, with the less negatively charged bis(catechol) complex (-1) potentially favoured. On loss of SO<sub>2</sub>, the free amine group of the aminochelin unit will be protonated at biological pH (7.4), so the tris(catecholate) complex will be a zwitterion with an overall charge of 0; this may be more favourable for tris(catecholate) formation.

When the SO<sub>2</sub> release kinetics of **2-9** and **2-15** are examined in the presence of Fe(NTA), a clear increase in release rate compared to the iron-free version is observed in both cases, with the absorbance reaching a plateau in a shorter time span (**Figure 2.32**). As there is no change in the mean absorbance at the plateau for the reactions containing Fe(NTA) compared to those without, this suggests the faster rate stems from formation of the glutathione conjugate, and not from formation of a different species absorbing around the same wavelength in the Fe(NTA) reactions.

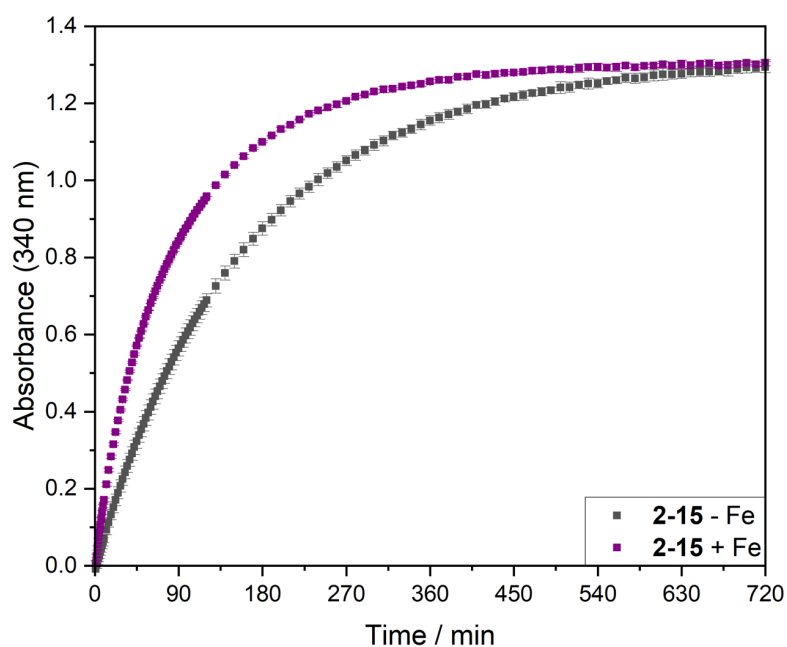
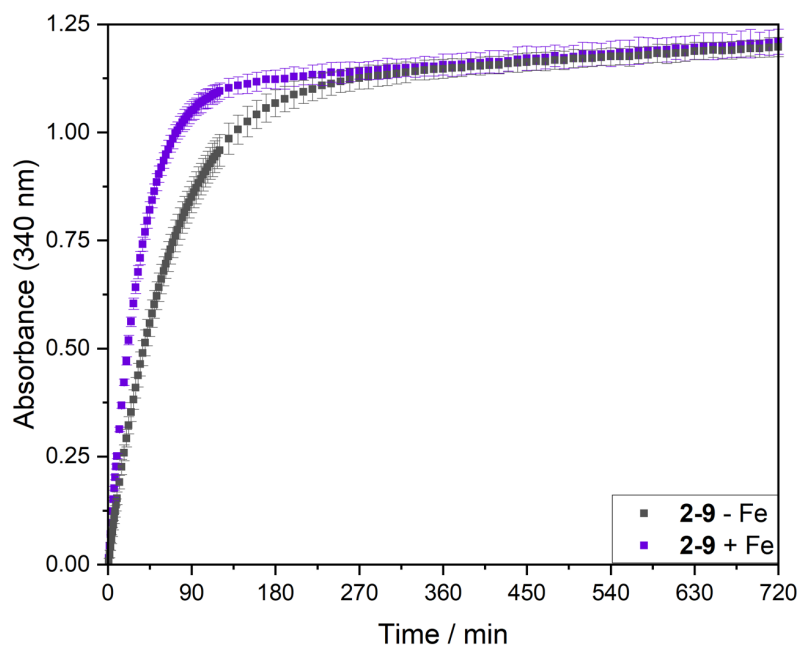


Figure 2.32 Plots of absorbance at 340 nm vs. time for conjugates **2-9** and **2-15** on reaction with glutathione (10 eq.) in the presence and absence of 0.33 eq. Fe(NTA).

This increase in rate is intriguing, and potentially points to the formation of an iron complex making the sulfonamide more accessible to glutathione, allowing for easier nucleophilic attack on the 2,4-dinitrobenzene ring, and therefore faster  $\text{SO}_2$  release. It is possible that the formation of an iron complex disrupts existing intramolecular interactions within the conjugate structures that create steric hindrance around the sulfonamide; for example

hydrogen bonding between the catechol OH groups and the sulfonamide and/or the nitro groups would hinder the approach of glutathione from certain angles. With the catechol groups bound to iron, this would free up the 2,4-dinitrobenzene ring for easier glutathione access. This also correlates with the existing difference in SO<sub>2</sub> release rate between **2-9** and **2-15**. In **2-15**, the catechol groups and the 2,4-dinitrobenzene ring are closer together, allowing for a greater degree of intramolecular interactions between the two; formation of an iron complex has a larger effect on the rate of release from **2-15** than **2-9**, suggesting greater intramolecular interactions between the catechol and the 2,4-dinitrobenzenesulfonamide in **2-15**. It is also possible that the high positive charge of the Fe<sup>3+</sup> cation exerts a strong electron-withdrawing effect on the whole ligand, making the 2,4-dinitrobenzenesulfonamide ring more electron-deficient, and hence increasing the rate of the S<sub>N</sub>Ar reaction.

## 2.7 Biological Studies

*All of the antimicrobial assays detailed in this section were carried out by Dr Adrian J. Chu, a postdoctoral researcher in the AKDK group. Experimental design was shared between CMB, AJC, and AKDK, with input from Prof. Gavin H. Thomas.*

Three compounds were screened against bacteria: aminochelin-sulfonamide **2-9**, Chakrapani's prodrug **2-22**, and "SO<sub>2</sub>-free" control **2-23**, which lacks the ability to produce SO<sub>2</sub>, but mimics the general structural features of **2-9** (Figure 2.33).

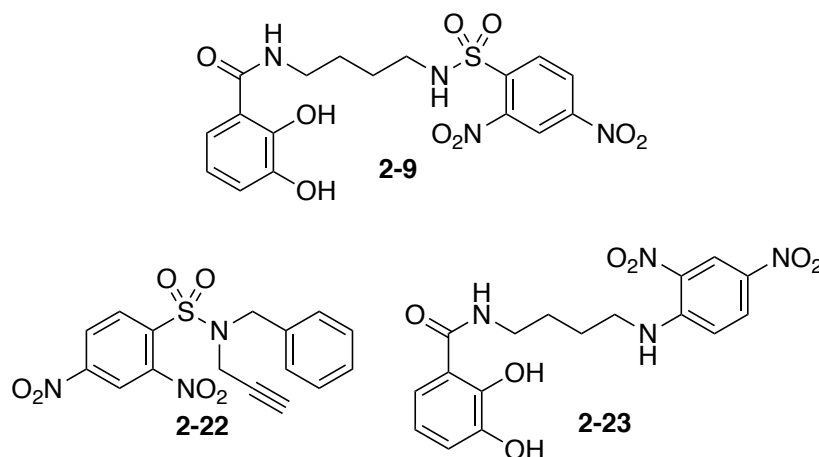


Figure 2.33 Structures of compounds that underwent biological screening.

## 2.7.1 Assays vs. *Staphylococcus aureus*

### 2.7.1.1 *S. aureus* and Siderophore Utilisation

The conjugates were initially tested for their biological activity vs. *Staphylococcus aureus* (NCTC 6571) to allow for comparison of **2-9** and **2-23** with the Chakrapani prodrug **2-22**, which has activity against MRSA.<sup>304</sup> *S. aureus* is a Gram-positive bacteria widely associated with human disease and infection, with a number of strains displaying extensive antibiotic resistance, including to the last resort antibiotic vancomycin.<sup>384</sup> However, around 30% of the human population are carriers of *S. aureus*, often with no ill effects.<sup>385</sup>

In terms of siderophores, *S. aureus* can produce two carboxylate-type siderophores, staphyloferrins A and B,<sup>103</sup> and a further metallophore, staphylopine (**Figure 2.34**), which may have a role in iron uptake, but is mostly involved in uptake of other vital metal ions ( $\text{Cu}^{2+}/\text{Ni}^{2+}/\text{Co}^{2+}/\text{Zn}^{2+}$ ).<sup>386</sup> Two further potential siderophores, named aureochelin and staphylobactin, have been identified but not characterised.<sup>103,387,388</sup> In addition to these mechanisms, *S. aureus* can utilise hydroxamate-type siderophores as xenosiderophores,<sup>104</sup> and even scavenge haem from haemoglobin in the body.<sup>103</sup> They also appear to be able to utilise catechol-containing molecules as xenosiderophores, although they only appear to offer significant growth promotion for strains unable to produce the native staphyloferrins.<sup>389</sup> Although catechol utilisation by *S. aureus* appears possible, it is unclear whether the catechol-sulfonamide will enter the cells via the siderophore uptake pathway, or via a similar uptake mechanism to Chakrapani's prodrugs.

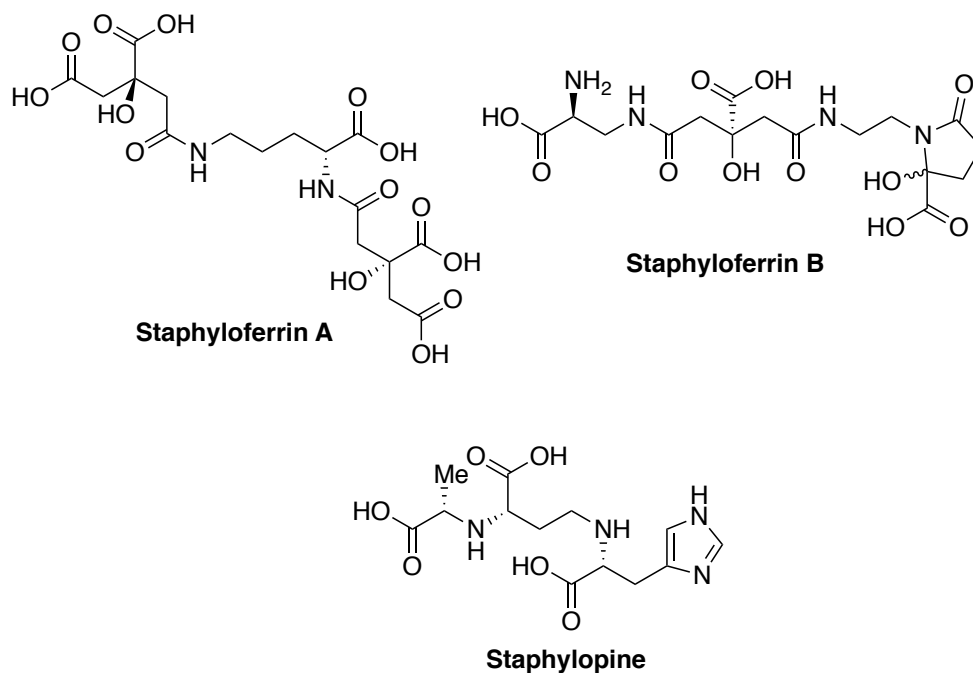


Figure 2.34 Siderophores produced by *S. aureus*.

### 2.7.1.2 Biological Screening and Results

The *S. aureus* cultures were grown overnight in tryptic soy broth (TSB), a nutrient-rich medium. From these overnight cultures, a master mix containing further TSB medium and a defined quantity of cultured cells was made up. Assays were carried out using an automatic plate reader method: a range of concentrations of the compounds to be tested are pipetted into a 96-well plate, along with the *S. aureus* master mix. The plate is maintained at 37 °C in a plate reader, and the OD<sub>600</sub> (the optical density at 600 nm) for each well is recorded at 30-minute intervals. The OD can be used as a measure of bacterial growth; a higher OD indicates higher bacterial growth. A range of concentrations between 500 μM and 100 nM were examined for each compound; initial stock solutions of **2-9**, **2-22** and **2-23** were made up in MeCN. Plain TSB solutions containing no cells were used as a negative control, with wells containing TSB and cells either with or without MeCN provided further controls. It should also be noted that **2-9** partially precipitates at the highest concentration used when added to the plate; to minimise this, it was often added just before beginning incubation.

Initial results proved promising: the first plate run involved only **2-9** and **2-22**, with **2-9** displaying antimicrobial activity at high concentrations (500  $\mu\text{M}$  to 50  $\mu\text{M}$ , **Figure 2.35**), although with a noticeable drop-off in activity for the 100  $\mu\text{M}$  and 50  $\mu\text{M}$  wells after 10 hours. The biphasic/diauxic shape of the growth curves is also different to the typical sigmoidal curves observed for bacterial growth.<sup>390</sup> This shape of growth curve can indicate a change in the metabolism of a bacteria,<sup>391</sup> or indicate the bacteria are able to tolerate the presence of an antimicrobial, and even overcome it completely.<sup>392,393</sup> **2-22** displays a similar profile, but with a much more significant drop-off in activity; the 50  $\mu\text{M}$  wells grow normally after 10 hours, and even the 500  $\mu\text{M}$  wells were not much different in OD to the plain TSB control after 24 hours. This is in contrast to the reported MIC value for prodrug **2-22** of 4  $\mu\text{g}/\text{mL}$ , which translates to c.10  $\mu\text{M}$ .<sup>304</sup> It should be noted that prodrug **2-22** was tested using a different assay method in the original paper, and evaluated against a different strain of *S. aureus*, which could be the reasons for this difference in activity. The  $\text{SO}_2$ -free control, **2-23**, was tested later, and showed no antimicrobial activity.

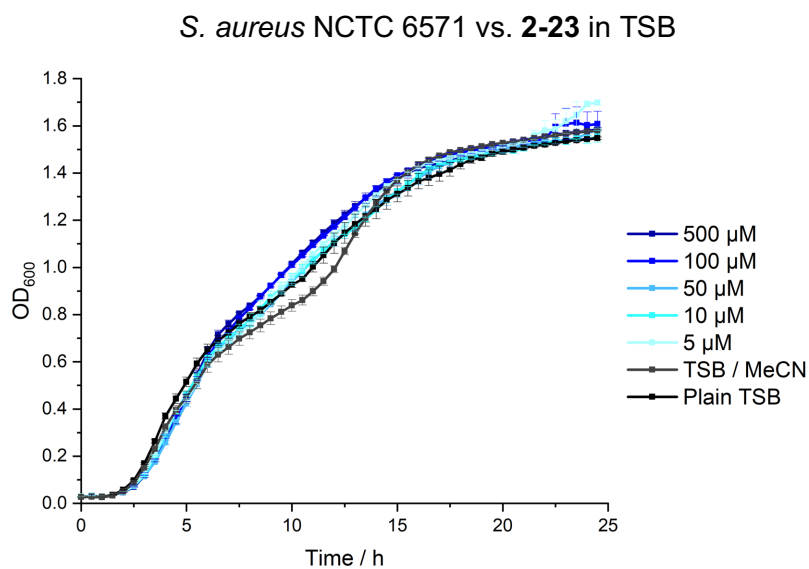
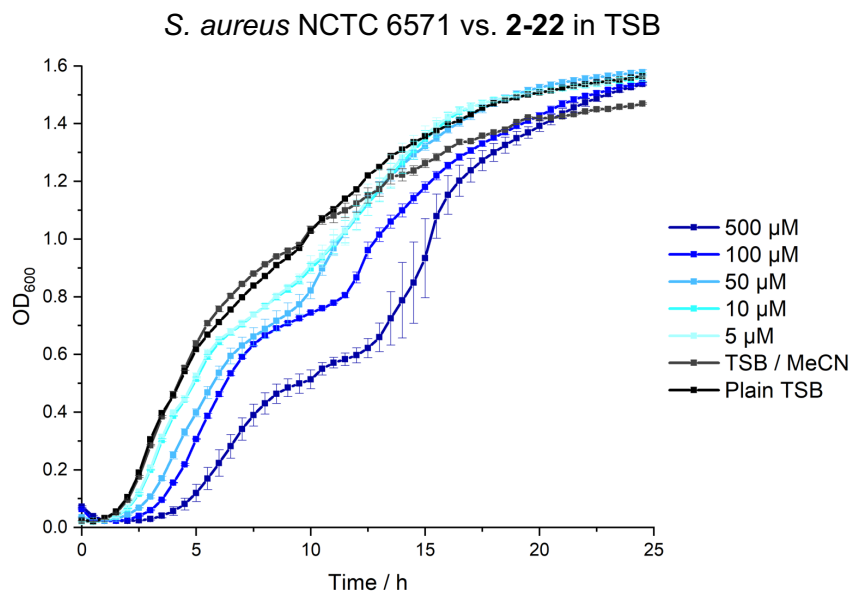
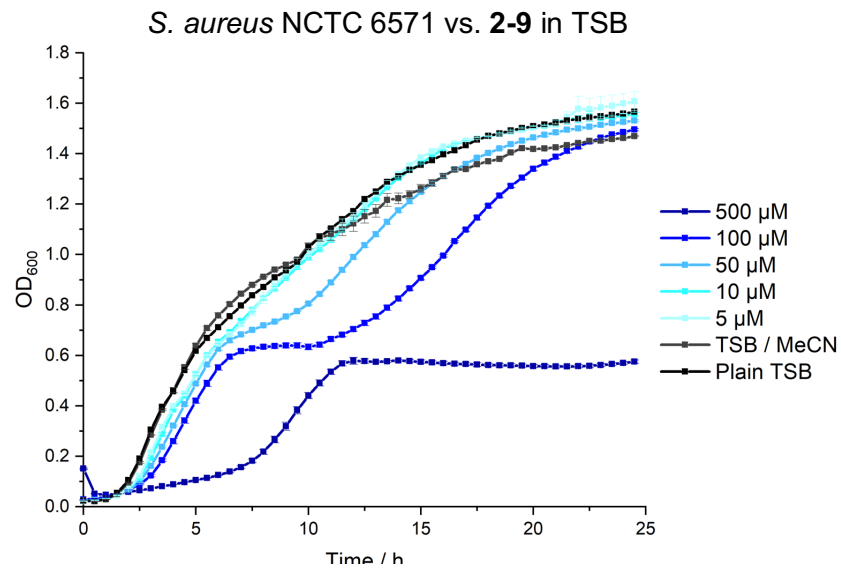


Figure 2.35 Growth curves for selected concentrations of **2-9**, **2-22** and **2-23** vs. *S. aureus* in Tryptic Soy Broth. Experiments for **2-9** and **2-22** are a mean average of 3 wells, **2-23** is a mean average of two wells. Error bars are calculated as the standard error of the mean.

The activity of **2-9** vs. *S. aureus* was probed for concentrations between 500 and 50  $\mu\text{M}$ , with a steady decrease in inhibition as the concentration of **2-9** decreases (**Figure 2.36**). The inhibition remains good up until 100  $\mu\text{M}$ . Following this plate, extracts from the 500  $\mu\text{M}$  and 250  $\mu\text{M}$  wells were spread out onto an agar plate to examine the viability of the bacteria remaining in the wells, and whether **2-9** is acting as a bacteriostatic or bacteriocidal antimicrobial. The extracts from both concentrations displayed good bacterial growth on the plate, demonstrating that the *S. aureus* is not completely killed, and pointing towards **2-9** acting in a bacteriostatic fashion (**Figure 2.37**).

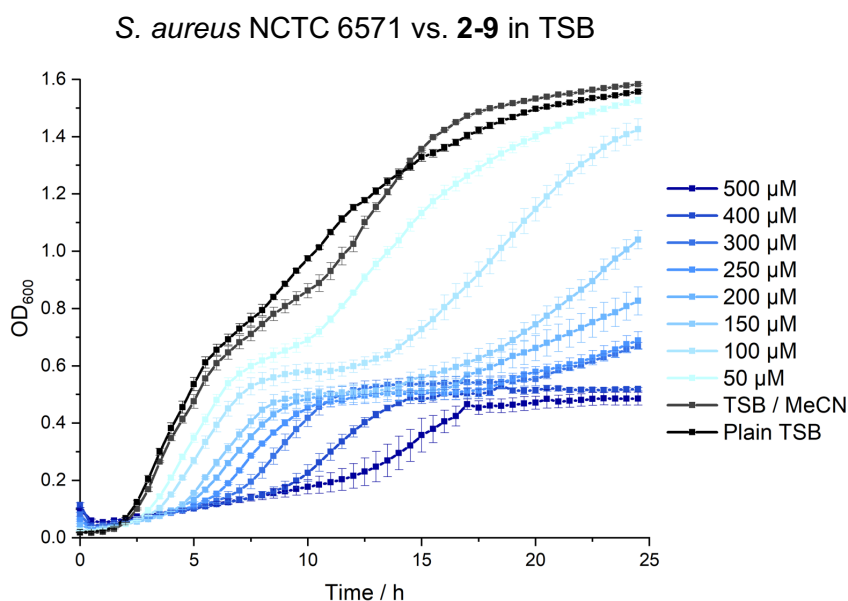


Figure 2.36 Growth curves for intermediate concentrations between 500 and 50  $\mu\text{M}$  of **2-9** vs. *S. aureus*. Curves are a mean average of three wells. Error bars are calculated as the standard error of the mean.

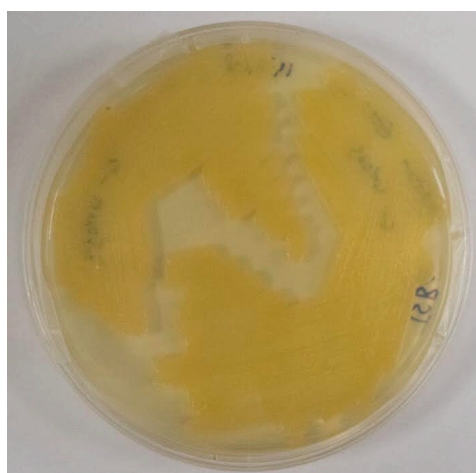


Figure 2.37 Photo of 500  $\mu\text{M}$  and 250  $\mu\text{M}$  wells plated onto agar at end of assay. Growth of golden *S. aureus* cultures can be observed.



As a rich and poorly-defined medium, TSB could potentially contain a number of components that could react with **2-9**, including cysteine. The stability of **2-9** in TSB was tested by replicating the original SO<sub>2</sub> release tests. 100 μM **2-9**, SO<sub>2</sub>-detecting dye **2-11** and TSB were combined in a cuvette and the UV-vis spectrum was observed over a 14-hour period. This showed minimal changes in the absorbance of the dye, indicating that **2-9** is stable in TSB, and suggests that any observed antimicrobial effects come from intracellular release of SO<sub>2</sub>, and not extracellular release in the medium. Although the UV-vis experiment is unable to replicate the biological conditions of the plate reader (37 °C, high stirring), the low rate of reaction suggests this wouldn't make a major difference.

## **2.7.2 Assays vs. *Bacillus subtilis***

### **2.7.2.1 *B. subtilis* and Siderophore Utilisation**

The compounds were also tested against *Bacillus subtilis* (strain 168), a non-pathogenic Gram-positive bacterium.<sup>394</sup> *B. subtilis* was chosen as it primarily makes and uses the catechol-type siderophore bacillibactin, an analogue of enterobactin, and its precursor 2,3-dihydroxybenzoylglycine (**Figure 2.38**).<sup>395</sup> In addition it can utilise a range of xenosiderophores, including hydroxamates like desferrioxamine and ferrichrome,<sup>396</sup> citrates,<sup>396</sup> and other catechols like enterobactin and petrobactin.<sup>397,398</sup> This use of catechol-type siderophores means *B. subtilis* is more likely than *S. aureus* to possess the required outer membrane receptors required for uptake of catechol-sulfonamide **2-9**.

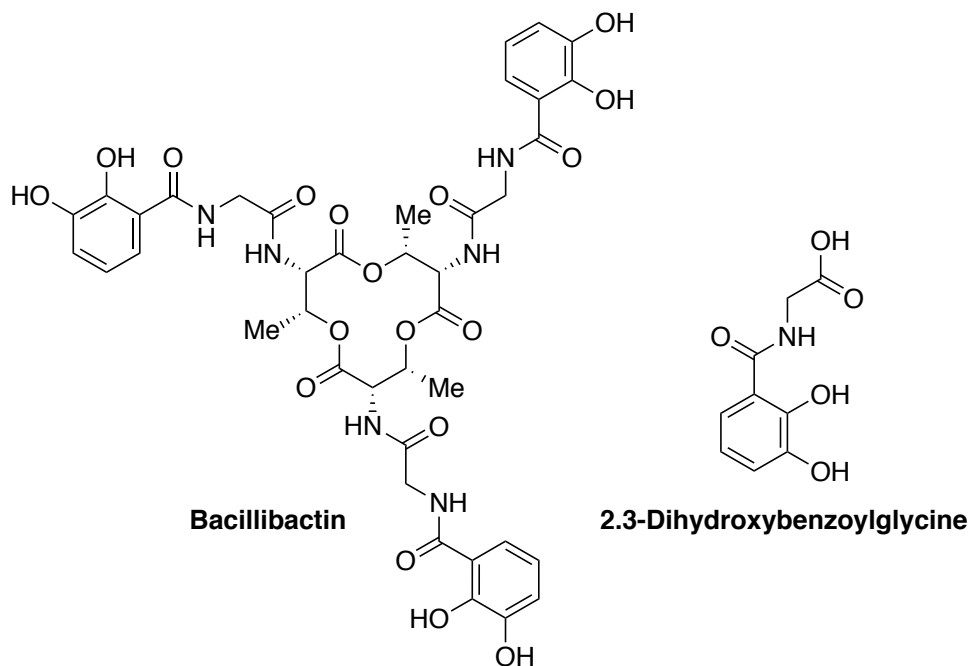
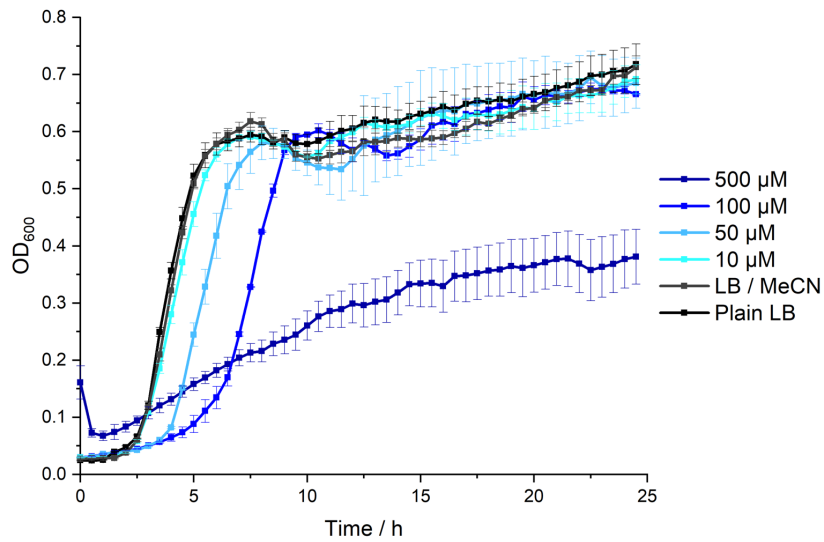


Figure 2.38 Structures of bacillibactin and *N*-2,3-dihydroxybenzoylglycine, native siderophores of *B. subtilis*.

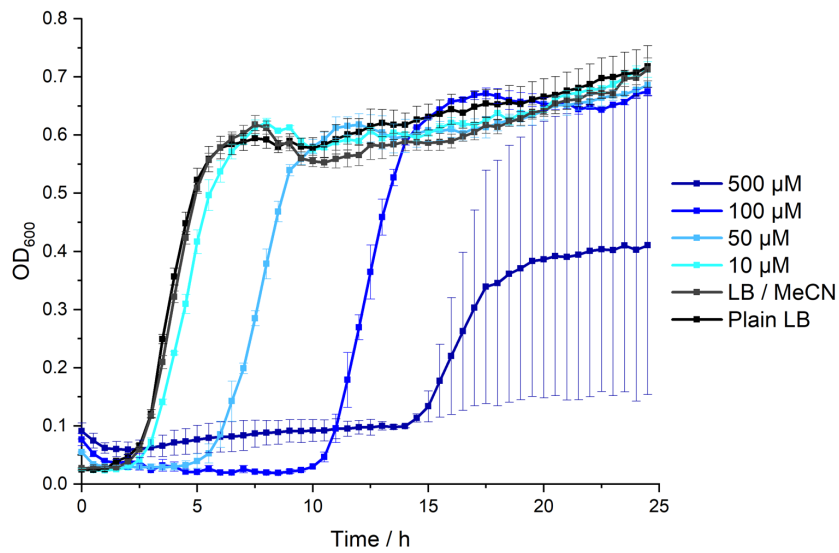
### 2.7.2.2 Biological Screening and Results

The main difference between the *S. aureus* and *B. subtilis* assays was the use of Lysogeny broth (LB) medium, another rich medium preferred over TSB for growing *Bacillus*. The results of the assay are similar to those for *S. aureus*. **2-9** is weakly active, with the 50 and 100  $\mu\text{M}$  wells displaying growth inhibition for 4 and 7 hours respectively, before reverting to normal growth, and the 500  $\mu\text{M}$  wells maintained a steady level of inhibition throughout. **2-22** proves slightly more active, with the 50 and 100  $\mu\text{M}$  wells showing growth inhibition for 6 and 11 hours respectively, and a longer delay for 500  $\mu\text{M}$  (the large error bars are the result of differing growth profiles for the duplicate **2-22** wells). The  $\text{SO}_2$  control **2-23** was again inactive (**Figure 2.39**).

*B. subtilis* 168 vs. **2-9** in LB



*B. subtilis* 168 vs. **2-22** in LB



*B. subtilis* 168 vs. **2-23** in LB

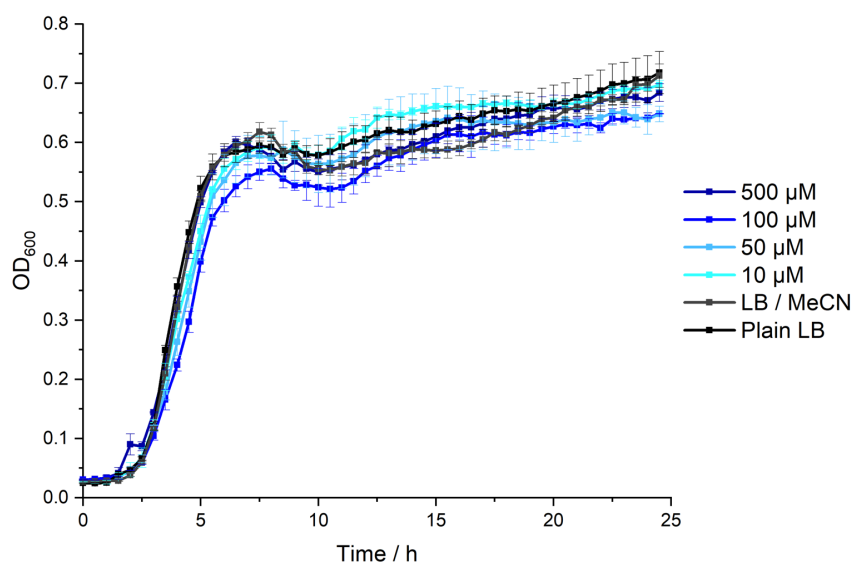


Figure 2.39 Growth curves for selected concentrations of **2-9**, **2-22** and **2-23** vs. *B. subtilis* in LB media. Experiments are an average of two wells. Error bars are calculated as the standard error of the mean.

## 2.7.3 Assays vs. Wild-Type *Escherichia coli*

### 2.7.3.1 *E. coli* and Siderophore Utilisation

Following the experiments with the two Gram-positive species, the compounds were then examined against *Escherichia coli* (BW25113), a Gram-negative bacterium. *E. coli* is considered the most widely-studied prokaryotic organism, perhaps due to the ease of culturing it in a laboratory environment; in favourable growth conditions *E. coli* can divide up to once every 20 minutes.<sup>399</sup> Like *S. aureus* it can be both a commensal and a pathogenic bacterium; it is often widely present in the gut microbiome in humans,<sup>400</sup> but certain strains can cause food poisoning and urinary tract infections.<sup>401</sup>

*E. coli* can produce and utilise a range of catechol-type siderophores consisting mainly of the widely-studied tris(catecholate) siderophore enterobactin and its breakdown products, such as 2,3-dihydroxybenzoylserine and 2,3-dihydroxybenzoic acid (**Figure 2.40**).<sup>105,402</sup> A further catecholate siderophore, the glycosylated enterobactin derivative salmochelin, is produced by some strains, and has been heavily linked to pathogenicity, as the glycosylation prevents recognition and binding of the siderophore by proteins in the immune system.<sup>403–406</sup> A number of strains also produce the hydroxamate siderophore aerobactin and the mixed siderophore yersiniabactin<sup>407–410</sup>; like with salmochelin, production of these two siderophores is often associated with pathogenicity, although non-pathogenic *E. coli* can also synthesise and use them.<sup>410</sup>

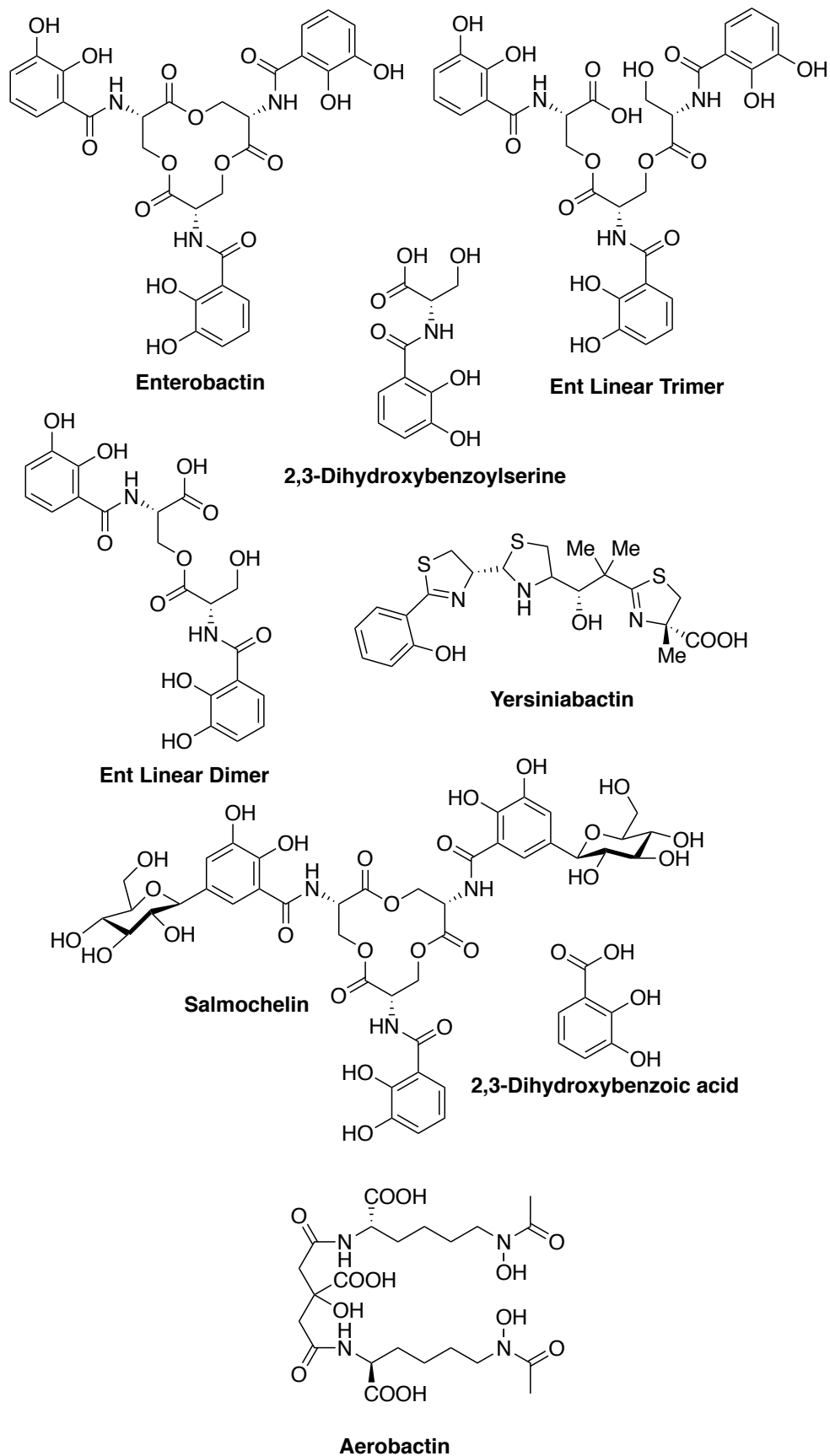


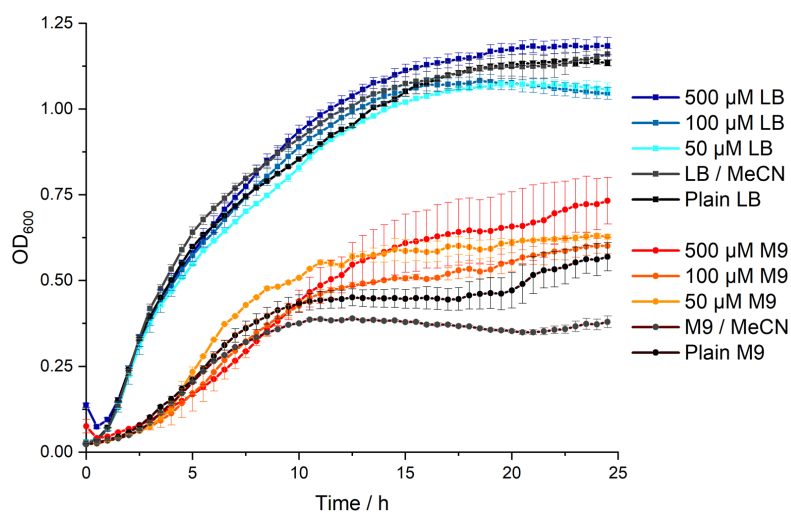
Figure 2.40 Native siderophores that can be biosynthesised by various *E. coli* strains. Production of siderophores is strain-dependent (i.e. Not all strains will be able to make all of these siderophores).

### 2.7.3.2 Biological Screening and Results

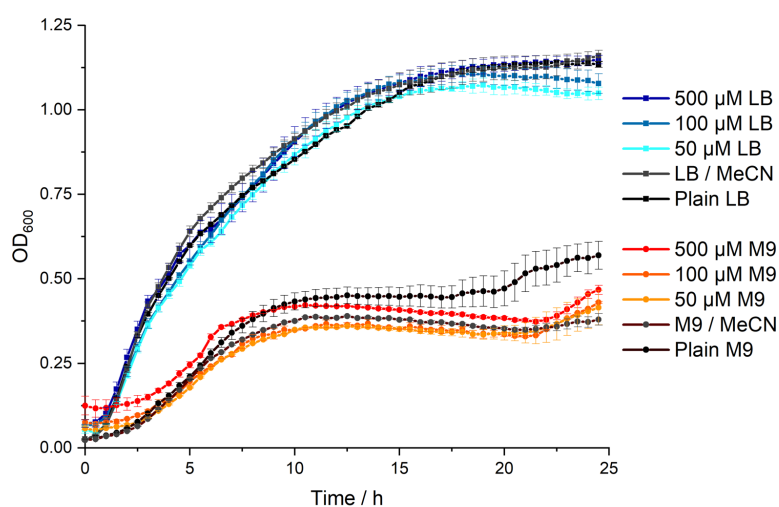
The SO<sub>2</sub> prodrugs and controls were initially tested against *E. coli* cultured overnight in LB medium, which is likely to be rich in iron. Unfortunately, none of the compounds tested were active against *E. coli* (**Figure 2.41**). This could be due to the relative abundance of iron in the medium, resulting in the depletion of outer membrane receptors, which are generally not present in iron-rich conditions),<sup>85</sup> or due to the presence of native siderophores with higher affinity for iron, which could outcompete **2-9** and **2-23** for iron binding, and therefore prevent uptake.

To try and create conditions where **2-9** might be taken up, and to better mimic the iron-poor growth conditions that would be present in the body, the *E. coli* were cultured in M9 minimal medium. As described in Section 2.5, M9 is a nutrient-poor and chemically well-defined medium consisting only of essential salts plus a carbon source (glucose) and a nitrogen source (NH<sub>4</sub>Cl). It lacks the undefined protein digests or yeast extracts present in LB or TSB, which are likely to be a major source of iron. However, similar to the results in LB, all three compounds tested again proved to be inactive against *E. coli*, with the graphs for **2-9** and **2-22** broadly similar to those for the M9 + MeCN control (**Figure 2.41**). Interestingly, all of the wells containing **2-9** and **2-23** grew better than the M9 + MeCN control, with even the 100 nm well reaching a final OD<sub>600</sub> greater than 0.55, compared to 0.40 for the MeCN control. This potentially suggests the catechols of these conjugates can engage in growth promotion, although there is little differentiation in growth between the different siderophore concentrations, so it is hard to say if this is a true effect.

*E. coli* BW25113 vs. **2-9** in LB/M9 Media



*E. coli* BW25113 vs. **2-22** in LB/M9 Media



*E. coli* BW25113 vs. **2-23** in LB/M9 Media

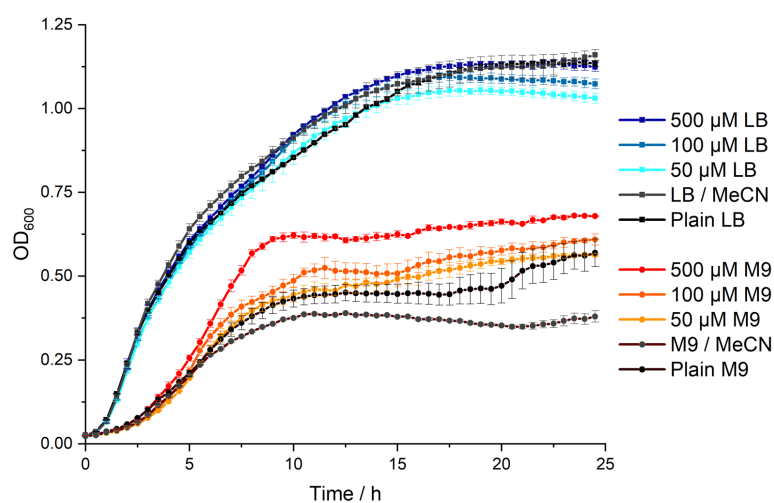
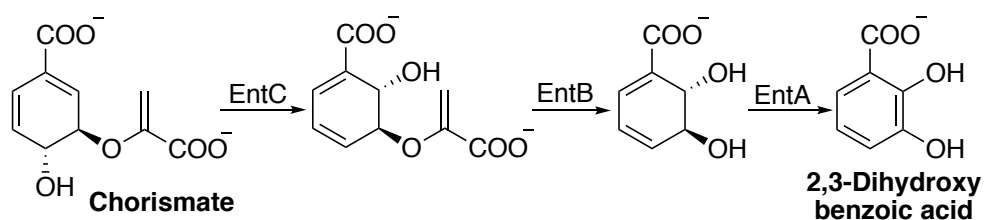


Figure 2.41 Growth curves for selected concentrations of **2-9**, **2-22** and **2-23** vs. *E. coli* in both LB media (blue, squares) and M9 media (red, circles). Experiments are an average of two wells. Error bars are calculated as the standard error of the mean.

It is possible that compound uptake is still taking place at a reduced rate compared to *S. aureus* or *B. subtilis*; combined with the weak antimicrobial activity observed against Gram-positive bacteria, this could result in any detrimental effects on the cells being attenuated due to the reduced concentrations present inside the cells. It is also possible that in the iron-poor conditions of M9, *E. coli* is producing high-affinity siderophores like enterobactin, or its linear forms, which will outcompete the monocatechol for iron binding. As iron binding is required for siderophore uptake, this would prevent any uptake of **2-9** via siderophore active transport pathways.

#### 2.7.4 Assays vs. *entA*-deficient *Escherichia coli*

To examine whether the siderophores produced by *E. coli* were outcompeting **2-9**, further assays were carried out on an *entA*-deficient strain of *E. coli*, JW0588-1. This strain lacks the gene for production of the EntA enzyme, which is responsible for catalysing the final step in the biosynthesis of 2,3-dihydroxybenzoic acid from chorismate (**Scheme 2.24**).<sup>411,412</sup> As all of the strongest native siderophores, and all of the catechol-type siderophores produced by *E. coli* stem from 2,3-dihydroxybenzoic acid, the mutant should be unable to produce and secrete any siderophores that will vastly outcompete the catechol-sulfonamides (it is unclear whether this strain can produce aerobactin or yersiniabactin). Previous research from the AKDK group has shown that the mutant retains the ability to take up siderophores, as growing the bacteria on iron-poor agar plates in the presence of enterobactin and other known siderophores offers excellent growth recovery compared to negative controls.<sup>413</sup>



Scheme 2.24 Pathway for biosynthesis of 2,3-dihydroxybenzoic acid from chorismate.<sup>412</sup>

Previous work carried out in the AKDK group with the *entA* mutant also showed that it fails to grow when cultured in plain M9, but grows



successfully when cultured in M9 supplemented with casamino acids,<sup>413</sup> a mixture of almost all of the essential amino acids (apart from tryptophan) and some small peptides obtained from acid hydrolysis of the protein casein.<sup>414</sup> It was suggested that some of the amino acids present had the potential to act as weak siderophores, and therefore help to restore growth of the mutant, although it may also be possible that trace iron is present in the casamino acids. Replication of this behaviour in the *entA* mutant was attempted, however, growth of the *entA* mutant in overnight cultures in plain M9 media proves inconsistent, with confluent growth observed c. 50% of the time. It is possible the mutant is very sensitive to slight changes in the culture medium, and hence is hard to grow consistently.

The activity of **2-9** was tested against cultures of the *entA* mutant. No activity was observed for **2-9** vs. the *entA* mutant in the casamino acid culture, but when **2-9** is screened against confluent cultures of plain M9, growth inhibition can be observed at 250  $\mu$ M and 50  $\mu$ M, suggesting that in the absence of siderophores in these conditions **2-9** can be taken up and provide an antimicrobial effect (**Figure 2.42**). Despite the inconsistent nature of the overnight growth of the *entA* mutant, this result is reproducible when *entA* cultures in M9 present with confluence in overnight growth.

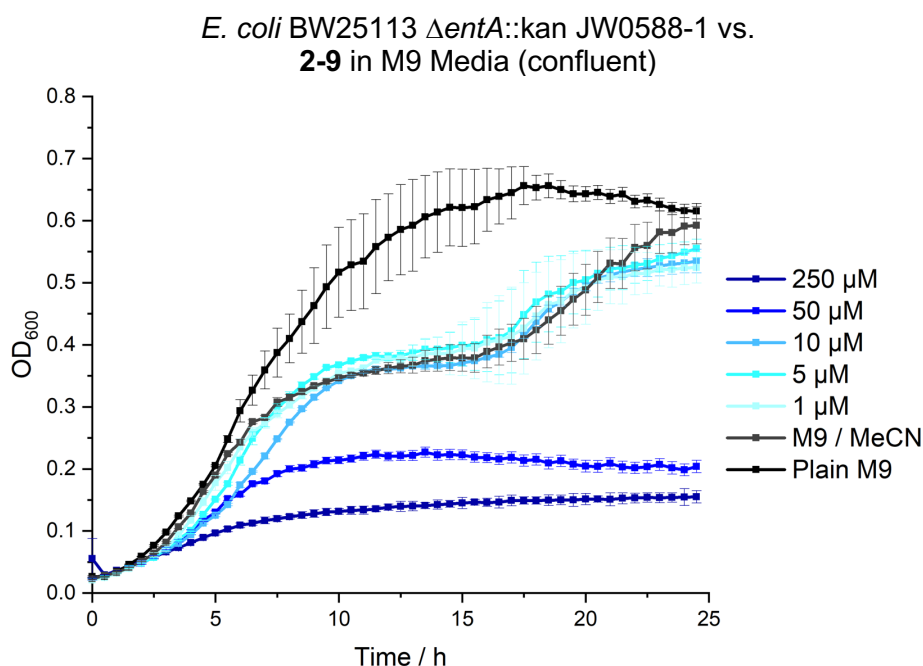


Figure 2.42 Growth curves for concentrations of **2-9** vs. *E. coli entA* mutant in plain M9 media (confluent overnight growth). Experiments are an average of two wells. Error bars are calculated as the standard error of the mean.

To try and find reproducible results in the media, a Chelex-treated M9 medium was utilised instead. Chelex is a polymeric resin containing iminodiacetic acid groups, which can form complexes with transition metal ions. By treating the salt and glucose solutions used to make up the M9 medium with Chelex, trace transition metals, including any iron present, should be removed from the medium, leaving it as close to iron-free as possible. This allows the amount of iron present to be precisely controlled.

A 4-way overnight culture experiment was carried out with wild-type *E. coli* and the *entA* mutant to observe how well they grow in Chelex-treated cultures; this time both were grown in Chelexed M9, and Chelexed M9 with 10  $\mu\text{M}$  Fe(NTA) added. Fe(NTA) provides a soluble source of iron, and shouldn't interfere with the complexation behaviour of **2-9** or **2-23**. After incubating overnight at 37  $^{\circ}\text{C}$ , both of the strains in M9 with 10  $\mu\text{M}$  Fe(NTA) displayed good growth, reaching OD<sub>600</sub>'s of 3.00 for the wild type and 2.88 for the mutant, whereas the cultures in Chelexed M9 only displayed hindered/no growth, with the wild type reaching an OD<sub>600</sub> of 0.28, and the *entA* mutant displaying no growth (**Figure 2.43**).



Figure 2.43 Photo of overnight cultures for wild-type (1 and 3) and *entA* mutant (2 and 4) in Chelex-treated M9 (left) and Chelex-treated M9 + 10  $\mu\text{M}$  Fe(NTA) (right).

Plate assays with **2-9** and **2-23**, were carried out for the *entA* mutant culture grown overnight in M9 + 10  $\mu\text{M}$  Fe(NTA); the clear culture in plain Chelex M9 was avoided due to the lack of overnight growth. To try and create iron-free conditions for the cells grown in Chelex M9 plus Fe(NTA), an aliquot of the overnight culture was taken and centrifuged to pellet the cells, then the iron-containing media removed and fresh iron-free Chelex M9 added before adding the cells to the plate medium. This ensures the cells are growing in an iron-free medium, and allows addition of a defined number of cells, unlike in the assays where a clear culture is used. The cells, despite being present in an iron-free medium on the plate, displayed remarkably good growth in the M9 control, although they showed an increased sensitivity to the MeCN control, such that no further growth was seen after 10 hours (**Figure 2.44**). For **2-9**, no significant inhibitory activity beyond that observed for the MeCN control could be seen. The wells containing **2-23** however displayed growth promotion to a much higher level than the MeCN control for the highest concentrations. This suggests that **2-23** can potentially act as a siderophore, and promote growth recovery. The good growth observed despite the lack of iron in the media is likely down to iron storage by the bacteria during their overnight growth in the relatively iron-rich overnight culture.

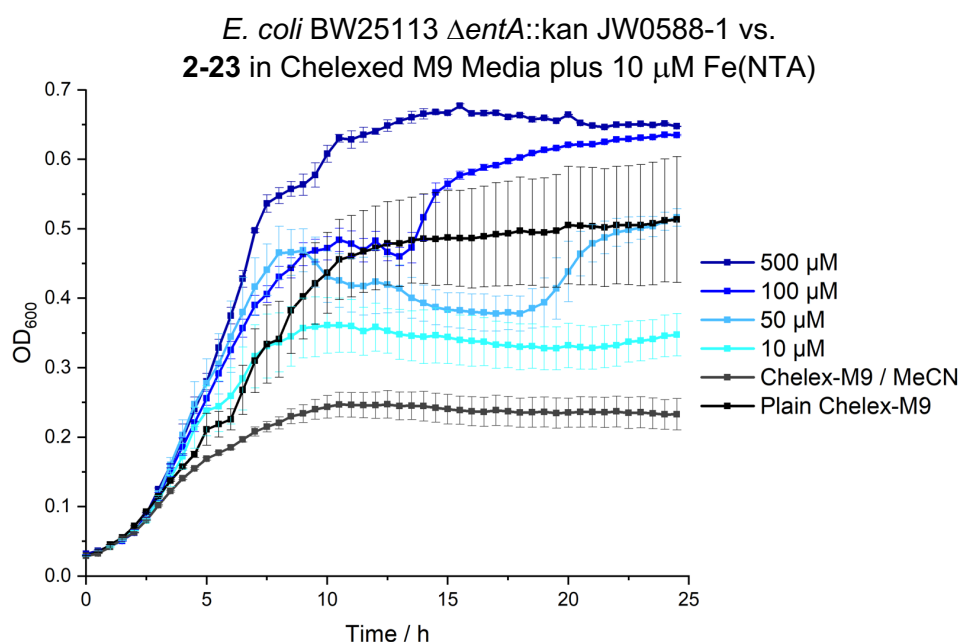


Figure 2.44 Growth curves for selected concentrations of **2-23** vs. *entA* mutant cultured overnight in Chelex M9 plus 10  $\mu\text{M}$  Fe(NTA). Experiments are an average of two wells. Error bars are calculated as the standard error of the mean.

### 2.7.5 Discussion of Biological Results

From the results obtained, it is clear that catechol-sulfonamide **2-9** is a poor to moderate antimicrobial when used against Gram-positive bacteria, and a very poor one when used against Gram-negative bacteria. Activity is potentially possible under certain conditions of iron limitation and only with an *E. coli* mutant unable to produce its own siderophores, although the exact conditions to yield reproducible results have proved hard to find. As SO<sub>2</sub>-free control **2-23** shows no inhibitory properties in any of the plate reader assays, it can be concluded that SO<sub>2</sub> release is the main mode of action for **2-9**. The biphasic growth, and the bacteriostatic nature of the inhibition, observed for bacteria treated with **2-9** and **2-22** indicates a degree of tolerance to SO<sub>2</sub> release, or the development of resistance over time.

This is a result comparable to an existing literature result with an aminochelin conjugate of linezolid (**1-14**), an oxazolidinone antibiotic usually inactive against Gram-negative bacteria (**Figure 2.13**).<sup>187</sup> This conjugate displayed increased activity compared to the parent drug against *P. aeruginosa*, but only up to 8 times (from 1024 μM to 128 μM). The activity of linezolid against Gram-positive bacteria is between 1 and 26 μM, depending on the strain, but often tends towards 1 to 6 μM.<sup>52</sup> This means a 100-fold difference in the activity between linezolid in Gram-positive bacteria and the aminochelin conjugate in Gram-negative bacteria; a similar difference in activity for catechol-sulfonamide **2-9** would place its MIC in Gram-negative bacteria outside the range of concentrations tested (>500 μM), hence no observed growth inhibition.

In terms of iron transport, it is hard to conclude that **2-9** exploits iron transport pathways in Gram-positive bacteria without further experimentation, however the results for **2-23** in M9 with the *entA* mutant suggest that the monocatechol moiety is capable of acting as a siderophore and boosting growth, so could potentially provide the siderophore component of a Trojan Horse conjugate given the right system. It should also be noted here that further research in the AKDK group carried out by James Southwell found M9 media to retain a high concentration of iron even post-treatment with Chelex (>100 μM), likely due to the strong iron binding ability

of phosphate groups present in the media (see Section 2.5). This leads to doubts other whether M9 can be considered an iron-poor media with such a high iron content, and other iron-deficient media should be explored for the study of these conjugates.

## 2.8 Summary and Conclusions

Aminochelin-bearing 2,4-dinitrobenzenesulfonamide conjugate **2-9**, and two related analogues **2-15** and **2-19** (Figure 2.45), have been successfully synthesised and characterised by  $^1\text{H}/^{13}\text{C}$  NMR and ESI mass spectrometry. The  $\text{SO}_2$ -releasing ability of each conjugate on reaction with the biological thiol glutathione was studied via UV-vis spectroscopy in aqueous buffer. The presence of aminochelin does not significantly impair the rate of  $\text{SO}_2$  release from **2-9** compared to catechol-free conjugate **2-19** or benzylamine conjugate **1-56**, however slower release is observed for conjugate **2-15**, which contains a shorter linker between the catechol and 2,4-dinitrobenzenesulfonamide units. Iron conjugates of **2-9** and **2-15** display a faster rate of  $\text{SO}_2$  release, potentially indicating the reduced  $\text{SO}_2$  release rate for **2-15** stems from an interaction between the catechol group and the 2,4-dinitrobenzenesulfonamide, although the faster rates could be due to the electron-withdrawing ability of the coordinated iron.

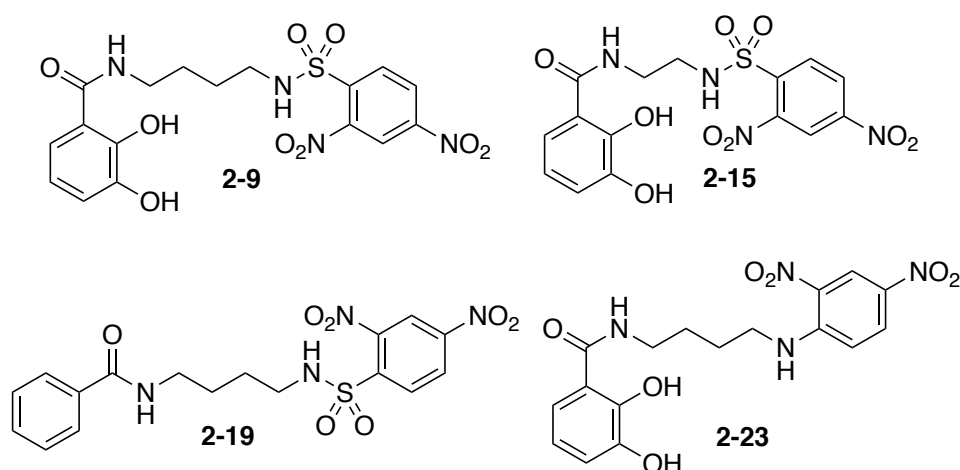


Figure 2.45 Structures of synthesised 2,4-dinitrobenzenesulfonamide conjugates **2-9**, **2-15** and **2-19**, and microbiological “ $\text{SO}_2$ -free” control **2-23**.

The antimicrobial activity of aminochelin conjugate **2-9** was evaluated against three bacterial species, *S. aureus*, *B. subtilis* and *E. coli*. **2-9** proved

active at high concentrations vs. *S. aureus* and *B. subtilis*, both Gram-positive bacteria, but inactive against Gram-negative *E. coli* at the concentrations tested. Antimicrobial activity can be observed against an *entA* mutant of *E. coli* incapable of producing its own siderophores, suggesting the lack of activity against wild-type *E. coli* stems from stronger native siderophores outcompeting the aminochelin unit of **2-9** for iron binding, preventing sufficient uptake. An SO<sub>2</sub>-free control with a similar structure, **2-23**, proved inactive against all bacteria tested, indicating SO<sub>2</sub> as the source of antimicrobial activity. In some cases, **2-9** and **2-23** can be shown to mediate growth promotion of *E. coli*, suggesting aminochelin can act as a siderophore for *E. coli* under certain conditions.

Some notable conclusions can be made from the work presented above. The ability of conjugates like **2-9** to undergo successful reaction with thiols, and subsequent SO<sub>2</sub> release, in the presence of siderophore units like aminochelin is promising for the development of future SO<sub>2</sub>-releasing siderophore conjugates. Likewise, the presence of a siderophore component appears to offer some weak benefits to the antimicrobial activity of SO<sub>2</sub>-releasing prodrugs, most notably in *S. aureus*, where greater activity is observed for **2-9** than Chakrapani prodrug **2-22**. However, the overall activity of **2-9** is disappointing, with high concentrations required to exert antimicrobial activity against Gram-positive bacteria, and a lack of activity vs. Gram-negative bacteria, likely due to the aminochelin unit of **2-9** being outcompeted for iron binding, and therefore uptake, by native siderophores.

## 2.9 Future Work

In terms of future work with the existing conjugates, the main aim would be to obtain consistency in the biological results, which has proved somewhat difficult so far. Alternate methods of enforcing iron deficiency, for example the use of 2,2'-bipyridine (bpy) to complex and withhold and iron present, could be explored.<sup>163</sup> The activity of the iron-complexed forms of **2-9** and **2-23** could also be examined. Iron complexation is vital for uptake of the siderophores, as studies like that by Zamora *et al.* have shown.<sup>362</sup> By pre-

forming the siderophore-iron complexes, either with an equimolar amount of iron, or a fixed concentration across all of the siderophore concentrations, the uptake in *E. coli* may be improved, and any growth promoting/inhibiting effects will become clearer to see. In a similar vein, the activity of gallium complexes of **2-9** and **2-23** could be examined. Ga(III) ions have a similar ionic radius to Fe(III), and can therefore form strong complexes with siderophores.<sup>193,415</sup> However, they lack the redox properties of Fe(III) ions, and as such can exert an inhibitory effect on bacterial growth.<sup>193</sup> The activity of **2-15** and **2-19** vs. bacteria should also be assessed; it would be interesting to examine whether the reduced SO<sub>2</sub> release rate seen for **2-15** translates into a significant change in antimicrobial activity.

As well as this, the effects of **2-9** and **2-23** could also be explored vs. other bacterial species, for example *Campylobacter jejuni*. This Gram-negative bacterium is unable to produce its own siderophores, but possesses several xenosiderophore uptake pathways, including one for enterobactin and its derivatives.<sup>362</sup> Zamora *et al.* carried out a study on *C. jejuni* where they examined growth recovery on addition of enterobactin and its hydrolysis products to the growth media. The results show similar or equal growth recovery when the bacteria were cultured with enterobactin and its monocatechol hydrolysis product, 2,3-dihydroxybenzoylserine, or other monocatechol containing analogues.<sup>362</sup> This suggests that *C. jejuni* is equally as good at utilising monocatechols as xenosiderophores as it is in using enterobactin, so **2-9** may be taken up more efficiently compared to in *E. coli*, and hence exert a greater antimicrobial effect.

The poor antimicrobial activity observed for the synthesised conjugates, and the relatively poor activity against *E. coli* and *S. aureus* of the prodrugs developed by Chakrapani and colleagues,<sup>304</sup> likely precludes the future development of SO<sub>2</sub>-releasing prodrugs of this type for targeting bacteria, especially Gram-negative bacteria. However, the use of stronger iron-binding siderophore units like the hexadentate hydroxamate desferrioxamine B over the monocatechol used in this case would be essential to reduce the issue of poor activity due to out-competition of the

conjugates for iron binding by native siderophores (**Figure 2.46**). In a similar fashion, the use of bis/tris(catecholate) siderophores could also be explored.

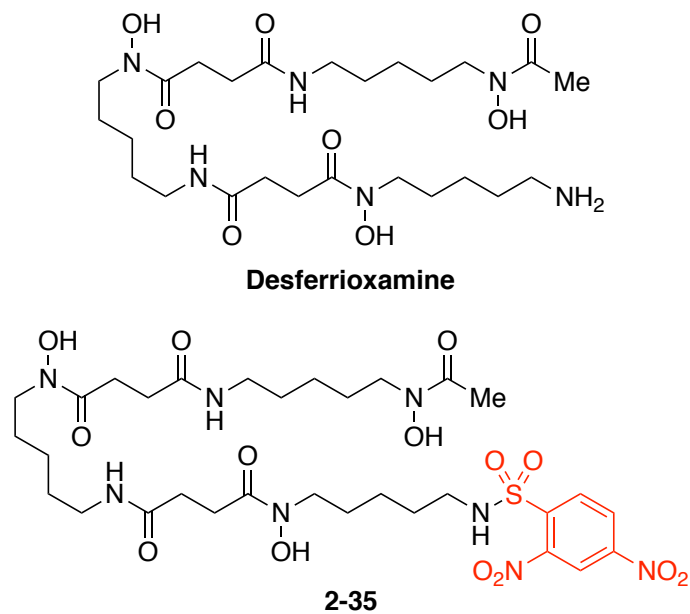


Figure 2.46 Structure of hydroxamate siderophore desferrioxamine B, and potential structure of a future SO<sub>2</sub>-releasing prodrug **2-35** based on desferrioxamine B.



**Chapter 3 :  
Synthesis and  
Characterisation  
of a SO<sub>2</sub>-Releasing  
Ciprofloxacin-Based  
Trojan Horse Conjugate**

### 3.1 Introduction

Following the studies discussed in Chapter 2, the focus moved away from the use of SO<sub>2</sub> as the sole antimicrobial source in a Trojan Horse conjugate, and towards utilising a SO<sub>2</sub>-releasing biolabile linker for release of an additional antimicrobial component. While the initial studies suggest antimicrobial activity with SO<sub>2</sub>-releasing conjugates can be achieved under certain conditions (Chapter 2), the antimicrobial activity was not sufficiently strong against the bacterial strains examined to be used as the sole mechanism of antimicrobial action in a Trojan Horse conjugate. However, SO<sub>2</sub> release may be sufficient to offer some additional activity in combination with an additional antimicrobial, making such a conjugate a dual-action antibiotic. The studies in Chapter 2 also suggest that the presence of a siderophore component is compatible with rapid SO<sub>2</sub> release, which is ideal for the design of a biolabile linker, although optimisation of the siderophore component for maximal uptake of SO<sub>2</sub>-releasing conjugates is required. In this Chapter, the synthesis and investigation of SO<sub>2</sub>-releasing conjugates containing a 4-carboxyl-2-nitrobenzenesulfonamide unit as the biolabile linker, and the fluoroquinolone antibiotic ciprofloxacin as the antimicrobial component, is discussed.

#### 3.1.1 Structure of SO<sub>2</sub>-Releasing Linker

As discussed in Chapter 2, the high release rates of SO<sub>2</sub> from 2,4-dinitrobenzenesulfonamides are well established,<sup>301,303,304,319</sup> and the release mechanism appears to be compatible with the presence of siderophores. Therefore, the first choice of potential biolabile SO<sub>2</sub>-releasing linker for the synthesis of a siderophore-antimicrobial conjugate aimed to deviate as little as possible from the 2,4-dinitrobenzene structure. In a biolabile SO<sub>2</sub>-releasing linker, the antimicrobial component needs to be bound to the sulfonamide of the SO<sub>2</sub>-releasing ring (**Figure 3.1**). This creates the need for an additional functional group on the ring for conjugation of the siderophore component. To maintain the electron-withdrawing abilities of the ring, this functional group should ideally also be an electron-withdrawing group. A good choice for this was considered to be a carboxylic acid group; while not as electron-withdrawing as a nitro group, it is still

reasonably electron-withdrawing, with a Hammett parameter  $\sigma_p = 0.45$ , compared to  $\sigma_p = 0.78$  for a nitro group.<sup>416</sup> It also offers a range of potential chemistries for attachment of a siderophore unit.

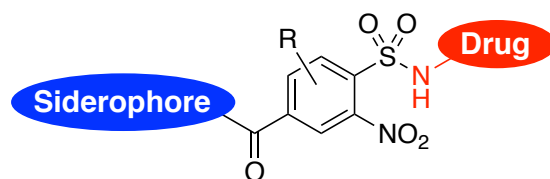
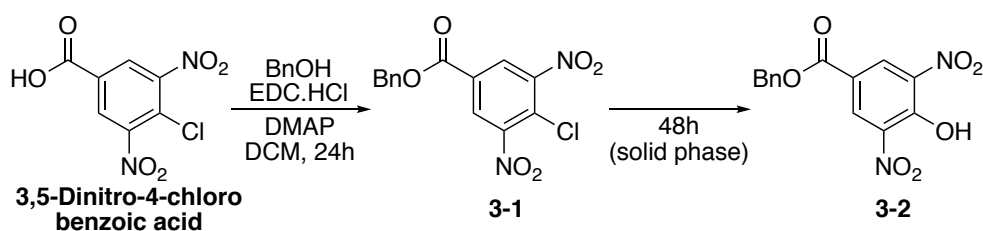


Figure 3.1 Schematic to demonstrate generic structure of target siderophore-sulfonamide-antimicrobial conjugate.

Initially, the design aimed to maintain the two nitro groups on the benzene ring and introduce an additional carboxylic acid group. However, brief experimentation with a route starting from 3,5-dinitro-4-chlorobenzoic acid disfavoured this idea; the product formed after initial esterification of the carboxylic acid (**3-1**) decomposes over a couple of days (in the solid state), with replacement of the chloro group with a hydroxy group, suggesting a reaction with water (**Scheme 3.1**). This high reactivity demonstrates the unsuitability of the 3,5-dinitrobenzoic acid ring for this design; even if a sulfonamide could be synthesised without significant decomposition, it is likely to be highly unstable in aqueous media, or even in air, especially with the greater electron-withdrawing ability of the sulfonamide compared to the chloro group.



Scheme 3.1 Esterification and subsequent decomposition of 3,5-dinitro-4-chlorobenzoic acid.

The decision was taken to try and construct a linker with one nitro group to reduce the overall electron-withdrawing character of the ring, whilst still retaining its ability to release  $\text{SO}_2$ . The most obvious route to this is the replacement of one of the nitro groups with the intended carboxyl group to give a 4-carboxyl-2-nitrobenzene ring (**Figure 3.2**). This maintains the *ortho*, *para* positioning of the electron-withdrawing groups, as seen in the 2,4-

dinitrobenzenesulfonamides, allowing maximal activation of the sulfonamide carbon towards nucleophilic aromatic substitution.

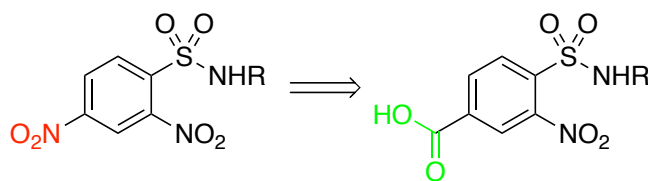
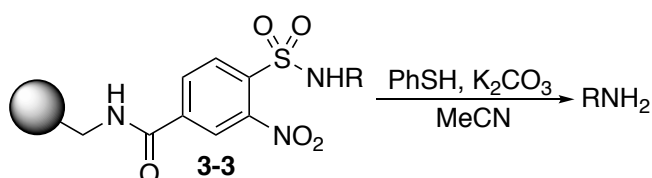


Figure 3.2 Exchange of nitro group for carboxylic acid group in biolabile linker design.

A number of examples of sulfonamides based on the 4-carboxyl-2-nitrobenzene ring, or a similar system, exist in the literature, often acting as cleavable linkers for various constructs. To the best of the author's knowledge, the first example of a cleavable 4-carboxyl-2-nitrobenzenesulfonamide unit was published by Kay *et al.* in 1997.<sup>417</sup> Inspired by the nosyl protecting groups developed by Fukuyama *et al.*,<sup>418</sup> they aimed to develop similar chemistry for linkers in solid-phase synthesis, with thiol-mediated cleavage of the sulfonamide as a release mechanism for an amine-bearing product. The sulfonamides were bound to a resin via an amide linkage (**3-3**, **Scheme 3.2**). Cleavage was achieved at room temperature on treatment of the solid-phase linker with 1-2 equivalents of potassium thiophenoxide (formed in situ from thiophenol/ $K_2CO_3$ ).



Scheme 3.2 Structure of solid-phase linker employed by Kay *et al.*, and method of cleavage to generate free amine.<sup>417</sup>

Further examples of solid state linkers of this type have been widely used in the construction of “reporter resins”, where the sulfonamide nitrogen is alkylated with a highly UV-active derivative such as anthracene (**3-4**, **Figure 3.3**),<sup>419–423</sup> or in synthetic methodology, for example by Pattarawarapan *et al.* for the synthesis of bifunctionalised scaffolds (**3-5**, **Figure 3.4**),<sup>424,425</sup> and by Xin *et al.* for their synthesis of cyclic tetrapeptides (**3-6**).<sup>426</sup>

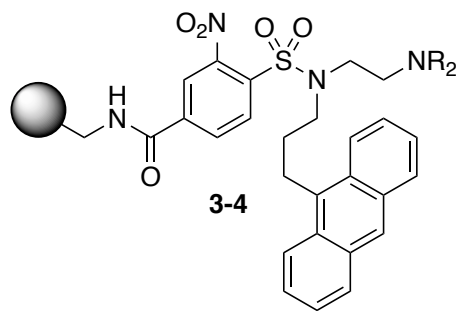


Figure 3.3 General structure of "reporter resins" containing anthracene.

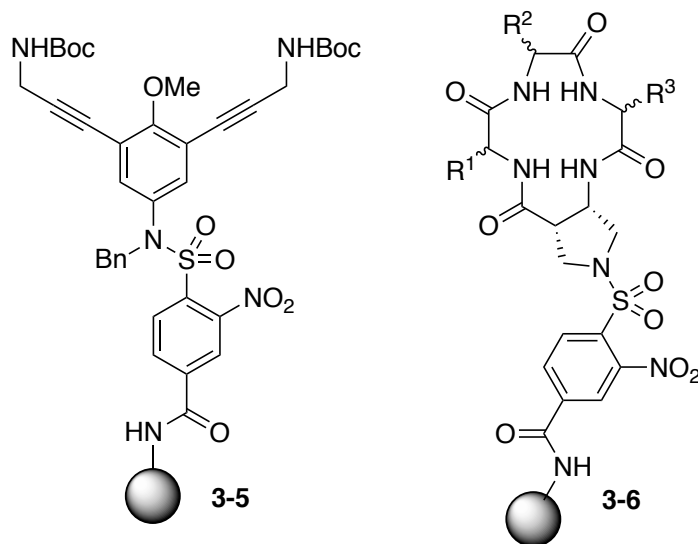


Figure 3.4 Two examples of solid-phase synthesis products achieved via strategies involving the 4-carboxyl-2-nitrobenzenesulfonamide group as a cleavable linker.<sup>424–426</sup>

### 3.1.1.1 4-Carboxyl-2-nitrobenzenesulfonamide Linkers in Biology

There are also notable examples of 4-carboxyl-2-nitrobenzenesulfonamide linkers being used in a biological context. Yokoshima *et al.* used a 4-carboxyl-2-nitrobenzenesulfonamide for synthesis of photoaffinity probe **3-7** (Figure 3.5).<sup>427</sup> In this case cleavage of the conjugate can be achieved with 2-mercaptoethanol in aqueous buffer, with cleavage over 7 to 12 hours in a NaHCO<sub>3</sub>-Na<sub>2</sub>CO<sub>3</sub> buffer (pH 9.2), and 24 to 33 hours in a KH<sub>2</sub>PO<sub>4</sub>-NaHPO<sub>4</sub> buffer (pH 7.4).<sup>427</sup>

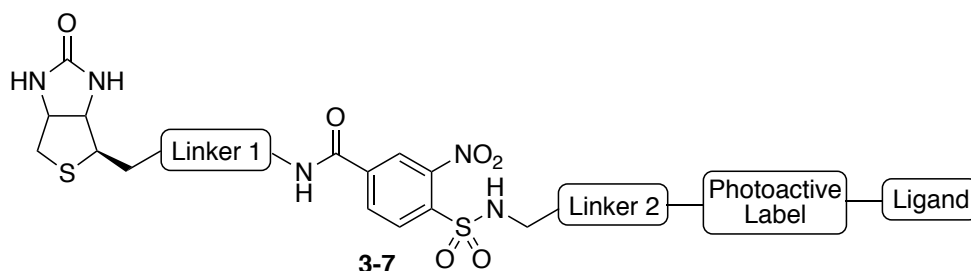


Figure 3.5 General structure of probes developed by Yokoshima *et al.*<sup>427</sup>

Ito *et al.* utilised a similar linker conjugated to a  $^{19}\text{F}$ -active coumarin dye (**3-8**) and a bioluminogenic probe (**3-9**) for the study of glutathione transferase enzymes inside cells.<sup>428</sup> Glutathione transferases (GSTs) are responsible for catalysing the nucleophilic attack of glutathione on a variety of molecules, primarily for the purposes of reducing their toxicity and facilitating their removal from cells.<sup>429,430</sup> In this case, the sulfonamide/sulfonate esters synthesised bear an acetyl group *para* to the sulfonamide, as opposed to the amides seen in previous examples (**Figure 3.6**). Both compounds were successfully examined *in vivo* in *E. coli*, where clear differences can be observed in both fluorescence,  $^{19}\text{F}$  NMR and bioluminescence between strains capable or incapable of expressing GSTs. Lee *et al.* also employed a similar method for examining the presence of reactive cysteine residues in proteins post-exposure to reactive oxygen species (ROS), with biotin-appended sulfonamide **3-10** designed as a probe for their detection.<sup>431</sup>

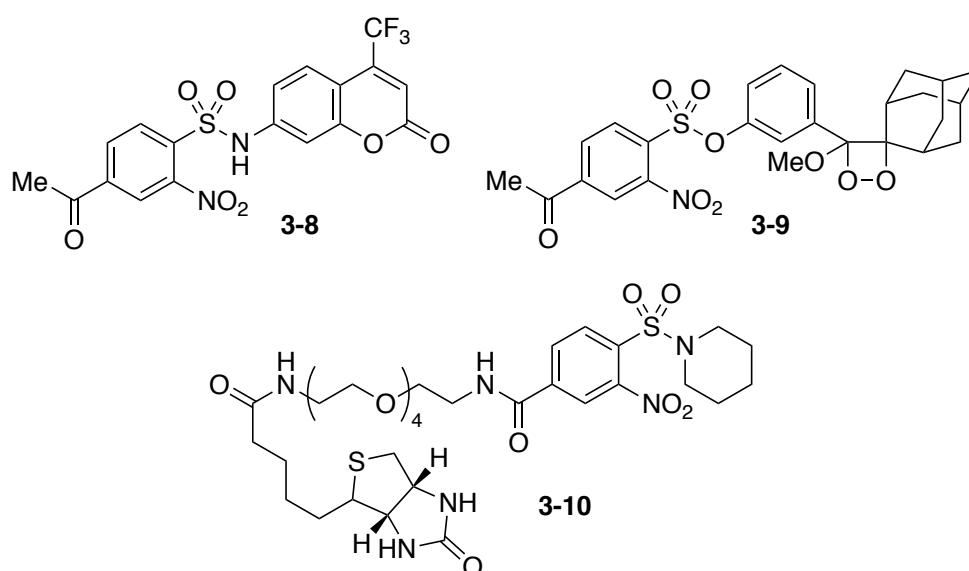


Figure 3.6 Fluorescent/ $^{19}\text{F}$ -active (**3-8**) and bioluminogenic (**3-9**) probes synthesised by Ito *et al.*, and probe for detecting reactive cysteine residues in proteins developed by Lee *et al.* (**3-10**).<sup>428,431</sup>

Van Gisbergen *et al.* have synthesised anticancer prodrugs containing 4-acetyl-2-nitrobenzenesulfonamide/sulfonyl ester groups in combination with the anticancer agents etoposide (**3-11**) and doxorubicin (**3-12**, **Figure 3.7**),<sup>432</sup> having previously synthesised 2,4-dinitrobenzenesulfonamide prodrugs of doxorubicin (**DNS-DOX**).<sup>305</sup> **3-12** displays slower release of doxorubicin than 2,4-dinitrobenzenesulfonamide equivalent **DNS-DOX**,

which allows for a greater selectivity for cancer cells overexpressing certain glutathione-S-transferases.

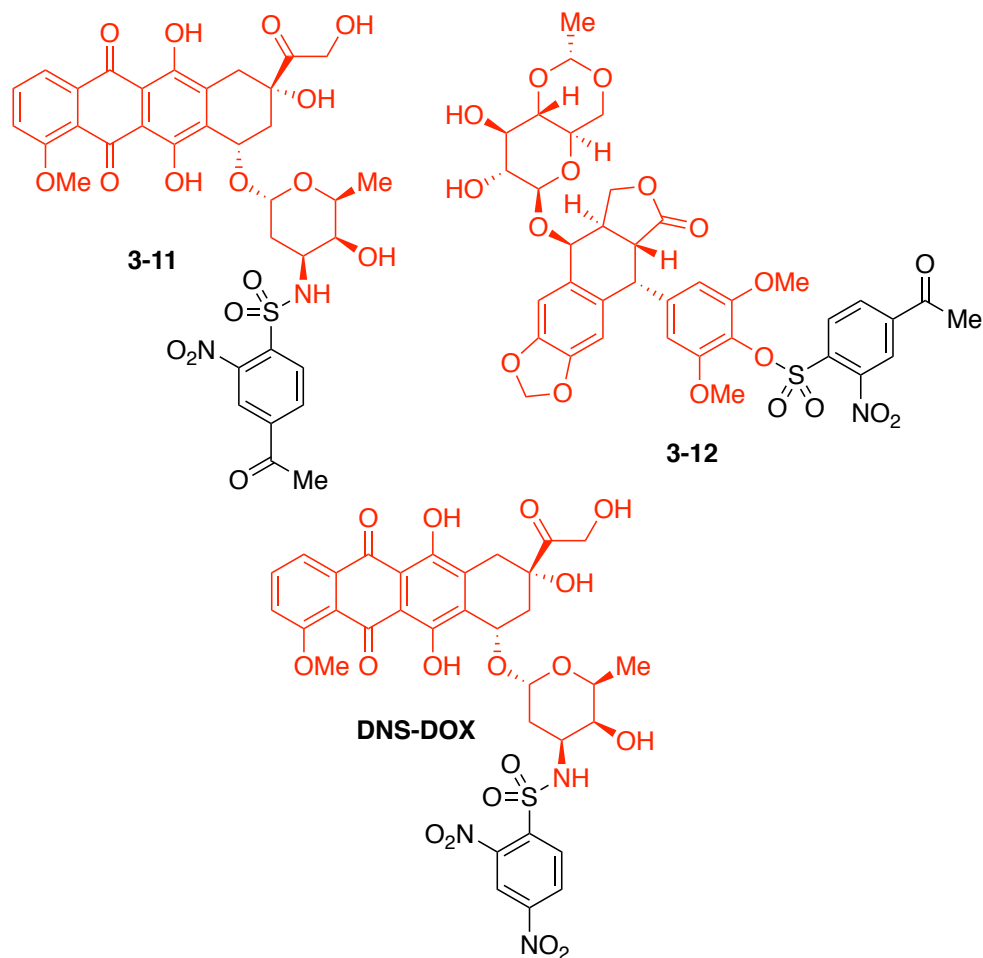
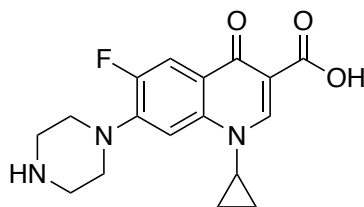


Figure 3.7 Structures of anticancer prodrugs containing etoposide (**3-11**) and doxorubicin (**3-12**), and 2,4-dinitrobenzenesulfonamide prodrug **DNS-DOX**. Drug moieties highlighted in red.<sup>432</sup>

### 3.1.2 Antimicrobial Component

As can be seen in the above examples, there is a literature precedent for the usage of 4-carboxyl-2-nitrobenzenesulfonamide as a thiol-reactive linker in a variety of scenarios. For formation of a biolabile linker based on the 4-carboxyl-2-nitrobenzenesulfonamide template, an antimicrobial containing a suitable amine for sulfonamide formation is required. With this in mind, the antimicrobial unit chosen for incorporation into the biolabile linker construct was ciprofloxacin, a second-generation antibiotic of the fluoroquinolone class (**Figure 3.8**). In ciprofloxacin, the secondary amine of the piperazine ring provides a convenient site for attachment to a biolabile linker. Ciprofloxacin can be active against both Gram-positive and Gram-negative bacteria.<sup>28,29</sup>



**Ciprofloxacin**

Figure 3.8 Structure of second-generation fluoroquinolone ciprofloxacin.

As discussed in Chapter 1, fluoroquinolones have been used extensively in the design of previous siderophore conjugates both with and without biolabile linkers, although antimicrobial activity is often reduced in conjugates lacking biolabile linkers.<sup>189–192,194,195,261–263,342,433–436</sup> Conjugation to the carboxylic acid group present in fluoroquinolones tends to be avoided; this moiety is key to the antimicrobial activity of ciprofloxacin,<sup>30,437</sup> and there are a limited number of biolabile linkers capable of releasing carboxylic acids (the linkers that do exist tend to contain ester linkages, which may prove labile in aqueous conditions).<sup>224,438,439</sup> Another reason for the use of ciprofloxacin in this case is its clinical relevance; it is widely prescribed across many healthcare systems, including in the USA, where it was the 109<sup>th</sup> most commonly prescribed drug in 2018 (and the 6<sup>th</sup> most prescribed antibiotic).<sup>440,441</sup> This widespread use has led to increasing resistance to ciprofloxacin, and fluoroquinolones in general.<sup>442–444</sup> Incorporating ciprofloxacin in a Trojan Horse conjugate may act to mitigate mechanisms of resistance associated with uptake.

One potential drawback of ciprofloxacin is its solubility; while not hydrophobic from a partition coefficient standpoint, with a calculated logP of  $-1.53$  (clogP, OSIRIS property explorer),<sup>445</sup> and an experimental logD (logP at pH 7.40) of between  $-0.78$ <sup>446,447</sup> and  $-1.13$ ,<sup>447–449</sup> it does display poor aqueous solubility in non-acidic conditions.<sup>181,450</sup>

### 3.1.3 Siderophore Component

The siderophore component selected for the design of this Trojan Horse conjugate was the hydroxamate-type siderophore desferrioxamine (DFO). As was noted in Chapter 2, the success of Trojan Horse conjugates vs. bacteria hinges on their ability of their siderophore component to bind iron



to allow for siderophore recognition and uptake. This in turn requires the siderophore component to compete effectively with native bacterial siderophores for acquisition of iron; weaker siderophores like the monocatechols employed in Chapter 2 can easily be outcompeted by higher denticity siderophores. As a hexadentate siderophore able to strongly coordinate iron, DFO is likely to be better able to compete with these native siderophores. Indeed, DFO has a  $pFe(III)$  value of 25.0, compared to 15.0 for the bidentate monocatechol *N,N*-dimethyl-2,3-dihydroxybenzamide (**3-13**), or 26.0 for the tetradentate bis(catechol) amonabactin T (**Figure 3.9**); it remains a weaker chelator than hexadentate catechol siderophores like enterobactin ( $pFe(III) = 35.5$ ).<sup>96</sup> A further consideration is the widespread uptake of DFO as a xenosiderophore by many bacterial species, including *P. aeruginosa*,<sup>451–453</sup> *S. aureus*,<sup>104</sup> and *Klebsiella pneumoniae*,<sup>454,455</sup> which may grant the proposed conjugate a relatively broad spectrum of activity.

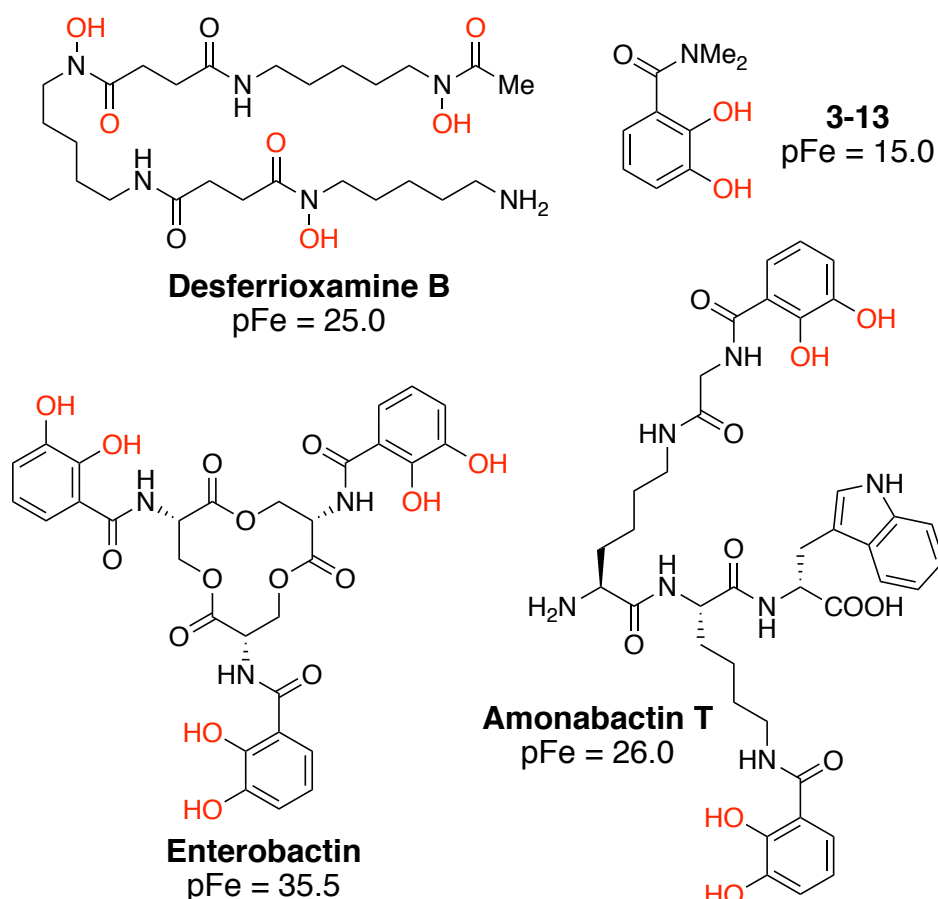


Figure 3.9 Structures of hexadentate hydroxamate siderophore desferrioxamine, and three examples of catecholate siderophores of varying denticity, plus associated  $pFe(III)$  values at pH 7.40. Groups involved in iron coordination are highlighted in red.

Another advantage of DFO is its hydrophilicity. The hydrophobic nature of the chosen biolabile linker and poor aqueous solubility of ciprofloxacin may have implications for the aqueous solubility of the final compounds, and it was hoped the incorporation of DFO may go some way to balancing out any solubility issues. From a synthetic standpoint, DFO possesses a free amine group, ideal for coupling to the carboxylic acid in the 4-carboxyl-2-nitrobenzenesulfonamide linker. Finally, unlike most tetra/hexadentate siderophores, DFO is commercially available, likely due to its use as a treatment for iron overload. This removes the need for a synthesis of the siderophore component at this early stage of developing a potential Trojan Horse system.

### 3.2 Conjugate Design and Synthetic Plan

A first synthetic target, **3-14**, with ciprofloxacin as the antimicrobial component and DFO as the siderophore component, was proposed. Ciprofloxacin is attached to the potential SO<sub>2</sub>-releasing linker via the secondary amine of the piperazine ring, and DFO is attached via the carboxylic acid of the sulfonamide ring (**Figure 3.10**).

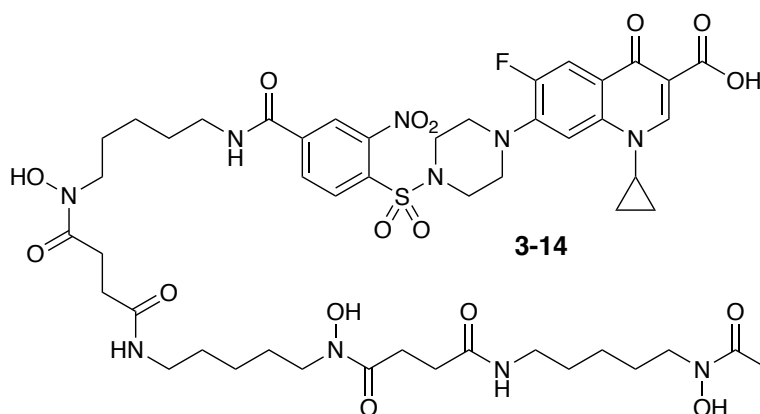
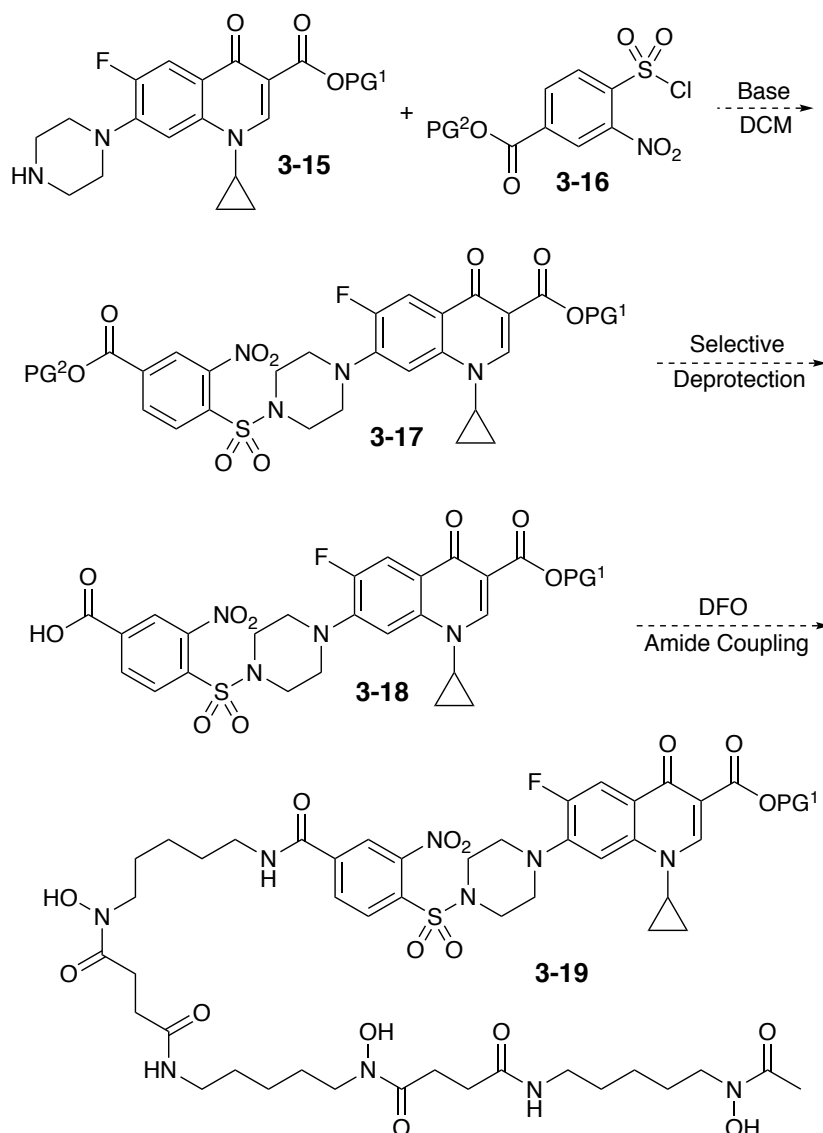


Figure 3.10 Structure of proposed ciprofloxacin-desferrioxamine conjugate **3-14**.

As mentioned above, DFO is commercially available, but in a form with no protection of its hydroxyl groups. To save adding extra protection/deprotection steps to the synthesis, and minimise the potential for degradation of the DFO component, the decision was made to start by coupling a protected ciprofloxacin moiety **3-15** with a protected 4-carboxyl-

2-nitrobenzenesulfonyl chloride **3-16** to form a sulfonamide (**3-17**), followed by deprotection of the carboxyl group on the sulfonamide ring. The DFO component can then be incorporated via an amide coupling reaction with the primary amine unit of DFO (**3-19**, **Scheme 3.3**).

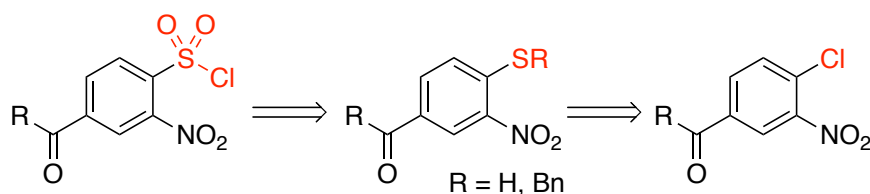


Scheme 3.3 Key reaction sequence in proposed synthesis of DFO conjugate **3-14**.

### 3.2.1 Synthetic Considerations for Sulfonyl Chlorides

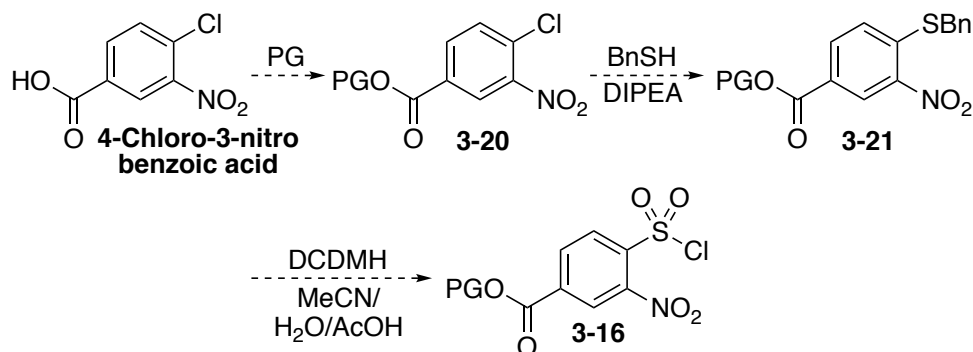
A key intermediate in the synthesis of 4-carboxyl-2-nitrobenzenesulfonyl chloride-based prodrugs is sulfonyl chloride **3-16**. Unlike the 2,4-dinitrobenzenesulfonyl chloride utilised for synthesis of the conjugates discussed in Chapter 2, sulfonyl chlorides based on the 4-carboxyl-2-nitrobenzene scaffold are not commercially available, so need to be synthesised. There are a number of routes existing in the literature for

the synthesis of 4-carboxyl-2-nitrobenzenesulfonyl chloride derivatives, all of which employ oxidative chlorination of a thiol or benzyl thioether component to generate the sulfonyl chloride target.<sup>417,422,423,426,456</sup> Given the electron-deficient nature of the 4-carboxyl-2-nitrobenzene ring, the required thiols/thioethers can be easily installed via nucleophilic aromatic substitution of the corresponding aryl halides (**Scheme 3.4**).<sup>423,426,456</sup>



Scheme 3.4 Retrosynthetic analysis of sulfonyl chlorides.

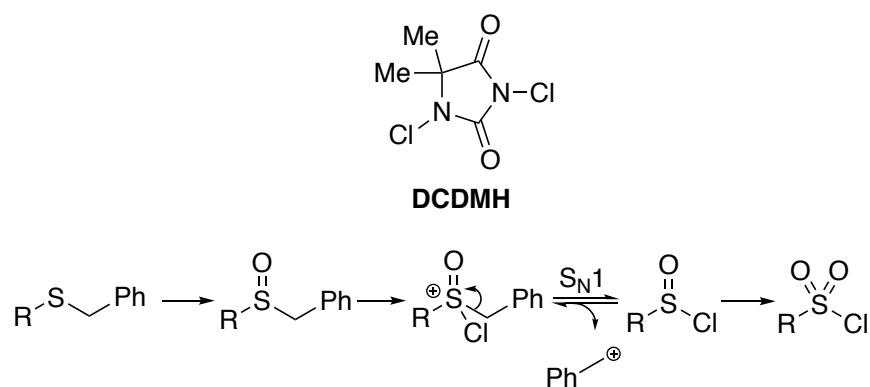
Synthesis of the sulfonyl chloride component was therefore envisaged to start from 4-chloro-3-nitrobenzoic acid, with protection of the carboxylic acid group followed by nucleophilic aromatic substitution of the chloro group with benzyl mercaptan to generate benzyl thioether **3-21** (**Scheme 3.6**).<sup>423,426,431</sup> While thiols can be installed in this position instead, and used for oxidative chlorination with a variety of reagents,<sup>456–458</sup> concerns about disulfide formation and problems with thiol synthesis led to the choice of benzyl thioether **3-21** as a shelf-stable alternative.



Scheme 3.5 Proposed synthetic route to sulfonyl chloride **3-16**.

Here, 1,3-dichloro-5,5'-dimethylhydantoin (DCDMH) was proposed as a reagent for oxidative chlorination of **3-21** (**Scheme 3.6**). DCDMH is used in industry as a bleaching agent and a disinfectant (notably in swimming pools); perhaps because of this it is remarkably affordable (£12.50 for 250 g). It is also relatively mild compared to most reagents used for oxidative chlorination. DCDMH was first used for the oxidative chlorination of benzyl

thioethers in 2010 by Pu *et al.*,<sup>459</sup> and has since been used in a number of other synthetic routes requiring sulfonyl chloride synthesis.<sup>460–462</sup> It has also been previously used with the 4-carboxyl-2-nitrobenzene ring system, with an amide at the 4-position rather than an ester.<sup>426</sup> While these benzyl thioethers come with the benefit of increased stability compared to their thiol counterparts, there is the risk of byproduct formation due to the reactivity of the benzyl cation believed to be formed in the reaction.<sup>459</sup>



Scheme 3.6 Structure of oxidative chlorination agent 1,3-dichloro-5,5'-dimethylhydantoin (DCDMH) and the potential mechanism for oxidative chlorination of benzyl thioethers proposed by Pu *et al.*<sup>459</sup>

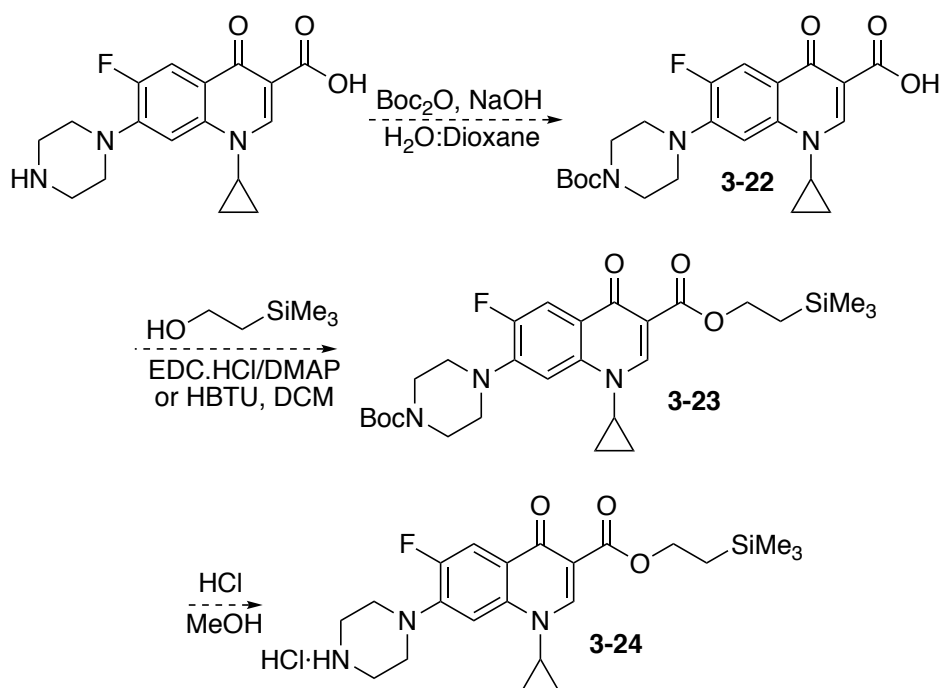
### 3.2.2 Protecting Groups and Planned Synthetic Route to 3-14

The choice of protecting groups for the synthetic route requires careful consideration, with the carboxylic acid groups on ciprofloxacin and the 4-carboxyl-2-nitrobenzene ring both needing to be protected in an orthogonal fashion. In addition, with the deprotection of ciprofloxacin's carboxylic acid being the last step of the synthesis, the conditions used for protecting group removal need to be compatible with all of the other functional groups present, including those on the DFO component. Helpfully, other DFO conjugates in the literature have proved stable to a range of conditions, including hydrogenation and TFA deprotection.<sup>463,464</sup>

Due to the presence of the nitro group on the aromatic ring, hydrogenation cannot be used. Although DFO has been shown to be stable to basic deprotection conditions (e.g. LiOH, MeOH:H<sub>2</sub>O),<sup>263</sup> and sulfonamides based on the 4-carboxyl-2-nitrobenzene ring are stable to similar conditions,<sup>424,465</sup> other SO<sub>2</sub>-releasing rings that could be used in future conjugates might be

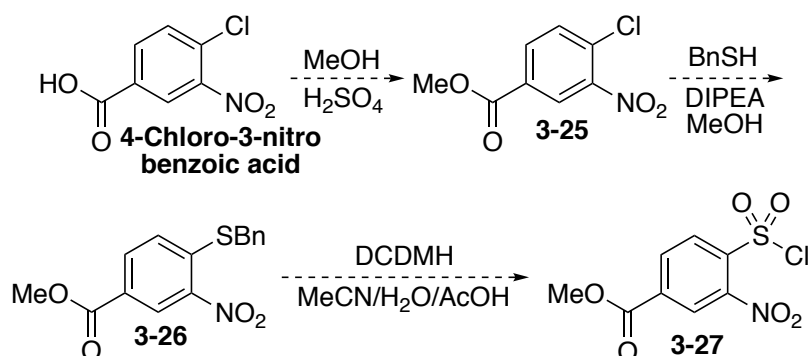
less stable to basic conditions, so use of base-labile protecting groups for the ciprofloxacin component (e.g. OMe) was initially avoided in pursuit of a ciprofloxacin derivative that could be used for the synthesis of any SO<sub>2</sub>-ciprofloxacin conjugate.

Based on the stability of DFO to trifluoroacetic acid (TFA), two TFA-labile protecting groups were suggested for ciprofloxacin protection: the *t*-butyl ester group (*t*BuO), and the trimethylsilylethanol group (TMSE). Based on the literature, the TMSE group appeared to offer more flexibility; it can be deprotected via TFA and also via a source of F<sup>-</sup> ions (e.g. TBAF),<sup>466</sup> can be installed by simple ester coupling with trimethylsilylethanol,<sup>467,468</sup> and even appears stable to other acidic deprotection conditions e.g. HCl.<sup>469–471</sup> To install this protecting group, the piperazine nitrogen of ciprofloxacin must first be protected to avoid the amine reacting under ester coupling conditions. A simple Boc group was suggested for this purpose, which can be installed via reaction with Boc anhydride in the presence of sodium hydroxide to give **3-22**,<sup>468,472</sup> and removed post-coupling via reaction with e.g. HCl/MeOH, which should leave the trimethylsilyl group intact (**Scheme 3.7**).<sup>471,473</sup>



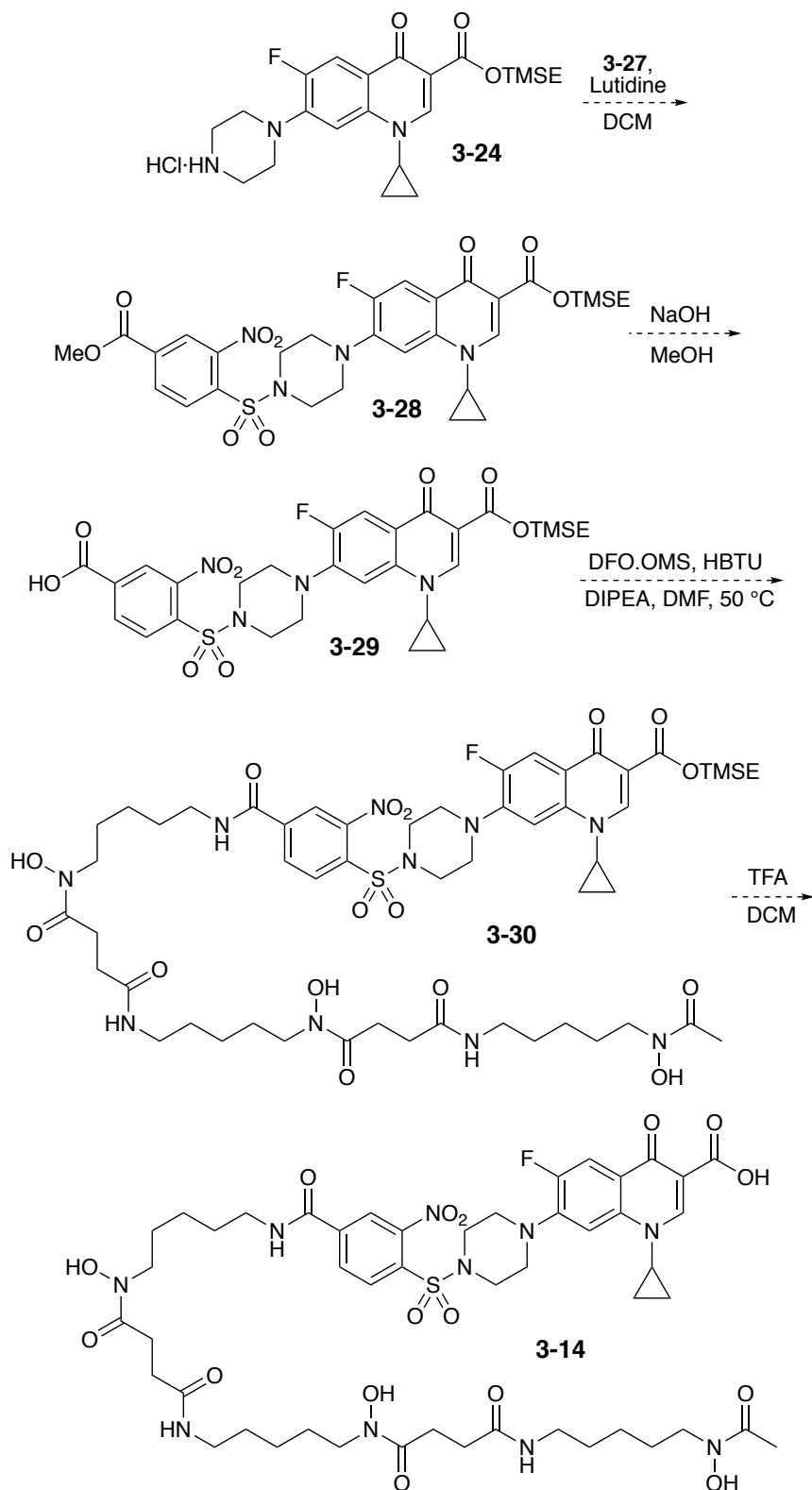
Scheme 3.7 Proposed synthetic route to TMSE-protected ciprofloxacin **3-24**.

To complement this choice of protecting group for ciprofloxacin, a methyl ester group was selected to protect the 4-carboxyl group of the benzene ring (**Scheme 3.8**). The methyl ester group is easy to install via acid-catalysed esterification,<sup>474</sup> can be deprotected under weakly basic conditions, is widely used for protection of 4-chloro-3-nitrobenzoic acid,<sup>423,474,475</sup> and has already featured in a synthesis of the sulfonyl chloride derived from this aromatic ring.<sup>456</sup> As mentioned above, sulfonamides derived from the 4-carboxyl-2-nitrobenzene ring have also been shown to be stable to OMe deprotection in the literature.<sup>465</sup>



Scheme 3.8 Proposed synthetic route to methyl ester-protected sulfonyl chloride component **3-27**.

Finally, the choice of amide coupling conditions for installation of desferrioxamine must be considered. A number of amide coupling reagents have been applied for synthesis of DFO derivatives in the literature, including EDC/HOBt,<sup>476</sup> CDI,<sup>477</sup> and HBTU.<sup>478</sup> Any of these would likely be suitable for the synthesis, with HBTU proposed for the first synthetic plan (**Scheme 3.9**).



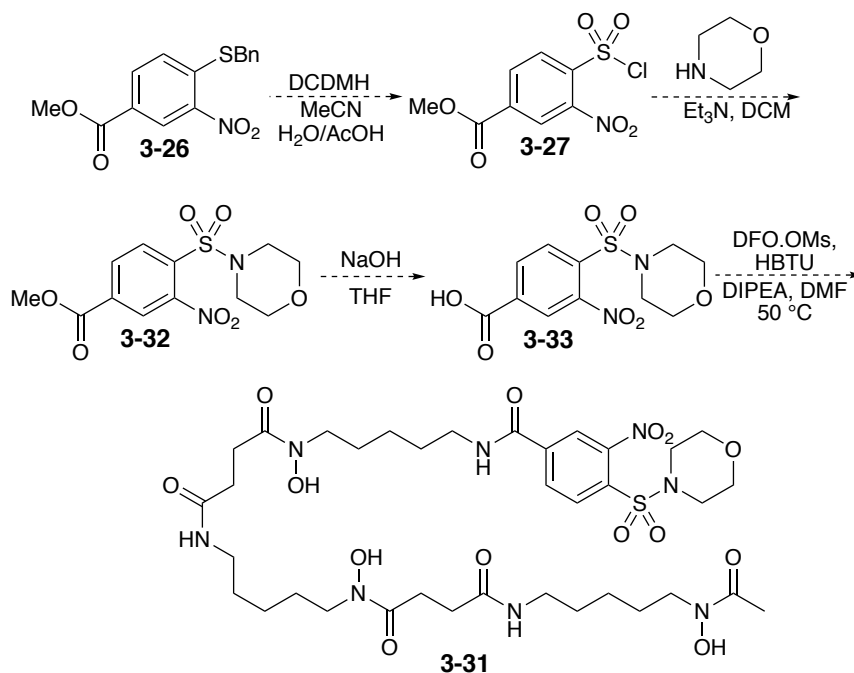
Scheme 3.9 Proposed synthetic route from sulfonyl chloride **3-27** to DFO conjugate **3-14**.

### 3.2.3 Synthetic Routes to Control Compounds

A series of microbiological controls were also designed. As demonstrated in Chapter 2, SO<sub>2</sub> release from a siderophore conjugate can have an antimicrobial effect under certain conditions, therefore the possibility of

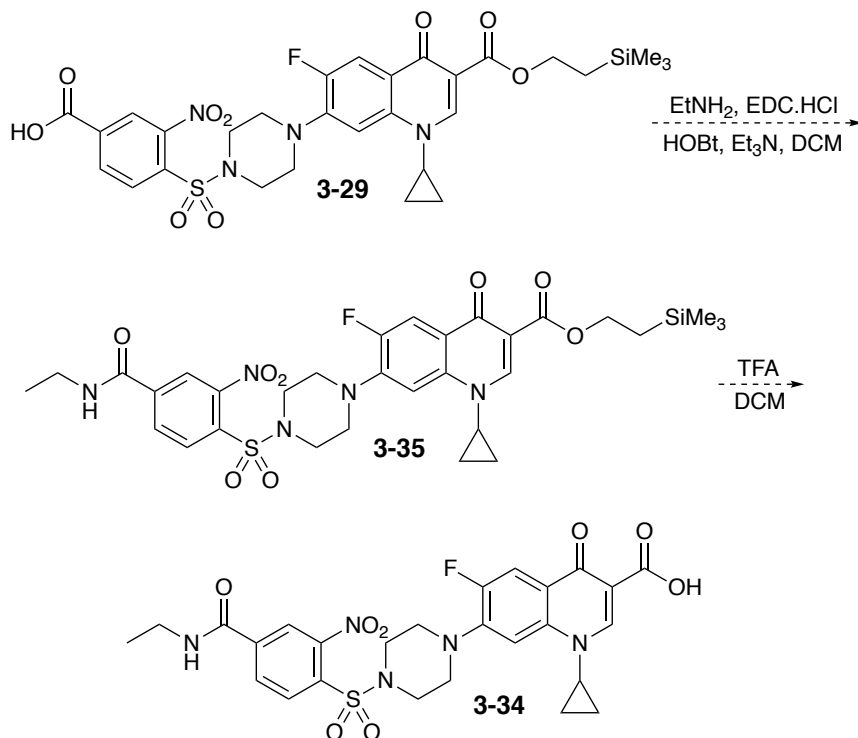


antimicrobial activity from SO<sub>2</sub> release alone should be examined to give a better idea whether any antimicrobial activity observed for **3-14** comes primarily from ciprofloxacin release, or from both ciprofloxacin and SO<sub>2</sub> release. To this end DFO conjugate **3-31** was designed as a “ciprofloxacin-negative” (Cipro –) control. This follows the same synthetic route as **3-14**, with the exception being the incorporation of morpholine in place of the ciprofloxacin structure as a partial mimic for the 6-membered piperazine ring found in ciprofloxacin (**Scheme 3.10**).



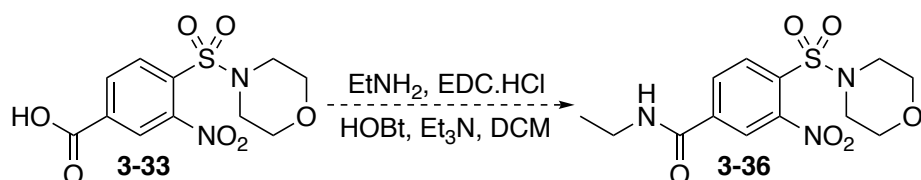
Scheme 3.10 Planned synthetic route to morpholine-containing DFO +, Cipro – control **3-31**.

A third control, **3-34**, was designed to try and determine whether ciprofloxacin conjugated to a 4-carboxyl-2-nitrobenzenesulfonamide unit could display good antimicrobial activity without the presence of DFO or another siderophore (a Cipro +, DFO – control). Here, the presence of an ethyl amide group should act as a good mimic of the amide bond in the DFO conjugates, and its electron-withdrawing ability for activation of the sulfonamide towards nucleophilic aromatic substitution. Control **3-34** could be synthesised via reaction of TMSE-protected **3-29** with ethylamine, followed by removal of the TMSE protecting group (**Scheme 3.11**).



Scheme 3.11 Planned synthetic route to Cipro +, DFO – control **3-34**.

Finally, ethyl amide **3-36** was designed as both a “ciprofloxacin-negative” and a “DFO-negative” control (Cipro –, DFO –). This would allow the effects of SO<sub>2</sub> release from 4-carboxyl-2-nitrobenzene rings to be examined independent of ciprofloxacin release or the presence of siderophores. The synthesis of **3-36** was envisaged in one step from carboxylic acid **3-33** (Scheme 3.12).



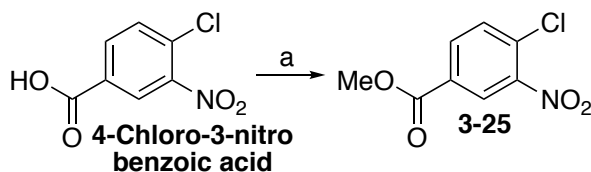
Scheme 3.12 Proposed synthetic route to Cipro –, DFO – control **3-36**.

### 3.3 Conjugate Syntheses

#### 3.3.1 Sulfonyl Chloride Component

The first step of the synthesis of the sulfonyl chloride component, methyl ester protection of the carboxylic acid of 4-chloro-3-nitrobenzoic acid (Scheme 3.13) proceeded smoothly. The <sup>1</sup>H NMR spectrum of **3-25** is consistent with the literature,<sup>474</sup> and the successful methylation is supported by the presence of a peak at *m/z* = 216.0055 in the ESI mass

spectrum, corresponding to an  $[M+H]^+$  molecular ion peak with a formula of  $C_8H_7ClNO_4$ .



Scheme 3.13 Methyl ester protection of 4-chloro-3-nitrobenzoic acid. a)  $H_2SO_4$ , MeOH, reflux, 18 h, 96%.

The  $^1H$  NMR spectrum for **3-25**, and indeed all subsequent 4-carboxyl-2-nitrobenzene derivatives, displays a characteristic doublet/doublet of doublets/doublet multiplet pattern for the aromatic protons (**Figure 3.11**), consistent with the substitution pattern of the aromatic ring. The two doublets are easily recognisable from each other from their distinct coupling constants of 8.5 Hz and 2.0 Hz.

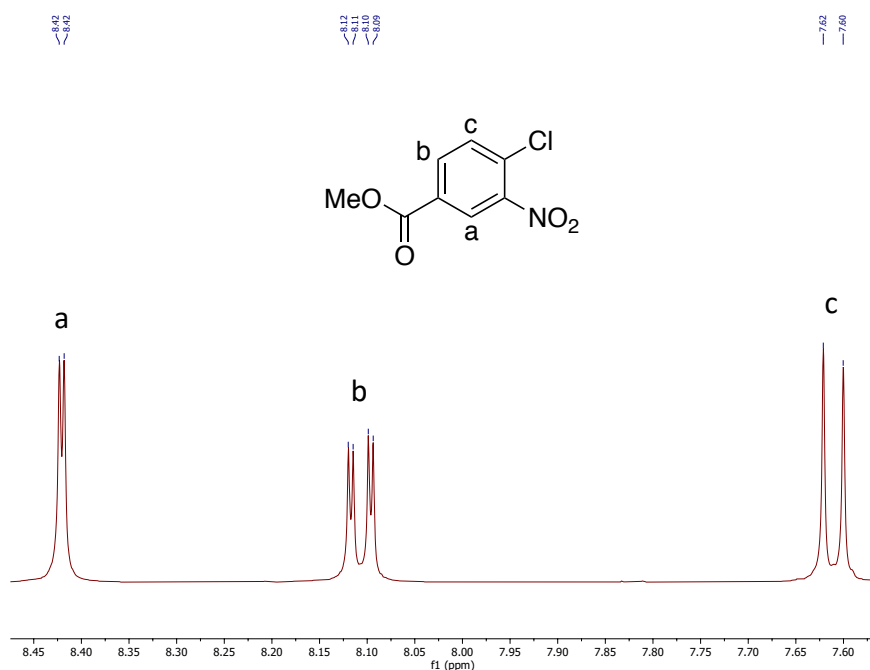
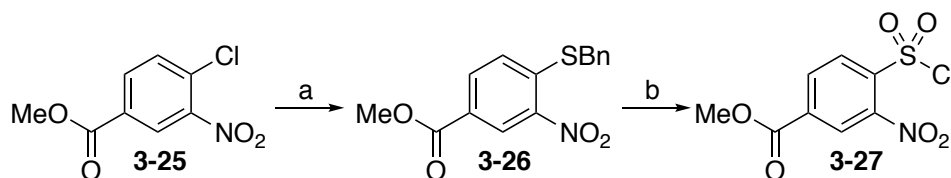


Figure 3.11 Aromatic region of the  $^1H$  NMR spectrum of **3-25**, demonstrating the characteristic multiplet pattern observed for the aromatic protons of 4-carboxyl-2-nitrobenzene rings with substituents at the 1-position.

Benzyl thioether **3-26** was synthesised in 91% yield from **3-25**. The  $^1H$  NMR spectrum obtained for the product is consistent with the literature,<sup>431</sup> and the ESI mass spectrum displays a peak at  $m/z = 326.0459$ , consistent with a

sodium adduct of the product (expected  $m/z = 326.0457$  for  $[M+Na]^+$ ). The oxidative chlorination of **3-26** was carried out according to the methodology of Pu *et al.*, utilising MeCN:AcOH:H<sub>2</sub>O as a solvent system (**Scheme 3.14**).<sup>459</sup> This proved successful in generating sulfonyl chloride **3-27**, with the <sup>1</sup>H NMR spectrum matching reported literature values for **3-27**.<sup>423,456</sup>



Scheme 3.14 Synthesis of benzyl thioether **3-26** and sulfonyl chloride **3-27**.  
a) BnSH, DIPEA, MeOH (anhydrous), 0 °C to rt, 22 h, 91%; b) DCDMH, MeCN:AcOH:H<sub>2</sub>O (40:1.5:1), 0 °C, 3 h.

Alongside the sulfonyl chloride, other byproducts are present (**Figure 3.12**). These stem from the proposed mechanism of the oxidative chlorination procedure (**Scheme 3.6**), which generates a benzyl cation from debenzylation of the thioether. This can then react with DCDMH, or the reaction solvents. The most obvious of these is benzyl chloride, from reaction of any chloride ions/chlorine formed with the benzylic cation; this displays a <sup>1</sup>H NMR singlet at 4.59 ppm, consistent with literature spectral data.<sup>479,480</sup> *N*-benzylacetamide, formed via a Ritter reaction between the benzyl cation and the acetonitrile solvent,<sup>459</sup> is also present. This can be identified via a <sup>1</sup>H NMR doublet at 4.44 ppm (2H) and a singlet at 2.04 ppm (3H), plus peaks in the ESI mass spectrum at  $m/z = 150.0913$  and  $172.0733$ , corresponding to the molecular ions  $[M+H]^+$  and  $[M+Na]^+$  respectively, which are consistent with adducts of formula C<sub>9</sub>H<sub>12</sub>NO and C<sub>9</sub>H<sub>11</sub>NNaO. Both of these byproducts were previously identified by Pu *et al.*<sup>459</sup> The likely presence of benzyl acetate can also be observed via <sup>1</sup>H NMR resonances at 5.11 and 2.11 ppm, consistent with literature spectra, although its presence is not observed via ESI mass spectrometry.<sup>481,482</sup>

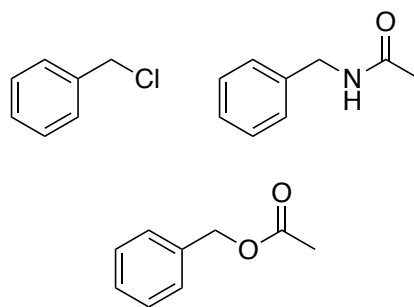
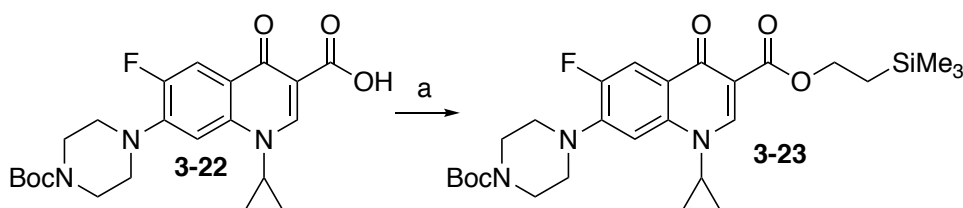


Figure 3.12 Identified byproducts from synthesis of sulfonyl chloride **3-27**.

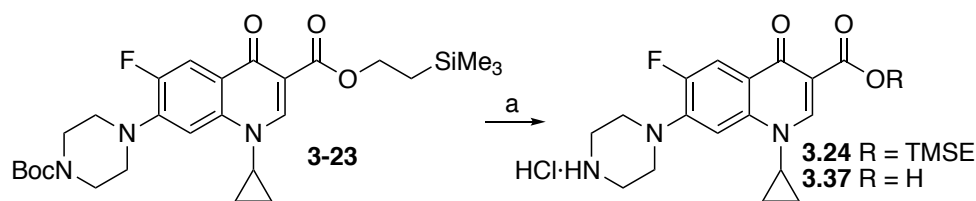
### 3.3.2 Ciprofloxacin Component and Linker Coupling

Before installation of the TMSE protecting group, the piperazine nitrogen of ciprofloxacin must first be protected; initially a Boc group was used. Boc-ciprofloxacin **3-22** (previously synthesised by Nick Kyriacou) was subjected to ester coupling with trimethylsilylethanol in the presence of EDC.HCl/DMAP. This failed to yield any product after 24 hours, so a second coupling reagent, HBTU, was trialled instead. This proved successful, with TMSE-protected **3-23** isolated in 78% yield after column chromatography (**Scheme 3.15**). A small proportion (estimated 15-20% by  $^{19}\text{F}$  NMR) of a  $\text{PF}_6$  salt derived from the HBTU coupling reagent, most likely  $\text{NaPF}_6$ , remains present after the column. The success of the coupling reaction can be observed in the  $^1\text{H}$  NMR spectrum by the presence of the distinctive coupling pattern for the  $\text{CH}_2$  groups present in the TMSE group, which stems from restricted rotation around the central C-C bond.<sup>483</sup> There is also a small upfield shift in the fluorine resonance observed in the  $^{19}\text{F}$  NMR spectrum from  $-120.9$  ppm for **3-22** to  $-123.8$  ppm for **3-23**, and two peaks observed at  $m/z = 532.3647$  and  $554.2467$  in the ESI mass spectrum, corresponding to molecular ions  $[\text{M}+\text{H}]^+$  and  $[\text{M}+\text{Na}]^+$  respectively. These are consistent with adducts of the expected molecular formula for **3-23** ( $\text{C}_{27}\text{H}_{38}\text{FN}_3\text{O}_5\text{Si}$ ).



Scheme 3.15 Synthesis of TMSE-protected Boc-ciprofloxacin **3-23**. a) Trimethylsilylethanol, HBTU, DMAP, DIPEA, DCM (anhydrous), 24 h, 78%.

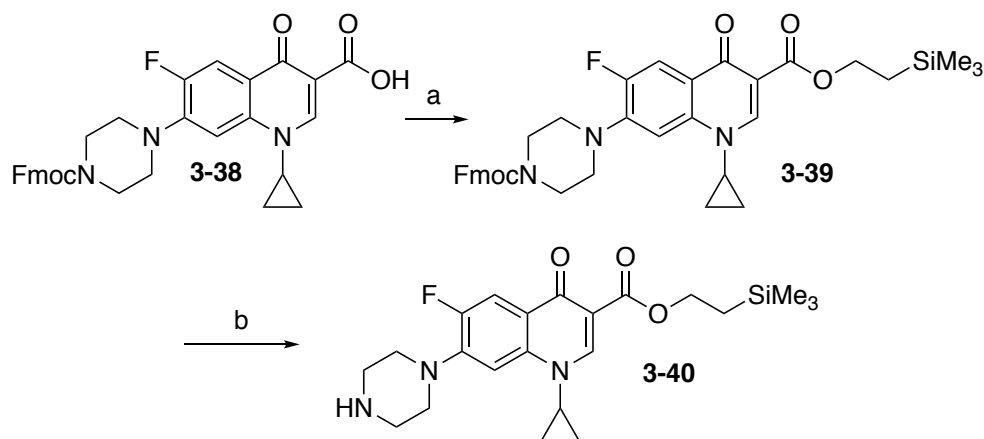
Removal of the Boc group on **3-23** to give **3-24** was initially attempted with HCl/MeOH (**Scheme 3.16**). Complete removal of the Boc group can be observed in the  $^1\text{H}$  NMR spectrum, with loss of the characteristic 9H singlet at 1.40 ppm. However, this reaction was hard to control, with the TMSE group also being partially removed under the reaction conditions to give fully deprotected ciprofloxacin hydrochloride **3-37**. This can be seen clearly by comparison of the  $^{19}\text{F}$  NMR for starting material **3-23** with the sample containing **3-24** and **3-37**; the minor peak at  $-121.7$  ppm corresponds to the expected literature value for fully deprotected ciprofloxacin.<sup>484</sup> The presence of both species can also be observed in the ESI mass spectrum, with peaks at  $m/z = 332.1407$ , corresponding to an  $[\text{M}+\text{H}]^+$  molecular ion of formula  $\text{C}_{17}\text{H}_{19}\text{FN}_3\text{O}_3$ , consistent with the formation of fully deprotected ciprofloxacin, as well as  $m/z = 432.2121$ , consistent with an  $[\text{M}+\text{H}]^+$  molecular ion of formula  $\text{C}_{22}\text{H}_{31}\text{FN}_3\text{O}_3\text{Si}$ , corresponding to product **3-24**.



**Scheme 3.16** Synthesis of deprotected TMSE-ciprofloxacin **3-24**, and formation of ciprofloxacin hydrochloride **3-37**. a) 3 M HCl in MeOH, 0 °C, 1 to 3.5 h.

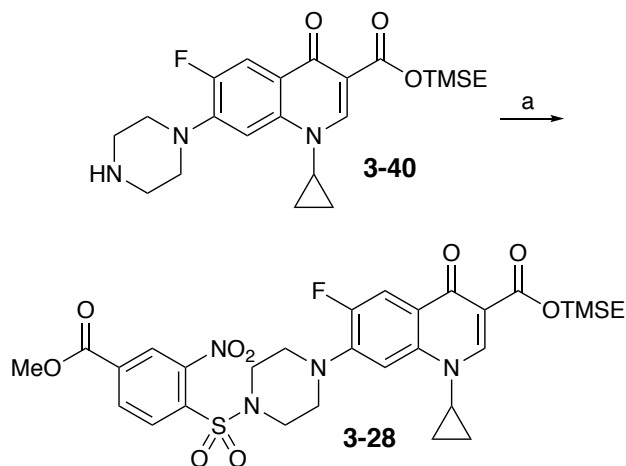
The Fmoc group was also trialed as an alternative to the Boc group. Fmoc ciprofloxacin **3-38** (previously synthesised by Holly Clarke) was protected with TMSE using equivalent conditions to the protection of **3-22**, resulting in a yield of 86% after purification by column chromatography (**Scheme 3.17**). The  $^1\text{H}$  NMR spectrum displays the expected TMSE  $\text{CH}_2$  proton patterns, and two peaks are observed at  $m/z = 654.2805$  and  $676.2625$  in the ESI mass spectrum, corresponding to  $[\text{M}+\text{H}]^+ / [\text{M}+\text{Na}]^+$  molecular ions consistent with the molecular formulas  $\text{C}_{37}\text{H}_{41}\text{FN}_3\text{O}_5\text{Si}$  and  $\text{C}_{37}\text{H}_{40}\text{FN}_3\text{NaO}_5\text{Si}$  respectively. TMSE-protected **3-39** was then subjected to typical Fmoc deprotection conditions (20% v/v piperidine in DCM), with the resulting free amine **3-40** isolated in 68% yield after column chromatography. This column also removes any  $\text{PF}_6$  salt that remains after the ester coupling. The aromatic

environments and CH<sub>2</sub> peak corresponding to the Fmoc group in the <sup>1</sup>H NMR spectrum are not observed in **3-40**, indicating successful deprotection, and the ESI mass spectrum contains peaks at  $m/z = 432.2119$  and  $454.1940$  corresponding to  $[M+H]^+/[M+Na]^+$  adducts of the desired molecular formula C<sub>22</sub>H<sub>30</sub>FN<sub>3</sub>O<sub>3</sub>Si.



Scheme 3.17 Synthesis of TMSE-protected ciprofloxacin **3-40** from Fmoc-protected ciprofloxacin **3-39**. a) Trimethylsilylethanol, HBTU, DMAP, DIPEA, DCM (anhydrous), 24 h, 86%; b) Piperidine, DCM, 0 °C, 90 min, 68%.

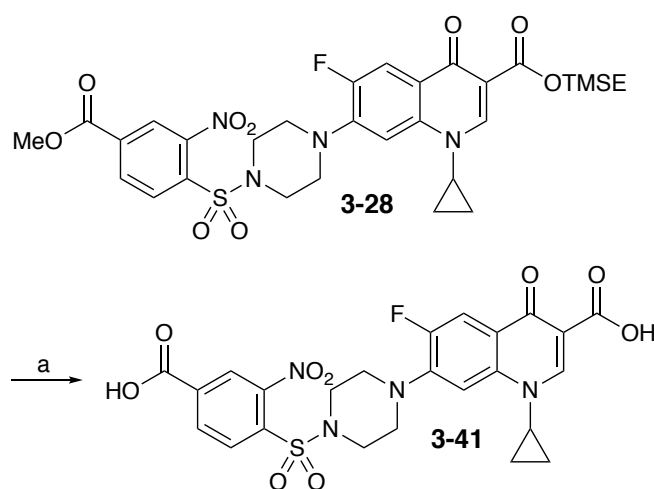
The synthesis of ciprofloxacin-sulfonamide unit **3-28** was carried out successfully via reaction of **3-27** and **3-40** in DCM with lutidine as a base (**Scheme 3.18**). The positions of all three protons on the 4-carboxyl-2-nitrobenzene ring in the <sup>1</sup>H NMR spectrum shift relative to their position in the sulfonyl chloride; the doublets from 8.48 and 8.34 ppm to 8.28 and 8.10 ppm respectively, and the doublet of doublets from 8.45 to 8.34 ppm. Furthermore, the ESI mass spectrum contains  $[M+H]^+$  and  $[M+Na]^+$  peaks at  $m/z = 675.1947$  and  $697.1765$ , consistent with the molecular formula C<sub>30</sub>H<sub>35</sub>FN<sub>4</sub>O<sub>9</sub>SSi. The crude product was purified by column chromatography; a portion of the *N*-benzyl acetamide byproduct from the synthesis of **3-27** also co-eluted and was carried through to the next step.



Scheme 3.18 Synthesis of TMSE-protected ciprofloxacin-sulfonamide **3-28**.

a) **3-27**, lutidine, DCM (anhydrous), 0 °C to rt, 72 h, 53%.

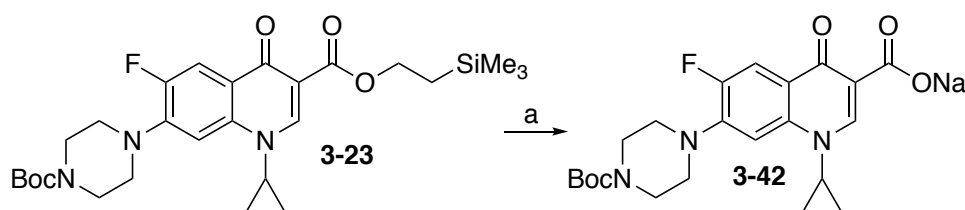
Hydrolysis of the methyl ester of **3-28** was attempted using four equivalents of aqueous sodium hydroxide in 2:1 THF:MeOH. After stirring for one hour, the reaction mixture was neutralised with 1 M aqueous HCl, yielding a precipitate that proved sparingly soluble in organic solvents. Analysis by  $^1\text{H}$  NMR spectroscopy and ESI mass spectrometry revealed that, in addition to the methyl ester hydrolysis, the TMSE ester had also been hydrolysed to give dicarboxylic acid **3-41** (Scheme 3.19); the resonances corresponding to all three proton environments in the TMSE group are absent from the  $^1\text{H}$  NMR spectrum, and the ESI mass spectrum reveals a peak at  $m/z = 561.1098$ , consistent with the presence of an  $[\text{M}+\text{H}]^+$  molecular ion with the formula  $\text{C}_{24}\text{H}_{22}\text{FN}_4\text{O}_9\text{S}$ , indicating the hydrolysis of both esters to form **3-41**.



Scheme 3.19 Outcome of attempted selective hydrolysis of methyl ester of **3-28**, resulting in formation of dicarboxylic acid **3-41**. a) NaOH (aq.), 2:1 THF:MeOH, 1 h, then HCl (aq.).



This result was somewhat unexpected, given the stability of the TMSE group in a number of reactions carried out under aqueous basic conditions in the literature.<sup>485–489</sup> To determine which part of the protocol (the deprotection with NaOH, or the subsequent addition of HCl) was responsible for the TMSE ester cleavage, the basic conditions were replicated using Boc-protected ciprofloxacin TMSE (**3-23**); in this case the solvent was removed under vacuum without performing the neutralisation step with HCl (**Scheme 3.20**). Cleavage of the TMSE ester was observed by <sup>1</sup>H NMR spectroscopy, with the loss of the CH<sub>2</sub> resonances and 9H singlet for the TMSE group, and ESI mass spectrometry, with a peak observed at *m/z* = 454.1753, corresponding to an [M+Na]<sup>+</sup> adduct of molecular formula C<sub>22</sub>H<sub>26</sub>FN<sub>3</sub>NaO<sub>5</sub>, consistent with the formation of a derivative of Boc ciprofloxacin **3-22** (likely sodium-bound **3-42**). This indicates the basic conditions alone were responsible for the TMSE ester hydrolysis.

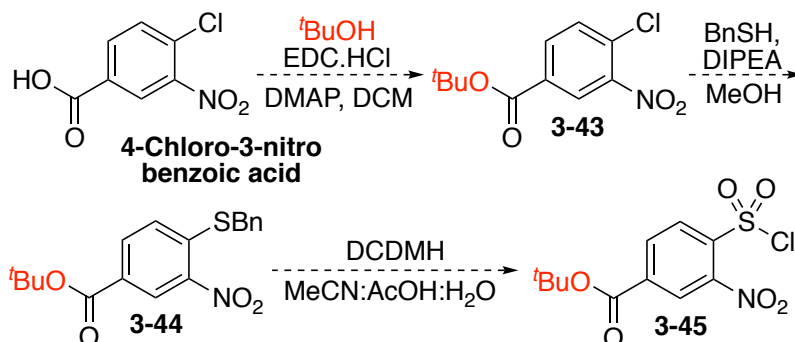


Scheme 3.20 Examination of conditions resulting in the hydrolysis of TMSE ester. a) NaOH (aq.), 2:1 THF:MeOH, 1 h, quantitative.

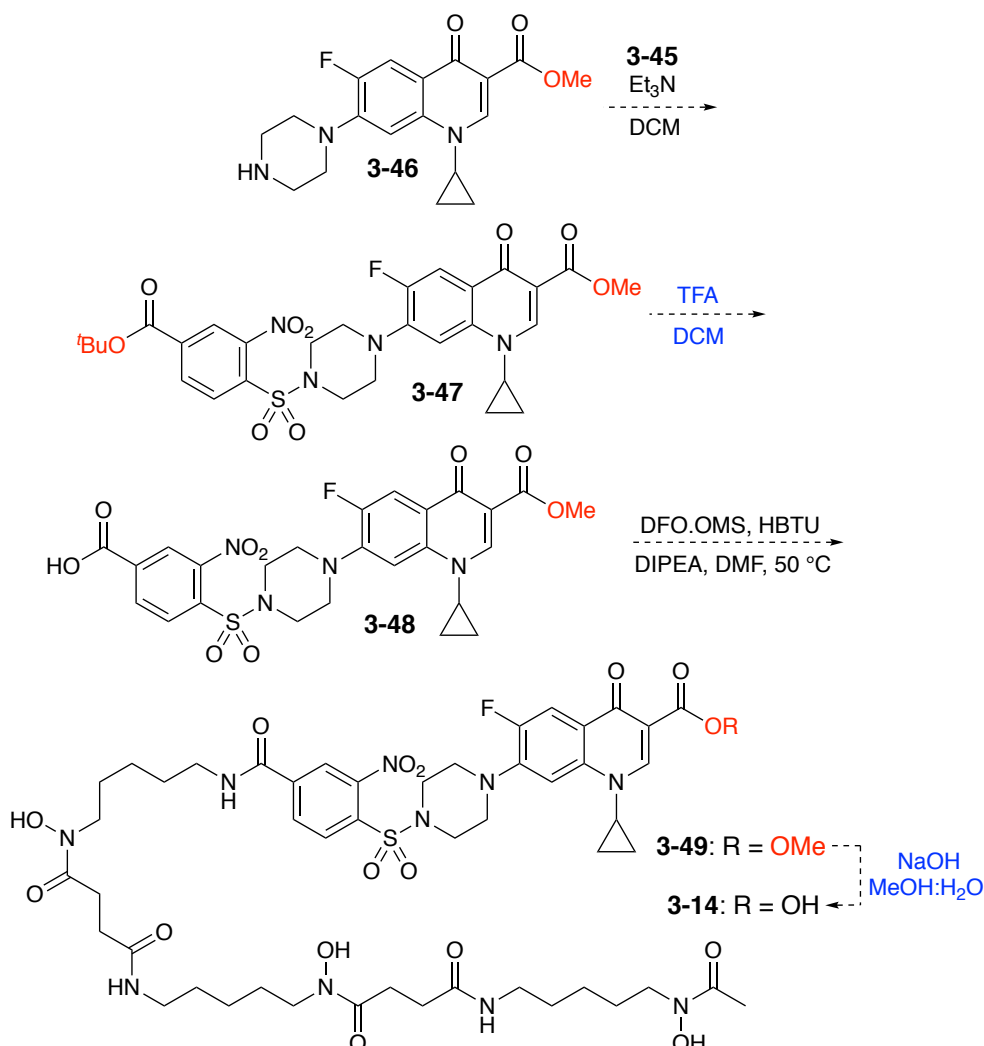
### 3.3.3 Revised Synthetic Route to 3-14

Following the problems with the TMSE protecting group, a new synthetic route with altered protecting group chemistry was devised. The methyl ester on the sulfonamide ring was replaced with a *tert*-butyl ester (**Scheme 3.21**), which is labile under acidic conditions (e.g. TFA/DCM),<sup>466</sup> and the TMSE ester on ciprofloxacin with a methyl ester (**Scheme 3.22**). One of the main reasons for the original choice of the TMSE ester was its potential versatility; it has been shown in the literature to be orthogonal to a range of other protecting groups, allowing variation of the protecting group on the sulfonamide ring without needing to change the protecting group on ciprofloxacin. While 4-carboxyl-2-nitrobenzenesulfonamides have been shown to be stable towards typical OMe ester deprotection conditions (aqueous NaOH),<sup>424,465,490</sup> other aromatic sulfonamides, especially heterocyclic ones,

may not possess this same stability, requiring another change in ciprofloxacin protecting group to accommodate them, as will be seen in Chapter 4.

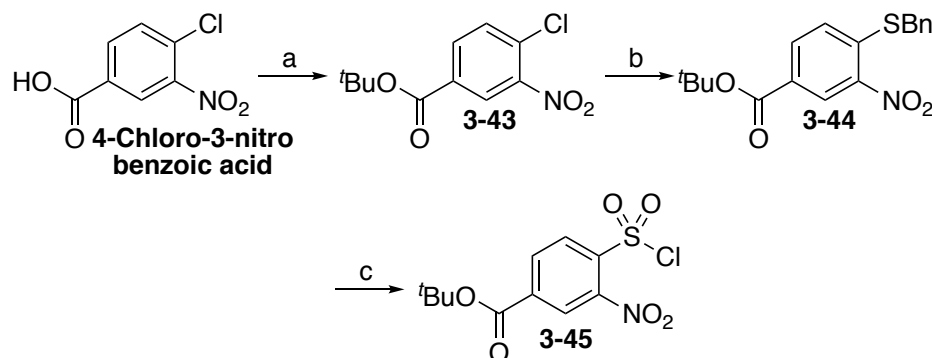


Scheme 3.21 Revised synthetic route to sulfonyl chloride **3-45**. Key protecting group changes are highlighted in red.



Scheme 3.22 Revised synthetic route to DFO conjugate **3-14**. Key protecting group changes are highlighted in red, and deprotection conditions in blue.

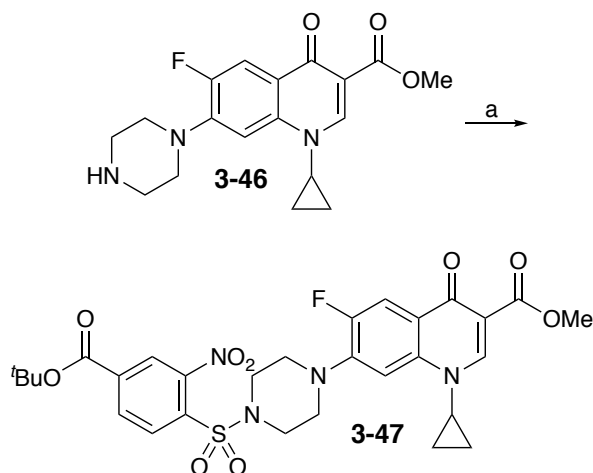
Synthesis of the new *tert*-butyl protected sulfonyl chloride **3-45** proceeded in 32% yield over 3 steps (**Scheme 3.23**). It followed a similar path to the original sulfonyl chloride synthesis: esterification of 4-chloro-3-nitrobenzoic acid with *tert*-butyl alcohol to give **3-43** was followed by reaction with benzyl mercaptan to yield thioether **3-44**. Successful formation of **3-43** can be confirmed by the presence of a *tert*-butyl singlet at 1.60 ppm in the  $^1\text{H}$  NMR spectrum, and synthesis of **3-44** can be confirmed by the presence of benzyl aromatic peaks between 7.45 and 7.28 ppm and a benzyl  $\text{CH}_2$  peak at 4.24 ppm, as well as the presence of a peak at  $m/z = 368.0924$  in the ESI mass spectrum, corresponding to an  $[\text{M}+\text{Na}]^+$  adduct of molecular formula  $\text{C}_{18}\text{H}_{19}\text{NNaO}_4\text{S}$ . Oxidative chlorination of **3-44** with DCDMH gave the desired sulfonyl chloride **3-45**; the *t*-Bu ester proved stable to the small amounts of aqueous acid present in the solvent system. The  $^1\text{H}$  NMR resonances corresponding to the benzyl ether are lost, alongside changes in the chemical shifts of the protons on the 4-carboxyl-2-nitrobenzene ring compared to thioether **3-44**, most notably the proton *ortho* to the sulfonyl chloride, which appears at 8.30 ppm in the  $^1\text{H}$  NMR spectrum of **3-45** compared to 7.49 ppm in the  $^1\text{H}$  NMR spectrum of **3-44**.



Scheme 3.23 Synthesis of *t*-Bu ester protected sulfonyl chloride **3-45**. a) *t*-BuOH, EDC.HCl, DMAP, DCM, 18 h, 52%; b) BnSH, DIPEA, MeOH (anhydrous), 0 °C to rt, 18 h, 71%; c) 1,3-dichloro-5,5'-dimethylhydantoin, MeCN:AcOH:H<sub>2</sub>O (40:1.5:1), 0 °C to rt, 3 h, 86%.

Coupling of the sulfonyl chloride to ciprofloxacin methyl ester **3-46** (previously synthesised by Dr Thomas Sanderson) yielded sulfonamide **3-47** (**Scheme 3.24**). The  $^1\text{H}$  NMR spectrum of **3-47** contains the three resonances corresponding to both the 4-carboxyl-2-nitrobenzene ring, and resonances corresponding to ciprofloxacin (most notably the singlet at 8.57 ppm, and

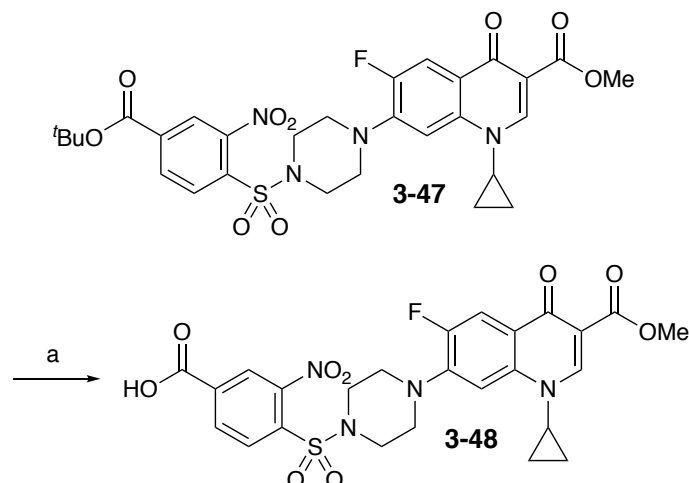
the fluorine-coupled doublet at 8.08 ppm, with a large coupling constant of 13.0 Hz), suggesting successful formation of **3-47**. Further supportive evidence comes from ESI mass spectrometry, which displays peaks at  $m/z = 631.1870$  and  $653.1689$  that can be assigned to  $[M+H]^+$  and  $[M+Na]^+$  molecular ions consistent with molecular formulas of  $C_{29}H_{32}FN_4O_9S$  and  $C_{29}H_{31}FN_4NaO_9S$  respectively.



Scheme 3.24 Synthesis of protected ciprofloxacin-sulfonamide **3-47**. a) **3-45**,  $Et_3N$ , DCM (anhydrous),  $0\text{ }^\circ\text{C}$  to rt, 24 h, 86%.

Due to the similarities in  $R_f$  (TLC) between some of the byproducts carried through from the synthesis of **3-45** and **3-47** itself, the crude product was used without purification for the next step, cleavage of the *t*-Bu ester with TFA/DCM (**Scheme 3.25**). Successful cleavage can be observed from the loss of the characteristic *tert*-butyl singlet in the  $^1H$  NMR spectrum (9H, 1.56 ppm in  $DMSO-d_6$ ), as well as the presence of peaks at  $m/z = 575.1248$  and  $597.1064$  in the ESI mass spectrum, corresponding to molecular ions  $[M+H]^+$  and  $[M+Na]^+$  respectively. These are both consistent with ESI adducts of molecular formula  $C_{25}H_{23}FN_4O_9S$ . The resulting carboxylic acid can be purified by column chromatography to successfully remove these byproducts, however this returned <50% yield of **3-48**, and residual acetic acid from the eluent proved hard to remove, even after repeated drying steps. Further experimentation with purification conditions determined that trituration of the solid with 10% v/v MeOH in  $Et_2O$  facilitated removal of remaining TFA from the ester cleavage, and the byproducts from the sulfonyl chloride synthesis, returning **3-48** in 54% yield. This can be observed from the loss of the aromatic resonances corresponding to benzyl chloride/*N*-

benzylacetamide/benzyl acetate in the  $^1\text{H}$  NMR spectrum, and the disappearance of the TFA peak at  $-74.3$  ppm in the  $^{19}\text{F}$  NMR spectrum.



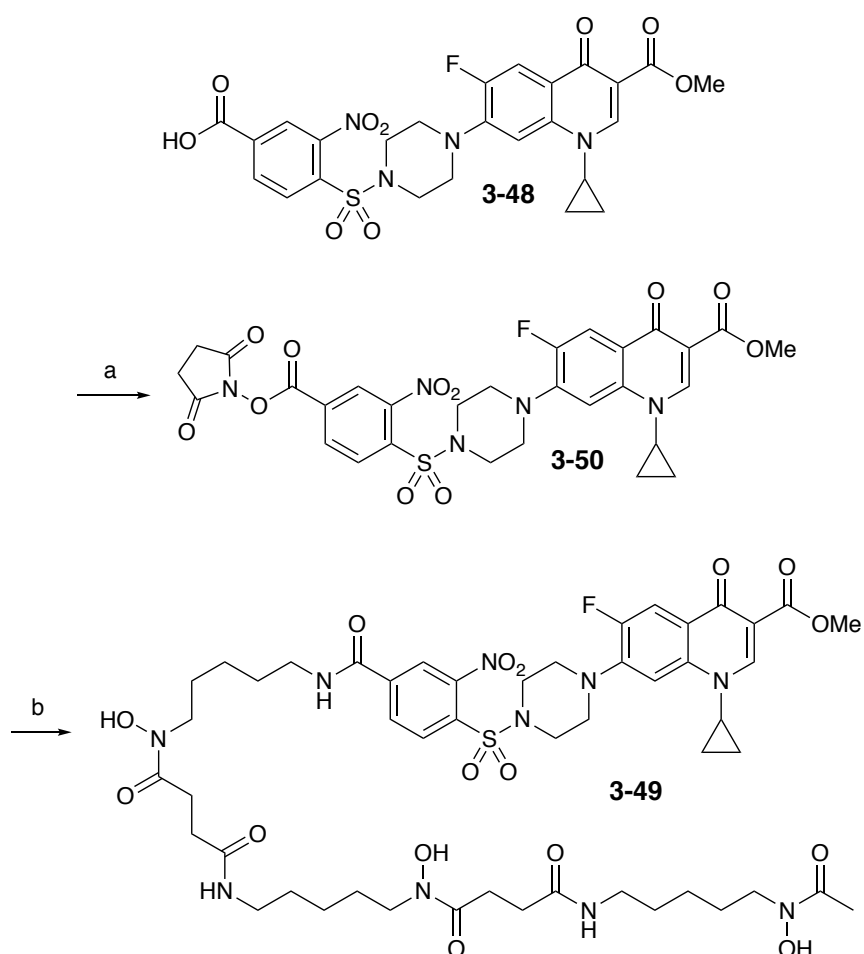
Scheme 3.25 Synthesis of deprotected ciprofloxacin-sulfonamide **3-48**. a) TFA (25% v/v), DCM (anhydrous), 4 h, 54%.

The coupling of DFO to **3-48** was initially attempted with HBTU as a coupling agent, but this proved unsuccessful, with a low yield and an impure product obtained. It was decided to instead synthesise an NHS ester of **3-48**, and carry out an amide coupling avoiding the use of coupling reagents.

The synthesis of NHS ester **3-50** was carried out using EDC.HCl as a coupling agent (**Scheme 3.26**). The presence of the NHS ester can be observed as a broad singlet in the  $^1\text{H}$  NMR spectrum at 2.95 ppm, and the ESI mass spectrum for the product displays peaks at  $m/z = 672.1396$  and  $694.1211$  which can be assigned as  $[\text{M}+\text{H}]^+ / [\text{M}+\text{Na}]^+$  adducts of molecular formula  $\text{C}_{29}\text{H}_{27}\text{FN}_5\text{O}_{11}\text{S}$  and  $\text{C}_{29}\text{H}_{26}\text{FN}_5\text{NaO}_{11}\text{S}$  respectively. **3-50** is unstable, with  $^1\text{H}$  NMR spectroscopic analysis showing it decomposing back to the parent carboxylic acid over a period of days (this instability can also be seen in the HPLC trace in **Figure 3.13**), and also decomposes when purification is attempted by column chromatography.

Therefore batches of **3-50** were reacted with DFO mesylate immediately following the EDC-mediated coupling, with **3-50** used in slight excess to ensure 100% consumption of the DFO component. The reaction of **3-50** with DFO mesylate is carried out in the presence of triethylamine in DMF at  $50^\circ\text{C}$ . Following removal of the DMF *in vacuo*, trituration of the resulting

residue in MeCN yields **3-49** as a yellow solid. Successful coupling was confirmed via  $^1\text{H}$  NMR spectroscopic analysis, with a shift in the quartet corresponding to the  $\text{CH}_2$  group adjacent to the terminal DFO amine from 2.76 ppm in the  $^1\text{H}$  NMR spectrum of DFO mesylate to 3.27 ppm in **3-49**, suggesting successful formation of an amide. In addition the ESI mass spectrum displayed a peak at  $m/z = 1117.4746$ , consistent with an  $[\text{M}+\text{H}]^+$  molecular ion of formula  $\text{C}_{50}\text{H}_{70}\text{FN}_{10}\text{O}_{16}\text{S}$ , and a peak at  $m/z = 1139.4508$ , consistent with an  $[\text{M}+\text{Na}]^+$  molecular ion of formula  $\text{C}_{50}\text{H}_{69}\text{FN}_{10}\text{NaO}_{16}\text{S}$ . HPLC also suggested successful conversion of **3-50** to a new product, with no trace of the NHS peak at a retention time of 8.64 minutes, and a new peak present at a retention time of 6.12 minutes (**Figure 3.13**).



Scheme 3.26 Synthesis of DFO conjugate **3-49** via NHS ester **3-50**. a) NHS, EDC.HCl, DCM (anhydrous), 21 h; b) Desferrioxamine mesylate (0.95 eq.),  $\text{Et}_3\text{N}$ , DMF,  $50^\circ\text{C}$ , 24 h, 83% over two steps.

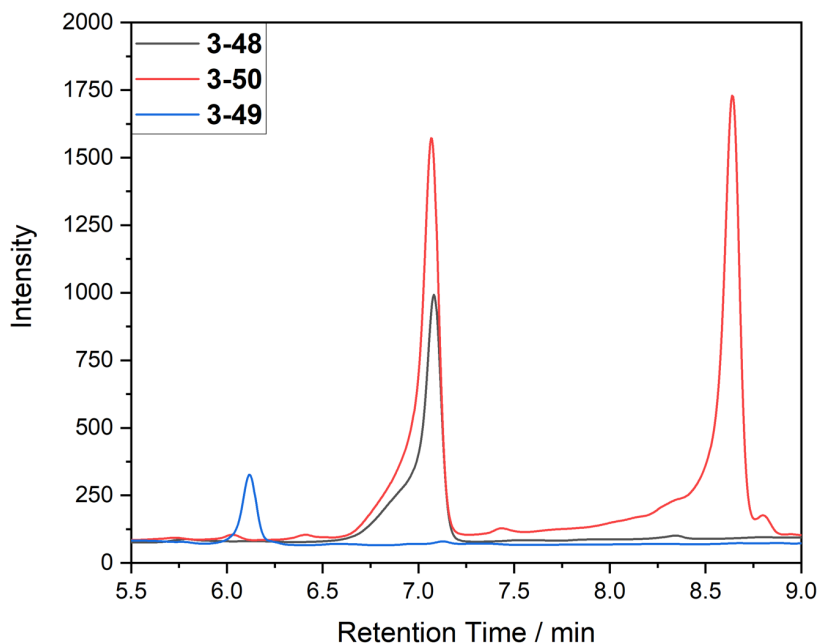
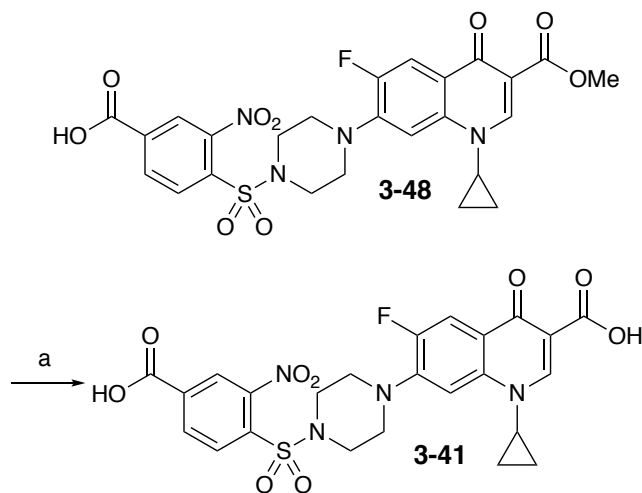


Figure 3.13 Overlaid HPLC traces for compounds **3-48**, **3-50** and **3-49**. Recorded on an Agilent HPLC, Eclipse XDB-C18 column, 30-70% MeCN:H<sub>2</sub>O, 220 nm wavelength.

### 3.3.4 Final Methyl Ester Deprotection and Attempted Purification

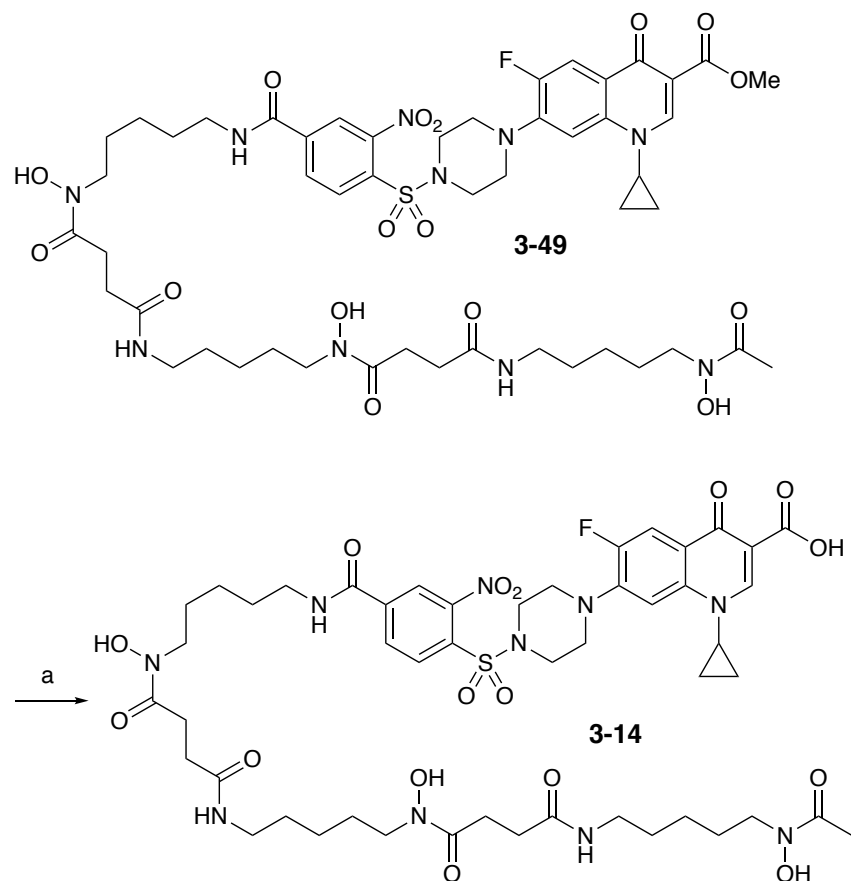
The final ester hydrolysis step to give conjugate **3-14** required optimisation of the equivalents of NaOH needed to remove the methyl ester; an initial reaction failed to achieve complete deprotection, so the deprotection conditions were trialed on the carboxylic acid **3-48** (**Scheme 3.27**). Addition of 10 equivalents of NaOH led to complete deprotection when the reaction was stirred for 24 hours, yielding dicarboxylic acid **3-41** following neutralisation with 1 M aq. HCl. This is evidenced by shifts in the aromatic region, and the observed loss of the methyl singlet resonance in the <sup>1</sup>H NMR spectrum, a shift of the fluorine resonance from -124.6 ppm to -121.8 ppm in the <sup>19</sup>F NMR spectrum, with the lower shift consistent with deprotected ciprofloxacin, and finally by ESI mass spectrometry, with peaks at *m/z* = 561.1086, 583.0890 and 605.0715 assigned to molecular ions [M+H]<sup>+</sup>, [M+Na]<sup>+</sup> and [M+2Na-H]<sup>+</sup> respectively, all of which are consistent with the desired product.



Scheme 3.27 Test of NaOH-mediated deprotection conditions carried out on **3-48**. a) 1 M aq. NaOH (10 eq.), 3:1 MeOH:H<sub>2</sub>O, 21 h.

These conditions transferred successfully to the deprotection of **3-49**. Addition of HCl post-reaction of **3-49** with NaOH resulted in the formation of a yellow-white precipitate; centrifugation, followed by removal of the solvent gave **3-14** as a yellow-white solid (**Scheme 3.28**). Successful deprotection of **3-14** was confirmed in a similar fashion to **3-48**, with observed loss of the methyl ester singlet at 3.73 ppm in the <sup>1</sup>H NMR spectrum, a shift in the ciprofloxacin fluorine resonance in <sup>19</sup>F NMR from –124.6 ppm to –121.8 ppm, and peaks at *m/z* = 1103.4534, 1125.4342 and 1147.4177 in the ESI mass spectrum, which can be assigned to [M+H]<sup>+</sup>, [M+Na]<sup>+</sup> and [M+2Na-H]<sup>+</sup> molecular ion peaks consistent with adducts of molecular formula C<sub>49</sub>H<sub>67</sub>FN<sub>10</sub>O<sub>16</sub>S. HPLC analysis appeared to suggest the compound contained a small amount of dicarboxylic acid **3-41** (among other small impurities), likely from deprotection of any remaining starting material from the DFO coupling step; this is supported by the presence of small peaks corresponding to **3-41** observed in the <sup>1</sup>H NMR spectrum, and a peak at the same retention time as **3-41** in the analytical HPLC (**Figure 3.14**).





Scheme 3.28 NaOH-mediated methyl ester hydrolysis to yield **3-14**. a) NaOH (aq., 10 eq.), 3:1 MeOH:H<sub>2</sub>O, 24 h, c. 60%.

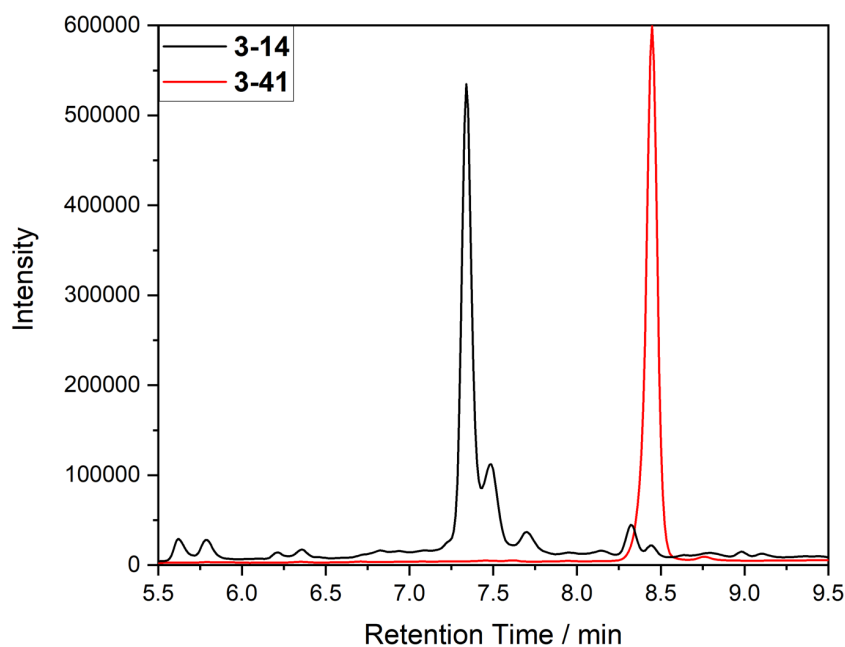


Figure 3.14 Overlaid HPLC traces for deprotected DFO conjugate **3-14** and dicarboxylic acid **3-41**. Recorded on a Shimadzu HPLC at 254 nm detection on an Eclipse XDB-C18 column, 25-70% MeCN:H<sub>2</sub>O.

The HPLC trace for conjugate **3-14** can be seen to contain two overlapping peaks between 7.25 and 7.50 minutes; these both have identical UV-vis

spectra (as measured via the HPLC), and later LCMS analysis of the peaks revealed ESI mass spectra with peaks observed at  $m/z = 1178.3463$  and  $1178.3464$  for each HPLC peak respectively, consistent with an  $[M+Na]^+$  molecular ion of the iron-bound DFO conjugate, with a molecular formula of  $C_{49}H_{64}FFeN_{10}NaO_{16}S$ . The presence of these peaks could indicate the presence of two different species of **3-14**, possibly an iron-bound and an iron-unbound version.

With a clear difference in peak elution times between **3-14** and the impurities observed in the HPLC traces, preparative HPLC was chosen as a purification method. Three batches of **3-14** were sent to an external company, Reach Separations, for purification. Their analysis of the batches also displayed two peaks at retention times of 7.15 and 7.34 minutes in each sample by HPLC; these were analysed further by LCMS. The second of the two HPLC peaks (7.34 min) contains mass spectral peaks at  $m/z = 578.96$  and  $1156.33$  respectively (both averages of the three batches, ranges =  $578.94$ - $578.97$  and  $1156.28$ - $1156.35$ ). The peak at  $1156.33$  is consistent with an  $[M+H]^+$  molecular ion peak for an iron-bound version of conjugate **3-14** (expected  $m/z = 1156.3629$ , **Figure 3.15**). The peak at  $578.96$  is close to the  $[M+2H]^{2+}$  peak (expected  $m/z = 578.6851$ ), but not an exact mass.

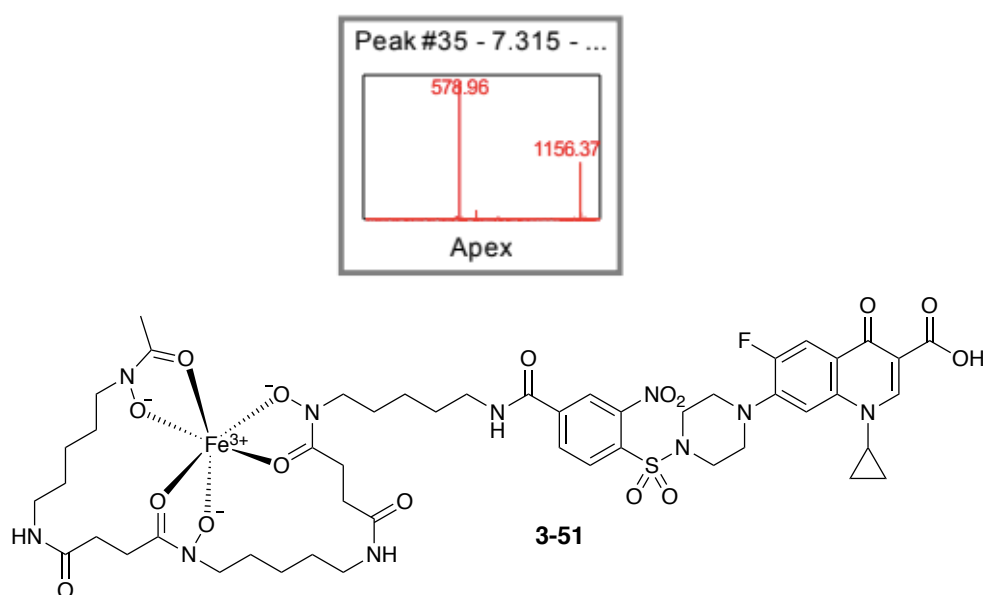


Figure 3.15 Observed peaks in LCMS analysis of second overlapping HPLC peak at 7.34 min, and structure of iron conjugate **3-51** consistent with observed mass (data obtained by Reach Separations).

The origin of the first HPLC peak at 7.15 minutes is a little less clear, although there are various possibilities. Again, two mass spectral peaks are observed at  $m/z = 564.50$  and  $1127.42$  respectively (averages of 3 batches, ranges =  $564.49$ - $564.51$  and  $1127.37$ - $1127.51$ ). The closest plausible structures to this mass are aluminium and silicon-bound versions of conjugate **3-14** (**Figure 3.16**). Desferrioxamine has previously been shown to bind Al(III) ions, albeit with a lower stability constant than iron,<sup>491</sup> and silicon conjugates of enterobactin/salmochelin have been observed in the literature.<sup>492</sup> Predicted aluminium (Al<sup>3+</sup>) conjugate **3-52** has an expected  $m/z = 1127.4095$  for the [M+H]<sup>+</sup> molecular ion, and silicon (Si<sup>4+</sup>) conjugate **3-53** has an expected  $m/z = 1127.3971$  for the [M]<sup>+</sup> molecular ion. The corresponding 2+ molecular ion peaks, [M+2H]<sup>2+</sup> and [M+H]<sup>2+</sup>, have expected  $m/z = 564.2084$  and  $564.2022$  respectively, so could potentially correlate to the peak at 564.50.

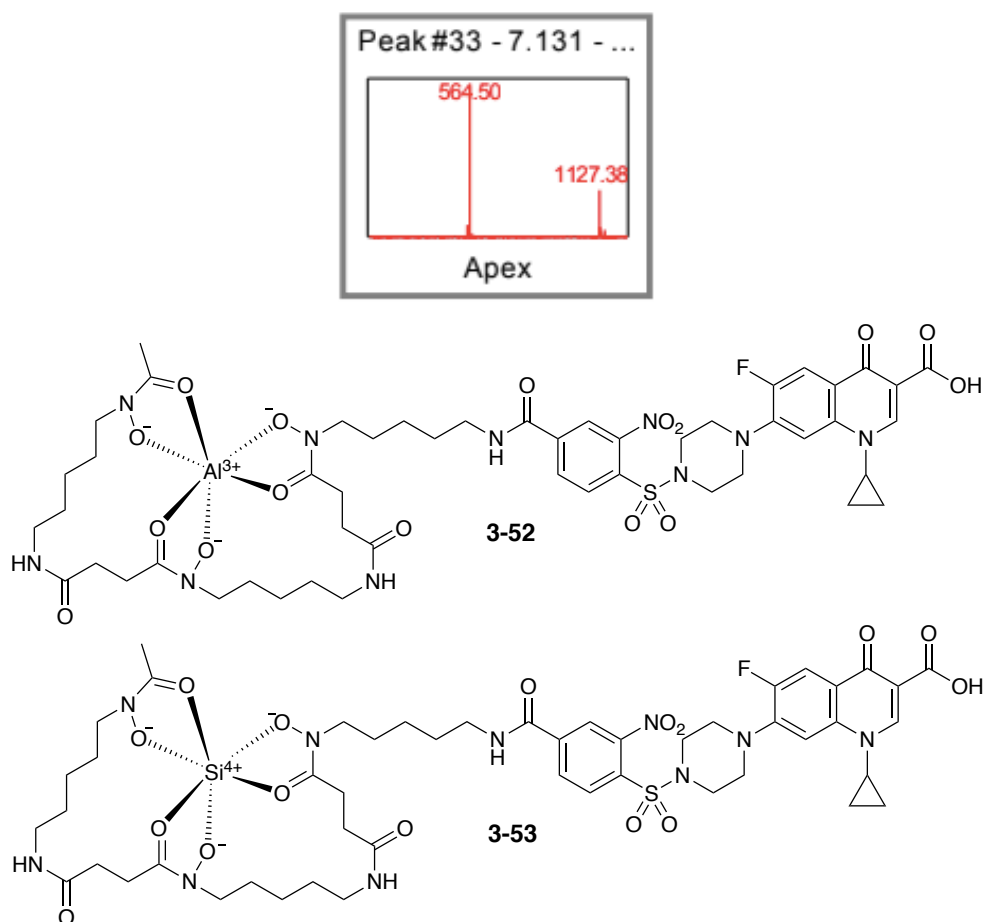


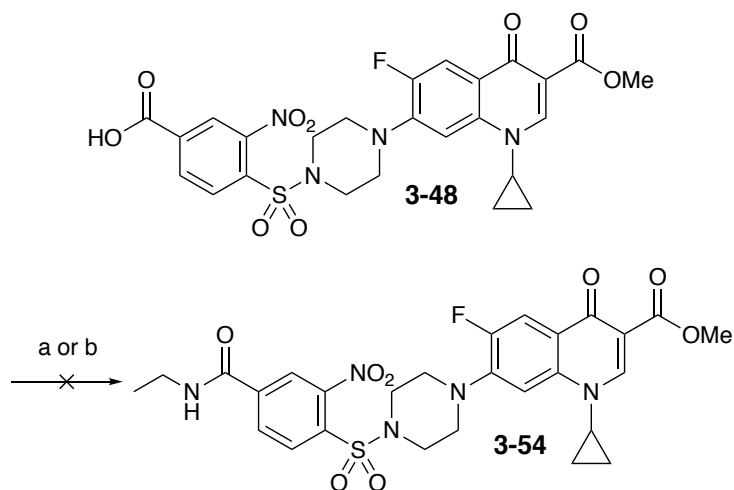
Figure 3.16 Observed peaks in LCMS analysis of first overlapping HPLC peak at 7.15 min, and structure of aluminium/silicon conjugates consistent with observed mass (data obtained by Reach Separations).

Reach Separations were unable to purify conjugate **3-14** by preparative HPLC, with collected fractions from **3-14** displaying an HPLC profile very similar to the crude analysis, suggesting poor separation of **3-14** from the impurities present. In addition, they reported “decomposition” of the compound when in solution over a 24-hour period (although they don’t state how this was observed). In the author’s hands, no decomposition was observed by HPLC when a solution of **3-14** in DMSO with a concentration of 12 mg/mL was left over a 42-hour period (equivalent to the concentration used for their purification attempts), with no new peaks emerging in the HPLC trace. There is a slight change in the appearance of the peak for **3-14**, from a broad peak after 15 minutes (possibly from two overlapping peaks), to a single defined peak after 19 hours, possibly indicating conversion of the unbound DFO to one of the complexed species seen above.

The purity of the crude **3-14** was examined by quantitative  $^1\text{H}/^{19}\text{F}$  NMR spectroscopy to determine its suitability for further studies. Stock solutions of **3-14** and fluorobenzene in DMSO- $d_6$  were made up, and combined to give a solution which should contain a 1:1 ratio of **3-14** to fluorobenzene if **3-14** is 100% pure. Comparison of the integration of the fluorobenzene protons in the  $^1\text{H}$  NMR spectrum to the resonances corresponding to aromatic protons in **3-14** suggested a purity of 90%. The resonances at 2.99 ppm, 2.57 ppm and 2.26 ppm suggest a similar purity (average 89%), while the methyl singlet at 1.96 ppm suggests a purity of 76%. It should be noted that the methyl resonance consistently displays a lower integration than expected when compared to other peaks in DFO, both in samples of pure DFO mesylate, and in other literature studies, so this may account for the lower purity estimate, and it can likely be discounted.<sup>493,494</sup> Surprisingly, the  $^{19}\text{F}$  NMR spectrum suggests an excess of **3-14** is present compared to fluorobenzene; this was also discounted as an anomalous result. The purity was considered high enough for biological studies of the unpurified conjugate to take place.

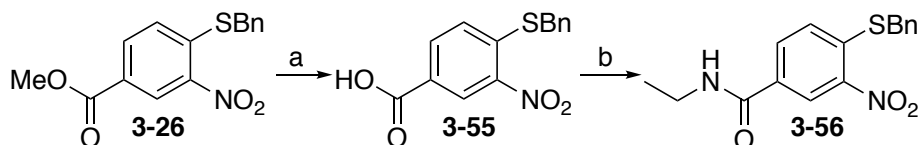
### 3.3.5 Synthesis of Microbiological Control Compounds

The synthesis of Cipro +, DFO – control **3-34** was initially attempted from ciprofloxacin-sulfonamide conjugate **3-48**, with amide coupling to yield intermediate **3-54** attempted with EDC.HCl, HOBT and ethylamine. When this proved unsuccessful, a reaction of ethylamine with NHS ester **3-50** was also attempted, again with no success (**Scheme 3.29**).



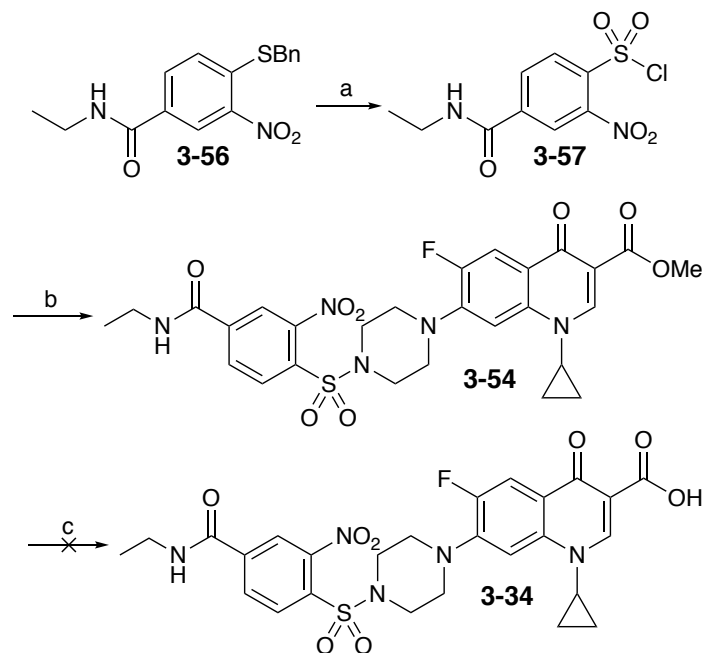
Scheme 3.29 Attempted synthesis of **3-54** from **3-48**. a) EtNH<sub>2</sub> (2 M in THF), EDC.HCl, HOBT, Et<sub>3</sub>N, DCM, 48 h; b) 1) NHS, EDC.HCl, DCM (anhydrous), 24 h; 2) EtNH<sub>2</sub> (2 M in THF), Et<sub>3</sub>N, THF, 48 h.

An alternate route to **3-34** was envisaged from benzyl thioether **3-26**. NaOH-mediated deprotection of the thioether according to literature conditions<sup>426</sup> yields carboxylic acid **3-55** in 81% yield. Successful formation can be confirmed by the observed loss of the methyl ester singlet in the <sup>1</sup>H NMR spectrum, and the ESI negative mass spectrum, with a peak at  $m/z = 288.0340$ , consistent with an  $[M-H]^-$  peak corresponding to a molecular formula of C<sub>14</sub>H<sub>10</sub>NO<sub>4</sub>S. **3-55** can then be coupled to ethylamine to give amide **3-56** (**Scheme 3.30**). The <sup>1</sup>H NMR spectrum of **3-56** displays a broad amide NH resonance at 6.13 ppm, and the characteristic ethyl triplet/quartet (in this case a dq) pattern at 1.27 and 3.51 ppm respectively. A molecular ion peak  $[M+H]^+$  can be observed at  $m/z = 317.0955$  in the ESI positive ion mass spectrum of **3-56**, corresponding to the molecular formula C<sub>16</sub>H<sub>17</sub>N<sub>2</sub>O<sub>3</sub>S. This is replicated in the ESI negative ion mass spectrum, with an  $[M-H]^-$  peak at  $m/z = 315.0813$ , which is consistent with a molecular formula of C<sub>16</sub>H<sub>15</sub>N<sub>2</sub>O<sub>3</sub>S.



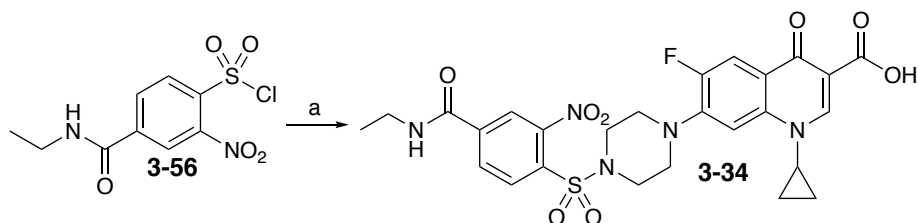
Scheme 3.30 Synthesis of ethyl amide **3-56**. a) NaOH, 1:1 THF:MeOH, 15 h, 81%; b) EtNH<sub>2</sub>.HCl, EDC.HCl, HOBT, Et<sub>3</sub>N, DCM (anhydrous), 20 h, 80%.

Ethyl amide **3-56** was subjected to oxidative chlorination to form sulfonyl chloride **3-57** using the DCDMH-based conditions employed earlier. Successful formation of **3-57** is supported via the observed loss of the benzyl CH<sub>2</sub> singlet at 4.24 ppm in the <sup>1</sup>H NMR spectrum, and the presence of peaks at *m/z* = 292.9982 and 314.9808 observed in the ESI mass spectrum, which can be assigned as [M+H]<sup>+</sup> and [M+Na]<sup>+</sup> molecular ions consistent with molecular formulas C<sub>9</sub>H<sub>10</sub><sup>35</sup>ClN<sub>2</sub>O<sub>5</sub>S and C<sub>9</sub>H<sub>9</sub><sup>35</sup>ClN<sub>2</sub>NaO<sub>5</sub>S respectively. **3-57** was then coupled to ciprofloxacin methyl ester (**3-46**) to give **3-54** (Scheme 3.31). Successful formation of **3-54** is supported by observed shifts in the positions of the characteristic d/dd/d resonances for the 4-ethylamide-2-nitrobenzenesulfonamide compared to sulfonyl chloride **3-57**; the doublets display shifts from 8.31 to 8.17 ppm and 8.25 to 8.38 ppm, and the doublet of doublets from 8.19 to 8.26 ppm. Furthermore, observed peaks in the ESI mass spectrum at *m/z* = 602.1724 and 624.1547, which can be assigned as [M+H]<sup>+</sup> and [M+Na]<sup>+</sup> molecular ions consistent with molecular formulas of C<sub>27</sub>H<sub>29</sub>FN<sub>5</sub>O<sub>8</sub>S and C<sub>27</sub>H<sub>28</sub>FN<sub>5</sub>NaO<sub>8</sub>S. Unfortunately, attempting NaOH-mediated deprotection of **3-54** under similar conditions to those employed for **3-14** (10 eq. NaOH, MeOH:H<sub>2</sub>O) failed to give control **3-34**, and instead resulted in decomposition over an extended reaction time, with a number of different peaks observed in the <sup>19</sup>F NMR spectrum, and the aromatic region of the <sup>1</sup>H NMR spectrum, indicating the formation of multiple products.



Scheme 3.31 Attempted synthesis of control compound **3-34**. a) 1,3-dichloro-5,5'-dimethylhydantoin, MeCN:AcOH:H<sub>2</sub>O (40:1.5:1), 0 to 20 °C, 24 h; b) **3-46**, Et<sub>3</sub>N, DCM (anhydrous), 26 h, 78% over 2 steps; c) NaOH (1 M aq., 10 eq.), MeOH:H<sub>2</sub>O (3:1), 96 h.

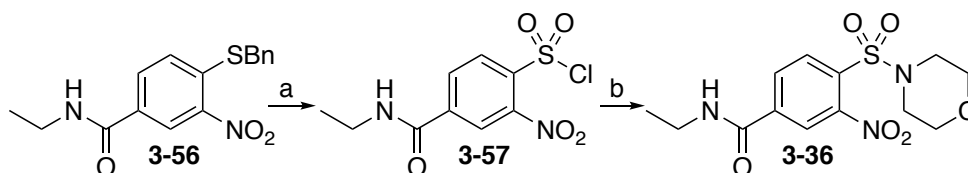
The use of unprotected ciprofloxacin in the sulfonamide formation was then trialled, with sulfonyl chloride **3-57** present in excess. This resulted in the successful formation of control **3-34** (Scheme 3.32). The chemical shifts of the protons on the sulfonamide ring shift in an analogous pattern to those for **3-54** (doublets from 8.31 to 8.17 ppm and 8.25 to 8.38 ppm, and the doublet of doublets from 8.19 to 8.26 ppm). In addition, a peak can be observed at  $m/z = 610.1383$  in the ESI mass spectrum, corresponding to an  $[M+Na]^+$  adduct of molecular formula C<sub>26</sub>H<sub>26</sub>FN<sub>5</sub>NaO<sub>8</sub>S.



Scheme 3.32 Synthesis of Cipro +, DFO – control **3-34**. a) Ciprofloxacin, Et<sub>3</sub>N, DCM, 22 h, 78%.

The synthesis of Cipro –, DFO – control **3-36** was initially attempted via a similar route to **3-34**. Instead of ciprofloxacin, sulfonyl chloride **3-57** was reacted with morpholine to successfully yield control **3-36** (Scheme 3.33).

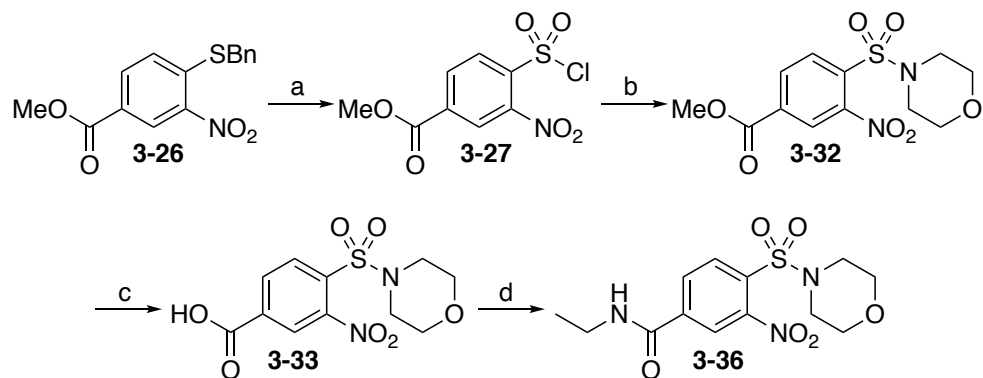
Successful synthesis can be supported by the presence of multiplets at 3.74 and 3.30 ppm in the  $^1\text{H}$  NMR spectrum, which can be assigned to the morpholine protons, and a peak at  $m/z = 366.0727$  in the ESI mass spectrum, consistent with an  $[\text{M}+\text{Na}]^+$  adduct of molecular formula  $\text{C}_{13}\text{H}_{17}\text{N}_3\text{NaO}_6\text{S}$ . However, separation of **3-36** from the byproducts of the sulfonyl chloride synthesis proved problematic, especially in the case of *N*-benzylacetamide, which co-elutes with **3-36** after column chromatography.



Scheme 3.33 Initial synthetic route to Cipro-, DFO – control **3-36** from **3-57**.  
 a) DCDMH, MeCN:AcOH:H<sub>2</sub>O, (40:1.5:1), 0 °C, 24 h; b) Morpholine, Et<sub>3</sub>N, DCM (anhydrous), 0 °C to rt, 23 h.

A new route was devised, with the order of synthesis steps altered. Benzyl thioether **3-26** was reacted with DCDMH to generate methyl ester protected sulfonyl chloride **3-27**, which was then reacted with morpholine to yield sulfonamide **3-32** (Scheme 3.34). Multiplets corresponding to the morpholine protons can be observed at 3.75 and 3.32 ppm in the  $^1\text{H}$  NMR spectrum, and the ESI mass spectrum displays peaks at  $m/z = 331.0594$  and  $353.0415$ , which can be assigned as  $[\text{M}+\text{H}]^+$  and  $[\text{M}+\text{Na}]^+$  peaks consistent with molecular formulas  $\text{C}_{12}\text{H}_{15}\text{N}_2\text{O}_7\text{S}$  and  $\text{C}_{12}\text{H}_{14}\text{N}_2\text{NaO}_7\text{S}$  respectively. The crude product was then subjected to NaOH-mediated ester hydrolysis to give carboxylic acid **3-33**. The loss of the methyl ester singlet in the  $^1\text{H}$  NMR spectrum supported successful hydrolysis, as does peaks observed at  $m/z = 292.9982$  and  $314.9808$  in the ESI mass spectrum, consistent with  $[\text{M}+\text{H}]^+$  and  $[\text{M}+\text{Na}]^+$  adducts with molecular formulas of  $\text{C}_{11}\text{H}_{13}\text{N}_2\text{O}_7\text{S}$  and  $\text{C}_{11}\text{H}_{12}\text{N}_2\text{NaO}_7\text{S}$ . The product **3-33** can now be subjected to amide coupling with ethylamine to give control **3-36**, which was obtained in 52% yield following column chromatography.

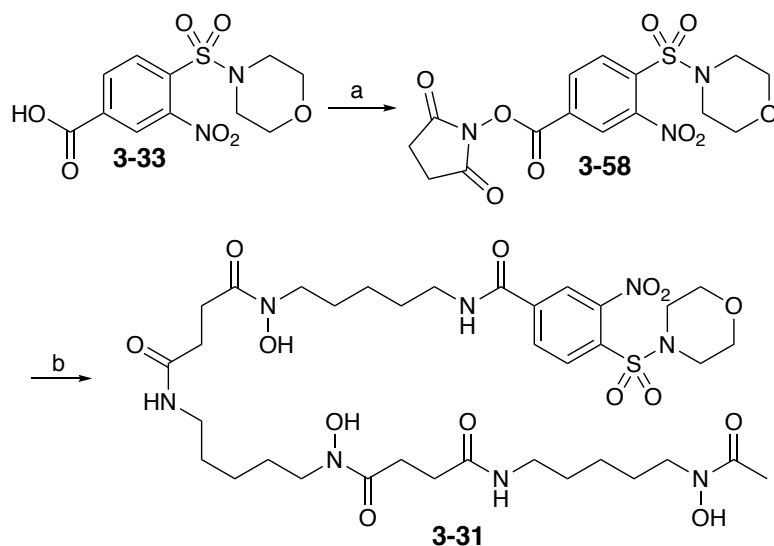




Scheme 3.34 Alternative synthesis of Cipro-, DFO- control **3-36** from **3-26**.

a) DCDMH, MeCN:AcOH:H<sub>2</sub>O, (40:1.5:1), 0 °C, 3 h; b) Morpholine, Et<sub>3</sub>N, DCM (anhydrous), 0 °C to rt, 18 h; c) NaOH (aq.), THF:MeOH (1:1), 24 h, 71% over 3 steps; d) EtNH<sub>2</sub>.HCl, EDC.HCl, HOBT, Et<sub>3</sub>N, DCM (anhydrous), 23 h, 52%.

**3-33** was also used for the synthesis of Cipro-, DFO + control **3-31**. Here, **3-33** was first converted to NHS ester **3-58**, which undergoes reaction with DFO mesylate in a similar fashion to **3-50**, resulting in the successful synthesis of control **3-31** (Scheme 3.35). Evidence for formation of NHS ester **3-58** comes from the presence of a broad singlet observed at 2.94 ppm in the <sup>1</sup>H NMR spectrum with a relative integration of 4H, corresponding to the NHS protons, and a peak in the ESI mass spectrum at  $m/z = 436.0419$ , corresponding to an [M+Na]<sup>+</sup> molecular ion of formula C<sub>15</sub>H<sub>15</sub>N<sub>3</sub>NaO<sub>9</sub>S. Formation of control **3-31** is supported by a shift in the CH<sub>2</sub> protons adjacent to the terminal DFO amine from 2.76 ppm in the <sup>1</sup>H NMR spectrum of DFO mesylate to 3.27 ppm in the <sup>1</sup>H NMR spectrum of **3-31**, and furthermore the presence of a peak at  $m/z = 881.3715$  in the ESI mass spectrum, consistent with an [M+Na]<sup>+</sup> molecular ion of molecular formula C<sub>36</sub>H<sub>58</sub>N<sub>8</sub>NaO<sub>14</sub>S.



Scheme 3.35 Synthesis of Cipro -, DFO + control **3-31**. a) NHS, EDC.HCl, DCM (anhydrous), 25 h; b) Desferrioxamine mesylate, Et<sub>3</sub>N, DMF, 50 °C, 24 h, 72% over 2 steps.

The purities of Cipro -, DFO + control **3-31** and Cipro +, DFO - control **3-34** were assessed by quantitative <sup>1</sup>H NMR spectroscopy in a similar manner to **3-14**. Maleic acid was used instead of fluorobenzene as a quantitative NMR standard. Comparison of integrations for the aromatic region of **3-31** (Cipro -, DFO +) suggests a purity of 94%; integrations in the alkyl region suggested an excess of **3-31** vs. maleic acid, but this likely comes from a poorly-resolved baseline. Similar results were obtained for **3-34**, with an average purity of 96% based on integrations for the aromatic protons. Cipro -, DFO - control **3-36** displayed high purity via <sup>1</sup>H NMR spectroscopy and elemental analysis.

### 3.4 Aqueous Solubility of Compounds

Before undertaking SO<sub>2</sub> release studies or biological studies of conjugate **3-14** and the associated control compounds, their solubility in aqueous media was examined. The solubility of the compounds determines whether they can be successfully studied further in liquid media, especially in the case of antibacterial studies, where compound precipitation can interfere with assay results. With the hydrophobic 4-carboxyl-2-nitrobenzene and ciprofloxacin components of conjugate **3-14**, poor solubility in aqueous media is a potential concern.

The solubility of the conjugates was examined in Mueller-Hinton II Broth (MHII). This medium consists of casein hydrolysate, beef extract and starch, plus  $\text{MgSO}_4$  and  $\text{CaCl}_2$ . MHII is often recommended as a growth medium for standardised MIC testing protocols,<sup>495–499</sup> and is widely used for the study of Trojan Horse conjugates,<sup>118,170,187,193,264</sup> with the addition of supplemental 2,2'-bipyridine (bpy) to enforce iron-limited conditions. Experiments by James Southwell in the AKDK group have demonstrated that treating MHII broth with a Chelex resin, and then adding bpy to complex any remaining iron, yields a medium in which bacterial growth displays “true” iron limited behaviour (i.e. the rate of bacterial growth differs significantly between the iron-limited and iron-rich conditions).

Controls **3-31** and **3-36** are soluble in DMSO at a concentration of 10 mM. Control **3-34** is less soluble, with a maximum concentration around 5 mM following sonication; some minor precipitation of the compound at this concentration was observed after three months. Conjugate **3-14** is only partially soluble at 10 mM, with an insoluble film persisting around the edges of the solution; complete dissolution is achieved upon dilution to 1.25 mM. The solubility of **3-14** and the three controls in MHII was examined at two DMSO concentrations relevant to biological studies: 2% DMSO in MHII, which is the percentage of organic solvent employed in 96-well plate growth assays, and 50% v/v DMSO:MHII broth, which is required for the determination of MIC values by broth dilution. Solubility was assessed visually, with a clear solution taken to indicate full solubility of the compounds. MHII was syringe filtered before the solubility tests to remove any solid particles from the media. The solubilities of the compounds are displayed in **Table 3.1**.

Compound	Solubility (2% DMSO:MHII)	Solubility (50% DMSO:MHII)
<b>3-14</b>	< 25 $\mu$ M	125 to 312.5 $\mu$ M
<b>3-31</b>	> 200 $\mu$ M	ND
<b>3-34</b>	< 25 $\mu$ M	125 to 250 $\mu$ M
<b>3-36</b>	> 200 $\mu$ M	ND

Table 3.1 Solubilities observed for **3-14** and control compounds in 2% DMSO in MHII and 50% v/v DMSO in MHII. ND = not determined.

As can be seen from the data in **Table 3.1**, both ciprofloxacin conjugates **3-14** and **3-34** display limited solubility in MHII. Given the sub-micromolar activity of ciprofloxacin,<sup>189,264,435</sup> these limited solubilities may not be a problem in antimicrobial assays, but they indicate a significant limitation on the use of the 4-carboxyl-2-nitrobenzene linkers in systems containing other hydrophobic or poorly soluble components like ciprofloxacin.

### 3.5 Iron Complexation Studies via Native ESI Mass Spectrometry

As a hexadentate siderophore, DFO is expected to coordinate Fe(III) in a 1:1 ratio.<sup>500,501</sup> To examine the iron-coordinating ability of the DFO conjugates, native ESI mass spectrometry was used to probe the species formed when a DFO conjugate was mixed with FeCl<sub>3</sub> in solution. Native ESI mass spectrometry is an approach to mass spectrometry where the analytes, typically biomolecules, are sprayed into the spectrometer from a non-denaturing solvent;<sup>502</sup> this has the advantage of maintaining the structures present in solution to a greater extent than traditional ESI mass spectrometry, minimising events like protein unfolding. This technique can also be applied to the study of siderophore-iron complexes.<sup>436,503,504</sup>

Cipro -, DFO + control **3-31** was selected for this experiment due to its high aqueous solubility. The buffer selected for the native ESI mass spectrometry was ammonium acetate, a volatile buffer that is commonly used for native ESI experiments.<sup>505</sup> Stock solutions of FeCl<sub>3</sub> (1 mM aq.) and control **3-31** (1 mM in DMSO) are combined to yield an orange solution, suggesting formation of the desired Fe(III) complex (**3-59**, **Figure 3.17**). The solvent was removed under vacuum, and the resulting residue re-dissolved in

ammonium acetate buffer at pH 7.40, yielding a slightly cloudy suspension, which was filtered and the filtrate submitted for analysis. The resulting ESI mass spectrum displays three peaks at  $m/z = 912.3023$ ,  $934.2840$  and  $950.2591$  respectively, consistent with  $[M+H]^+$ ,  $[M+Na]^+$  and  $[M+K]^+$  adducts of molecular formulas  $C_{36}H_{56}FeN_8O_{14}S$ ,  $C_{36}H_{55}FeN_8NaO_{14}S$  and  $C_{36}H_{55}FeKN_8O_{14}S$  respectively, all of which display the expected 1:1 DFO:Fe(III) coordination.

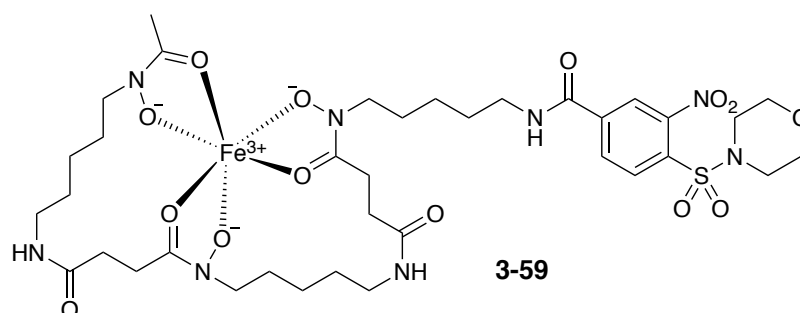
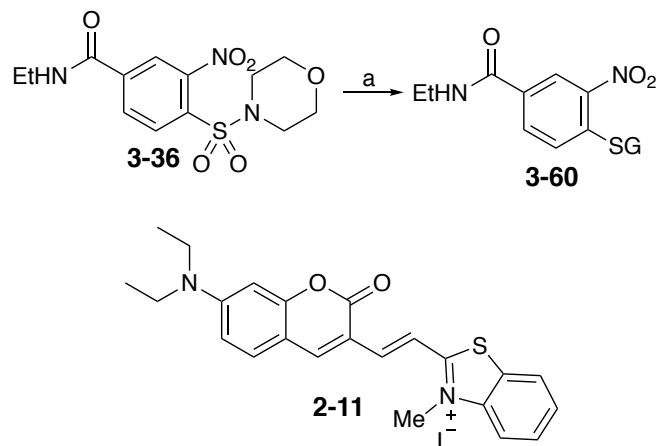


Figure 3.17 Structure of complex **3-59** observed by native ESI mass spectrometry.

### 3.6 SO<sub>2</sub> Release Studies

As with the conjugates studied in Chapter 2, examining SO<sub>2</sub> release from the 4-carboxyl-2-nitrobenzene-based linkers is a key part of their evaluation. If the linkers are unable to undergo efficient reaction with biological thiols to release ciprofloxacin and SO<sub>2</sub>, then they will be unable to function as effective antimicrobials.

A qualitative study of SO<sub>2</sub> release was carried out using the SO<sub>2</sub>-detecting dye **2-11** previously described in Chapter 2, and Cipro –, DFO – control **3-36**, which displays high aqueous solubility. The experiment was carried out under analogous conditions to the SO<sub>2</sub> release experiments described in Chapter 2 (10 eq. GSH, 0.1 eq. **2-11**, 10% MeCN in HEPES buffer, pH 7.4, **Scheme 3.36**).



Scheme 3.36 Reaction of **3-36** with glutathione in HEPES buffer in presence of dye **2-11**. a) GSH (10 eq.), **2-11** (0.1 eq.), 10% MeCN:HEPES, pH 7.4, rt, 24 h.

The UV-vis spectrum obtained shows gradual loss of the dye absorbance band at 545 nm over a period of 24 hours (**Figure 3.18**), indicating release of SO<sub>2</sub>, albeit at a much slower rate than the previously-studied 2,4-dinitrobenzenesulfonamide conjugates, which see loss of the dye absorbance band in around 30 minutes.

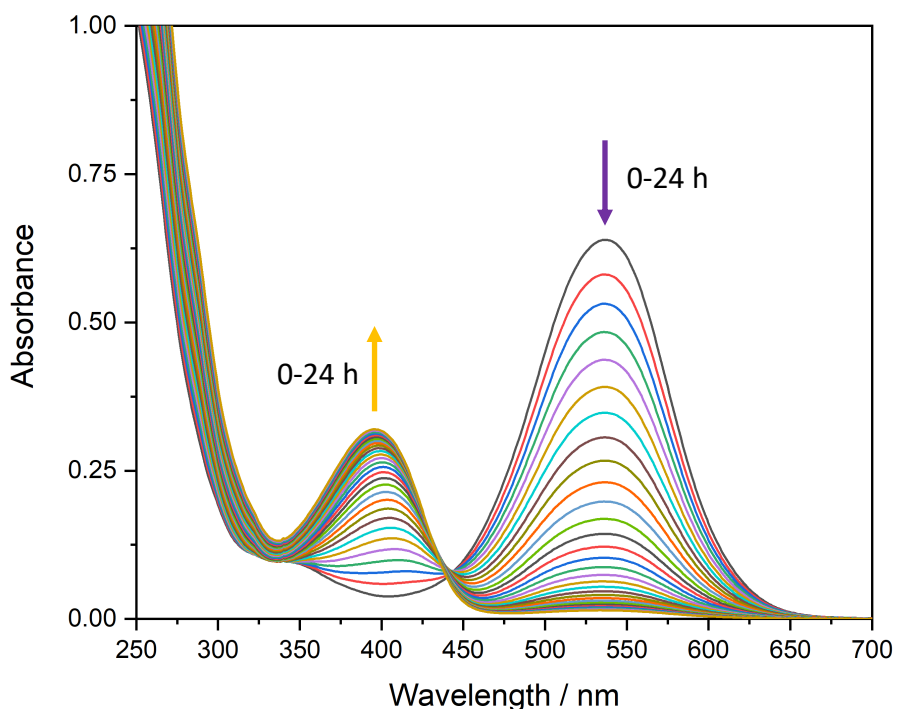
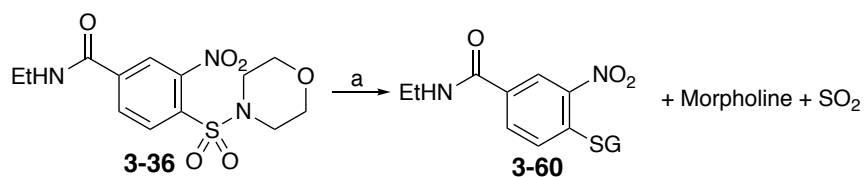


Figure 3.18 UV-visible spectra for the reaction of **3-36** with glutathione in the presence of dye **2-11**, recorded over 24 hours. The spectra displayed are at intervals of 50 minutes.

The slow rate of SO<sub>2</sub> release observed in the experiments with dye **2-11**, and the much lower extinction coefficient for the 4-carboxyl-2-nitrobenzene-glutathione conjugate compared to the 2,4-dinitrobenzene-glutathione conjugate previously studied (1000 to 3000 M<sup>-1</sup> cm<sup>-1</sup> vs. 10500 M<sup>-1</sup> cm<sup>-1</sup>)<sup>506-508</sup> disfavoured the use of UV-vis experiments for obtaining quantitative data of the release rate. Instead, the rate of release was examined using an HPLC assay. This has the added benefit of allowing elevated temperatures to be used, in this case experiments were carried out at 37 °C. Caffeine was added to the reaction as an internal standard to allow quantification of the amount of control **3-36** present as the reaction progresses. A calibration curve for the experiment was prepared by examining the ratio of HPLC integrations between caffeine and **3-36**; the caffeine concentration remained fixed, while the concentration of **3-36** was varied. All other conditions were maintained from the SO<sub>2</sub> release assays previously carried out. Aliquots were taken from the reaction mixture at various intervals throughout the reaction for HPLC analysis.



Scheme 3.37 Reaction of **3-36** with glutathione in HEPES buffer. a) GSH (10 eq.), caffeine (5 eq.), 10% MeCN:HEPES, pH 7.4, 37 °C, 74 h.

The HPLC experiment shows a moderately fast initial reaction, with c. 25% of **3-36** reacting over the first two hours, and 45% after c. 10 hours (**Figure 3.19**). However, the rate of reaction drops off significantly, with conversion only reaching 59% after 21 hours, and 73% after 52 hours. As the reaction was carried out under aerobic conditions, a likely cause of this is oxidation of the glutathione to its corresponding disulfide in the reaction mixture, removing some or all of the free thiol present in the reaction mixture and preventing the reaction from going to completion. Oxidation of glutathione on incubation at 37 °C in aqueous buffer has previously been observed in the literature to varying extents (for example, Nomi *et al.* report 30% conversion over 24 hours, while Petruzzella *et al.* report full conversion).<sup>509,510</sup> A similar experiment was attempted with DFO conjugate

**3-14**, but this proved impossible due to its poor aqueous solubility, with a negligible amount of **3-14** visible in the HPLC trace.

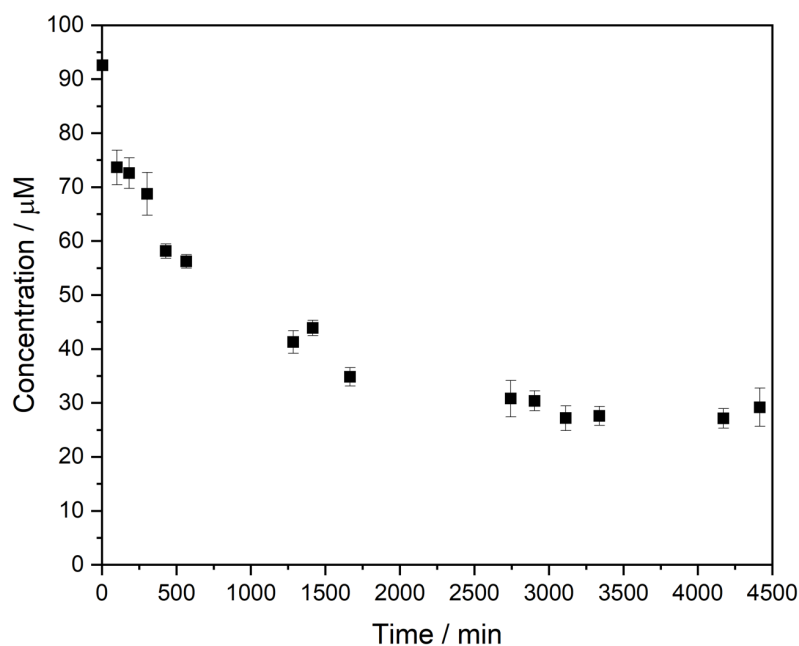


Figure 3.19 Change in concentration of **3-36** over 74 hours on reaction with glutathione in HEPES buffer as determined by HPLC.

This slow rate of release is not unexpected, given the reduction in electron-withdrawing ability provided by the carboxylic acid of **3-36** compared to the nitro group present in 2,4-dinitrobenzenesulfonamides. Even if the initial reaction rate observed by HPLC had remained constant, this would still represent a significant decrease on the rate of  $\text{SO}_2$  release from 2,4-dinitrobenzenesulfonamides. Slow rates of  $\text{SO}_2$  release were observed in other 4-carboxyl-2-nitrobenzenesulfonamide-based systems (**Section 3.1.1.1**). Photoaffinity probe **3-7**, synthesised by Yokoshima *et al.*, displayed 100% conversion over 33 hours on reaction with 10 equivalents of 2-mercaptoethanol in phosphate buffer,<sup>427</sup> while Ito *et al.* observed only 5% conversion over 60 minutes for coumarin conjugate **3-8** on reaction with 80 equivalents of glutathione at 37 °C in phosphate buffer.<sup>428</sup> These slow rates are also not entirely representative of the situation inside the bacterial cytoplasm. Here, the presence of glutathione transferase (GST) enzymes has the potential to accelerate the nucleophilic aromatic substitution reaction with glutathione. For example, Ito *et al.* see a 17-fold increase in conversion over the same time period when 10  $\mu\text{g}/\text{mL}$  of a GST enzyme is present.<sup>428</sup>



While the examination of the reactivity of **3-36** in the presence of GST enzymes was considered, bacterial GST enzymes are not commercially available, and the purchase of an alternate GST enzyme was considered an inadequate substitute.

### 3.7 Biological Studies

*The antimicrobial assays detailed in this section were carried out by Cerys Orritt and Dr Angela Oates at the Hull York Medical School.*

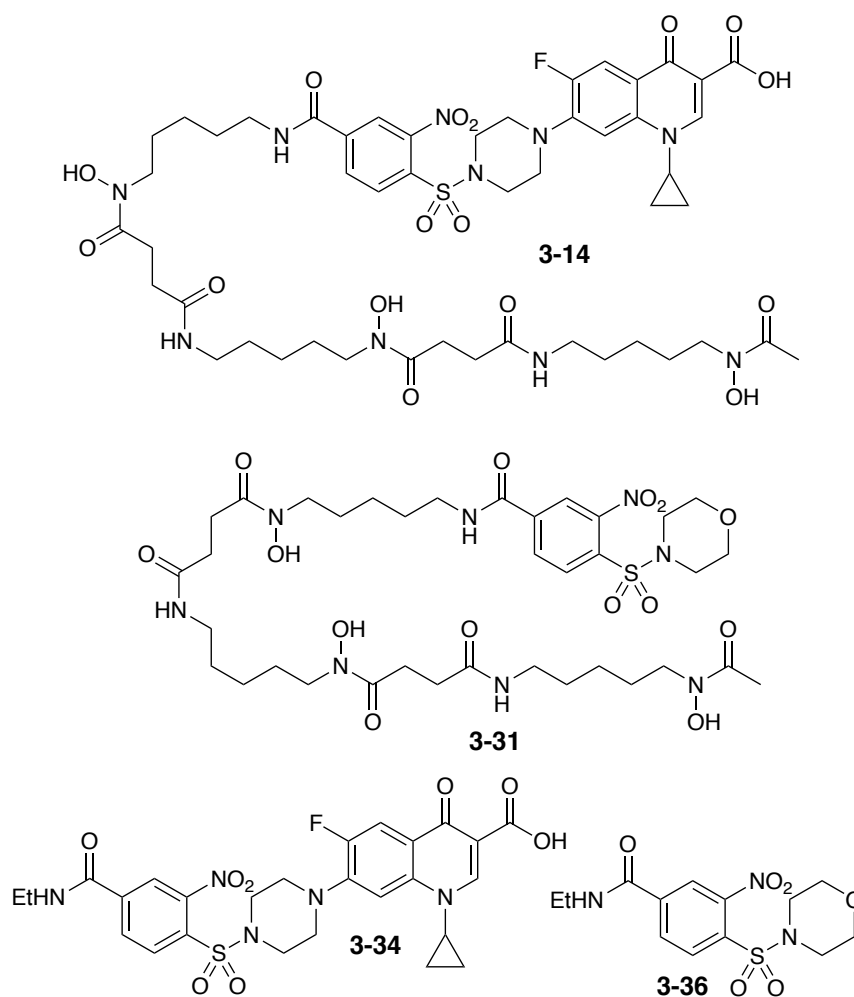


Figure 3.20 Structures of conjugate **3-14** and microbiological controls assessed in antimicrobial assays.

Examination of the antimicrobial activity of conjugate **3-14**, and the microbiological controls (**Figure 3.20**), was carried out against a panel of bacterial species (**Table 3.2**), including both Gram-positive and Gram-negative bacteria, and four of the six ESKAPE bacterial species. The ESKAPE bacteria are responsible for the majority of hospital-acquired infections,

often via resistant strains, and are considered key targets for new antimicrobial development.<sup>511,512</sup> The panel also includes strains with a variety of sensitivities to ciprofloxacin as defined by Vitek-2 screening,<sup>513–515</sup> and confirmed by disk diffusion assays compared to EUCAST breakpoint data.<sup>516</sup> This may allow evaluation of the ability of **3-14** to bypass ciprofloxacin resistance, although the mechanisms of resistance in the strains selected are not known, so it is possible that none possess uptake-mediated resistance.

<b>Bacterial Strain Number</b>	<b>Species</b>	<b>Ciprofloxacin Sensitivity</b>
AC2	<i>Acinetobacter baumannii</i>	Resistant
PS2	<i>Pseudomonas aeruginosa</i>	Ciprofloxacin susceptible with increased exposure
PS3	<i>Pseudomonas aeruginosa</i>	Sensitive
EC1	<i>Escherichia coli</i>	Sensitive
EC3	<i>Escherichia coli</i>	Resistant
CN1	<i>Staphylococcus epidermidis</i>	Sensitive
CN3	<i>Staphylococcus epidermidis</i>	Resistant
CN4	<i>Staphylococcus epidermidis</i>	Resistant
MR2	<i>Staphylococcus aureus</i>	Sensitive
MR3	<i>Staphylococcus aureus</i>	Resistant
KL3	<i>Klebsiella pneumoniae</i>	Sensitive
KL5	<i>Klebsiella pneumoniae</i>	Resistant

Table 3.2 Panel of bacterial species selected for antimicrobial testing.

As mentioned in Section 3.1.3, a wide range of bacteria are able to uptake DFO as a xenosiderophore. Of the bacteria in this panel, DFO uptake has been demonstrated in *S. aureus*,<sup>104,517</sup> *A. baumannii*,<sup>518,519</sup> *P. aeruginosa*<sup>451,452</sup> and *K. pneumoniae*<sup>454,455</sup> (although in the latter two uptake has been shown to vary between strains).<sup>453</sup> Growth of *S. epidermidis* is inhibited by DFO,<sup>520–522</sup> suggesting it possesses no mechanism for DFO uptake. There is some evidence for DFO uptake by *E. coli* strains. Some strains have been shown to possess an uptake system for DFO, with

competing reports identifying different outer membrane receptors FhuE<sup>523</sup> or FoxB<sup>524</sup> as responsible for DFO uptake. However, other reports suggest that other strains are unable to utilise DFO, with no growth promotion observed for six strains in an agar plate assay,<sup>525</sup> and no uptake of <sup>68</sup>Ga-labelled DFO in three other strains.<sup>453</sup>

### 3.7.1 Screening on Agar Plates

Conjugate **3-14** and associated controls were first screened against the bacterial panel on Mueller-Hinton agar plates, with the compounds loaded onto discs via stock solutions in DMSO. Each disc was loaded to a concentration equivalent to 5 µg of ciprofloxacin. The agar plates were incubated at 37 °C overnight, and the zone of inhibition surrounding the discs was measured to give an indication of the antimicrobial activity. The results are displayed in **Table 3.3**, with zones of inhibition observed for ciprofloxacin for comparison.

<b>Bacterial Strain Number</b>	<b>Cipro</b>	<b>3-14</b>	<b>3-31</b>	<b>3-34</b>	<b>3-36</b>
AC2 (R)	0	0	0	0	0
PS2 (I)	23.5	0	0	0	0
PS3 (S)	32.4	15.3	0	8.6	0
EC1 (S)	34.8	23.6	0	21.4	0
EC3 (R)	0	0	0	0	0
CN1 (S)	36.5	14.9	8.3	26.5	0
CN3 (R)	0	0	8.4	0	0
CN4 (R)	15.9	0	11.4	13.1	0
MR2 (S)	24.5	0	0	16.3	0
MR3 (R)	0	0	0	0	0
KL3 (S)	29.6	18.6	0	14.4	0
KL5 (R)	18.7	0	0	0	0

Table 3.3 Zones of inhibition (mm) for each compound against bacterial panel. R = ciprofloxacin-resistant, S = ciprofloxacin-sensitive, I = ciprofloxacin-susceptible with increased exposure (i.e. Less sensitive, but higher doses still effective).

Conjugate **3-14** proved less active than ciprofloxacin against all the strains examined, with activity only observed against four strains, PS3, EC1, CN1 and KL3. Of these, activity vs. CN1 (*S. epidermidis*) can likely be assigned to the DFO unit rather than ciprofloxacin, with DFO known to inhibit *S. epidermidis* growth on agar plates,<sup>520</sup> and a lack of DFO uptake in *S. epidermidis* as discussed above. This is supported further by the weak activity for Cipro –, DFO + control **3-31** observed vs. all three strains of *S. epidermidis*. As both **3-14** and **3-31** are above the c. 600 Da cutoff for passive uptake via porins like OmpF (the primary uptake pathway for ciprofloxacin),<sup>526–529</sup> it is also unlikely that they would be taken up into cells unless there is a DFO transporter present, so the activity could not be mediated by either ciprofloxacin or SO<sub>2</sub> release. Given the evidence against *E. coli* utilisation of DFO discussed above, the activity vs. EC1 is also a little surprising, although it is possible that this particular *E. coli* strain is an example that does possess DFO transporters. Isolation and characterisation of this strain, and examination of its ability to take up DFO would help inform whether this activity comes from conjugate uptake, or from another source.

The activity of **3-14** remains higher than Cipro +, DFO – control **3-34** in all but two cases, those of CN1 and MR2. With a mass of 587.15 Da, **3-34** is smaller than the c. 600 Da cutoff for passive uptake via porins, so can potentially be taken up via this route. This explains the difference in activity for CN1, and may explain the observed differences in activity in MR2. It is possible that MR2 lacks a transporter for DFO, hence the lack of activity for **3-14**. The increased hydrophobicity of **3-34** compared to ciprofloxacin (calculated logP = 0.58 vs. –1.53 for ciprofloxacin, OSIRIS property explorer)<sup>445</sup> may also aid passive diffusion through the cell membrane, an alternative uptake route that has been suggested for fluoroquinolones.<sup>530,531</sup> This would correlate well with the activity in Gram-positive strains; the outer membrane of Gram-negative bacteria acts as a barrier to more hydrophobic antibiotics, hence an increase in diffusion of **3-34** through membranes would not lead to increased activity in Gram-negative strains.<sup>531,532</sup> Cipro –, DFO – control **3-36** is inactive against all the strains tested, indicating either a lack of uptake, or

that SO<sub>2</sub> release is unable to exert a significant antimicrobial effect on its own at low concentrations, as per Chapter 2.

### 3.7.2 MIC/MBC Screening

Following the initial screening of conjugate **3-14** and the microbiological controls, the minimum inhibitory concentration (MIC) and minimum bactericidal concentration (MBC) of **3-14** were determined for two of the strains for which activity was observed, CN1 and KL3, and compared to those for ciprofloxacin.

The MIC of an antimicrobial compound is defined as the lowest concentration that will inhibit growth of a microorganism after overnight incubation.<sup>533</sup> This is commonly assessed by serial dilution of the antimicrobial on a well plate, and observing the concentrations at which there is no growth by eye (i.e. overnight incubation yields a clear solution). The MBC is the lowest concentration of an antimicrobial that prevents growth after sub-culturing of the incubated bacteria onto antimicrobial-free media. Here, MHII broth is used as the media for the MIC/MBC experiments. The obtained MIC and MBC values for **3-14** and ciprofloxacin are recorded in **Table 3.4**.

Strain	Ciprofloxacin		<b>3-14</b>	
	MIC / $\mu$ M	MBC / $\mu$ M	MIC / $\mu$ M	MBC / $\mu$ M
CN1	5.89	23.57	56.65	ND
KL3	0.24	5.89	113.31	113.31

Table 3.4 MIC and MBC values of ciprofloxacin and **3-14** for strains of *S. epidermidis* (CN1) and *K. pneumoniae* (KL3). ND = not determined.

The MIC data obtained for **3-14** displays a 10-fold reduction for activity vs. *S. epidermidis*, and a 500-fold reduction for activity vs. *K. pneumoniae*, with a decrease of 19x also seen for the MBC vs. *K. pneumoniae*. As discussed above, it is unclear whether the activity vs. *S. epidermidis* is ciprofloxacin-mediated, with DFO and Cipro –, DFO + control **3-31** able to exert an antimicrobial effect on CN1 as well. The drop-off in activity of **3-14** compared

to ciprofloxacin for KL3 could be related to the slow release observed from the biolabile linker of **3-14**, or a lack of uptake. This perhaps merits further investigation, with a number of methods available for determining the level of uptake of Trojan Horse conjugates in bacteria that could be applied to KL3.<sup>163</sup>

Further screening of MIC/MBC values was carried out against isolates of CN1 and KL3 that had been subjected to a forced adaptation assay. This assay involves repeated exposure of bacteria to an antimicrobial to induce exposure-related resistance.<sup>534</sup> This is carried out by plating the bacteria on agar in the presence of a disc containing the desired antimicrobial, then following overnight incubation those bacteria growing closest to the disc are removed and transferred to a new agar plate. This cycle is repeated x10, or until bacterial growth reaches the discs. The bacteria were repeatedly exposed to either ciprofloxacin or conjugate **3-14**, with the resulting MICs/MBCs displayed in **Table 3.5**.

Strain	Ciprofloxacin		<b>3-14</b>	
	MIC / $\mu$ M	MBC / $\mu$ M	MIC / $\mu$ M	MBC / $\mu$ M
CN1	5.89	23.57	56.65	ND
CN1* (Cip)	47.17	188.62	113.31	ND
CN1* ( <b>3-14</b> )	11.80	94.31	56.65	ND
KL3	0.24	5.89	113.31	113.31
KL3* (Cip)	377.25	ND	113.31	ND
KL3* ( <b>3-14</b> )	ND	ND	113.31	113.31

Table 3.5 MIC and MBC values of ciprofloxacin and **3-14** for strains of *S. epidermidis* (CN1) and *K. pneumoniae* (KL3), including strains subjected to forced adaptation assays with ciprofloxacin or **3-14**, which are indicated by \*. ND = not determined.

As can be seen from the data, *S. epidermidis* subjected to forced adaptation with ciprofloxacin displays an 8-fold increase in the MIC and MBC of ciprofloxacin, indicating increased resistance. A 2-fold decrease in the effectiveness of **3-14** is observed vs. the same bacteria, which may suggest

some role of ciprofloxacin in activity vs. CN1. This is supported by a 2-fold increase in the MIC, and 4-fold increase in the MBC for ciprofloxacin against *S. epidermidis* subjected to forced adaptation with **3-14**, which could indicate successful uptake and ciprofloxacin-mediated activity for **3-14**, or a general decrease in the permeability of the bacteria.

KL3 shows greater resistance development on forced adaptation assays with ciprofloxacin, with a c. 1,500-fold decrease in ciprofloxacin activity against KL3\*(Cip). In contrast, the activity of **3-14** remains unchanged. This could indicate that the increased resistance to ciprofloxacin is related to decreased uptake, while the uptake pathways for DFO conjugate **3-14** are still present, hence no change in activity. For the KL3 strain that underwent forced adaptation with **3-14**, the MIC and MBC values for ciprofloxacin could not be determined using the dilution series employed.

### 3.8 Summary and Conclusions

A Trojan Horse conjugate, **3-14**, containing desferrioxamine as a siderophore unit, a 4-carboxyl-2-nitrobenzenesulfonamide as a biolabile SO<sub>2</sub>-releasing linker, and ciprofloxacin as an antimicrobial component has been synthesised and characterised by <sup>1</sup>H/<sup>13</sup>C/<sup>19</sup>F NMR spectroscopy and ESI mass spectrometry. In addition, three microbiological control compounds, **3-31**, **3-34** and **3-36**, have been synthesised and characterised (**Figure 3.21**). Conjugate **3-14** is poorly soluble in aqueous media, as is control **3-34**, whereas **3-31** and **3-36** display good solubility. The SO<sub>2</sub>-releasing ability of control **3-36** was examined in an HPLC study, with slow release of SO<sub>2</sub> observed on reaction with glutathione, although this study was partially compromised by oxidation of the glutathione during the reaction, preventing the reaction from going to completion. The iron-coordinating ability of control **3-31** was also probed via native ESI mass spectrometry, with a 1:1 complex with Fe(III) detected.

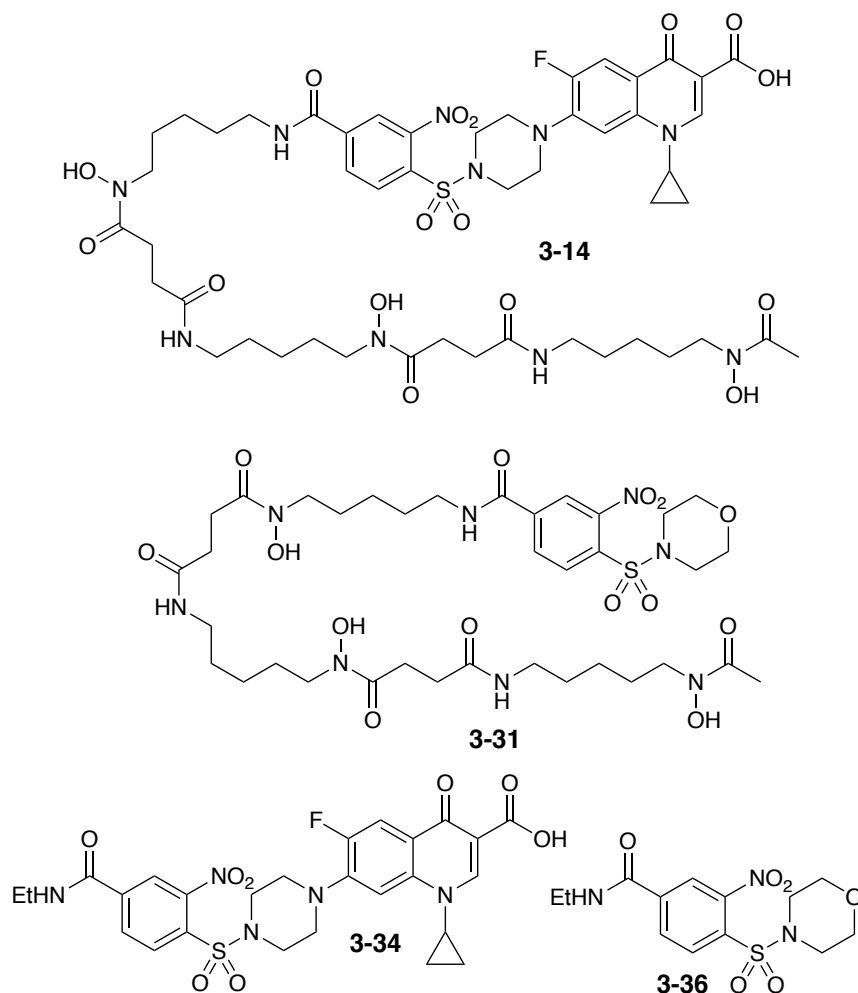


Figure 3.21 Structures of DFO conjugate **3-14**, and microbiological controls **3-31**, **3-34** and **3-36**.

The antimicrobial activity of **3-14** and the three controls were evaluated via a panel of bacterial species in an agar plate-based assay. For bacterial strains that were susceptible to ciprofloxacin, **3-14** proved less active than ciprofloxacin in all cases. Possible “ciprofloxacin-mediated” activity was observed against three strains, PS3 (*P. aeruginosa*), EC1 (*E. coli*) and KL3 (*K. pneumoniae*); activity vs. a fourth strain, CN1 (*S. epidermidis*), is likely to be primarily DFO-mediated, with activity also observed for Cipro –, DFO + control **3-31** against the same strain. This DFO-mediated activity is likely to source from the DFO component binding extracellular iron in competition with native siderophores, limiting the amount of iron that is available for uptake by the bacteria.

The weaker activity for **3-14** compared to ciprofloxacin for these three strains suggests issues with the uptake of **3-14**, or that the slow release of



ciprofloxacin fails to provide a high enough intracellular concentration for good antimicrobial activity. While it may be possible that conjugate **3-14** could bind to DNA gyrase/topoisomerase IV without ciprofloxacin release, the large DFO component is likely to interfere with target binding.

Cipro +, DFO – control **3-34** displays some additional activity above that of conjugate **3-14**, proving more active than **3-14** vs. two Gram-positive strains, CN1 and MR2 (*S. aureus*); this is potentially related to the size of **3-34**, which is below the c. 600 Da cut-off for uptake via porins, and/or the increased hydrophobicity compared to ciprofloxacin, which may allow diffusion through the lipid bilayer of cell membranes. The enhanced activity of **3-34** in MR2 vs. DFO conjugate **3-14** indicates that poor uptake of **3-14** (DFO conjugate) is likely to be the cause of the lack of antimicrobial activity in this case. However, the activity of **3-34** remains weaker than that of ciprofloxacin, indicating that the rate of ciprofloxacin release from the 4-carboxyl-2-nitrobenzenesulfonamide linker remains a general problem for **3-14** and **3-34**. Cipro –, DFO – control **3-36** displayed no activity in the screening, indicating SO<sub>2</sub> release is too slow, or insufficiently potent to effect antimicrobial activity at the concentrations tested.

Conjugate **3-14** also has a high MIC in liquid cultures of 56.65 μM vs. CN1 (10-fold worse than ciprofloxacin) and 113.31 μM vs. KL3 (500-fold worse than ciprofloxacin). In KL3, this loss of activity compared to ciprofloxacin could be due to either slow ciprofloxacin release, or a lack of uptake of **3-14**; further investigation is required. Finally, forced adaptation assays of CN1 and KL3 carried out with ciprofloxacin and **3-14** indicate a portion of the activity vs. CN1 may be ciprofloxacin-mediated, and a significant drop-off in activity for ciprofloxacin in KL3 post-assay is not mirrored by that of **3-14**, suggesting the resistance mechanisms developed for ciprofloxacin are related to uptake, with **3-14** likely being taken up via the iron transport pathway, and hence avoiding any uptake-related resistance associated with ciprofloxacin.

Some key conclusions can be drawn from the work presented above. While it can be demonstrated to successfully release SO<sub>2</sub>, the usage of 4-carboxyl-2-nitrobenzenesulfonamide linkers appears a poor fit for these types of conjugate. While the slow rate of SO<sub>2</sub> release, and hence ciprofloxacin release, may be beneficial in some circumstances, it does not appear to be sufficient to generate a high enough intracellular concentration of ciprofloxacin for good antimicrobial activity.

The hydrophobic nature of the linker also creates problems for the design of conjugates, especially when antimicrobials with poor aqueous solubility like ciprofloxacin are used. The use of desferrioxamine as a siderophore unit gives a reasonable spectrum of activity; excluding the *S. epidermidis* strains, conjugate **3-14** is active against three of the six ciprofloxacin-susceptible strains. However, it is not hydrophilic enough to balance out the other components and give sufficient aqueous solubility.

### **3.9 Future Work**

In terms of future work with the existing conjugates, there exist a number of areas for further investigation. Firstly, the further purification of conjugate **3-14** is required. Given the failure of initial attempts at preparative HPLC purification, there are likely limited options, but it is possible that on exploration of further conditions purification of **3-14** may become possible. Another possibility is the formation of the iron complex of **3-14**, which may alter the properties of the conjugate in a way that facilitates further purification.

The rate of SO<sub>2</sub> release from the 4-carboxyl-2-nitrobenzenesulfonamide linkers could be probed further, with measurements carried out under inert atmosphere to prevent glutathione oxidation, or incorporation of glutathione transferases to accelerate the rate of reaction and provide a closer picture of SO<sub>2</sub> release within cells.

Some trends in the biological results could be explored further if desired. The uptake of DFO in each of the strains in the bacterial panel could be

examined, for example by uptake of radiolabelled iron or gallium complexes of DFO,<sup>163,453</sup> a similar approach could be employed to measure the uptake of conjugate **3-14** in these strains, which would allow evaluation of the compatibility of the biolabile linker/ciprofloxacin attachment with uptake via siderophore-dependent uptake pathways. The activity of the compounds could also be explored in iron-deficient conditions.

In terms of further chemical modifications to the conjugate system, there is scope for optimisation of each component. Optimisation of the SO<sub>2</sub>-releasing linker offers the greatest opportunity for improvement, with a higher rate of SO<sub>2</sub> release potentially offering more active conjugates via faster ciprofloxacin release. This would require synthesis of a more electron-deficient aromatic ring, most likely by inclusion of an additional electron-withdrawing functionality in the position *ortho* to the sulfonamide. With the high reactivity with water observed for inclusion of a nitro group ( $\sigma_p = 0.78$ ) at this position (**Scheme 3.1**), a weaker electron-withdrawing group like fluorine ( $\sigma_p = 0.06$ ), chlorine ( $\sigma_p = 0.23$ ) or acetyl ( $\sigma_p = 0.50$ ) could be employed (**Figure 3.22**).

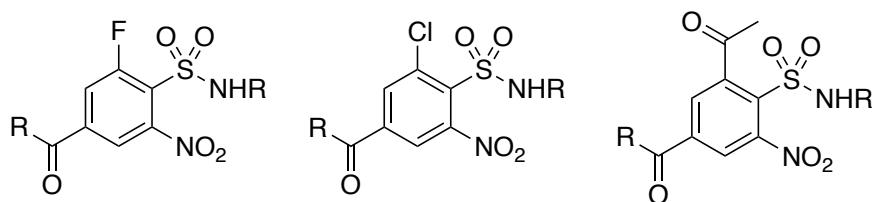


Figure 3.22 Potential alternative SO<sub>2</sub>-releasing linkers.

For optimisation of the antimicrobial component, a more water-soluble fluoroquinolone like moxifloxacin could be utilised (**Figure 3.23**). In a similar manner, a more hydrophilic siderophore unit may also aid with the solubility issues; this could even be achieved with modifications to the DFO structure, as demonstrated by Richardson-Sanchez *et al.*, who were able to alter the biosynthesis of DFO in *Streptomyces pilosus* to produce a DFO analogue containing ether-bridged carbon chains, resulting in a 45x increase in aqueous solubility.<sup>493</sup>

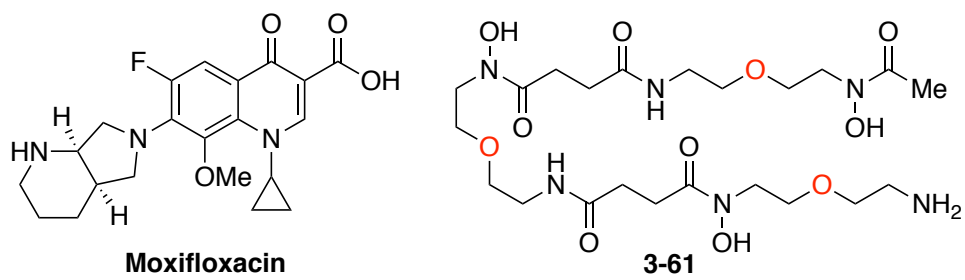


Figure 3.23 Structure of potential replacements for optimisation of the fluoroquinolone and siderophore units. For **3-61**, the inserted ethers are highlighted in red.

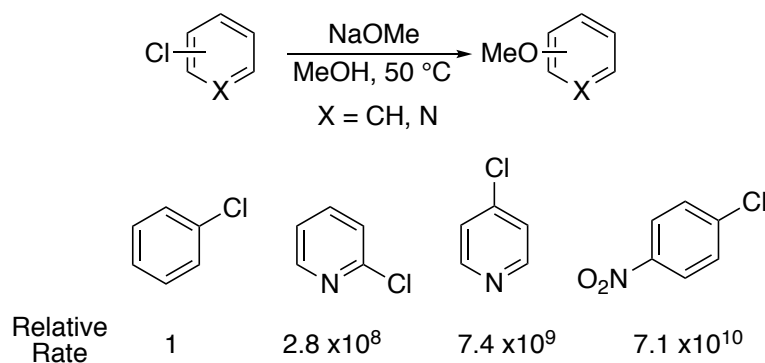
**Chapter 4 :**  
**Heterocyclic Systems for**  
**SO<sub>2</sub> Release, and**  
**Synthesis of an**  
**Azotochelin Conjugate**

## 4.1 Introduction

The compatibility of any biolabile linker design with biological conditions is key to the development of successful Trojan Horse antimicrobials, as is the rapid release of the bound antimicrobial component. The 4-carboxyl-2-nitrobenzenesulfonamide linkers used in Trojan Horse conjugate **3-14**, as detailed in Chapter 3, offer relatively slow SO<sub>2</sub> release rates (and hence ciprofloxacin release) on reaction with glutathione, which might contribute to the poor antimicrobial activity of the resulting conjugates. These conjugates also have significant problems with aqueous solubility, likely due in part to the hydrophobicity of the linker units. The development of a SO<sub>2</sub>-releasing linker with more rapid SO<sub>2</sub> release and reduced hydrophobicity may offer a route to more active conjugates. The usage of sulfonamides based on heterocyclic rings for the development of biolabile linkers was proposed as a solution to both of these problems. In this Chapter, the synthesis and investigation of SO<sub>2</sub>-releasing conjugates containing a novel pyrazine-based sulfonamide as a biolabile linker is discussed.

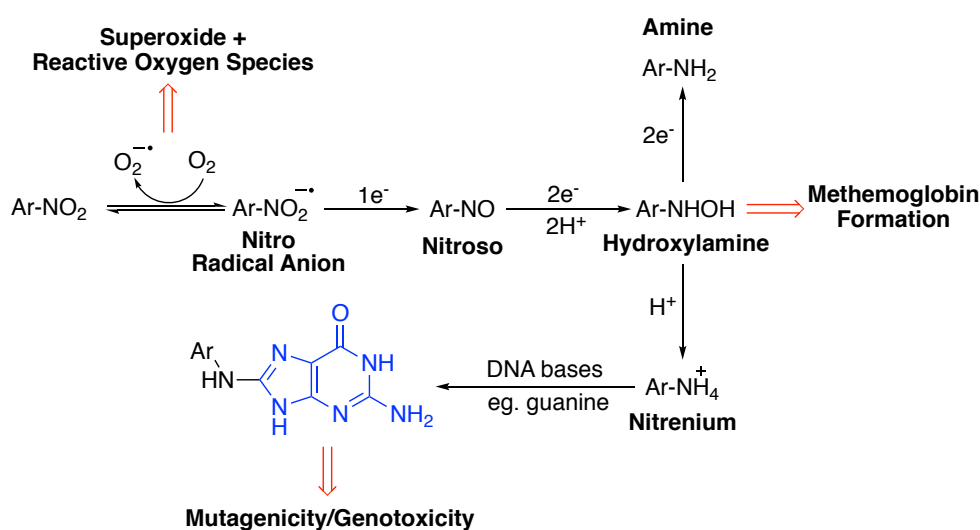
### 4.1.1 The Potential of Heterocyclic Sulfonamides

The development of sulfonamides based on heterocyclic rings could offer a solution to some of the key problems with the nitrobenzene-based rings used in Chapter 3. Aromatic rings containing electronegative heteroatoms are more electron-deficient than the comparable benzene-based equivalents, and are therefore better electrophiles in S<sub>N</sub>Ar reactions. This can be clearly demonstrated by the reactivity of 2- and 4-chloropyridines with sodium methoxide (**Scheme 4.1**).<sup>535–537</sup> These show 10<sup>8</sup> and 10<sup>9</sup> fold enhancements in nucleophilic aromatic substitution rates, respectively, when compared to chlorobenzene, comparable to the rate enhancement observed for 4-nitrochlorobenzene (10<sup>10</sup>).



Scheme 4.1 Reactivity of selected aryl and heteroaryl chlorides with sodium methoxide, and relative  $S_NAr$  rates. Adapted from Joule and Mills.<sup>537</sup>

A further advantage of utilising heterocyclic sulfonamides is the potential to reduce or eliminate the reliance on nitro groups for creating electron-deficient aromatic rings. Nitro groups are used in a number of drugs, perhaps most notably in the nitroimidazole class of antibiotics.<sup>538</sup> They can undergo reduction *in vivo* to form a number of reactive metabolites (**Scheme 4.2**), which are often responsible for the biological activity observed.<sup>538</sup> The metabolites can go on to react with DNA or other cellular components, or inflict damage on target organisms via ROS production inside cells.<sup>538–540</sup> However, these metabolites can also damage the human body, with carcinogenic, hepatotoxic, or mutagenic effects.<sup>538,540</sup> Their use is therefore avoided unless the nitro functionality is vital to activity, and the mutagenicity of such compounds is carefully monitored.<sup>538</sup>



Scheme 4.2 Reduction pathways of nitro groups, and some mechanisms of toxicity associated with reduced species (indicated with red arrows).<sup>538,541–</sup>

<sup>543</sup> Partially adapted from Nepali *et al.*<sup>538</sup>

Finally, heterocyclic rings offer a more hydrophilic alternative to the benzene-based rings employed in Chapters 2 and 3. A 2012 study by Ritchie *et al.* of a GSK compound library found notable increases in aqueous solubility for compounds containing heteroaromatic rings compared to benzene-based compounds.<sup>544</sup> A similar study by Ritchie and Macdonald demonstrated between a 2 to 8.5 fold enhancement of aqueous solubility on replacement of a benzene ring with the equivalent heterocyclic ring.<sup>545</sup> With ciprofloxacin forming relatively hydrophobic conjugates, as seen in Chapter 3, the incorporation of a more hydrophilic linker offers an opportunity to counterbalance this hydrophobicity, which may result in a higher aqueous solubility for any synthesised conjugates. It may also help to facilitate the incorporation of more hydrophobic siderophores in the conjugates.

## 4.1.2 Existing Heterocyclic Sulfonamides and Reactivity with Thiols

### 4.1.2.1 6-Membered Heterocycles Sulfonamides

There are a number of examples of electron-deficient heterocyclic-based systems that have been shown to undergo reactions with biological thiols under biologically-relevant conditions (37 °C, pH 7.4), including a number of sulfonamide-containing systems. An early example of this comes from a study published in 1958 into the metabolism of 6-uracilsulfonamide (**4-1**, **Figure 4.1**), a potential anticancer agent, which was shown to undergo reaction with biological thiols in aqueous buffer on incubation at 37 °C.<sup>546</sup>

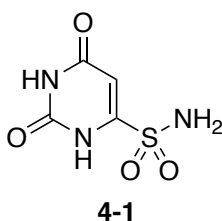
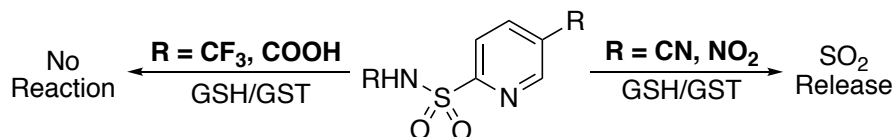


Figure 4.1 Structure of 6-uracilsulfonamide (**4-1**).<sup>546</sup>

Similar thiol reactivity was observed in two 1999 studies on analogues of a HIV-1 protease inhibitor.<sup>547,548</sup> In these studies, a series of pyridine-2-sulfonamides substituted with a *para*-cyano or nitro groups were shown to undergo reaction with glutathione (catalysed by the enzyme glutathione-S-transferase), resulting in SO<sub>2</sub> release (**Scheme 4.3**).<sup>548</sup> Pyridines substituted

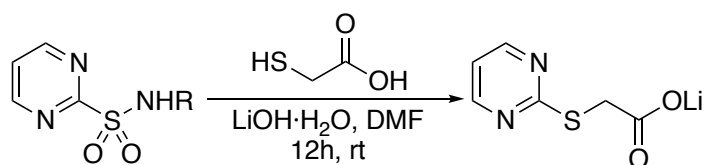


with weaker electron-withdrawing groups e.g.  $\text{CF}_3$  or  $\text{COOH}$  showed no reaction with glutathione.



Scheme 4.3 Varying reactivity of pyridine sulfonamides with glutathione/glutathione-S-transferase (GST).<sup>547,548</sup>

To the best of this author's knowledge, there are no examples of other non-fused 6-membered heterocyclic rings (e.g. pyrazine, pyrimidine) bearing sulfonamides reacting with biological thiols, although Bornholdt *et al.* were able to demonstrate the successful reaction of a 2-pyrimidinesulfonamide group with 2-mercaptoacetic acid under basic conditions in DMF (**Scheme 4.4**).<sup>549</sup>

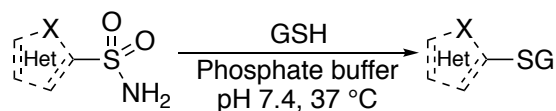


Scheme 4.4 Reaction of 2-pyrimidinesulfonamides with thioglycolic acid.<sup>549</sup>

#### 4.1.2.2 5-Membered Heterocyclic Sulfonamides

5-membered heterocyclic sulfonamides have been more widely studied, with a number of examples in the literature. The reaction of benzothiazole-2-sulfonamide with glutathione has been noted as a key step in its metabolism in various animals.<sup>550–552</sup> A range of studies on similar structures, including 6-hydroxybenzothiazole-2-sulfonamide (**4-2**) revealed some interesting reactivity trends (**Table 4.1**). Loss of the nitrogen in the thiazole ring to give benzothiophene **4-3** renders the sulfonamide unreactive to glutathione.<sup>552,553</sup> The corresponding benzofuran (**4-4**) and indole (**4-5**) analogues of **4-2** display higher reactivity, likely related to the higher electronegativity and hence electron-withdrawing ability of the heteroatoms involved.<sup>552,554</sup> A further study on derivatives of benzothiazole-2-sulfonamide also looked at the glutathione reactivity of acetazolamide (**4-6**) and methazolamide (**4-7**), two sulfonamide-containing carbonic anhydrase inhibitors based on a 1,3,4-thiadiazole scaffold, with slower

release observed compared with the parent benzothiazole (significantly so in the case of acetazolamide).<sup>555</sup>



Scheme 4.5 Reaction of 5-membered heterocyclic sulfonamides with glutathione. 0.5 mM sulfonamide, and 5/20 equivalents of glutathione were employed, and the percentage reactivity after 16-22 h was determined by HPLC after quenching with 1% H<sub>3</sub>PO<sub>4</sub> in MeCN.

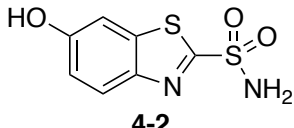
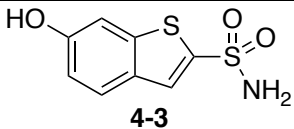
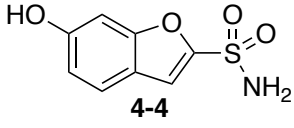
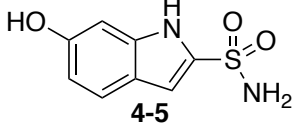
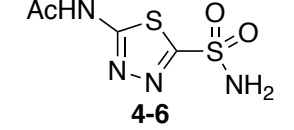
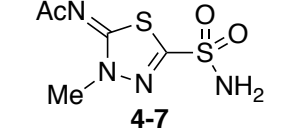
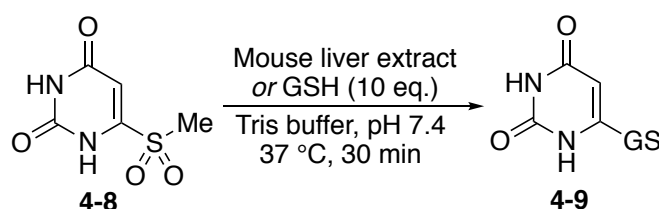
Structure	% Reacted (5 eq. GSH)	% Reacted (20 eq. GSH)	Ref
 4-2	27	ND	555
 4-3	0	2.9	553,554
 4-4	4.9	23	554
 4-5	2.9	17	554
 4-6	3	ND	555
 4-7	27	ND	555

Table 4.1 Percentage reactivity of selected 5-membered heterocyclic sulfonamides with glutathione.

#### 4.1.2.3 5/6-Membered Heterocyclic Sulfones

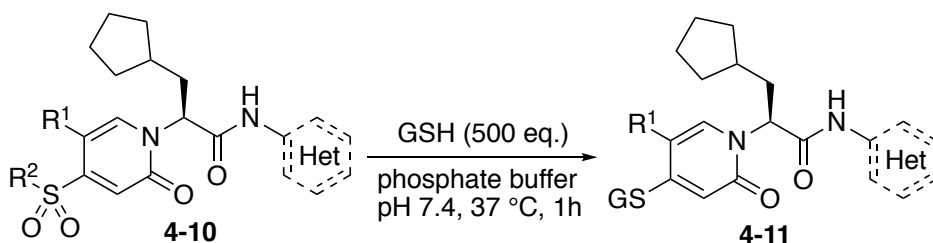
The ability to undergo reactions with biological thiols under biologically-relevant conditions is not limited to heterocyclic sulfonamides. Other sulfur-based groups, particularly sulfones and sulfoxides, can also undergo

displacement in a similar fashion. One of the first examples of this comes from a study by Cooper in 1958, who demonstrated the reactivity of 6-uracilmethylsulfone (**4-8**) with biological thiols while studying its degradation by liver enzymes (**Scheme 4.6**).<sup>546</sup> The product formed on reaction with liver enzymes displayed identical properties to the product formed on reaction with glutathione (**4-9**), with loss of the methylsulfonyl group demonstrated via the lack of sulfone bands in the IR spectrum of the product, and via labelling of the methyl group with carbon-14 (to demonstrate loss of the radioactivity). The reactivity of similar nucleotide-based mercaptopurine derivatives with biological thiols has also been demonstrated.<sup>556,557</sup> The reaction likely proceeds via loss of methylsulfinic acid (MeSO<sub>2</sub>H) as a leaving group.<sup>558</sup>



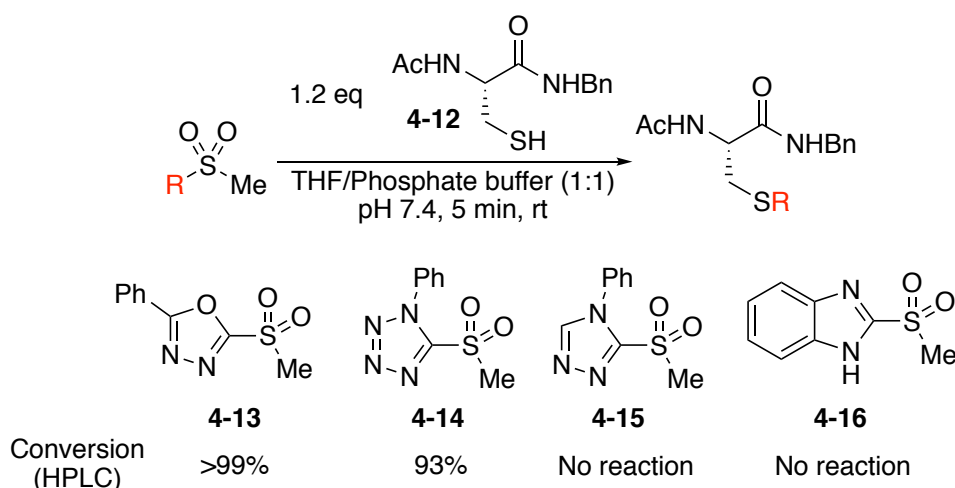
Scheme 4.6 Reaction of 6-uracilmethylsulfone **4-8** with mouse liver homogenate or glutathione, with loss of methylsulfone group.<sup>546</sup>

The reactivity of two 4-sulfonyl-2-pyridone-based systems was noted in two papers published by Pfefferkorn *et al.* and Litchfield *et al.* in 2009 and 2010.<sup>559,560</sup> A range of molecules containing this motif were noted to undergo rapid metabolism and clearance when they were examined in a rat model.<sup>559</sup> Analysis of the metabolites produced revealed formation of a glutathione conjugate **4-11**. This was followed by incubation of selected examples with a large excess of GSH at 37 °C, with partial conversion to **4-11** observed after 1 hour (**Scheme 4.7**).<sup>559,560</sup> This conversion was accelerated in the presence of liver enzymes, or human glutathione transferase.<sup>560</sup> The steric bulk around the sulfonyl group also had no major impact on reactivity, indicating a general reactivity specific to this type of structural motif.<sup>559</sup>



Scheme 4.7 Reaction of 4-sulfonyl-2-pyridones with glutathione.<sup>559,560</sup>

Toda *et al.* examined the reaction of protected cysteine **4-12** with four further ring types, oxadiazole **4-13**, tetrazole **4-14**, triazole **4-15**, and benzimidazole **4-16**.<sup>561</sup> The triazole and benzimidazole compounds proved inactive, while the tetrazole and the oxadiazole display 93% and <99% conversion over 5 minutes respectively (**Scheme 4.8**). Toda *et al.* go on to demonstrate reactivity of oxadiazole **4-13** with cysteine residues in human serum albumin.<sup>561</sup> Oxadiazoles similar to **4-13** have since been used in a number of applications, including attachment of radioactive probes to antibody conjugates and peptides.<sup>562–564</sup>



Scheme 4.8 Reactivity of four heterocyclic methylsulfones with cysteine derivative **4-12** as studied by Toda *et al.*<sup>561</sup>

Similar thiol reactivity has been observed for 6-membered heterocyclic rings bearing sulfone groups. Bauer *et al.* discovered 2-methylsulfonylpyrimidine **4-17** was capable of binding to cysteine residues while screening a fragment library for ligands to bind to a mutant p53 protein.<sup>565</sup> Further investigation revealed **4-17** and similar 2-sulfonylpyrimidines can act as effective inhibitors of cancer cell growth *in vitro*, while displaying low toxicity towards normal cells.<sup>565</sup> A number of similar sulfones have since emerged as

promising anticancer leads and apoptosis inhibitors, including pyrimidines **4-18** to **4-20**,<sup>566–568</sup> and pyridine **4-21** (Figure 4.2).<sup>569</sup>

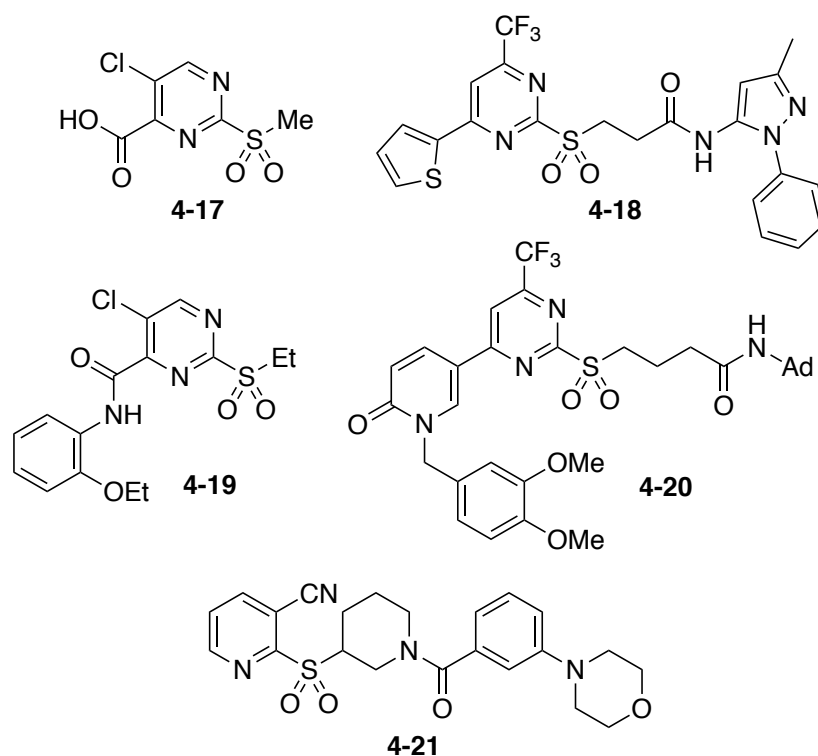


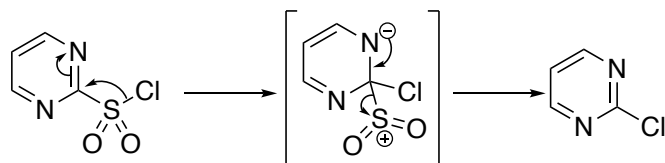
Figure 4.2 Structures of heterocyclic sulfones that can act as anticancer/anti-apoptosis agents, and undergo reaction with biological thiols. For structure **4-20**, Ad = adamantane.

These examples demonstrate the ability of heterocyclic compounds containing sulfonamides or oxidised sulfur-based groups to undergo  $S_NAr$  reactions with biological thiols, giving confidence that they can successfully be utilised for  $SO_2$  release. The rapid thiol conjugation observed in some examples also suggests that with the right choice of heterocycle, these compounds could potentially offer release rates comparable with the 2,4-dinitrobenzenesulfonamide-based compounds previously discussed.

### 4.1.3 Synthesis of Heterocyclic Sulfonamides

The synthesis of heterocyclic sulfonamides is notably more challenging than their non-heterocyclic counterparts. The sulfonyl chloride intermediates required for the typical sulfonamide synthesis route are difficult to synthesise, often decomposing *in situ* to their corresponding heteroaryl chlorides.<sup>570–572</sup> Even if the formed sulfonyl chlorides can be successfully isolated from the reaction mixture, the resulting products can decompose

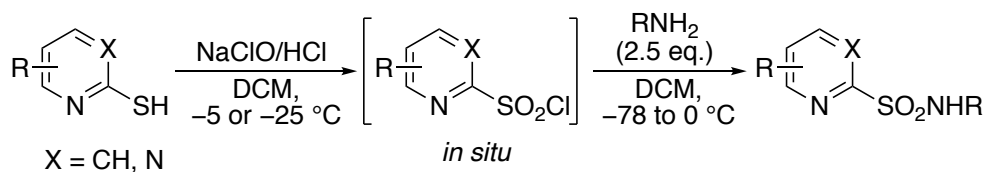
post-reaction to form the corresponding heteroaryl chlorides with loss of SO<sub>2</sub> (this is believed to be via an S<sub>N</sub>i-type process, **Scheme 4.9**).<sup>573–575</sup>



Scheme 4.9 Suggested S<sub>N</sub>i decomposition mechanism for pyrimidine-2-sulfonyl chloride (based on Kwart and Body, 1965).<sup>574</sup>

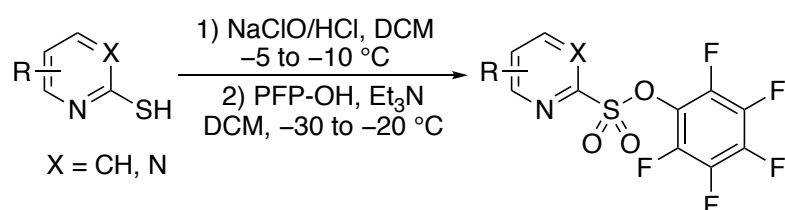
The traditional method of sulfonyl chloride synthesis involves oxidative chlorination with chlorine gas in acidic solution. For heterocycles, this has been limited to pyridine rings,<sup>570,571</sup> and even then those with strongly electron-withdrawing groups are produced in low yields.<sup>576</sup> Diazine heterocycles like pyrimidine or pyrazine often return sub-20% yields via this methodology.<sup>570,571</sup>

In recent years this area has seen the development of new synthetic methods aimed at circumventing this problem. In 2006, Wright and Hallström published a synthesis of heterocyclic sulfonamides, with heteroaromatic thiols being converted to their sulfonyl chlorides *in situ* with aqueous sodium hypochlorite (NaClO) as an oxidising agent. The reaction employs a biphasic mixture, with DCM added to provide a water-immiscible organic layer, which the sulfonyl chlorides should enter upon formation, reducing their exposure to the NaClO/HCl mixture utilised for the oxidative chlorination reaction (**Scheme 4.10**). The DCM layer can then be separated from the aqueous layer, and transferred to a fresh flask cooled to –78 °C, followed by addition of an amine to form the desired sulfonamides.<sup>571</sup> The synthesis required reaction temperatures to be kept below 0 °C throughout the oxidative chlorination reaction; in some cases further cooling to –25 °C was required to prevent sulfonyl chloride decomposition.



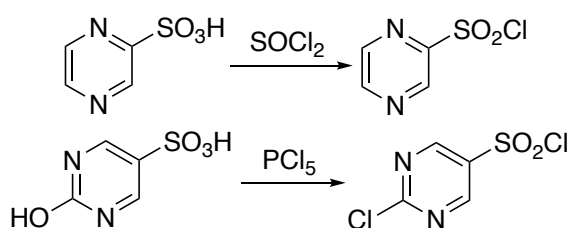
Scheme 4.10 Synthetic methodology employed by Wright and Hallström for the synthesis of heterocyclic sulfonamides.<sup>571</sup>

A later publication by Bornholdt *et al.* adopted the same methodology with some minor modifications to synthesise pentafluorophenolsulfonyl esters of selected heterocyclic rings. Instead of trapping the formed sulfonyl chlorides with amines, pentafluorophenol (PFP-OH) was added to create a stable sulfonate ester (**Scheme 4.11**). These sulfonate esters are stable as solids at room temperature, and can be reacted further with amines to give the desired heterocyclic sulfonamides.<sup>575</sup>



Scheme 4.11 Bornholdt *et al.*'s adaptation of Wright and Hallström's methodology to produce stable activated sulfonate esters.<sup>575</sup>

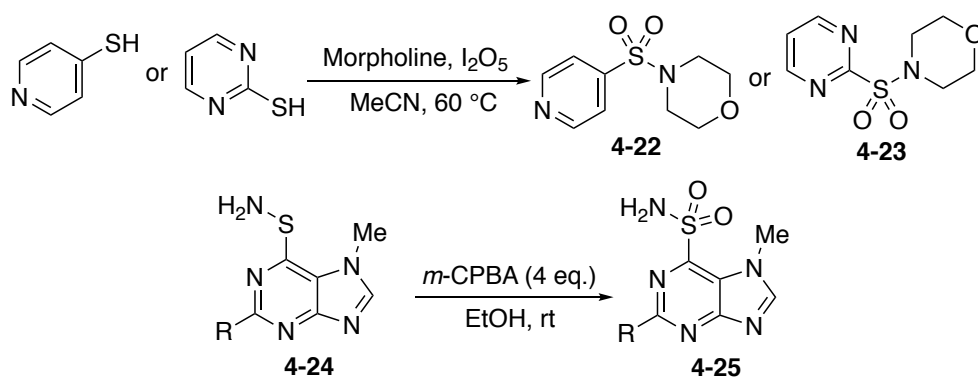
A couple of other oxidative chlorination methods have been demonstrated to be effective with pyridine-based heterocycles, including the use of DCDMH (as used previously in Chapter 3),<sup>459,460,577</sup> *N*-chlorosuccinimide,<sup>578–580</sup> or sulfuryl dichloride;<sup>581</sup> these are effective for both thiols and benzyl thioethers. Chlorinating agents such as phosphorus pentachloride<sup>582</sup> or thionyl chloride<sup>583</sup> may also be used for conversion of heterocyclic sulfonic acids to the corresponding sulfonyl chlorides (**Scheme 4.12**), although this tends to result in low-yielding reactions.



Scheme 4.12 Conversion of heterocyclic sulfonic acids to the corresponding sulfonyl chlorides.<sup>582,583</sup>

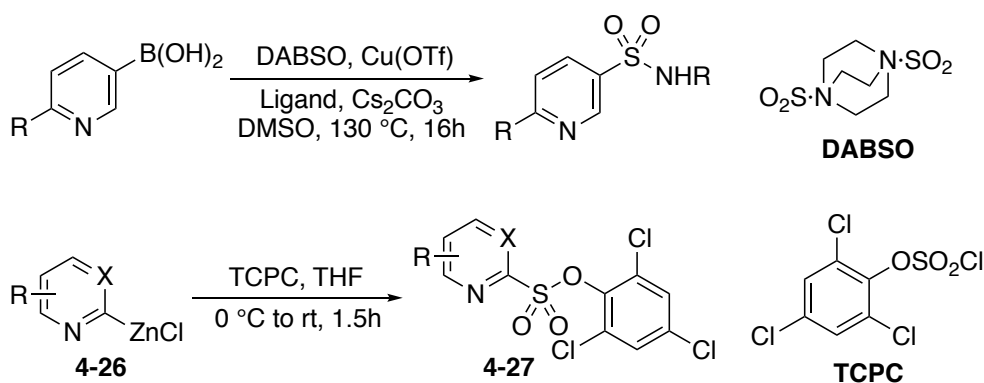
Other oxidative methods have also been employed for the synthesis of heterocyclic sulfonamides. Iodine pentoxide ( $\text{I}_2\text{O}_5$ ) has been shown to effect oxidative conversion of 4-pyridinethiol to the corresponding morpholine sulfonamide **4-22** in a one-pot process (believed to occur via *in situ* formation of a sulfonyl iodide).<sup>584</sup> The use of  $\text{I}_2\text{O}_5$  has also proved successful

in the formation of a pyrimidine-sulfonamide **4-23** (Scheme 4.13). Sulfonamide formation via oxidation of the corresponding heterocyclic sulfenamides with *m*-CPBA has also been shown to be a viable pathway (e.g. for synthesis of purine derivative **4-25**),<sup>585,586</sup> although the synthesis of sulfenamides is complicated by the requirement for potentially toxic and/or unstable chloramine or sulfenyl chloride intermediates.<sup>587–589</sup>



Scheme 4.13 Examples of other oxidative routes to heterocyclic sulfonamides.<sup>584–586</sup>

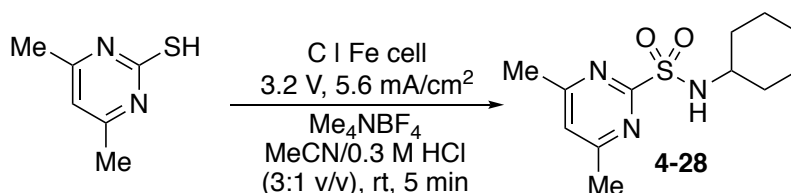
Organometallic coupling routes to sulfonamides are another area to have seen developments in recent years, with transition metal catalysts (e.g. Pd, Cu) being combined with sources of SO<sub>2</sub> and traditional cross coupling substrates like aryl halides or boronic acids to generate a range of SO<sub>2</sub>-functionalised aromatics.<sup>590–594</sup> However, few of these papers utilise heterocyclic substrates. Shavnya *et al.*,<sup>595</sup> and the Willis group,<sup>596–598</sup> have experimented with pyridine substrates, with yields ranging from 15 to 60%. In addition, Colombe *et al.* synthesised a pyrimidine-based activated sulfonate ester **4-27** in 31% yield from an organozinc pyrimidine starting material (**4-26**, Scheme 4.14).<sup>599</sup>



Scheme 4.14 Selected examples of organometallic coupling routes to sulfonamides/activated sulfonate esters.



Laudadio *et al.* have published an electrochemical synthesis of sulfonamides from their corresponding thiols/disulfides and amines, with pyridine and pyrimidine derivatives like **4-28** successfully synthesised in their substrate scope. This transformation does not require addition of any additional reagents (**Scheme 4.15**).<sup>600</sup> Other studies have since utilised similar methods for heterocyclic sulfonamide synthesis.<sup>601</sup>



Scheme 4.15 Electrochemical synthesis of pyrimidine-sulfonamide **4-28**.<sup>600</sup>

Finally, another sulfonyl halide functional group, the sulfonyl fluoride group, has gained increasing popularity in recent years as an alternative to sulfonyl chlorides in various roles, including in sulfonamide synthesis. The sulfonyl fluoride (SO<sub>2</sub>F) functionality has been known since the early 20<sup>th</sup> Century,<sup>602</sup> but had not found widespread use in synthetic organic chemistry until its potential as a versatile functional group in ‘click chemistry’ reactions was highlighted by the group of K. Barry Sharpless in 2014.<sup>603</sup> Sulfonyl fluorides are much more stable to hydrolysis and nucleophilic attack than their corresponding chlorides,<sup>603–605</sup> with the S-F bond around 172 kJmol<sup>-1</sup> stronger than the S-Cl bond in hexavalent sulfur compounds.<sup>603</sup>

#### 4.1.4 Selection of Heterocyclic Sulfonamide Target

There are a large range of heterocyclic sulfonamides that can undergo reaction with biological thiols, as detailed above. This allows a wide scope for the design of linker units for heterocyclic sulfonamides. As with the 4-carboxyl-2-nitrobenzene-based linkers studied in Chapter 3, the chosen linker requires a reactive functional group, ideally electron-withdrawing, for conjugation to the siderophore component of the overall conjugate; a carboxylic acid was again preferred here. The chosen linker must also maintain a sufficiently electron-deficient environment to allow nucleophilic aromatic substitution to take place.

To minimise the complexity of the first linker systems developed, only 5- or 6-membered rings were considered for the first attempts at linker design. As more synthetic routes exist for the synthesis of 6-membered rings, these were initially favoured over 5-membered rings. Here, the choice of a diazine ring for initial study was favoured, with the two heteroaromatic nitrogens present expected to create a strongly electron-deficient environment.

A 5-pyrazinecarboxylic acid derivative **4-29** was initially selected for linker development. The *para*-positioning of the carboxylic acid group to the sulfonamide position, similar to that seen in the 4-carboxyl-2-nitrobenzene linkers, is maintained (**Figure 4.3**). As well as maximising the electron-withdrawing ability of the carboxylic acid to the *para* position, this also ensures maximal distance between the sulfonamide linker and the siderophore unit, which should act to prevent any steric hindrance of nucleophilic attack on the sulfonamide.

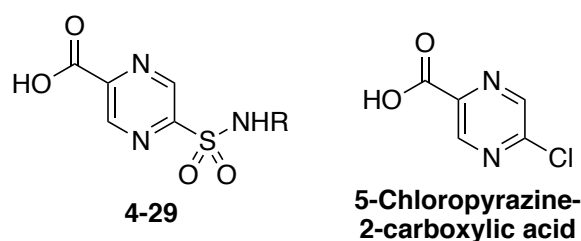


Figure 4.3 Structure of initial 5-pyrazinecarboxylic acid group for design of a first heterocyclic sulfonamide biolabile linker (**4-29**), and desired 5-chloropyrazine-2-carboxylic acid starting material.

#### 4.1.5 Selection of Siderophore Component

The choice of heterocyclic sulfonamides as linker units for siderophore conjugates may allow the use of more hydrophobic siderophore units. Therefore, the decision was taken to incorporate a tetradentate catecholate siderophore, azotochelin, as the siderophore unit (**Figure 4.4**). This might allow a different bacterial target profile to that seen for conjugate **3-14** in Chapter 3. Despite the presence of the four catechol groups and the carboxylic acid, the structure remains reasonably hydrophobic, with a calculated logP of 1.10 (clogP, OSIRIS property explorer).<sup>445</sup> In contrast, the hexadentate hydroxamate siderophore desferrioxamine (DFO) employed in Chapter 3 has a clogP of -0.31.

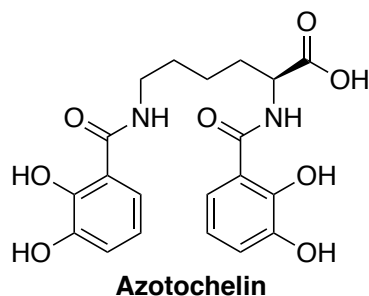


Figure 4.4 Structure of tetradentate catechol siderophore azotochelin.

Azotochelin has previously found use in three Trojan Horse conjugates. The first two were  $\beta$ -lactam (**4-30**) and monobactam conjugates (**4-31**) designed by McKee *et al.* (**Figure 4.5**).<sup>606</sup> The azotochelin component alone was shown to enhance bacterial growth, suggesting successful uptake, while  $\beta$ -lactam conjugate **4-30** proved effective vs. *E. coli* in initial studies (**4-31** proved inactive).<sup>606,607</sup> However, later studies of **4-30** with a wider range of bacteria displayed excellent growth promotion instead of the expected antimicrobial activity, perhaps due to the azotochelin component hindering  $\beta$ -lactam-target binding.<sup>608</sup> The second is a phenothiazine conjugate, **1-11**, synthesised by Tarapdar *et al.* (**Figure 4.6**).<sup>185</sup> As mentioned in Chapter 1, a biological evaluation of this conjugate has not yet been published.

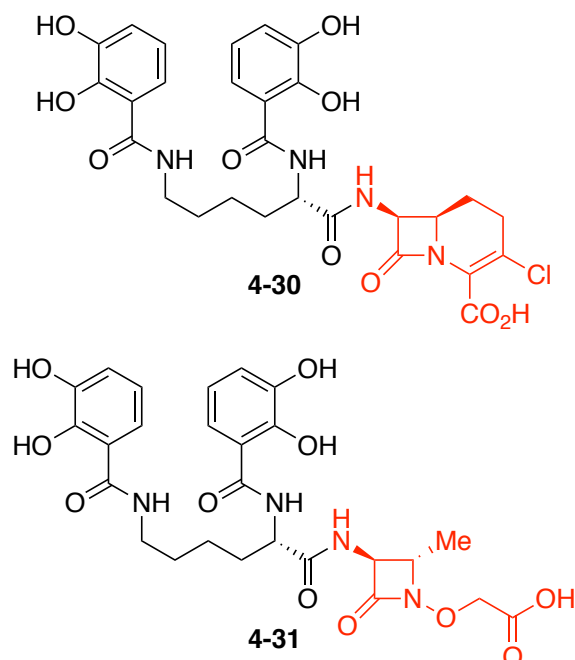


Figure 4.5 Structures of previous azotochelin conjugates synthesised by McKee *et al.*<sup>606</sup>

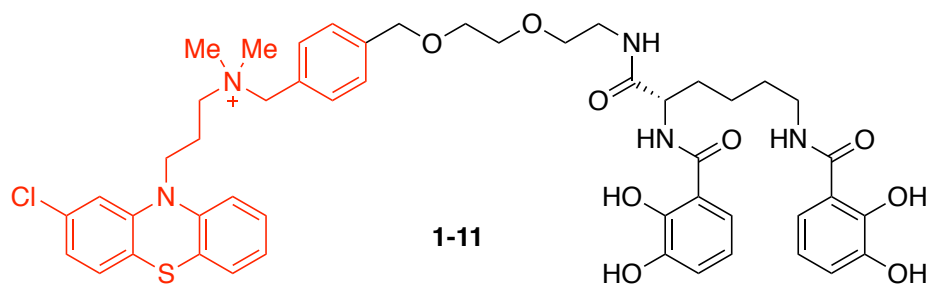


Figure 4.6 Structure of previous phenthiazine-azotochelin conjugate synthesised by Tarapdar *et al.*<sup>185</sup>

The use of azotochelin as a potential Trojan Horse siderophore component is also supported by further studies of its uptake, and its ability to bind to siderophore transport components in a range of species. Stintzi *et al.* demonstrated successful uptake of radiolabelled azotochelin in the bacterium *Aeromonas hydrophila*,<sup>609</sup> while Naikare *et al.* observed growth promotion for azotochelin vs. *Campylobacter jejuni*.<sup>610</sup> The Duhme-Klair group were later able to demonstrate binding of an azotochelin-based metalloenzyme conjugate to CeuE, the periplasmic binding protein of *C. jejuni*.<sup>611</sup> Finally, Moynié *et al.* followed up a 2016 report that azotochelin could be taken up by *P. aeruginosa* via the PfeA outer membrane transporter by obtaining a crystal structure of azotochelin bound to PfeA.<sup>612,613</sup>

## 4.2 Conjugate Design and Synthetic Plan

A first synthetic target, **4-32**, containing ciprofloxacin as the antimicrobial component and azotochelin as the siderophore component, was proposed. Similar to conjugate **3-14**, discussed in Chapter 3, the ciprofloxacin is coordinated to the pyrazine-sulfonamide via the secondary amine of the piperazine ring, and azotochelin attached to the carboxylic acid on the pyrazine ring via an aliphatic diamine linkage (**Figure 4.7**).

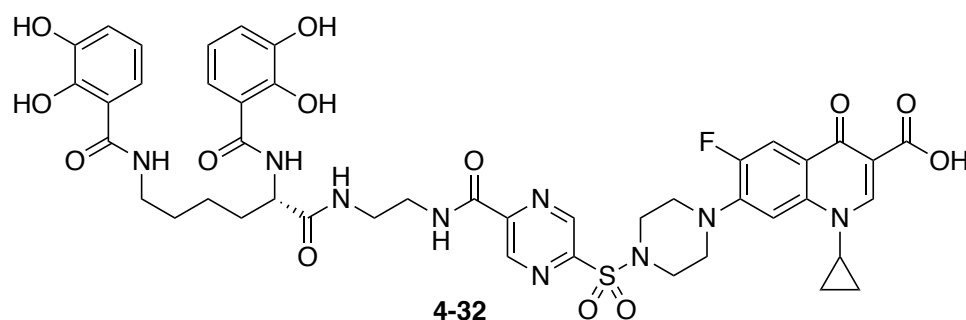
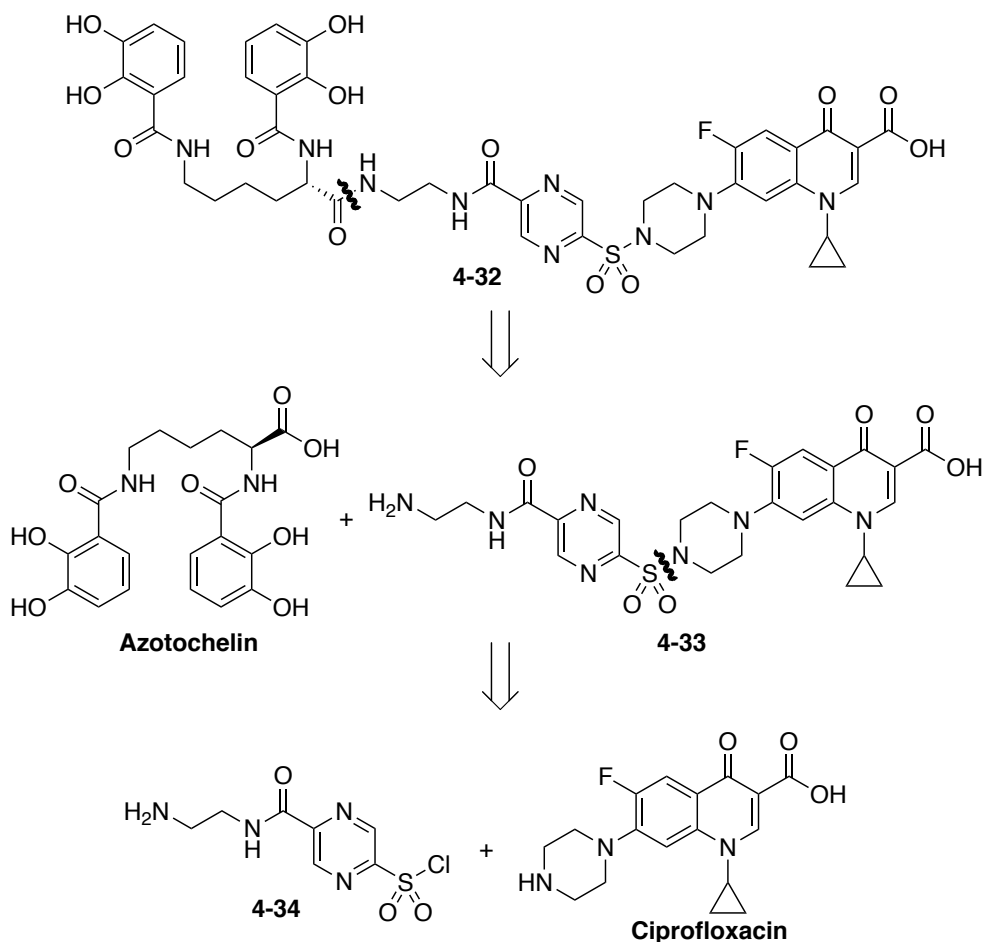


Figure 4.7 Structure of initial synthetic target **4-32**.

The two key steps in this synthesis are the formation of a sulfonamide of ciprofloxacin (**4-33**), and the coupling to the siderophore unit (**Scheme 4.16**). As with conjugate **3-14** in Chapter 3, attachment of the siderophore unit was planned to take place after synthesis of the sulfonamide to avoid exposure to the sulfonamide formation conditions. Initially, a sulfonyl chloride-based strategy via **4-34** to sulfonamide formation was pursued.



Scheme 4.16 A retrosynthetic analysis of the key coupling steps to **4-32**, and identification of the three key coupling components.

#### 4.2.1 Planned Synthetic Route to Sulfonyl Chloride

Before the selection of conditions for the synthetic route, the scope of the protecting group chemistry that can be applied to the pyrazine-sulfonamide ring must be considered, in particular the potential use of the methyl ester protecting group as in Chapter 3. Methyl esters can easily be incorporated on either the pyrazine carboxyl group or the ciprofloxacin component, however there were concerns about the stability of the heterocyclic sulfonamide unit to the basic deprotection conditions required for methyl ester hydrolysis.

The potential instability of the sulfonamide group to basic conditions led to the choice of an acid-labile protecting group, similar to the protection strategy utilised for the 4-carboxyl-2-nitrobenzene ring in Chapter 3. This could take two forms, a *tert*-butyl ester group for direct protection of the carboxylic acid group of the pyrazine ring (**4-35**), or a Boc protecting group on a linker unit coupled to the pyrazine ring via e.g. an amide of the carboxylic acid group (**4-36**, Figure 4.8).

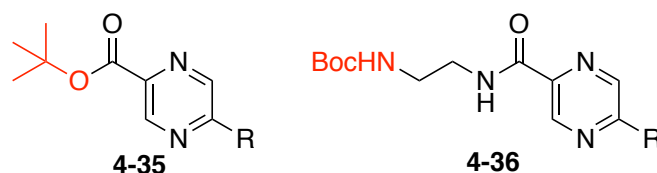
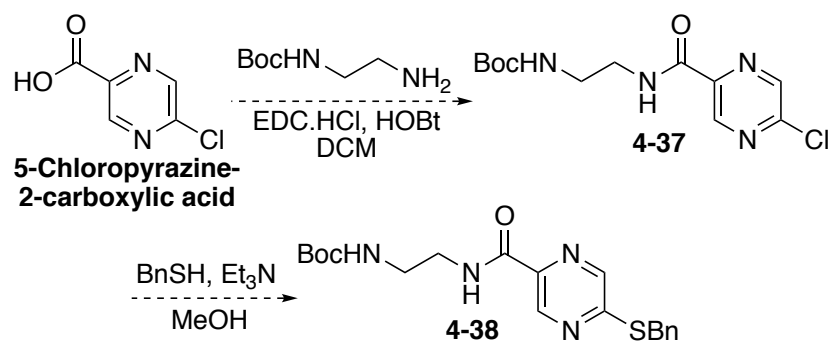


Figure 4.8 Protecting group strategies for carboxylic acid of pyrazine.

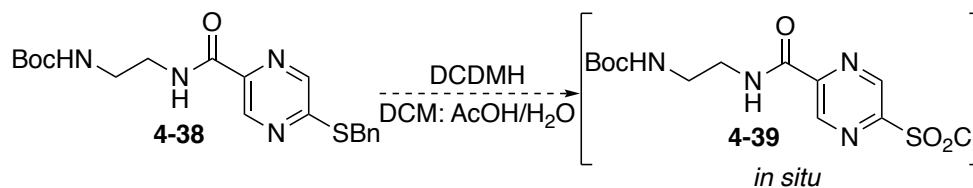
With the desired siderophore, azotochelin, containing a carboxylic acid group, the decision was made to pursue the second strategy. This could be achieved via incorporation of the commercially available *N*-Boc-ethylenediamine via an amide coupling reaction to give **4-37**. Synthesis of the target pyrazine sulfonyl chloride **4-39** from a benzyl thioether (**4-38**) was envisaged, similar to the strategy employed in Chapter 3 (Scheme 4.17).



Scheme 4.17 Proposed synthetic route to benzyl thioether **4-38**.

Oxidative chlorination of benzyl thioether **4-38** with 1,3-dichloro-5,5'-dimethylhydantoin (DCDMH) was selected as a first method to attempt sulfonyl chloride formation. As mentioned above, DCDMH has previously been used for the synthesis of heterocyclic sulfonyl chlorides, although it has not previously been employed with pyrazine rings.<sup>460,577,614–616</sup> It was decided to employ biphasic DCM/AcOH:H<sub>2</sub>O reaction conditions for this step, similar to those employed for the synthesis of 3-nitropyridine-2-sulfonyl chloride in the literature.<sup>614–616</sup> This may help to protect the formed

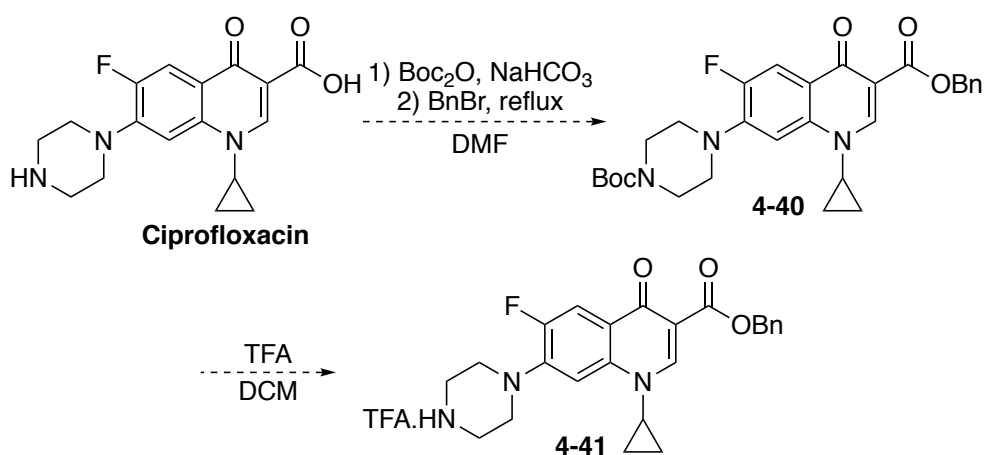
sulfonyl chloride from aqueous acid, and the DCM layer can be separated out, keeping the sulfonyl chloride *in situ* (Scheme 4.18).



Scheme 4.18 Proposed conditions for *in situ* synthesis of sulfonyl chloride **4-39**.

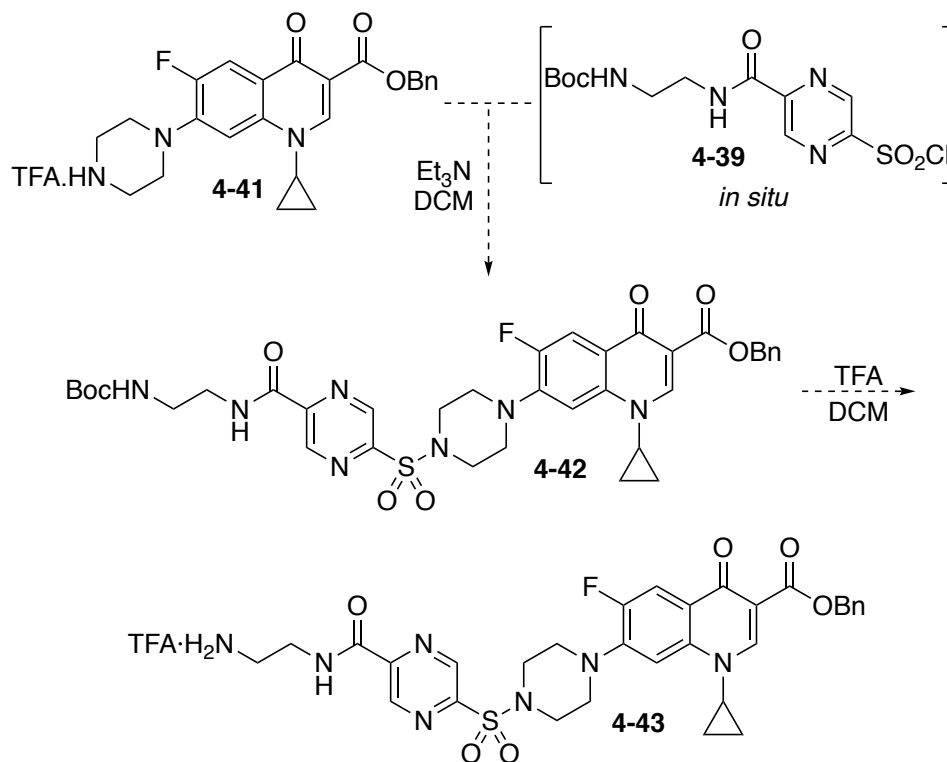
#### 4.2.2 Proposed Synthetic Route to Sulfonamide **4-43**

With the methyl ester group deemed unsuitable for use in the synthesis of pyrazine-sulfonamide conjugate **4-32**, a different protecting group was sought for the ciprofloxacin component. Here, a benzyl ester protecting group was envisaged; these are usually removed via hydrogenation,<sup>466</sup> which was hoped to be compatible with the desired pyrazine-sulfonamide linker. Synthetic strategies involving protection of ciprofloxacin with a benzyl ester have been employed a number of times in the literature, with the piperazine nitrogen of ciprofloxacin first being protected with a Boc group, then installation of the benzyl ester via alkylation with BnBr,<sup>195,435,436</sup> or via ester coupling.<sup>468</sup> The Boc group can then be removed via reaction with HCl<sup>195,435</sup> or TFA<sup>436,468</sup> in organic solvents to give the target ciprofloxacin component **4-41** for coupling to sulfonyl chloride **4-39** (Scheme 4.19).



Scheme 4.19 Proposed synthetic route to benzyl-protected ciprofloxacin **4-41**.

A similar coupling reaction to that employed in Chapter 3 was proposed, with formation of sulfonamide **4-42** via reaction of **4-41** and sulfonyl chloride **4-39** in DCM, plus triethylamine as a base. Following successful formation of **4-42**, removal of the Boc group on the diamine linker via reaction with TFA/DCM was envisaged to give TFA salt **4-43** in preparation for coupling to the azotochelin component (**Scheme 4.20**).

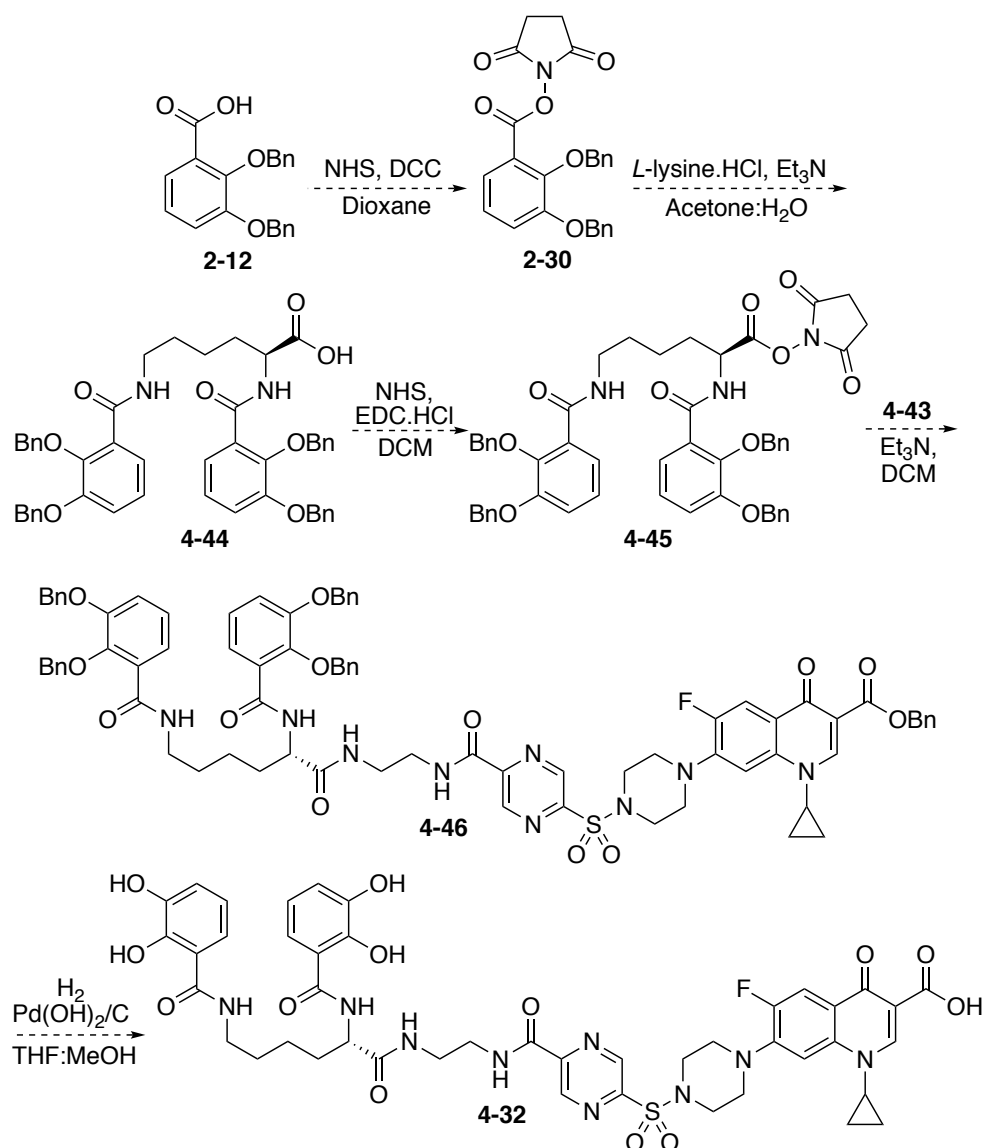


Scheme 4.20 Proposed synthetic route to pyrazine-sulfonamide **4-43**.

### 4.2.3 Proposed Installation of Azotochelin and Final Deprotection

Benzyl protecting groups were also envisaged for the synthesis of the azotochelin component, in this case benzyl ethers for protection of the four catechol hydroxyl groups. As with their benzyl ester counterparts, these can also be removed via hydrogenation. The synthesis of benzylated azotochelin starting from 2,3-bis(benzyloxy)benzoic acid (**2-12**) is well established in the Duhme-Klair group.<sup>349</sup> **2-12** is first converted to NHS ester **2-30** via a DCC-mediated reaction with *N*-hydroxysuccinimide. Two equivalents of **2-30** can then be reacted with *L*-lysine hydrochloride to generate the desired benzyl protected azotochelin **4-44**. Formation of NHS ester **4-45** was envisaged for amide coupling to TFA salt **4-43** to give **4-46** (**Scheme 4.21**).

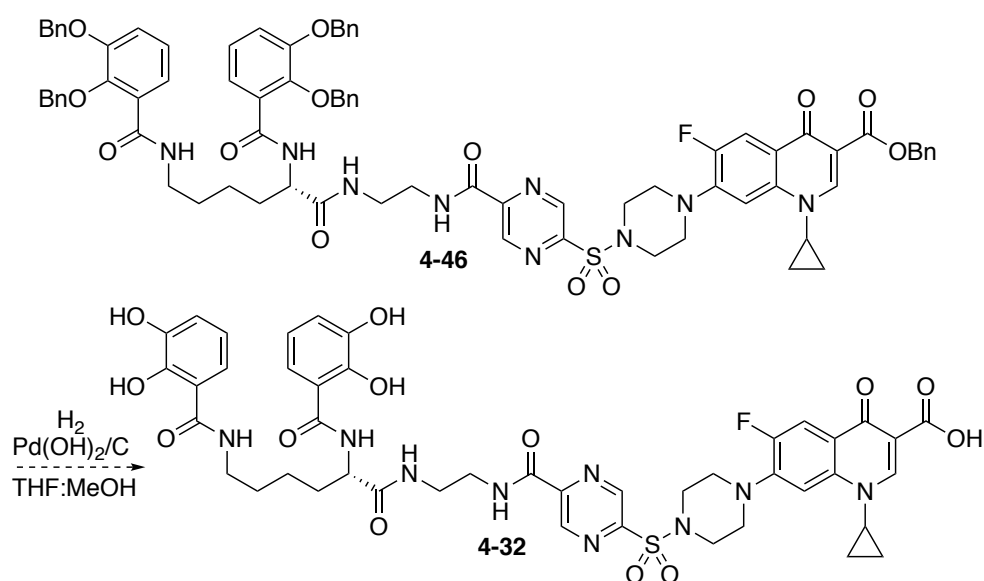




Scheme 4.21 Proposed synthesis of benzyl-protected azotochelin NHS ester **4-45**, and coupling to pyrazine-sulfonamide component **4-43**.

Finally, a global benzyl deprotection was proposed to reach target conjugate **4-32**. The typical conditions employed for benzyl group deprotection are hydrogenolysis with palladium on carbon as a catalyst. The stability of the central pyrazine ring to these conditions is not clear from the literature; there are examples of halogen replacement,<sup>617,618</sup> and even full hydrogenation of the pyrazine ring<sup>619</sup> for carboxyl-substituted pyrazines (although the latter tends to occur under high pressure).<sup>620</sup> However, these reactions have not been described for pyrazine rings as electron-deficient as the pyrazine-sulfonamide linker, so there is every chance it will be stable to hydrogenation conditions.

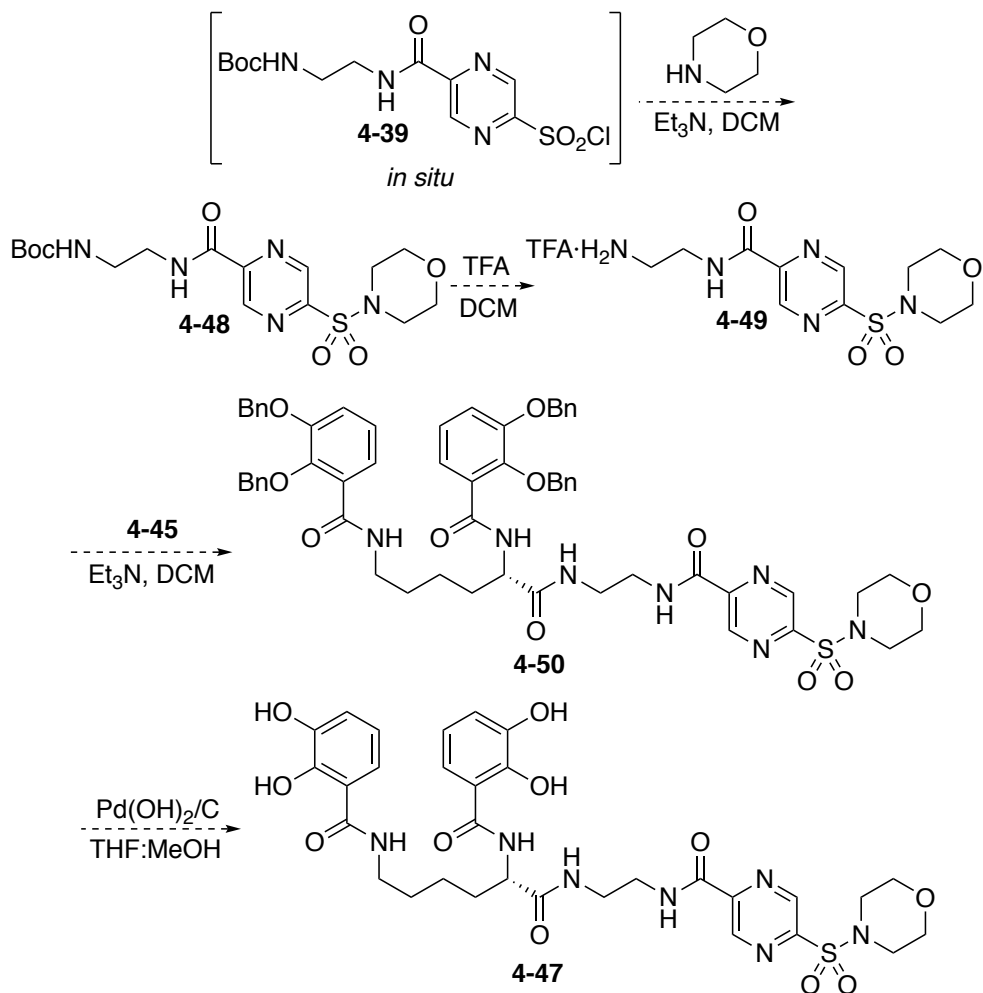
While a range of conditions have been used in the literature for hydrogenation of ciprofloxacin-containing compounds<sup>189,435,436</sup> previous studies have demonstrated poor yields and mass recovery when palladium on charcoal is utilised, potentially due to adsorption of the product or starting material to the charcoal surface.<sup>621,622</sup> Palladium hydroxide on carbon (Pearlman's catalyst) has been shown to facilitate benzyl group removal in the presence of ciprofloxacin without significant impact on yields, so this was suggested as a reagent for global debenzylation of **4-46** (Scheme 4.22).<sup>266,435,436</sup>



Scheme 4.22 Proposed global debenzylation to yield target conjugate **4-32**.

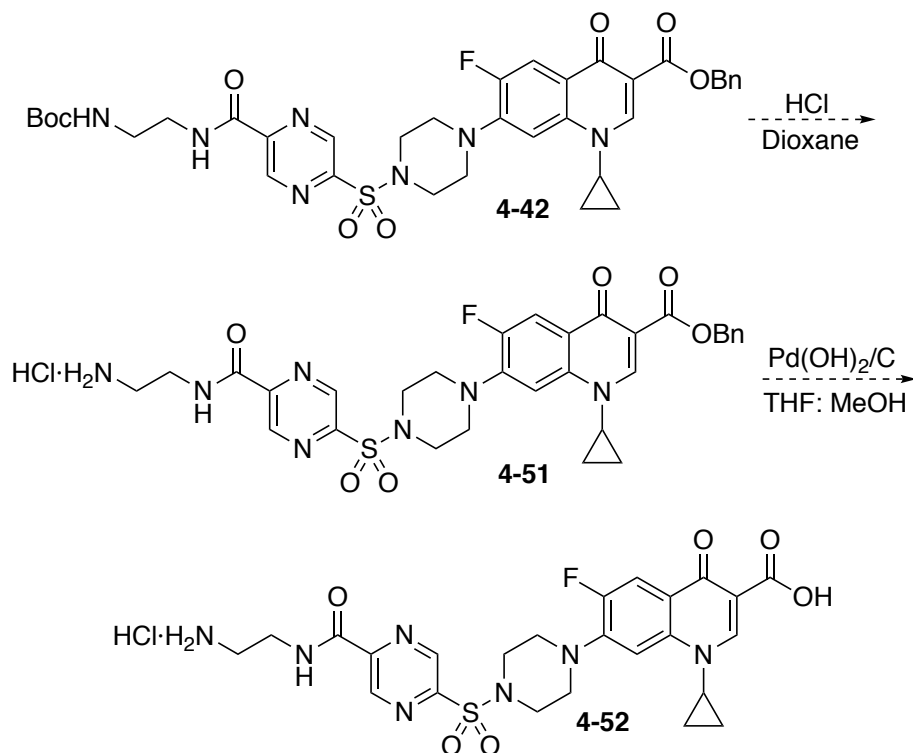
#### 4.2.4 Proposed Synthetic Routes to Control Compounds

A series of control compounds for microbiological screening were also designed analogous to the control compounds synthesised in Chapter 3. The first of these is a Cipro –, Azoto + control **4-47**, designed to examine antimicrobial activity stemming from  $\text{SO}_2$  release alone. Likewise with the Cipro –, DFO + control utilised in Chapter 3, a morpholine group was selected to act as a mimic of the 6-membered piperazine ring of ciprofloxacin. The synthetic route therefore follows a similar pathway to the synthesis of **3-31** (Scheme 4.23).



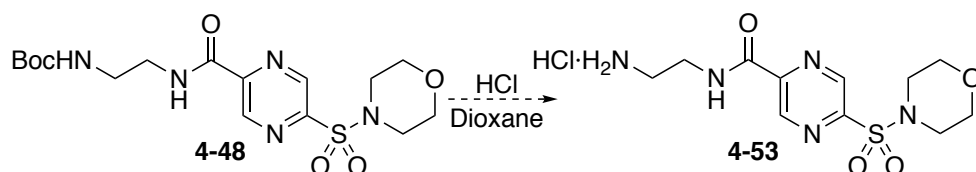
Scheme 4.23 Proposed synthesis of Cipro –, Azoto + control **4-47**.

The synthesis of a Cipro +, Azoto – control was also envisaged to examine the change in antimicrobial activity on loss of the siderophore unit. Here, pyrazine-sulfonamide salt **4-43** could offer an appropriate control. However, the use of TFA salts in biological experiments is sometimes avoided, as the presence of TFA can sometimes generate toxic effects beyond those of the parent compounds.<sup>623,624</sup> Therefore, the synthesis of a hydrochloric acid salt **4-51** from Boc-protected **4-42** was proposed instead, with a final benzyl deprotection of the ciprofloxacin unit leading to Cipro +, Azoto – control **4-52** (Scheme 4.24).



Scheme 4.24 Proposed synthesis of Cipro +, Azoto – control **4-52**.

Finally, the synthesis of a Cipro –, Azoto – control was imagined from Boc-protected morpholine-sulfonamide **4-48**. Again, a HCl salt was proposed to avoid any toxic effects from TFA. A HCl-mediated deprotection of **4-48** was envisaged to give the target control **4-53** (**Scheme 4.25**).



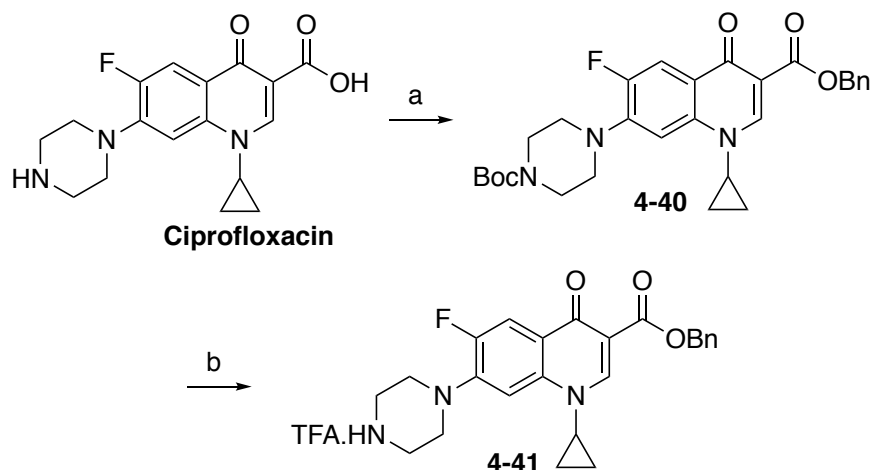
Scheme 4.25 Proposed synthesis of Cipro –, Azoto – control **4-53**.

## 4.3 Synthesis

### 4.3.1 Synthesis of Ciprofloxacin Component

In accordance with the synthetic strategy outlined above, ciprofloxacin was reacted with Boc anhydride, then benzyl bromide to give Boc-ciprofloxacin benzyl ester **4-40** in a one-pot reaction (**Scheme 4.26**). The presence of the Boc group can be observed as a 9H singlet at 1.42 ppm in the  $^1\text{H}$  NMR spectrum; likewise successful installation of the benzyl group can be seen via a benzyl  $\text{CH}_2$  resonance at 5.39 ppm, and aromatic resonances between 7.53 and 7.26 ppm. Further structural confirmation comes from the ESI mass spectrum, where a peak at  $m/z = 544.2223$  can be assigned as an  $[\text{M}+\text{Na}]^+$

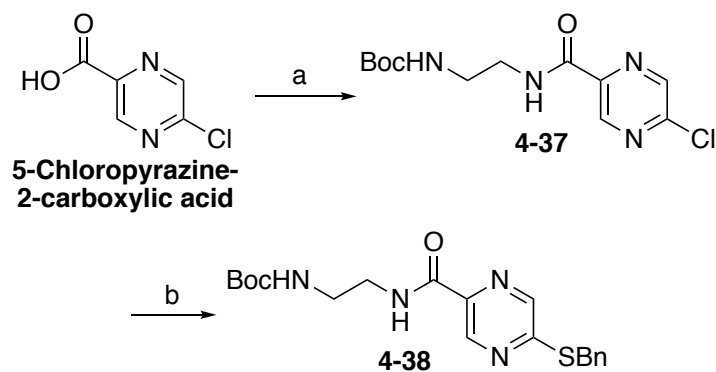
molecular ion consistent with a molecular formula of  $C_{29}H_{32}FN_3NaO_5$ . Removal of the Boc group was achieved with TFA in DCM, with formation of **4-41** confirmed via the observed loss of the Boc singlet in the  $^1H$  NMR spectrum, and the presence of peaks in the ESI mass spectrum at  $m/z = 422.1881$  and  $444.1703$ , consistent with  $[M+H]^+$  and  $[M+Na]^+$  molecular ions with molecular formulae  $C_{26}H_{26}F_4N_3O_5$  and  $C_{26}H_{25}F_4N_3NaO_5$  respectively.



Scheme 4.26 Synthesis of benzyl-protected ciprofloxacin **4-41**. a)  $Boc_2O$ ,  $NaHCO_3$ , DMF (anhydrous), 18 h, then  $BnBr$ ,  $90\text{ }^\circ C$ , 26 h, 83%; b) TFA (10% v/v), DCM, 17 h, 96%.

### 4.3.2 Synthesis of Pyrazine Sulfonamide

The synthesis of pyrazine benzyl thioether **4-38** proceeded smoothly in 84% yield over two steps (Scheme 4.27). Successful amide coupling to give **4-37** is confirmed by the presence of quartets corresponding to the  $CH_2$  groups in ethylenediamine at 3.59 and 3.41 ppm in the  $^1H$  NMR spectrum, and the presence of a peak at  $m/z = 323.0888$  in the ESI mass spectrum, consistent with an  $[M+Na]^+$  molecular ion of formula  $C_{12}H_{17}^{35}ClN_4NaO_3$ . Elemental analysis is consistent with a pure product. Installation of a benzyl thioether can be seen from an observed shift in the aromatic proton *ortho* to the thioether from 8.52 ppm in **4-37** to 8.31 ppm in **4-38**, consistent with the more electron-donating nature of the thioether compared to chlorine. In addition, the ESI mass spectrum displays a peak at  $m/z = 411.1452$ , which can be assigned as an  $[M+Na]^+$  molecular ion of formula  $C_{19}H_{24}N_4NaO_3S$ , consistent with the desired product.



Scheme 4.27 Synthesis of pyrazine benzyl thioether **4-38**. a) *N*-Boc ethylenediamine, EDC.HCl, HOBT, DCM (anhydrous), 24 h, 84%; b) BnSH, Et<sub>3</sub>N, MeOH (anhydrous), 0 °C to rt, 24 h, 78%.

In both **4-37** and **4-38**, the presence of two distinct isomers can be seen in the <sup>1</sup>H NMR spectrum in a ratio of c. 90:10; these can be assigned to the *anti* and *syn* forms of the carbamate bond, which similar to amides display partial double bond character (**Figure 4.9**).<sup>625,626</sup> The *anti* form is typically more stable, and therefore likely to be the major isomer.<sup>625</sup> The isomeric nature of these resonances can be demonstrated by variable temperature <sup>1</sup>H NMR spectroscopy of **4-37**, with the two singlet carbamate proton resonances coalescing to give a single broad resonance at high temperature.

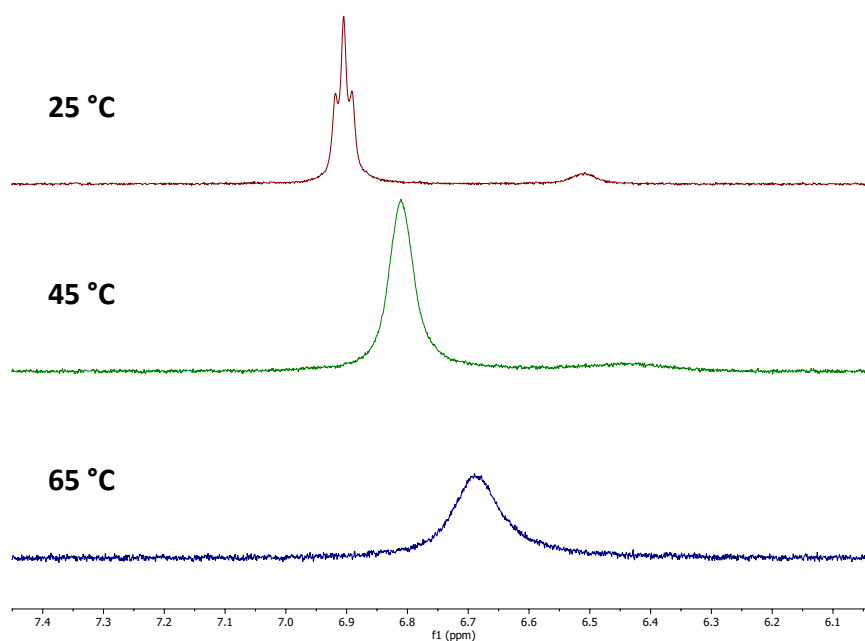
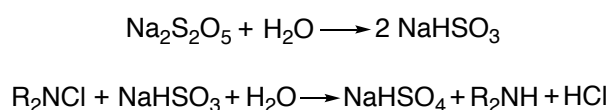


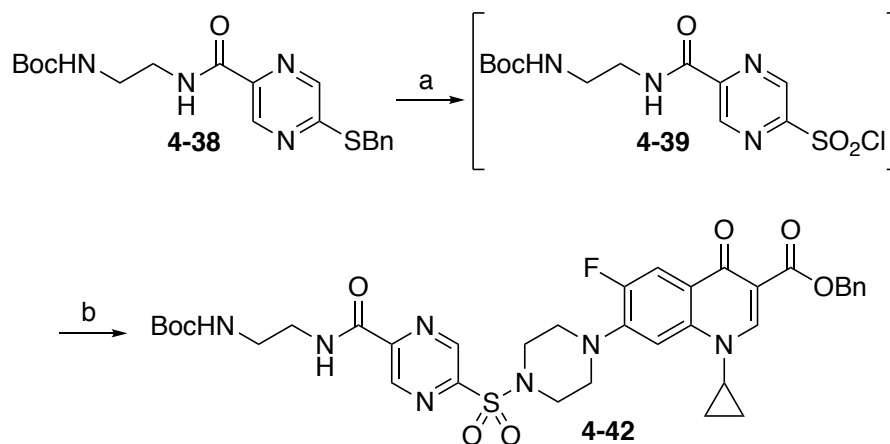
Figure 4.9 Overlaid <sup>1</sup>H NMR spectra for variable temperature experiments for **4-37** in DMSO-d<sub>6</sub> to show coalescing of potential rotameric carbamate resonances.

The initial conditions for the oxidative chlorination reaction of **4-38** were based on the literature for 3-nitro-2-pyridinesulfonyl chloride,<sup>614-616</sup> namely 3 equivalents of DCDMH, solvent ratios of between 11 and 7 parts DCM to 2 parts H<sub>2</sub>O and 1 part AcOH, and quenching of remaining DCDMH by pouring the reaction mixture into a dilute solution of sodium metabisulfite, followed by vigorous agitation (**Scheme 4.28**). The dechlorinated hydantoin derivatives can then be removed in the subsequent basic aqueous workup. The DCM layer is kept cold throughout the workup, then transferred to a new flask after drying with MgSO<sub>4</sub>, and reagents for the sulfonamide formation are immediately added to the solution.



Scheme 4.28 Chemical equations for quenching of chloramines by sodium metabisulfite.

The oxidative chlorination reaction of **4-38**, followed by subsequent addition of TFA salt **4-41**, proved successful in synthesising pyrazine-sulfonamide **4-42** (**Scheme 4.29**). Sulfonyl chloride formation can be observed by <sup>1</sup>H NMR spectroscopy, with the chemical shifts of the pyrazine protons moving from 9.14 and 8.31 ppm in thioether **4-38** to 9.56 and 9.24 ppm in **4-39**. Coupling of the ciprofloxacin unit can be confirmed by <sup>1</sup>H NMR spectroscopy, with the pyrazine protons shifting to 9.45 and 9.09 ppm, and the presence of proton resonances corresponding to the quinoline ring of ciprofloxacin observed at 8.54, 8.05 and 7.30 ppm. The ESI mass spectrum of **4-42** also contains a peak at  $m/z = 772.2541$ , which can be assigned as an [M+Na]<sup>+</sup> molecular ion of formula C<sub>36</sub>H<sub>40</sub>FN<sub>7</sub>NaO<sub>8</sub>S. Around 0.825 equivalents of **4-41** was found to give the least amount of unreacted ciprofloxacin derivative at the end of the reaction, suggesting that around 15-20% of the pyrazine sulfonyl chloride is being lost during the aqueous workup, or not reacting during the sulfonamide formation step. **4-42** can be obtained in 61% yield following purification by column chromatography.



Scheme 4.29 Synthesis of pyrazine-sulfonamide **4-42**. a) 1,3-dichloro-5,5'-dimethylhydantoin, DCM/AcOH:H<sub>2</sub>O (biphasic), 0 to 20 °C, 7.5 h; b) **4-41**, Et<sub>3</sub>N, DCM, 24 h, 61% over two steps.

Over a number of repeats, some key factors in the progress of the reaction became apparent. If the oxidative chlorination reaction time is too short (< 6 hours), the presence of pyrazine sulfoxide **4-54** may be observed in the final product (**Figure 4.10**). The same outcome is observed if fewer than three equivalents of DCDMH are used. The presence of sulfoxide **4-54** can be observed by <sup>1</sup>H NMR spectroscopy in CDCl<sub>3</sub>, with two doublets at 4.46 and 4.16 ppm, both with an integration of 1H; these can be assigned to the diastereotopic CH<sub>2</sub> protons adjacent to the chiral sulfoxide. **4-54** can also be observed in the ESI mass spectrum, with a peak at *m/z* = 427.1415, which can be assigned as an [M+Na]<sup>+</sup> adduct of formula C<sub>19</sub>H<sub>24</sub>N<sub>4</sub>NaO<sub>4</sub>S, consistent with the formation of the sulfoxide. **4-54** is expected to be an intermediate in the oxidative chlorination reaction,<sup>459</sup> so its presence is not unexpected, but it provides an indicator as to the progress of the reaction.

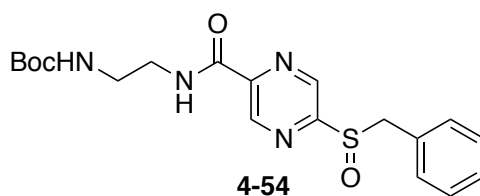


Figure 4.10 Sulfoxide intermediate **4-54** observed in some oxidative chlorination reactions of benzyl thioether **4-38**.

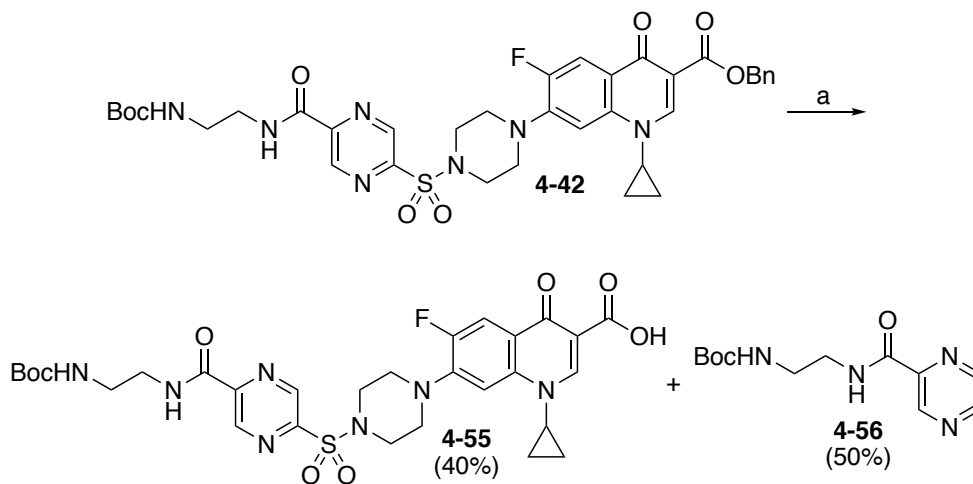
The sulfonyl chloride (**4-39**) appears to tolerate extended reaction times of up to 18 hours, although the formation of small amounts (<0.05 eq.) of pyrazine chloride **4-37** can be observed after longer reaction times,



indicating a small amount of decomposition over time. The sulfonyl chloride also tolerates temperatures above 0 °C, with the reaction mixture allowed to warm slowly to room temperature over the course of the reaction. Finally, although it was not observed for examples of pyrazine sulfonyl chloride **4-39**, DCDMH can mediate formation of chloramine derivatives of the sulfonyl chloride product,<sup>627,628</sup> so the use of more than three equivalents is not advisable.

### 4.3.3 Instability of Pyrazine-Sulfonamide **4-42** to Hydrogenation

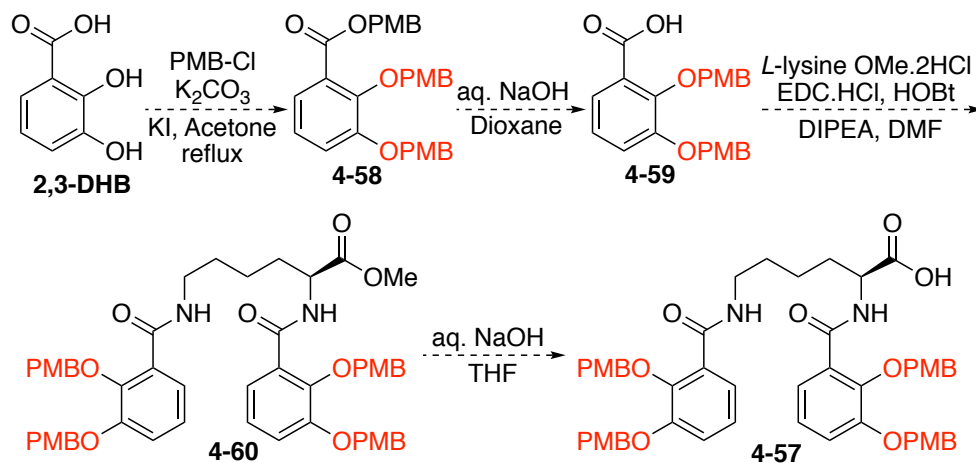
Before proceeding to the amide coupling with benzyl-protected azotochelin **4-45**, the stability of pyrazine-sulfonamide **4-42** to the intended hydrogenolysis conditions with Pd(OH)<sub>2</sub> was explored (**Scheme 4.30**). A mixture of products was observed by <sup>1</sup>H/<sup>19</sup>F NMR spectroscopy. The major product appeared to be the debenzylated pyrazine-sulfonamide **4-55**, with almost complete loss of the benzyl aromatic peaks between 7.52 and 7.27 ppm, and the CH<sub>2</sub> peak at 5.38 ppm, and a corresponding shift in the proton adjacent to the ciprofloxacin carboxylic acid from 8.54 ppm to 8.80 ppm. There is also an observed shift in the fluoroquinolone <sup>19</sup>F resonance from -123.9 ppm in **4-42** to -121.3 ppm in **4-55**. The ESI mass spectrum also contains a peak at *m/z* = 682.2055, which can be assigned as an [M+Na]<sup>+</sup> molecular ion of formula C<sub>29</sub>H<sub>34</sub>FN<sub>7</sub>NaO<sub>8</sub>S. Some starting material (c. 10%) remains present. However, a significant amount (50%) of a third product was also present, with doublets at 9.40 and 8.75 ppm, and a doublet of doublets at 8.54 ppm. The coupling pattern for this product in the <sup>1</sup>H NMR spectrum could indicate a pyrazine ring bearing 3 hydrogens, suggesting that **4-42** has undergone hydrogenation at the sulfonamide position to yield **4-56**. This is confirmed via comparison of the <sup>1</sup>H NMR chemical shifts with a literature spectrum of **4-56**,<sup>629</sup> and the presence of a peak at *m/z* = 289.1265 in the ESI mass spectrum, corresponding to an [M+Na]<sup>+</sup> molecular ion of formula C<sub>12</sub>H<sub>18</sub>N<sub>4</sub>NaO<sub>3</sub>.



Scheme 4.30 Testing of hydrogenolysis conditions. a)  $\text{H}_2$ ,  $\text{Pd}(\text{OH})_2/\text{C}$ ,  $\text{THF}:\text{MeOH}$ , 20 h.

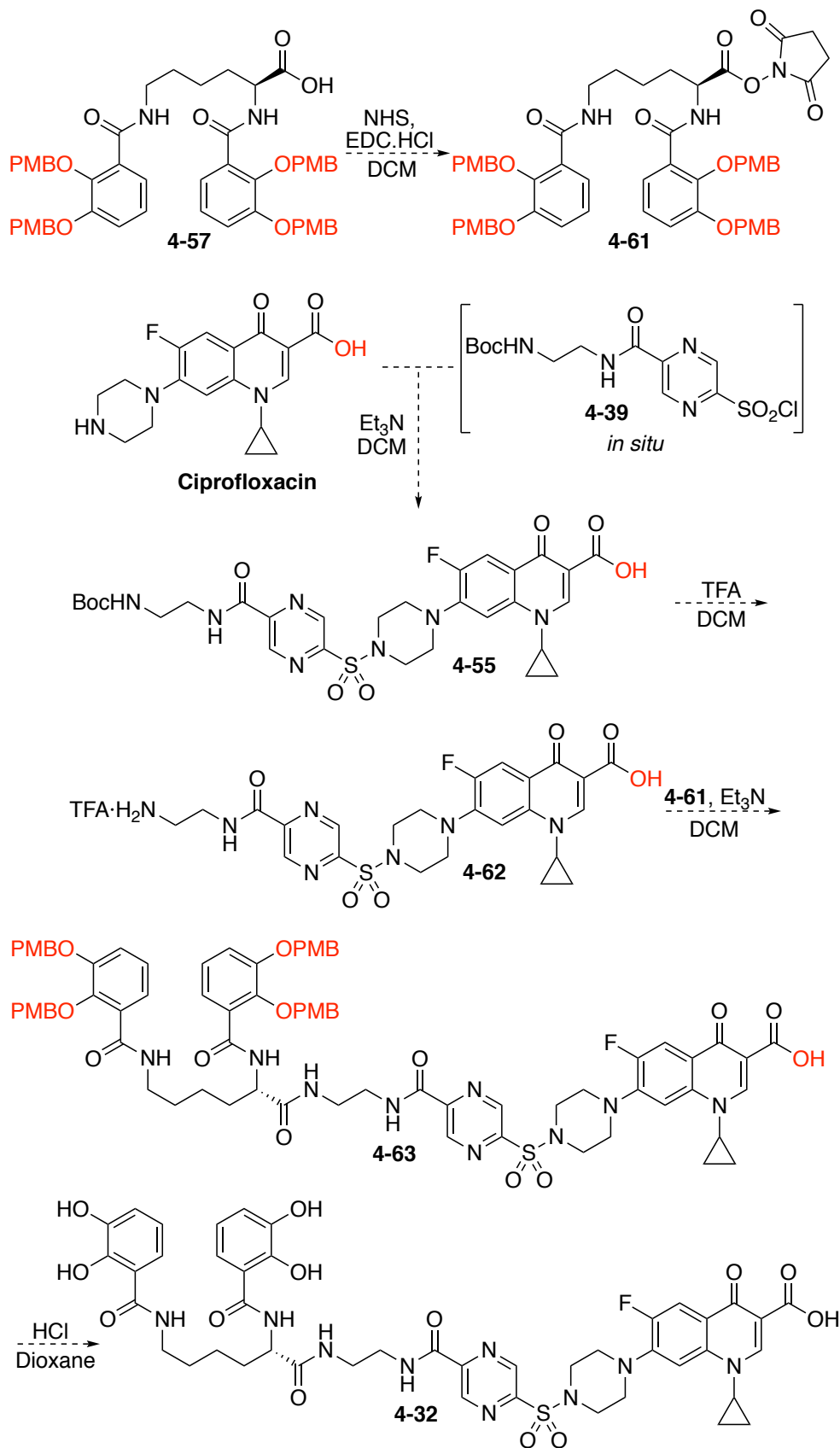
#### 4.3.4 Revised Synthetic Route to 4-32

As the hydrogenation conditions examined were not suitable to fully deprotect **4-42** and yielded a significant amount of hydrogenated pyrazine **4-56**, a change to the synthetic route was required. The planned benzyl groups on the catechol groups of azotochelin were replaced with *para*-methoxybenzyl (PMB) groups; these have previously been used in the literature for protection of azotochelin, with deprotection of the catechols via reaction with TFA.<sup>185</sup> Further studies in the AKDK research group have also identified  $\text{HCl}/\text{dioxane}$  as a suitable reagent for PMB removal from azotochelin.<sup>630</sup> The proposed synthetic route to PMB-protected azotochelin **4-57** was originally carried out by James Southwell, using a method based on Tarapdar *et al.*<sup>185</sup> Reaction of 2,3-dihydroxybenzoic acid (**2,3-DHB**) with *para*-methoxybenzyl chloride (PMB-Cl) followed by hydrolysis of the formed PMB ester **4-58** with sodium hydroxide yields PMB-protected benzoic acid **4-59**. This can then be coupled to *L*-lysine methyl ester with  $\text{EDC}\cdot\text{HCl}/\text{HOBT}$ , followed by a further deprotection with sodium hydroxide to yield PMB-protected azotochelin **4-57** (**Scheme 4.31**).



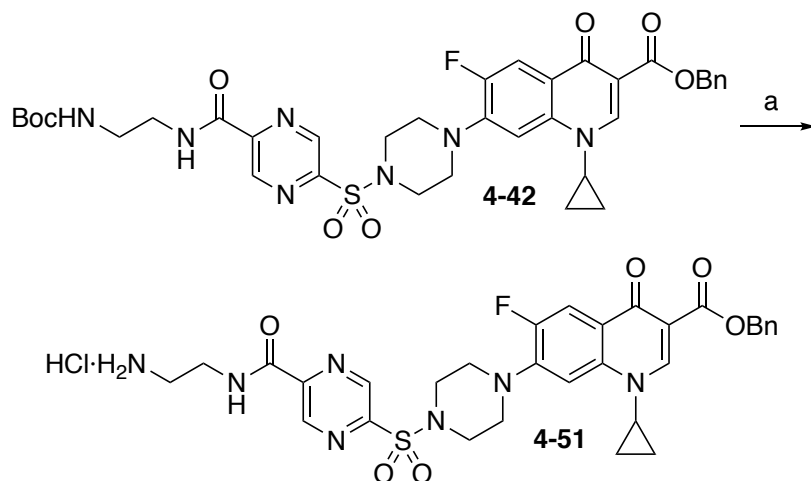
Scheme 4.31 Proposed synthetic route to PMB-protected azotochelin **4-57**. New protecting groups highlighted in red.

Ciprofloxacin was also incorporated into the new route without carboxylic acid protection (**Scheme 4.32**). This minimises the deprotection steps required for the final conjugate, and precludes the need to develop a new protecting strategy for ciprofloxacin. This strategy has been used before for other conjugates.<sup>262,433,435,631,632</sup> The main drawback is a limitation of the routes possible for amide coupling of pyrazine-sulfonamide **4-62** to the protected azotochelin, however, this should still be achievable with the NHS ester strategy intended for benzyl-protected azotochelin, with the amine of pyrazine-sulfonamide **4-62** much more reactive than the unprotected carboxylic acid.



Scheme 4.32 Revised synthetic route to target conjugate **4-32**. Protecting group changes are highlighted in red.

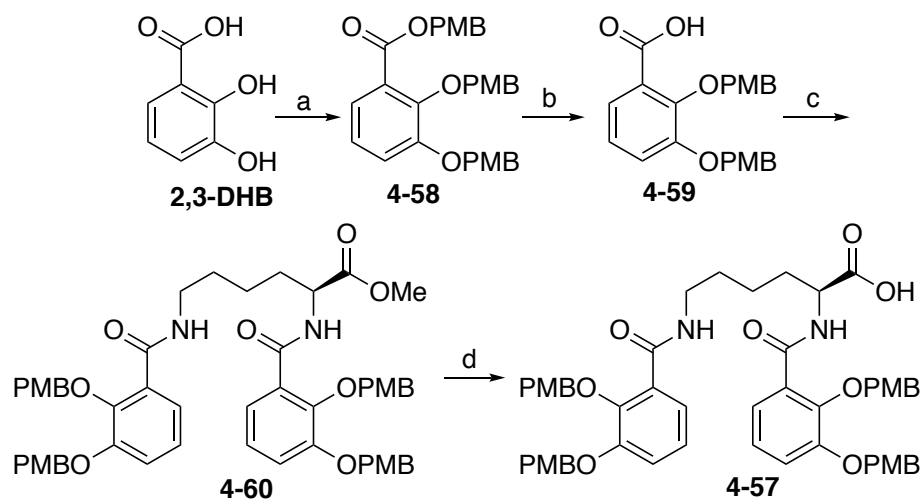
The compatibility of pyrazine-sulfonamide **4-42** with the strong acid deprotection conditions required for PMB removal was examined before proceeding with this route, with no decomposition observed (**Scheme 4.33**).



Scheme 4.33 Testing of PMB deprotection conditions on pyrazine-sulfonamide **4-42**. a) HCl (129 eq.), dioxane, 0 to 20 °C, 17 h.

#### 4.3.5 Synthesis of New Azotochelin Component

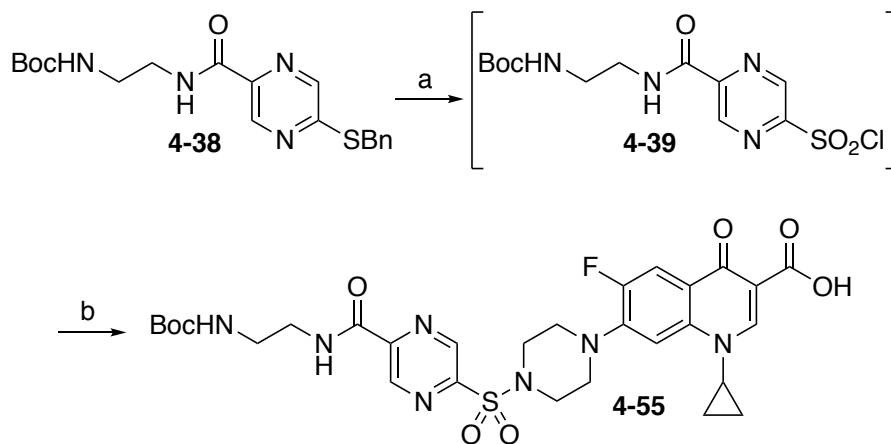
Alkylation of 2,3-dihydroxybenzoic acid (**2,3-DHB**) with *para*-methoxybenzylchloride gave **4-58**, which was subjected to subsequent ester hydrolysis with aqueous NaOH in dioxane to give carboxylic acid **4-59** (**Scheme 4.34**). **4-59** can then be subjected to an amide coupling reaction with *L*-lysine methyl ester dihydrochloride to yield **4-60**. Finally, **4-60** can undergo methyl ester hydrolysis with aqueous NaOH to give the target PMB-protected azotochelin **4-57** (**Scheme 4.34**). All of the characterisation data for the compounds in this route are consistent with the literature.<sup>185</sup> Successful synthesis of **4-57** can be observed from the <sup>1</sup>H NMR spectrum, with the loss of the OMe ester singlet, and from the ESI mass spectrum, which contains a peak at  $m/z = 921.3593$ , consistent with an  $[M+Na]^+$  molecular ion of formula  $C_{52}H_{54}N_2NaO_{12}$ .



Scheme 4.34 Synthesis of PMB-protected azotochelin **4-57**. a) PMB-Cl,  $K_2CO_3$ , KI, acetone (anhydrous), reflux, 72 h, 91%; b) aq. NaOH, dioxane, 72 h, 90%; c) *L*-lysine methyl ester dihydrochloride, EDC.HCl, HOBT, DIPEA, DMF, 50 °C, 40 h, 55%; d) aq. NaOH, THF, 23 h, 71%.

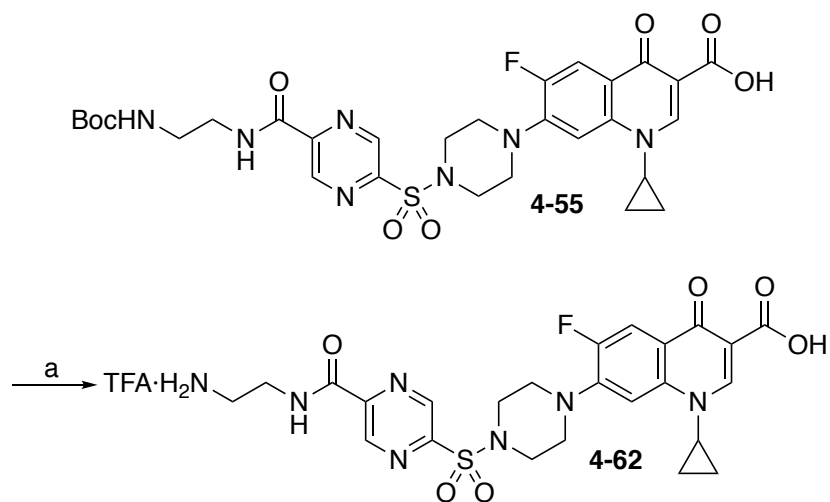
#### 4.3.6 Synthesis of New Pyrazine-Sulfonamide Component

New pyrazine-sulfonamide target **4-55** was successfully synthesised from sulfonyl chloride **4-39** and ciprofloxacin. **4-55** precipitates from the reaction mixture as a white solid, and can be isolated pure by Buchner filtration when washed with further DCM, and 1 M HCl to remove any remaining ciprofloxacin (**Scheme 4.35**). Formation of **4-55** can be supported by observed changes in the chemical shifts of the piperazine protons in the  $^1H$  NMR spectrum, from 3.23 and 2.89 ppm in ciprofloxacin to 3.48 and 3.42 ppm in **4-55**, and the presence of peaks at  $m/z = 682.2051$  in the ESI positive ion mass spectrum and  $m/z = 658.2113$  in the ESI negative ion mass spectrum, corresponding to  $[M+Na]^+$  and  $[M-H]^-$  molecular ions of formula  $C_{29}H_{34}FN_7NaO_8S$  and  $C_{29}H_{33}FN_7O_8S$  respectively, consistent with the expected molecular formula of **4-55** ( $C_{29}H_{34}FN_7O_8S$ ).



Scheme 4.35 Synthesis of key pyrazine-sulfonamide **4-55**. a) 1,3-dichloro-5,5'-dimethylhydantoin, DCM/AcOH:H<sub>2</sub>O (biphasic), 0 to 20 °C, 15 h; b) ciprofloxacin, DIPEA, DCM, 0 to 20 °C, 18-24 h, 52% over two steps.

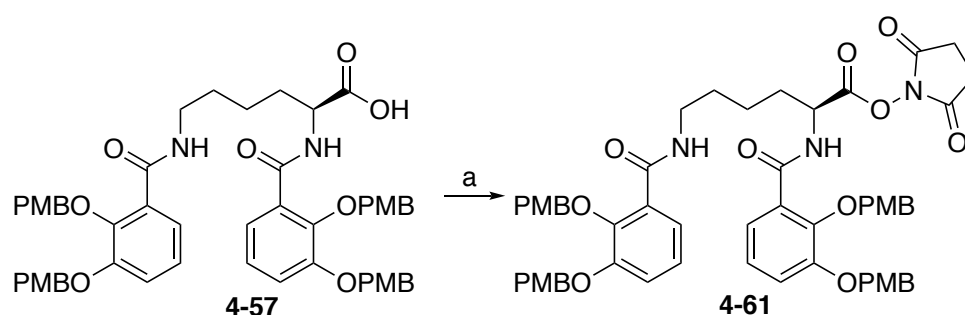
Removal of the Boc group on the ethylenediamine linker to give deprotected TFA salt **4-62** can be achieved with 10% v/v TFA in DCM (**Scheme 4.36**). Successful deprotection can be confirmed by observation of the <sup>1</sup>H NMR spectrum, with loss of the *tert*-butyl singlet at 1.34 ppm, and the ESI mass spectrum, which displays a peak at *m/z* = 582.1538, consistent with an [M+Na]<sup>+</sup> molecular ion of formula C<sub>24</sub>H<sub>26</sub>FN<sub>7</sub>NaO<sub>6</sub>S. The presence of a TFA counterion can also be observed by <sup>19</sup>F NMR spectroscopy, with a resonance at -73.4 ppm in a c. 3:1 integration ratio to the fluoroquinolone <sup>19</sup>F resonance.



Scheme 4.36 Synthesis of TFA salt **4-62**. a) TFA (10% v/v), DCM (anhydrous), 5 h, 73%.

### 4.3.7 Coupling of 4-55 and 4-61 and Final Deprotection

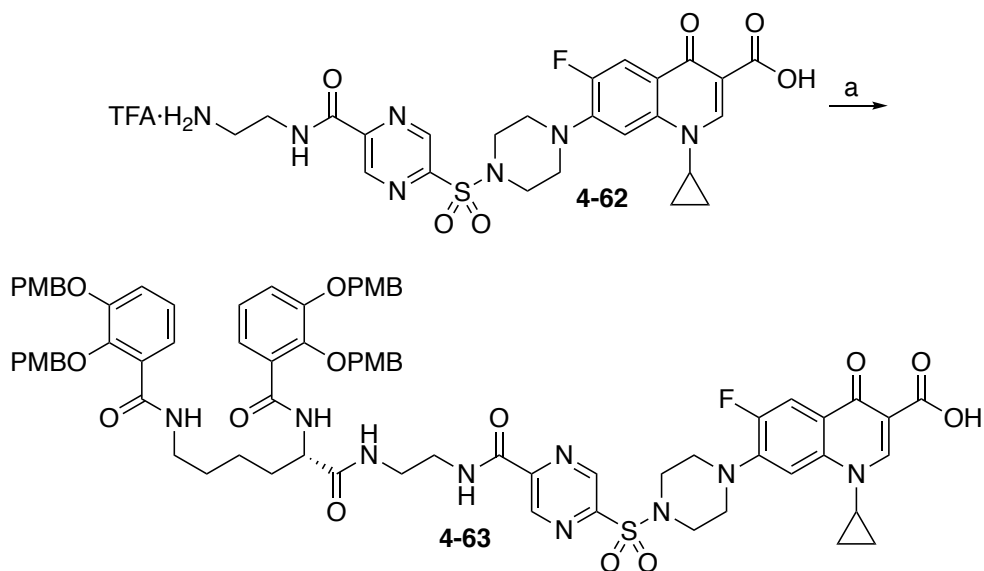
The required NHS ester **4-61** for coupling of the azotochelin and pyrazine-sulfonamide components can be synthesised via EDC-mediated amide coupling (**Scheme 4.37**). Successful formation of **4-61** is supported by  $^1\text{H}$  NMR spectroscopy, with the NHS ester observed as a singlet with an integration of 4 at 2.78 ppm. An additional C=O resonance is observed at 168.7 ppm in the  $^{13}\text{C}$  NMR spectrum, which can be assigned to the two carbonyl groups of the NHS ester. The ESI mass spectrum also contains a peak at  $m/z = 1018.3765$ , which can be assigned as an  $[\text{M}+\text{Na}]^+$  adduct of molecular formula  $\text{C}_{56}\text{H}_{57}\text{N}_3\text{NaO}_{14}$ . The NHS ester decomposes slowly over time, so is used immediately after purification.



Scheme 4.37 Synthesis of PMB-protected azotochelin NHS ester **4-61**. a) *N*-hydroxysuccinimide, EDC.HCl, DCM, 18 h, 55%.

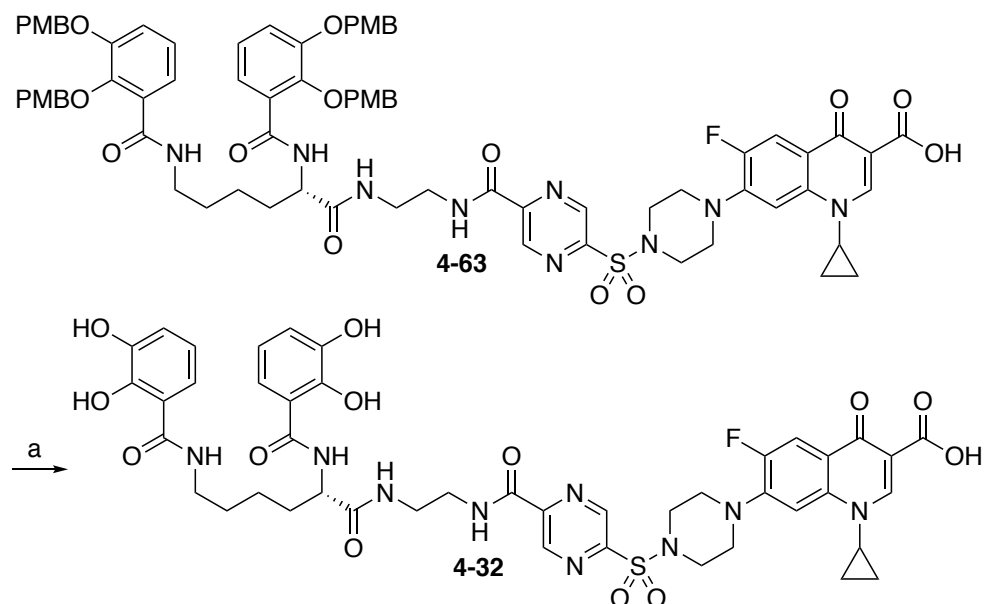
Coupling of NHS ester **4-61** and TFA salt **4-62** was carried out with  $\text{Et}_3\text{N}$  as a base, with **4-63** successfully isolated in 91% yield (**Scheme 4.38**). The  $^1\text{H}$  NMR spectrum of **4-63** contains resonances corresponding to the pyrazine-sulfonamide and the azotochelin in a 1:1 ratio, with a new amide resonance at 172.9 ppm in the  $^{13}\text{C}$  NMR spectrum (compared to the carboxylic acid peak at 166.2 ppm in **4-57**, or the NHS ester peak at 168.2 ppm in **4-61**). The ESI mass spectrum also supports the formation of **4-63**, with a peak at  $m/z = 1462.5112$ , consistent with an  $[\text{M}+\text{Na}]^+$  molecular ion of formula  $\text{C}_{76}\text{H}_{78}\text{FN}_9\text{NaO}_{17}\text{S}$ .





Scheme 4.38 Coupling of PMB-protected azotochelin NHS ester **4-61** and TFA salt **4-62**. a) **4-61**, Et<sub>3</sub>N, DCM, 24 h, 91%.

**4-63** was subjected to HCl-mediated removal of the PMB groups in dioxane to give target conjugate **4-32** (Scheme 4.39). Successful formation of **4-32** is supported by the observed loss of the PMB aromatic resonances between 7.46 and 6.71 ppm, the PMB CH<sub>2</sub> singlets between 5.12 and 4.85 ppm and the PMB methyl groups between 3.78 and 3.65 ppm in the <sup>1</sup>H NMR spectrum. Further evidence comes from the ESI positive ion mass spectrum, with a peak observed at  $m/z = 982.2852$ , consistent with an [M+Na]<sup>+</sup> molecular ion of formula C<sub>44</sub>H<sub>46</sub>FN<sub>9</sub>O<sub>13</sub>S, and the ESI negative ion mass spectrum, where a peak was observed at  $m/z = 958.2845$ , consistent with an [M-H]<sup>-</sup> molecular ion of formula C<sub>44</sub>H<sub>45</sub>FN<sub>9</sub>NaO<sub>13</sub>S. A portion of the deprotected conjugate precipitates from the reaction mixture as a yellow solid; on analysis of the <sup>1</sup>H NMR spectrum, this appears to contain an equivalent of dioxane, even after it was subjected to drying under vacuum, suggesting it may be present trapped in the crystal lattice.



Scheme 4.39 HCl-mediated PMB removal to give target conjugate **4-32**. a) HCl, dioxane, 4.5 h, 33%.

The progress of the reaction was monitored by HPLC. No starting material remained after 21 minutes, with three main fractions eluting at retention times of 3.11, 5.33 and 7.51 minutes respectively, with an integration ratio of 3:5:2. The compound eluting at 3.11 minutes was later shown to be the fully-deprotected product **4-32**, while the other two compounds likely correspond to the mono- and di-protected products **4-64** and **4-65** (Figure 4.11), loss of the less hindered PMB group is suggested to occur first to form **4-64** from **4-65**, but there is no evidence to support this). Previous studies with a range of protecting groups and substrates have revealed selective deprotection of the *ortho*-hydroxy group of 1-carbonyl and carboxyl-substituted catechols is possible without deprotection of the *meta*-hydroxy group, hence the assignment of **4-64** and **4-65** as the two *meta*-protected isomers.<sup>633–636</sup> The compound eluting at 7.51 minutes is mostly lost after 61 minutes of reaction, although a small remnant is still visible while the peak at 5.33 minutes reduces in intensity more slowly over 4 hours.

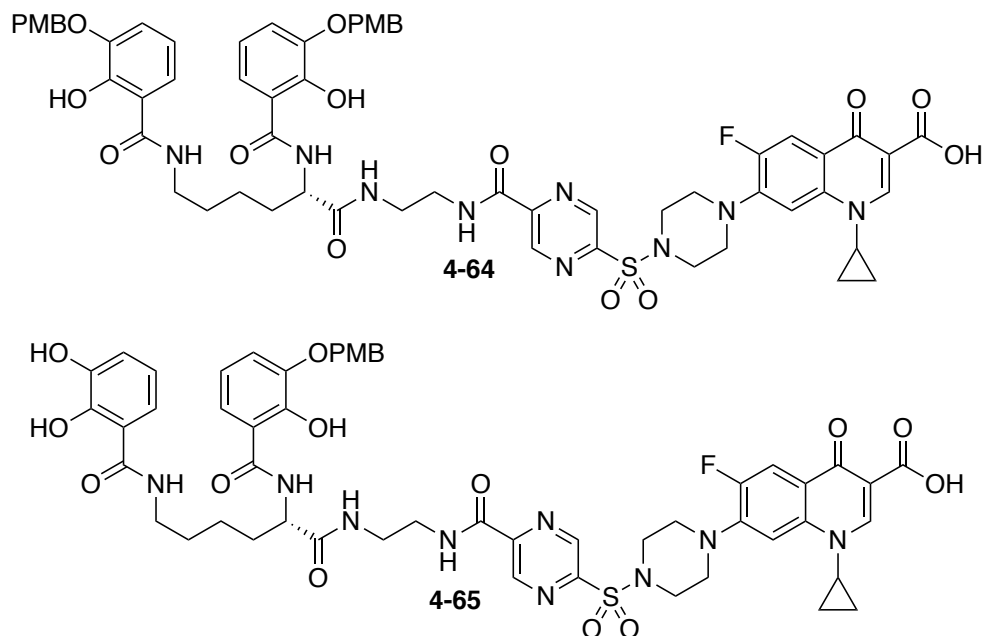


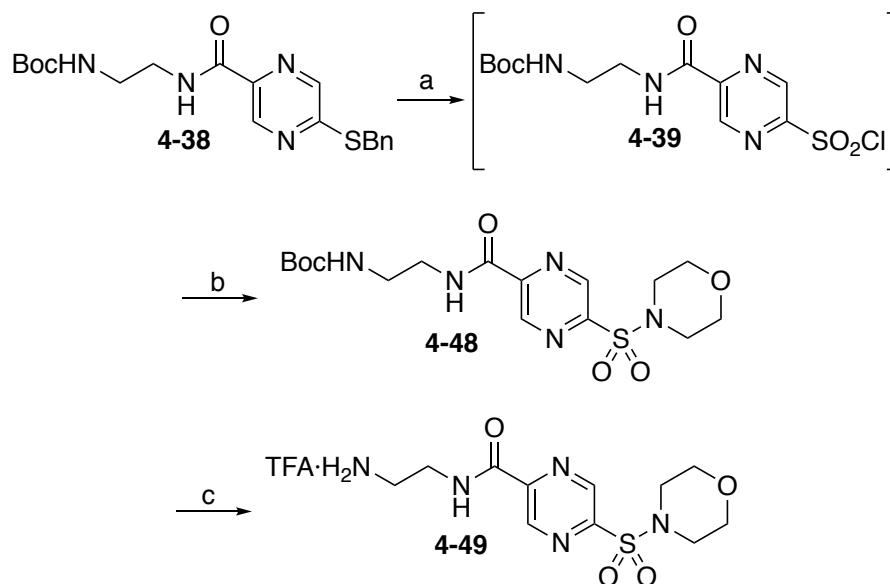
Figure 4.11 Structure of proposed intermediates in HCl-mediated deprotection of **4-63**.

The purity of **4-32** was assessed via quantitative  $^1\text{H}$  NMR spectroscopy in a similar manner to the conjugates described in Chapter 3. Maleic acid was again used as a quantitative NMR standard. Comparison of the integration between maleic acid, and proton resonances in the aromatic region of the  $^1\text{H}$  NMR spectrum of **4-32** suggested a purity of 81%. If the presence of an equivalent of dioxane in the product is factored into the calculations a purity of 89% is obtained. This was deemed of sufficiently purity for preliminary biological screening.

### 4.3.8 Synthesis of Control Compounds

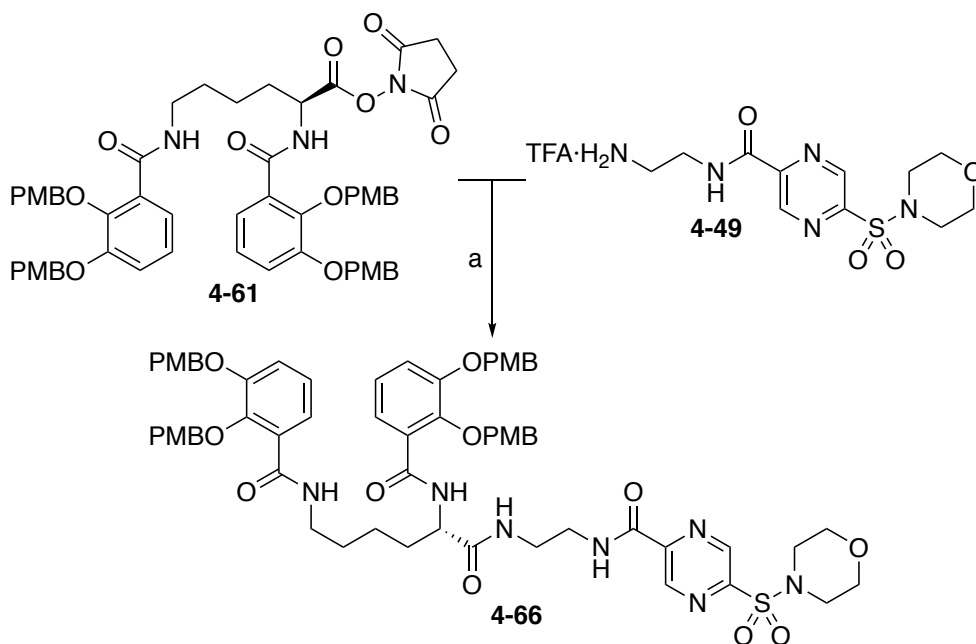
The first step towards the synthesis of Cipro –, Azoto + control **4-47** was the synthesis of morpholine-sulfonamide **4-48** via reaction of morpholine with sulfonyl chloride **4-39**, followed by purification to yield pure **4-48** (Scheme 4.40). Multiplets corresponding to the morpholine protons can be observed at 3.76 and 3.40 ppm in the  $^1\text{H}$  NMR spectrum, and the ESI mass spectrum displays peaks at  $m/z = 416.1601$  and  $438.1421$ , which can be assigned as  $[\text{M}+\text{H}]^+$  and  $[\text{M}+\text{Na}]^+$  peaks consistent with molecular formulae  $\text{C}_{16}\text{H}_{26}\text{N}_5\text{O}_6\text{S}$  and  $\text{C}_{16}\text{H}_{25}\text{N}_5\text{NaO}_6\text{S}$  respectively. **4-48** can then undergo TFA-mediated removal of the Boc group to yield TFA salt **4-49**. The  $^1\text{H}$  NMR spectrum in  $\text{DMSO-d}_6$  lacks the *tert*-butyl singlet at 1.35 ppm, indicating successful Boc

cleavage, while the ESI positive ion mass spectrum contains a peak at  $m/z = 316.1073$ , which can be assigned to an  $[M+H]^+$  molecular ion of formula  $C_{11}H_{18}N_5O_4S$ , consistent with the free amine of **4-49**. The ESI negative ion mass spectrum also contains a peak at  $m/z = 428.0864$ , which can be assigned to an  $[M-H]^-$  molecular ion of formula  $C_{13}H_{17}F_3N_5O_6S$ , consistent with the molecular formula of the desired TFA salt.



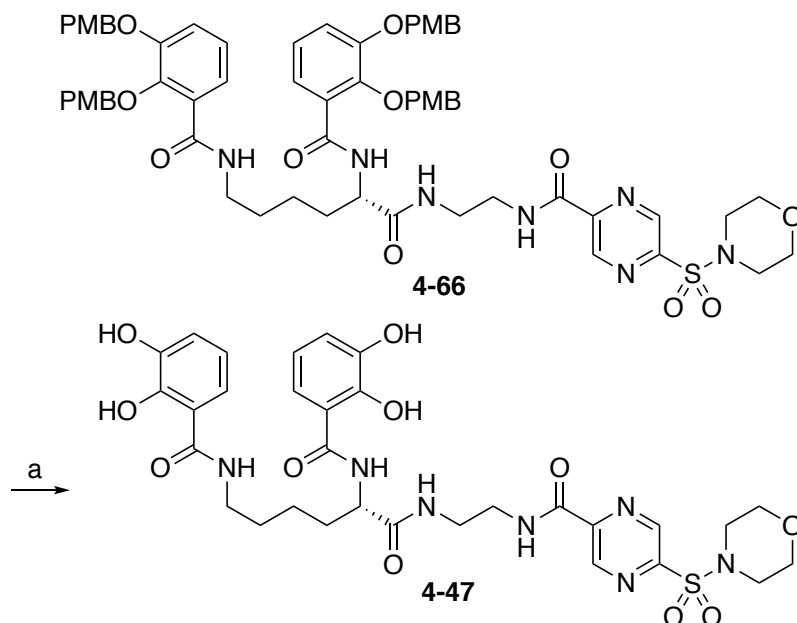
Scheme 4.40 Synthesis of morpholine-sulfonamide TFA salt **4-49**. a) 1,3-dichloro-5,5'-dimethylhydantoin, DCM/AcOH:H<sub>2</sub>O (biphasic), 0 to 20 °C, 15 h; b) morpholine, Et<sub>3</sub>N, DCM, 0 °C to rt, 18 h, 40% over two steps; c) TFA (10% v/v), DCM, 0 °C, 5 h, 68%.

TFA salt **4-49** undergoes reaction with NHS ester **4-61** in a similar fashion to ciprofloxacin-sulfonamide **4-62** to yield conjugate **4-66** (Scheme 4.41). The formation of the new amide bond can be seen from the observed presence of a new amide proton resonance at 6.88 ppm in the <sup>1</sup>H NMR spectrum, and a resonance at 172.8 ppm in the <sup>13</sup>C NMR spectrum, consistent with an amide C=O. The ESI mass spectrum also contains a peak at  $m/z = 1218.4517$ , consistent with an  $[M+Na]^+$  molecular ion of formula  $C_{63}H_{69}N_7NaO_{15}S$ .



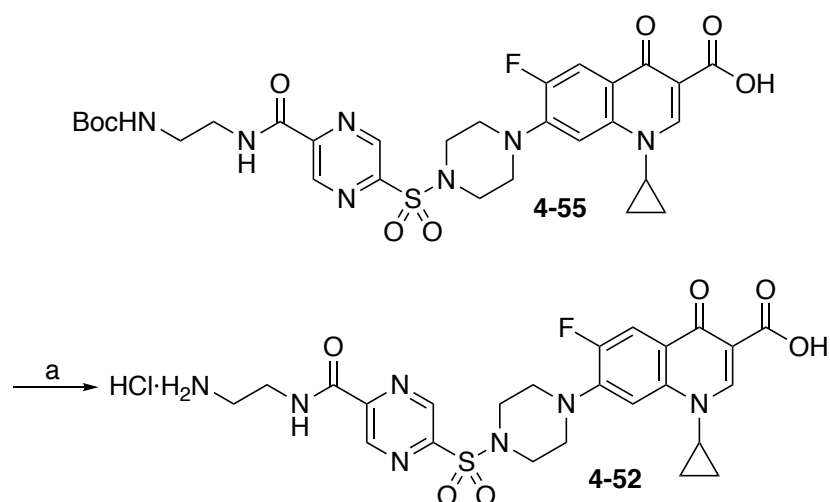
Scheme 4.41 Coupling of TFA salt **4-49** and NHS ester **4-61**. a) Et<sub>3</sub>N, DCM, 16 h, 87%.

Finally, **4-66** can be subjected to HCl-mediated removal of the PMB groups (**Scheme 4.42**). Purification of **4-47** was attempted by automated reverse-phase column chromatography, which resulted in removal of the main impurity present post-reaction (the 4-methoxybenzyl chloride formed as a byproduct of the deprotection), however some minor impurities remained post-column. The purity of the product was considered sufficient (estimated 89% by HPLC) for preliminary biological studies. Successful formation of **4-47** is supported by the absence of the PMB aromatic resonances between 7.44 and 6.74 ppm, the PMB CH<sub>2</sub> singlets between 5.14 and 4.95 ppm and the PMB methyl groups between 3.83 and 3.73 ppm in the <sup>1</sup>H NMR spectrum. Formation of **4-47** is further supported by the presence of a peak observed at  $m/z = 738.2161$  in the ESI positive ion mass spectrum, consistent with an [M+Na]<sup>+</sup> molecular ion of formula C<sub>31</sub>H<sub>37</sub>N<sub>7</sub>NaO<sub>11</sub>S, and a peak at  $m/z = 714.2192$  in the ESI negative ion mass spectrum, consistent with an [M-H]<sup>-</sup> molecular ion of formula C<sub>31</sub>H<sub>36</sub>N<sub>7</sub>O<sub>11</sub>S.



Scheme 4.42 Synthesis of Cipro –, Azoto + control **4-47**. a) HCl, dioxane, 26 h, 36%.

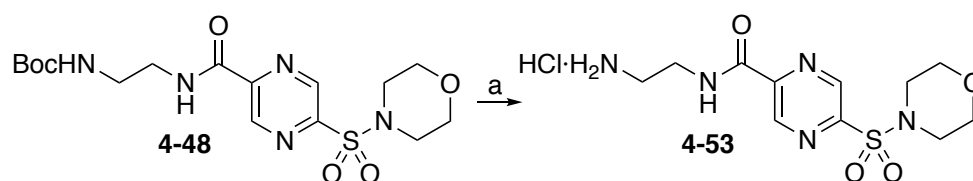
Cipro +, Azoto – control **4-52** can be synthesised from pyrazine-sulfonamide **4-55** via HCl-mediated removal of the Boc group (**Scheme 4.43**). Successful formation of **4-52** can be confirmed by the loss of the *tert*-butyl group at 1.34 ppm in the  $^1\text{H}$  NMR spectrum, and the presence of a peak at  $m/z = 560.1717$  in the ESI mass spectrum, consistent with an  $[\text{M}+\text{Na}]^+$  molecular ion of formula  $\text{C}_{24}\text{H}_{27}\text{aFN}_7\text{O}_6\text{S}$ .



Scheme 4.43 Synthesis of Cipro +, Azoto – control **4-52**. a) HCl, DCM:dioxane (3:1), 0 °C to rt, 24 h, 60%.

Cipro –, Azoto – control **4-53** can be synthesised from morpholine-sulfonamide **4-48** in a similar fashion (**Scheme 4.44**). Again, successful removal of the Boc group can be observed by the loss of the *tert*-butyl singlet

at 1.35 ppm in the  $^1\text{H}$  NMR spectrum, and via the presence of a peak observed at  $m/z = 316.1061$  in the ESI mass spectrum, consistent with an  $[\text{M}+\text{Na}]^+$  molecular ion for the deprotected amine, with a formula of  $\text{C}_{11}\text{H}_{18}\text{N}_5\text{O}_4\text{S}$ .



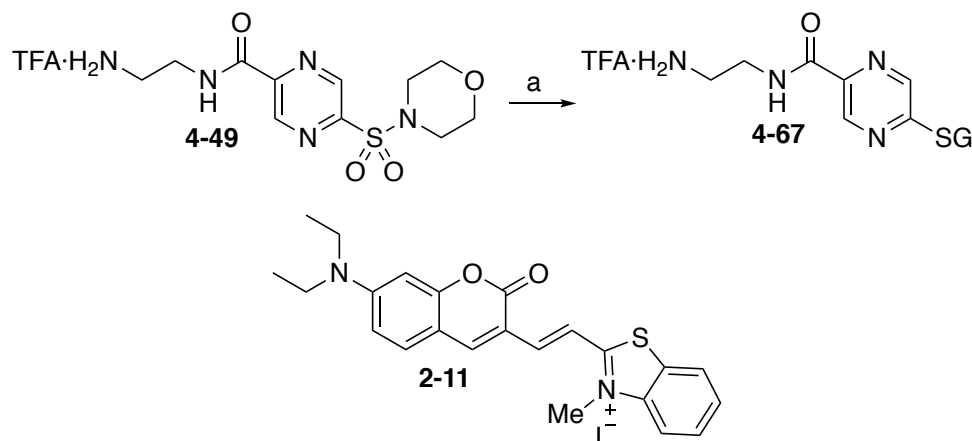
Scheme 4.44 Synthesis of Cipro-, Azoto- control **4-53**. a) HCl, EtOH, rt, 48 h, 61%.

The purities of control compounds **4-52** and **4-53** were assessed by quantitative  $^1\text{H}$  NMR spectroscopy. In both cases, small additional pyrazine resonances are evident on the shoulder of the old resonances. For **4-52** a new resonance appears at 9.33 ppm next to the original resonance at 9.34 ppm, and for **4-53** a new resonance appears at 9.36 ppm, with the original resonance at 9.37 ppm. This potentially indicates partial counterion exchange between maleic acid and HCl. Including both sets of peaks in the quantitative analysis gives an estimated purity of 98% for **4-53**; all other resonances corresponding to **4-53** overlap with the H<sub>2</sub>O resonance present in the DMSO-d<sub>6</sub>, so cannot be used for comparison. Applying a similar approach to **4-52** gives an average estimated purity of 96% from the integrations of the aromatic protons, and 98% from the two cyclopropane CH<sub>2</sub> groups; overlap with H<sub>2</sub>O and problems with the spectral baseline prevented comparison with any other resonances.

#### 4.4 SO<sub>2</sub> Release Studies

As the pyrazine-sulfonamides synthesised represent a novel set of compounds, evaluation of whether they are capable of undergoing reaction with biological thiols to release SO<sub>2</sub> is vital for determining their potential as biolabile linkers. Pyrazine-sulfonamide TFA salt **4-49** was initially selected for studying SO<sub>2</sub> release from the pyrazine-sulfonamide linker due to its high aqueous solubility. Initial qualitative studies of SO<sub>2</sub> release from **4-49** were carried out in the presence of SO<sub>2</sub>-detecting dye **2-21** and glutathione in 10% DMSO:HEPES buffer (Scheme 4.45). This demonstrated a high rate of

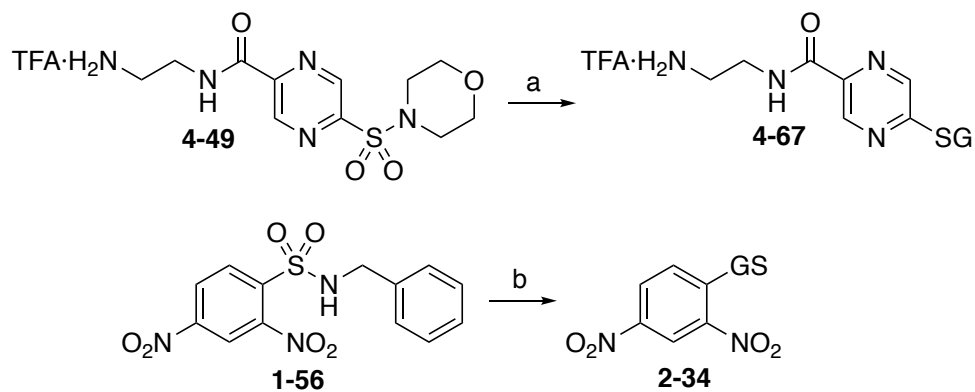
release, with the dye absorbance band at 540 nm decreasing to zero absorbance over 10 minutes.



Scheme 4.45 Reaction of **4-49** with glutathione in the presence of  $\text{SO}_2$ -detecting dye **2-11**. a) GSH (10 eq.), **2-11** (0.1 eq.), 10% DMSO/HEPES buffer, pH 7.4, rt, 30 min.

The rate of  $\text{SO}_2$  release from **4-49** proved too rapid to monitor via HPLC studies, with the starting material consumed after 17 minutes of reaction at 37 °C. Therefore, the rate of reaction was instead examined via UV-vis spectroscopy (**Scheme 4.46**). On reaction with GSH, a new UV-vis band emerges with a maximum at 329 nm, likely due to the pyrazine-glutathione conjugate **4-67**. Plotting the absorbance at 329 nm over time allows the rate of formation of the glutathione conjugate, and hence the rate of  $\text{SO}_2$  release, to be examined. Pyrazine-sulfonamide **4-49** displays a rapid rate of release, reaching a plateau in around 25 minutes (**Figure 4.12**). This is faster than the previously-studied 2,4-dinitrobenzenesulfonamide conjugates, for example benzylamine conjugate **1-56**, which take around 2 hours to reach a plateau. **4-49** appears to remain stable in HEPES buffer in the absence of glutathione; no increase in absorbance is observed at 329 nm over a period of 6.5 hours, indicating glutathione is required for the  $\text{SO}_2$  release reaction to take place. A similar rate of release is seen in experiments with ciprofloxacin conjugate TFA salt **4-62**.





Scheme 4.46 Reaction of **4-49** and **1-56** with glutathione in HEPES buffer. a) GSH (10 eq.), 10% DMSO/HEPES, pH 7.4, rt, 60 min; b) GSH (10 eq.), 10% MeCN/HEPES, pH 7.4, rt, 12 h.

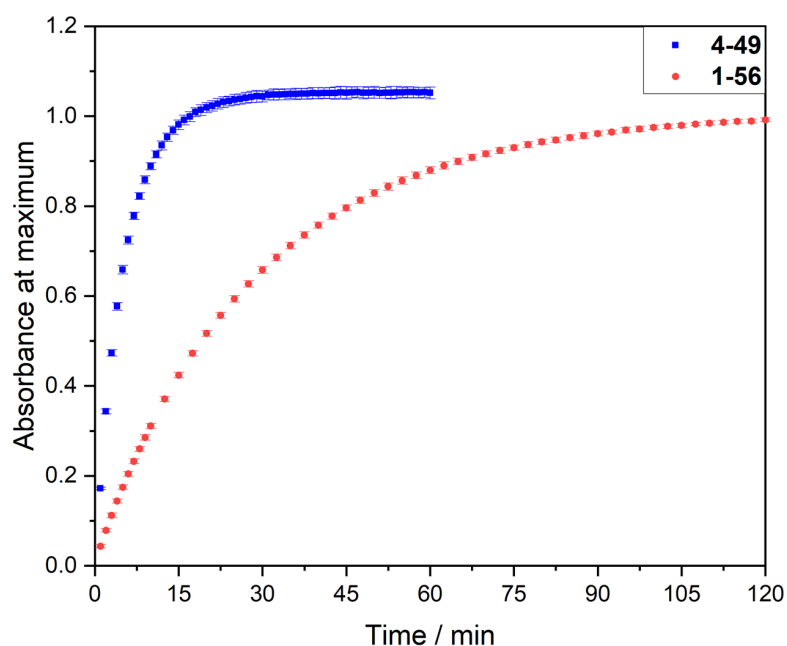
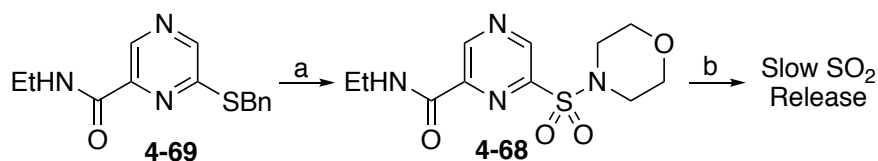


Figure 4.12 Plot of absorbance vs. time for pyrazine-sulfonamide **4-49** and 2,4-dinitrobenzenesulfonamide **1-56** at their respective absorbance maximum (329 and 340 nm) on reaction with glutathione (10 eq.) at pH 7.40.

The synthesis and evaluation of SO<sub>2</sub> release from other diazine sulfonamides was also considered. Different diazine structures may offer varying release profiles, giving a range of potential linkers that could be tailored towards a desired release profile. A morpholine-sulfonamide **4-68** based on a 2-carboxyl-6-sulfonamidopyrazine structure was successfully synthesised from thioether **4-69**, which had previously been synthesised by Luke Stirland (Scheme 4.47). Interestingly, when subjected to identical SO<sub>2</sub> release conditions to previous morpholine-sulfonamides, no change in the UV-vis spectrum was observed. Experiments with SO<sub>2</sub>-detecting dye **2-11** displayed

a 9% decrease in dye absorbance at 535 nm over 150 minutes, indicating very slow SO<sub>2</sub> release. This difference in SO<sub>2</sub> release rates between the two pyrazine isomers perhaps merits further investigation.



Scheme 4.47 Synthesis of morpholine sulfonamide **4-68** and subsequent SO<sub>2</sub> release. a) 1) 1,3-dichloro-5,5'-dimethylhydantoin, DCM/AcOH:H<sub>2</sub>O (biphasic), 0 to 20 °C, 14 h; 2) morpholine, Et<sub>3</sub>N, DCM, 0 °C to rt, 5.5 h, 59% over two steps; b) GSH (10 eq.), **2-11** (0.1 eq.), 10% DMSO/HEPES, pH 7.4, rt, 2.5 h.

#### 4.5 Conjugate Solubility and Stability

As with the conjugates examined in Chapter 3, the solubility of **4-32** and the associated microbiological controls was determined before undertaking biological studies. This determines what biological experiments can be carried out on **4-32** and the controls, in particular those carried out in liquid media. In addition, given the high glutathione reactivity observed for the pyrazine-sulfonamide linker, the stability of the compounds in aqueous media was also probed. If the biolabile linkers are unstable in liquid media, this could lead to premature extracellular release of the ciprofloxacin from **4-32** and **4-52** in biological studies, which has been observed in previous examples of Trojan Horse conjugates.<sup>187,194,210,262</sup> This would make it hard to determine if any observed antimicrobial activity stems from the conjugates, or from free ciprofloxacin released into the media and then taken up by bacteria.

Both **4-32**, and controls **4-52** and **4-53** display high solubility in DMSO (up to 10 mM); there was not sufficient stock of pure **4-47** to carry out solubility/stability testing. The solubility of **4-32**, and controls **4-52** and **4-53** was tested under identical conditions to the conjugates in Chapter 3, with two DMSO:MHII broth ratios relevant to biological studies employed (2% DMSO in MHII and 50% v/v DMSO in MHII). Solubility was again assessed visually, with a clear solution taken to indicate full solubility of the

compounds. The solubilities of the three compounds are displayed in **Table 4.2**.

Compound	Solubility (2% DMSO in MHII)	Solubility (50% DMSO in MHII)
<b>4-32</b>	10 to 20 $\mu$ M	100 to 250 $\mu$ M
<b>4-52</b>	50 to 75 $\mu$ M	150 to 200 $\mu$ M
<b>4-53</b>	> 100 $\mu$ M	ND

Table 4.2 Solubilities observed for **4-32**, **4-52**, and **4-53** in 2% DMSO in MHII and 50% DMSO in MHII. ND = not determined.

The solubility results indicate that the hydrophilic pyrazine-sulfonamide linker is unable to balance out the hydrophobicity of the azotochelin siderophore and the ciprofloxacin on its own, as might have been hoped. This should be taken into account for the design of any future conjugates.

The stability of conjugate **4-32**, and the Cipro +, Azoto – control **4-52** in MHII media were assessed by analytical HPLC studies. A number of components in the MHII media absorb at 254 nm, so the use of the two conjugates with the strongly UV-absorbing ciprofloxacin unit was considered to give the best visibility of the compounds. The use of the ciprofloxacin conjugates also allows the amount of free ciprofloxacin released, if any, to be determined, which is not possible with the morpholine released from the Cipro –, Azoto – control **4-53**. Selected concentrations of **4-32** and **4-52** were incubated at 37 °C in DMSO:MHII media, with 500  $\mu$ M caffeine added as an internal standard. The ratio of HPLC peak integrations between the caffeine peak and the peaks for **4-32**, **4-52** or ciprofloxacin was used to determine their concentrations in the stability studies from plotted calibration curves.

Cipro +, Azoto – control **4-52** was examined over 23 hours at a concentration of 50  $\mu$ M in 2% DMSO:MHII, with aliquots taken from the reaction mixture over four hours, then a final aliquot after heating overnight. At the first HPLC time point (c. 5 minutes after addition of **4-52**), the detectable concentration of **4-52** has already dropped to 40  $\mu$ M, dropping further to 20  $\mu$ M after around 4 hours, and around 5  $\mu$ M overnight. While this could indicate

decomposition of **4-52**, the concentration of ciprofloxacin in the media does not increase at the same rate, with around 5  $\mu\text{M}$  formed by the end of the reaction (**Figure 4.13**). This indicates instead that **4-52** might be precipitating from solution over time. The solubility of ciprofloxacin was also examined in a similar assay to determine if ciprofloxacin could be being released, then precipitating from the reaction mixture. This proved not to be the case, with incubation of 20  $\mu\text{M}$  ciprofloxacin in 2% DMSO:MHII at 37  $^{\circ}\text{C}$  displaying no loss of analyte over the same time period (**Figure 4.14**).

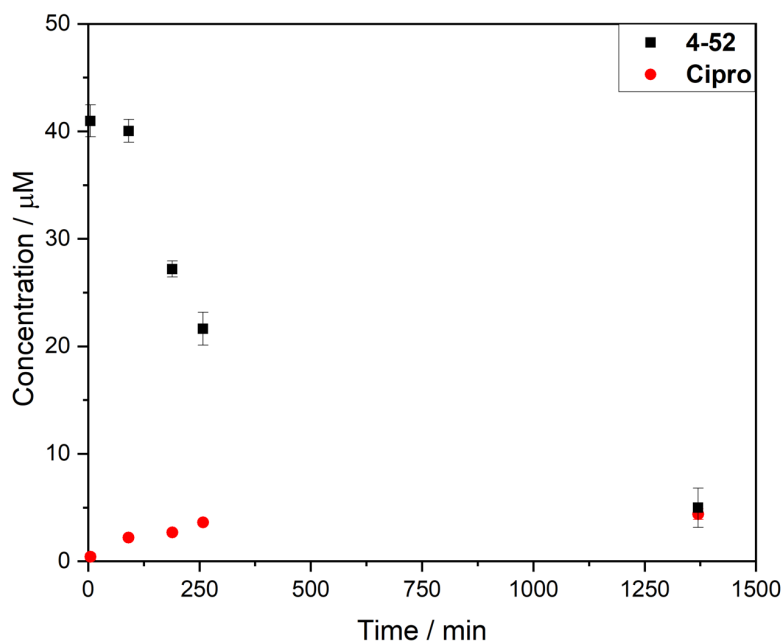


Figure 4.13 Stability and solubility of **4-52** in Mueller-Hinton II media over 23 hours at 37  $^{\circ}\text{C}$  as determined by HPLC analysis.

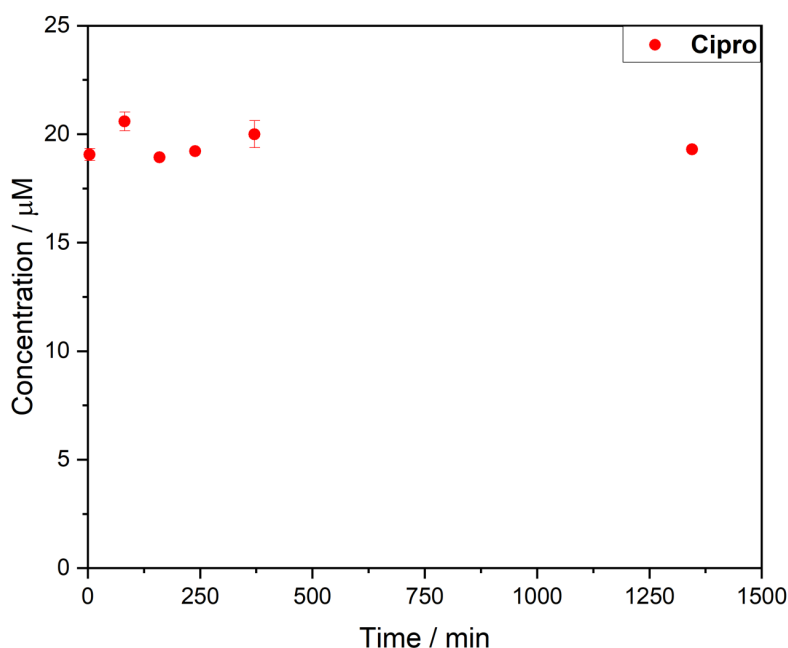


Figure 4.14 Solubility of ciprofloxacin in Mueller-Hinton II media over 23 hours at 37  $^{\circ}\text{C}$  as determined by HPLC analysis.

Poorer solubility is observed for conjugate **4-32**, which was tested at 10  $\mu\text{M}$  in 2% DMSO:MHII over 27 hours. At the first HPLC time point (ca. 9 minutes after addition of **4-32**), the concentration of **4-32** visible by HPLC was 0.1  $\mu\text{M}$ , 100x lower than the solubility observed in the basic solubility tests. This rises to around 1  $\mu\text{M}$  over six hours, but drops back to a negligible amount overnight. Again, formation of ciprofloxacin is observed, with the concentration increasing slowly over the first six hours, but reaching 7  $\mu\text{M}$  by the end of the reaction (**Figure 4.15**).

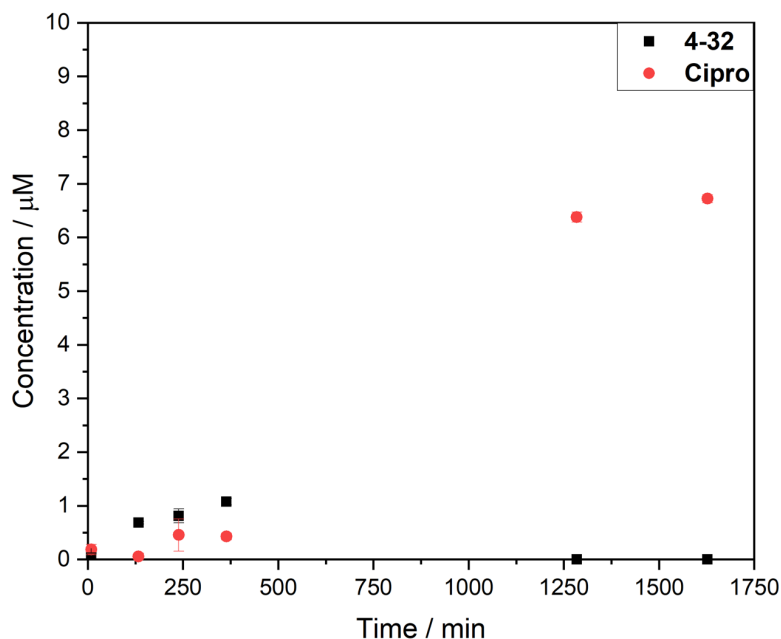


Figure 4.15 Stability and solubility of **4-32** in Mueller-Hinton II media over 27 hours at 37  $^{\circ}\text{C}$  as determined by HPLC analysis.

The formation of ciprofloxacin in both stability tests indicates some breakdown of the conjugates in MHII media. Given the presence of protein hydrolysates in MHII, it is likely to contain a quantity of thiols in the form of cysteine, so some reactivity of **4-32** and **4-52** may not be surprising given their fast breakdown on reaction with glutathione. However, to ensure the pyrazine-sulfonamides were fully stable in aqueous media, Cipro +, Azoto – control **4-52** and morpholine TFA salt **4-49** were also subjected to HPLC stability tests in aqueous HEPES buffer (pH 7.4). In both cases, 50  $\mu\text{M}$  of the compounds was incubated in 5% DMSO:HEPES buffer overnight at 37  $^{\circ}\text{C}$ . The concentration of **4-49** remains close to 50  $\mu\text{M}$  over 24 hours, indicating no solubility issues or decomposition (**Figure 4.16**). For **4-52**, a faster

concentration drop-off to that in MHII is observed, with 43  $\mu\text{M}$  present after 5 minutes, falling to 7  $\mu\text{M}$  after 83 minutes, and 5  $\mu\text{M}$  overnight. There is no significant increase in the amount of ciprofloxacin observed in the reaction, which remains around 0.5  $\mu\text{M}$  throughout, indicating no decomposition with associated ciprofloxacin release of **4-52** in HEPES buffer (**Figure 4.17**).

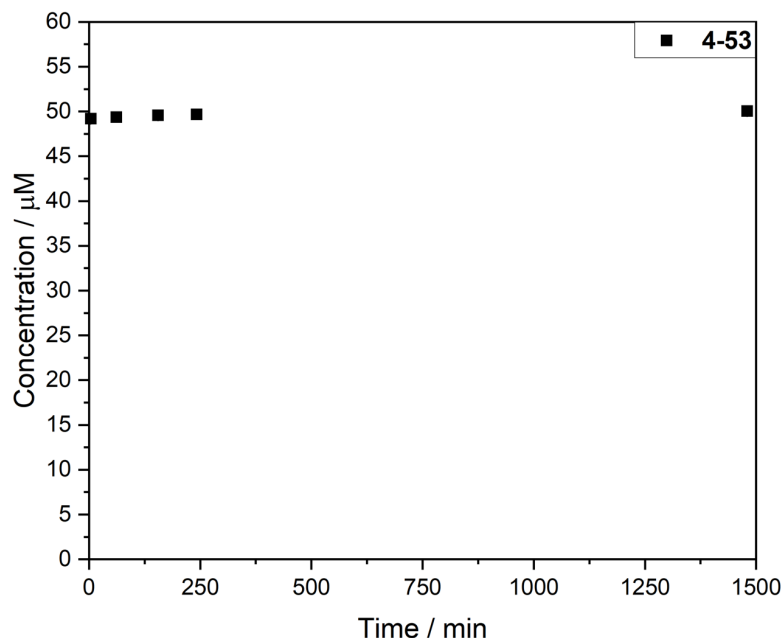


Figure 4.16 Stability of **4-49** in aqueous HEPES buffer (pH 7.4) over 24 hours at 37 °C as determined by HPLC analysis.

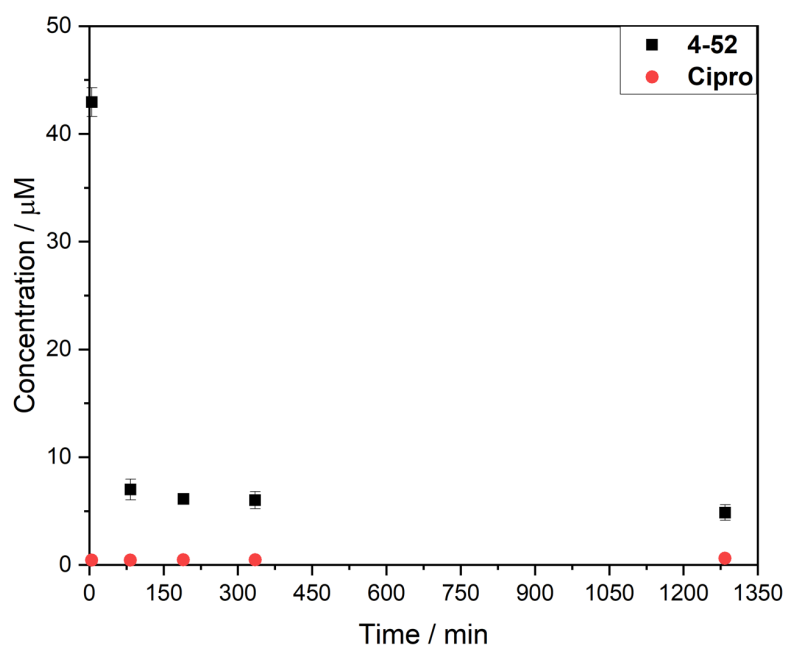


Figure 4.17 Stability of **4-52** in aqueous HEPES buffer (pH 7.4) over 22 hours at 37 °C as determined by HPLC analysis.

The addition of DMSO to the aliquots taken from the reaction mixture did not increase the concentration of **4-52** present in the HPLC traces; this could

indicate loss of the HCl counterion in solution, and formation of the free amine of **4-52**, which other experiments have shown to be insoluble even in 100% DMSO. It could also indicate aggregation of the molecules in solution via e.g. pi-pi stacking between ciprofloxacin or azotochelin units in **4-32**, or ionic interactions between the carboxylic acid and amine present in **4-52**. The solutions containing **4-32** and **4-52** are cloudy when aliquots are removed, providing further evidence of the precipitation of the conjugates in the media examined. The role of caffeine in the precipitation can be ruled out; it appears to stay present at roughly the same intensity throughout the reaction. If it was involved in an aggregation process with **4-32** or **4-52**, loss of the caffeine peak would also be observed. Preliminary UV-vis solubility studies with **4-52** in the absence of caffeine also indicate a poor solubility in HEPES not apparent from the visual analysis carried out previously.

The stability studies of **4-32** and **4-52** indicate that carrying out solubility tests for these compounds by visual analysis is not a suitable method, given the low solubility observed in the HPLC experiments; a new method for evaluating this needs to be developed. The poor solubility also has implications for biological studies, as does the instability of the conjugates. Thiol-containing growth media like MHII broth should be avoided if at all possible to prevent premature decomposition of **4-32**; a possible alternative is a phosphate-based minimal media like M9, or MOPS minimal media. These issues both need to be taken into account for the design of any future conjugates of this type.

## **4.6 Biological Studies**

*All of the antimicrobial assays detailed in this section were carried out by Cerys Orritt and Dr Angela Oates at the Hull York Medical School.*

The antimicrobial activity of conjugate **4-32** and the microbiological controls were examined in an identical manner to the biological screening described in Chapter 3, with the same panel of bacterial species used to assess the spectrum of activity (**Table 4.3**).

Bacterial Strain Number	Species	Ciprofloxacin Sensitivity
AC2	<i>Acinetobacter baumannii</i>	Resistant
PS2	<i>Pseudomonas aeruginosa</i>	Ciprofloxacin susceptible with increased exposure
PS3	<i>Pseudomonas aeruginosa</i>	Sensitive
EC1	<i>Escherichia coli</i>	Sensitive
EC3	<i>Escherichia coli</i>	Resistant
CN1	<i>Staphylococcus epidermidis</i>	Sensitive
CN3	<i>Staphylococcus epidermidis</i>	Resistant
CN4	<i>Staphylococcus epidermidis</i>	Resistant
MR2	<i>Staphylococcus aureus</i>	Sensitive
MR3	<i>Staphylococcus aureus</i>	Resistant
KL3	<i>Klebsiella pneumoniae</i>	Sensitive
KL5	<i>Klebsiella pneumoniae</i>	Resistant

Table 4.3 Panel of bacterial species selected for antimicrobial testing.

Of the bacterial strains in this panel, *E. coli* and *K. pneumoniae* both produce the catechol siderophore enterobactin and its derivatives as their primary siderophores, so would likely be able to utilise the catechol azotochelin.<sup>105,165,637</sup> As discussed above, uptake of azotochelin in *P. aeruginosa* has also been demonstrated.<sup>612,613</sup> In addition, Möllman *et al.* demonstrated strain-dependent growth promotion in all three of these bacteria when treated with  $\beta$ -lactam conjugate **4-30**, indicating their ability to transport and utilise azotochelin derivatives as siderophores.<sup>608</sup> *A. baumannii* has been shown to possess receptors that facilitate the uptake of monocatechol-based Trojan Horse conjugates,<sup>638</sup> and similar bis(catechols) to azotochelin have been shown to form effective Trojan Horse conjugates.<sup>267,639</sup> *S. aureus* has shown the ability to utilise catechol siderophores like petrobactin, enterobactin, and 2,3-dihydroxybenzoic acid as xenosiderophores, although this uptake pathway does not seem to be vital for virulence (apart from in a murine heart model).<sup>389</sup> Catechol siderophore uptake is less well documented in *S. epidermidis*, although catecholamine drugs like noradrenaline or dopamine have been shown to



mediate growth promotion of some strains, possibly indicating the presence of a transport pathway for catechols.<sup>640,641</sup>

#### 4.6.1 Initial Screening on Agar Plates

Conjugate **4-32**, and the associated controls, were screened against the bacterial panel on Mueller-Hinton agar plates, with the compounds loaded to discs via stock solutions in DMSO at a concentration equivalent to 5 µg of ciprofloxacin. Following overnight incubation at 37 °C, the zone of inhibition surrounding the discs was measured, and the results displayed in **Table 4.4**. Zones of inhibition for ciprofloxacin are again displayed for comparison.

<b>Bacterial Strain Number</b>	<b>Cipro</b>	<b>4-32</b>	<b>4-47</b>	<b>4-52</b>	<b>4-53</b>
AC2 (R)	0	0	0	0	0
PS2 (I)	23.5	13.8	0	0	0
PS3 (S)	32.4	19.7	0	13.2	0
EC1 (S)	34.8	25.9	0	20.1	0
EC3 (R)	0	0	0	0	0
CN1 (S)	36.5	15.4	0	12.6	0
CN3 (R)	0	0	0	0	0
CN4 (R)	15.9	0	0	0	0
MR2 (S)	24.5	10.7	0	0	0
MR3 (R)	0	0	0	0	0
KL3 (S)	29.6	22.7	12.5	18.6	0
KL5 (R)	18.7	0	0	0	0

Table 4.4 Zones of inhibition (mm) for each compound against bacterial panel. R = ciprofloxacin-resistant, S = ciprofloxacin-sensitive, I = ciprofloxacin-susceptible with increased exposure (i.e. Less sensitive, but higher doses still effective).

Similar to DFO conjugate **3-14**, azotochelin conjugate **4-32** proved less active than ciprofloxacin against all of the strains examined, although it displays a wider activity profile than **3-14**, with additional activity vs. PS2 and MR2. Cipro –, Azoto + control **4-47** only displays activity vs. KL3; this could be an

erroneous result, or could indicate a role for azotochelin-induced iron limitation in activity vs. KL3 (similar to the DFO-mediated activity for Cipro –, DFO + control **3-31** against *S. epidermidis* strains in Chapter 3). In theory, the activity could also source from SO<sub>2</sub> release, but given the lack of activity of Cipro –, Azoto – control **4-53** against the full bacterial panel, this seems unlikely.

Some activity is observed for Cipro +, Azoto – control **4-52**; with a mass of 596 Da (560 for the free amine), uptake via porins like OmpF is possible,<sup>526–529</sup> and the primary amine may help mediate uptake in the Gram-negative strains.<sup>642</sup> In comparison to the Cipro +, DFO – control **3-34**, no activity for Cipro +, Azoto – control **4-52** is observed against MR2 (*S. aureus*). This could add further weight to the hypothesis that the hydrophobicity of Cipro +, DFO – control **3-34** contributes to its uptake in MR2, with Cipro +, Azoto – control **4-52** much more hydrophilic (clogP = –3.40 vs. 0.58 for **3-34**).<sup>445</sup>

It should also be noted that the results will be affected by the ability of the conjugates to diffuse through the agar, with higher molecular weight compounds likely to diffuse slower than lower molecular weight compounds,<sup>643</sup> and differences observed for antibiotics of different hydrophobicities.<sup>644</sup> These may account for some of the results observed. It is not known what role the poor aqueous solubility of **4-32** or the instability in MHII media will play in results obtained on agar plates; the loading of the compounds in DMSO may have helped to mitigate some of the solubility issues.

## 4.7 Summary and Conclusions

Prospective Trojan Horse conjugate **4-32**, containing a novel 5-carboxyl-2-pyrazinesulfonamide as a biolabile SO<sub>2</sub>-releasing linker, plus azotochelin as a siderophore unit and ciprofloxacin as an antimicrobial component has been successfully synthesised and characterised by <sup>1</sup>H/<sup>13</sup>C/<sup>19</sup>F NMR and ESI mass spectrometry, although full purification was not achieved. The synthetic route involves a novel method for the synthesis of pyrazine sulfonyl chlorides, although similar conditions have previously been

employed in the literature. In addition, three microbiological controls, **4-47**, **4-52** and **4-53**, have been synthesised and characterised (**Figure 4.18**).

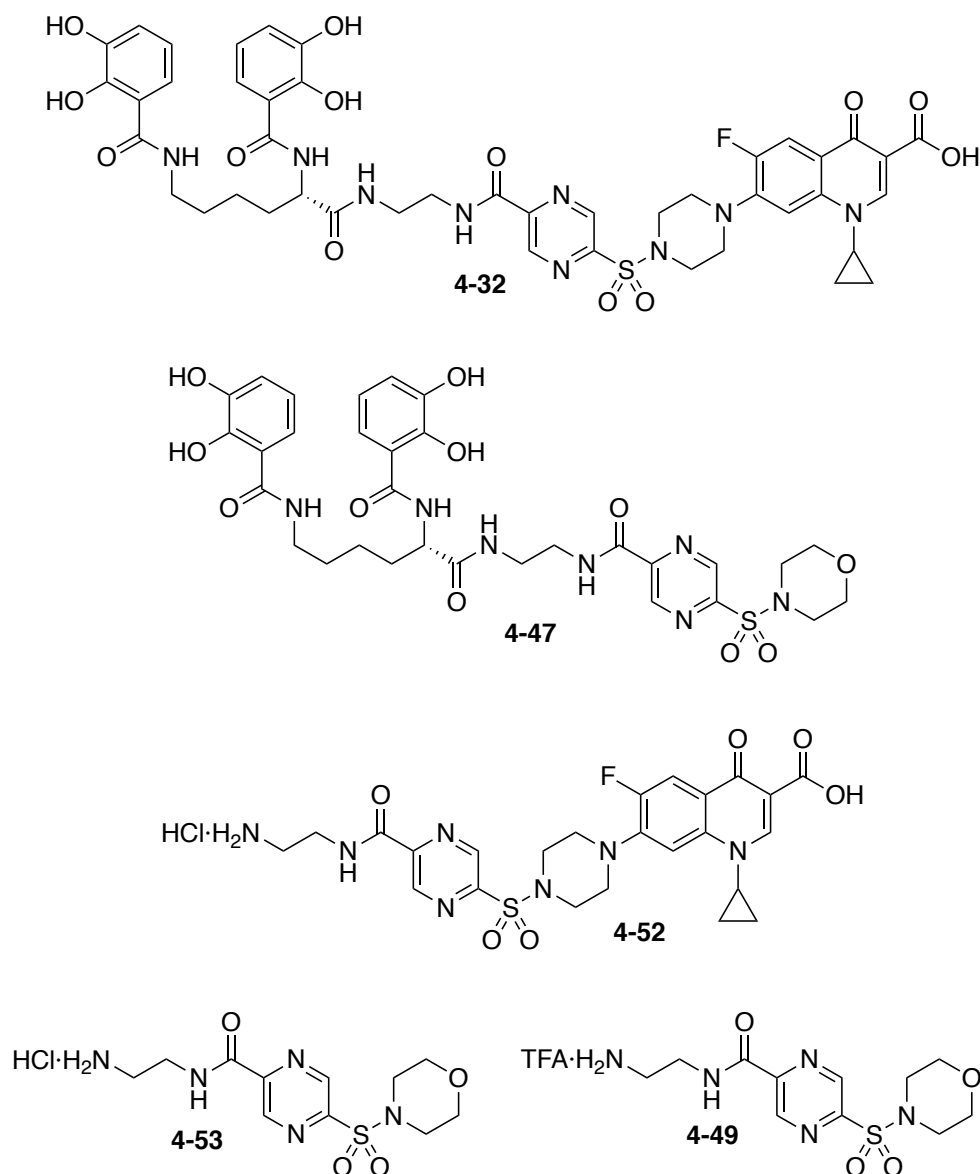


Figure 4.18 Structure of Trojan Horse conjugate **4-32** and related microbiological controls, plus TFA salt **4-49**.

SO<sub>2</sub> release experiments with TFA salt **4-49** demonstrated rapid release of SO<sub>2</sub> from the novel pyrazine linker of reaction with glutathione, with the reaction going to completion in around 25 minutes. A related 6-carboxyl-2-pyrazinesulfonamide **4-68** displayed much slower release of SO<sub>2</sub> on reaction with GSH. Azotochelin conjugate **4-32** and control **4-52** were found to be poorly soluble in aqueous media, while salts **4-49** and **4-53** display good solubility. In addition to their lack of solubility, **4-32** and **4-52** display instability in Mueller-Hinton broth, a common biological growth medium, with ciprofloxacin release observed on incubation at 37 °C; this is likely due

to reaction with cysteine residues or other nucleophiles present in the medium. **4-32** and **4-52** are also observed to be insoluble in MHII, with **4-52** in particular losing solubility over time (going from c. 40  $\mu$ M present at the start to 5  $\mu$ M at the end). This likely indicates aggregation and/or precipitation of **4-52** in solution over time.

The antimicrobial activity of **4-32** and the three controls were evaluated via agar-based culture methods, with screening against a panel of bacterial species in a Mueller-Hinton agar plate-based assay. **4-32** proved less active than ciprofloxacin in all cases. It is unclear whether conjugate **4-32** is stable on Mueller-Hinton agar; if it is, then given the fast release rates demonstrated for the biolabile linker, the lower activity of **4-32** compared to ciprofloxacin likely indicates a lack of uptake, or that ciprofloxacin modification/efflux occurs faster than uptake of **4-32**. Activity for Cipro +, Azoto – control **4-52** is observed for some strains, although this is reduced again compared to conjugate **4-32**. Cipro –, Azoto + control **4-47** only displays activity vs. *K. pneumoniae* KL3, which could indicate some role for azotochelin-mediated iron starvation of the bacteria, and Cipro –, Azoto – control **4-53** proved inactive vs. all bacterial strains.

Drawing overall conclusions about the efficacy of **4-32** as a Trojan Horse conjugate is hard, given its instability in MHII broth. However, conclusions can be drawn about some parts of the conjugate. The novel 5-carboxyl-2-pyrazinesulfonamide linker does display rapid release of SO<sub>2</sub> on reaction with glutathione as intended, with the electron-deficient environment of the pyrazine ring offering a favourable replacement for the previously-employed nitro-based sulfonamides. The sulfonamide linker appears to be stable in aqueous buffer at pH 7.4 in the absence of thiols. Unfortunately, the greater hydrophilicity of the pyrazine component is unable to balance out the poor solubility of the ciprofloxacin component in **4-52**, or both the ciprofloxacin and azotochelin components in **4-32**.

## 4.8 Future Work

Of the work discussed in this thesis, this area of research provides the greatest potential for further development. The pyrazine-based sulfonamide linker is only one of a wide range of heterocyclic structures that could be employed for the design of new biolabile linkers, and the area presents much scope for expansion.

Like with DFO conjugate **3-14**, further purification of conjugate **4-32** is required, with preparative HPLC a potential method to explore. The iron-binding ability of conjugate **4-32** and control **4-47** could also be examined, although the poor solubility of **4-32** prevented efforts to characterise its corresponding iron complex by native ESI mass spectrometry. The reactivity of the 5-carboxyl-2-pyrazinesulfonamide linker with other biological nucleophiles like lysine or serine should also be examined to determine whether the instability observed in MHII broth comes solely from reaction with any thiols present. Given the limited solubility that was observed in the HPLC experiments compared to the rudimentary solubility testing carried out, a better method of measuring the solubility of conjugates like **4-32** must be employed for any future studies, for example a method utilising HPLC or UV-vis measurements to gain a quantitative evaluation of solubility.<sup>645</sup>

Any future biological studies must move away from the use of MHII media, and towards the use of non-thiol containing alternatives, for example M9. Some of the trends observed in the current results may also merit investigation, especially if they can be replicated in different media. For example, the uptake of both azotochelin and conjugate **4-32** into the different strains in the agar panel could be probed; a number of methods exist in the literature for evaluation of uptake, including mutant studies, growth recovery assays and siderophore radiolabelling.<sup>163</sup>

To overcome the solubility problems observed for conjugate **4-32**, a more hydrophilic siderophore like DFO ( $\text{clogP} = -0.31$ ) or staphyloferrin A ( $\text{clogP} = -4.52$ ) could be employed.<sup>445</sup>

The synthesis and evaluation of other heterocyclic sulfonamide systems as SO<sub>2</sub>-releasing linkers also offers an intriguing avenue of research. Luke Stirland, an MChem student in the group, was tasked with synthesising a set of diazine sulfonamides/sulfonate esters containing a fluorescent coumarin dye. By examining the release rate of the coumarin dye via fluorimetry, the rates of SO<sub>2</sub> release from each of the desired conjugates could easily be compared.

Synthesis and evaluation of a 5-carboxypyrazine-2-sulfonate ester (**4-70**, **Figure 4.19**) was attempted as part of the studies described here. Interestingly, when subjected to a stability study in HEPES buffer, c. 50% decomposition of **4-70** is observed over three hours, with formation of both 7-hydroxycoumarin and a new species apparent in the HPLC. It is possible that released 7-hydroxycoumarin, which has a pKa of 7.5,<sup>646</sup> could act as a nucleophile to attack further sulfonate ester **4-70**, accelerating the decomposition. The use of 7-hydroxycoumarin in any future dye release studies is therefore discouraged.

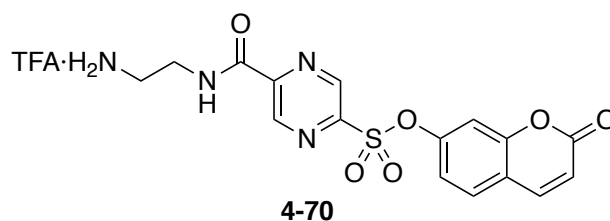
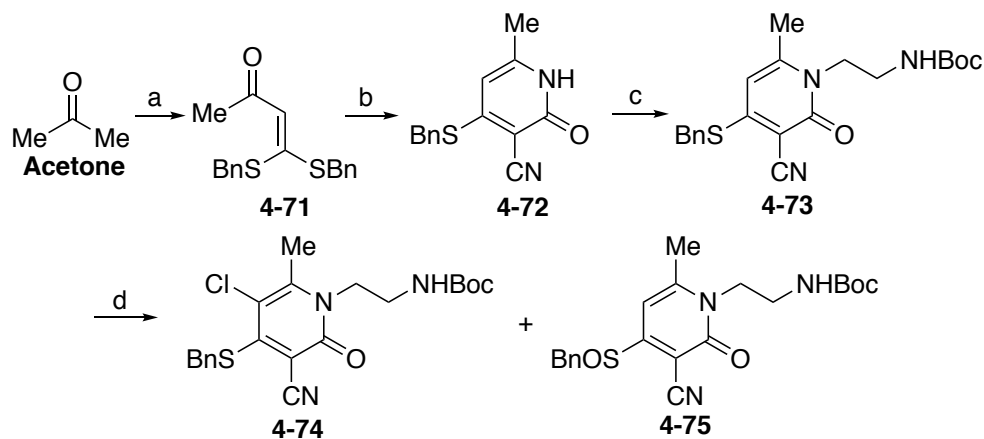


Figure 4.19 Structure of coumarin sulfonate ester **4-70**.

An attempt was also made at synthesising a linker based on a pyridone core, similar to those seen in **Scheme 4.7**. Briefly, coupling of ketone **4-71**, synthesised from reaction of acetone with CS<sub>2</sub> and BnBr, with cyanoacetamide yielded pyridone thioether **4-72**, with a Boc-protected amine linker installed on the pyridone nitrogen via reaction with *N*-Boc-2-bromoethylamine (**Scheme 4.48**). However, attempted formation of a sulfonyl chloride with DCDMH led to chlorination of the pyridone ring and/or oxidation of the thioether. Optimisation of these conditions was not attempted due to time constraints, but could provide a route to a further novel biolabile linker.



Scheme 4.48 Synthesis of pyridone thioether **4-73** and attempted oxidative chlorination reaction. a)  $\text{CS}_2$ ,  $t\text{BuOK}$ , THF,  $0\text{ }^\circ\text{C}$ , 1.5 h, then  $\text{BnBr}$ , 18 h, 58%; b) cyanoacetamide,  $t\text{BuOK}$ ,  $t\text{BuOH}$ ,  $80\text{ }^\circ\text{C}$ , 24 h, 52%; c) *N*-Boc-2-bromoethylamine,  $\text{K}_2\text{CO}_3$ , DMF, rt, 20 h, 50%; d) 1,3-dichloro-5,5'-dimethylhydantoin, DCM/AcOH:H<sub>2</sub>O (biphasic), 7 h,  $0\text{ }^\circ\text{C}$  to rt.

Conjugates containing other antimicrobial units could be synthesised and evaluated. The alternative antimicrobial units could take the form of more water-soluble fluoroquinolones like moxifloxacin, or other antibiotic classes, like the oxazolidinones. One of the advantages of using oxazolidinones in the development of Trojan Horse conjugates containing biolabile linkers is their lack of uptake and activity vs. many species of Gram-negative bacteria. If activity is observed for oxazolidinone conjugates, this indicates successful cytoplasmic uptake and/or release of the conjugates must be occurring.<sup>267</sup>

# **Chapter 5 : Experimental**



## 5.1 General Considerations

### 5.1.1 Materials

Unless otherwise stated, all chemicals and solvents were purchased from commercial sources and used without further purification. Dry DCM and THF were obtained from department solvent stills (Prosolv MD 7 solvent purification system) and stored over 4 Å activated molecular sieves. EtOH and acetone were dried using 4 Å activated molecular sieves, MeOH was dried using 3 Å molecular sieves. Dry DMF and DIPEA were purchased from Acros Organics.

When thiol-containing reagents were employed for synthesis, all contaminated equipment/disposables were placed in a covered bleach bath (1:1 mixture of bleach and H<sub>2</sub>O) overnight to ensure oxidation and neutralisation of any remaining thiols.

### 5.1.2 Instrumentation

Analytical TLC was used to monitor some reactions; it was performed on Merck Silica gel 60 F<sub>254</sub> aluminium-backed plates and observed under UV light at 254 nm or 365 nm. Column chromatography was performed with Sigma-Aldrich high-purity silica gel, pore size 60 Å, 220-440 mesh particle size, 35-75 µm particle size. Potassium permanganate, vanillin, ninhydrin, or iodine staining was used whenever no UV signal presented; the choice depended on the reaction reagents.

<sup>1</sup>H/<sup>13</sup>C/<sup>19</sup>F NMR and variable temperature <sup>1</sup>H NMR spectra were recorded on JeolECX or JeolECS 400 MHz spectrometers at 298K. Further NMR spectra were recorded on a Bruker AV 500 MHz or a Bruker AV 600 MHz by Thorsten Dreher, or a Bruker AVIII 300 MHz by Dr Charlotte Lee, Dr Phil Helliwell or Mrs Helen Burrell. Where necessary, NMR assignments were confirmed using DEPT 135, 2D HMQC (<sup>1</sup>H-<sup>13</sup>C single bond) and HMBC (<sup>1</sup>H-<sup>13</sup>C multiple bond) correlation experiments. NMR spectra analysis and presentation was carried out using MestReNova software.

FTIR spectra were recorded using a Perkin-Elmer FT-IR Spectrum Two spectrometer (ATIR).

High-resolution mass spectra were recorded on a Thermo-Finnigan LCQ Spectrometer or a Bruker microTOF by Mr Karl Heaton, Dr Rosaria Cercola or Mr Angelo Lopez.

Elemental analysis was carried out by Dr Graeme McAllister on an Exeter CE-440 elemental analyser.

UV-vis spectra were recorded on a Shimadzu UV-1800 Spectrophotometer using Starna Scientific quartz cuvettes (3/Q/10 or 21/Q/10, path lengths = 1 cm).

Uncorrected melting points were recorded using a Stuart Scientific SMP3 instrument.

### **5.1.3 HPLC/LCMS Analysis and Purification**

Analytical HPLC was performed on a Shimadzu HPLC system (Prominence) with a LC-20AD pump, SIL-20A autosampler, DGU-20AS degasser, CTO-20AC column oven, CBM-20A communication bus module and SPD-M20A diode array detector, or an Agilent 1100 Series HPLC system, with a G1311A QuatPump, G1313A ALS, G1316A ColCom and a G1322A Degasser.

Preparative HPLC was performed on a Varian ProStar HPLC system with two 210 series pumps (25 mL), a 325 series UV detector, a model 701 fraction collector and a model 410 autosampler using a SunFire Prep C18 column (10  $\mu\text{m}$ , 19 x 250 mm).

LCMS (analytical and preparative) was performed on a Waters LCMS, with a Water 3100 Mass Detector, Waters 996 Photodiode Array Detector, Waters 2525 Binary Gradient Module, Waters 515 HPLC Pump, Waters SFO (System Fluidics Organiser) and a Waters 2767 Sample Manager. Analytical runs were performed using a SunFire C<sub>18</sub> column (5  $\mu\text{m}$ , 4.6 x 150 mm), and Preparative

runs were performed using a SunFire Prep C18 column (10  $\mu\text{m}$ , 19 x 250 mm).

Preparative HPLC Method A:

(Varian ProStar HPLC)

Starting ratio is 40:60 MeCN + 0.1% Formic Acid (FA): H<sub>2</sub>O + 0.1% FA. Over 20 minutes the ratio is increased to 70:30 MeCN + FA: H<sub>2</sub>O + FA. The ratio was then reduced to 40:60 MeCN + FA: H<sub>2</sub>O + FA for 5 minutes to re-equilibrate the column. Flow rate 20 mL/minute.

Preparative LCMS Method A:

(Waters LCMS)

Starting ratio is 50:50 MeCN + 0.1% Formic Acid (FA): H<sub>2</sub>O + 0.1% FA. Over 20 minutes the ratio is increased to 68:32 MeCN + FA: H<sub>2</sub>O + FA. The ratio was then reduced to 50:50 MeCN + FA: H<sub>2</sub>O + FA for 5 minutes to re-equilibrate the column. Flow rate 20 mL/minute

Analytical HPLC Method A. Agilent HPLC, Eclipse XDB-C18 column (5  $\mu\text{m}$ , 4.6 x 150 mm). Oven temperature of 40 °C. Injection volume 20  $\mu\text{L}$ . Starting ratio of 30:70 MeCN + 0.1% FA: H<sub>2</sub>O + 0.1% FA. Over 12 minutes the ratio is increased to 70:30 MeCN + 0.1% FA: H<sub>2</sub>O + 0.1% FA. The ratio was then reduced to 30:70 MeCN + 0.1% FA: H<sub>2</sub>O + 0.1% FA for 5 minutes to re-equilibrate the column. Flow rate 1 mL/minute.

Analytical HPLC Method B. Shimadzu HPLC, Eclipse XDB-C18 column (5  $\mu\text{m}$ , 4.6 x 150 mm). Oven temperature of 40 °C. Injection volume 10  $\mu\text{L}$ . Starting ratio of 25:75 MeCN + 0.1% FA: H<sub>2</sub>O + 0.1% FA. Over 10 minutes the ratio is increased to 70:30 MeCN + 0.1% FA: H<sub>2</sub>O + 0.1% FA. The ratio was then reduced to 25:75 MeCN + 0.1% FA: H<sub>2</sub>O + 0.1% FA for 5 minutes to re-equilibrate the column. Flow rate 1 mL/minute.

Analytical HPLC Method C. Shimadzu HPLC, SunFire C<sub>18</sub> column (5  $\mu\text{m}$ , 4.6 x 150 mm). Oven temperature of 40 °C. Injection volume 20  $\mu\text{L}$ . Starting ratio of 10:90 MeCN: H<sub>2</sub>O + 0.1% FA. Over 10 minutes the ratio is increased to

75:25 MeCN: H<sub>2</sub>O + 0.1% FA. The ratio was then reduced to 10:90 MeCN: H<sub>2</sub>O + 0.1% FA for 5 minutes to re-equilibrate the column. Flow rate 1 mL/minute.

Analytical HPLC Method D. Shimadzu HPLC, SunFire C<sub>18</sub> column (5 μm, 4.6 x 150 mm). Oven temperature of 40 °C. Injection volume 25 μL. Starting ratio of 50:50 MeCN: H<sub>2</sub>O + 0.1% FA. Over 10 minutes the ratio is increased to 95:5 MeCN: H<sub>2</sub>O + 0.1% FA. The ratio was then reduced to 50:50 MeCN: H<sub>2</sub>O + 0.1% FA for 5 minutes to re-equilibrate the column. Flow rate 1 mL/minute.

Analytical HPLC Method E. Shimadzu HPLC, SunFire C<sub>18</sub> column (5 μm, 4.6 x 150 mm). Oven temperature of 40 °C. Injection volume 20 μL. Starting ratio of 5:95 MeCN: H<sub>2</sub>O + 0.1% FA. Over 10 minutes the ratio is increased to 75:25 MeCN: H<sub>2</sub>O + 0.1% FA. The ratio was then reduced to 5:95 MeCN: H<sub>2</sub>O + 0.1% FA for 5 minutes to re-equilibrate the column. Flow rate 1 mL/minute.

#### 5.1.4 Specific Glassware Setups

Reactions with BBr<sub>3</sub> were performed under constant flow of nitrogen in three-necked round bottomed flasks equipped with a condenser as shown below. One neck is used as a nitrogen inlet, with the flow routed to a gas washing bottle containing 1 M aqueous sodium hydroxide via the condenser to eliminate any acidic gases produced.

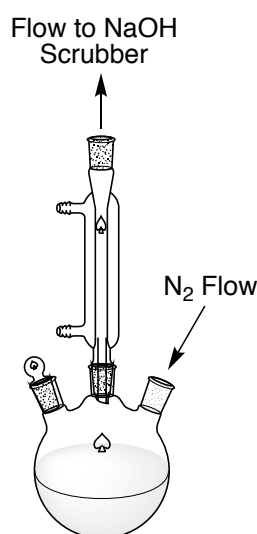
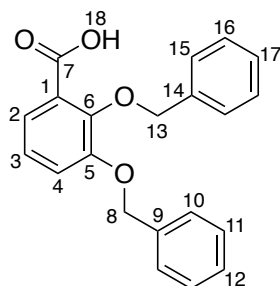


Figure 5.1 Glassware setup for reactions carried out with BBr<sub>3</sub>.

## 5.2 Synthesis

### 2,3-Bis(benzyloxy)benzoic acid (2-12)



Molecular Formula: C<sub>21</sub>H<sub>18</sub>O<sub>4</sub>

Molecular Mass: 334.37 g mol<sup>-1</sup>

Prepared according to a literature procedure adapted by Dr Ellis Wilde.<sup>647</sup>

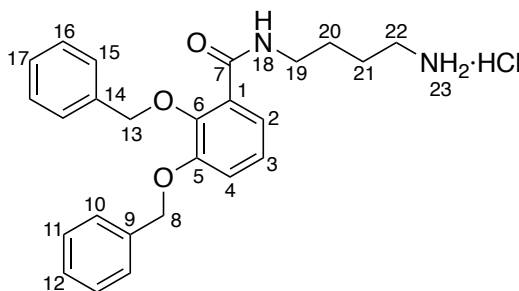
2,3-Dihydroxybenzaldehyde (3.00 g, 21.7 mmol) was dissolved in anhydrous EtOH (65 mL), then benzyl chloride (6.25 mL, 54.3 mmol) and potassium carbonate (7.51 g, 54.4 mmol) added. The resulting mixture was stirred at reflux for 24 hours under anhydrous conditions. The reaction was allowed to cool to room temperature, then cooled further in an ice bath. The solid formed was isolated via Buchner filtration and washed with water. This solid was dissolved in EtOAc (110 mL), and then washed with water (2 x 40 mL) and brine (2 x 40 mL). The organic layer was dried over MgSO<sub>4</sub> and the solvent removed under vacuum. The crude aldehyde obtained was dissolved in 5:4 acetone: H<sub>2</sub>O (65 mL). A solution of sulfamic acid (3.29 g, 33.9 mmol) in H<sub>2</sub>O was made up and a portion (5 mL) added to the aldehyde solution. Solid sodium chlorite (2.69 g, 29.8 mmol) and the remainder of the sulfamic acid solution were added alternately to the reaction mixture over 30 minutes, then the reaction was stirred for two hours in air. The acetone was removed *in vacuo*, and the resulting mixture was cooled in a fridge overnight, then the solid was isolated by Buchner filtration, washed with ice-cold H<sub>2</sub>O and recrystallised from hot EtOH to yield a white solid (4.90 g, 14.7 mmol, 68%). M.p. = 123-124 °C (lit. = 124-126 °C).<sup>648</sup>

Characterisation data consistent with literature.<sup>647</sup>

**<sup>1</sup>H NMR:** (400 MHz, DMSO-d<sub>6</sub>) δ<sub>H</sub> ppm: 12.87 (1H, br s, H18), 7.51-7.47 (2H, m, Ar H), 7.43-7.29 (9H, m, Ar H), 7.22 (1H, dd, J = 7.5, 1.5 Hz, H2 or 4), 7.15 (1H, t, J = 8.0 Hz, H3), 5.19 (2H, s, H8 or 13), 5.00 (2H, s, H8 or 13).

**HRMS (ESI):** Calcd. [M+Na]<sup>+</sup> (C<sub>21</sub>H<sub>18</sub>NaO<sub>4</sub>) m/z = 357.1097; Obs. [M+Na]<sup>+</sup> m/z = 357.1089, Mean err 2.0 ppm.

***N*-(4-Aminobutyl)-2,3-bis(benzyloxy)benzamide hydrochloride (2-13)**



Molecular Formula: C<sub>25</sub>H<sub>29</sub>ClN<sub>2</sub>O<sub>3</sub>

Molecular Mass: 440.97 g mol<sup>-1</sup>

Prepared according to a literature procedure.<sup>349,647</sup>

2,3-Bis(benzyloxy)benzoic acid (**2-12**, 0.554 g, 1.66 mmol) was placed under N<sub>2</sub> then dissolved in dry THF (10 mL). 1,1'-Carbonyldiimidazole (CDI, 0.556 g, 3.43 mmol) was added and the reaction stirred until any bubbling observed ceased. In a separate flask, 1,4-diaminobutane (0.42 mL, 4.18 mmol) was dissolved in dry THF (10 mL) with vigorous stirring. The benzoic acid solution was added dropwise over 75 minutes, and the reaction stirred at room temperature for 22 hours. The THF was then removed *in vacuo*, and the residue redissolved in CHCl<sub>3</sub> (30 mL). The organic layer was washed with saturated NaHCO<sub>3</sub> solution (15 mL), brine (15 mL), 1 M aq. HCl (20 mL) and brine (20 mL), dried over MgSO<sub>4</sub> and the solvent reduced to around 5 mL *in vacuo*. Addition of EtOAc (10 mL) failed to precipitate a solid, so the resulting viscous brown oil was recrystallised from 2:1 EtOAc:CHCl<sub>3</sub> to give a white solid, which was isolated by Buchner filtration and washed with EtOAc to obtain **2-13** (0.281 g, 0.636 mmol, 38%). M.p. = 131-133 °C (lit. = 137 °C).<sup>349</sup>

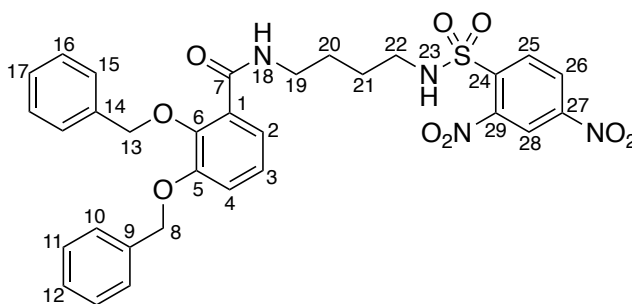
Characterisation data consistent with literature.<sup>647</sup>

**<sup>1</sup>H NMR:** (400 MHz, DMSO-d<sub>6</sub>) δ<sub>H</sub> ppm: 8.24 (1H, t, *J* = 6.0 Hz, *H*18), 7.73 (3H, br s, *H*23), 7.52-7.48 (2H, m, *Ar H*), 7.43-7.30 (8H, m, *Ar H*), 7.28 (1H, dd, *J* = 7.5, 2.0 Hz, *H*2 or 4), 7.14 (1H, t, *J* = 8.0 Hz, *H*3), 7.11 (1H, dd, *J* = 8.0, 2.0 Hz, *H*2 or 4)\*, 5.20 (2H, s, *H*8 or 13), 5.02 (2H, s, *H*8 or 13), 3.19 (2H, app. q, *J* = 6.0 Hz, *H*19), 2.73 (2H, t, *J* = 7.0 Hz, *H*22), 1.56-1.41 (4H, m, *H*20 and 21).

\*Overlapping with t at 7.14

**HRMS (ESI):** Calcd. [M+H]<sup>+</sup> (C<sub>25</sub>H<sub>29</sub>N<sub>2</sub>O<sub>3</sub>) *m/z* = 405.2173; Obs. [M+H]<sup>+</sup> *m/z* = 405.2180, Mean err -1.7 ppm. Calcd. [M+Na]<sup>+</sup> (C<sub>25</sub>H<sub>28</sub>N<sub>2</sub>NaO<sub>3</sub>) *m/z* = 427.1992; Obs. [M+Na]<sup>+</sup> *m/z* = 427.1997, Mean err -1.4 ppm.

**2,3-Bis(benzyloxy)-*N*-(4-(2,4-dinitrobenzenesulfonamido)butyl)benzamide (2-14)**



Molecular Formula: C<sub>31</sub>H<sub>30</sub>N<sub>4</sub>O<sub>9</sub>S

Molecular Mass: 634.66 g mol<sup>-1</sup>

2,4-Dinitrobenzenesulfonyl chloride (0.147 g, 0.549 mmol) was placed under N<sub>2</sub>, then dissolved in dry DCM (25 mL). The solution was cooled to 0 °C, then *N*-(2,3-Bis(benzyloxy)benzoyl)diaminobutane hydrochloride (**2-13**, 0.221 g, 0.500 mmol) and lutidine (0.25 mL, 2.15 mmol) added. The reaction was stirred at 0 °C for 5 hours, and then allowed to warm to room temperature overnight. After stirring for 28 hours, water (25 mL) was added and the organic layer separated. The aqueous layer was extracted with DCM (2 x 20 mL), then the combined organic layers were washed with 1 M aq. HCl (40 mL), water (40 mL) and brine (40 mL), dried over MgSO<sub>4</sub> and the DCM removed *in vacuo* to give a beige solid (0.312 g, 0.491 mmol, 98%). M.p. = 169-170 °C. R<sub>f</sub> = 0.17 (8:1 DCM:EtOAc).

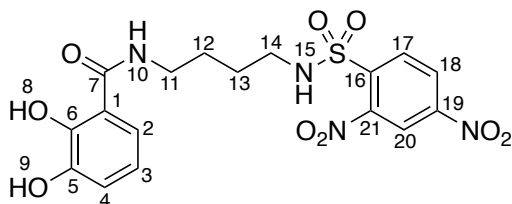
**<sup>1</sup>H NMR:** (400 MHz, DMSO-d<sub>6</sub>) δ<sub>H</sub> ppm: 8.89 (1H, d, *J* = 2.5 Hz, *H*<sub>28</sub>), 8.62 (1H, dd, *J* = 9.0, 2.5 Hz, *H*<sub>26</sub>), 8.48 (1H, t, *J* = 6.0 Hz, *H*<sub>23</sub>), 8.22 (1H, d, *J* = 9.0 Hz, *H*<sub>25</sub>), 8.16 (1H, t, *J* = 6.0 Hz, *H*<sub>18</sub>), 7.50-7.49 (2H, m, *Ar H*), 7.43-7.23 (9H, m, *Ar H*), 7.12 (1H, t, *J* = 8.0 Hz, *H*<sub>3</sub>), 7.08 (1H, dd, *J* = 7.5, 2.0 Hz, *H*<sub>4</sub>), 5.20 (2H, s, *H*<sub>8 or 13</sub>), 4.99 (2H, s, *H*<sub>8 or 13</sub>), 3.13 (2H, app. q, *J* = 6.5 Hz, *H*<sub>19</sub>), 2.90 (2H, app. q, *J* = 6.5 Hz, *H*<sub>22</sub>), 1.44-1.36 (4H, m, *H*<sub>20 and 21</sub>).

**<sup>13</sup>C NMR:** (100 MHz, DMSO-d<sub>6</sub>) δ<sub>C</sub> ppm: 165.6 (*C*<sub>7</sub>), 151.6 (*C*<sub>5</sub>), 149.6 (*C*<sub>27</sub>), 147.7 (*C*<sub>29</sub>), 145.1 (*C*<sub>6</sub>), 137.8 (*C*<sub>24</sub>), 137.1, 136.8 (*C*<sub>9 and 14</sub>), 131.2 (*C*<sub>25</sub>), 131.1 (*C*<sub>1</sub>), 128.5, 128.3, 128.2, 128.0, 127.8 (*C*<sub>10-12 and 15-17</sub>), 127.3 (*C*<sub>26</sub>), 124.2 (*C*<sub>3</sub>), 120.7 (*C*<sub>4</sub>), 120.1 (*C*<sub>28</sub>), 115.8 (*C*<sub>2</sub>), 75.1, 70.2 (*C*<sub>8 and 13</sub>), 42.5 (*C*<sub>22</sub>), 38.3 (*C*<sub>19</sub>), 26.6, 26.1 (*C*<sub>20 and 21</sub>).

**HRMS (ESI):** Calcd. [M+H]<sup>+</sup> (C<sub>31</sub>H<sub>31</sub>N<sub>4</sub>O<sub>9</sub>S) *m/z* = 635.1806; Obs. [M+H]<sup>+</sup> *m/z* = 635.1824, Mean err -2.2 ppm. Calcd. [M+Na]<sup>+</sup> (C<sub>31</sub>H<sub>31</sub>N<sub>4</sub>NaO<sub>9</sub>S) *m/z* = 657.1626; Obs. [M+Na]<sup>+</sup> *m/z* = 657.1642, Mean err -2.5 ppm.

**IR (ATIR, cm<sup>-1</sup>):** 3375 (amide NH stretch, m), 3159 (sulfonamide NH stretch, m), 3130-2870 (C-H stretching, w), 1633 (C=O stretch, s), 1573 (N=O/C=C stretches, m), 1554 (N=O/C=C stretches, s), 1538 (N=O/C=C stretches, s), 1348 (S=O/N=O stretch, s), 1165 (S=O stretch, s).

***N*-(4-((2,4-Dinitrophenyl)sulfonamido)butyl)-2,3-dihydroxybenzamide  
(2-9)**



Molecular Formula: C<sub>17</sub>H<sub>18</sub>N<sub>4</sub>O<sub>9</sub>S

Molecular Mass: 454.41 g mol<sup>-1</sup>

**2-14** (0.200 g, 0.315 mmol) was placed in a 3-necked RBF, then the flask purged with N<sub>2</sub>, and dry DCM (7.5 mL) added. Boron tribromide (1 M in DCM, 0.79 mL, 0.790 mmol) was added dropwise and the reaction stirred under



flow of N<sub>2</sub> at room temperature for 7 hours. Wet methanol (25 mL) was added to quench any remaining BBr<sub>3</sub>, then the solvent removed *in vacuo*. MeOH (3 x 15 mL) was added and removed under vacuum to try and remove volatile borate salts, giving an orange-brown solid. The crude product was purified by preparative HPLC chromatography using Prep. HPLC Method A to give **2-9** as a yellow solid (63.4 mg, 0.140 mmol, 40%). M.p. = 133-134 °C.

**<sup>1</sup>H NMR:** (400 MHz, MeCN-d<sub>3</sub>) δ<sub>H</sub> ppm: 12.99 (1H, s, H8), 8.59 (1H, d, J = 2.0 Hz, H20), 8.48 (1H, dd, J = 8.5, 2.0 Hz, H18), 8.24 (1H, d, J = 8.5 Hz, H17), 7.39-7.25 (1H, m, H10 or 15), 7.03 (1H, dd, J = 8.0, 1.0 Hz, H2), 6.96 (1H, dd, J = 8.0, 1.0 Hz, H4), 6.73 (1H, app. t, J = 8.0 Hz, H3), 6.55 (1H, br s, H9), 6.19 (1H, br t, J = 6.0 Hz, H10 or 15), 3.31 (2H, app. q, J = 6.0 Hz, H14), 3.13 (2H, app. q, J = 6.0 Hz, H11), 1.61-1.49 (4H, m, H12 and 13).

**<sup>13</sup>C NMR:** (100 MHz, MeCN-d<sub>3</sub>) δ<sub>C</sub> ppm: 171.2 (C7), 151.0 (C19), 150.5 (C6), 148.9 (C21), 146.8 (C5), 139.4 (C16), 133.1 (C17), 128.1 (C18), 121.3 (C20), 119.2, 119.1 (C3 and 4), 117.6 (C2), 115.2 (C1), 44.0 (C14), 39.3 (C11), 27.5, 26.9 (C12 and 13).

**HRMS (ESI):** Calcd. [M+H]<sup>+</sup> (C<sub>17</sub>H<sub>19</sub>N<sub>4</sub>O<sub>9</sub>S) *m/z* = 455.0867; Obs. [M+H]<sup>+</sup> *m/z* = 455.0869, Mean err -3.4 ppm. Calcd. [M+Na]<sup>+</sup> (C<sub>17</sub>H<sub>18</sub>N<sub>4</sub>NaO<sub>9</sub>S) *m/z* = 477.0687; Obs. [M+Na]<sup>+</sup> *m/z* = 477.0680, Mean err 1.0 ppm.

**IR (ATIR, cm<sup>-1</sup>):** 3527 (OH stretch, w), 3444 (amide NH stretch, w), 3258 (OH stretch – H bonded, w br), 3104 (sulfonamide NH stretch, w), 3100-2850 (C-H stretching, w), 1641 (C=O stretch, m), 1599 (N=O/C=C stretches, m), 1532 (N=O/C=C stretches, s), 1346 (S=O stretch, s), 1333 (N=O stretch, s), 1164 (S=O stretch, s).

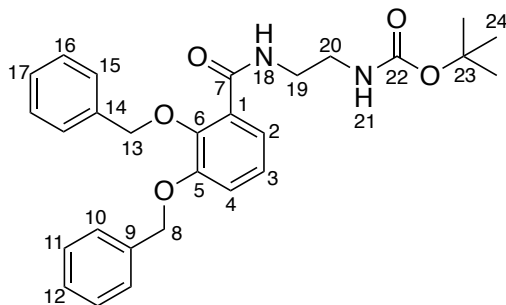
#### Elemental Analysis:

For [C<sub>17</sub>H<sub>18</sub>N<sub>4</sub>O<sub>9</sub>S · 0.29 H<sub>2</sub>O]:

*Calculated:* %C, 44.42; %H, 4.07; %N, 12.19.

*Measured:* %C, 44.58, %H, 4.05, %N, 12.03.

***N*-(*N'*-*tert*-Butyloxycarbonyl)ethane diamino)-2,3-bis(benzyloxy)benzamide (**2-16**)**



Molecular Formula: C<sub>28</sub>H<sub>32</sub>N<sub>2</sub>O<sub>5</sub>

Molecular Mass: 476.57 g mol<sup>-1</sup>

Prepared according to a literature procedure.<sup>351</sup>

2,3-Bis(benzyloxy)benzoic acid (**2-12**, 1.18 g, 3.53 mmol) was dissolved in dry DCM (50 mL), then 1-hydroxybenzotriazole (HOBT, 0.471 g, 3.49 mmol) and 1-ethyl-3-(3-dimethylaminopropyl)carbodiimide hydrochloride (EDC.HCl, 0.814 g, 4.25 mmol) added. The solution was placed under N<sub>2</sub>, then *N*-Boc-ethylene diamine (0.59 mL, 3.73 mmol) added dropwise and the solution was stirred overnight. Additional DCM (50 mL) was added, then the organic layer was washed with 0.1 M aqueous formic acid (35 mL), saturated NaHCO<sub>3</sub> solution (35 mL), water (50 mL) and brine (50 mL). The organic layer was dried over MgSO<sub>4</sub> and the solvent removed under vacuum to give a white solid (1.42 g, 2.98 mmol, 84%). M.p. = 134-135 °C (lit = 135 °C).<sup>649</sup> R<sub>f</sub> = 0.81 (EtOAc).

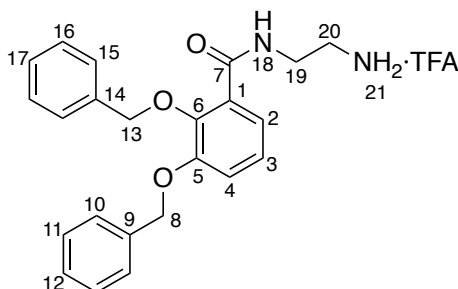
Characterisation data consistent with literature.<sup>351</sup>

<sup>1</sup>H NMR: (400 MHz, CDCl<sub>3</sub>) δ<sub>H</sub> ppm: 8.07 (1H, br t, *J* = 5.5 Hz, H<sub>21</sub>), 7.71 (1H, app. quintet, *J* = 5.0 Hz, H<sub>18</sub>), 7.49-7.46 (2H, m, Ar H), 7.44-7.32 (9H, m, Ar H), 7.17-7.13 (2H, m, H<sub>3</sub> and 4), 5.17 (2H, s, H<sub>8</sub> or 13), 5.09 (2H, s, H<sub>8</sub> or 13), 3.35 (2H, app. q, *J* = 5.5 Hz, H<sub>19</sub>), 3.16 (2H, app. q, *J* = 5.5 Hz, H<sub>20</sub>), 1.40 (9H, s, H<sub>24</sub>).

**<sup>13</sup>C NMR:** (100 MHz, CDCl<sub>3</sub>) δ<sub>C</sub> ppm: 166.4 (C7), 156.5 (C3), 152.2, 147.2 (C5 and 6), 136.8, 136.7 (C9 and 14), 129.33, 129.30, 129.25, 129.2, 128.8, 128.2 (C10-12 and 15-17), 127.6 (C1), 124.9, 123.7, 117.6 (C2/3/4), 79.7 (C23), 77.0, 71.8 (C8 and 13), 41.4 (C20), 40.3 (C19), 28.8 (C24).

**HRMS (ESI):** Calcd. [M+H]<sup>+</sup> (C<sub>28</sub>H<sub>33</sub>N<sub>2</sub>O<sub>5</sub>) *m/z* = 477.2384; Obs. [M+H]<sup>+</sup> *m/z* = 477.2391, Mean err -1.1 ppm. Calcd. [M+Na]<sup>+</sup> (C<sub>28</sub>H<sub>32</sub>N<sub>2</sub>NaO<sub>5</sub>) *m/z* = 499.2203; Obs. [M+Na]<sup>+</sup> *m/z* = 499.2205, Mean err -0.2 ppm.

***N*-(Aminoethyl)-2,3-bis(benzyloxy)benzamide, TFA salt (2-17)**



Molecular Formula: C<sub>25</sub>H<sub>25</sub>F<sub>3</sub>N<sub>2</sub>O<sub>5</sub>

Molecular Mass: 490.48 g mol<sup>-1</sup>

Prepared according to a literature procedure.<sup>351</sup>

**2-16** (1.02 g, 2.15 mmol) was dissolved in DCM (16 mL) and cooled to 0 °C. A solution of 20% v/v trifluoroacetic acid in DCM (16 mL; 10% v/v TFA in final solution) was added dropwise, then the reaction allowed to warm to room temperature and stirred for 4 hours. The solvent was removed under vacuum and the residue redissolved in hot EtOH (0.5 mL). Diethyl ether (30-40 mL) was added to precipitate the product, which was isolated by Buchner filtration to give a white solid (0.808 g, 1.65 mmol, 77%). M.p. = 152-154 °C. R<sub>f</sub> = 0.00 (EtOAc).

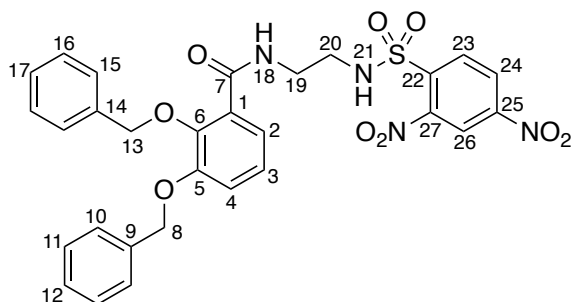
**<sup>1</sup>H NMR:** (400 MHz, MeOD) δ<sub>H</sub> ppm: 7.53-7.50 (2H, m, *Ar H* or *H18*), 7.43-7.30 (11H, m, *Ar H* or *H18*), 7.17 (1H, t, *J* = 8.0 Hz, *H3*), 5.22 (2H, s, *H8* or *13*), 5.13 (2H, s, *H8* or *13*), 3.47 (2H, t, *J* = 6.0 Hz, *H19*), 2.98 (2H, t, *J* = 6.0 Hz, *H20*).

**<sup>13</sup>C NMR:** (100 MHz, MeOD)  $\delta_c$  ppm: 169.9 (C7), 153.6, 147.9 (C5 and 6), 138.4, 138.3 (C9 and 14), 130.3, 129.89, 129.84, 129.80, 129.5, 129.3 (C10-12 and 15-17), 125.8 (C3), 123.7, 117.6 (C2 and 4), 77.6, 72.4 (C8 and 13), 41.0 (C20), 38.8 (C19).

C1 is not observed, but may be overlapping with other aryl peaks in the 131-129 ppm region.

**HRMS (ESI):** Calcd.  $[M+H]^+$  (C<sub>23</sub>H<sub>25</sub>N<sub>2</sub>O<sub>3</sub>)  $m/z$  = 377.1860; Obs.  $[M+H]^+$   $m/z$  = 377.1863, Mean err -1.3 ppm.

**2,3-Bis(benzyloxy)-N-(4-(2,4-dinitrobenzenesulfonamido)ethyl)benzamide (2-18)**



Molecular Formula: C<sub>29</sub>H<sub>26</sub>N<sub>4</sub>O<sub>9</sub>S

Molecular Mass: 606.61 g mol<sup>-1</sup>

**2-17** (77.9 mg, 0.159 mmol) was dissolved in 1 M aq. NaOH solution (4 mL), and stirred for 30 minutes, then the solution extracted with DCM (3 x 5 mL), dried over MgSO<sub>4</sub> and the solvent removed to give a clear pale yellow oil. The oil was dissolved in anhydrous DCM (10 mL), and the solution cooled to 0 °C, then 2,4-dinitrobenzenesulfonyl chloride (45.6 mg, 0.171 mmol) and lutidine (71  $\mu$ L, 0.613 mmol) were added, and the reaction was allowed to warm to room temperature and stirred for 24 hours. Water (10 mL) was added and the organic layer separated. The aqueous layer was extracted with DCM (2 x 10 mL), then the combined organic layers were washed with 1 M aq. HCl (15 mL), water (20 mL) and brine (15 mL), dried over MgSO<sub>4</sub> and the DCM removed *in vacuo* to give a yellow-green oil (83.4 mg, 0.137 mmol, 86%). M.p. = 137-139 °C. R<sub>f</sub> = 0.36 (DCM).

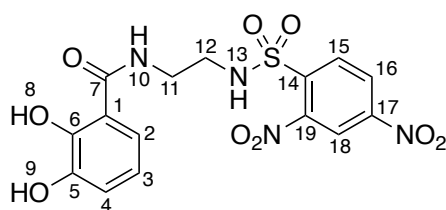
**<sup>1</sup>H NMR:** (400 MHz, MeOD)  $\delta_{\text{H}}$  ppm: 8.46 (1H, d,  $J = 2.5$  Hz, *H*26), 8.22 (1H, dd,  $J = 8.5, 2.5$  Hz, *H*24), 8.11 (1H, d,  $J = 8.5$  Hz, *H*23), 7.57-7.54 (2H, m, *Ar H*), 7.45-7.35 (3H, m, *Ar H*), 7.32-7.20 (7H, m, *Ar H*), 7.10 (1H, t,  $J = 8.0$  Hz, *H*3), 5.17 (2H, s, *H*8 or 13), 4.99 (2H, s, *H*8 or 13). The peaks for *H*19 and *H*20 were hidden under the methanol solvent peak, but were visible on HMQC and HMBC spectra.

**<sup>13</sup>C NMR:** (100 MHz, MeOD)  $\delta_{\text{C}}$  ppm: 167.9 (*C*7), 153.1 (*C*5 or 6), 150.5, 149.0 (*C*25 and 27), 147.4 (*C*5 or 6), 140.8 (*C*22), 138.0, 137.7 (*C*9 and 14), 133.0 (*C*23), 130.1, 129.7, 129.6, 129.4, 129.3 (*C*10-12 and 15-17), 128.0 (*C*24), 127.9 (*C*1), 125.5 (*C*3), 123.0 (*C*2), 121.4 (*C*26), 118.3 (*C*4), 77.2, 72.1 (*C*8 and 13), 44.0, 40.5 (*C*19 and 20).

**HRMS (ESI):** Calcd.  $[\text{M}+\text{Na}]^+$  ( $\text{C}_{29}\text{H}_{26}\text{N}_4\text{NaO}_9\text{S}$ )  $m/z = 629.1313$ ; Obs.  $[\text{M}+\text{Na}]^+$   $m/z = 629.1300$ , Mean err 2.8 ppm.

**IR (ATIR,  $\text{cm}^{-1}$ ):** 3360 (amide NH stretch, w), 3099 (sulfonamide NH stretch, w), 3050-2850 (C-H stretching, w), 1644 (C=O stretch, m), 1575 (N=O/C=C stretches, m), 1537 (N=O/C=C stretches, s), 1454 (N=O/C=C stretches, s), 1346 (S=O stretch, s), 1165 (S=O stretch, s).

***N*-[2-(2,4-Dinitrobenzenesulfonamido)ethyl]-2,3-dihydroxybenzamide (2-15)**



Molecular Formula:  $\text{C}_{15}\text{H}_{14}\text{N}_4\text{O}_9\text{S}$

Molecular Mass:  $426.36 \text{ g mol}^{-1}$

**2-18** (0.118 g, 0.195 mmol) was dissolved in dry DCM (5 mL) and placed in a 3-necked RBF, then the flask purged with  $\text{N}_2$ . Boron tribromide (1 M in DCM, 0.488 mL, 0.488 mmol) was added dropwise and the reaction stirred under flow of  $\text{N}_2$  at room temperature overnight. Extra DCM (5 mL) was added in

the morning as the reaction had almost dried out. Wet methanol (25 mL) was added to quench any remaining BBr<sub>3</sub>, then the solvent removed *in vacuo*. MeOH (3 x 20 mL) was added and removed under vacuum, giving a yellow-orange oil. The crude product was purified by preparative LCMS chromatography using Prep. LCMS Method A to give a yellow solid (45.6 mg, 0.107 mmol, 55%). M.p. = 175-177 °C.

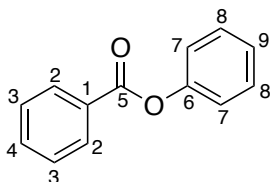
**<sup>1</sup>H NMR:** (400 MHz, MeCN-d<sub>3</sub>) δ<sub>H</sub> ppm: 12.59 (1H, br s, *H8*), 8.45 (1H, d, *J* = 2.0 Hz, *H18*), 8.32 (1H, dd, *J* = 8.5, 2.5 Hz, *H16*), 8.18 (1H, d, *J* = 8.5 Hz, *H15*), 7.41 (1H, br s, *H10 or 13*), 6.88 (1H, d, *J* = 8.0 Hz, *H4*), 6.84 (1H, d, *J* = 8.0 Hz, *H2*), 6.66 (1H, app. t, *J* = 8.0 Hz, *H3*), 6.60-6.30 (2H, m, *H9 and H10 or 13*), 3.50-3.40 (4H, m, *H11 and 12*).

**<sup>13</sup>C NMR:** (100 MHz, MeCN-d<sub>3</sub>) δ<sub>C</sub> ppm: 171.5 (*C7*), 150.39, 150.36 (*C6 and 17*), 148.6 (*C19*), 146.7 (*C5*), 139.7 (*C14*), 132.8 (*C15*), 128.2 (*C16*), 121.2 (*C18*), 119.5 (*C4*), 119.3 (*C3*), 117.7 (*C2*), 114.7 (*C1*), 43.9, 39.7 (*C11 and 12*).

**HRMS (ESI):** Calcd. [M+Na]<sup>+</sup> (C<sub>15</sub>H<sub>14</sub>N<sub>4</sub>NaO<sub>9</sub>S) *m/z* = 449.0374; Obs. [M+Na]<sup>+</sup> *m/z* = 499.0376, Mean err -1.1 ppm.

**IR (ATIR, cm<sup>-1</sup>):** 3436 (OH stretch, m), 3407 (amide NH stretch, m), 3114 (sulfonamide NH stretch, w), 3110-2850 (C-H stretching, w), 1639 (C=O stretch, m), 1599 (N=O/C=C stretches, m), 1546 (N=O/C=C stretches, s), 1534 (N=O/C=C stretches, s), 1346 (S=O stretch, s), 1336 (N=O stretch, s), 1163 (S=O stretch, s).

## Phenyl Benzoate



Molecular Formula:  $C_{13}H_{10}O_2$

Molecular Mass:  $198.22 \text{ g mol}^{-1}$

Prepared according to a literature procedure.<sup>650</sup>

Phenol (0.720 g, 7.63 mmol) was dissolved in 10% w/v aqueous NaOH solution (7 mL), then benzoyl chloride (0.89 mL, 7.63 mmol) added and the resulting mixture stirred for 2 hours. The white solid formed was isolated via Buchner filtration and washed with distilled water. The solid was recrystallized from hot EtOH to give a white crystalline solid over two crops (0.530 g, 2.68 mmol, 35%). M.p. = 69-70 °C (lit. 69-70 °C).<sup>651</sup>

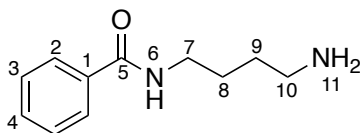
Characterisation data consistent with literature.<sup>651</sup>

**<sup>1</sup>H NMR:** (400 MHz,  $CDCl_3$ )  $\delta_H$  ppm: 8.24-8.19 (2H, m, *H2*), 7.65 (1H, tt, *J* = 7.5, 1.5 Hz, *H4*), 7.54-7.50 (2H, m, *H3*), 7.47-7.41 (2H, m, *H8*), 7.28 (1H, tt, *J* = 7.5, 1.5 Hz, *H9*), 7.24-7.20 (2H, m, *H7*).

**<sup>13</sup>C NMR:** (100 MHz,  $CDCl_3$ )  $\delta_C$  ppm: 165.4 (*C5*), 151.1 (*C6*), 133.7 (*C4*), 130.3 (*C2*), 129.7 (*C1*), 129.6 (*C8*), 128.7 (*C3*), 126.0 (*C9*), 121.9 (*C7*).

**HRMS (APCI):** Calcd.  $[M+H]^+$  ( $C_{13}H_{11}O_2$ )  $m/z$  = 199.0754; Obs.  $[M+H]^+$   $m/z$  = 199.0748, Mean err 1.9 ppm.

### ***N*-(4-Aminobutyl)-benzamide (2-20)**



Molecular Formula: C<sub>11</sub>H<sub>16</sub>N<sub>2</sub>O

Molecular Mass: 192.26 g mol<sup>-1</sup>

Prepared according to a literature procedure.<sup>354</sup>

Phenyl benzoate (0.396 g, 2.00 mmol) was placed under N<sub>2</sub>, then H<sub>2</sub>O (0.1 mL) added. 1,4-Diaminobutane (0.201 mL, 2.00 mmol) was added and the reaction stirred under N<sub>2</sub> for 30 minutes, before heating at 50 °C for 24 hours. The resulting pink slurry was purified by column chromatography (silica gel, 5:3:1:1 Et<sub>2</sub>O:MeCN:MeOH:aq. NH<sub>3</sub>). The product was initially obtained as a pink oil; after drying under vacuum for 3 hours, it partially solidified to give 0.231 g of **2-19** (1.20 mmol, 60%). R<sub>f</sub> = 0.39 (5:3:1:1 Et<sub>2</sub>O:MeCN:MeOH: aq. NH<sub>3</sub>).

Characterisation data consistent with literature.<sup>355</sup>

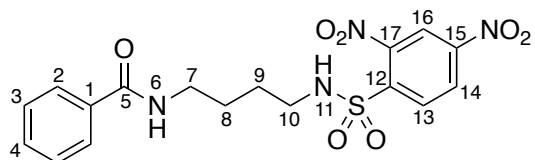
**<sup>1</sup>H NMR:** (400 MHz, MeOD) δ<sub>H</sub> ppm: 7.83-7.80 (2H, m, *H*<sub>2</sub>), 7.53 (1H, tt, *J* = 7.0, 1.5 Hz, *H*<sub>4</sub>), 7.45 (2H, tt, *J* = 7.0, 1.5 Hz, *H*<sub>3</sub>), 3.40 (2H, t, *J* = 7.0 Hz, *H*<sub>7</sub>), 2.70 (2H, t, *J* = 7.0 Hz, *H*<sub>10</sub>), 1.70-1.52 (4H, m, *H*<sub>8</sub> and *9*).

**<sup>13</sup>C NMR:** (100 MHz, MeOD) δ<sub>C</sub> ppm: 170.3 (*C*<sub>5</sub>), 135.8 (*C*<sub>1</sub>), 132.6 (*C*<sub>4</sub>), 129.5 (*C*<sub>3</sub>), 128.2 (*C*<sub>2</sub>), 42.1 (*C*<sub>9</sub>), 40.7 (*C*<sub>7</sub>), 30.8, 27.9 (*C*<sub>8</sub> and *9*).

**HRMS (ESI):** Calcd. [M+H]<sup>+</sup> (C<sub>11</sub>H<sub>17</sub>N<sub>2</sub>O) *m/z* = 193.1335; Obs. [M+H]<sup>+</sup> *m/z* = 193.1335, Mean err 0.8 ppm.



## ***N*-[4-(2,4-Dinitrobenzenesulfonamido)butyl]benzamide (2-19)**



Molecular Formula: C<sub>17</sub>H<sub>18</sub>N<sub>4</sub>O<sub>7</sub>S

Molecular Mass: 422.41 g mol<sup>-1</sup>

2,4-Dinitrobenzenesulfonyl chloride (0.157 g, 0.590 mmol) was placed under N<sub>2</sub>, then dissolved in dry DCM (10 mL). The solution was cooled to 0 °C, then **2-20** (0.107 g, 0.555 mmol) was dissolved in in dry DCM (10 mL) and added. Lutidine (0.26 mL, 2.23 mmol) was then added, and the reaction was allowed to warm to room temperature and stirred for 24 hours. As the reaction had not gone to completion, extra sulfonyl chloride (0.02 g, 0.07 mmol) and lutidine (0.08 mL, 0.69 mmol) were added and the reaction stirred for an additional 72 hours. Water (20 mL) was added and the organic layer separated. The aqueous layer was extracted with DCM (2 x 20 mL), then the combined organic layers were washed with 1 M aq. HCl (35 mL), water (30 mL) and brine (30 mL), dried over MgSO<sub>4</sub> and the DCM removed *in vacuo* to give a viscous orange oil, which solidified overnight to form a brown solid (0.112 g, 0.264 mmol, 48%). M.p. = 145 °C.

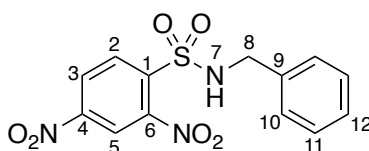
**<sup>1</sup>H NMR:** (400 MHz, MeOD) δ<sub>H</sub> ppm: 8.68 (1H, d, *J* = 2.5 Hz, *H*16), 8.55 (1H, dd, *J* = 8.5, 2.5 Hz, *H*14), 8.31 (1H, d, *J* = 8.5 Hz, *H*13), 7.77 (2H, dt, *J* = 7.0, 1.5 Hz, *H*2), 7.53 (1H, tt, *J* = 7.0, 1.5 Hz, *H*4), 7.45 (2H, tt, *J* = 7.0, 1.5 Hz, *H*3), 3.35 (2H, t, *J* = 7.0 Hz, *H*7), 3.16 (2H, t, *J* = 7.0 Hz, *H*10), 1.69-1.54 (4H, m, *H*8 and 9).

**<sup>13</sup>C NMR:** (100 MHz, MeOD) δ<sub>C</sub> ppm: 170.2 (*C*5), 151.3, 149.5 (*C*15 and 17), 140.3 (*C*12), 135.7 (*C*1), 133.2 (*C*13), 132.6 (*C*4), 129.6 (*C*3), 128.2 (*C*2), 127.9 (*C*14), 1121.4 (*C*16), 44.1 (*C*10), 40.2 (*C*7), 28.3, 27.6 (*C*8 and 9).

**HRMS (ESI):** Calcd. [M+H]<sup>+</sup> (C<sub>17</sub>H<sub>19</sub>N<sub>4</sub>O<sub>7</sub>S) *m/z* = 423.0969; Obs. [M+H]<sup>+</sup> *m/z* = 423.0967, Mean err -0.3 ppm. Calcd. [M+Na]<sup>+</sup> (C<sub>17</sub>H<sub>18</sub>N<sub>4</sub>NaO<sub>7</sub>S) *m/z* = 445.0788; Obs. [M+Na]<sup>+</sup> *m/z* = 445.0784, Mean err 1.1 ppm.

**IR (ATR,  $\text{cm}^{-1}$ ):** 3452 (amide NH stretch, w), 3159 (amide NH stretch II, w br), 3105 (sulfonamide NH stretch, w), 3050-2800 (C-H stretching, w), 1654 (C=O stretch, s), 1603 (N=O/C=C stretches, w), 1580 (N=O/C=C stretches, w), 1550 (N=O/C=C stretches, s), 1524 (N=O/C=C stretches, s), 1361 (N=O stretch, s), 1343 (S=O stretch, s), 1164 (S=O stretch, s).

***N*-Benzyl-2,4-dinitrobenzenesulfonamide (1-56)**



Molecular Formula:  $\text{C}_{13}\text{H}_{11}\text{N}_3\text{O}_6\text{S}$

Molecular Mass:  $337.31 \text{ g mol}^{-1}$

Prepared according to a literature procedure.<sup>301</sup>

2,4-Dinitrobenzenesulfonyl chloride (0.504 g, 1.89 mmol) was dissolved in dry DCM (30 mL) and cooled to 0 °C in an ice bath. Benzylamine (0.25 mL, 2.25 mmol) and pyridine (0.23 mL, 2.81 mmol) were added. The mixture, which turned orange after 10 minutes of stirring, was stirred for 4 hours in an ice bath before it was allowed to warm to room temperature and stirred overnight.  $\text{H}_2\text{O}$  (15 mL) was added, and the layers separated. The aqueous layer was extracted with DCM (2 x 20 mL), then the combined organic layers washed with brine (2 x 60 mL), dried ( $\text{MgSO}_4$ ) and the solvent removed. The crude product was purified by column chromatography (silica gel, 1:1 40-60 pet. ether:EtOAc) to give **1-56** as an orange-yellow solid (0.412 g, 1.22 mmol, 65%). M.p. = 149-150 °C (lit. = 150-151 °C).<sup>301</sup>

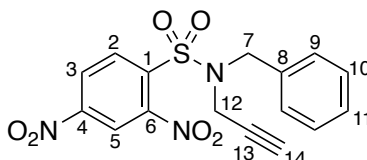
Characterisation data consistent with literature.<sup>301</sup>

**$^1\text{H NMR}$ :** (400 MHz,  $\text{DMSO-d}_6$ )  $\delta_{\text{H}}$  ppm: 9.06 (1H, t,  $J = 6.0 \text{ Hz}$ , H7), 8.86 (1H, d,  $J = 2.5 \text{ Hz}$ , H5), 8.51 (1H, dd,  $J = 8.5, 2.5 \text{ Hz}$ , H3), 8.12 (1H, d,  $J = 8.5 \text{ Hz}$ , H2), 7.26-7.20 (5H, m, H10-12), 4.20 (2H, d,  $J = 6.0 \text{ Hz}$ , H8).

**<sup>13</sup>C NMR:** (100 MHz, DMSO-d<sub>6</sub>) δ<sub>C</sub> ppm: 149.5, 147.4 (*C4 and 6*), 138.1 (*C1*), 137.0 (*C9*), 131.4 (*C2*), 128.4, 127.7, 127.4, 127.1 (*C3 and C10/11/12*), 120.1 (*C5*), 46.3 (*C8*).

**HRMS (ESI):** Calcd. [M+Na]<sup>+</sup> (C<sub>13</sub>H<sub>11</sub>N<sub>3</sub>NaO<sub>6</sub>S) *m/z* = 360.0261; Obs. [M+Na]<sup>+</sup> *m/z* = 360.0254, Mean err 1.8 ppm.

***N*-Benzyl-2,4-dinitro-*N*-(prop-2-yn-1-yl)benzenesulfonamide (2-22)**



Molecular Formula: C<sub>16</sub>H<sub>13</sub>N<sub>3</sub>O<sub>6</sub>S

Molecular Mass: 375.36 g mol<sup>-1</sup>

Prepared according to a literature procedure.<sup>304</sup>

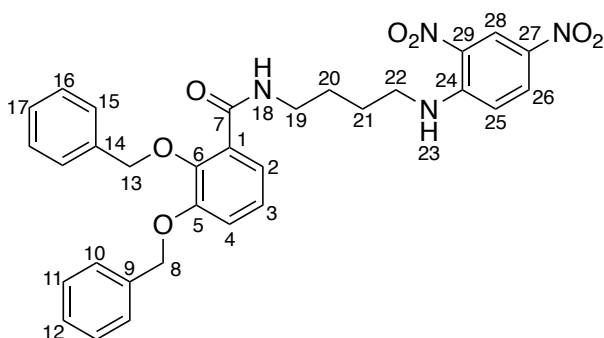
*N*-Benzyl-2,4-dinitrobenzenesulfonamide (**1-56**, 0.147 g, 0.436 mmol) was dissolved in dry DMF (10 mL), then K<sub>2</sub>CO<sub>3</sub> (0.182 g, 1.32 mmol) added. The resulting brown solution was treated with propargyl bromide (80% in toluene, 0.26 mL, 2.33 mmol) and stirred at room temperature overnight. The reaction mixture was poured into H<sub>2</sub>O (110 mL) and extracted with DCM (3 x 35 mL). The combined organic layers were washed with H<sub>2</sub>O (50 mL) and brine (50 mL), dried over MgSO<sub>4</sub> and the solvent removed under vacuum. The crude product was purified via column chromatography (silica gel, 2:1 40-60 °C pet. ether:EtOAc) and dried under vacuum to give **2-22** as an orange solid (0.107 g, 0.297 mmol, 68%). M.p. = 95-97 °C (lit. = 91-92 °C).<sup>652</sup> R<sub>f</sub> = 0.42 (2:1 40-60 °C pet. ether:EtOAc).

**<sup>1</sup>H NMR:** (400 MHz, CDCl<sub>3</sub>) δ<sub>H</sub> ppm: 8.50 (1H, d, *J* = 2.0 Hz, *H5*), 8.48 (1H, dd, *J* = 8.5, 2.0 Hz, *H3*), 8.26 (1H, d, *J* = 8.5 Hz, *H2*), 7.39-7.35 (5H, m, *H9-11*), 4.62 (2H, s, *H7*), 4.06 (2H, d, *J* = 2.5 Hz, *H12*), 2.21 (1H, t, *J* = 2.5 Hz, *H14*).

**<sup>13</sup>C NMR:** (100 MHz, CDCl<sub>3</sub>) δ<sub>c</sub> ppm: 149.9 (C4), 148.5 (C6), 138.6 (C1), 133.9 (C8), 132.9 (C2), 129.1, 129.0 (C9 and 10), 128.8 (C11), 126.1 (C3), 119.9 (C5), 76.2 (C14), 74.9 (C13), 51.0 (C7), 36.3 (C12).

**HRMS (ESI):** Calcd. [M+Na]<sup>+</sup> (C<sub>16</sub>H<sub>13</sub>N<sub>3</sub>NaO<sub>6</sub>S) *m/z* = 398.0417; Obs. [M+Na]<sup>+</sup> *m/z* = 398.0412, Mean err 3.1 ppm.

**2,3-Bis(benzyloxy)-N-{4-[(2,4-dinitrophenyl)amino]butyl}benzamide  
(2-21)**



Molecular Formula: C<sub>31</sub>H<sub>30</sub>N<sub>4</sub>O<sub>7</sub>

Molecular Mass: 570.60 g mol<sup>-1</sup>

**2-13** (0.109 g, 0.247 mmol) was placed under N<sub>2</sub>, then dissolved in dry DCM (6 mL). 1-Chloro-2,4-dinitrobenzene (50.9 mg, 0.251 mmol) and Et<sub>3</sub>N (0.105 mL, 0.753 mmol) were added, and the resulting yellow solution was stirred at room temperature for 24 hours. Extra DCM (5 mL) and water (10 mL) were added and the layers separated. The aqueous layer was extracted with DCM (2 x 10 mL), then the combined organic layers were washed with 1 M aq. HCl (15 mL), water (15 mL), 1 M NaHCO<sub>3</sub> solution (5 mL) and brine (15 mL), dried over MgSO<sub>4</sub> and the DCM removed *in vacuo*. The crude product was purified by column chromatography (silica gel, 2:1 EtOAc:40-60 °C pet. ether) to give **2-21** as a yellow-orange glassy solid (92.0 mg, 0.161 mmol, 65%). M.p. = 113-114 °C. R<sub>f</sub> = 0.71 (EtOAc); 0.62 (9:1 DCM:MeOH); 0.31 (2:1 EtOAc:40-60 °C pet. ether).

**<sup>1</sup>H NMR:** (400 MHz, DMSO-d<sub>6</sub>) δ<sub>H</sub> ppm: 8.85-8.82 (2H, m, H<sub>23</sub> and 28), 8.24-8.18 (2H, m\*, H<sub>18</sub> and 26), 7.51-7.48 (2H, m, Ar H), 7.43-7.31 (5H, m, Ar H), 7.29-7.25 (4H, m, Ar H), 7.17 (1H, d, *J* = 10.0 Hz, H<sub>25</sub>), 7.12 (1H, t, *J* = 8.0 Hz,

H3), 7.08 (1H, dd,  $J = 8.0, 2.0$  Hz, H2 or 4), 5.20 (2H, s, H8 or 13), 4.99 (2H, s, H8 or 13), 3.43 (2H, app. q,  $J = 6.5$  Hz, H22), 3.24 (2H, app. q,  $J = 6.5$  Hz, H19), 1.63-1.46 (4H, m, H20 and 21).

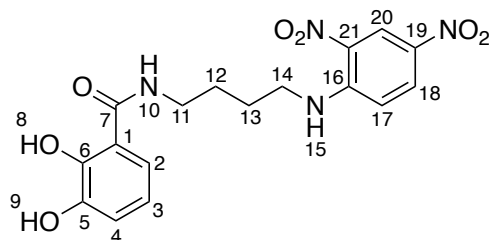
\*Looks to be t and dd overlapping.

**$^{13}\text{C}$  NMR:** (100 MHz, DMSO- $d_6$ )  $\delta_c$  ppm: 165.7 (C7), 151.6 (C5), 148.1 (C27), 145.1 (C6), 137.1, 136.8 (C9 and 14), 134.6 (C1), 131.3 (C24), 129.9 (C26), 129.6 (C29), 128.5, 128.23, 128.16, 128.02, 127.97, 127.8 (C10-12 and 15-17), 124.2, 123.7 (C28 and C2 or 4), 120.7 (C3), 115.7, 115.3 (C25 and C2 or 4), 75.1, 70.1 (C8 and 13), 42.3 (C22), 38.6 (C19), 26.3, 25.5 (C20 and 21).

**HRMS (ESI):** Calcd.  $[\text{M}+\text{H}]^+$  ( $\text{C}_{31}\text{H}_{31}\text{N}_4\text{O}_7$ )  $m/z = 571.2187$ ; Obs.  $[\text{M}+\text{H}]^+$   $m/z = 571.2192$ , Mean err  $-1.1$  ppm. Calcd.  $[\text{M}+\text{Na}]^+$  ( $\text{C}_{31}\text{H}_{30}\text{N}_4\text{NaO}_7$ )  $m/z = 593.2007$ ; Obs.  $[\text{M}+\text{Na}]^+$   $m/z = 593.2015$ , Mean err  $-0.2$  ppm. Calcd.  $[\text{M}+\text{K}]^+$  ( $\text{C}_{31}\text{H}_{30}\text{KN}_4\text{O}_7$ )  $m/z = 609.1746$ ; Obs.  $[\text{M}+\text{K}]^+$   $m/z = 609.1749$ , Mean err  $-1.0$  ppm.

**IR (ATIR,  $\text{cm}^{-1}$ ):** 3376 (amide NH stretch, m), 3115-2875 (C-H stretching, w), 1651 (C=O stretch, s), 1617 (N=O/C=C stretches, s), 1586 (N=O/C=C stretches, s), 1575 (N=O/C=C stretches, s), 1520 (N=O/C=C stretches, s), 1336 (N=O stretch, s).

### ***N*-{4-[(2,4-Dinitrophenyl)amino]butyl}-2,3-dihydroxybenzamide (2-23)**



Molecular Formula:  $\text{C}_{17}\text{H}_{18}\text{N}_4\text{O}_7$

Molecular Mass:  $390.35 \text{ g mol}^{-1}$

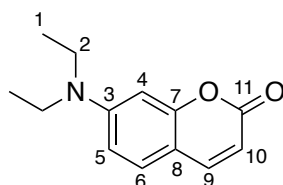
**2-21** (0.067 g, 0.117 mmol) was placed in a 3-necked RBF, then the flask purged with  $\text{N}_2$ , and dry DCM (3.5 mL) added. Boron tribromide (1 M in DCM,

0.40 mL, 0.400 mmol) was added dropwise and the reaction stirred at room temperature for 22 hours. Wet methanol (15 mL) was added to quench any remaining BBr<sub>3</sub>, then the solvent removed *in vacuo*. MeOH (3 x 15 mL) was added and removed under vacuum to try and remove volatile borate salts, giving an orange-black solid. The crude product was purified by preparative HPLC chromatography using Prep. LCMS Method A to give **2-23** as a brown solid (9.9 mg, 0.025 mmol, 22%).

**<sup>1</sup>H NMR:** (400 MHz, DMSO-d<sub>6</sub>) δ<sub>H</sub> ppm: 12.80 (1H, s, H8), 9.13 (1H, br s, H9), 8.91 (1H, br t, *J* = 6.0 Hz, H10 or 15), 8.84 (1H, d, *J* = 2.5 Hz, H20), 8.80 (1H, br t, *J* = 6.0 Hz, H10 or 15), 8.23 (1H, dd, *J* = 9.5, 2.5 Hz, H18), 7.26-7.22 (2H, m, H17 and H2 or 4), 6.88 (1H, dd, *J* = 8.0, 2.0 Hz, H2 or 4), 6.64 (1H, t, *J* = 8.0 Hz, H3), 3.53 (2H, app. q, *J* = 6.0 Hz, H14), 3.37-3.20 (2H, m, H11), 1.71-1.59 (4H, m, H12 and 13).

**HRMS (ESI):** Calcd. [M+H]<sup>+</sup> (C<sub>17</sub>H<sub>19</sub>N<sub>4</sub>O<sub>7</sub>) *m/z* = 391.1248; Obs. [M+H]<sup>+</sup> *m/z* = 391.1251, Mean err -0.7 ppm.

### 7-(Diethylamino)coumarin (**2-26**)



Molecular Formula: C<sub>13</sub>H<sub>15</sub>NO<sub>2</sub>

Molecular Mass: 217.27 g mol<sup>-1</sup>

Prepared according to a literature procedure.<sup>361</sup>

4-(Diethylamino)salicylaldehyde (2.05 g, 10.6 mmol) was dissolved in dry EtOH (40 mL). Diethyl malonate (3.30 mL, 21.6 mmol) and piperidine (1.05 mL, 10.6 mmol) were added and the resulting dark purple-red solution was heated at reflux overnight. The solvent was removed under vacuum, then concentrated hydrochloric acid (20 mL) and glacial acetic acid (20 mL) were added, and stirred at reflux overnight. The solution was allowed to cool to

room temperature, then poured into ice-cold H<sub>2</sub>O (100 mL). NaOH (10 M) was added to neutralize the mixture, then DCM (30 mL) added. The organic layer was separated and washed with H<sub>2</sub>O (3 x 10 mL) and brine (10 mL), then dried over MgSO<sub>4</sub> and the solvent removed. The crude product was purified via column chromatography (silica gel, 1:1 EtOAc:40-60 °C pet. ether) to give an orange solid (1.19 g, 5.47 mmol, 52%). R<sub>f</sub> = 0.41 (1:1 EtOAc:40-60 °C pet. ether), spot fluorescent blue under both short and long-wavelength UV.

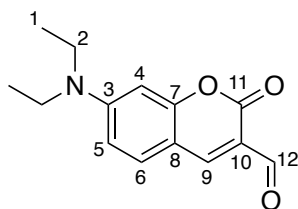
Characterisation data consistent with literature.<sup>361</sup>

**<sup>1</sup>H NMR:** (400 MHz, CDCl<sub>3</sub>) δ<sub>H</sub> ppm: 7.54 (1H, dd, *J* = 9.5, 0.5 Hz, *H*9), 7.24 (1H, d, *J* = 9.0 Hz, *H*6), 6.56 (1H, dd, *J* = 9.0, 2.5 Hz, *H*5), 6.49 (1H, d, *J* = 2.5 Hz, *H*4), 6.03 (1H, d, *J* = 9.0 Hz, *H*10), 3.41 (4H, q, *J* = 7.0 Hz, *H*2), 1.21 (6H, t, *J* = 7.0 Hz, *H*1).

**<sup>13</sup>C NMR:** (100 MHz, CDCl<sub>3</sub>) δ<sub>C</sub> ppm: 162.4 (*C*11), 156.9 (*C*7), 150.7 (*C*3), 143.8 (*C*9), 128.9 (*C*6), 109.4 (*C*10), 108.8 (*C*5), 108.4 (*C*8), 97.7 (*C*4), 45.0 (*C*2), 12.6 (*C*1).

**HRMS (ESI):** Calcd. [M+H]<sup>+</sup> (C<sub>13</sub>H<sub>15</sub>NO<sub>2</sub>) *m/z* = 218.1176; Obs. [M+H]<sup>+</sup> *m/z* = 218.1177, Mean err -1.2 ppm. Calcd. [M+Na]<sup>+</sup> (C<sub>13</sub>H<sub>15</sub>NNaO<sub>2</sub>) *m/z* = 240.0995; Obs. [M+Na]<sup>+</sup> *m/z* = 240.0997, Mean err -1.1 ppm.

### 7-(Diethylamino)-3-formylcoumarin (2-27)



Molecular Formula: C<sub>14</sub>H<sub>15</sub>NO<sub>3</sub>

Molecular Mass: 245.28 g mol<sup>-1</sup>

Prepared according to a literature procedure.<sup>361</sup>

A 50 mL RBF was placed under N<sub>2</sub> then POCl<sub>3</sub> (1.30 mL, 14.0 mmol) added. Dry DMF (1.27 mL, 16.5 mmol) was added dropwise and the solution stirred for 30 minutes. 7-(Diethylamino)coumarin (**2-26**, 1.19 g, 5.46 mmol) in dry DMF (7.5 mL) was added dropwise, and the solution was stirred at 70 °C for 23 hours. The final red-black solution was poured into ice-cold H<sub>2</sub>O (100 mL) and neutralized with aqueous NaOH solution (5 M). Ethyl acetate (60 mL) added, and the organic layer extracted and washed with H<sub>2</sub>O (3 x 20 mL) and brine (10 mL). The organic layer was dried over MgSO<sub>4</sub> and the solvent removed to give an orange crystalline solid (0.910 g, 3.71 mmol, 68%). The solid becomes a lime-green fluorescent solution when dissolved in CDCl<sub>3</sub>. M.p. = 164-165 °C (lit. = 162-165 °C).<sup>653,654</sup> R<sub>f</sub> = 0.34 (1:2 EtOAc:hexane), poorly visible under short-wave UV, fluorescent green under long-wave UV.

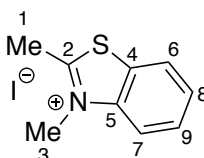
Characterisation data consistent with literature.<sup>361</sup>

**<sup>1</sup>H NMR:** (400 MHz, CDCl<sub>3</sub>) δ<sub>H</sub> ppm: 10.13 (1H, s, H12), 8.26 (1H, s, H9), 7.41 (1H, d, *J* = 9.0 Hz, H6), 6.64 (1H, dd, *J* = 9.0, 2.5 Hz, H5), 6.49 (1H, d, *J* = 2.5 Hz, H4), 3.48 (4H, q, *J* = 7.0 Hz, H2), 1.25 (6H, t, *J* = 7.0 Hz, H1).

**<sup>13</sup>C NMR:** (100 MHz, CDCl<sub>3</sub>) δ<sub>C</sub> ppm: 188.1 (C12), 162.1 (C11), 159.1 (C7), 153.5 (C3), 145.5 (C9), 132.7 (C6), 114.3 (C10), 110.3 (C5), 108.4 (C8), 97.3 (C4), 45.4 (C2), 12.6 (C1).

**HRMS (ESI):** Calcd. [M+Na]<sup>+</sup> (C<sub>14</sub>H<sub>15</sub>NNaO<sub>3</sub>) *m/z* = 268.0944; Obs. [M+Na]<sup>+</sup> *m/z* = 268.0947, Mean err -0.6 ppm.

### 2,3-Dimethylbenzothiazolium iodide (**2-28**)



Molecular Formula: C<sub>9</sub>H<sub>10</sub>INS

Molecular Mass: 291.15 g mol<sup>-1</sup>

Prepared according to a literature procedure.<sup>345</sup>



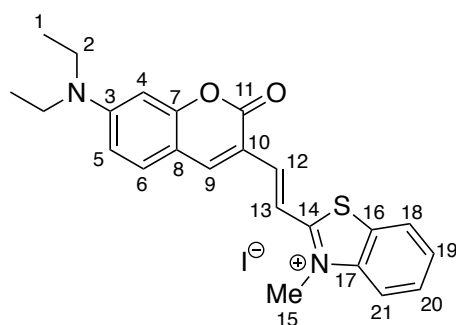
2-Methylbenzothiazole (2.14 mL, 16.8 mmol) and methyl iodide (1.05 mL, 16.8 mmol) were dissolved in MeCN (25 mL) and placed under N<sub>2</sub>. The solution was heated at 75 °C for 24 hours, then allowed to cool to room temperature. The formed solid isolated via Buchner filtration and washed three times with MeCN to give a white solid with a slight blue tinge (2.10 g, 7.23 mmol). The filtrate was moved to a fridge, with precipitation of further product over two weeks (0.468 g, 1.61 mmol) to give a total yield of 2.57 g (8.83 mmol, 53%). M.p. = 223-224 °C (lit. = 220-230 °C).<sup>655,656</sup>

Characterisation data consistent with literature.<sup>656</sup>

<sup>1</sup>H NMR: (400 MHz, DMSO-d<sub>6</sub>) δ<sub>H</sub> ppm: 8.46 (1H, dd, *J* = 8.5, 1.0 Hz, *H*6 or 7), 8.30 (1H, d, *J* = 8.5 Hz, *H*6 or 7), 7.89 (1H, ddd, *J* = 8.5, 7.5, 1.0 Hz, *H*8 or 9), 7.80 (1H, ddd, *J* = 8.5, 7.5, 1.0 Hz, *H*8 or 9), 4.21 (3H, s, *H*3), 3.19 (3H, s, *H*1).

HRMS (ESI): Calcd. [M]<sup>+</sup> (C<sub>9</sub>H<sub>10</sub>NS) *m/z* = 164.0528; Obs. [M]<sup>+</sup> *m/z* = 164.0534, Mean err -3.2 ppm.

**(*E*)-2-(2-(7-(Diethylamino)-2-oxo-2*H*-chromen-3-yl)vinyl)-3-methyl benzo[*d*]thiazol-3-ium iodide (2-11)**



Molecular Formula: C<sub>23</sub>H<sub>23</sub>IN<sub>2</sub>O<sub>2</sub>S

Molecular Mass: 518.41 g mol<sup>-1</sup>

Prepared according to a literature procedure.<sup>345</sup>

**2-28** (1.07 g, 3.66 mmol) and **2-27** (0.899 g, 3.66 mmol) were dissolved in EtOH (55 mL), and then heated at reflux for 18 hours. The resulting dark purple solution was allowed to cool to room temperature, then the solid

formed was isolated via Buchner filtration and washed with EtOH to give a dark green solid with an occasional metallic sheen (1.71 g, 3.31 mmol, 90%). The solid forms a dark red-purple solution when dissolved in ethanol, acetonitrile or DMSO. M.p. = 238-240 °C (dec.).

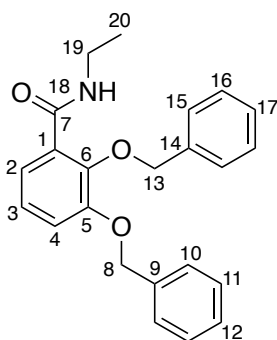
Characterisation data consistent with literature.<sup>345</sup>

**<sup>1</sup>H NMR:** (400 MHz, DMSO-d<sub>6</sub>) δ<sub>H</sub> ppm: 8.60 (1H, s, *H9*), 8.37 (1H, dd, *J* = 8.5, 1.0 Hz, *H21*), 8.21 (1H, d, *J* = 8.5 Hz, *H18*), 8.06-7.97 (2H, m, *H12 and 13*), 7.83 (1H, td, *J* = 7.5, 1.5 Hz, *H20*), 7.74 (1H, td, *J* = 7.0, 1.0 Hz, *H19*), 7.57 (1H, d, *J* = 9.5 Hz, *H6*), 6.87 (1H, dd, *J* = 9.0, 2.5 Hz, *H5*), 6.67 (1H, d, *J* = 2.5 Hz, *H4*), 4.21 (3H, s, *H15*), 3.52 (4H, q, *J* = 7.0 Hz, *H2*), 1.15 (6H, t, *J* = 7.0 Hz, *H1*).

**<sup>13</sup>C NMR:** (100 MHz, DMSO-d<sub>6</sub>) δ<sub>C</sub> ppm: 171.7 (*C14*), 159.6 (*C11*), 157.2 (*C7*), 153.3 (*C3*), 148.4 (*C9*), 144.4 (*C12*), 142.1 (*C17*), 131.8 (*C6*), 129.3 (*C20*), 128.2 (*C19*), 127.5 (*C16*), 124.2 (*C21*), 116.6 (*C18*), 112.0 (*C10*), 111.4 (*C13*), 110.9 (*C5*), 108.9 (*C8*), 96.5 (*C4*), 44.7 (*C2*), 35.9 (*C15*), 12.5 (*C1*).

**HRMS (ESI):** Calcd. [M]<sup>+</sup> (C<sub>23</sub>H<sub>23</sub>N<sub>2</sub>O<sub>2</sub>S) *m/z* = 391.1475; Obs. [M]<sup>+</sup> *m/z* = 391.1472, Mean err 1.1 ppm.

### 2,3-Bis(benzyloxy)-*N*-ethylbenzamide (2-31)



Molecular Formula: C<sub>23</sub>H<sub>23</sub>NO<sub>3</sub>

Molecular Mass: 361.44 g mol<sup>-1</sup>

Prepared according to a literature procedure.<sup>370</sup>

2,3-Bis(benzyloxy)benzoic acid NHS ester (**2-30**, 0.460 g, 1.06 mmol) was dissolved in THF (25 mL), then Et<sub>3</sub>N (0.185 mL, 1.33 mmol) and ethylamine (2 M in THF, 0.67 mL, 1.34 mmol) added and the reaction stirred under air for 72 hours, before the THF was removed under vacuum. The resulting oil was taken up in DCM (30 mL) and washed with 0.1 M aq. HCl (7.5 mL), saturated NaHCO<sub>3</sub> solution (7.5 mL) and H<sub>2</sub>O (3 x 10 mL). The organic layer was dried over MgSO<sub>4</sub>, and the solvent removed to give a golden oil (0.360 g, 0.996 mmol, 94%).

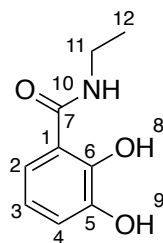
Characterisation data consistent with literature.<sup>370</sup>

**<sup>1</sup>H NMR:** (400 MHz, DMSO-d<sub>6</sub>) δ<sub>H</sub> ppm: 8.17 (1H, t, *J* = 5.5 Hz, *H18*), 7.52-7.25 (11H, m, *Ar H*), 7.14-7.01 (2H, m, *Ar H*), 5.20 (2H, s, *H8*), 5.01 (2H, s, *H13*), 3.20 (2H, dq, *J* = 7.0, 5.5 Hz, *H19*), 1.00 (3H, t, *J* = 7.0 Hz, *H20*).

**<sup>13</sup>C NMR:** (100 MHz, DMSO-d<sub>6</sub>) δ<sub>C</sub> ppm: 165.3 (*C7*), 151.2 (*C5*), 145.2 (*C6*), 137.1, 136.9 (*C13/17*), 131.1 (*C1*), 128.5, 128.4, 128.3, 128.1, 128.0, 127.8 (*C9-11, 14-16*), 124.2, 120.8, 115.8 (*C2/3/4*), 75.1 (*C13*), 70.2 (*C8*), 33.8 (*C19*), 14.5 (*C20*).

**HRMS (ESI):** Calcd. [M+H]<sup>+</sup> (C<sub>23</sub>H<sub>24</sub>NO<sub>3</sub>) *m/z* = 362.1751; Obs. [M+H]<sup>+</sup> *m/z* = 362.1751, Mean err 0.1 ppm. Calcd. [M+Na]<sup>+</sup> (C<sub>23</sub>H<sub>23</sub>NNaO<sub>3</sub>) *m/z* = 384.1570; Obs. [M+Na]<sup>+</sup> *m/z* = 384.1570, Mean err -0.3 ppm.

### ***N*-Ethyl-2,3-dihydroxybenzamide (**2-29**)**



Molecular Formula: C<sub>9</sub>H<sub>11</sub>NO<sub>3</sub>

Molecular Mass: 181.19 g mol<sup>-1</sup>

Prepared according to a literature procedure.<sup>370</sup> All glassware in use was

pre-soaked in 6 M HCl overnight before use in order to remove any iron adsorbed to surface of glassware.

**2-31** (0.28 g, 0.775 mmol) was dissolved in dry EtOH (45 mL), then two small spatula tips of 10% Pd-C added. Three balloons of H<sub>2</sub> gas were passed through the system to purge, then another balloon added to create a positive pressure of hydrogen. The reaction was stirred for 4 days under positive pressure, then the solution filtered twice through microfiber filters (Whatman, 47 mm) to remove the palladium. The solvent was removed under vacuum, and the resulting oil dried under vacuum for 6 hours to give a viscous orange-brown oil (0.121 g, 0.666 mmol, 86%). R<sub>f</sub> = 0.44 (4:1 DCM:EtOAc).

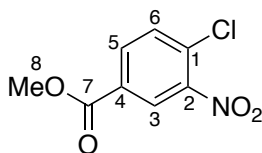
Characterisation data consistent with literature.<sup>370</sup>

**<sup>1</sup>H NMR:** (400 MHz, DMSO-d<sub>6</sub>) δ<sub>H</sub> ppm: 12.90 (1H, br s, *H8*), 9.13 (1H, br s, *H9*), 8.81 (1H, br t, *J* = 5.0 Hz, *H10*), 7.26 (1H, dd, *J* = 8.0, 1.0 Hz, *H2*), 6.89 (1H, dd, *J* = 8.0, 1.0 Hz, *H4*), 6.67 (1H, t, *J* = 8.0 Hz, *H3*), 3.33-3.28 (2H, m, overlap with H<sub>2</sub>O peak, *H11*), 1.13 (3H, t, *J* = 7.5 Hz, *H12*).

**<sup>13</sup>C NMR:** (100 MHz, DMSO-d<sub>6</sub>) δ<sub>C</sub> ppm: 169.6 (*C7*), 149.8 (*C6*), 146.2 (*C5*), 118.8 (*C4*), 117.9 (*C3*), 117.0 (*C2*), 114.9 (*C1*), 33.8 (*C11*), 14.5 (*C12*).

**HRMS (ESI):** Calcd. [M+H]<sup>+</sup> (C<sub>9</sub>H<sub>12</sub>NO<sub>3</sub>) *m/z* = 182.0812; Obs. [M+H]<sup>+</sup> *m/z* = 182.0811, Mean err -1.1 ppm. Calcd. [M+Na]<sup>+</sup> (C<sub>9</sub>H<sub>11</sub>NNaO<sub>3</sub>) *m/z* = 204.0631; Obs. [M+Na]<sup>+</sup> *m/z* = 204.0630, Mean err -4.5 ppm.

### Methyl 4-chloro-3-nitrobenzoate (**3-25**)



Molecular Formula: C<sub>8</sub>H<sub>6</sub>ClNO<sub>4</sub>

Molecular Mass: 215.59 g mol<sup>-1</sup>

Prepared according to a literature procedure.<sup>474</sup>

4-Chloro-3-nitrobenzoic acid (1.12 g, 5.58 mmol) was suspended in MeOH (8.5 mL) to give a cloudy white solution. Concentrated H<sub>2</sub>SO<sub>4</sub> (0.25 mL) was added to give a pale green-yellow solution, which was heated at reflux for 18 hours. The solution was allowed to cool to room temperature, before the solvent was removed under vacuum, giving a white crystalline mass. H<sub>2</sub>O (10 mL) was added, and extracted with EtOAc (3 x 15 mL). The combined organic layers were dried over MgSO<sub>4</sub> and the solvent removed to give **3-25** as a crystalline white solid (1.14 g, 5.26 mmol, 95%). Average yield = 96% (n = 3). M.p. = 78-80 °C (lit = 78-81 °C).<sup>423,657</sup>

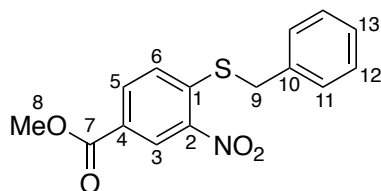
Characterisation data consistent with literature.<sup>474</sup>

**<sup>1</sup>H NMR:** (400 MHz, CDCl<sub>3</sub>) δ<sub>H</sub> ppm: 8.48 (1H, d, *J* = 2.0 Hz, *H*3), 8.14 (1H, dd, *J* = 8.5, 2.0 Hz, *H*5), 7.63 (1H, d, *J* = 2.0 Hz, *H*6), 3.95 (3H, s, *H*8).

**<sup>13</sup>C NMR:** (100 MHz, CDCl<sub>3</sub>) δ<sub>C</sub> ppm: 164.3 (*C*7), 147.9 (*C*2), 133.7 (*C*5), 132.3 (*C*6), 131.7 (*C*1), 130.1 (*C*4), 126.7 (*C*3), 53.0 (*C*8).

**HRMS (ESI):** Calcd. [M+H]<sup>+</sup> (C<sub>8</sub>H<sub>7</sub><sup>35</sup>ClNO<sub>4</sub>) *m/z* = 216.0058; Obs. [M+H]<sup>+</sup> *m/z* = 216.0055, Mean err -1.9 ppm.

### Methyl 4-(benzylsulfanyl)-3-nitrobenzoate (3-26)



Molecular Formula: C<sub>15</sub>H<sub>13</sub>NO<sub>4</sub>S

Molecular Mass: 303.33 g mol<sup>-1</sup>

Prepared according to a literature procedure.<sup>431</sup>

**3-25** (0.889 g, 4.12 mmol) was suspended in dry MeOH (4 mL) and cooled to 0 °C to give a cloudy white solution. Dry DIPEA (0.90 mL, 5.17 mmol) and benzyl mercaptan (0.60 mL, 5.11 mmol) were added, giving a cloudy orange solution. The mixture was allowed to heat to room temperature, and stirred for 22 hours, with the precipitate thickening over time. The precipitate was isolated by Buchner filtration, and washed with ice-cold MeOH (17.5 mL) and ice-cold hexane (40 mL) to give a lime green-yellow solid (1.15 g, 3.80 mmol, 91%). Average yield = 91% (n = 4). M.p. = 137-138 °C (lit. = 138-139 °C).<sup>423</sup>  
R<sub>f</sub> = 0.61 (DCM).

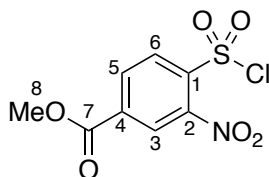
Characterisation data consistent with literature.<sup>431</sup>

**<sup>1</sup>H NMR:** (400 MHz, CDCl<sub>3</sub>) δ<sub>H</sub> ppm: 8.87 (1H, d, *J* = 2.0 Hz, *H*3), 8.14 (1H, dd, *J* = 8.5, 2.0 Hz, *H*5), 7.53 (1H, d, *J* = 8.5 Hz, *H*6), 7.45-7.41 (2H, m, *H*11 or 12), 7.38-7.29 (3H, m, *H*13 and *H*11 or 12), 4.25 (2H, s, *H*9), 3.95 (3H, s, *H*8).

**<sup>13</sup>C NMR:** (100 MHz, CDCl<sub>3</sub>) δ<sub>C</sub> ppm: 165.1 (*C*7), 145.2 (*C*2), 144.0 (*C*1), 134.3 (*C*10), 133.8 (*C*5), 129.2, 129.1 (*C*11/12), 128.2 (*C*13), 127.5 (*C*3), 126.8 (*C*4), 126.6 (*C*6), 52.8 (*C*8), 37.7 (*C*9).

**HRMS (ESI):** Calcd. [M+Na]<sup>+</sup> (C<sub>15</sub>H<sub>13</sub>NNaO<sub>4</sub>S) *m/z* = 326.0457; Obs. [M+Na]<sup>+</sup> *m/z* = 326.0459, Mean err 0.2 ppm. Calcd. [M+K]<sup>+</sup> (C<sub>15</sub>H<sub>13</sub>KNO<sub>4</sub>S) *m/z* = 342.0197; Obs. [M+K]<sup>+</sup> *m/z* = 342.0198, Mean err 0.1 ppm.

### Methyl 4-(chlorosulfonyl)-3-nitrobenzoate (3-27)



Molecular Formula: C<sub>8</sub>H<sub>6</sub>ClNO<sub>6</sub>S

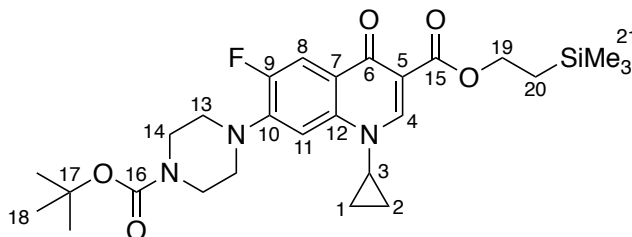
Molecular Mass: 279.65 g mol<sup>-1</sup>

**3-26** (0.304 g, 1.00 mmol) was placed under N<sub>2</sub> and dissolved in MeCN (5 mL), then AcOH (0.18 mL) and H<sub>2</sub>O (0.12 mL) were added and the cloudy yellow solution cooled to 0 °C. 1,3-Dichloro-5,5'-dimethylhydantoin (0.409 g, 2.08 mmol) was added in portions to give a clear yellow solution, which was stirred at 0 °C for 3 hours. The solvent was removed under vacuum, and the residue redissolved in DCM (25 mL). The resulting solution was cooled to 0 °C, then ice-cold saturated NaHCO<sub>3</sub> solution (25 mL) was added with stirring. The biphasic mixture was stirred for 20 minutes, then the layers partitioned and the organic layer washed with ice-cold brine (25 mL), dried over MgSO<sub>4</sub> and the solvent removed to give a yellow solid (0.363 g, c. 72% desired product by mass, 93%), which was used in the next step without any further purification.

Characterisation data consistent with literature.<sup>456</sup>

<sup>1</sup>H NMR: (400 MHz, CDCl<sub>3</sub>) δ<sub>H</sub> ppm: 8.48 (1H, d, *J* = 1.5 Hz, *H*3), 8.45 (1H, dd, *J* = 8.5, 1.5 Hz, *H*5), 8.34 (1H, d, *J* = 8.5 Hz, *H*6), 4.04 (3H, s, *H*8).

### 2-(Trimethylsilyl)ethyl 7-[4-[(*tert*-butoxy)carbonyl]piperazin-1-yl]-1-cyclopropyl-6-fluoro-4-oxo-1,4-dihydroquinoline-3-carboxylate (3-23)



Molecular Formula: C<sub>27</sub>H<sub>38</sub>FN<sub>3</sub>O<sub>5</sub>Si

Molecular Mass: 531.70 g mol<sup>-1</sup>

Boc ciprofloxacin (**3-22**, 0.613 g, 1.42 mmol) placed under N<sub>2</sub> then dissolved in dry DCM (45 mL). Trimethylsilylethanol (0.255 mL, 1.78 mmol), HBTU (1.35 g, 3.55 mmol), DMAP (17.3 mg, 0.142 mmol) and dry DIPEA (0.65 mL, 3.73 mmol) were added and the reaction was stirred at room temperature for 24 hours. Extra DCM (20 mL) was added, then the organic layer washed with 0.1 M aqueous formic acid (45 mL), H<sub>2</sub>O (45 mL), saturated NaHCO<sub>3</sub> solution (45 mL) and brine (45 mL), dried over MgSO<sub>4</sub> and the solvent removed. The resulting beige solid was purified by column chromatography (silica gel, 6.5:1 EtOAc:40-60 °C pet. ether) to give **3-23** as a pale yellow crystalline powder (0.640 g, est. 92% product by mass, 1.11 mmol, 78%).\*

\*<sup>19</sup>F NMR revealed presence of some remaining PF<sub>6</sub> salt, assumed to be NaPF<sub>6</sub>. This is accounted for in the final yield.

<sup>1</sup>H NMR: (400 MHz, CDCl<sub>3</sub>) δ<sub>H</sub> ppm: 8.44 (1H, s, H4), 7.90 (1H, d, <sup>3</sup>J<sub>F-H</sub> = 13.5 Hz, H8), 7.29 (1H, d, J = 6.5, 1.5 Hz, H11), 4.39-4.31 (2H, TMSE m, H19), 3.68-3.59 (4H, m, H14), 3.50-3.42 (1H, m, H3), 3.26-3.18 (4H, m, H13), 1.48 (9H, s, H18), 1.37-1.31 (2H, m, H1 or 2), 1.15-1.08 (2H, TMSE m, H20), 1.05-0.99 (2H, m, H1 or 2), 0.03 (9H, s, H21).

<sup>13</sup>C NMR: (100 MHz, CDCl<sub>3</sub>) δ<sub>C</sub> ppm: 174.0 (C6), 165.6 (C15), 154.8 (C16), 153.5 (d, <sup>1</sup>J<sub>F-C</sub> = 249 Hz, C9), 148.2 (C4), 144.9 (d, <sup>2</sup>J<sub>F-C</sub> = 10 Hz, C10), 138.2 (C12), 122.6 (d, <sup>3</sup>J<sub>F-C</sub> = 7 Hz, C7), 113.1 (d, <sup>2</sup>J<sub>F-C</sub> = 23 Hz, C8), 109.6 (C5), 105.3 (C11), 80.4 (C17), 63.2 (C19), 49.9 (C13), 44.3-42.5 (m, C14), 35.0 (C3), 28.5 (C18), 17.5 (C20), 8.2 (C1 and 2), 1.4 (C21).

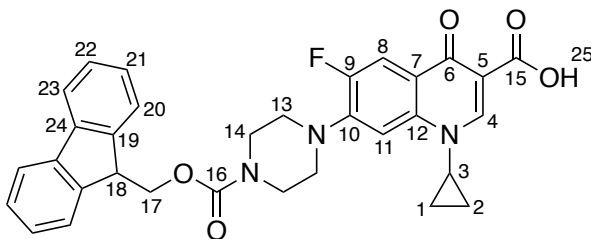
<sup>19</sup>F NMR: (376 MHz, CDCl<sub>3</sub>) δ<sub>F</sub> ppm: -123.15 (1F, br s).

Also presence of PF<sub>6</sub> salt: δ<sub>F</sub> ppm: -73.30 (1F, d, J = 712 Hz).

**HRMS (ESI):** Calcd. [M+H]<sup>+</sup> (C<sub>27</sub>H<sub>39</sub>FN<sub>3</sub>O<sub>5</sub>Si) m/z = 532.2638; Obs. [M+H]<sup>+</sup> m/z = 532.2647, Mean err -1.5 ppm. Calcd. [M+Na]<sup>+</sup> (C<sub>27</sub>H<sub>38</sub>FN<sub>3</sub>NaO<sub>5</sub>Si) m/z = 554.2457; Obs. [M+Na]<sup>+</sup> m/z = 554.2467, Mean err -1.5 ppm.



**1-Cyclopropyl-7-(4-[[[9H-fluoren-9-yl)methoxy]carbonyl]piperazin-1-yl]-6-fluoro-4-oxo-1,4-dihydroquinoline-3-carboxylic acid (3-38)**



Molecular Formula: C<sub>32</sub>H<sub>28</sub>FN<sub>3</sub>O<sub>5</sub>

Molecular Mass: 553.59 g mol<sup>-1</sup>

Ciprofloxacin (0.566 g, 1.71 mmol) was suspended in sodium carbonate solution (6.5 mL, 0.85 M solution, 9% w/v) and cooled to 0 °C. A solution of FmocOSu (0.707 g, 2.10 mmol) in DMF:dioxane (3:1, 10.5 mL) was added and the mixture was stirred vigorously for 20 minutes, then allowed to warm to room temperature. The resulting precipitate was filtered and washed with water (c. 50 mL), then taken up in 95:4.5:0.5 CHCl<sub>3</sub>:EtOH:AcOH and purified by column chromatography (silica gel, 80-90 g, 95:4.5:0.5 CHCl<sub>3</sub>:EtOH:AcOH) to give **3-38** as a white-cream solid (0.432 g, 0.781 mmol, 46%). Average yield = 39% (n = 2). R<sub>f</sub> = 0.46 (95:4.5:0.5 CHCl<sub>3</sub>:EtOH:AcOH).

**<sup>1</sup>H NMR:** (400 MHz, CDCl<sub>3</sub>) δ<sub>H</sub> ppm: 14.93 (1H, br s, H<sub>25</sub>), 8.78 (1H, s, H<sub>4</sub>), 8.05 (1H, d, <sup>3</sup>J<sub>F-H</sub> = 12.5 Hz, H<sub>8</sub>), 7.78 (2H, app. d, J = 7.5 Hz, H<sub>23</sub>), 7.59 (2H, app. d, J = 7.5 Hz, H<sub>20</sub>), 7.41 (2H, app. t, J = 7.5 Hz, H<sub>22</sub>), 7.38-7.30 (3H, m\*, H<sub>11</sub> and H<sub>21</sub>), 4.52 (2H, d, J = 6.5 Hz, H<sub>17</sub>), 4.27 (1H, t, J = 6.5 Hz, H<sub>18</sub>), 3.80-3.60 (4H, m, H<sub>14</sub>), 3.60-3.50 (1H, m, H<sub>3</sub>), 3.35-3.19 (4H, m, H<sub>13</sub>), 1.44-1.38 (2H, m, H<sub>1</sub> or H<sub>2</sub>), 1.24-1.10 (2H, m, H<sub>1</sub> or H<sub>2</sub>).

\*Overlapping d and dt

**<sup>13</sup>C NMR:** (100 MHz, CDCl<sub>3</sub>) δ<sub>C</sub> ppm: 177.30-177.27 (d, J = 3 Hz, C<sub>6</sub>), 167.1 (C<sub>15</sub>), 155.2 (C<sub>16</sub>), 153.8 (d, <sup>1</sup>J<sub>F-C</sub> = 251 Hz, C<sub>9</sub>), 147.7 (C<sub>4</sub>), 145.8 (d, <sup>2</sup>J<sub>F-C</sub> = 10 Hz, C<sub>10</sub>), 144.0 (C<sub>19</sub>), 141.5 (C<sub>24</sub>), 139.2 (C<sub>12</sub>), 127.9 (C<sub>22</sub>), 127.2 (C<sub>21</sub>), 125.0 (C<sub>20</sub>), 120.5 (d, <sup>3</sup>J<sub>F-C</sub> = 8 Hz, C<sub>7</sub>), 120.2 (C<sub>23</sub>), 112.9 (d, <sup>2</sup>J<sub>F-C</sub> = 24 Hz, C<sub>8</sub>),

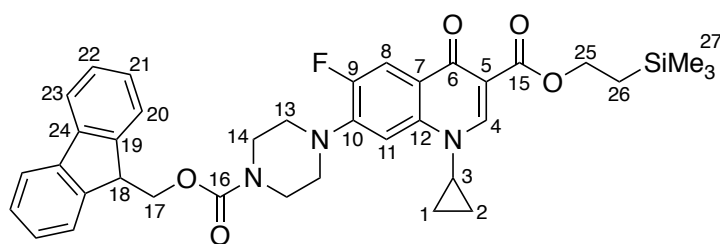
108.4 (C5), 105.2 (d,  $^3J_{F-C} = 3$  Hz, C11), 67.6 (C17), 49.8 (m, C13), 47.5 (C18), 43.8 (m, C14), 35.4 (C3), 8.4 (C1 and 2).

$^{19}\text{F}$  NMR: (376 MHz,  $\text{CDCl}_3$ )  $\delta_{\text{F}}$  ppm: -120.95 (1F, dd,  $J = 12.5, 6.5$  Hz).

**HRMS (ESI Pos.):** Calcd.  $[\text{M}+\text{Na}]^+$  ( $\text{C}_{32}\text{H}_{29}\text{FN}_3\text{O}_5$ )  $m/z = 554.2086$ ; Obs.  $[\text{M}+\text{H}]^+$   $m/z = 554.2079$ , Mean err 3.5 ppm. Calcd.  $[\text{M}+\text{Na}]^+$  ( $\text{C}_{32}\text{H}_{28}\text{FN}_3\text{NaO}_5$ )  $m/z = 576.1905$ ; Obs.  $[\text{M}+\text{Na}]^+$   $m/z = 576.1906$ , Mean err 1.3 ppm.

**HRMS (ESI Neg.):** Calcd.  $[\text{M}-\text{H}]^-$  ( $\text{C}_{32}\text{H}_{27}\text{FN}_3\text{O}_5$ )  $m/z = 552.1940$ ; Obs.  $[\text{M}-\text{H}]^-$   $m/z = 552.1923$ , Mean err 2.6 ppm.

**2-(Trimethylsilyl)ethyl-1-cyclopropyl-7-((9H-fluoren-9-yl)methoxy) carbonyl)piperazin-1-yl)-6-fluoro-4-oxo-1,4-dihydroquinoline-3-carboxylate (3-39)**



Molecular Formula:  $\text{C}_{37}\text{H}_{40}\text{FN}_3\text{O}_5\text{Si}$

Molecular Mass:  $653.83 \text{ g mol}^{-1}$

Fmoc ciprofloxacin (**3-38**, 0.257 g, 0.465 mmol) was placed under  $\text{N}_2$ , then dry DCM (20 mL) added. Trimethylsilyl ethanol (0.10 mL, 1.03 mmol), HBTU (0.444 g, 1.17 mmol), DMAP (5.5 mg, 0.045 mmol) and DIPEA (0.25 mL, 1.44 mmol) were added sequentially, and the reaction was stirred at room temperature for 24 hours. Extra DCM (20 mL) added, then washed with 1 M aq. HCl (20 mL),  $\text{H}_2\text{O}$  (2 x 20 mL) and brine (20 mL). The organic layer was dried over  $\text{MgSO}_4$  and the solvent removed to give a yellow oil. The product was purified by column chromatography (silica gel, c. 40 g, 6:1 EtOAc:40-60 °C pet. ether) to give a white crystalline powder (0.262 g, 0.401 mmol, 86%).\*  $R_f = 0.50$  (6:1 EtOAc:40-60 °C pet. ether).

\*<sup>19</sup>F NMR revealed presence of some remaining PF<sub>6</sub> salt, assumed to be NaPF<sub>6</sub>. This is accounted for in the final yield.

**<sup>1</sup>H NMR:** (400 MHz, CDCl<sub>3</sub>) δ<sub>H</sub> ppm: 8.47 (1H, s, *H4*), 7.97 (1H, d, <sup>3</sup>J<sub>F-H</sub> = 13.0 Hz, *H8*), 7.76 (2H, app. d, *J* = 7.5 Hz, *H23*), 7.59 (2H, app. d, *J* = 7.0 Hz, *H20*), 7.40 (2H, app. t, *J* = 7.5 Hz, *H22*), 7.33 (2H, td, *J* = 7.5, 1.5 Hz, *H21*), 7.31-7.28 (1H, m\*, *H11*), 4.48 (2H, d, *J* = 6.5 Hz, *H17*), 4.39 (2H, TMSE m, *H25*), 4.26 (1H, t, *J* = 6.5 Hz, *H18*), 3.75-3.65 (4H, m, *H14*), 3.50-3.43 (1H, m, *H3*), 3.28-3.18 (4H, m, *H13*), 1.38-1.32 (2H, m, *H1 or 2*), 1.15 (2H, TMSE m, *H17*), 1.09-1.02 (2H, m, *H1 or 2*), 0.06 (9H, s, *H18*).

\*d overlapping with dt

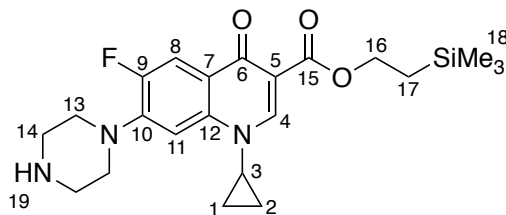
**<sup>13</sup>C NMR:** (100 MHz, CDCl<sub>3</sub>) δ<sub>C</sub> ppm: 173.9 (*C6*), 165.7 (*C15*), 155.3 (*C16*), 153.5 (d, <sup>1</sup>J<sub>F-C</sub> = 247 Hz, *C9*), 148.2 (*C4*), 144.7 (d, <sup>2</sup>J<sub>F-C</sub> = 10 Hz, *C10*), 144.0 (*C19*), 141.5 (*C24*), 138.2 (*C12*), 127.9 (*C22*), 127.2 (*C21*), 125.0 (*C20*), 122.9 (*C7*), 120.1 (*C23*), 113.3 (d, <sup>2</sup>J<sub>F-C</sub> = 23 Hz, *C8*), 109.7 (*C5*), 105.4 (*C11*), 67.7 (*C17*), 63.3 (*C25*), 49.8 (d, *J* = 3.5 Hz, *C13*), 47.4 (*C18*), 44.0-43.5 (m, *C14*), 34.9 (*C3*), 17.6 (*C26*), 8.3 (*C1 and 2*), 1.4 (*C27*).

**<sup>19</sup>F NMR:** (376 MHz, CDCl<sub>3</sub>) δ<sub>F</sub> ppm: -123.37 (1F, br s).

Also presence of PF<sub>6</sub> salt: δ<sub>F</sub> ppm: -73.00 (1F, d, *J* = 712 Hz).

**HRMS (ESI):** Calcd. [M+H]<sup>+</sup> (C<sub>37</sub>H<sub>41</sub>FN<sub>3</sub>O<sub>5</sub>Si) *m/z* = 654.2794; Obs. [M+H]<sup>+</sup> *m/z* = 654.2805, Mean err -1.6 ppm. Calcd. [M+Na]<sup>+</sup> (C<sub>37</sub>H<sub>40</sub>FN<sub>3</sub>NaO<sub>5</sub>Si) *m/z* = 676.2613; Obs. [M+Na]<sup>+</sup> *m/z* = 676.2625, Mean err -1.6 ppm.

**2-(Trimethylsilyl)ethyl-1-cyclopropyl-6-fluoro-4-oxo-7-(piperazin-1-yl)-1,4-dihydroquinoline-3-carboxylate (3-40)**



Molecular Formula: C<sub>22</sub>H<sub>30</sub>FN<sub>3</sub>O<sub>3</sub>Si

Molecular Mass: 431.58 g mol<sup>-1</sup>

**3-39** (0.128 g, 0.196 mmol) was dissolved in dry DCM (2.5 mL) and cooled to 0 °C. Piperidine (16.6% v/v, 0.50 mL) was added and the reaction was stirred at 0 °C for 90 minutes. Extra DCM (15 mL) was added and the solution washed with saturated aq. NH<sub>4</sub>Cl (15 mL). The DCM layer was dried over MgSO<sub>4</sub> and the solvent removed. The crude product was purified by column chromatography (silica gel, 18:2:1 CHCl<sub>3</sub>:MeOH:aq. NH<sub>3</sub>) to give **3-40** (57.7 mg, 0.134 mmol, 68%) as a beige solid. R<sub>f</sub> = 0.44 (9:1:1 CHCl<sub>3</sub>:MeOH:aq. NH<sub>3</sub>).

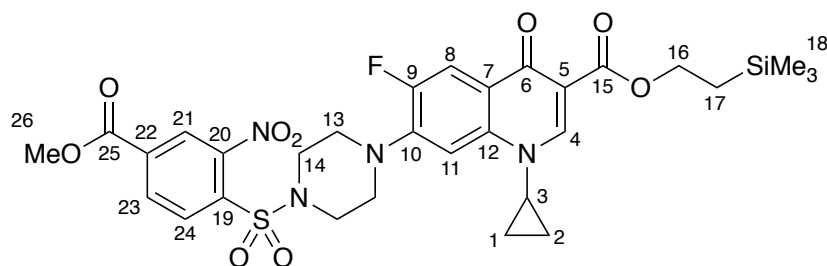
**<sup>1</sup>H NMR:** (400 MHz, CDCl<sub>3</sub>) δ<sub>H</sub> ppm: 8.51 (1H, s, H<sub>4</sub>), 8.04 (1H, d, <sup>3</sup>J<sub>F-H</sub> = 13.5 Hz, H<sub>8</sub>), 7.26 (1H, d, J = 7.0 Hz, H<sub>11</sub>), 4.40 (2H, TMSE m, H<sub>16</sub>), 3.46-3.38 (1H, m, H<sub>3</sub>), 3.25-3.21 (4H, m, H<sub>13</sub> or 14), 3.12-3.07 (4H, m, H<sub>13</sub> or 14), 1.34-1.28 (2H, m, H<sub>1</sub> or 2), 1.18 (2H, TMSE m, H<sub>17</sub>), 1.14-1.10 (2H, m, H<sub>1</sub> or 2), 0.07 (9H, s, H<sub>18</sub>).

**<sup>13</sup>C NMR:** (100 MHz, CDCl<sub>3</sub>) δ<sub>C</sub> ppm: 173.3 (C<sub>6</sub>), 166.1 (C<sub>15</sub>), 153.6 (d, <sup>1</sup>J<sub>F-C</sub> = 248 Hz, C<sub>9</sub>), 148.2 (C<sub>4</sub>), 145.1 (d, <sup>2</sup>J<sub>F-C</sub> = 11 Hz, C<sub>10</sub>), 138.2 (C<sub>12</sub>), 123.3 (d, <sup>3</sup>J<sub>F-C</sub> = 7 Hz, C<sub>7</sub>), 113.5 (d, <sup>2</sup>J<sub>F-C</sub> = 23 Hz, C<sub>8</sub>), 110.7 (C<sub>5</sub>), 104.8 (d, <sup>3</sup>J<sub>F-C</sub> = 3 Hz, C<sub>11</sub>), 63.2 (C<sub>16</sub>), 51.1 (d, <sup>4</sup>J<sub>F-C</sub> = 5 Hz, C<sub>13</sub>), 46.0 (C<sub>14</sub>), 34.6 (C<sub>3</sub>), 17.8 (C<sub>17</sub>), 8.3 (C<sub>1</sub> and 2), -1.4 (C<sub>18</sub>).

**<sup>19</sup>F NMR:** (376 MHz, CDCl<sub>3</sub>) δ<sub>F</sub> ppm: -123.61 (1F, dd, J = 13.5, 7.0 Hz).

**HRMS (ESI):** Calcd. [M+H]<sup>+</sup> (C<sub>22</sub>H<sub>31</sub>FN<sub>3</sub>O<sub>3</sub>Si) m/z = 432.2113; Obs. [M+H]<sup>+</sup> m/z = 432.2119, Mean err -1.3 ppm. Calcd. [M+Na]<sup>+</sup> (C<sub>22</sub>H<sub>30</sub>FN<sub>3</sub>NaO<sub>3</sub>Si) m/z = 454.1933; Obs. [M+Na]<sup>+</sup> m/z = 454.1940, Mean err -1.8 ppm.

**2-(Trimethylsilyl)ethyl 1-cyclopropyl-6-fluoro-7-{4-[4-(methoxycarbonyl)-2-nitrobenzenesulfonyl]piperazin-1-yl}-4-oxo-1,4-dihydroquinoline-3-carboxylate (3-28)**



Molecular Formula: C<sub>30</sub>H<sub>35</sub>FN<sub>4</sub>O<sub>9</sub>SSi

Molecular Mass: 674.77 g mol<sup>-1</sup>

**3-40** (46.6 mg, 0.108 mmol) was placed under N<sub>2</sub>, then dissolved in dry DCM (5 mL). The solution was cooled to 0 °C, then **3-27** (38.3 mg, 0.137 mmol) and lutidine (27 μL, 0.232 mmol) added and the reaction allowed to warm to room temperature. The clear yellow solution was stirred for 72 hours, then extra DCM (5 mL) and water (10 mL) were added and the organic layer separated. The aqueous layer was extracted with DCM (2 x 8 mL), then the combined organic layers were washed with 1 M aq. HCl (15 mL), water (12.5 mL), saturated NaHCO<sub>3</sub> solution (12.5 mL) and brine (12.5 mL), dried over MgSO<sub>4</sub> and the DCM removed *in vacuo*. The resulting residue was purified by column chromatography (silica gel, gradient: 3:1 EtOAc:40-60 °C pet. ether to 100% EtOAc) to give a yellow white solid (40.9 mg, est. 94% product by mass, 0.057 mmol, 53%). R<sub>f</sub> = 0.40 (5:1 EtOAc:40-60 °C pet. ether).

**<sup>1</sup>H NMR:** (400 MHz, CDCl<sub>3</sub>) δ<sub>H</sub> ppm: 8.52 (1H, s, H<sub>4</sub>), 8.34 (1H, dd, *J* = 8.5, 1.5 Hz, H<sub>23</sub>), 8.28 (1H, d, *J* = 1.5 Hz, H<sub>21</sub>), 8.10 (1H, d, *J* = 8.0 Hz, H<sub>24</sub>), 8.06 (1H, d, <sup>3</sup>*J*<sub>F-H</sub> = 13.0 Hz, H<sub>8</sub>), 7.28 (1H, d, *J* = 7.0 Hz, H<sub>11</sub>), 4.40 (2H, TMSE m, H<sub>16</sub>), 4.01 (3H, s, H<sub>26</sub>), 3.58-3.53 (4H, m, H<sub>14</sub>), 3.45-3.38 (1H, m, H<sub>3</sub>), 3.36-3.31 (4H, m, H<sub>13</sub>), 1.37-1.29 (2H, m, H<sub>1</sub> or 2), 1.17 (2H, TMSE m, H<sub>17</sub>), 1.17-1.10 (2H, m, H<sub>1</sub> or 2), 0.06 (9H, s, H<sub>18</sub>).

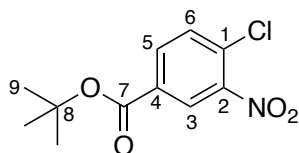
**<sup>13</sup>C NMR:** (100 MHz, CDCl<sub>3</sub>) δ<sub>C</sub> ppm: 173.2 (C<sub>6</sub>), 166.0 (C<sub>15</sub>), 163.7 (C<sub>25</sub>), 153.4 (d, <sup>1</sup>*J*<sub>F-C</sub> = 267 Hz, C<sub>9</sub>), 148.5 (C<sub>20</sub>), 148.4 (C<sub>4</sub>), 143.8 (d, <sup>2</sup>*J*<sub>F-C</sub> = 11 Hz, C<sub>10</sub>), 138.1 (C<sub>12</sub>), 135.6 (C<sub>22</sub>), 134.8 (C<sub>19</sub>), 132.5 (C<sub>23</sub>), 131.5 (C<sub>24</sub>), 125.4

(C19), 124.1 (d,  $^3J_{F-C} = 7$  Hz, C7), 113.8 (d,  $^2J_{F-C} = 22$  Hz, C8), 110.0 (C5), 105.5 (d,  $^3J_{F-C} = 2$  Hz, C11), 63.4 (C16), 53.5 (C26), 50.0 (d,  $^4J_{F-C} = 5$  Hz, C13), 46.1 (C14), 34.6 (C3), 17.8 (C17), 8.3 (C1 and 2), -1.4 (C18).

$^{19}\text{F}$  NMR: (376 MHz,  $\text{CDCl}_3$ )  $\delta_{\text{F}}$  ppm: -124.31 (1F, dd,  $J = 13.0, 7.0$  Hz).

**HRMS (ESI):** Calcd.  $[\text{M}+\text{H}]^+$  ( $\text{C}_{30}\text{H}_{36}\text{FN}_4\text{O}_9\text{SSi}$ )  $m/z = 675.1951$ ; Obs.  $[\text{M}+\text{H}]^+$   $m/z = 675.1947$ , Mean err 0.1 ppm. Calcd.  $[\text{M}+\text{Na}]^+$  ( $\text{C}_{30}\text{H}_{35}\text{FN}_4\text{NaO}_9\text{SSi}$ )  $m/z = 697.1770$ ; Obs.  $[\text{M}+\text{Na}]^+$   $m/z = 697.1765$ , Mean err 0.5 ppm. Calcd.  $[\text{M}+\text{K}]^+$  ( $\text{C}_{30}\text{H}_{35}\text{FKN}_4\text{O}_9\text{SSi}$ )  $m/z = 713.1510$ ; Obs.  $[\text{M}+\text{Na}]^+$   $m/z = 713.1504$ , Mean err -1.0 ppm.

### ***tert*-Butyl 4-chloro-3-nitrobenzoate (3-43)**



Molecular Formula:  $\text{C}_{11}\text{H}_{12}\text{ClNO}_4$

Molecular Mass:  $257.67 \text{ g mol}^{-1}$

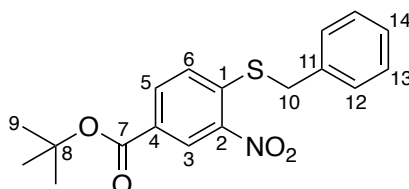
4-Chloro-3-nitrobenzoic acid (1.50 g, 7.43 mmol) was placed under  $\text{N}_2$  and dissolved in dry DCM (50 mL) to give a cloudy white solution. *tert*-Butyl alcohol (0.80 mL, 8.37 mmol) and DMAP (89.7 mg, 0.734 mmol) were added and the reaction cooled to  $0^\circ\text{C}$ . EDC.HCl (1.57 g, 8.18 mmol) was added, giving a clear yellow-green solution after 5 minutes. The solution was allowed to warm to room temperature and stirred for 18 hours, then the solvent removed under vacuum; the resulting oil was redissolved in the minimum amount of DCM and purified by column chromatography (silica gel, 7:1 40-60  $^\circ\text{C}$  pet. ether:EtOAc) to give **3-43** (1.00 g, 3.89 mmol, 52%) as a white crystalline solid. M.p. =  $68^\circ\text{C}$  (lit =  $70\text{-}71^\circ\text{C}$ ).<sup>658</sup>  $R_f = 0.47$  (7:1 40-60  $^\circ\text{C}$  pet. ether:EtOAc); 0.78 (DCM).

Characterisation data consistent with literature.<sup>658</sup>

**<sup>1</sup>H NMR:** (400 MHz, CDCl<sub>3</sub>) δ<sub>H</sub> ppm: 8.42 (1H, d, *J* = 2.0 Hz, *H*3), 8.10 (1H, dd, *J* = 8.5, 2.0 Hz, *H*5), 7.61 (1H, d, *J* = 8.5 Hz, *H*6), 1.60 (9H, s, *H*9).

**<sup>13</sup>C NMR:** (100 MHz, CDCl<sub>3</sub>) δ<sub>C</sub> ppm: 162.9 (*C*7), 148.0 (*C*2), 133.6 (*C*5), 132.1 (*C*4), 132.0 (*C*6), 131.2 (*C*1), 126.5 (*C*3), 83.2 (*C*8), 28.2 (*C*9).

***tert*-Butyl 4-(benzylsulfanyl)-3-nitrobenzoate (3-44)**



Molecular Formula: C<sub>18</sub>H<sub>19</sub>NO<sub>4</sub>S

Molecular Mass: 345.41 g mol<sup>-1</sup>

**3-43** (0.471 g, 1.83 mmol) was placed under N<sub>2</sub>, then dissolved in dry MeOH (4 mL), and cooled to 0 °C. Benzyl mercaptan (0.240 mL, 2.04 mmol) and dry DIPEA (0.385 mL, 2.21 mmol) were added. The reaction was allowed to warm to room temperature and stirred for 18 hours. A yellow precipitate crashes out after around two hours; extra MeOH may be added to allow stirring to continue. The precipitate was isolated by Buchner filtration, and washed with ice-cold MeOH (10 mL), followed by ice-cold hexane (30 mL) to give a lime green-yellow solid (0.518 g, 1.50 mmol, 82%). Average yield = 71% (*n* = 5). M.p. = 118-119 °C. R<sub>f</sub> = 0.73 (DCM).

Analytical sample obtained via column chromatography, gradient: 9:1 40-60 °C pet. ether:EtOAc to 4:1 40-60 °C pet. ether:EtOAc.

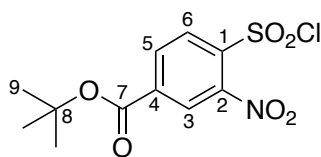
**<sup>1</sup>H NMR:** (400 MHz, CDCl<sub>3</sub>) δ<sub>H</sub> ppm: 8.77 (1H, d, *J* = 2.0 Hz, *H*3), 8.08 (1H, dd, *J* = 8.5, 2.0 Hz, *H*5), 7.49 (1H, d, *J* = 8.5 Hz, *H*6), 7.45-7.40 (2H, m, *H*12 or 13), 7.38-7.28 (3H, m, *H*14 and *H*12 or 13), 4.24 (2H, s, *H*10), 1.60 (9H, s, *H*9).

**<sup>13</sup>C NMR:** (100 MHz, CDCl<sub>3</sub>) δ<sub>C</sub> ppm: 163.7 (*C*7), 145.2 (*C*2), 143.2 (*C*1), 134.5 (*C*11), 133.7 (*C*5), 129.2, 129.1 (*C*12/13), 128.8 (*C*4), 128.1 (*C*14), 127.2 (*C*3), 126.5 (*C*6), 82.5 (*C*8), 37.7 (*C*10), 28.3 (*C*9).

**HRMS (ESI):** Calcd.  $[M+NH_4]^+$  ( $C_{18}H_{23}N_2O_4S$ )  $m/z = 363.1373$ ; Obs.  $[M+NH_4]^+$   $m/z = 363.1369$ , Mean err 3.2 ppm. Calcd.  $[M+Na]^+$  ( $C_{18}H_{19}NNaO_4S$ )  $m/z = 368.0927$ ; Obs.  $[M+Na]^+$   $m/z = 368.0924$ , Mean err 0.3 ppm.

**IR (ATIR,  $cm^{-1}$ ):** 3000-2750 (C-H stretching, w), 1716 (ester C=O stretch, s), 1702 (ester C=O stretch, s), 1605 (C=C stretch, m), 1550 (N=O/C=C stretches, m), 1521 (N=O/C=C stretches, m), 1497 (N=O/C=C stretches, m).

***tert*-Butyl 4-(chlorosulfonyl)-3-nitrobenzoate (3-45)**



Molecular Formula:  $C_{11}H_{12}ClNO_6S$

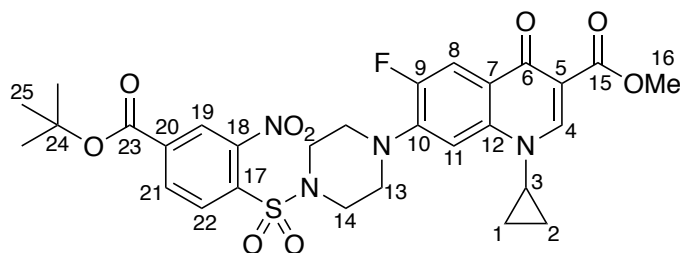
Molecular Mass:  $321.73 \text{ g mol}^{-1}$

**3-44** (0.341 g, 0.986 mmol) was placed under  $N_2$  and dissolved in MeCN (5 mL), then 3:2 AcOH:H<sub>2</sub>O (0.32 mL) added and the cloudy yellow solution cooled to 0 °C. 1,3-Dichloro-5,5'-dimethylhydantoin (0.397 g, 2.01 mmol) added in portions to give a clear yellow solution, which was stirred at 0 °C for 2.5 hours. The solvent was removed under vacuum, and the residue redissolved in dry DCM (20 mL). The resulting solution was cooled to 0 °C, then ice-cold saturated  $NaHCO_3$  solution (15 mL) was added with stirring. The biphasic mixture was stirred for 25 minutes, then the layers partitioned and the organic layers washed with ice-cold brine (16 mL), dried over  $MgSO_4$  and the solvent removed to give a viscous yellow green oil (0.373 g, c. 73% desired product by mass, 86%).

**$^1H$  NMR:** (400 MHz,  $CDCl_3$ )  $\delta_H$  ppm: 8.40-8.37 (2H, m, *H3 and 5*), 8.30 (1H, d,  $J = 8.5 \text{ Hz}$ , *H6*), 1.63 (9H, s, *H9*).



**Methyl 7-(4-{4-[(*tert*-butoxy)carbonyl]-2-nitrobenzenesulfonyl}piperazin-1-yl)-1-cyclopropyl-6-fluoro-4-oxo-1,4-dihydroquinoline-3-carboxylate (3-47)**



Molecular Formula: C<sub>29</sub>H<sub>31</sub>FN<sub>4</sub>O<sub>9</sub>S

Molecular Mass: 630.64 g mol<sup>-1</sup>

**3-45** (0.814 g, est. 73% SO<sub>2</sub>Cl by mass, 1.86 mmol) was placed under N<sub>2</sub>, then dissolved in dry DCM (45 mL). The solution was cooled to 0 °C, then ciprofloxacin methyl ester (**3-46**, 0.600 g, 1.74 mmol) and Et<sub>3</sub>N (0.37 mL, 2.62 mmol) added and the resulting clear yellow solution allowed to warm to room temperature, and stirred for 18 hours. Extra DCM (20 mL) and water (50 mL) were added and the organic layer separated. The aqueous layer was extracted with DCM (2 x 35 mL), then the combined organic layers were washed with 1 M aq. HCl (55 mL), water (50 mL), saturated NaHCO<sub>3</sub> solution (55 mL) and brine (50 mL), dried over MgSO<sub>4</sub> and the DCM removed *in vacuo* to give a bubbly yellow solid (1.14 g, est. 89% product by mass, 1.61 mmol, 86%). The product was used for future reaction steps with no further purification. R<sub>f</sub> = 0.22 (EtOAc).

**<sup>1</sup>H NMR:** (400 MHz, CDCl<sub>3</sub>) δ<sub>H</sub> ppm: 8.57 (1H, s, H<sub>4</sub>), 8.28 (1H, dd, J = 8.0, 1.5 Hz, H<sub>21</sub>), 8.19 (1H, d, J = 1.5 Hz, H<sub>19</sub>), 8.08 (1H, d, <sup>3</sup>J<sub>F-H</sub> = 13.0 Hz, H<sub>8</sub>), 8.07 (1H, d, J = 8.0 Hz, H<sub>22</sub>)\*, 7.30-7.28 (1H, m, H<sub>11</sub>)\*\*, 3.92 (3H, s, H<sub>16</sub>), 3.57-3.52 (4H, m, H<sub>14</sub>), 3.46-3.39 (1H, m, H<sub>3</sub>), 3.37-3.30 (4H, m, H<sub>13</sub>), 1.62 (9H, s, H<sub>25</sub>), 1.38-1.31 (2H, m, H<sub>1</sub> or 2), 1.17-1.12 (2H, m, H<sub>1</sub> or 2).

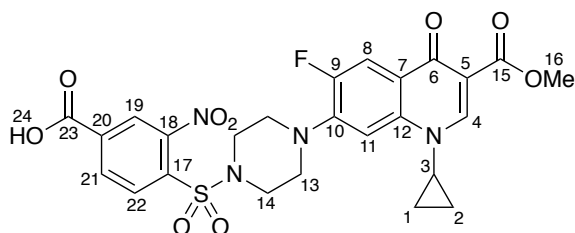
\*Doublets at 8.08 and 8.07 overlap

\*\*Overlaps with *N*-benzyl acetamide and benzyl chloride aromatics

**<sup>19</sup>F NMR:** (376 MHz, CDCl<sub>3</sub>) δ<sub>F</sub> ppm: -124.05 (1F, dd, *J* = 13.0, 7.0 Hz).

**HRMS (ESI):** Calcd. [M+H]<sup>+</sup> (C<sub>29</sub>H<sub>32</sub>FN<sub>4</sub>O<sub>9</sub>S) *m/z* = 631.1869; Obs. [M+H]<sup>+</sup> *m/z* = 631.1870, Mean err -0.3 ppm. Calcd. [M+Na]<sup>+</sup> (C<sub>29</sub>H<sub>31</sub>FN<sub>4</sub>NaO<sub>9</sub>S) *m/z* = 653.1688; Obs. [M+Na]<sup>+</sup> *m/z* = 653.1689, Mean err -0.7 ppm.

**4-({4-[1-Cyclopropyl-6-fluoro-3-(methoxycarbonyl)-4-oxo-1,4-dihydroquinolin-7-yl]piperazin-1-yl}sulfonyl)-3-nitrobenzoic acid (3-48)**



Molecular Formula: C<sub>25</sub>H<sub>23</sub>FN<sub>4</sub>O<sub>9</sub>S

Molecular Mass: 574.54 g mol<sup>-1</sup>

**3-47** (0.453 g, est. 89% product by mass, 0.640 mmol) was dissolved in dry DCM (15 mL) to give a clear yellow solution, then trifluoroacetic acid (5 mL) was added. The resulting clear orange solution was stirred for 4 hours, then the solvent was removed under vacuum. DCM (7 x 30 mL) was added and removed under vacuum, resulting in a yellow-orange solid. This was ground into a powder, and triturated in 10% v/v MeOH in Et<sub>2</sub>O (135 mL) with sonication for 45 minutes at 30 °C. The resulting beige powdery solid was isolated by Buchner filtration and washed with 10% v/v MeOH in Et<sub>2</sub>O (50 mL) and dried under vacuum to give 0.263 g of **3-48** (0.458 mmol, 72%). Over three steps from thioether **3-44**, the yield of **3-48** was 52%. M.p. = 201-204 °C (dec.). R<sub>f</sub> = 0.18 (90:10:1 CHCl<sub>3</sub>:MeOH:AcOH).

**<sup>1</sup>H NMR:** (400 MHz, DMSO-d<sub>6</sub>) δ<sub>H</sub> ppm: 8.46-8.43 (2H, m, *H4 and H19*), 8.33 (1H, dd, *J* = 8.0, 1.5 Hz, *H21*), 8.18 (1H, d, *J* = 8.0 Hz, *H22*), 7.77 (1H, d, <sup>3</sup>*J*<sub>F-H</sub> = 13.5 Hz, *H8*), 7.47 (1H, d, <sup>4</sup>*J*<sub>F-H</sub> = 7.0 Hz, *H11*), 3.73 (3H, s, *H16*), 3.67-3.59 (1H, m, *H3*), 3.48-3.42 (4H, m, *H13 or 14*), 3.34 (4H, m\*, *H13 or 14*), 1.30-1.22 (2H, m, *H1 or 2*), 1.12-1.04 (2H, m, *H1 or 2*).

\*Overlaps with H<sub>2</sub>O peak

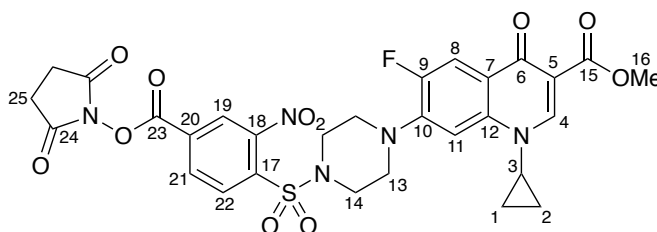
**<sup>13</sup>C NMR:** (100 MHz, DMSO-d<sub>6</sub>) δ<sub>C</sub> ppm: 171.7 (C6), 165.0 (C15), 164.7 (C23), 152.7 (d, <sup>1</sup>J<sub>F-C</sub> = 247 Hz, C9), 148.5 (C4), 148.0 (C18), 143.2 (d, <sup>2</sup>J<sub>F-C</sub> = 11 Hz, C10), 138.1 (C12), 137.2 (C20), 132.8 (C21), 132.3 (C17), 131.2 (C22), 124.9 (C19), 122.5 (d, <sup>3</sup>J<sub>F-C</sub> = 7 Hz, C7), 111.7 (d, <sup>2</sup>J<sub>F-C</sub> = 22 Hz, C8), 109.1 (C5), 107.2 (C11), 51.4 (C16), 49.3 (C13 or 14), 45.6 (C13 or 14), 34.9 (C3), 7.6 (C1 and 2).

**<sup>19</sup>F NMR:** (376 MHz, DMSO-d<sub>6</sub>) δ<sub>F</sub> ppm: -124.64 (1F, dd, J = 13.5, 7.5 Hz).

**HRMS (ESI):** Calcd. [M+H]<sup>+</sup> (C<sub>25</sub>H<sub>24</sub>FN<sub>4</sub>O<sub>9</sub>S) *m/z* = 575.1243; Obs. [M+H]<sup>+</sup> *m/z* = 575.1248, Mean err -0.9 ppm. Calcd. [M+Na]<sup>+</sup> (C<sub>25</sub>H<sub>23</sub>FN<sub>4</sub>NaO<sub>9</sub>S) *m/z* = 597.1062; Obs. [M+Na]<sup>+</sup> *m/z* = 597.1064, Mean err -0.6 ppm.

**IR (ATIR, cm<sup>-1</sup>):** 3450 (OH stretch, w br), 3100-2750 (C-H stretching, w), 1718 (ester C=O stretch, s), 1695 (carboxylic acid C=O stretch, s), 1620 (C=O quinolone stretch, s), 1547 (N=O/C=C stretches, s), 1492 (N=O/C=C stretches, s), 1480 (N=O/C=C stretches, s), 1364 (S=O stretch, s), 1168 (S=O stretch, s).

**Methyl 1-cyclopropyl-7-[4-(4-[[2,5-dioxopyrrolidin-1-yl]oxy]carbonyl)-2-nitrobenzenesulfonyl]piperazin-1-yl]-6-fluoro-4-oxo-1,4-dihydroquinoline-3-carboxylate (3-50)**



Molecular Formula: C<sub>29</sub>H<sub>26</sub>FN<sub>5</sub>O<sub>11</sub>S

Molecular Mass: 671.61 g mol<sup>-1</sup>

**3-48** (0.106 g, 0.184 mmol) was placed under N<sub>2</sub>, then suspended in dry DCM (8 mL), giving a cloudy white solution. *N*-Hydroxysuccinimide (27 mg, 0.234 mmol) and EDC.HCl (45 mg, 0.236 mmol) were added and the now clear yellow solution stirred for 21 hours at room temperature. A further portion of DCM (15 mL) was added, then the solution was washed with 1 M aq. HCl (12 mL), H<sub>2</sub>O (12 mL), and brine (12 mL), dried over MgSO<sub>4</sub>, and the solvent

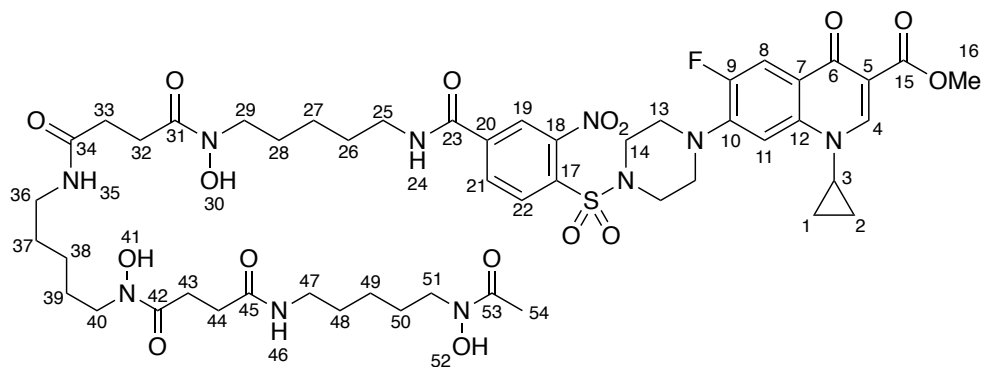
removed to give a yellow bubbly solid (0.122 g). Due to its instability, the product was used without further purification.

**<sup>1</sup>H NMR:** (400 MHz, CDCl<sub>3</sub>) δ<sub>H</sub> ppm: 8.57 (1H, s, H<sub>4</sub>), 8.44 (1H, dd, *J* = 8.0, 1.5 Hz, H<sub>21</sub>), 8.38 (1H, d, *J* = 1.5 Hz, H<sub>19</sub>), 8.21 (1H, d, *J* = 8.0 Hz, H<sub>22</sub>), 8.08 (1H, d, <sup>3</sup>*J*<sub>F-H</sub> = 13.0 Hz, H<sub>8</sub>), 7.29 (1H, d, <sup>4</sup>*J*<sub>F-H</sub> = 7.0 Hz, H<sub>11</sub>), 3.92 (3H, s, H<sub>16</sub>), 3.61-3.56 (4H, m, H<sub>14</sub>), 3.47-3.40 (1H, m, H<sub>3</sub>), 3.36-3.30 (4H, m, H<sub>13</sub>), 2.95 (4H, br s, H<sub>25</sub>), 1.38-1.31 (2H, m, H<sub>1</sub> or 2), 1.17-1.11 (2H, m, H<sub>1</sub> or 2).

**<sup>19</sup>F NMR:** (376 MHz, CDCl<sub>3</sub>) δ<sub>F</sub> ppm: -123.97 (1F, dd, *J* = 13.0, 7.0 Hz).

**HRMS (ESI):** Calcd. [M+H]<sup>+</sup> (C<sub>29</sub>H<sub>27</sub>FN<sub>5</sub>O<sub>11</sub>S) *m/z* = 672.1406; Obs. [M+H]<sup>+</sup> *m/z* = 672.1396, Mean err 0.3 ppm. Calcd. [M+Na]<sup>+</sup> (C<sub>29</sub>H<sub>26</sub>FN<sub>5</sub>NaO<sub>11</sub>S) *m/z* = 694.1226; Obs. [M+Na]<sup>+</sup> *m/z* = 694.1211, Mean err 1.6 ppm.

**Methyl 1-cyclopropyl-6-fluoro-7-[4-(4-[[5-(*N*-hydroxy-3-[[5-(*N*-hydroxy-3-[[5-(*N*-hydroxyacetamido)pentyl]carbamoyl]propanamido)pentyl]carbamoyl]propanamido)pentyl]carbamoyl]-2-nitrobenzenesulfonyl]piperazin-1-yl]-4-oxo-1,4-dihydroquinoline-3-carboxylate (3-49)**



Molecular Formula: C<sub>50</sub>H<sub>69</sub>FN<sub>10</sub>O<sub>16</sub>S

Molecular Mass: 1117.21 g mol<sup>-1</sup>

**3-50** (0.119 g, 0.178 mmol) dissolved in dry DMF (20 mL), then desferrioxamine mesylate (0.114 g, 0.173 mmol) and triethylamine (75 μL, 0.538 mmol) were added. The resulting cloudy white-yellow solution was heated to 50 °C for 24 hours, then allowed to cool to room temperature and the solvent removed *in vacuo*. MeCN (45 mL) was added, and the mixture

sonicated for 40 minutes at 40 °C, then transferred to a Falcon tube and centrifuged for 10 minutes (4400 rpm). The solvent was removed carefully via syringe, then further MeCN (35 mL) was added and the mixture sonicated for a further 30 minutes at 40 °C. After further centrifugation (10 minutes, 4400 rpm), the solvent was again removed via syringe, and the product left to dry in air to give **3-49** as a yellow solid. The product was used without further purification. M.p. = 165-169 °C (dec.).

**<sup>1</sup>H NMR:** (400 MHz, DMSO-d<sub>6</sub>) δ<sub>H</sub> ppm: 9.71 (1H, br s, H30 or 41 or 52), 9.67 (1H, br s, H30 or 41 or 52), 9.66 (1H, br s, H30 or 41 or 52), 8.87 (1H, br t, *J* = 5.5 Hz, H24), 8.45 (1H, s, H4), 8.37 (1H, d, *J* = 1.5 Hz, H19), 8.25 (1H, dd, *J* = 8.5, 1.5 Hz, H21), 8.17 (1H, d, *J* = 8.5 Hz, H22), 7.85-7.72 (3H, m, H8/35/46), 7.47 (1H, d, <sup>4</sup>*J*<sub>F-H</sub> = 7.5 Hz, H11), 3.72 (3H, s, H16), 3.67-3.60 (1H, m, H3), 3.58-3.36 (10H, m, H29/40/51 and H13 or 14), 3.36-3.30 (4H, m, H13 or 14), 3.27 (2H, app. q, *J* = 6.0 Hz, H25), 3.05-2.93 (4H, m, H36 and 47), 2.57 (4H, t, *J* = 7.0 Hz, H32 and 43), 2.26 (4H, t, *J* = 7.0 Hz, H33 and 44), 1.96 (3H, s, H54), 1.60-1.43 (8H, m, H26/28/39/50), 1.43-1.31 (4H, m, H37 and 48), 1.31-1.14 (8H, m, H27/38/49 and H1 or 2), 1.14-1.02 (2H, m, H1 or 2).

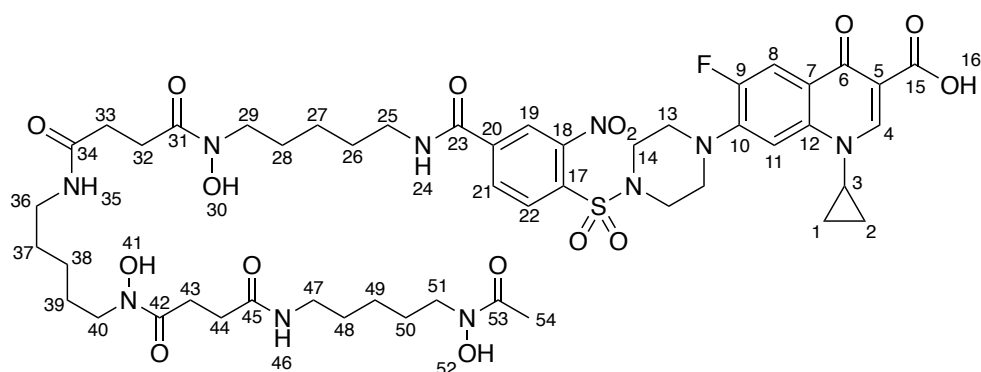
**<sup>13</sup>C NMR:** (100 MHz, DMSO-d<sub>6</sub>) δ<sub>C</sub> ppm: 172.1 (C31 and 42), 171.8 (C6), 171.5 (C34 and 45), 170.3 (C53), 165.1 (C15), 163.1 (C23), 152.7 (d, <sup>1</sup>*J*<sub>F-C</sub> = 247 Hz, C9), 148.6 (C4), 147.9 (C18), 143.3 (d, <sup>2</sup>*J*<sub>F-C</sub> = 10 Hz, C10), 140.3 (C20), 138.1 (C12), 131.0, 130.9 (C17/21/22), 123.1 (C19), 122.5 (d, <sup>3</sup>*J*<sub>F-C</sub> = 7 Hz, C7), 111.7 (d, <sup>2</sup>*J*<sub>F-C</sub> = 24 Hz, C8), 109.1 (C5), 107.2 (C11), 51.4 (C16), 49.4 (C13 or 14), 47.2, 46.9 (C29/40/51), 45.7 (C13 or 14), 40.1 (C25), 38.5 (C36 and 47), 34.9 (C3), 30.0 (C33 and 44), 28.9 (C37 and 48), 28.6 (C26), 27.7 (C32 and 43), 26.1 (C28/39/50), 23.6 (C27/38/49), 20.5 (C54), 7.7 (C1 and 2).

Some desferrioxamine NMR assignments are partially based on those made by Richardson-Sanchez *et al.*<sup>493</sup>

**HRMS (ESI):** Calcd. [M+H]<sup>+</sup> (C<sub>50</sub>H<sub>70</sub>FN<sub>10</sub>O<sub>16</sub>S) *m/z* = 1117.4671; Obs. [M+H]<sup>+</sup> *m/z* = 1117.4746, Mean err -3.8 ppm. Calcd. [M+Na]<sup>+</sup> (C<sub>50</sub>H<sub>69</sub>FN<sub>10</sub>NaO<sub>16</sub>S) *m/z* = 1139.4490; Obs. [M+Na]<sup>+</sup> *m/z* = 1139.4508, Mean err -1.5 ppm.

**IR (ATIR, cm<sup>-1</sup>):** 3500-3150 (OH/NH stretches, m br), 3100-2750 (C-H stretching, m), 1723 (ester C=O stretch, w), 1618 (C=O amide and quinolone stretches, br s), 1547 (N=O/C=C stretches, s), 1459 (N=O/C=C stretches, m), 1369 (S=O stretch, m), 1162 (S=O stretch, m).

**1-Cyclopropyl-6-fluoro-7-[4-(4-[[5-(N-hydroxy-3-[[5-(N-hydroxy-3-[[5-(N-hydroxyacetamido)pentyl]carbamoyl]propanamido)pentyl]carbamoyl]propanamido)pentyl]carbamoyl]-2-nitrobenzenesulfonyl)piperazin-1-yl]-4-oxo-1,4-dihydroquinoline-3-carboxylic acid (3-14)**



Molecular Formula: C<sub>49</sub>H<sub>67</sub>FN<sub>10</sub>O<sub>16</sub>S

Molecular Mass: 1103.19 g mol<sup>-1</sup>

**3-49** (0.166 g, 0.149 mmol) was suspended in MeOH:H<sub>2</sub>O (3:1, 25 mL) to give a yellow cloudy solution. Aqueous NaOH (1 M, 1.50 mL, 1.50 mmol) was added with stirring, and the resulting clear yellow solution was stirred for 24 hours. Aqueous HCl (1 M, 3.00 mL) was added to give a cloudy yellow solution. The solution was transferred to a 50 mL Falcon tube and centrifuged for 20 minutes (4400 rpm). The solution was removed carefully via syringe and the resultant white-yellow solid left to dry in air, and then further dried under vacuum to give **3-14** as a yellow solid (99.6 mg, 0.090 mmol, 61%). Average yield = 60% (n = 3). M.p. = 159-164 °C (dec.).

**<sup>1</sup>H NMR:** (400 MHz, DMSO-d<sub>6</sub>) δ<sub>H</sub> ppm: 9.69 (1H, br s, H<sub>30</sub> or 41 or 52), 9.66 (1H, br s, H<sub>30</sub> or 41 or 52), 9.64 (1H, br s, H<sub>30</sub> or 41 or 52), 8.89 (1H, br t, J = 5.5 Hz, H<sub>24</sub>), 8.67 (1H, s, H<sub>4</sub>), 8.38 (1H, d, J = 1.5 Hz, H<sub>19</sub>), 8.26 (1H, dd, J = 8.0, 1.5 Hz, H<sub>21</sub>), 8.17 (1H, d, J = 8.0 Hz, H<sub>22</sub>), 7.92 (1H, d, <sup>3</sup>J<sub>F-H</sub> = 13.0 Hz, H<sub>8</sub>), 7.85-7.72 (2H, m, H<sub>35</sub> and 46), 7.60 (1H, d, <sup>4</sup>J<sub>F-H</sub> = 7.5 Hz, H<sub>11</sub>), 3.84-3.77 (1H,

m, H3), 3.50-3.40 (14H, m, H13/14/29/40/51), 3.30-3.21 (2H, m, H25), 3.05-2.94 (4H, m, H36 and 47), 2.57 (4H, t,  $J = 7.0$  Hz, H32 and 43), 2.26 (4H, t,  $J = 7.0$  Hz, H33 and 44), 1.96 (3H, s, H54), 1.62-1.43 (8H, m, H26/28/39/50), 1.42-1.12 (14H, m, H1/2/27/37/38/48/49).

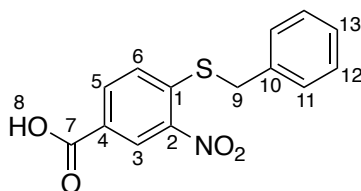
**$^{13}\text{C}$  NMR:** (100 MHz, DMSO- $d_6$ )  $\delta_{\text{C}}$  ppm: 176.5 (C6), 172.0 (C31 and 42), 171.4 (C34 and 45), 170.2 (C53), 166.0 (C15), 163.0 (C23), 153.4 (d,  $^1J_{\text{F-C}} = 251$  Hz, C9), 148.2 (C4), 147.8 (C18), 144.7 (C10), 140.2 (C20), 139.1 (C12), 131.0, 130.9 (C17/21/22), 123.1 (C19), 119.4 (C7), 111.0 (C8), 107.3 (C11), 106.9 (C5), 49.2 (C13 or 14), 47.1, 46.8 (C29/40/51), 45.5 (C13 or 14), 39.9 (C25), 38.5 (C36 and 47), 36.0 (C3), 29.9 (C33 and 44), 28.9 (C37 and 48), 28.5 (C26), 27.6 (C32 and 43), 26.1 (C28/39/50), 23.5 (C27/38/49), 20.4 (C54), 7.7 (C1 and 2).

Some desferrioxamine NMR assignments are partially based on those made by Richardson-Sanchez *et al.*<sup>493</sup>

**HRMS (ESI):** Calcd.  $[\text{M}+\text{H}]^+$  ( $\text{C}_{49}\text{H}_{68}\text{FN}_{10}\text{O}_{16}\text{S}$ )  $m/z = 1103.4514$ ; Obs.  $[\text{M}+\text{H}]^+$   $m/z = 1103.4534$ , Mean err  $-1.2$  ppm. Calcd.  $[\text{M}+\text{Na}]^+$  ( $\text{C}_{49}\text{H}_{67}\text{FN}_{10}\text{NaO}_{16}\text{S}$ )  $m/z = 1125.4333$ ; Obs.  $[\text{M}+\text{Na}]^+$   $m/z = 1125.4342$ , Mean err  $-0.4$  ppm. Calcd.  $[\text{M}+2\text{Na}-\text{H}]^+$  ( $\text{C}_{49}\text{H}_{66}\text{FN}_{10}\text{Na}_2\text{O}_{16}\text{S}$ )  $m/z = 1147.4153$ ; Obs.  $[\text{M}+2\text{Na}-\text{H}]^+$   $m/z = 1147.4177$ , Mean err  $0.7$  ppm.

**IR (ATIR,  $\text{cm}^{-1}$ ):** 3500-3150 (OH/NH stretches, w br), 3100-2750 (C-H stretching, w), 1725 (carboxylic acid C=O stretch, w), 1623 (C=O amide and quinolone stretches, br s), 1545 (N=O/C=C stretches, s), 1495 (N=O/C=C stretches, s), 1455 (N=O/C=C stretches, s), 1374 (S=O stretch, m), 1162 (S=O stretch, m).

#### 4-(Benzylsulfanyl)-3-nitrobenzoic acid (**3-55**)



Molecular Formula: C<sub>14</sub>H<sub>11</sub>NO<sub>4</sub>S

Molecular Mass: 289.31 g mol<sup>-1</sup>

Preparation adapted from a literature procedure.<sup>426</sup>

Methyl 4-(benzylsulfanyl)-3-nitrobenzoate (**3-26**, 0.215 g, 0.710 mmol) was placed under N<sub>2</sub>, then suspended in THF:MeOH (1:1, 4 mL). Aqueous NaOH (1 M, 1.3 mL) was added, with the solution changing from cloudy orange to cloudy yellow. The reaction was stirred for 18 hours, then the solvent removed under vacuum. Aqueous HCl (1 M, 3 mL) was added to give an orange precipitate, which was isolated via Buchner filtration. The resulting solid was dried in a vacuum desiccator for 3 days to give **3-55** as a crystalline orange solid (0.170 g, 0.588 mmol, 83%). Average yield = 81% (n = 4). M.p. = 295-297 °C.

Characterisation data consistent with literature.<sup>426</sup>

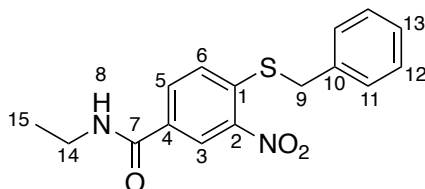
**<sup>1</sup>H NMR:** (400 MHz, DMSO-d<sub>6</sub>) δ<sub>H</sub> ppm: 8.55 (1H, d, *J* = 2.0 Hz, *H*3), 8.08 (1H, dd, *J* = 8.5, 2.0 Hz, *H*5), 7.66 (1H, d, *J* = 8.5 Hz, *H*6), 7.47-7.43 (2H, m, *H*11 or 12), 7.37-7.31 (2H, m, *H*11 or 12), 7.31-7.25 (1H, m, *H*13), 4.35 (2H, s, *H*9).

**<sup>13</sup>C NMR:** (100 MHz, DMSO-d<sub>6</sub>) δ<sub>C</sub> ppm: 166.2 (*C*7), 144.6 (*C*2), 138.7 (*C*4), 136.7 (*C*1), 135.8 (*C*10), 134.4 (*C*5), 129.4, 128.7 (*C*11/12), 127.6 (*C*13), 126.6 (*C*6), 125.9 (*C*3), 36.6 (*C*9).

**HRMS (ESI Neg.):** Calcd. [M-H]<sup>-</sup> (C<sub>14</sub>H<sub>10</sub>NO<sub>4</sub>S) *m/z* = 288.0336; Obs. [M-H]<sup>-</sup> *m/z* = 288.0340, Mean err -0.5 ppm.



#### 4-(Benzylsulfanyl)-*N*-ethyl-3-nitrobenzamide (3-56)



Molecular Formula: C<sub>16</sub>H<sub>16</sub>N<sub>2</sub>O<sub>3</sub>S

Molecular Mass: 316.38 g mol<sup>-1</sup>

**3-55** (0.206 g, 0.711 mmol) was placed under N<sub>2</sub> and dissolved in dry DCM (20 mL), then HOBt (97.6 mg, 0.722 mmol), EDC.HCl (0.210 g, 1.09 mmol) and Et<sub>3</sub>N (0.30 mL, 2.15 mmol) were added, yielding a cloudy yellow-orange solution. EtNH<sub>2</sub>.HCl (98.0 mg, 1.20 mmol) was added, and the solution was stirred for 28 hours, then extra DCM (20 mL) added, and the solution washed with 1 M aq. HCl (30 mL), H<sub>2</sub>O (30 mL), saturated NaHCO<sub>3</sub> solution (30 mL), and brine (30 mL), dried over MgSO<sub>4</sub> and the solvent removed under vacuum. The crude product was purified by column chromatography (silica gel, 26 g, 2:1 EtOAc:40-60 °C pet. ether to 100% EtOAc) to give **3-56** as a fluffy yellow solid (0.180 g, 0.570 mmol, 80%). M.p. = 196-197 °C. R<sub>f</sub> = 0.77 (9:1:0.1 EtOAc:MeOH:AcOH); 0.56 (3:1 EtOAc:40-60 °C pet. ether).

**<sup>1</sup>H NMR:** (400 MHz, CDCl<sub>3</sub>) δ<sub>H</sub> ppm: 8.56 (1H, d, *J* = 2.0 Hz, *H*<sub>3</sub>), 8.00 (1H, dd, *J* = 8.5, 2.0 Hz, *H*<sub>5</sub>), 7.53 (1H, d, *J* = 8.5 Hz, *H*<sub>6</sub>), 7.45-7.40 (2H, m, *H*<sub>11</sub> or *H*<sub>12</sub>), 7.39-7.28 (3H, m, *H*<sub>13</sub> and *H*<sub>11</sub> or *H*<sub>12</sub>), 6.22-6.12 (1H, m, *H*<sub>8</sub>), 4.24 (2H, s, *H*<sub>9</sub>), 3.52 (2H, dq, *J* = 7.5, 5.5 Hz, *H*<sub>14</sub>), 1.28 (3H, t, *J* = 7.5 Hz, *H*<sub>15</sub>).

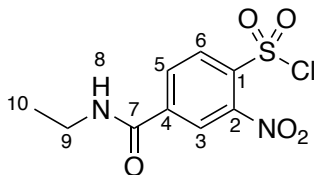
**<sup>13</sup>C NMR:** (100 MHz, CDCl<sub>3</sub>) δ<sub>C</sub> ppm: 164.7 (*C*<sub>7</sub>), 145.0 (*C*<sub>2</sub>), 142.2 (*C*<sub>1</sub>), 134.5 (*C*<sub>10</sub>), 132.3 (*C*<sub>5</sub>), 131.2 (*C*<sub>4</sub>), 129.2, 129.1 (*C*<sub>11/12</sub>), 128.2 (*C*<sub>13</sub>), 127.0 (*C*<sub>6</sub>), 124.1 (*C*<sub>3</sub>), 37.7 (*C*<sub>9</sub>), 35.4 (*C*<sub>14</sub>), 15.0 (*C*<sub>15</sub>).

**HRMS (ESI Pos.):** Calcd. [M+H]<sup>+</sup> (C<sub>16</sub>H<sub>17</sub>N<sub>2</sub>O<sub>3</sub>S) *m/z* = 317.0954; Obs. [M+H]<sup>+</sup> *m/z* = 317.0955, Mean err -1.5 ppm. Calcd. [M+Na]<sup>+</sup> (C<sub>16</sub>H<sub>16</sub>N<sub>2</sub>NaO<sub>3</sub>S) *m/z* = 339.0774; Obs. [M+Na]<sup>+</sup> *m/z* = 339.0771, Mean err 0.6 ppm.

**HRMS (ESI Neg.):** Calcd. [M-H]<sup>-</sup> (C<sub>16</sub>H<sub>15</sub>N<sub>2</sub>O<sub>3</sub>S) *m/z* = 315.0809; Obs. [M-H]<sup>-</sup> *m/z* = 315.0813, Mean err -1.4 ppm.

**IR (ATIR,  $\text{cm}^{-1}$ ):** 3330 (NH stretch, m), 3100-2850 (C-H stretching, m), 1633 (C=O stretch, s), 1603 (C=C stretch, s), 1542 (N=O/C=C stretches, s), 1512 (C=C stretch, s), 1496 (C=C stretch, s).

#### 4-(Ethylcarbamoyl)-2-nitrobenzene-1-sulfonyl chloride (3-57)



Molecular Formula:  $\text{C}_9\text{H}_9\text{ClN}_2\text{O}_5\text{S}$

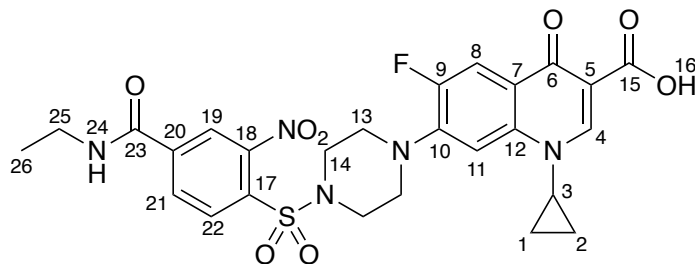
Molecular Mass:  $292.69 \text{ g mol}^{-1}$

**3-56** (0.367 g, 1.16 mmol) was placed under  $\text{N}_2$  and dissolved in MeCN (8.5 mL), then 3:2 AcOH:H<sub>2</sub>O (0.54 mL) added and the cloudy yellow solution cooled to 0 °C. 1,3-Dichloro-5,5'-dimethylhydantoin (0.523 g, 2.65 mmol) was added in portions to give a clear yellow solution, which was allowed to warm to room temperature and stirred over 24 hours. The solvent was removed under vacuum, and the residue redissolved in dry DCM (30 mL). The resulting solution was cooled to 0 °C, then ice-cold saturated  $\text{NaHCO}_3$  solution (20 mL) was added with stirring. The biphasic mixture was stirred for 15 minutes, then the layers partitioned and the organic layer washed with ice-cold brine (20 mL), dried over  $\text{MgSO}_4$  and the solvent removed to give a white-yellow solid (0.401 g, est. 78% desired product by mass, 92%).

**$^1\text{H NMR}$ :** (400 MHz,  $\text{CDCl}_3$ )  $\delta_{\text{H}}$  ppm: 8.31 (1H, d,  $J = 8.5 \text{ Hz}$ , H6), 8.25 (1H, d,  $J = 2.0 \text{ Hz}$ , H3), 8.19 (1H, dd,  $J = 8.5, 2.0 \text{ Hz}$ , H5), 6.47-6.35 (1H, m, H8), 3.55 (2H, dq,  $J = 7.5, 5.5 \text{ Hz}$ , H9), 1.30 (3H, t,  $J = 7.5 \text{ Hz}$ , H10).

**HRMS (ESI):** Calcd.  $[\text{M}+\text{H}]^+$  ( $\text{C}_9\text{H}_{10}^{35}\text{ClN}_2\text{O}_5\text{S}$ )  $m/z = 292.9993$ ; Obs.  $[\text{M}+\text{H}]^+$   $m/z = 292.9982$ , Mean err 2.6 ppm. Calcd.  $[\text{M}+\text{Na}]^+$  ( $\text{C}_9\text{H}_9^{35}\text{ClN}_2\text{NaO}_5\text{S}$ )  $m/z = 314.9813$ ; Obs.  $[\text{M}+\text{Na}]^+$   $m/z = 314.9808$ , Mean err 0.8 ppm. Calcd.  $[\text{M}+\text{K}]^+$  ( $\text{C}_9\text{H}_9^{35}\text{ClKN}_2\text{O}_5\text{S}$ )  $m/z = 330.9552$ ; Obs.  $[\text{M}+\text{K}]^+$   $m/z = 330.9546$ , Mean err -3.9 ppm.

**1-Cyclopropyl-7-{4-[4-(ethylcarbamoyl)-2-nitrobenzenesulfonyl]piperazin-1-yl}-6-fluoro-4-oxo-1,4-dihydroquinoline-3-carboxylic acid (3-34)**



Molecular Formula: C<sub>26</sub>H<sub>26</sub>FN<sub>5</sub>O<sub>8</sub>S

Molecular Mass: 587.58 g mol<sup>-1</sup>

**3-57** (81.8 mg, c. 75% by mass, 0.210 mmol) was placed under N<sub>2</sub>, then dry DCM (10 mL) was added, and the resulting cloudy beige solution was cooled to 0 °C. Ciprofloxacin (51.8 mg, 0.156 mmol) and Et<sub>3</sub>N (33 μL, 0.237 mmol) were added, and the cloudy white solution was allowed to warm to room temperature and stirred for 23 hours. The product was isolated by Buchner filtration and washed with 1 M HCl (10 mL) and DCM (15 mL) to give **3-34** as an off-white solid (38.8 mg, 0.066 mmol, 42%). M.p. = 300-303 °C (dec.).

**<sup>1</sup>H NMR:** (400 MHz, DMSO-d<sub>6</sub>) δ<sub>H</sub> ppm: 8.89 (1H, br t, *J* = 5.0 Hz, *H*<sub>24</sub>), 8.67 (1H, s, *H*<sub>4</sub>), 8.37 (1H, d, *J* = 1.5 Hz, *H*<sub>19</sub>), 8.26 (1H, dd, *J* = 8.5, 1.5 Hz, *H*<sub>21</sub>), 8.17 (1H, d, *J* = 8.5 Hz, *H*<sub>22</sub>), 7.93 (1H, d, <sup>3</sup>*J*<sub>F-H</sub> = 13.0 Hz, *H*<sub>8</sub>), 7.60 (1H, d, <sup>4</sup>*J*<sub>F-H</sub> = 7.5 Hz, *H*<sub>11</sub>), 3.85-3.77 (1H, m, *H*<sub>3</sub>), 3.50-3.40 (8H, m, *H*<sub>13</sub> and *H*<sub>14</sub>), 3.40-3.25 (2H, m, *H*<sub>25</sub>\*), 1.35-1.28 (2H, m, *H*<sub>1</sub> or *H*<sub>2</sub>), 1.19-1.13 (2H, m, *H*<sub>1</sub> or *H*<sub>2</sub>), 1.13 (3H, t, *J* = 7.0 Hz, *H*<sub>26</sub>).

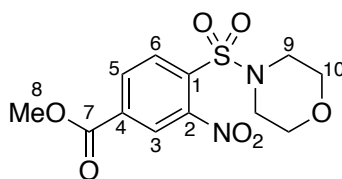
\*Hidden underneath H<sub>2</sub>O peak

**<sup>13</sup>C NMR:** (100 MHz, DMSO-d<sub>6</sub>) δ<sub>C</sub> ppm: 176.6 (*C*<sub>6</sub>), 166.0 (*C*<sub>15</sub>), 162.8 (*C*<sub>23</sub>), 153.1 (d, <sup>1</sup>*J*<sub>F-C</sub> = 249 Hz, *C*<sub>9</sub>), 148.3 (*C*<sub>4</sub>), 147.8 (*C*<sub>18</sub>), 140.2 (*C*<sub>20</sub>), 139.2 (*C*<sub>10</sub>), 139.1 (*C*<sub>12</sub>), 130.96, 130.92, 130.88 (*C*<sub>17/21/22</sub>), 123.0 (*C*<sub>19</sub>), 119.4 (*C*<sub>7</sub>), 111.7 (*C*<sub>8</sub>), 107.2, 106.9 (*C*<sub>5/11</sub>), 49.1 (*C*<sub>13</sub> and *C*<sub>14</sub>), 45.5 (*C*<sub>16</sub>), 36.0 (*C*<sub>3</sub>), 34.5 (*C*<sub>25</sub>), 14.5 (*C*<sub>26</sub>), 7.6 (*C*<sub>1</sub> and *C*<sub>2</sub>).

**HRMS (ESI):** Calcd.  $[M+Na]^+$  ( $C_{26}H_{26}FN_5NaO_8S$ )  $m/z = 610.1378$ ; Obs.  $[M+Na]^+$   $m/z = 610.1383$ , Mean err  $-0.9$  ppm.

**IR (ATIR,  $cm^{-1}$ ):** 3600-3300 (NH/OH stretching, w br), 3372 (amide NH stretch/OH stretch, w), 3100-2750 (C-H stretching, w), 1706 (carboxylic acid C=O stretch, s), 1659 (amide C=O stretch, s), 1615 (C=O quinolone stretch, s), 1537 (N=O/C=C stretches, s), 1492 (N=O/C=C stretches, s), 1473 (N=O/C=C stretches, s), 1367 (S=O stretch, m), 1162 (S=O stretch, m).

### Methyl 4-(morpholine-4-sulfonyl)-3-nitrobenzoate (3-32)



Molecular Formula:  $C_{12}H_{14}N_2O_7S$

Molecular Mass:  $330.31$  g mol $^{-1}$

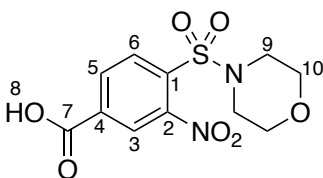
**3-27** (0.279 g, 71% product by mass, 0.711 mmol) was placed under  $N_2$ , then dissolved in dry DCM (20 mL) to give a clear yellow solution. The solution was cooled to  $0$  °C, then morpholine (97  $\mu$ L, 1.11 mmol) and  $Et_3N$  (175  $\mu$ L, 1.26 mmol) added, resulting in the production of a white vapour. The reaction was allowed to warm to room temperature and stirred for 18 hours. Extra DCM (10 mL) was added, and the solution washed with 1 M aq. HCl (25 mL), water (25 mL), saturated  $NaHCO_3$  solution (25 mL) and brine (25 mL), dried over  $MgSO_4$  and the DCM removed *in vacuo* to give a powdery orange solid (0.340 g), which was used in the next step without further purification.

**$^1H$  NMR:** (400 MHz,  $CDCl_3$ )  $\delta_H$  ppm: 8.31 (1H, dd,  $J = 8.0, 1.5$  Hz,  $H_5$ ), 8.26 (1H, d,  $J = 1.5$  Hz,  $H_3$ ), 8.05 (1H, d,  $J = 8.0$  Hz,  $H_6$ ), 4.00 (3H, s,  $H_8$ ), 3.77-3.73 (4H, m,  $H_{10}$ ), 3.34-3.30 (4H, m,  $H_9$ ).

**$^1H$  NMR:** (400 MHz,  $DMSO-d_6$ )  $\delta_H$  ppm: 8.50 (1H, d,  $J = 1.5$  Hz,  $H_3$ ), 8.33 (1H, dd,  $J = 8.5, 1.5$  Hz,  $H_5$ ), 8.15 (1H, d,  $J = 8.5$  Hz,  $H_6$ ), 3.93 (3H, s,  $H_8$ ), 3.67-3.62 (4H, m,  $H_{10}$ ), 3.22-3.17 (4H, m,  $H_9$ ).

**HRMS (ESI):** Calcd.  $[M+H]^+$  ( $C_{12}H_{15}N_2O_7S$ )  $m/z = 331.0594$ ; Obs.  $[M+H]^+$   $m/z = 331.0594$ , Mean err  $-0.6$  ppm. Calcd.  $[M+Na]^+$  ( $C_{12}H_{14}N_2NaO_7S$ )  $m/z = 353.0414$ ; Obs.  $[M+Na]^+$   $m/z = 353.0415$ , Mean err  $-0.4$  ppm. Calcd.  $[M+K]^+$  ( $C_{12}H_{14}KN_2O_7S$ )  $m/z = 369.0153$ ; Obs.  $[M+K]^+$   $m/z = 369.0156$ , Mean err  $-0.6$  ppm.

#### 4-(Morpholine-4-sulfonyl)-3-nitrobenzoic acid (**3-33**)



Molecular Formula:  $C_{11}H_{12}N_2O_7S$

Molecular Mass:  $316.28 \text{ g mol}^{-1}$

**3-32** (0.779 g) was suspended in THF:MeOH (1:1, 35 mL) to give a cloudy yellow mixture. Aqueous NaOH (2.5 M, 5 mL) was added with stirring, and the resulting cloudy dark orange solution was stirred for 24 hours. Aqueous HCl (3 M, 5 mL) was added to give a clear yellow solution. The solvent was removed *in vacuo*, and the resulting light brown solid isolated via Buchner filtration and washed with  $H_2O$  (80 mL) and DCM (80 mL) to give **3-33** (0.527 g, 1.67 mmol, 71% yield over 3 steps from thioether **3-26**).

A portion of the product (0.1997 g) was purified further for analysis via column chromatography (25 g silica gel, 9:1:0.1  $CHCl_3$ :MeOH:AcOH; dry loading of compound). The resulting product was dissolved x3 in  $CHCl_3$ :toluene:MeOH (25 mL, 2:2:1) and the solvent removed to remove residual AcOH, giving **3-33** as white microneedles (0.128 g, 0.405 mmol). M.p. =  $280-282 \text{ }^\circ\text{C}$  (dec.).  $R_f = 0.33$  (9:1:0.1  $CHCl_3$ :MeOH:AcOH).

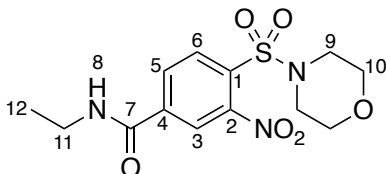
**$^1H$  NMR:** (400 MHz, DMSO- $d_6$ )  $\delta_H$  ppm: 14.00 (1H, br s, H8), 8.44 (1H, d,  $J = 1.5$  Hz, H3), 8.31 (1H, dd,  $J = 8.5, 1.5$  Hz, H5), 8.13 (1H, d,  $J = 8.5$  Hz, H6), 3.69-3.60 (4H, m, H10), 3.23-3.15 (4H, m, H9).

**$^{13}C$  NMR:** (100 MHz, DMSO- $d_6$ )  $\delta_C$  ppm: 164.6 (C7), 148.0 (C2), 136.7 (C4), 132.6 (C5), 132.1 (C1), 131.3 (C6), 124.8 (C3), 66.6 (C10), 45.8 (C9).

**HRMS (ESI):** Calcd.  $[M+Na]^+$  ( $C_{11}H_{12}N_2NaO_7S$ )  $m/z = 339.0257$ ; Obs.  $[M+Na]^+$   $m/z = 339.0259$ , Mean err  $-1.7$  ppm.

**IR (ATIR,  $cm^{-1}$ ):** 3100-2500 (OH stretch, w br and C-H stretching, w), 1721 (C=O stretch, s), 1544 (N=O/C=C stretches, s), 1492 (N=O/C=C stretches, s), 1370 (S=O stretch, s), 1161 (S=O stretch, s).

***N*-Ethyl-4-(morpholine-4-sulfonyl)-3-nitrobenzamide (3-36)**



Molecular Formula:  $C_{13}H_{17}N_3O_6S$

Molecular Mass:  $343.35$  g mol $^{-1}$

**3-33** (100 mg, 0.316 mmol) was placed under  $N_2$ , then suspended in dry DCM (10 mL), giving a cloudy white solution. HOBT (44.9 mg, 0.332 mmol) and EDC.HCl (94.4 mg, 0.492 mmol) were added to give a clear yellow solution, then  $Et_3N$  (0.133 mL, 0.954 mmol) and ethylamine hydrochloride (53.1 mg, 0.651 mmol) were added and the solution stirred for 23 hours at room temperature. Further DCM (15 mL) was added, then the solution was washed with 1 M aq. HCl (18 mL),  $H_2O$  (18 mL), saturated  $NaHCO_3$  solution (18 mL) and brine (18 mL), dried over  $MgSO_4$ , and the solvent removed under vacuum. The resulting yellow-orange oil was purified by column chromatography (silica gel, 25 g, 39:1  $CHCl_3$ :MeOH, flow rate c. 5 mL/min) to give **3-36** as a white solid (56.3 mg, 0.164 mmol, 52%). M.p. = 156-157 °C.  $R_f = 0.10$  (39:1  $CHCl_3$ :MeOH); 0.18 (29:1  $CHCl_3$ :MeOH).

**$^1H$  NMR:** (400 MHz,  $CDCl_3$ )  $\delta_H$  ppm: 8.03 (1H, dd,  $J = 8.5, 1.5$  Hz,  $H_5$ ), 8.00 (1H, d,  $J = 8.5$  Hz,  $H_6$ ), 7.99 (1H, d,  $J = 1.5$  Hz,  $H_3$ ), 6.35 (1H, br t,  $J = 5.5$  Hz,  $H_8$ ), 3.76-3.72 (4H, m,  $H_{10}$ ), 3.52 (2H, dq,  $J = 7.5, 5.5$  Hz,  $H_{11}$ ), 3.32-3.27 (4H, m,  $H_9$ ), 1.28 (3H, t,  $J = 7.5$  Hz,  $H_{12}$ ).

**<sup>13</sup>C NMR:** (100 MHz, CDCl<sub>3</sub>) δ<sub>c</sub> ppm: 163.7 (C7), 148.5 (C2), 140.4 (C4), 133.0 (C1), 131.6 (C6), 129.9 (C5), 123.1 (C3), 66.5 (C10), 46.1 (C9), 35.7 (C11), 14.8 (C12).

**HRMS (ESI):** Calcd. [M+Na]<sup>+</sup> (C<sub>13</sub>H<sub>17</sub>N<sub>3</sub>NaO<sub>6</sub>S) *m/z* = 366.0730; Obs. [M+Na]<sup>+</sup> *m/z* = 366.0727, Mean err 1.1 ppm.

**IR (ATIR, cm<sup>-1</sup>):** 3323 (amide NH stretch, m), 3090-2850 (C-H stretching, w), 1645 (C=O stretch, s), 1545 (N=O/C=C stretches, s), 1349 (S=O stretch, s), 1163 (S=O stretch, s).

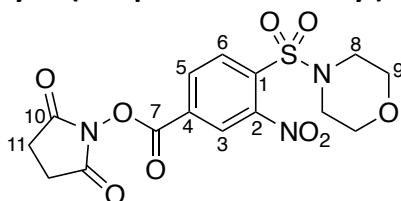
#### Elemental Analysis:

For [C<sub>13</sub>H<sub>17</sub>N<sub>3</sub>O<sub>6</sub>S . 0.10 CHCl<sub>3</sub> . 0.05 CH<sub>3</sub>OH]:

*Calculated:* %C, 44.26; %H, 4.89; %N, 11.77.

*Measured:* %C, 44.49, %H, 4.89, %N, 11.54.

#### 2,5-Dioxopyrrolidin-1-yl 4-(morpholine-4-sulfonyl)-3-nitrobenzoate (3-58)



Molecular Formula: C<sub>15</sub>H<sub>15</sub>N<sub>3</sub>O<sub>9</sub>S

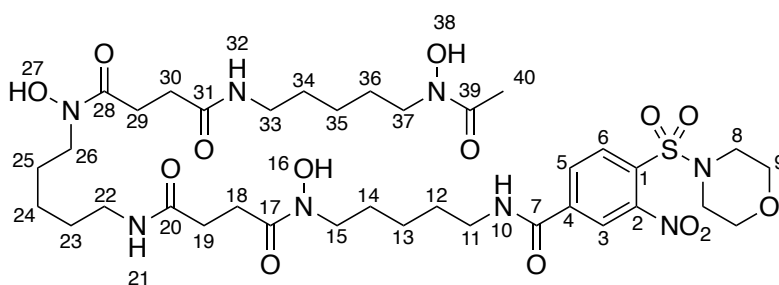
Molecular Mass: 413.36 g mol<sup>-1</sup>

**3-33** (85 mg, 0.269 mmol) was placed under N<sub>2</sub>, then suspended in dry DCM (8 mL), giving a cloudy beige solution. *N*-Hydroxysuccinimide (43 mg, 0.371 mmol) and EDC.HCl (70 mg, 0.365 mmol) were added and the now clear solution stirred for 25 hours at room temperature. A further portion of DCM (12.5 mL) was added, then the solution was washed with 1 M aq. HCl (15 mL), H<sub>2</sub>O (15 mL), saturated NaHCO<sub>3</sub> solution (15 mL) and brine (15 mL), dried over MgSO<sub>4</sub>, and the solvent removed to give a white-yellow bubbly solid (0.112 g). Due to its instability, the product was used without further purification. R<sub>f</sub> = 0.48 (19:1 CHCl<sub>3</sub>:MeOH).

**<sup>1</sup>H NMR:** (400 MHz, CDCl<sub>3</sub>) δ<sub>H</sub> ppm: 8.41 (1H, dd, *J* = 8.5, 1.5 Hz, *H*5), 8.35 (1H, d, *J* = 1.5 Hz, *H*6), 8.14 (1H, d, *J* = 8.5 Hz, *H*3), 3.78-3.72 (4H, m, *H*9), 3.37-3.30 (4H, m, *H*8), 2.94 (4H, br s, *H*11).

**HRMS (ESI):** Calcd. [M+Na]<sup>+</sup> (C<sub>15</sub>H<sub>15</sub>N<sub>3</sub>NaO<sub>9</sub>S) *m/z* = 436.0421; Obs. [M+Na]<sup>+</sup> *m/z* = 436.0419, Mean err -0.8 ppm.

***N*-Hydroxy-*N'*-[5-(*N*-hydroxy-3-{[5-(*N*-hydroxyacetamido)pentyl]carbamoyl}propanamido)pentyl]-*N*-(5-{[4-(morpholine-4-sulfonyl)-3-nitrophenyl]formamido}pentyl)butanediamide (3-31)**



Molecular Formula: C<sub>36</sub>H<sub>58</sub>N<sub>8</sub>O<sub>14</sub>S

Molecular Mass: 858.96 g mol<sup>-1</sup>

**3-58** (63.5 mg, 0.153 mmol) was placed under N<sub>2</sub>, then suspended in dry DMF (10 mL) to give a yellow solution. Desferrioxamine mesylate (93.6 mg, 0.143 mmol) and Et<sub>3</sub>N (60 μL, 0.430 mmol) were added to give a cloudy white solution, which was heated to 50 °C. The resulting clear yellow solution was stirred at 50 °C for 24 hours, then the solvent removed under vacuum. MeCN (35 mL) was added, and the product sonicated at 40 °C for 30 minutes. The solution was transferred to a Falcon tube and centrifuged for 10 minutes (4400 rpm). The solvent was removed carefully via syringe, then further MeCN (30 mL) added and the mixture sonicated for a further 30 minutes at 40 °C. After further centrifugation (10 minutes, 4400 rpm), the solvent was again removed via syringe, and the product left to dry in air to give **3-31** as a yellow solid (88.2 mg, 0.103 mmol, 72%). M.p. = 168-170 °C.

**<sup>1</sup>H NMR:** (400 MHz, DMSO-*d*<sub>6</sub>) δ<sub>H</sub> ppm: 9.66 (1H, br s, *H*16 or 27 or 38), 9.63 (1H, br s, *H*16 or 27 or 38), 9.61 (1H, br s, *H*16 or 27 or 38), 8.87 (1H, br t, *J* = 5.5 Hz, *H*10), 8.35 (1H, d, *J* = 2.0 Hz, *H*3), 8.24 (1H, dd, *J* = 8.5, 2.0 Hz, *H*5),



8.10 (1H, d,  $J = 8.5$  Hz,  $H_6$ ), 7.78 (2H, br t,  $J = 5.5$  Hz,  $H_{21}$  and  $32$ ), 3.66-3.62 (4H, m,  $H_9$ ), 3.53-3.41 (6H, m,  $H_{15/26/37}$ ), 3.27 (2H, t,  $J = 6.0$  Hz,  $H_{11}$ ), 3.20-3.15 (4H, m,  $H_8$ ), 3.03-2.94 (4H, m,  $H_{22}$  and  $33$ ), 2.57 (4H, t,  $J = 7.5$  Hz,  $H_{18}$  and  $29$ ), 2.26 (4H, t,  $J = 7.5$  Hz,  $H_{19}$  and  $30$ ), 1.96 (3H, s,  $H_{40}$ ), 1.60-1.43 (8H, m,  $H_{12/14/25/36}$ ), 1.42-1.13 (10H, m,  $H_{13/23/24/34/35}$ ).

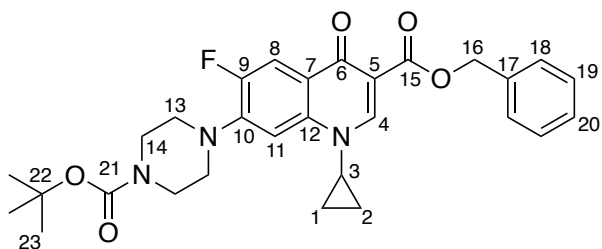
$^{13}\text{C}$  NMR: (100 MHz, DMSO- $d_6$ )  $\delta_c$  ppm: 172.0 ( $C_{17}$  and  $28$ ), 171.4 ( $C_{20}$  and  $31$ ), 170.2 ( $C_{39}$ ), 163.0 ( $C_7$ ), 147.9 ( $C_2$ ), 140.2 ( $C_4$ ), 131.0, 130.8 ( $C_{5/6}$ ), 130.5 ( $C_1$ ), 123.0 ( $C_3$ ), 65.6 ( $C_9$ ), 47.1 ( $C_{26}$  and  $37$ ), 46.8 ( $C_{15}$ ), 45.8 ( $C_8$ ), 39.1 ( $C_{11}$ ), 38.5 ( $C_{22}$  and  $33$ ), 29.9 ( $C_{19}$  and  $30$ ), 28.9 ( $C_{23}$  and  $34$ ), 28.5 ( $C_{12}$ ), 27.6 ( $C_{18}$  and  $29$ ), 26.1 ( $C_{14/25/36}$ ), 23.5 ( $C_{13/24/35}$ ), 20.4 ( $C_{40}$ ).

Some desferrioxamine NMR assignments are partially based on those made by Richardson-Sanchez *et al.*<sup>493</sup>

**HRMS (ESI):** Calcd.  $[M+Na]^+$  ( $C_{36}H_{58}N_8NaO_{14}S$ )  $m/z = 881.3685$ ; Obs.  $[M+Na]^+$   $m/z = 881.3715$ , Mean err  $-3.4$  ppm.

**IR (ATIR,  $\text{cm}^{-1}$ ):** 3304 (OH/NH stretches, w br), 3300-3100 (OH/NH stretches, w br), 3000-2750 (C-H stretching, w), 1618 (C=O amide stretches, s), 1547 (N=O/C=C stretches, s), 1459 (N=O/C=C stretches, s), 1368 (S=O stretch, m), 1161 (S=O stretch, m).

**Benzyl 7-{4-[(*tert*-butoxy)carbonyl]piperazin-1-yl}-1-cyclopropyl-6-fluoro-4-oxo-1,4-dihydroquinoline-3-carboxylate (4-40)**



Molecular Formula:  $C_{29}H_{32}FN_3O_5$

Molecular Mass:  $521.59 \text{ g mol}^{-1}$

Prepared according to a literature procedure.<sup>195</sup>

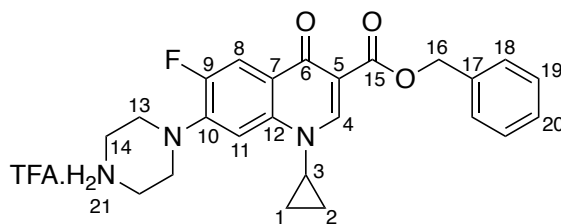
Ciprofloxacin (0.993 g, 3.00 mmol), Boc anhydride (0.848 g, 3.89 mmol) and NaHCO<sub>3</sub> (1.27 g, 15.2 mmol) were suspended in dry DMF (25 mL), and the resulting white cloudy solution was stirred at room temperature for 18 hours, then benzyl bromide (1.610 mL, 13.54 mmol) was added and the reaction heated at 90 °C for 25 ½ hours, initially turning cloudy brown, then orange over a 6 hour period. The DMF was removed under vacuum, and the resulting solid dissolved in CHCl<sub>3</sub> (75 mL) and H<sub>2</sub>O (50 mL). The layers were separated, and the organic layer washed with H<sub>2</sub>O (25 mL) and brine (25 mL), dried over MgSO<sub>4</sub> and the solvent removed under vacuum. The resulting solid was suspended in Et<sub>2</sub>O, isolated by Buchner filtration, and washed with several further portions of Et<sub>2</sub>O to give an orange solid with white patches. This was further purified via column chromatography (silica, c. 55 g, 1:1 EtOAc:CHCl<sub>3</sub>, loading with eluent/DCM) to give **4-40** as a white solid (1.20 g, 2.31 mmol, 77%). Average yield = 83% (n = 2). M.p. = 195-196 °C (lit = 191-193 °C).<sup>195</sup> R<sub>f</sub> = 0.38 (1:1 EtOAc:CHCl<sub>3</sub>).

Characterisation data consistent with literature.<sup>195</sup>

**<sup>1</sup>H NMR:** (400 MHz, CDCl<sub>3</sub>) δ<sub>H</sub> ppm: 8.54 (1H, s, H4), 8.08 (1H, d, <sup>3</sup>J<sub>F-H</sub> = 13.0 Hz, H8), 7.53-7.49 (2H, m, H11/18/19/20), 7.40-7.34 (2H, m, H11/18/19/20), 7.33-7.26 (2H, m, H11/18/19/20), 5.39 (2H, s, H16), 3.67-3.62 (4H, m, H14), 3.44-3.36 (1H, m, H3), 3.24-3.18 (4H, m, H13), 1.42 (9H, s, H23), 1.33-1.27 (2H, m, H1 or 2), 1.14-1.08 (2H, m, H1 or 2).

**HRMS (ESI):** Calcd. [M+H]<sup>+</sup> (C<sub>29</sub>H<sub>33</sub>FN<sub>3</sub>O<sub>5</sub>) *m/z* = 522.2399; Obs. [M+H]<sup>+</sup> *m/z* = 522.2402, Mean err 0.0 ppm. Calcd. [M+Na]<sup>+</sup> (C<sub>29</sub>H<sub>32</sub>FN<sub>3</sub>NaO<sub>5</sub>) *m/z* = 544.2218; Obs. [M+Na]<sup>+</sup> *m/z* = 544.2223, Mean err -1.2 ppm.

**Benzyl 1-cyclopropyl-6-fluoro-4-oxo-7-(piperazin-1-yl)-1,4-dihydroquinoline-3-carboxylate (4-41)**



Molecular Formula: C<sub>26</sub>H<sub>25</sub>F<sub>4</sub>N<sub>3</sub>O<sub>5</sub>

Molecular Mass: 535.50 g mol<sup>-1</sup>

Prepared according to a literature procedure.<sup>266</sup>

**4-40** (0.528 g, 1.01 mmol) was dissolved in DCM (25 mL) to give a pale yellow solution, then trifluoroacetic acid (2 mL) was added, giving an instant change to an orange solution. The reaction was stirred for 18 hours, then the solvent removed under vacuum. Residual TFA was removed by addition and removal of EtOH under vacuum (10 x 20 mL), yielding **4-41** as a powdery white solid\* (0.541 g, quantitative). Average yield = 96% (n = 3). M.p. = 223-227 °C (dec.).

\*Colour can range from white to off/white, and even pink.

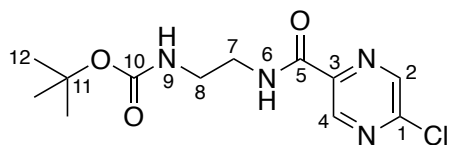
Characterisation data consistent with literature.<sup>659</sup>

**<sup>1</sup>H NMR:** (400 MHz, DMSO-d<sub>6</sub>) δ<sub>H</sub> ppm: 8.50 (1H, s, *H4*), 7.83 (1H, d, <sup>3</sup>J<sub>F-H</sub> = 13.0 Hz, *H8*), 7.50-7.45 (3H, m, *H11 and H18 or 19*), 7.42-7.36 (2H, m, *H18 or 19*), 7.35-7.32 (1H, m, *H20*), 5.27 (2H, s, *H16*), 3.72-3.65 (1H, m, *H3*), 3.48-3.42 (4H, m, *H13 or 14*), 3.36-3.30 (4H, m, *H13 or 14*), 1.29-1.22 (2H, m, *H1 or 2*), 1.13-1.07 (2H, m, *H1 or 2*).

**<sup>13</sup>C NMR:** (100 MHz, DMSO-d<sub>6</sub>) δ<sub>C</sub> ppm: 171.8 (*C6*), 164.6 (*C15*), 152.6 (d, <sup>1</sup>J<sub>F-C</sub> = 247 Hz, *C9*), 148.8 (*C4*), 142.9 (d, <sup>2</sup>J<sub>F-C</sub> = 11 Hz, *C10*), 138.2 (*C12*), 136.7 (*C17*), 128.6 (*C18 or 19*), 128.0 (*C20*), 127.8 (*C18 or 19*), 122.7 (d, <sup>3</sup>J<sub>F-C</sub> = 6 Hz, *C7*), 111.9 (d, <sup>2</sup>J<sub>F-C</sub> = 22 Hz, *C8*), 109.1 (*C5*), 106.9 (*C11*), 65.4 (*C16*), 46.7 (*C13 or 14*), 42.9 (*C13 or 14*), 35.1 (*C3*), 7.7 (*C1 and 2*).

**HRMS (ESI):** Calcd.  $[M+H]^+$  ( $C_{24}H_{25}FN_3O_3$ )  $m/z = 422.1874$ ; Obs.  $[M+H]^+$   $m/z = 422.1881$ , Mean err  $-1.2$  ppm. Calcd.  $[M+Na]^+$  ( $C_{24}H_{24}FN_3NaO_3$ )  $m/z = 444.1694$ ; Obs.  $[M+Na]^+$   $m/z = 444.1703$ , Mean err  $-2.3$  ppm. Calcd.  $[M+K]^+$  ( $C_{24}H_{24}FKN_3O_3$ )  $m/z = 460.1433$ ; Obs.  $[M+K]^+$   $m/z = 460.1438$ , Mean err  $-0.8$  ppm.

***tert*-Butyl *N*-{2-[(5-chloropyrazin-2-yl)formamido]ethyl}carbamate (**4-37**)**



Molecular Formula:  $C_{12}H_{17}ClN_4O_3$

Molecular Mass:  $300.74 \text{ g mol}^{-1}$

5-chloropyrazine-2-carboxylate (0.309 g, 1.95 mmol) was placed under  $N_2$  and dissolved in dry DCM (11.5 mL) to give a cloudy white solution. Boc-ethylenediamine (0.335 mL, 2.12 mmol) and HOBt (0.265 g, 1.96 mmol\*) were added, followed by EDC.HCl (0.444 g, 2.32 mmol) was added, giving a clear solution with a slight green tinge after 5 minutes. The solution was stirred for 24 hours, then extra DCM (30 mL) added, and the solution washed with 1 M aq. HCl (15 mL),  $H_2O$  (15 mL),  $NaHCO_3$  (15 mL), and brine (15 mL), then dried over  $MgSO_4$  and the solvent removed under vacuum. The resulting pale beige-white solid was purified by column chromatography (silica, 4:3 EtOAc:40-60 °C pet. ether) to give **4-37** as a fluffy white solid (0.447 g, 1.488 mmol, 76%). Average yield = 84% ( $n = 4$ ). M.p. = 151 °C.  $R_f = 0.24$  (4:3 EtOAc:40-60 °C pet. ether); 0.79 (9:1:0.1 EtOAc:MeOH:AcOH).\*\*

\*A later repeat of the reaction with 0.75 eq. of HOBt also gave complete conversion after 24 h.

\*\*This solvent system provides clear differentiation from HOBt ( $R_f = 0.37$ ) and 5-chloropyrazine-2-carboxylic acid ( $R_f = 0.14$ ) under the same conditions.

**<sup>1</sup>H NMR:** (400 MHz, CDCl<sub>3</sub>) δ<sub>H</sub> ppm: 9.16 (1H, d, *J* = 1.5 Hz, *H*4), 8.52 (1H, d, *J* = 1.5 Hz, *H*2), 8.15-8.01 (1H, m, *H*6), 4.99-4.83 (1H, m, *H*9), 3.59 (2H, app. q, *J* = 5.5 Hz, *H*7), 3.41 (2H, app. q, *J* = 5.5 Hz, *H*8), 1.41 (9H, s, *H*12).

**<sup>13</sup>C NMR:** (100 MHz, CDCl<sub>3</sub>) δ<sub>C</sub> ppm: 163.0 (*C*5), 156.7 (*C*10), 152.2 (*C*1), 144.0 (*C*4), 142.7 (*C*2 and 3), 79.9 (*C*11), 40.6 (*C*7), 40.2 (*C*8), 28.4 (*C*12).

**HRMS (ESI):** Calcd. [M+Na]<sup>+</sup> (C<sub>12</sub>H<sub>17</sub><sup>35</sup>ClN<sub>4</sub>NaO<sub>3</sub>) *m/z* = 323.0881; Obs. [M+Na]<sup>+</sup> *m/z* = 323.0888, Mean err -1.6 ppm.

**IR (ATIR, cm<sup>-1</sup>):** 3346 (NH amide stretch, m), 3322 (NH carbamate stretch, m), 3070-2900 (C-H stretching, w), 1683 (carbamate C=O stretch, s), 1659 (amide C=O stretch, s), 1531 (C=N/C=C stretches, s), 1455 (C=N/C=C stretches, m).

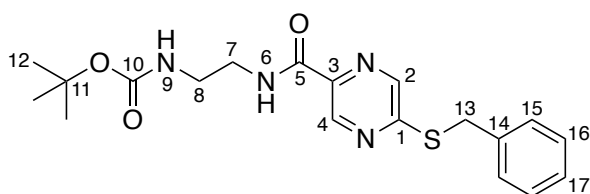
#### Elemental Analysis:

For [C<sub>12</sub>H<sub>17</sub>ClN<sub>4</sub>O<sub>3</sub>]:

*Calculated:* %C, 47.93; %H, 5.70; %N, 18.63.

*Measured:* %C, 47.91, %H, 5.66, %N, 18.58.

#### ***tert*-Butyl *N*-(2-{{[5-(benzylsulfanyl)pyrazin-2-yl]formamido}ethyl) carbamate (4-38)**



Molecular Formula: C<sub>19</sub>H<sub>24</sub>N<sub>4</sub>O<sub>3</sub>S

Molecular Mass: 388.49 g mol<sup>-1</sup>

**4-37** (0.773 g, 2.57 mmol) was placed under N<sub>2</sub>, and suspended in dry MeOH (7.5 mL), giving a cloudy white solution, then cooled to 0 °C. Benzyl mercaptan (0.386 mL, 3.29 mmol) and triethylamine (0.450 mL, 3.23 mmol) were added to give a cloudy beige-orange solution, which was left to warm to room temperature, and began to go clear over two hours. A yellow-white

solid precipitates over 24 hours of stirring. The solid was isolated via Buchner filtration, and washed with ice-cold MeOH (15 mL) and ice-cold hexane (40 mL) to give the product as a white solid (0.438 g, 1.13 mmol, 44%). The filtrate was reduced to dry under vacuum, and purified by column chromatography (silica gel, gradient: 35% EtOAc in 40-60 °C pet. ether to 100% EtOAc) to isolate further **4-38** as a yellow-white crystalline solid (0.396 g, 1.02 mmol, 40%). Combined average yield = 78% (n = 5). M.p. = 139-140 °C.  $R_f$  = 0.86 (EtOAc); 0.45 (1:1 40-60 °C pet. ether:EtOAc); 0.20 (2:1 40-60 °C pet. ether:EtOAc).

**$^1\text{H}$  NMR:** (400 MHz,  $\text{CDCl}_3$ )  $\delta_{\text{H}}$  ppm: 9.14 (1H, d,  $J$  = 1.5 Hz,  $H_4$ ), 8.31 (1H, d,  $J$  = 1.5 Hz,  $H_2$ ), 8.06-7.91 (1H, m,  $H_6$ ), 7.43-7.37 (2H, m,  $H_{15}$  or  $H_{16}$ ), 7.34-7.23 (3H, m,  $H_{17}$  and  $H_{15}$  or  $H_{16}$ ), 4.99-4.84 (1H, m,  $H_9$ ), 4.48 (2H, s,  $H_{13}$ ), 3.57 (2H, app. q,  $J$  = 5.5 Hz,  $H_7$ ), 3.38 (2H, app. q,  $J$  = 5.5 Hz,  $H_8$ ), 1.41 (9H, s,  $H_{12}$ ).

**$^{13}\text{C}$  NMR:** (100 MHz,  $\text{CDCl}_3$ )  $\delta_{\text{C}}$  ppm: 164.3 ( $C_5$ ), 160.3 ( $C_1$ ), 156.7 ( $C_{10}$ ), 143.4 ( $C_4$ ), 141.1 ( $C_2$ ), 139.6 ( $C_3$ ), 136.9 ( $C_{14}$ ), 129.2, 128.8 ( $C_{15/16}$ ), 127.7 ( $C_{17}$ ), 79.8 ( $C_{11}$ ), 40.5 ( $C_8$ ), 40.2 ( $C_7$ ), 34.1 ( $C_{13}$ ), 28.5 ( $C_{12}$ ).

**HRMS (ESI):** Calcd.  $[\text{M}+\text{H}]^+$  ( $\text{C}_{19}\text{H}_{25}\text{N}_4\text{O}_3\text{S}$ )  $m/z$  = 389.1642; Obs.  $[\text{M}+\text{H}]^+$   $m/z$  = 389.1633, Mean err 2.1 ppm. Calcd.  $[\text{M}+\text{Na}]^+$  ( $\text{C}_{19}\text{H}_{24}\text{N}_4\text{NaO}_3\text{S}$ )  $m/z$  = 411.1461; Obs.  $[\text{M}+\text{Na}]^+$   $m/z$  = 411.1452, Mean err 2.5 ppm.

**IR (ATIR,  $\text{cm}^{-1}$ ):** 3366 (NH amide stretch, m), 3323 (NH carbamate stretch, m), 3000-2880 (C-H stretching, w), 1691 (carbamate C=O stretch, s), 1651 (amide C=O stretch, s), 1530 (C=N/C=C stretches, s), 1455 (C=N/C=C stretches, m).

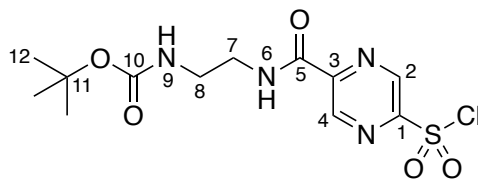
#### Elemental Analysis:

For  $[\text{C}_{19}\text{H}_{24}\text{N}_4\text{O}_3\text{S} \cdot 0.2 \text{H}_2\text{O} \cdot 0.05 \text{EtOAc} \cdot 0.05 \text{C}_6\text{H}_{14}]$ :

*Calculated:* %C, 58.44; %H, 6.41; %N, 13.98.

*Measured:* %C, 58.45, %H, 6.41, %N, 13.95.

***tert*-Butyl *N*-(2-{{[5-(chlorosulfonyl)pyrazin-2-yl]formamido}ethyl) carbamate (4-39)**



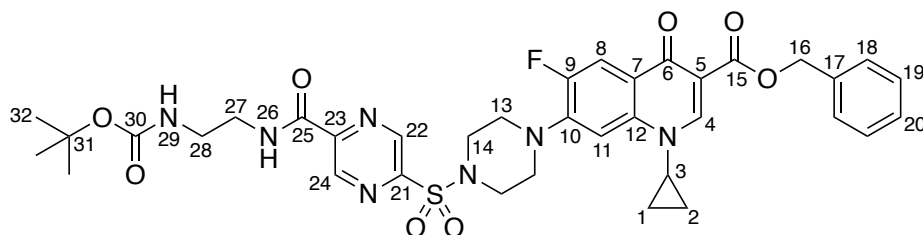
Molecular Formula: C<sub>12</sub>H<sub>17</sub>ClN<sub>4</sub>O<sub>5</sub>S

Molecular Mass: 364.80 g mol<sup>-1</sup>

**4-38** (0.559 g, 1.44 mmol) placed under N<sub>2</sub>, then dissolved in DCM (8 mL), then glacial AcOH (0.71 mL) and H<sub>2</sub>O (1.42 mL) were added, and the resulting pale yellow biphasic solution cooled to 0 °C. 1,3-Dichloro-5,5'-dimethylhydantoin (0.873 g, 4.43 mmol) added in portions with vigorous stirring to initially give a cloudy off-white solution, with a green-yellow tinge appearing after two minutes. The solution was stirred at 0 °C for between 12 to 15 hours, then additional DCM (30 mL) was added and the solution poured into ice-cold sodium metabisulfite solution (5% w/v, 45 mL). The resulting mixture was stirred for 10 minutes, then the layers were shaken and separated, and the metabisulfite layer extracted with further DCM (2 x 25 mL). The combined organic layers were washed with ice-cold saturated NaHCO<sub>3</sub> solution (45 mL) and brine (50 mL), dried over MgSO<sub>4</sub> and filtered to give a clear solution, which was used without further purification. A sample was taken from the solution for analysis.

**<sup>1</sup>H NMR:** (400 MHz, CDCl<sub>3</sub>) δ<sub>H</sub> ppm: 9.56 (1H, d, *J* = 1.5 Hz, *H2* or 4), 9.24 (1H, d, *J* = 1.5 Hz, *H2* or 4), 8.41-8.28 (1H, m, *H6*), 4.94-4.81 (1H, m, *H9*), 3.64 (2H, app. q, *J* = 6.0 Hz, *H7*), 3.44 (2H, app. q, *J* = 6.0 Hz, *H8*), 1.42 (9H, s, *H12*).

**Benzyl 7-[4-{{5-[[2-{{(tert-butoxy)carbonyl]amino}ethyl)carbamoyl]pyrazin-2-yl)sulfonyl]piperazin-1-yl]-1-cyclopropyl-6-fluoro-4-oxo-1,4-dihydroquinoline-3-carboxylate (4-42)**



Molecular Formula: C<sub>36</sub>H<sub>40</sub>FN<sub>7</sub>O<sub>8</sub>S

Molecular Mass: 749.82 g mol<sup>-1</sup>

**4-38** (0.559 g, 1.44 mmol) was placed under N<sub>2</sub>, then DCM (10 mL), acetic acid (0.71 mL) and H<sub>2</sub>O (1.42 mL) were added, and the resulting pale beige-yellow biphasic solution was cooled to 0 °C. 1,3-Dichloro-5,5'-dimethylhydantoin (0.873 g, 4.43 mmol) was added in portions with vigorous stirring to give a cloudy beige solution, which was allowed to warm slowly in the ice bath and stirred for 7 hours. Extra DCM (30 mL) was added, and the reaction mixture poured into ice-cold aqueous sodium metabisulfite solution (5% w/v, 45 mL). The layers were shaken well and separated, then the aqueous layer was extracted with DCM (2 x 25 mL). The combined organic layers were washed with ice-cold saturated NaHCO<sub>3</sub> solution (45 mL) and ice-cold brine (45 mL), dried over MgSO<sub>4</sub>, transferred to a fresh round-bottomed flask, and cooled back to 0 °C. **4-41** (0.827 eq., 0.637 g, 1.19 mmol) was added, followed by triethylamine (0.50 mL, 3.59 mmol). The solution was allowed to warm to room temperature and stirred for 24 hours. Additional DCM (20 mL) was added, and the solution washed with 1 M aq. HCl (50 mL), H<sub>2</sub>O (50 mL), saturated NaHCO<sub>3</sub> solution (50 mL) and brine (50 mL), dried over MgSO<sub>4</sub> and the solvent removed to give an off-white solid. The product was purified by column chromatography (silica gel, c. 100 g, DCM used for loading), using a gradient from 17:3 EtOAc:CHCl<sub>3</sub> to 100% EtOAc, followed by 100% EtOAc to 8:2 EtOAc:MeOH, to give **4-42** as a white solid (0.542 g, 0.723 mmol, 61%)\*. M.p. = 206-207 °C. R<sub>f</sub> = 0.18 (17:3 EtOAc:CHCl<sub>3</sub>).



\*The product is poorly soluble in the eluent, with white spots, potentially precipitated product, appearing near the top of the column. These can be removed by flushing the column with 8:2 DCM: MeOH, which yields further impure product.

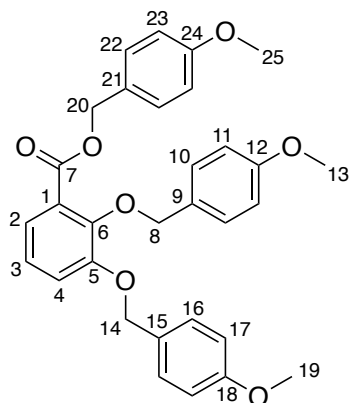
**<sup>1</sup>H NMR:** (400 MHz, CDCl<sub>3</sub>) δ<sub>H</sub> ppm: 9.45 (1H, d, *J* = 1.5 Hz, *H*22 or 24), 9.09 (1H, d, *J* = 1.5 Hz, *H*22 or 24), 8.54 (1H, s, *H*4), 8.29 (1H, br s, *H*26), 8.05 (1H, d, <sup>3</sup>*J*<sub>F-H</sub> = 13.0 Hz, *H*8), 7.52-7.45 (2H, m, *H*18 or 19), 7.39-7.34 (2H, m, *H*18 or 19), 7.33-7.27 (2H, m, *H*11 and 20), 5.38 (2H, s, *H*16), 4.93 (1H, br s, *H*29), 3.66-3.59 (6H, m, *H*14 and 27), 3.46-3.37 (3H, m, *H*3 and 28), 3.37-3.29 (4H, m, *H*13), 1.42 (9H, s, *H*32), 1.35-1.29 (2H, m, *H*1 or 2), 1.15-1.09 (2H, m, *H*1 or 2).

**<sup>13</sup>C NMR:** (100 MHz, CDCl<sub>3</sub>) δ<sub>C</sub> ppm: 173.0 (*C*6), 165.6 (*C*15), 162.1 (*C*25), 156.8 (*C*30), 154.6 (*C*21), 153.4 (d, <sup>1</sup>*J*<sub>F-C</sub> = 249 Hz, *C*9), 148.6 (*C*4), 146.7 (*C*23), 144.1 (*C*22 or 24), 143.9 (d, <sup>2</sup>*J*<sub>F-C</sub> = 11 Hz, *C*10), 141.5 (*C*22 or 24), 138.1 (*C*12), 136.5 (*C*17), 128.7, 128.12 (*C*18/19), 128.08 (*C*20), 123.8 (d, <sup>3</sup>*J*<sub>F-C</sub> = 7 Hz, *C*7), 113.8 (d, <sup>2</sup>*J*<sub>F-C</sub> = 24 Hz, *C*8), 111.0 (*C*5), 105.5 (*C*11), 80.1 (*C*31), 66.6 (*C*16), 49.9 (*C*13 or 14), 46.6 (*C*13 or 14), 41.0 (*C*27), 40.1 (*C*28), 34.7 (*C*3), 28.4 (*C*32), 8.3 (*C*1 and 2).

**<sup>19</sup>F NMR:** (376 MHz, CDCl<sub>3</sub>) δ<sub>F</sub> ppm: -123.99 (1F, dd, *J* = 13.0, 7.0 Hz).

**HRMS (ESI):** Calcd. [M+H]<sup>+</sup> (C<sub>36</sub>H<sub>41</sub>FN<sub>7</sub>O<sub>8</sub>S) *m/z* = 750.2716; Obs. [M+H]<sup>+</sup> *m/z* = 750.2718, Mean err -0.3 ppm. Calcd. [M+Na]<sup>+</sup> (C<sub>36</sub>H<sub>40</sub>FN<sub>7</sub>NaO<sub>8</sub>S) *m/z* = 772.2535; Obs. [M+Na]<sup>+</sup> *m/z* = 772.2541, Mean err 0.2 ppm.

**(4-Methoxyphenyl)methyl 2,3-bis[(4-methoxyphenyl)methoxy]benzoate  
(4-58)**



Molecular Formula: C<sub>31</sub>H<sub>30</sub>O<sub>7</sub>

Molecular Mass: 514.57 g mol<sup>-1</sup>

Prepared according to a literature procedure.<sup>185</sup>

2,3-Dihydroxybenzoic acid (3.86 g, 25.07 mmol) was suspended in dry acetone (200 mL) to give an orange suspension\*, then *para*-methoxybenzyl chloride (10.9 mL, 80.39 mmol), KI (13.35 g, 80.45 mmol) and K<sub>2</sub>CO<sub>3</sub> (24.27 g, 175.6 mmol) were added. The resulting cloudy white mixture was stirred at reflux under a CaCl<sub>2</sub> guard column for three days, changing to pink over 10 hours of stirring. The acetone was removed under vacuum, and the resulting residue re-dissolved in H<sub>2</sub>O (200 mL) and extracted with DCM (3x240 mL). The combined organic layers were dried over MgSO<sub>4</sub>, and the solvent removed. The resulting orange-brown oil was purified by column chromatography (silica gel, 5 cm column diameter, 6 inches silica height, 2:3 EtOAc:40-60 °C pet. ether) to give **4-58** as a white solid (11.73 g, 22.80 mmol, 91%). R<sub>f</sub> = 0.52 (2:3 EtOAc:40-60 °C pet. ether).

\*reasonable solubility, but not full solubility

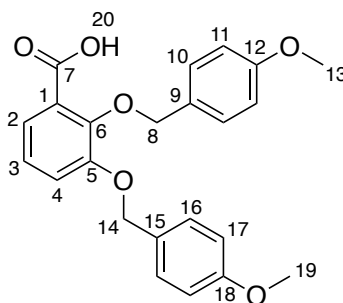
Characterisation data consistent with literature.<sup>185</sup>

<sup>1</sup>H NMR: (400 MHz, CDCl<sub>3</sub>) δ<sub>H</sub> ppm: 7.38-7.32 (5H, m, H<sub>2</sub> and H<sub>10</sub> or 16 or 22), 7.20-7.16 (2H, m, H<sub>10</sub> or 16 or 22), 7.12 (1H, dd, J = 8.0, 1.5 Hz, H<sub>4</sub>), 7.05 (1H, t, J = 8.0 Hz, H<sub>3</sub>), 6.92-6.89 (2H, m, H<sub>11</sub> or 17 or 23), 6.89-6.85 (2H, m,

H11 or 17 or 23), 6.78-6.74 (2H, m, H11 or 17 or 23), 5.25 (2H, s, H8 or 14 or 20), 5.05 (2H, s, H8 or 14 or 20), 4.95 (2H, s, H8 or 14 or 20), 3.82 (3H, s, H13 or 19 or 25), 3.81 (3H, s, H13 or 19 or 25), 3.79 (3H, s, H13 or 19 or 25).

**HRMS (ESI):** Calcd.  $[M+Na]^+$  ( $C_{31}H_{30}NaO_7$ )  $m/z = 537.1884$ ; Obs.  $[M+Na]^+$   $m/z = 537.1895$ , Mean err  $-1.6$  ppm.

### 2,3-Bis[(4-methoxyphenyl)methoxy]benzoic acid (**4-59**)



Molecular Formula:  $C_{23}H_{22}O_6$

Molecular Mass:  $394.42 \text{ g mol}^{-1}$

Prepared according to a literature procedure.<sup>185</sup>

**4-58** (11.75 g, 22.84 mmol) was dissolved in dioxane (110 mL) to give a yellow solution, then aqueous NaOH (2.5 M, 49 mL, 122.5 mmol) was added and the reaction stirred at room temperature for 19 hours. As the reaction appeared incomplete on TLC, a further portion of aqueous NaOH (10 M, 10 mL) was added, followed by a subsequent portion (10 M, 5 mL) after a further 24 hours. After 72 hours, the cloudy orange solution was concentrated under vacuum to remove dioxane, then  $H_2O$  (100 mL) was added, and the resulting cloudy brown solution acidified to pH 3 by dropwise addition of aqueous HCl (2 M) with rapid stirring, with precipitation of a white solid observed around pH 9. The precipitate was isolated via Buchner filtration and washed with hexane (3 x 50 mL), then dried in a desiccator for one week to give **4-59** as a white solid (8.121 g, 20.59 mmol, 90%). M.p. =  $107-108 \text{ }^\circ\text{C}$  (lit. =  $110 \text{ }^\circ\text{C}$ ).<sup>660</sup>

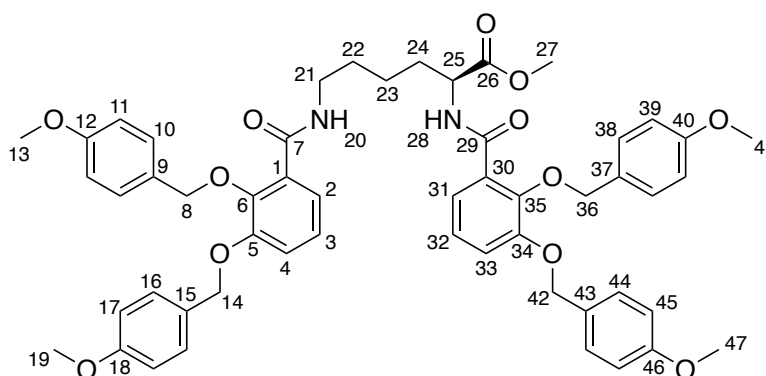
Characterisation data consistent with literature.<sup>185</sup>

**<sup>1</sup>H NMR:** (400 MHz, CDCl<sub>3</sub>) δ<sub>H</sub> ppm: 11.46 (1H, br s, H<sub>20</sub>), 7.73 (1H, dd, *J* = 8.0, 1.5 Hz, H<sub>2</sub>), 7.44-7.39 (2H, m, H<sub>10</sub> or 16), 7.28-7.21 (3H, m, H<sub>4</sub> and H<sub>10</sub> or 16), 7.18 (1H, t, *J* = 8.0 Hz, H<sub>3</sub>), 6.99-6.94 (2H, m, H<sub>11</sub> or 17), 6.86-6.81 (2H, m, H<sub>11</sub> or 17), 5.20 (2H, s, H<sub>8</sub> or 14), 5.12 (2H, s, H<sub>8</sub> or 14), 3.85 (3H, s, H<sub>13</sub> or 19), 3.80 (3H, s, H<sub>13</sub> or 19).

**HRMS (ESI Pos.):** Calcd. [M+Na]<sup>+</sup> (C<sub>23</sub>H<sub>22</sub>NaO<sub>6</sub>) *m/z* = 417.1309; Obs. [M+Na]<sup>+</sup> *m/z* = 417.1302, Mean err 1.5 ppm.

**HRMS (ESI Neg.):** Calcd. [M-H]<sup>-</sup> (C<sub>23</sub>H<sub>21</sub>O<sub>6</sub>) *m/z* = 393.1344; Obs. [M-H]<sup>-</sup> *m/z* = 393.1344, Mean err -0.3 ppm.

**Methyl (2S)-2,6-bis({2,3-bis[(4-methoxyphenyl)methoxy]phenyl}formamido)hexanoate (4-60)**



Molecular Formula: C<sub>53</sub>H<sub>56</sub>N<sub>2</sub>O<sub>12</sub>

Molecular Mass: 913.03 g mol<sup>-1</sup>

**4-59** (5.317 g, 13.48 mmol) was placed under nitrogen, then DMF (50 mL) added. EDC.HCl (7.72, 40.26 mmol) and HOBT (5.48 g, 40.55 mmol) were added, and the resulting cloudy orange mixture was cooled to 0 °C and stirred for 10 minutes. DIPEA (7.00 mL, 40.19 mmol) and *L*-lysine methyl ester dihydrochloride (1.397 g, 5.994 mmol) were added, plus further DMF (20 mL), and the mixture allowed to warm to room temperature and stirred overnight, then heated at 50 °C for a further 18 hours. The solvent was removed under vacuum to give an orange-brown syrup. The syrup was re-dissolved in 1 M HCl (2 x 200 mL) and EtOAc (5 x 50 mL), then the aqueous layer extracted with further EtOAc (2 x 50 mL). The combined organic layers

were washed with NaHCO<sub>3</sub> (2 x 200 mL) and brine (150 mL), dried over MgSO<sub>4</sub> and the solvent removed *in vacuo*. The resulting orange-brown paste was purified by column chromatography (15.5 cm silica in 5 cm diameter column, 1:1 EtOAc: 40-60 °C pet. ether to 4:1 EtOAc: 40-60 °C pet. ether\*, loaded with 1:1 eluent:DCM) to give **4-60** as a colourless paste\*\* (2.99 g, 3.27 mmol, 55%). R<sub>f</sub> = 0.18 (1:1 EtOAc:40-60 °C pet. ether); 0.45 (4:1 EtOAc:40-60 °C pet. ether).

\*Solvent volumes: 180 mL 1:1 EtOAc:pet. ether, then 550 mL 3:2 EtOAc:pet. ether, then 900 mL 7:3 EtOAc:pet. ether, then 600 mL 4:1 EtOAc:pet. ether.

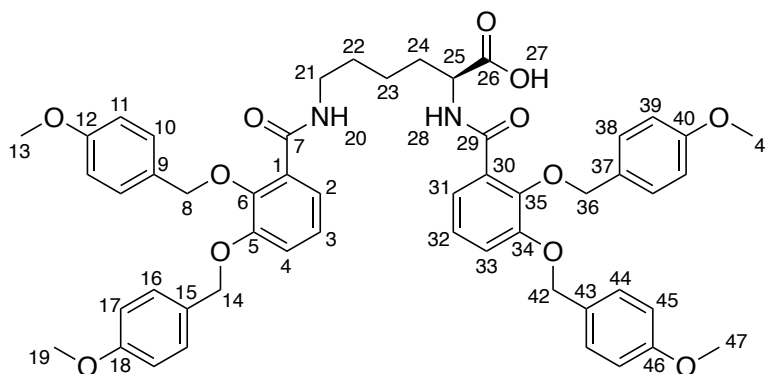
\*\*Prolonged drying may result in the formation of a white bubbly solid, which returns to a paste over time.

Characterisation data consistent with literature.<sup>185</sup>

**<sup>1</sup>H NMR:** (400 MHz, CDCl<sub>3</sub>) δ<sub>H</sub> ppm: 8.56 (1H, d, *J* = 7.5 Hz, *H*28), 7.96 (1H, br t, *J* = 5.5 Hz, *H*20), 7.74-7.68 (2H, m, *H*2 and *H*31), 7.42-7.36 (4H, m, *H*10/16/38/44), 7.31-7.25 (2H, m, *H*10/16/38/44), 7.22-7.18 (2H, m, *H*10/16/38/44), 7.15-7.09 (4H, m, *H*3/4/32/33), 6.95-6.90 (4H, m, *H*11/17/39/45), 6.84-6.79 (2H, m, *H*11/17/39/45), 6.79-6.75 (2H, m, *H*11/17/39/45), 5.10-5.01 (6H, m, *H*8/14/36/42), 4.97 (2H, s, *H*8/14/36/42), 4.63 (1H, td, *J* = 7.5, 5.5 Hz, *H*25), 3.83 (2 x 3H, s, *H*13/19/41/47), 3.75 (3H, s, *H*13/19/41/47), 3.74 (3H, s, *H*13/19/41/47), 3.71 (3H, s, *H*27), 3.22-3.12 (2H, m, *H*21), 1.75-1.64 (1H, m, *H*24), 1.51-1.41 (1H, m, *H*24), 1.32-1.13 (4H, m, *H*22 and 23).

**HRMS (ESI):** Calcd. [M+H]<sup>+</sup> (C<sub>53</sub>H<sub>57</sub>N<sub>2</sub>O<sub>12</sub>) *m/z* = 913.3906; Obs. [M+H]<sup>+</sup> *m/z* = 913.3952, Mean err -4.9 ppm. Calcd. [M+Na]<sup>+</sup> (C<sub>53</sub>H<sub>56</sub>N<sub>2</sub>NaO<sub>12</sub>) *m/z* = 935,3725; Obs. [M+Na]<sup>+</sup> *m/z* = 935.3770, Mean err -4.9 ppm. Calcd. [M+K]<sup>+</sup> (C<sub>53</sub>H<sub>56</sub>KN<sub>2</sub>O<sub>12</sub>) *m/z* = 951.3465; Obs. [M+K]<sup>+</sup> *m/z* = 951.3489, Mean err -2.9 ppm.

**(2S)-2,6-Bis({2,3-bis[(4-methoxyphenyl)methoxy]phenyl}formamido)hexanoic acid (4-57)**



Molecular Formula: C<sub>52</sub>H<sub>54</sub>N<sub>2</sub>O<sub>12</sub>

Molecular Mass: 899.01 g mol<sup>-1</sup>

**4-60** (0.779 g, 0.853 mmol) was dissolved in THF (45 mL) to give a clear solution, then aqueous NaOH (2.5 M, 3.50 mL, 8.75 mmol) was added with vigorous stirring. The resulting beige solution was stirred for 23 hours, then acidified to pH 3 by dropwise addition of aqueous HCl (1 M, c. 9 mL). The solution was extracted with EtOAc (3 x 40 mL), dried over MgSO<sub>4</sub>, and the solvent removed under vacuum. The resulting pale yellow oil was purified by column chromatography (20.5 cm silica in 3.1 cm diameter column, 19:1 CHCl<sub>3</sub>:MeOH to 9:1 CHCl<sub>3</sub>:MeOH), and the product dried under vacuum to give **4-57** as a white solid (0.606 g, 0.674 mmol, 79%). Average yield = 71% (n = 2). R<sub>f</sub> = 0.28 (9:1 CHCl<sub>3</sub>:MeOH).

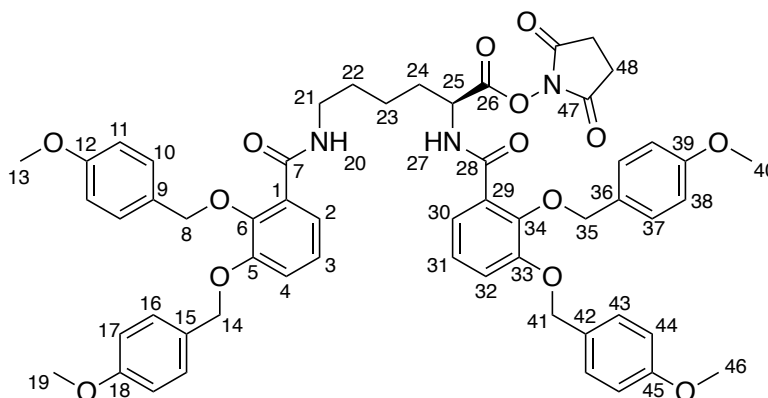
<sup>1</sup>H NMR: (400 MHz, CDCl<sub>3</sub>) δ<sub>H</sub> ppm: 8.66 (1H, d, J = 6.5 Hz, H<sub>28</sub>), 8.03 (1H, t, J = 5.5 Hz, H<sub>20</sub>), 7.74-7.66 (2H, m, H<sub>2</sub> and 31), 7.37 (4H, d, J = 8.0 Hz, H<sub>10/16/38/44</sub>), 7.24 (2H, d, J = 8.0 Hz, H<sub>10/16/38/44</sub>), 7.18 (2H, d, J = 8.5 Hz, H<sub>10/16/38/44</sub>), 7.15-7.04 (4H, m, H<sub>3/4/32/33</sub>), 6.92 (4H, app. d, J = 8.5 Hz, H<sub>11/17/39/45</sub>), 6.79 (2H, d, J = 8.5 Hz, H<sub>11/17/39/45</sub>), 6.74 (2H, d, J = 8.5 Hz, H<sub>11/17/39/45</sub>), 5.04 (6H, app. s, H<sub>8/14/36/42</sub>), 4.95 (2H, s, H<sub>8/14/36/42</sub>), 4.57 (1H, q, J = 6.5 Hz, H<sub>25</sub>), 3.82 (6H, s, H<sub>13/19/41/47</sub>), 3.73 (3H, s, H<sub>13/19/41/47</sub>), 3.69 (3H, s, H<sub>13/19/41/47</sub>), 3.15 (2H, q, J = 6.5 Hz, H<sub>21</sub>), 1.81-1.69 (1H, m, H<sub>24</sub>), 1.52-1.40 (1H, m, H<sub>24</sub>), 1.31-1.12 (4H, m, H<sub>22</sub> and 23).

<sup>13</sup>C NMR: (100 MHz, CDCl<sub>3</sub>) δ<sub>c</sub> ppm: 166.2 (C26), 165.4 (C7 and 29), 160.0, 159.9, 159.8, 159.7 (C12/18/40/46), 151.9, 151.8 (C5/34), 147.3, 147.0 (C6/35), 130.9, 130.6, 129.8, 129.6 (C10/16/38/44), 128.61, 128.58, 128.46, 128.40 (C9/15/37/43), 127.1, 126.1 (C1/30), 124.4 (C3/4/32/33), 123.3, 123.2 (C2/31), 117.6, 117.2 (C3/4/32/33), 114.13, 114.10, 114.0 (C11/17/39/45), 76.2, 76.1, 71.2 (C8/14/36/42), 55.44, 55.39, 55.31 (C13/19/41/47), 53.2 (C25), 39.5 (C21), 31.1 (C24), 29.0, 23.0 (C22/23).

HRMS (ESI Pos.): Calcd. [M+Na]<sup>+</sup> (C<sub>52</sub>H<sub>54</sub>N<sub>2</sub>NaO<sub>12</sub>) *m/z* = 921.3569; Obs. [M+Na]<sup>+</sup> *m/z* = 921.3593, Mean err -2.7 ppm.

HRMS (ESI Neg.): Calcd. [M-H]<sup>-</sup> (C<sub>52</sub>H<sub>53</sub>N<sub>2</sub>O<sub>12</sub>) *m/z* = 897.3604; Obs. [M-H]<sup>-</sup> *m/z* = 897.3626, Mean err -2.6 ppm.

**2,5-Dioxopyrrolidin-1-yl (2S)-2,6-bis({2,3-bis[(4-methoxyphenyl)methoxy]phenyl}formamido)hexanoate (4-61)**



Molecular Formula: C<sub>56</sub>H<sub>57</sub>N<sub>3</sub>O<sub>14</sub>

Molecular Mass: 996.08 g mol<sup>-1</sup>

**4-57** (0.207 g, 0.230 mmol) was placed under N<sub>2</sub>, and dissolved in dry DCM (25 mL), then NHS (33.1 mg, 0.288 mmol) and EDC.HCl (63.0 mg, 0.329 mmol) were added, and the clear solution stirred for 18 hours. Extra DCM (15 mL) was added, and the organic layer washed with 1 M HCl (35 mL), H<sub>2</sub>O (30 mL), saturated NaHCO<sub>3</sub> solution (30 mL) and brine (30 mL), dried over MgSO<sub>4</sub> and the solvent removed under vacuum. The resulting white paste/foam was purified by column chromatography (17 cm silica in 2.3 cm diameter column, 3:1 EtOAc:40-60 °C pet. ether to 4:1 EtOAc:40-60 °C pet.

ether, loaded with DCM) to give **4-61** as a colourless paste (0.124 g, 0.124 mmol, 54%), which was used as soon as possible due to its instability. Average yield = 55% (n = 4). R<sub>f</sub> = 0.51 (9:1 CHCl<sub>3</sub>:MeOH), 0.29 (4:1 EtOAc:40-60 °C pet. ether).

**<sup>1</sup>H NMR:** (400 MHz, CDCl<sub>3</sub>) δ<sub>H</sub> ppm: 8.61 (1H, d, *J* = 7.5 Hz, *H*27), 7.91 (1H, br t, *J* = 5.5 Hz, *H*20), 7.75 (1H, dd, *J* = 7.0, 2.5 Hz, *H*2 or 30), 7.68 (1H, m, *H*2 or 30), 7.42-7.36 (4H, m, *H*10/16/37/43), 7.24-7.21 (2H, m, *H*10/16/37/43), 7.20-7.18 (2H, m, *H*10/16/37/43), 7.15-7.14 (1H, m, *H*3/4/31/32), 7.13-7.09 (3H, m, *H*3/4/31/32), 6.95-6.91 (4H, m, *H*11/17/38/44), 6.83-6.80 (2H, m, *H*11/17/38/44), 6.79-6.76 (2H, m, *H*11/17/38/44), 5.09-5.00 (6H, m, *H*8/14/35/41), 4.99-4.92 (3H, m, *H*8/14/25/35/41), 3.84 (3H, s, *H*13/19/40/46), 3.83 (3H, s, *H*13/19/40/46), 3.75 (6H, two overlapping s, *H*13/19/40/46), 3.25-3.14 (2H, m, *H*21), 2.77 (4H, br s, *H*48), 1.84-1.72 (1H, m, *H*24), 1.59-1.51 (1H, m, *H*24), 1.38-1.27 (4H, m, *H*22 and 23).

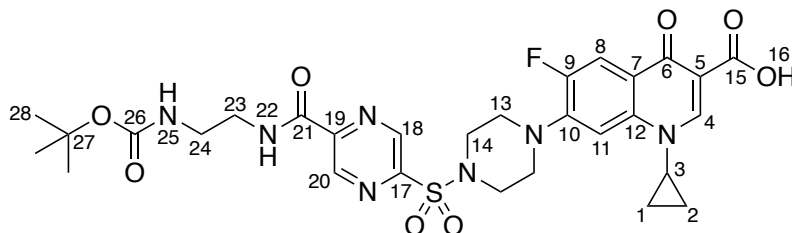
**<sup>13</sup>C NMR:** (100 MHz, CDCl<sub>3</sub>) δ<sub>C</sub> ppm: 168.7 (*C*47), 168.2 (*C*26), 165.2, 165.1 (*C*7/28), 160.04, 160.01, 159.82, 159.79 (*C*12/18/39/45), 151.9, 151.8 (*C*5/33), 147.2, 146.9 (*C*6/34), 130.9, 130.7, 129.8, 129.7 (*C*10/16/37/43), 128.7, 128.6, 128.5, 128.4 (*C*9/15/36/42), 127.6, 126.0 (*C*1/29), 124.4, 124.3 (*C*3/4/31/32), 123.6, 123.3 (*C*2/30), 117.6, 116.9 (*C*3/4/31/32), 114.18, 114.16, 114.10, 114.07 (*C*11/17/38/44), 76.2, 76.1, 71.2 (*C*8/14/35/41), 55.5, 55.42, 55.38 (*C*13/19/40/46), 50.8 (*C*25), 39.4 (*C*21), 31.7 (*C*24), 28.8 (*C*22 or 23) 25.7 (*C*48), 22.8 (*C*22 or 23).

**HRMS (ESI):** Calcd. [M+Na]<sup>+</sup> (C<sub>56</sub>H<sub>57</sub>N<sub>3</sub>NaO<sub>14</sub>) *m/z* = 1018.3733; Obs. [M+Na]<sup>+</sup> *m/z* = 1018.3765, Mean err -4.1 ppm.

**IR (ATIR, cm<sup>-1</sup>):** 3361 (NH stretches, w br), 3050-2800 (C-H stretching, w), 1816 (NHS ester C=O stretch, w), 1784 (NHS C=O symmetric stretch, w), 1738 (NHS C=O asymmetric stretch, s), 1655 (amide C=O stretch, br m), 1611 (amide C=O stretch, m) 1514 (C=C stretches, s), 1461 (C=C stretches, m), 1247 (C-O stretches, s).



**7-[4-({5-[(2-[(*tert*-Butoxy)carbonyl]amino}ethyl)carbamoyl]pyrazin-2-yl)sulfonyl)piperazin-1-yl]-1-cyclopropyl-6-fluoro-4-oxo-1,4-dihydroquinoline-3-carboxylic acid (4-55)**



Molecular Formula: C<sub>29</sub>H<sub>34</sub>FN<sub>7</sub>O<sub>8</sub>S

Molecular Mass: 659.69 g mol<sup>-1</sup>

**4-38** (0.741 g, 1.91 mmol) was placed under N<sub>2</sub>, then DCM (25 mL), acetic acid (1.9 mL) and H<sub>2</sub>O (3.8 mL) were added, and the resulting biphasic solution was cooled to 0 °C. 1,3-Dichloro-5,5'-dimethylhydantoin (1.13 g, 5.72 mmol) was added in portions with vigorous stirring to give a cloudy beige solution, which was allowed to warm slowly in the ice bath and stirred for 14 hours and 30 minutes. Extra DCM (80 mL) was added, followed by ice-cold aqueous sodium metabisulfite solution (5% w/v, 105 mL), and stirred for 10 minutes at 0 °C. The layers were transferred to a separating funnel, and shaken well, and separated, then the aqueous layer was extracted with DCM (2 x 60 mL). The combined organic layers were washed with ice-cold saturated NaHCO<sub>3</sub> solution (130 mL) and ice-cold brine (130 mL), dried over MgSO<sub>4</sub> and transferred to a fresh round-bottomed flask, and cooled back to 0 °C. Ciprofloxacin (0.511 g, 1.54 mmol) and DIPEA (0.81 mL, 4.65 mmol) were added to give a cloudy white solution, which was allowed to warm to room temperature and stirred for a further 24 hours. The volume was reduced to around 40 mL, and the resulting solid isolated via Buchner filtration, and washed with DCM (65 mL) and 1 M HCl (150 mL), then dried under vacuum to give **4-55** as a white solid (0.533 g, 0.808 mmol, 52%). M.p. = 228-229 °C (dec.), brown colour on heating to c. 160 °C.

<sup>1</sup>H NMR: (400 MHz, DMSO-d<sub>6</sub>) δ<sub>H</sub> ppm: 9.34 (1H, d, *J* = 1.5 Hz, *H*18 or 20), 9.17 (1H, d, *J* = 1.5 Hz, *H*18 or 20), 9.13 (1H, br t, *J* = 6.0 Hz, *H*22), 8.67 (1H, s, *H*4), 7.92 (1H, d, <sup>3</sup>*J*<sub>F-H</sub> = 13.0 Hz, *H*8), 7.59 (1H, d, <sup>4</sup>*J*<sub>F-H</sub> = 7.5 Hz, *H*11), 6.93 (1H, br t, *J* = 5.5 Hz, *H*25), 3.87-3.75 (1H, m, *H*3), 3.52-3.45 (4H, m, *H*13 or 14),

3.45-3.29 (6H, m, H13 or 14 and H23 or 24), 3.12 (2H, app. q,  $J = 6.0$  Hz, H23 or 24), 1.34 (9H, s, H27), 1.33-1.29 (2H, m, H1 or 2), 1.20-1.14 (2H, m, H1 or 2).

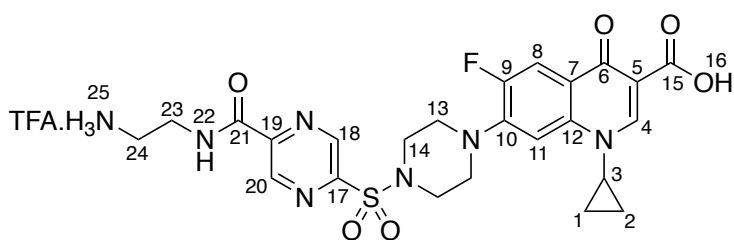
**$^{13}\text{C}$  NMR:** (100 MHz, DMSO- $d_6$ )  $\delta_{\text{C}}$  ppm: 176.4 (C6), 166.0 (C15), 162.0 (C21), 155.8 (C26), 152.8 (C9), 152.5 (C17 or 19), 148.2 (C4), 147.4 (C17 or 19), 144.0 (C10 and C18 or 20), 141.5 (C18 or 20), 139.1 (C12), 119.3 (C7), 111.2 (C8), 107.2 (C11), 106.8 (C5), 77.8 (C27), 49.1 (C13 or 14), 45.8 (C13 or 14), 39.3 (C24), 39.2 (C23), 36.0 (C3), 28.2 (C28), 7.6 (C1 and 2).

**HRMS (ESI Pos.):** Calcd.  $[\text{M}+\text{H}]^+$  ( $\text{C}_{29}\text{H}_{35}\text{FN}_7\text{O}_8\text{S}$ )  $m/z = 660.2246$ ; Obs.  $[\text{M}+\text{H}]^+$   $m/z = 660.2236$ , Mean err 2.8 ppm. Calcd.  $[\text{M}+\text{Na}]^+$  ( $\text{C}_{29}\text{H}_{34}\text{FN}_7\text{NaO}_8\text{S}$ )  $m/z = 682.2066$ ; Obs.  $[\text{M}+\text{Na}]^+$   $m/z = 682.2051$ , Mean err 3.3 ppm. Calcd.  $[\text{M}+\text{K}]^+$  ( $\text{C}_{29}\text{H}_{34}\text{FKN}_7\text{O}_8\text{S}$ )  $m/z = 698.1805$ ; Obs.  $[\text{M}+\text{K}]^+$   $m/z = 698.1782$ , Mean err 1.9 ppm.

**HRMS (ESI Neg.):** Calcd.  $[\text{M}-\text{H}]^-$  ( $\text{C}_{29}\text{H}_{33}\text{FN}_7\text{O}_8\text{S}$ )  $m/z = 658.2101$ ; Obs.  $[\text{M}-\text{H}]^-$   $m/z = 658.2113$ , Mean err 1.2 ppm. Calcd.  $[\text{M}+^{35}\text{Cl}]^-$  ( $\text{C}_{29}\text{H}_{34}^{35}\text{ClFN}_7\text{O}_8\text{S}$ )  $m/z = 694.1868$ ; Obs.  $[\text{M}+^{35}\text{Cl}]^-$   $m/z = 694.1872$ .

**IR (ATIR,  $\text{cm}^{-1}$ ):** 3513 (OH stretch, m), 3297 (NH amide/carbamate stretch, m), 3000-2750 (C-H stretching, w), 1705 (carboxylic acid/amide C=O stretch, br m), 1667 (carbamate C=O stretch, m), 1629 (quinolone C=O stretch, m), 1537 (C=N/C=C stretches, s), 1453 (C=N/C=C stretches, m), 1374 (S=O stretch, m), 1165 (S=O stretch, s).

**7-[4-({5-[(2-Aminoethyl)carbamoyl]pyrazin-2-yl}sulfonyl)piperazin-1-yl]-1-cyclopropyl-6-fluoro-4-oxo-1,4-dihydroquinoline-3-carboxylic acid (4-62)**



Molecular Formula:  $\text{C}_{26}\text{H}_{27}\text{F}_4\text{N}_7\text{O}_8\text{S}$

Molecular Mass:  $673.60 \text{ g mol}^{-1}$

**4-55** (0.325 g, 0.492 mmol) was suspended in dry DCM (6 mL) to give a cloudy white solution, which was cooled to 0 °C. A solution of 20% (v/v) trifluoroacetic acid in DCM (6.2 mL; 10% v/v TFA in final solution) was added slowly to give a clear yellow solution and stirred at 0 °C for 5 hours. The solvent was removed under vacuum to give an orange-yellow solid. The resulting residue was triturated in hot EtOH (6 mL), then Et<sub>2</sub>O (20 mL) was added and the resulting yellow-white solid was isolated via Buchner filtration and washed with Et<sub>2</sub>O (50 mL) to give **4-62** (0.262 g, 0.389 mmol, 79%). Average yield = 73% (n = 3). M.p. = 213-217 °C (dec.).

**<sup>1</sup>H NMR:** (400 MHz, DMSO-d<sub>6</sub>) δ<sub>H</sub> ppm: 9.37 (1H, d, *J* = 1.5 Hz, *H18 or 20*), 9.32 (1H, br t, *J* = 6.0 Hz, *H22*), 9.21 (1H, d, *J* = 1.5 Hz, *H18 or 20*), 8.66 (1H, s, *H4*), 7.90 (1H, d, <sup>3</sup>*J*<sub>F-H</sub> = 13.0 Hz, *H8*), 7.90 (3H, br s, *H25*)\*, 7.58 (1H, d, <sup>4</sup>*J*<sub>F-H</sub> = 7.5 Hz, *H11*), 3.84-3.76 (1H, m, *H3*), 3.59 (2H, app. q, *J* = 6.0 Hz, *H23*), 3.52-3.45 (4H, m, *H13 or 14*), 3.45-3.40 (4H, m, *H13 or 14*), 3.06-2.95 (2H, m, *H24*), 1.35-1.29 (2H, m, *H1 or 2*), 1.20-1.14 (2H, m, *H1 or 2*).

\*Chemical shift appears to be concentration-dependent, moves from 7.78 to 7.82 to 7.90 as the concentration in the NMR increases.

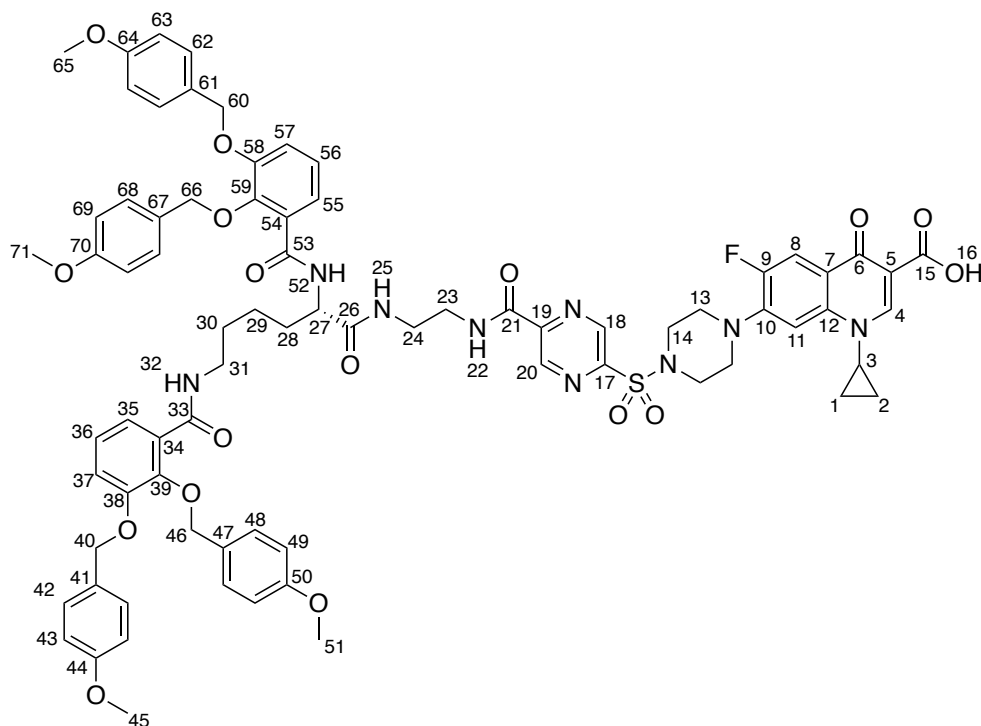
**<sup>13</sup>C NMR:** (100 MHz, DMSO-d<sub>6</sub>) δ<sub>C</sub> ppm: 176.4 (*C6*), 165.9 (*C15*), 162.5 (*C21*), 158.0 (q, <sup>2</sup>*J*<sub>F-C</sub> = 31 Hz, *TFA C=O*), 153.0 (d, <sup>1</sup>*J*<sub>F-C</sub> = 250 Hz, *C9*), 152.7 (*C17 or 19*), 148.2 (*C4*), 147.2 (*C17 or 19*), 144.6 (d, <sup>2</sup>*J*<sub>F-C</sub> = 10 Hz, *C10*), 144.1 (*C18 or 20*), 141.5 (*C18 or 20*), 139.1 (*C12*), 119.2 (d, <sup>3</sup>*J*<sub>F-C</sub> = 8 Hz, *C7*), 111.1 (d, <sup>2</sup>*J*<sub>F-C</sub> = 23 Hz, *C8*), 107.2 (d, <sup>3</sup>*J*<sub>F-C</sub> = 3 Hz, *C11*), 106.8 (*C5*), 49.1 (*C13 or 14*), 45.8 (*C13 or 14*), 38.5 (*C24*), 36.9 (*C23*), 36.0 (*C3*), 7.7 (*C1 and 2*).

**<sup>19</sup>F NMR:** (376 MHz, DMSO-d<sub>6</sub>) δ<sub>F</sub> ppm: -73.38 (3F, s, *TFA*), -121.91 (1F, dd, *J* = 13.0, 7.5 Hz).

**HRMS (ESI):** Calcd. [M+H]<sup>+</sup> (C<sub>24</sub>H<sub>27</sub>FN<sub>7</sub>O<sub>6</sub>S) *m/z* = 560.1722; Obs. [M+H]<sup>+</sup> *m/z* = 560.1713, Mean err 4.7 ppm. Calcd. [M+Na]<sup>+</sup> (C<sub>24</sub>H<sub>26</sub>FN<sub>7</sub>NaO<sub>6</sub>S) *m/z* = 582.1542; Obs. [M+Na]<sup>+</sup> *m/z* = 582.1538, Mean err 2.5 ppm.

**IR (ATIR,  $\text{cm}^{-1}$ ):** 3500-2700 ( $\text{NH}_3$  stretch, w br), 3416 (amide NH stretch, w), 3100-2850 (C-H stretching, w), 1683 (carboxylic acid C=O stretch/amide C=O stretch, br s), 1626 (C=O quinolone stretch, s), 1495 (N=C/C=C stretches, br s), 1451 (C=C stretches, s), 1359 (S=O stretch, m), 1175 (S=O stretch, s), 1128 (C-F stretches, s).

**7-(4-{[5-{{2-[[2S]-2,6-Bis({2,3-bis[(4-methoxyphenyl)methoxy]phenyl}formamido)hexanamido]ethyl}carbamoyl]pyrazin-2-yl]sulfonyl]piperazin-1-yl)-1-cyclopropyl-6-fluoro-4-oxo-1,4-dihydroquinoline-3-carboxylic acid (4-63)**



Molecular Formula:  $\text{C}_{76}\text{H}_{78}\text{FN}_9\text{O}_{17}\text{S}$

Molecular Mass:  $1440.56 \text{ g mol}^{-1}$

**4-61** (55.6 mg, 0.056 mmol) was placed under  $\text{N}_2$ , then dissolved in dry DCM (10 mL) to give a clear solution. TFA salt **4-62** (40.3 mg, 0.060 mmol) and  $\text{Et}_3\text{N}$  (25  $\mu\text{L}$ , 0.179 mmol) were added, along with an additional 10 mL DCM, yielding a cloudy yellow-white solution. The solution was stirred for 24 hours, then filtered into a separating funnel, and washed with extra DCM (10 mL). The solution was washed with 1 M aqueous HCl (22.5 mL),  $\text{H}_2\text{O}$  (20 mL) and brine (20 mL), dried over  $\text{MgSO}_4$  and the solvent removed under

vacuum to give **4-63** as a yellow glass, which becomes a powdery solid on scraping (73.1 mg, 0.051 mmol, 91%).  $R_f = 0.36$  (9:1  $\text{CHCl}_3$ :MeOH).

**$^1\text{H NMR}$** : (400 MHz,  $\text{CDCl}_3$ )  $\delta_{\text{H}}$  ppm: 14.90 (1H, br s, *H16*), 9.31 (1H, d,  $J = 1.5$  Hz, *H18 or 20*), 8.72 (1H, s, *H4*), 8.65 (1H, d,  $J = 1.5$  Hz, *H18 or 20*), 8.49 (1H, br d,  $J = 6.5$  Hz, *H52*), 8.38 (1H, br t,  $J = 6.0$  Hz, *H22*), 8.05 (1H, br t,  $J = 6.0$  Hz, *H32*), 7.97 (1H, d,  $^3J_{\text{F-H}} = 12.5$  Hz, *H8*), 7.57-7.51 (2H, m, *H35 and 55*), 7.45-7.37 (4H, m, *H42/48/62/68*), 7.36 (1H, d,  $^4J_{\text{F-H}} = 7.0$  Hz, *H11*), 7.30-7.24 (2H, m, *H42/48/62/68*), 7.23-7.17 (3H, m, *H37/42/48/57/62/68*), 7.15-7.09 (2H, m, *H36/37/56/57*), 7.08-7.01 (2H, m, *H25/36/56*), 6.97-6.91 (4H, m, *H43/49/63/69*), 6.84-6.79 (2H, m, *H43/49/63/69*), 6.79-6.75 (2H, m, *H43/49/63/69*), 5.14-5.02 (6H, m, *H40/46/60/66*), 4.97 (2H, s, *H40/46/60/66*), 4.30 (1H, q,  $J = 7.0$  Hz, *H27*), 3.84 (3H, s, *H45/51/65/71*), 3.83 (3H, s, *H45/51/65/71*), 3.76 (3H, s, *H45/51/65/71*), 3.74 (3H, s, *H45/51/65/71*), 3.69-3.63 (1H, m, *H23/24*), 3.62-3.47 (7H, m, *H3/13/14/23/24*), 3.46-3.32 (5H, m, *H13/14/23/24*), 3.18 (2H, app. q,  $J = 6.5$  Hz, *H31*), 1.79-1.68 (1H, m, *H28*), 1.58-1.49 (1H, m, *H28*), 1.45-1.15 (8H, m, *H1/2/29/30*).

**$^{13}\text{C NMR}$** : (100 MHz,  $\text{CDCl}_3$ )  $\delta_{\text{C}}$  ppm: 177.1 (*C6*), 172.9 (*C26*), 166.9 (*C15*), 166.1 (*C53*), 165.4 (*C33*), 162.2 (*C21*), 160.0, 159.8, 159.7 (*C44/50/64/70*), 154.2 (d,  $^1J_{\text{F-C}} = 252$  Hz, *C9*), 153.9 (*C17 or 19*), 151.83, 151.80 (*C38/58*), 147.7 (*C4*), 146.84, 146.80 (*C17/19/39/59*), 145.2 (d,  $^2J_{\text{F-C}} = 10$  Hz, *C10*), 144.0 (*C18 or 20*), 141.3 (*C18 or 20*), 139.0 (*C12*), 130.9, 130.6, 129.8, 129.6 (*C42/48/62/68*), 128.6, 128.5, 128.39, 128.37 (*C41/47/61/67*), 127.0, 126.6 (*C34/54*), 124.3 (*C36 and 56*), 123.0, 122.6 (*C35/55*), 120.6 (d,  $^3J_{\text{F-C}} = 8$  Hz, *C7*), 117.3, 117.0 (*C37/57*), 114.12, 114.06, 114.0 (*C43/49/63/69*), 112.6 (d,  $^2J_{\text{F-C}} = 23$  Hz, *C8*), 108.2 (*C5*), 105.6 (*C11*), 76.1, 75.7, 71.1 (*C40/46/60/66*), 55.4, 55.3 (*C45/51/65/71*), 54.3 (*C27*), 49.6 (*C13 or 14*), 46.3 (*C13 or 14*), 40.1, 39.2 (*C23/24*), 39.0 (*C31*), 35.5 (*C3*), 30.6 (*C28*), 29.0, 23.1 (*C29/30*), 8.3 (*C1 and 2*).

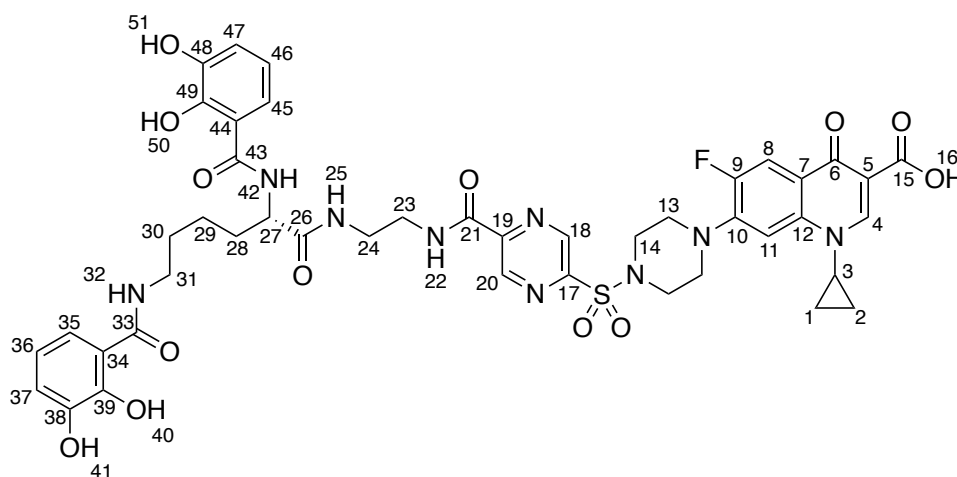
**$^{19}\text{F NMR}$** : (282 MHz,  $\text{DMSO-d}_6$ )  $\delta_{\text{F}}$  ppm: -121.34 (1F, dd,  $J = 13.0, 7.5$  Hz).

**HRMS (ESI Pos.):** Calcd.  $[M+Na]^+$  ( $C_{76}H_{78}FN_9NaO_{17}S$ )  $m/z = 1462.5113$ ; Obs.  $[M+Na]^+$   $m/z = 1462.5112$ , Mean err 0.6 ppm.

**HRMS (ESI Neg.):** Calcd.  $[M-H]^-$  ( $C_{76}H_{77}FN_9O_{17}S$ )  $m/z = 1438.5148$ ; Obs.  $[M-H]^-$   $m/z = 1438.5168$ , Mean err -0.7 ppm.

**IR (ATIR,  $cm^{-1}$ ):** 3360 (NH/OH stretches, w br), 3050-2800 (C-H stretching, w), 1726 (amide C=O stretch, w), 1649 (carboxylic acid C=O stretch/amide C=O stretch, br m), 1628 (C=O quinolone stretch, m), 1612 (amide C=O stretch, m) 1513 (N=C/C=C stretches, s), 1453 (N=C/C=C stretches, s), 1364 (S=O stretch, m), 1247 (C-O stretches, s), 1173 (S=O stretch, m).

**7-(4-{[5-{(2-[2,6-Bis[(2,3-dihydroxyphenyl)formamido]hexanamido]ethyl}carbamoyl)pyrazin-2-yl]sulfonyl}piperazin-1-yl)-1-cyclopropyl-6-fluoro-4-oxo-1,4-dihydroquinoline-3-carboxylic acid (4-32)**



Molecular Formula:  $C_{44}H_{46}FN_9O_{13}S$

Molecular Mass:  $959.96 \text{ g mol}^{-1}$

**4-63** (68.4 mg, 0.048 mmol) was dissolved in dioxane (8 mL) to give a clear solution. 4 M HCl in dioxane (1.75 mL, 7.00 mmol) was diluted in a further 4.5 mL dioxane, and added dropwise, with the solution changing to clear yellow one minute post the start of addition, and then cloudy yellow thereafter, with formation of a yellow precipitate. The solution was stirred for 5 hours, then the precipitate was isolated via Buchner filtration was washed with further dioxane (10 mL) and DCM (15 mL). The yellow solid was dried further under vacuum to give **4-32** (15.7 mg, 0.016 mmol, 34%).

The reaction may be monitored by HPLC by taking 20  $\mu$ L aliquots at regular intervals, followed by dilution in 980  $\mu$ L DMSO, and the corresponding HPLC trace recorded using Analytical HPLC method D.

**$^1\text{H}$  NMR:** (600 MHz, DMSO- $d_6$ )  $\delta_{\text{H}}$  ppm: 16.14 (1H, br s, *H16*), 12.83 (1H, br s, *H40 or 50*), 12.01 (1H, br s, *H40 or 50*), 9.32 (1H, d,  $J = 1.5$  Hz, *H18 or 20*), 9.13 (1H, d,  $J = 1.5$  Hz, *H18 or 20*), 9.09 (1H, br t,  $J = 6.0$  Hz, *H22*), 8.75 (1H, br t,  $J = 5.0$  Hz, *H32*), 8.71 (1H, br t,  $J = 7.5$  Hz, *H42*), 8.66 (1H, s, *H4*), 8.21 (1H, br t,  $J = 6.0$  Hz, *H25*), 7.89 (1H, d,  $^3J_{\text{F-H}} = 13.0$  Hz, *H8*), 7.56 (1H, d,  $^4J_{\text{F-H}} = 7.0$  Hz, *H11*), 7.39 (1H, d,  $J = 8.0$  Hz, *H45*), 7.24 (1H, d,  $J = 8.0$  Hz, *H35*), 6.92 (1H, dd,  $J = 7.5, 1.0$  Hz, *H47*), 6.86 (1H, dd,  $J = 8.0, 1.0$  Hz, *H37*), 6.67 (1H, t,  $J = 8.0$  Hz, *H46*), 6.62 (1H, t,  $J = 8.0$  Hz, *H36*), 4.41-4.35 (1H, m, *H27*), 3.82-3.76 (1H, m, *H3*), 3.50-3.45 (4H, m, *H13 or 14*), 3.45-3.20 (8H, m, *H23 and 24 and H13 or 14*)\*, 3.28-3.18 (2H, m, *H31*), 1.81-1.68 (2H, m, *H28*), 1.58-1.47 (2H, m, *H30*), 1.41-1.34 (1H, m, *H29*), 1.34-1.26 (3H, m, *H29 and H1 or 2*), 1.19-1.13 (2H, m, *H1 or 2*).

\*Overlap with residual  $\text{H}_2\text{O}$  peak in DMSO.

**$^{13}\text{C}$  NMR:** (100 MHz,  $\text{CDCl}_3$ )  $\delta_{\text{C}}$  ppm: 176.4 (*C6*), 171.7 (*C26*), 169.7 (*C33*), 168.9 (*C43*), 165.9 (*C15*), 162.0 (*C21*), 152.9 (d,  $^1J_{\text{F-C}} = 250$  Hz, *C9*), 152.6 (*C17 or 19*), 149.7 (*C39*), 148.7 (*C49*), 148.1 (*C4*), 147.3 (*C17 or 19*), 146.2 (*C38*), 146.0 (*C48*), 144.5 (d,  $^2J_{\text{F-C}} = 10$  Hz, *C10*), 143.9 (*C18 or 20*), 141.4 (*C18 or 20*), 139.1 (*C12*), 119.2 (d,  $^3J_{\text{F-C}} = 7$  Hz, *C7*), 118.8, 118.7 (*C37/47*), 118.3 (*C45*), 118.0 (*C46*), 117.8 (*C36*), 117.1 (*C35*), 115.7 (*C44*), 114.9 (*C34*), 111.1 (d,  $^2J_{\text{F-C}} = 23$  Hz, *C8*), 107.1 (*C11*), 106.8 (*C5*), 53.3 (*C27*), 49.0 (*C13 or 14*), 45.8 (*C13 or 14*), 39.1 (*C26*), 38.8 (*C31*), 38.2 (*C24*), 35.9 (*C3*), 31.3 (*C28*), 28.5 (*C30*), 23.1 (*C29*), 7.6 (*C1 and 2*).

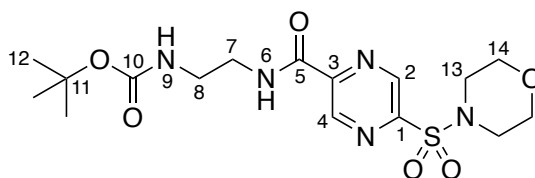
**$^{19}\text{F}$  NMR:** (470 MHz, DMSO- $d_6$ )  $\delta_{\text{F}}$  ppm: -121.91 (1F, dd,  $J = 12.5, 7.5$  Hz).

**HRMS (ESI Pos.):** Calcd.  $[\text{M}+\text{Na}]^+$  ( $\text{C}_{44}\text{H}_{46}\text{FN}_9\text{NaO}_{13}\text{S}$ )  $m/z = 982.2812$ ; Obs.  $[\text{M}+\text{Na}]^+$   $m/z = 982.2852$ , Mean err -2.4 ppm.

**HRMS (ESI Neg.):** Calcd.  $[M-H]^-$  ( $C_{44}H_{45}FN_9NaO_{13}S$ )  $m/z = 958.2847$ ; Obs.  $[M-H]^-$   $m/z = 958.2845$ , Mean err 0.2 ppm.

**IR (ATIR,  $cm^{-1}$ ):** 3650-3100 (NH/OH stretches, w br), 3100-2750 (C-H stretching, w), 1720 (amide C=O stretch, w), 1671 (carboxylic acid C=O stretch/amide C=O stretch, br m), 1626 (C=O quinolone stretch, w), 1535 (N=C/C=C stretches, s), 1495 (N=C/C=C stretches, w), 1450 (N=C/C=C stretches, s), 1263 (C-O stretches, s), 1156 (S=O stretch, m).

***tert*-Butyl *N*-(2-{{[5-(morpholine-4-sulfonyl)pyrazin-2-yl]formamido}ethyl) carbamate (4-48)**



Molecular Formula:  $C_{16}H_{25}N_5O_6S$

Molecular Mass:  $415.47 \text{ g mol}^{-1}$

**4-38** (0.112 g, 0.289 mmol) was placed under  $N_2$ , then DCM (1 mL), acetic acid (0.14 mL) and  $H_2O$  (0.28 mL) were added, and the resulting biphasic solution was cooled to  $0^\circ C$ . 1,3-Dichloro-5,5'-dimethylhydantoin (0.177 g, 0.870 mmol) was added in portions with vigorous stirring to give a cloudy beige solution, which was allowed to warm slowly in the ice bath and stirred for 7h30. Extra DCM (10 mL) was added, and the reaction mixture poured into ice-cold aqueous sodium metabisulfite solution (5% w/v, 15 mL). The layers were shaken well and separated, then the aqueous layer was extracted with DCM (2 x 12.5 mL). The combined organic layers were washed with ice-cold saturated  $NaHCO_3$  solution (15 mL) and ice-cold brine (15 mL), dried over  $MgSO_4$ , transferred to a fresh round-bottomed flask, and cooled back to  $0^\circ C$ , then morpholine (28  $\mu L$ , 0.320 mmol) and  $Et_3N$  (60  $\mu L$ , 0.430 mmol) added, giving a clear colourless solution. The reaction was allowed to warm to room temperature and stirred for 25 hours, changing to pale green over that time. The solution was washed with 1 M aq. HCl (20 mL), water (20 mL), saturated  $NaHCO_3$  solution (20 mL) and brine (20 mL), dried over  $MgSO_4$  and the DCM removed *in vacuo* to give a white solid. The product was



purified further by column chromatography (35g silica gel, 1:1 40-60 °C pet. ether:EtOAc followed by 1:1 CHCl<sub>3</sub>:EtOAc) to give **4-48** as a crystalline white solid (43 mg, 0.103 mmol, 36%). Average yield = 43% (n = 4). M.p. = 182 °C.

**<sup>1</sup>H NMR:** (400 MHz, CDCl<sub>3</sub>) δ<sub>H</sub> ppm: 9.45 (1H, d, *J* = 1.5 Hz, *H2 or 4*), 9.06 (1H, d, *J* = 1.5 Hz, *H2 or 4*), 8.34-8.18 (1H, m, *H6*), 4.95-4.80 (1H, m, *H9*), 3.80-3.73 (4H, m, *H14*), 3.62 (2H, app. q, *J* = 6.0 Hz, *H7*), 3.46-3.35 (6H, m, *H8 and 13*), 1.41 (9H, s, *H12*).

**<sup>13</sup>C NMR:** (100 MHz, CDCl<sub>3</sub>) δ<sub>C</sub> ppm: 162.3 (*C5*), 156.8 (*C10*), 154.5 (*C1 or 3*), 146.5 (*C1 or 3*), 144.0 (*C2 or 4*), 141.6 (*C2 or 4*), 80.1 (*C11*), 66.5 (*C14*), 46.7 (*C13*), 41.0, 40.1 (*C7/8*), 28.4 (*C12*).

**HRMS (ESI):** Calcd. [M+H]<sup>+</sup> (C<sub>16</sub>H<sub>26</sub>N<sub>5</sub>O<sub>6</sub>S) *m/z* = 416.1598; Obs. [M+H]<sup>+</sup> *m/z* = 416.1601, Mean err 0.2 ppm. Calcd. [M+Na]<sup>+</sup> (C<sub>16</sub>H<sub>25</sub>N<sub>5</sub>NaO<sub>6</sub>S) *m/z* = 438.1418; Obs. [M+Na]<sup>+</sup> *m/z* = 438.1421, Mean err -1.1 ppm.

**IR (ATIR, cm<sup>-1</sup>):** 3357 (NH stretches, m), 3000-2825 (C-H stretching, w), 1717 (carbamate C=O stretch, m), 1681 (amide C=O stretch, s), 1536 (C=N/C=C stretches, s), 1451 (C=N/C=C stretches, m), 1350 (S=O stretch, m), 1164 (S=O stretch, s).

#### Elemental Analysis:

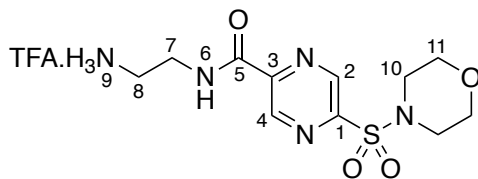
For [C<sub>16</sub>H<sub>25</sub>N<sub>5</sub>O<sub>6</sub>S . 0.02 CHCl<sub>3</sub> . 0.15 EtOAc]:

*Calculated:* %C, 46.31; %H, 6.13; %N, 16.25.

*Measured:* %C, 46.35, %H, 6.11, %N, 16.27.

***N*-(2-Aminoethyl)-5-(morpholine-4-sulfonyl)pyrazine-2-carboxamide**

**TFA salt (4-49)**



Molecular Formula: C<sub>13</sub>H<sub>18</sub>F<sub>3</sub>N<sub>5</sub>O<sub>6</sub>S

Molecular Mass: 429.37 g mol<sup>-1</sup>

**4-48** (0.111 g, 0.267 mmol) was dissolved in dry DCM (8 mL) to give a clear solution, which was cooled to 0 °C. A solution of 20% (v/v) trifluoroacetic acid in DCM (8 mL; 10% v/v TFA in final solution) was added slowly and the solution stirred at 0 °C for 5 hours. The solvent was removed under vacuum to give a pink residue, which was triturated in hot EtOH (1 mL), then Et<sub>2</sub>O (15 mL) was added and the resulting white powdery solid was isolated via Buchner filtration and washed with Et<sub>2</sub>O (25 mL) to give **4-49** (77.7 mg, 0.181 mmol, 68%). Average yield = 64% (n = 3). M.p. = 223-225 °C (dec.).

**<sup>1</sup>H NMR:** (400 MHz, DMSO-d<sub>6</sub>) δ<sub>H</sub> ppm: 9.37 (1H, d, *J* = 1.5 Hz, *H*2 or 4), 9.31 (1H, br t, *J* = 6.0 Hz, *H*6), 9.17 (1H, d, *J* = 1.5 Hz, *H*2 or 4), 7.80 (3H, br s, *H*9), 3.66-3.61 (4H, m, *H*11), 3.59 (2H, app. q, *J* = 6.0 Hz, *H*7), 3.25-3.19 (4H, m, *H*10), 3.02 (2H, t, *J* = 6.0 Hz, *H*8).

**<sup>13</sup>C NMR:** (100 MHz, DMSO-d<sub>6</sub>) δ<sub>C</sub> ppm: 162.5 (*C*5), 152.6 (*C*1 or 3), 147.1 (*C*1 or 3), 144.0 (*C*2 or 4), 141.5 (*C*2 or 4), 65.6 (*C*11), 46.1 (*C*10), 38.6 (*C*8), 36.9 (*C*7).

**<sup>19</sup>F NMR:** (376 MHz, DMSO-d<sub>6</sub>) δ<sub>F</sub> ppm: -73.42 (3F, s, TFA).

**IR (ATIR, cm<sup>-1</sup>):** 3272 (NH stretches, br w), 3100-2800 (C-H stretching, w), 1694 (amide C=O stretch, s), 1534 (C=N/C=C stretches, m), 1509 (NH<sub>3</sub><sup>+</sup> bending, m), 1454 (C=N/C=C stretches, m), 1359 (S=O stretch, s), 1172 (S=O stretch, m).

### Free Amine

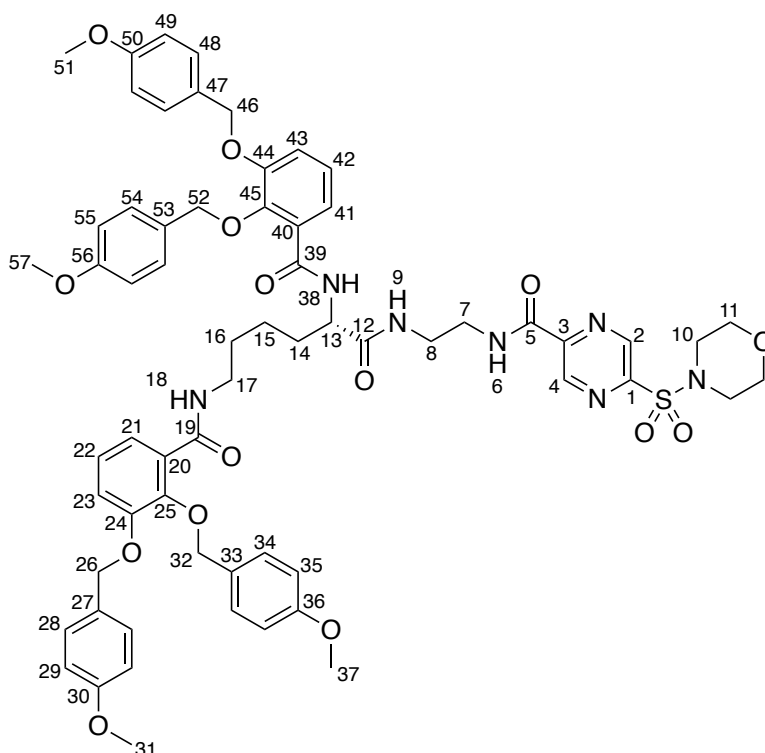
**HRMS (ESI Pos.):** Calcd.  $[M+H]^+$  ( $C_{11}H_{18}N_5O_4S$ )  $m/z = 316.1074$ ; Obs.  $[M+H]^+$   $m/z = 316.1073$ , Mean err  $-1.8$  ppm.

**HRMS (ESI Neg.):** Calcd.  $[M-H]^-$  ( $C_{11}H_{16}N_5O_4S$ )  $m/z = 314.0928$ ; Obs.  $[M-H]^-$   $m/z = 314.0949$ , Mean err  $-0.5$  ppm.

### TFA Salt

**HRMS (ESI Neg.):** Calcd.  $[M-H]^-$  ( $C_{13}H_{17}F_3N_5O_6S$ )  $m/z = 428.0857$ ; Obs.  $[M-H]^-$   $m/z = 428.0864$ , Mean err  $-3.4$  ppm.

### **(2S)-2,6-Bis({2,3-bis[(4-methoxyphenyl)methoxy]phenyl}formamido)-*N*- (2-{{[5-(morpholine-4-sulfonyl)pyrazin-2-yl]}formamido}ethyl)hexanamide (4-66)**



Molecular Formula:  $C_{63}H_{69}N_7O_{15}S$

Molecular Mass:  $1196.34 \text{ g mol}^{-1}$

**4-61** (50.8 mg, 0.051 mmol) was placed under  $N_2$ , then dissolved in dry DCM (8 mL) to give a clear solution. **4-49** (23.5 mg, 0.055 mmol) and  $Et_3N$  (22  $\mu$ L, 0.158 mmol), plus additional DCM (7 mL) were added, and the reaction stirred for 16 hours. Extra DCM (10 mL) was added, and the organic layers

washed with 1 M HCl (20 mL), H<sub>2</sub>O (15 mL), saturated NaHCO<sub>3</sub> solution (15 mL) and brine (15 mL), then dried over MgSO<sub>4</sub>\*, and the solvent removed to give **4-66** as a colourless glass, which scrapes to a powdery solid (52.2 mg, 0.044 mmol, 86%). Average yield = 87% (n = 2).

\*The RBF used post-aqueous workup was pre-soaked in 6 M HCl overnight to ensure removal of any traces of iron.

**<sup>1</sup>H NMR:** (400 MHz, CDCl<sub>3</sub>) δ<sub>H</sub> ppm: 9.29 (1H, d, *J* = 1.5 Hz, *H2 or 4*), 8.57 (1H, d, *J* = 1.5 Hz, *H2 or 4*), 8.44 (1H, br d, *J* = 7.0 Hz, *H38*), 8.30 (1H, br t, *J* = 5.0 Hz, *H6*), 8.04 (1H, br t, *J* = 5.5 Hz, *H18*), 7.55 (1H, dd, *J* = 8.0, 1.5 Hz, *H21 or 41*), 7.53 (1H, dd, *J* = 8.0, 1.5 Hz, *H21 or 41*), 7.44-7.37 (4H, m, *H28/34/48/54*), 7.26-7.22 (2H, m, *H28/34/48/54*), 7.22-7.16 (3H, m, *H23/28/34/43/48/54*), 7.15-7.09 (2H, m, *H22/23/42/43*), 7.03 (1H, t, *J* = 8.0 Hz, *H22 or 42*), 6.96-6.91 (4H, m, *H29/35/49/55*), 6.90-6.85 (1H, m, *H9*), 6.83-6.79 (2H, m, *H29/35/49/55*), 6.79-6.74 (2H, m, *H29/35/49/55*), 5.14-5.00 (6H, m, *H26/32/46/52*), 4.99-4.95 (2H, m, *H26/32/46/52*), 4.26 (1H, q, *J* = 7.0 Hz, *H13*), 3.83 (6H, two overlapping s, *H31/37/51/57*), 3.75 (3H, s, *H31/37/51/57*), 3.73 (3H, s, *H31/37/51/57*), 3.73-3.68 (4H, m, *H11*), 3.69-3.63 (1H, m, *H7 or 8*), 3.58-3.45 (2H, m, *H7 or 8*), 3.43-3.35 (1H, m, *H7 or 8*), 3.33-3.27 (4H, m, *H10*), 3.19 (2H, app. q, *J* = 6.5 Hz, *H17*), 1.80-1.67 (1H, m, *H14*), 1.43-1.34 (1H, m, *H14*), 1.34-1.15 (4H, m, *H15 and 16*).

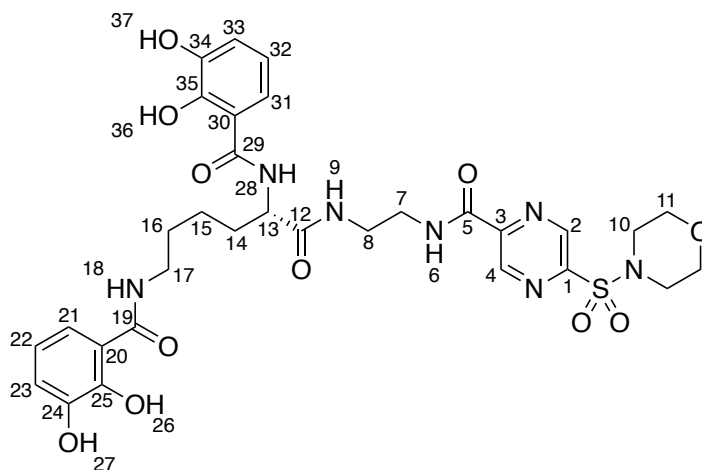
**<sup>13</sup>C NMR:** (100 MHz, CDCl<sub>3</sub>) δ<sub>C</sub> ppm: 172.8 (*C12*), 166.3 (*C39*), 165.4 (*C19*), 162.3 (*C5*), 160.05, 160.03, 159.83, 159.79 (*C30/36/50/56*), 153.9 (*C1 or 3*), 151.9 (*C24 and 44*), 146.9, 146.8 (*C25/45*), 146.6 (*C1 or 3*), 143.9 (*C2 or 4*), 141.5 (*C2 or 4*), 131.0, 130.7, 129.9, 129.7 (*C28/34/48/54*), 128.7, 128.6, 128.5, 128.4 (*C27/33/47/53*), 127.1, 126.7 (*C20/40*), 124.4 (*C22 and 42*), 123.1, 122.6 (*C21/41*), 117.3, 117.1 (*C23/43*), 114.2, 114.12, 114.07 (*C29/35/49/55*), 76.2, 75.8, 71.2, 71.1 (*C26/32/46/52*), 66.5 (*C11*), 55.46, 55.44, 55.38 (*C31/37/51/57*), 54.4 (*C13*), 46.6 (*C10*), 40.1, 39.3 (*C23/24*), 38.9 (*C17*), 30.4 (*C14*), 29.0, 23.2 (*C15/16*).

**HRMS (ESI Pos.):** Calcd.  $[M+Na]^+$  ( $C_{63}H_{69}N_7NaO_{15}S$ )  $m/z = 1218.4465$ ; Obs.  $[M+Na]^+$   $m/z = 1218.4517$ , Mean err  $-3.4$  ppm.

**HRMS (ESI Neg.):** Calcd.  $[M-H]^-$  ( $C_{63}H_{68}N_7O_{15}S$ )  $m/z = 1194.4500$ ; Obs.  $[M-H]^-$   $m/z = 1194.4483$ , Mean err  $0.5$  ppm.

**IR (ATIR,  $cm^{-1}$ ):** 3350 (NH stretches, w br), 3050-2800 (C-H stretching, w), 1646 (amide C=O stretches, br m), 1612 (amide C=O stretch, m), 1574 (C=N/C=C stretches, m), 1514 (C=N/C=C stretches, s), 1455 (C=N/C=C stretches, m), 1360 (S=O stretch, m), 1247 (C-O stretches, s), 1173 (S=O stretch, m).

**(2S)-2,6-Bis[(2,3-dihydroxyphenyl)formamido]-N-(2-[[5-(morpholine-4-sulfonyl)pyrazin-2-yl]formamido]ethyl)hexanamide (4-47)**



Molecular Formula:  $C_{31}H_{37}N_7O_{11}S$

Molecular Mass:  $715.74$  g mol $^{-1}$

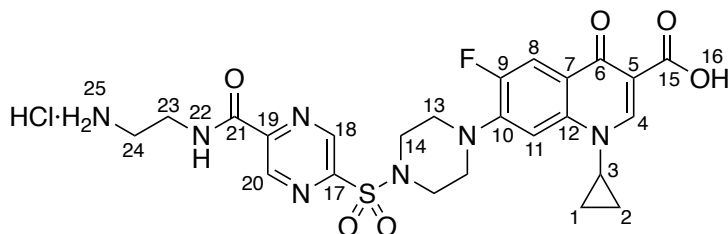
**4-66** (41.8 mg, 0.035 mmol) was dissolved in dioxane (7.5 mL) to give a clear solution. 4 M HCl in dioxane (2.5 mL, 10.0 mmol) was diluted in a further 2.5 mL dioxane, and added dropwise, with the solution changing to a pale yellow. The reaction was monitored by HPLC, and stirred for 24 hours, then the solvent was removed under vacuum. Purification of the residue was attempted by automated column (5-95% MeCN:H<sub>2</sub>O), yielding purer **4-47** as a purple solid (9.2 mg, 0.012 mmol, 36%).

**<sup>1</sup>H NMR:** (400 MHz, DMSO-d<sub>6</sub>) δ<sub>H</sub> ppm: 12.85 (1H, br s, *H36 or 37*), 12.07 (1H, br s, *H36 or 37*), 9.31 (1H, d, *J* = 1.5 Hz, *H2 or 4*), 9.26 (1H, br s, *H18/27/28/37*), 9.11 (1H, br t, *J* = 6.0 Hz, *H6*), 9.08 (1H, d, *J* = 1.5 Hz, *H2 or 4*), 8.82-8.67 (2H, m, *H18/27/28/37*), 8.21 (1H, br t, *J* = 5.5 Hz, *H9*), 7.40 (1H, d, *J* = 8.0 Hz, *H21 or 31*), 7.25 (1H, d, *J* = 8.0 Hz, *H21 or 31*), 6.96-6.85 (2H, m, *H22/23/32/33*), 6.72-6.62 (2H, m, *H22/23/32/33*), 4.43-4.35 (1H, m, *H13*), 3.66-3.56 (4H, m, *H11*), 3.46-3.39 (2H, m, *H7 or 8*), 3.40-3.17 (8H, m, *H10 and 17 and H7 or 8*), 1.80-1.67 (2H, m, *H14*), 1.59-1.45 (2H, m, *H16*), 1.40-1.25 (4H, m, *H15*).

**HRMS (ESI Pos.):** Calcd. [M+Na]<sup>+</sup> (C<sub>31</sub>H<sub>37</sub>N<sub>7</sub>NaO<sub>11</sub>S) *m/z* = 738.2164; Obs. [M+Na]<sup>+</sup> *m/z* = 738.2161, Mean err -0.4 ppm.

**HRMS (ESI Neg.):** Calcd. [M-H]<sup>-</sup> (C<sub>31</sub>H<sub>36</sub>N<sub>7</sub>O<sub>11</sub>S) *m/z* = 714.2199; Obs. [M-H]<sup>-</sup> *m/z* = 714.2192, Mean err 2.4 ppm.

**7-[4-({5-[(2-Aminoethyl)carbamoyl]pyrazin-2-yl)sulfonyl}piperazin-1-yl)-1-cyclopropyl-6-fluoro-4-oxo-1,4-dihydroquinoline-3-carboxylic acid hydrochloride (4-52)**



Molecular Formula: C<sub>24</sub>H<sub>27</sub>ClFN<sub>7</sub>O<sub>6</sub>S

Molecular Mass: 596.03 g mol<sup>-1</sup>

**4-55** (52.8 mg, 0.080 mmol) was suspended in dry DCM (3.5 mL) to give a cloudy white solution and cooled to 0 °C. 4 M HCl in dioxane (1.2 mL, 4.80 mmol) was added and the resulting clear yellow solution was allowed to warm to room temperature and stirred for 25 hours, turning cloudy again after 2 hours. The solvent was removed under vacuum, and the resulting yellow-white solid was triturated in hot EtOH (1.5 mL), then Et<sub>2</sub>O (8 mL) added and the product isolated by Buchner filtration and washed with

further Et<sub>2</sub>O (25 mL). The resulting pale yellow solid was dried further under vacuum to give **4-52** (28.6 mg, 0.048 mmol, 60%). M.p. = 245-250 °C (dec.).

**<sup>1</sup>H NMR:** (400 MHz, DMSO-d<sub>6</sub>) δ<sub>H</sub> ppm: 9.35 (1H, d, *J* = 1.5 Hz, *H18 or 20*), 9.31 (1H, br t, *J* = 6.0 Hz, *H22*), 9.20 (1H, d, *J* = 1.5 Hz, *H18 or 20*), 8.66 (1H, s, *H4*), 7.93 (1H, d, <sup>3</sup>*J*<sub>F-H</sub> = 13.0 Hz, *H8*), 7.80\* (3H, br s, *H25*), 7.59 (1H, d, <sup>4</sup>*J*<sub>F-H</sub> = 7.5 Hz, *H11*), 3.84-3.77 (1H, m, *H3*), 3.59 (2H, app. q, *J* = 6.0 Hz, *H23*), 3.52-3.45 (4H, m, *H13 or 14*), 3.45-3.40 (4H, m, *H13 or 14*), 3.06-2.96 (2H, m, *H24*), 1.35-1.28 (2H, m, *H1 or 2*), 1.20-1.14 (2H, m, *H1 or 2*).

\*Chemical shift is concentration-dependent

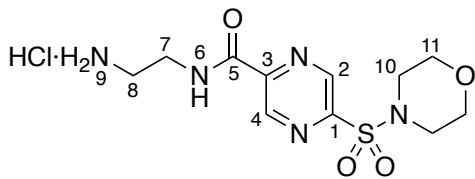
**<sup>13</sup>C NMR:** (100 MHz, DMSO-d<sub>6</sub>) δ<sub>C</sub> ppm: 176.6 (*C6*), 166.3 (*C15*), 162.8 (*C21*), 153.4 (d, <sup>1</sup>*J*<sub>F-C</sub> = 249 Hz, *C9*), 152.8 (*C17 or 19*), 148.4 (*C4*), 147.4 (*C17 or 19*), 144.8 (d, <sup>2</sup>*J*<sub>F-C</sub> = 10 Hz, *C10*), 144.2 (*C18 or 20*), 141.7 (*C18 or 20*), 139.3 (*C12*), 119.3 (d, <sup>3</sup>*J*<sub>F-C</sub> = 8 Hz, *C7*), 111.4 (d, <sup>2</sup>*J*<sub>F-C</sub> = 23 Hz, *C8*), 107.3 (*C11*), 106.9 (*C5*), 49.2, 46.0 (*C13/14*), 38.5 (*C24*), 37.1 (*C23*), 36.2 (*C3*), 7.8 (*C1 and 2*).

**<sup>19</sup>F NMR:** (470 MHz, DMSO-d<sub>6</sub>) δ<sub>F</sub> ppm: -122.00 (1F, dd, *J* = 13.0, 7.5 Hz).

**HRMS (ESI):** Calcd. [M+H]<sup>+</sup> (C<sub>24</sub>H<sub>27</sub>FN<sub>7</sub>O<sub>6</sub>S) *m/z* = 560.1722; Obs. [M+H]<sup>+</sup> *m/z* = 560.1717, Mean err -1.0 ppm.

**IR (ATIR, cm<sup>-1</sup>):** 3415 (NH amide stretch, w), 3100-2750 (O-H and C-H stretching, w), 1683 (carboxylic acid and amide C=O stretch, br s), 1627 (quinolone C=O stretch, m), 1496 (C=N/C=C stretches, s), 1452 (C=N/C=C stretches, s), 1359 (S=O stretch, m), 1130 (S=O stretch, s).

***N*-(2-Aminoethyl)-5-(morpholine-4-sulfonyl)pyrazine-2-carboxamide hydrochloride (4-53)**



Molecular Formula: C<sub>11</sub>H<sub>18</sub>ClN<sub>5</sub>O<sub>4</sub>S

Molecular Mass: 351.81 g mol<sup>-1</sup>

**4-49** (65.2 mg, 0.157 mmol) was suspended in dry EtOH (7 mL). 3 M HCl in EtOH (4.5 mL, 13.5 mmol) was added and the resulting solution was stirred at room temperature for 23 hours, turning clear after 2 hours. The reaction was not complete by TLC, so further 3 M HCl in EtOH (4 mL) was added and the reaction stirred for a further 25 hours, before the solvent was removed under vacuum. The resulting yellow-white solid was triturated in hot EtOH (2 mL), then Et<sub>2</sub>O (15 mL) added and the product isolated by Buchner filtration and washed with further Et<sub>2</sub>O (15 mL) to give **4-53** as a pale yellow solid (33.6 mg, 0.095 mmol, 61%). M.p. = 245-248 °C (dec.).

**<sup>1</sup>H NMR:** (400 MHz, DMSO-d<sub>6</sub>) δ<sub>H</sub> ppm: 9.36 (1H, d, *J* = 1.5 Hz, *H2* or 4), 9.32 (1H, br t, *J* = 6.0 Hz, *H6*), 9.16 (1H, d, *J* = 1.5 Hz, *H2* or 4), 8.02 (3H, br s, *H9*), 3.67-3.61 (4H, m, *H11*), 3.60 (2H, app. q, *J* = 6.0 Hz, *H7*), 3.25-3.18 (4H, m, *H10*), 3.01 (2H, t, *J* = 6.0 Hz, *H8*).

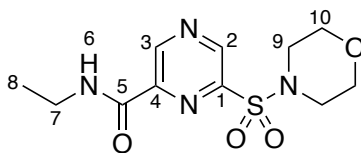
**<sup>13</sup>C NMR:** (100 MHz, DMSO-d<sub>6</sub>) δ<sub>C</sub> ppm: 162.5 (*C5*), 152.5 (*C1* or 3), 147.2 (*C1* or 3), 144.1 (*C2* or 4), 141.5 (*C2* or 4), 65.6 (*C11*), 46.1 (*C10*), 38.4 (*C8*), 36.9 (*C7*).

**HRMS (ESI):** Calcd. [M+H]<sup>+</sup> (C<sub>11</sub>H<sub>18</sub>N<sub>5</sub>O<sub>4</sub>S) *m/z* = 316.1074; Obs. [M+H]<sup>+</sup> *m/z* = 316.1081, Mean err -2.7 ppm.

**IR (ATIR, cm<sup>-1</sup>):** 3379 (NH stretches, w), 3050-2800 (C-H stretching, w), 1681 (amide C=O stretch, s), 1523 (C=N/C=C stretches, m), 1453 (C=N/C=C stretches, w), 1359 (S=O stretch, s), 1159 (S=O stretch, m).



### N-Ethyl-6-(morpholine-4-sulfonyl)pyrazine-2-carboxamide (4-68)



Molecular Formula: C<sub>11</sub>H<sub>16</sub>N<sub>4</sub>O<sub>4</sub>S

Molecular Mass: 300.33 g mol<sup>-1</sup>

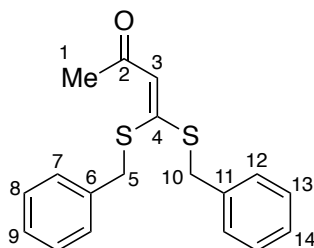
6-(Benzylsulfonyl)-N-ethylpyrazine-2-carboxamide (**4-69**, 92.9 mg, 0.340 mmol) was placed under N<sub>2</sub>, then DCM (5 mL), acetic acid (0.45 mL) and H<sub>2</sub>O (0.90 mL) were added, and the resulting biphasic solution was cooled to 0 °C. 1,3-Dichloro-5,5'-dimethylhydantoin (0.203 g, 1.03 mmol) was added in portions with vigorous stirring to give a cloudy beige solution, which was allowed to warm slowly in the ice bath and stirred for 14 hours. Extra DCM (10 mL) was added, followed by ice-cold aqueous sodium metabisulfite solution (5% w/v, 12.5 mL). The biphasic mixture was stirred for 15 minutes, then the layers were shaken well and separated. The aqueous layer was extracted with DCM (2 x 10 mL), then the combined organic layers were washed with ice-cold saturated NaHCO<sub>3</sub> solution (25 mL) and ice-cold brine (30 mL), dried over MgSO<sub>4</sub>, transferred to a fresh round-bottomed flask, and cooled back to 0 °C. Morpholine (32 μL, 0.366 mmol) and Et<sub>3</sub>N (62 μL, 0.445 mmol) were added, and the reaction was allowed to warm to room temperature and stirred for 5 hours and 30 minutes. The solution was washed with 1 M aq. HCl (25 mL), water (25 mL), saturated NaHCO<sub>3</sub> solution (25 mL) and brine (25 mL), dried over MgSO<sub>4</sub> and the DCM removed *in vacuo* to give a white solid. The product was purified by column chromatography (14 cm silica gel in 2.3 cm diameter column, 3:2 EtOAc:40-60 °C pet. ether followed by 2:1 EtOAc:40-60 °C pet. ether), and dried further under vacuum to give **4-68** as a white to light pink crystalline powder (60.3 mg, 0.201 mmol, 59%). M.p. = 161-162 °C. R<sub>f</sub> = 0.30 (2:1 EtOAc:40-60 °C pet. ether).

<sup>1</sup>H NMR: (400 MHz, CDCl<sub>3</sub>) δ<sub>H</sub> ppm: 9.62 (1H, s, H2 or 3), 9.27 (1H, s, H2 or 3), 7.65-7.43 (1H, m, H6), 3.84-3.71 (4H, m, H10), 3.56 (2H, app. quintet, J = 7.0 Hz, H7), 3.37-3.27 (4H, m, H9), 1.29 (3H, t, J = 7.0 Hz, H8).

<sup>13</sup>C NMR: (100 MHz, CDCl<sub>3</sub>) δ<sub>c</sub> ppm: 161.4 (C5), 149.5 (C1 or 4), 147.5 (C2 or 3), 145.8 (C2 or 3), 144.4 (C1 or 4), 66.4 (C10), 46.5 (C9), 34.9 (C7), 14.9 (C8).

HRMS (ESI): Calcd. [M+H]<sup>+</sup> (C<sub>11</sub>H<sub>17</sub>N<sub>4</sub>O<sub>4</sub>S) *m/z* = 301.0965; Obs. [M+H]<sup>+</sup> *m/z* = 301.0960, Mean err 0.2 ppm. Calcd. [M+Na]<sup>+</sup> (C<sub>11</sub>H<sub>16</sub>N<sub>4</sub>NaO<sub>4</sub>S) *m/z* = 323.0784; Obs. [M+Na]<sup>+</sup> *m/z* = 323.0787, Mean err -0.6 ppm. Calcd. [M+K]<sup>+</sup> (C<sub>11</sub>H<sub>16</sub>KN<sub>4</sub>O<sub>4</sub>S) *m/z* = 339.0524; Obs. [M+K]<sup>+</sup> *m/z* = 339.0529, Mean err -0.8 ppm.

#### 4,4-Bis(benzylsulfanyl)but-3-en-2-one (4-71)



Molecular Formula: C<sub>18</sub>H<sub>18</sub>OS<sub>2</sub>

Molecular Mass: 314.46 g mol<sup>-1</sup>

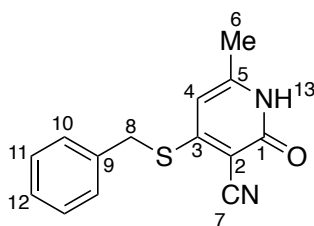
<sup>t</sup>BuOK (2.154 g, 19.20 mmol) was added to an oven-dried argon-flushed flask, and kept under Ar, then dry THF (20 mL) added, and the cloudy white solution cooled to 0 °C. Acetone (0.56 mL, 7.57 mmol) was added, then carbon disulfide (0.58 mL, 9.65 mmol), resulting in the formation of an orange precipitate. An additional 20 mL of dry THF was added and the reaction stirred at 0 °C for 1h30 min, then BnBr (2.00 mL, 16.82 mmol) was added slowly via syringe. The reaction was allowed to warm to room temperature and stirred for a further 18 hours, then poured into ice-cold H<sub>2</sub>O (60 mL) and acidified to pH 5, then extracted with DCM (3 x 60 mL). The combined organic layers were washed with H<sub>2</sub>O (2 x 90 mL) and brine (90 mL), dried over MgSO<sub>4</sub> and the solvent removed under vacuum. The product was purified further by column chromatography (silica gel, 23cm height in 3.7 cm diameter column, 2:1 40-60 °C pet. ether:Et<sub>2</sub>O to 1:1 40-60 °C pet. ether:Et<sub>2</sub>O, loaded with DCM) to give **4-71** as an orange-white solid (1.38 g, 4.38 mmol, 58%). M.p. = 116-117 °C.

**<sup>1</sup>H NMR:** (400 MHz, CDCl<sub>3</sub>) δ<sub>H</sub> ppm: 7.48-7.11 (10H, m, *H*7-9, *H*12-14), 6.18 (1H, s, *H*3), 4.22 (2H, s, *H*5 or 10), 4.13 (2H, s, *H*5 or 10), 2.14 (3H, s, *H*1).

**<sup>13</sup>C NMR:** (100 MHz, CDCl<sub>3</sub>) δ<sub>C</sub> ppm: 193.2 (*C*2), 160.3 (*C*4), 135.8, 134.1 (*C*6/11), 129.5, 129.3, 129.0, 128.7 (*C*7/8/12/13), 128.2, 127.7 (*C*9/14), 115.3 (*C*3), 39.3, 36.5 (*C*5/10), 30.5 (*C*1).

**HRMS (ESI):** Calcd. [M+H]<sup>+</sup> (C<sub>18</sub>H<sub>19</sub>OS<sub>2</sub>) *m/z* = 315.0872; Obs. [M+H]<sup>+</sup> *m/z* = 315.0873, Mean err -0.1 ppm. Calcd. [M+Na]<sup>+</sup> (C<sub>18</sub>H<sub>18</sub>NaOS<sub>2</sub>) *m/z* = 337.0691; Obs. [M+Na]<sup>+</sup> *m/z* = 337.0690, Mean err 0.1 ppm. Calcd. [M+K]<sup>+</sup> (C<sub>18</sub>H<sub>18</sub>KOS<sub>2</sub>) *m/z* = 353.0431; Obs. [M+K]<sup>+</sup> *m/z* = 353.0437, Mean err 0.4 ppm.

**4-(Benzylsulfanyl)-6-methyl-2-oxo-1,2-dihydropyridine-3-carbonitrile  
(4-72)**



Molecular Formula: C<sub>14</sub>H<sub>12</sub>N<sub>2</sub>OS

Molecular Mass: 256.32 g mol<sup>-1</sup>

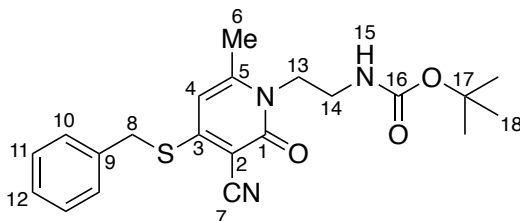
<sup>t</sup>BuOK (0.271 g, 2.42 mmol) was added to an oven-dried argon-flushed flask, and kept under Ar. <sup>t</sup>BuOH (25 mL) was added, followed by **4-71** (0.483 g, 1.54 mmol) and cyanoacetamide (0.130 g, 1.54 mmol), and the resulting deep brown solution was stirred at 80 °C for 24 hours, then allowed to cool to room temperature and H<sub>2</sub>O (10 mL) was added. The solution was acidified to pH 2 with 1 M aq. HCl, and the resulting beige-brown precipitate was isolated via Buchner filtration and washed with 40-60 °C pet. ether (70 mL) and dried under vacuum to give **4-72** (0.203 g, 0.792 mmol, 51%). M. p. = 275-280 °C (dec.).

**<sup>1</sup>H NMR:** (400 MHz, DMSO-d<sub>6</sub>) δ<sub>H</sub> ppm: 12.29 (1H, br s, H13), 7.49-7.43 (2H, m, H10 or 11), 7.40-7.34 (2H, m, H10 or 11), 7.33-7.27 (1H, m, H12), 6.46 (1H, s, H4), 4.45 (2H, s, H8), 2.24 (3H, s, H6).

**<sup>13</sup>C NMR:** (100 MHz, DMSO-d<sub>6</sub>) δ<sub>C</sub> ppm: 162.6 (C3), 160.1 (C1), 151.3 (C5), 135.4 (C9), 129.1, 128.8 (C10/11), 127.8 (C12), 115.3 (C7), 102.3 (C4), 93.4 (C2), 34.7 (C8), 19.2 (C6).

**HRMS (ESI):** Calcd. [M+H]<sup>+</sup> (C<sub>14</sub>H<sub>13</sub>N<sub>2</sub>OS) *m/z* = 257.0743; Obs. [M+H]<sup>+</sup> *m/z* = 257.0744, Mean err 0.1 ppm. Calcd. [M+Na]<sup>+</sup> (C<sub>14</sub>H<sub>12</sub>N<sub>2</sub>NaOS) *m/z* = 279.0563; Obs. [M+Na]<sup>+</sup> *m/z* = 279.0562, Mean err 1.3 ppm. Calcd. [M+K]<sup>+</sup> (C<sub>14</sub>H<sub>12</sub>KN<sub>2</sub>OS) *m/z* = 295.0302; Obs. [M+K]<sup>+</sup> *m/z* = 295.0301, Mean err 0.2 ppm.

***tert*-Butyl *N*-{2-[4-(benzylsulfanyl)-3-cyano-6-methyl-2-oxo-1,2-dihydro pyridin-1-yl]ethyl}carbamate (**4-73**)**



Molecular Formula: C<sub>21</sub>H<sub>25</sub>N<sub>3</sub>O<sub>3</sub>S

Molecular Mass: 399.51 g mol<sup>-1</sup>

Due to potential photodegradation of *N*-Boc-2-bromoethylamine, the reaction flask was covered in foil for the duration of the reaction.

*N*-Boc-2-bromoethylamine (0.243 g, 1.08 mmol), **4-72** (0.222 g, 0.865 mmol) and K<sub>2</sub>CO<sub>3</sub> (0.298 g, 2.15 mmol) were dissolved in dry DMF (12 mL), and the resulting dark brown solution stirred for 20 hours, then the solvent removed under vacuum. The residue was extracted with EtOAc (30 mL) and H<sub>2</sub>O (30 mL) and the layers separated. The H<sub>2</sub>O layer was further extracted with EtOAc (2 x 20 mL), and the combined organic layers washed with H<sub>2</sub>O (40 mL) and brine (40 mL), dried over MgSO<sub>4</sub> and the solvent removed *in vacuo*. The solid was purified further by column chromatography (16.5 cm silica gel

height in 2.8 cm diameter column, 1:1 EtOAc:40-60 °C pet. ether to 3:1 EtOAc:40-60 °C pet. ether, loaded with DCM) to give **4-73** as a colourless paste (0.173 g, 0.434 mmol, 50%).  $R_f = 0.44$  (3:1 EtOAc:40-60 °C pet. ether).

**<sup>1</sup>H NMR:** (400 MHz, CDCl<sub>3</sub>)  $\delta_H$  ppm: 7.40-7.27 (5H, m, *H10/11/12*), 6.07 (1H, s, *H4*), 5.12-5.00 (1H, m, *H15*), 4.25 (2H, s, *H8*), 4.11 (2H, t,  $J = 6.0$  Hz, *H13*), 3.40 (2H, app. q,  $J = 6.0$  Hz, *H14*), 2.45 (3H, s, *H6*), 1.41 (9H, s, *H18*).

**<sup>13</sup>C NMR:** (100 MHz, CDCl<sub>3</sub>)  $\delta_C$  ppm: 161.1 (*C3*), 160.6 (*C1*), 156.4 (*C16*), 151.0 (*C5*), 134.2 (*C9*), 129.2, 129.0 (*C10/11*), 128.3 (*C12*), 114.7 (*C7*), 104.3 (*C4*), 96.4 (*C2*), 80.0 (*C17*), 44.6 (*C13*), 38.8 (*C14*), 36.3 (*C8*), 28.4 (*C18*).

**HRMS (ESI):** Calcd. [M+H]<sup>+</sup> (C<sub>21</sub>H<sub>26</sub>N<sub>3</sub>O<sub>3</sub>S)  $m/z = 400.1689$ ; Obs. [M+H]<sup>+</sup>  $m/z = 400.1691$ , Mean err -1.4 ppm. Calcd. [M+Na]<sup>+</sup> (C<sub>21</sub>H<sub>25</sub>N<sub>3</sub>NaO<sub>3</sub>S)  $m/z = 422.1509$ ; Obs. [M+Na]<sup>+</sup>  $m/z = 422.1515$ , Mean err -1.8 ppm. Calcd. [M+K]<sup>+</sup> (C<sub>21</sub>H<sub>25</sub>KN<sub>3</sub>O<sub>3</sub>S)  $m/z = 438.1248$ ; Obs. [M+K]<sup>+</sup>  $m/z = 438.1254$ , Mean err -0.4 ppm.

## 5.3 UV-Visible Experiments

### 5.3.1 Job Plot Method

A series of aqueous solutions containing the ligand of interest and Fe(NTA) were prepared such that the sum of the concentrations of both remained constant (400  $\mu$ M).

Stock solutions were prepared as follows:

**110 mM TrisHCl pH 7.5:** Tris(hydroxymethyl)aminomethane (3.332 g, 27.5 mmol) was dissolved in c. 200 mL distilled water. The pH of the resulting solution was adjusted to 7.5 with 2 M HCl, then the volume of the solution was made up to 250 mL with a distilled water in a volumetric flask.

**Ligand Solution: 2-29** (0.0181 g, 0.1 mmol) was dissolved in 4-5 mL MeCN in a vial, then made up to 10 mL MeCN in a volumetric flask to give a 10 mM solution.

**Fe(NTA) Solution:** Nitrilotriacetic acid trisodium salt (0.1 mmol) dissolved in AAS absorption standard Fe(NO<sub>3</sub>)<sub>3</sub> solution (0.0179 M, 5.587 mL). This solution was made up to 10 mL with milliQ H<sub>2</sub>O, to give a final solution containing 0.01 M Fe(NO<sub>3</sub>)<sub>3</sub> and 0.01 M NTA.

### 5.3.2 UV-Based SO<sub>2</sub> Release Studies

Stocks of the compounds for SO<sub>2</sub> release study were made up in MeCN or DMSO; the concentrations and solvents utilised for each compound are detailed in **Table 5.1**.

Compound Code	Solvent	Concentration
<b>1-56</b>	MeCN	1 mM
<b>2-9</b>	MeCN	1 mM
<b>2-15</b>	MeCN	1 mM
<b>2-19</b>	MeCN	1 mM
<b>3-36</b>	MeCN	1 mM
<b>4-49</b>	DMSO	1 mM
<b>4-62</b>	DMSO	1 mM
<b>4-68</b>	DMSO	1 mM

Table 5.1 Solvents and concentrations used for preparation of stock solutions.

Other stock solutions were prepared as follows:

#### **HEPES Buffer 20 mM pH 7.4**

HEPES buffer was made fresh every three months. The pH of a stock solution of 100 mM HEPES was adjusted to pH 7.4 by addition of aqueous sodium hydroxide, then diluted to 20 mM.

#### **Cysteine/Glutathione**

10 mM stock solutions of cysteine or glutathione in 20 mM HEPES buffer (pH 7.4) were made fresh before every experiment, and the stocks renewed every day.

#### **Dye 2-11**

A 1 mM stock of SO<sub>2</sub>-releasing dye **2-11** was made up in MeCN via a 10-fold dilution from a 10 mM stock. A new stock was made up every 6 months.

SO<sub>2</sub> release experiments were carried out in quartz cuvettes. First, a 100 μM solution of the desired conjugate was made up from 250 μL conjugate stock solution (1 mM) + 2250 μL HEPES, and used to record a baseline on the on the UV-vis spectrometer. A second solution of the conjugate was made up from 250 μL 1 mM stock solution + 2000 μL HEPES buffer. 250 μL 10 mM cysteine or GSH was then added, and the solution mixed quickly via pipette, before being transferred to the UV-vis spectrometer for measurement of the absorption spectra at regular time intervals.

For experiments with dye **2-11**, a baseline cuvette was made up from 250 μL conjugate (1 mM) + 2225 μL HEPES buffer + 25 μL MeCN, and a reaction cuvette from 250 μL conjugate (1 mM) + 1975 μL HEPES buffer + 25 μL dye **2-11** (1 mM) + 250 μL GSH. For experiments with iron-bound conjugate, a baseline stock solution was made up from 250 μL conjugate (1 mM) + 2225 μL HEPES buffer + 25 μL 3.33 mM Fe(NTA), and a reaction solution from 250 μL conjugate (1 mM) + 1975 μL HEPES buffer + 25 μL 3.33 mM Fe(NTA) + 250 μL GSH.

### 5.3.3 Solubility Testing

Stock solutions of the compounds to be tested were made up in DMSO with sonication/vortexing to ensure complete dissolution. All compounds were dissolved to a concentration of 10 mM, with the exception of **3-34** (5 mM) and **3-14** (1.25 mM). Further dilutions were made from these stock solutions as necessary. MHII media was made up according to the manufacturer's instructions (22 g MHII salts/1000 mL distilled H<sub>2</sub>O) and sonicated for 45 minutes at 50 °C. 1 mL of freshly-made MHII media was syringe filtered into a vial, and the requisite compound added to give solutions containing either 2% DMSO or 50% DMSO. The vials were shaken, and observed by eye for any precipitation or cloudiness; absence of this was taken to indicate solubility.



## 5.4 HPLC-Based Methods

### 5.4.1 SO<sub>2</sub> Release by HPLC

A 2 mM stock solution of **3-36** was made up in MeCN (1.425 mg in 2.0751 mL MeCN). A 10 mM stock solution of glutathione was made up in 20 mM HEPES buffer (pH 7.4, 6.1464 mg in 2.0451 mL HEPES). A 10 mM stock solution of caffeine was made up in distilled H<sub>2</sub>O (48.52 mg in 25 mL H<sub>2</sub>O).

Reaction solutions were made up in triplicate in 7 mL vials, and the vials placed in a heating block (**Figure 5.2**), with the individual heating block wells filled with oil to a depth of c. 1/3<sup>rd</sup> of the height of the vials. The temperature controller of the hotplate was also immersed in one of the wells. The hot plate temperature controller was set to 37.7 °C; this gave a temperature of 37 °C in the vials when measured by the temperature probe of a WTW Profilab pH 597 pH meter.

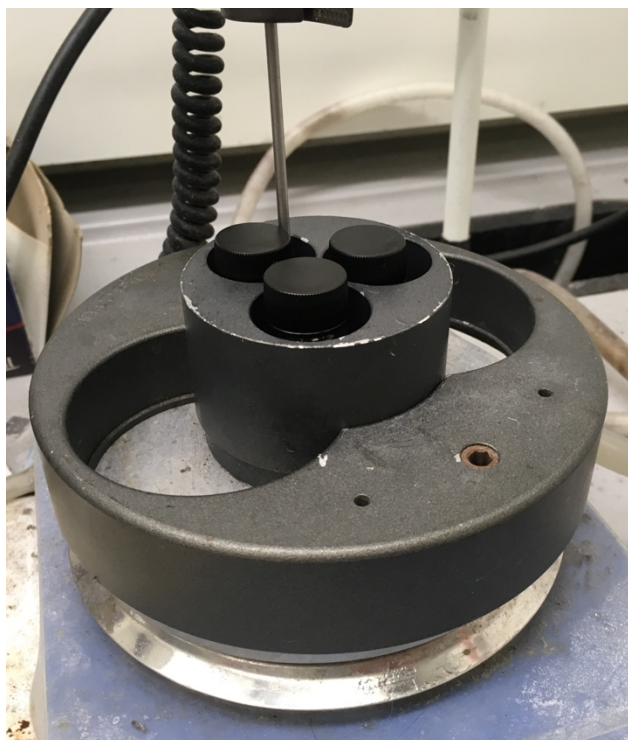


Figure 5.2 Photo of hotplate setup for HPLC reactions.

The reaction mixtures were made up from 4.5 mL HEPES buffer, 300 μL 10 mM caffeine, 300 μL 2 mM **3-36** and 300 μL MeCN. The solutions were heated to 37 °C before addition of 600 μL 10 mM GSH to give final concentrations of 100 μM **3-36**, 1 mM GSH and 500 μM caffeine (10% MeCN:HEPES). The reactions were timed from the addition of glutathione.

Aliquots of c. 200  $\mu\text{L}$  were removed from the reactions at regular intervals and the corresponding HPLC trace recorded using analytical HPLC method C.

A calibration curve was determined by varying the concentration of **3-36** in solutions with a fixed concentration of caffeine (500  $\mu\text{M}$ ). 1 mL solutions were made up according to the volumes in **Table 5.2**.

Concentration of <b>3-36</b> / $\mu\text{M}$	Vol. 2 mM <b>3-36</b> / $\mu\text{L}$	Vol. MeCN / $\mu\text{L}$	Vol. 10 mM caffeine / $\mu\text{L}$	Vol. HEPES buffer / $\mu\text{L}$
120	60	40	50	850
100	50	50	50	850
80	40	60	50	850
60	30	70	50	850
40	20	80	50	850
20	10	90	50	850
10	5	95	50	850
5	2.5	97.5	50	850

Table 5.2 Stock volumes used to prepare samples for calibration curve.

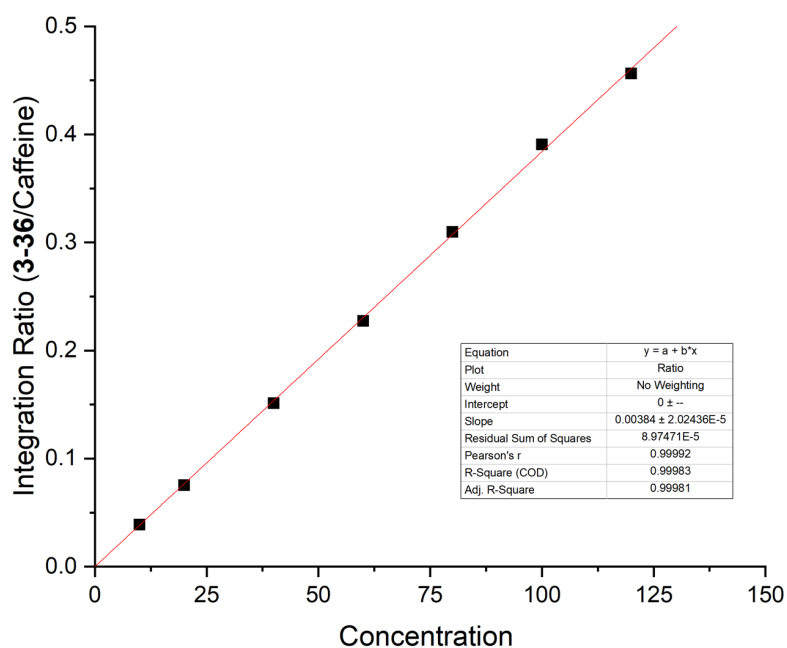


Figure 5.3 Calibration curve for determining the concentration of **3-36** relative to caffeine in  $\text{SO}_2$  release experiments.

#### 5.4.2 HPLC Stability Tests

Stock solutions of **4-32** (1 mM, 0.715 mg in 0.7371 mL), **4-49** (1 mM, 1.04 mg in 2.4221 mL) and **4-52** (2.5 mM, 3.095 mg in 2.0771 mL) were made up in DMSO. A stock of caffeine was made up as previously described (48.52 mg in 25 mL distilled H<sub>2</sub>O).

An identical setup to that in **Section 5.4.1** was used. Solutions containing the desired compound were made up in triplicate in 7 mL vials, and the vials placed in a heating block (**Figure 5.2**), with the individual heating block wells filled with oil to a depth of c. 1/3<sup>rd</sup> of the height of the vials. The temperature controller of the hotplate was also immersed in one of the wells. The hot plate temperature controller was set to 37.7 °C; this gave a temperature of 37 °C in the vials when measured by the temperature probe of a WTW Profilab pH 597 pH meter.

For the stability tests in various media, solutions were made up as follows:  
50 µM **4-52** in MHII media (2% DMSO): 2790 µL MHII media + 150 µL 10 mM caffeine + 60 µL 2.5 mM **4-52**.

10 µM **4-32** in MHII media (2% DMSO): 2790 µL MHII media + 150 µL 10 mM caffeine + 30 µL 1 mM **4-32** + 30 µL DMSO.

50 µM **4-52** in HEPES (5% DMSO): 2160 µL HEPES + 120 µL 10 mM caffeine + 48 µL 2.5 mM **4-52** + 72 µL DMSO.

50 µM **4-49** in HEPES (5% DMSO): 1800 µL HEPES + 100 µL 10 mM caffeine + 100 µL 1 mM **4-49**.

The solutions were heated to 37 °C before addition of the respective test compound. The reactions were timed from the addition of the compounds. Aliquots of c. 200 µL were removed from the reactions at regular intervals and the corresponding HPLC trace recorded using analytical HPLC method E. The calibration curves plotted for determination of the concentrations of the analytes present in solution are displayed below.

## Calibration Curves in MHII Media

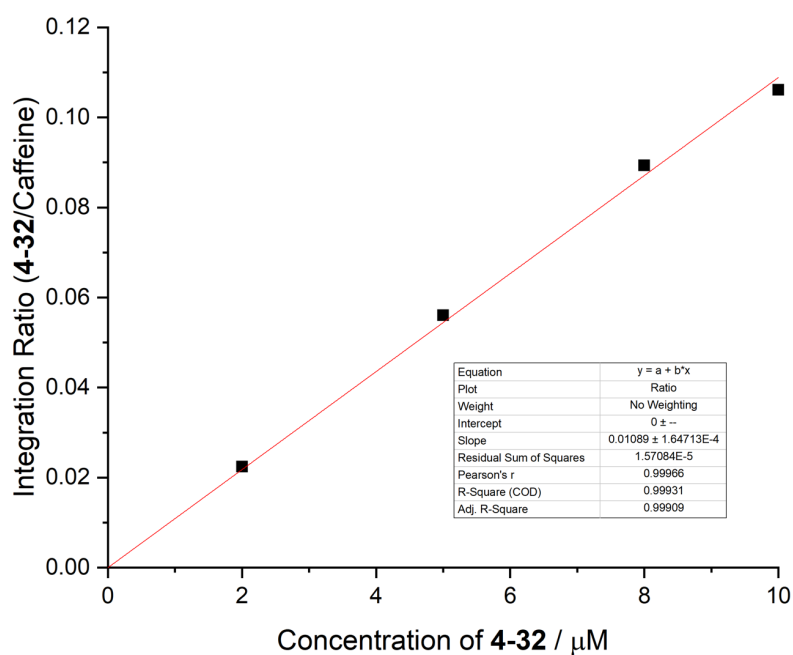


Figure 5.4 Calibration curve for determining the concentration of **4-32** relative to caffeine in stability experiments in MHII media.

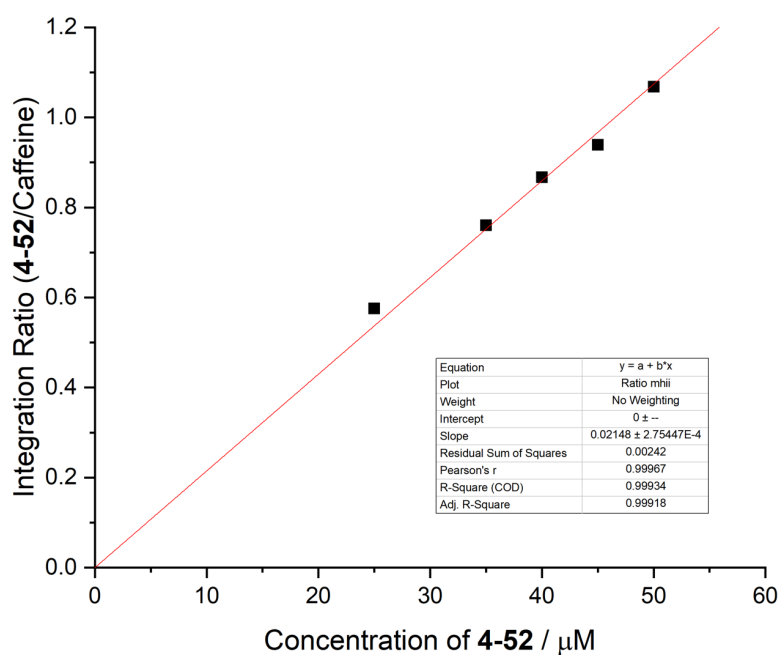


Figure 5.5 Calibration curve for determining the concentration of **4-52** relative to caffeine in stability experiments in MHII media.

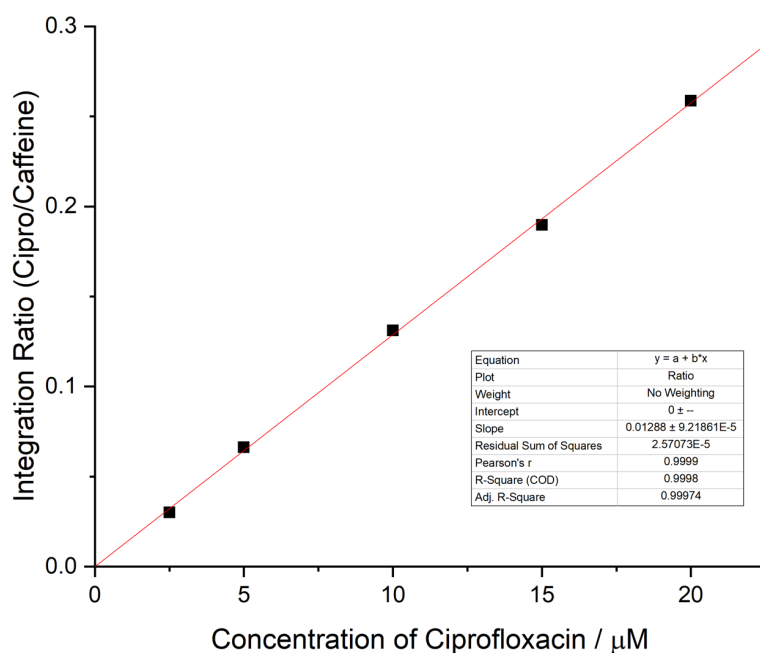


Figure 5.6 Calibration curve for determining the concentration of ciprofloxacin relative to caffeine in stability experiments in MHII media.

### Calibration Curves in HEPES

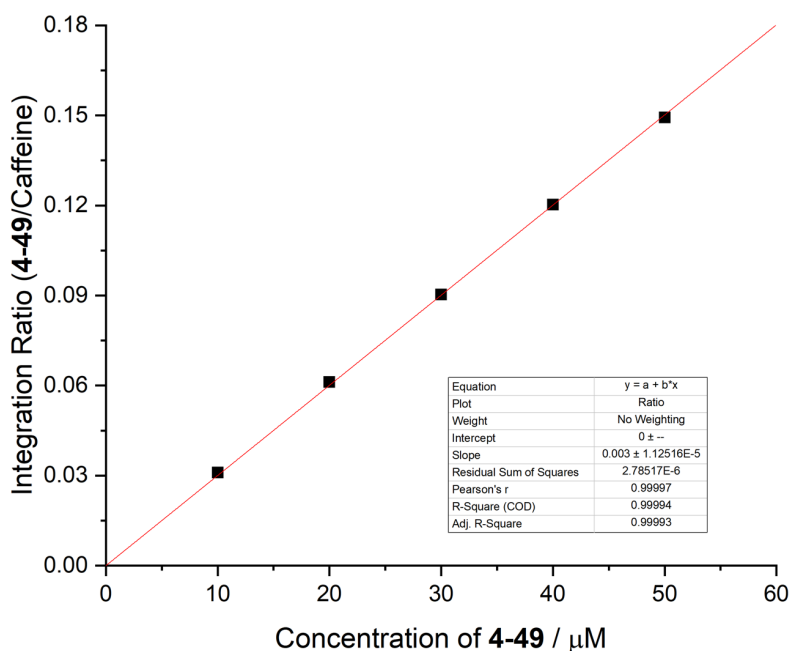


Figure 5.7 Calibration curve for determining the concentration of 4-49 relative to caffeine in stability experiments in HEPES buffer.

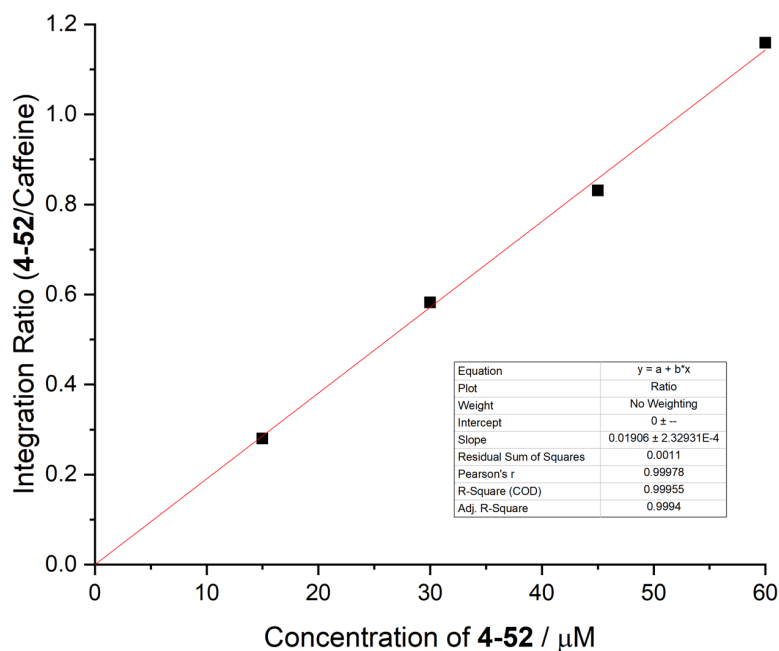


Figure 5.8 Calibration curve for determining the concentration of **4-52** relative to caffeine in stability experiments in HEPES buffer.

## 5.5 Native ESI Mass Spectrometry

Stock solutions were prepared as follows:

### 10 mM Ammonium acetate pH 7.40

NH<sub>4</sub>OAc (1.1580 g) was dissolved in 90 mL of distilled H<sub>2</sub>O, and the pH adjusted to 7.40 by addition of dilute AcOH and NH<sub>3</sub>(aq.). The solution was made up to 100 mL with distilled water in a volumetric flask to give a 150 mM solution of NH<sub>4</sub>OAc. A portion was taken and diluted further to 10 mM in a volumetric flask.

### 1 mM FeCl<sub>3</sub>.6H<sub>2</sub>O

FeCl<sub>3</sub>.6H<sub>2</sub>O (47.1 mg, 0.1743 mmol) was dissolved in 1.7425 mL distilled H<sub>2</sub>O to give a 100 mM solution. A 100 μL aliquot was diluted further in a 10 mL volumetric flask to give a 1 mM solution. Solutions of FeCl<sub>3</sub>.6H<sub>2</sub>O were always made up fresh immediately before an experiment.

### 10 mM 3-31

**3-31** (1.89 mg) was dissolved in DMSO (220 μL) to give a 10 mM stock solution.

Iron complexation was carried out by combining 10  $\mu\text{L}$  10 mM **3-31**, 90  $\mu\text{L}$  of DMSO and 100  $\mu\text{L}$  1 mM  $\text{FeCl}_3 \cdot 6\text{H}_2\text{O}$  solution. The resulting orange solution was stirred for two hours, then the solvent removed under high vacuum. 2 mL of 10 mM  $\text{NH}_4\text{OAc}$  was added, and the solution sonicated for 15 minutes at 25  $^\circ\text{C}$ , then filtered and submitted for native ESI analysis.

## 5.6 Biological Studies

### 5.6.1 Chapter 2

#### 5.6.1.1 Media

All solutions and media were prepared using distilled  $\text{H}_2\text{O}$  and sterilised by autoclave or filter sterilisation prior to use. The antibiotic kanamycin was added when required to select for mutant strains. TSB and LB solids were purchased from commercial sources and used as directed. M9 Minimal Medium was prepared from stock solutions of commercial SigmaAldrich 5X M9 salts, 20% glucose, 1 M  $\text{MgSO}_4$ , and 1 M  $\text{CaCl}_2$ . 10% casamino acids can also be added. To make Chelex-Treated M9 media, 5% w/v Chelex resin was stirred with each stock solution for 1 hour, before vacuum filtration through a Corning system (cellulose acetate membrane, 0.22  $\mu\text{M}$  pore size).

A total volume of 20 mL was used for both starter cultures and the master mixes used to load the well plates in bacterial growth curve experiments.

For M9 overnight cultures, this was made up as shown:

<b>Stock Solutions (autoclaved or filter-sterilised)</b>	<b>Volume</b>
d $\text{H}_2\text{O}$	14.725 ml
5X M9 Salts	4 ml
(Optional: 10% casamino acids)	(800 $\mu\text{l}$ )
20% glucose	400 $\mu\text{l}$
1 M $\text{MgSO}_4$	40 $\mu\text{l}$
1 M $\text{CaCl}_2$	2 $\mu\text{l}$
(Optional for mutant: 30 mg/ml kanamycin)	33.33 $\mu\text{l}$ (for 50 $\mu\text{g}/\text{ml}$ final)

Table 5.3 Stock solutions and volumes used for preparation of M9 media.

Composition of master mix: A conical flask containing the M9 components in their requisite volumes was made up, then distilled water (10.725 mL) added. 1 mL of the overnight starter culture was taken into a 1 mL Kartell cuvette and the OD<sub>600</sub> measured using a Jenway spectrophotometer or the cuvette mode of the Epoch 2 plate reader; if this value exceeded the dynamic range of the instrument, the culture was diluted by addition of 50 µl starter culture into 950 µl blank media, then the resulting value multiplied to give the OD<sub>600</sub> of the starter culture. From this OD<sub>600</sub>, the volume of starter culture required to give an OD<sub>600</sub> of 0.05 in the master mix was calculated, and this volume taken and added to the M9-containing flask. The resulting master mix is then made up to 20 mL with distilled water. Other additives e.g. Fe(NTA) can be added in place of an equivalent volume of distilled water.

#### **5.6.1.2 Growth of Cultures**

Starter cultures for bacterial growth curve experiments were prepared by making up 20 mL of the selected media in a 125 mL conical flask, followed by inoculation with partially frozen bacterial glycerol stocks. Inoculation can be carried out by pipetting 10 µl of the glycerol stock into the starter culture, or by dipping a full loop from the glycerol stocks into the culture. The cultures are incubated overnight at 37 °C with shaking at around 200 rpm.

#### **5.6.1.3 Bacterial Growth Assays**

Growth assays were carried out in 96-well plates using an Epoch 2 plate reader. A master mix was made up for the selected bacteria and media as detailed above. Wells were made up to a total volume of 200 µL, and no more than 2% organic solvents; both the moats (1.7 mL) and the edge wells (200 µL) were filled with distilled H<sub>2</sub>O. Control wells were made up containing blank media (cell-free, 200 µL) or master mix (drug-free, 200 µL); a solvent control containing master mix (196 µL) and the solvent used for the test compound (4 µL) was also made up. Master mix (196 µL) was added to the wells intended for testing, then 4 µL of the test compound stock solutions was added. The plates were incubated at 37 °C within the plate reader, and shaken continuously in a double orbital pattern. The OD<sub>600</sub> was



recorded initially after 5 seconds, then at 30 minute intervals for the following 24 hours.

## **5.6.2 Chapter 3 and 4**

*The experimental protocols in this section were provided by Dr Angela Oates.*

### **5.6.2.1 Disc Diffusion Assays**

Disc diffusion assays were conducted in accordance with the standardised EUCAST disk diffusion method for antimicrobial susceptibility testing. Briefly, colonies of fresh cultures of the selected bacterial strains were grown on Mueller-Hinton (MH) agar at 37 °C were picked off and emulsified in 5 mL of sterile phosphate buffered saline (PBS). Inocula were adjusted to a 0.5 McFarland's turbidity standard (0.08-0.1OD), the equivalent to  $1.5 \times 10^8$  CFU/ml. To allow for a uniform semi-confluent bacterial growth, adjusted inocula were evenly swabbed over the surface of MH agar using a sterile cotton swab. Sterile blank antibiotic disks (6 mm) (GE Healthcare, UK) were individually impregnated with 15 µL of 1 mM stock solutions of **3-14**, **4-32**, or associated controls. Disks were then placed in separate quadrants onto the surface of the agar. All plates were incubated overnight (>16 hrs) at 37 °C. After incubation any zones of inhibition present were measured using digital callipers to the greatest millimetre.

### **5.6.2.2 Forced Adaptation Assays**

A modified version of the adaption assay previously described by Henly *et al.*<sup>534</sup> was undertaken. In brief, colonies of KL3 and CN1 were emulsified in 3 mL of sterile PBS. The bacterial inocula were swabbed in a radial line from the edge of the plate to the centre using a sterile cotton swab. For compound adaptations, 6 mm sterile blank antibiotic disks (GE Healthcare, UK) were individually impregnated with 15 µL 1 mM **3-14**. For ciprofloxacin, 5 µg ciprofloxacin disks (Oxoid, UK) were used. All plates were inverted and incubated overnight (>16 hrs) at 37°C in anaerobic conditions.

After incubation any zones of inhibition present were measured using digital callipers to the greatest millimetre. The bacterial growth from inner edge, closest to the antimicrobial compounds was picked off used to inoculate a new agar plate with antimicrobial compounds as outlined above. This was repeated for 10 passages or until bacterial growth reached the compound. This generated forced adaptations in the selected strains via repeated exposure to the antimicrobial compounds.

To confirm if there were changes to the bacterial isolate's ciprofloxacin sensitivity after the final passage, a disk diffusion assay (ciprofloxacin 5 µg) was undertaken. The zones of inhibition of the adapted isolates were assessed against the EUCAST (2020) database.

#### **5.6.2.3 MIC/MBC Assays**

To confirm the minimum concentration that the compounds inhibit bacterial growth, a minimum inhibitory concentration (MIC) and minimum bactericidal concentration (MBC) assays were undertaken. The MIC of the compounds and ciprofloxacin were determined for selected bacterial strains; KL3 and CN1-starter strains and on the forced adapted KL3 and CN1 strains. The MIC and MBC assays were undertaken in accordance with a 2001 protocol.<sup>533</sup>

**3-14** was diluted to a clinically relevant concentration equivalent to a dose of 5 µg of ciprofloxacin to permit comparison to ciprofloxacin MIC/MBCs and biological triplicate testing. All other compounds were undertaken at stock concentrations. Briefly, double strength MHII broth (150 µL) were dispensed in the first column of 96 well microtiter plate. Overnight broth cultures (MH broth) of the selected strains, were adjusted to 0.5 McFarland's turbidity standard (0.08-0.1OD), the equivalent to  $1.5 \times 10^8$  CFU/mL in fresh sterile MHII and dispensed into the remaining wells (150 µL) for serial dilution. The selected compounds or ciprofloxacin was then added to the first column (150 µL) containing the double strength MHII broth. A series of doubling dilutions (150 µL) of the compounds or ciprofloxacin was undertaken across the rows of the 96 well plate. The concentration range across the MIC for

the compounds and ciprofloxacin was 250  $\mu\text{g}/\text{mL}$  to 0.0001  $\mu\text{g}/\text{mL}$ . Each bacterial isolate was replicated in biological triplicate. After serial dilutions, the plates were incubated under aerobic conditions at 37 °C for 24 hours. The MIC value was determined as the lowest concentration of the compound at which no visible bacterial growth was present on the microtiter plate. MIC assay plates were then used for MBC assays

The minimum bactericidal concentrations are the lowest concentration of the compounds or ciprofloxacin required to kill the selected bacteria. From the MIC microtiter plates 20  $\mu\text{L}$  was removed from each well where there was no bacterial growth observed and spot plated onto MH agar plates. The agar plates were inverted and incubated overnight (>16 hrs) at 37 °C in aerobic conditions. Following incubation agar plates were visually assessed for colonies. The MBC values were determined as the lowest concentration where no bacterial growth was observed on the agar plate.

## Abbreviations

°C	Degrees Celsius
μ (prefix)	Micro
λ <sub>max</sub>	Wavelength of Maximum Absorbance
2,4-DNS	2,4-Dinitrobenzenesulfonamide
<i>A. baumannii</i>	<i>Acinetobacter baumannii</i>
ABC	ATP-Binding Cassette
Abs	Absorbance
AcOH	Acetic Acid
AD	Anno Domini
ADC	Antibody-Drug Conjugate
Ala	Alanine
Aq.	Aqueous
ATP	Adenosine Triphosphate
<i>B. subtilis</i>	<i>Bacillus subtilis</i>
BBr <sub>3</sub>	Boron Tribromide
BnBr	Benzyl Bromide
BnOH	Benzyl Alcohol
BnSH	Benzyl Mercaptan
Boc	<i>tert</i> -Butyloxycarbonyl
bpy	2,2'-Bipyridine
<i>C. jejuni</i>	<i>Campylobacter jejuni</i>
CaCl <sub>2</sub>	Calcium Chloride
CDI	1,1'-Carbonyldiimidazole
CF <sub>3</sub>	Trifluoromethyl
Cip/Cipro	Ciprofloxacin
clog <i>P</i>	Calculated Partition Coefficient
CO	Carbon Monoxide
CO <sub>2</sub>	Carbon Dioxide
COMT	Catechol <i>O</i> -Methyltransferase
COOH	Carboxylic Acid
CORM	Carbon Monoxide Releasing Molecule
Da	Dalton

DBU	1,8-Diazabicyclo(5.4.0)undec-7-ene
DCEMH	1,3-Dichloro-5,5'-dimethylhydantoin
DCM	Dichloromethane
DFO	Desferrioxamine
DHPS	Dihydropteroate Synthase
DIPEA	Diisopropylethylamine
DMAP	4-Dimethylaminopyridine
DMF	<i>N,N'</i> -Dimethylformamide
DMSO	Dimethylsulfoxide
DNA	Deoxyribonucleic Acid
DNS-Cl	2,4-Dinitrobenzenesulfonyl Chloride
DOX	Doxorubicin
<i>E. cloacae</i>	<i>Enterobacter cloacae</i>
<i>E. coli</i>	<i>Escherichia coli</i>
<i>E. faecalis</i>	<i>Enterococcus faecalis</i>
EDC.HCl	1-Ethyl-3-(3'-dimethylaminopropyl)carbodiimide Hydrochloride
EMA	European Medicines Agency
ESI	Electrospray Ionisation
EtNH <sub>2</sub> .HCl	Ethylamine Hydrochloride
EtOH	Ethanol
EUCAST	European Committee on Antimicrobial Susceptibility Testing
EWG	Electron-Withdrawing Group
Et <sub>2</sub> O	Diethyl ether
FAEE	Ferulic Acid Ethyl Ester
FDA	US Food and Drug Administration
Fmoc	Fluorenylmethyloxycarbonyl
GSH	Glutathione
GSK	Glaxo Smith-Kline
GSSG	Oxidised Glutathione
GST	Glutathione-S-Transferase
HBTU	(2-(1H-benzotriazol-1-yl)-1,1,3,3-tetramethyluronium Hexafluorophosphate

HCl	Hydrochloric Acid/Hydrochloride
HEPES	(4-(2-Hydroxyethyl)-1-piperazineethanesulfonic acid
HOBt	1-Hydroxybenzotriazole
HPLC	High Performance Liquid Chromatography
HSA	Human Serum Albumin
IEDDA	Inverse-Electron Demand Diels Alder
<i>K. pneumoniae</i>	<i>Klebsiella pneumoniae</i>
K <sub>2</sub> CO <sub>3</sub>	Potassium carbonate
LB	Lysogeny Broth
LCMS	Liquid Chromatography Mass Spectrometry
LiOH	Lithium Hydroxide
LMCT	Ligand-to-Metal Charge Transfer
M	Molar
MBC	Minimum Bactericidal Concentration
MeCN	Acetonitrile
MeOH	Methanol
MgSO <sub>4</sub>	Magnesium Sulfate
MHII	Mueller-Hinton media
MHz	Megahertz
MIC	Minimum Inhibitory Concentration
MRSA	Methicillin-Resistant <i>S. aureus</i>
<i>N. gonorrhoeae</i>	<i>Neisseria gonorrhoeae</i>
<i>N. meningitidis</i>	<i>Neisseria meningitidis</i>
NaClO	Sodium Hypochlorite
NaOH	Sodium Hydroxide
NDM-1	New Delhi Metallo-Beta-Lactamase 1
NH <sub>4</sub> Cl	Ammonium Chloride
NHS	<i>N</i> -Hydroxysuccinimide
nm	Nanometer
NMR	Nuclear Magnetic Resonance
NO	Nitric Oxide
NTA	Nitrilotriacetic acid
OD <sub>x</sub>	Optical Density at Wavelength x
<i>P. aeruginosa</i>	<i>Pseudomonas aeruginosa</i>

PABA	<i>para</i> -Aminobenzoic acid
PABC	<i>para</i> -Aminobenzyloxycarbonyl
PBP	Penicillin Binding Protein
PBS	Phosphate Buffer Solution
PF <sub>6</sub>	Hexafluorophosphate anion
PFP-OH	Pentafluorophenol
PMB	<i>para</i> -Methoxybenzyl
ppm	Parts per Million
RNA	Ribonucleic Acid
RNOS	Reactive Nitrogen Oxygen Species
ROS	Reactive Oxygen Species
rt	Room Temperature
<i>S. aureus</i>	<i>Staphylococcus aureus</i>
<i>S. pneumoniae</i>	<i>Streptococcus pneumoniae</i>
S <sub>N</sub> Ar	Nucleophilic Aromatic Substitution
S <sub>N</sub> i	Internal Nucleophilic Substitution
TB	<i>Mycobacterium tuberculosis</i>
TBAF	Tetra- <i>n</i> -Butylammonium Fluoride
<sup>t</sup> BuO	<i>tert</i> -Butyl Ester
<sup>t</sup> BuOH	<i>tert</i> -Butyl Alcohol
<sup>t</sup> BuOK	Potassium <i>tert</i> -Butoxide
TFA	Trifluoroacetic Acid
THF	Tetrahydrofuran
TLC	Thin Layer Chromatography
TMSE	Trimethylsilylethanol
Tris	Tris(hydroxymethyl)aminomethane
tRNA	Transfer Ribonucleic Acid
TSB	Tryptic Soy Broth
UV/vis	Ultraviolet-visible
WHO	World Health Organisation
XDR	Extensively Drug-Resistant
<i>Y. enterocolitica</i>	<i>Yersinia enterocolitica</i>

## References

- 1 M. D. Iseman, *Eur. Respir. J.*, 2002, **20**, 87s-94s.
- 2 S. A. Waksman, *Mycologia*, 1947, **39**, 565–569.
- 3 S. A. Waksman, *J. Hist. Med. Allied Sci.*, 1973, **XXVIII**, 284–286.
- 4 S. D. Mills and T. J. Dougherty, in *Antibiotic Discovery and Development*, eds. T. J. Dougherty and M. J. Pucci, Springer US, Boston, MA, 2012, pp. 901–929.
- 5 R. Aminov, *Front. Microbiol.*, 2010, **1**, 134.
- 6 K. Gould, *J. Antimicrob. Chemother.*, 2016, **71**, 572–575.
- 7 E. J. Bassett, M. S. Keith, G. J. Armelagos, D. L. Martin and A. R. Villanueva, *Science*, 1980, **209**, 1532–1534.
- 8 M. Nelson, A. Dinardo, J. Hochberg and G. Armelagos, *Am. J. Phys. Anthropol.*, 2010, **143**, 151–154.
- 9 R. A. Milch, D. P. Rall and J. E. Tobie, *J. Bone Jt. Surg.*, 1958, **40**, 897–910.
- 10 D. D. Perrin, *Nature*, 1965, **208**, 787–788.
- 11 C. Pautke, S. Vogt, K. Kreutzer, C. Haczek, G. Wexel, A. Kolk, A. B. Imhoff, H. Zitzelsberger, S. Milz and T. Tischer, *J. Anat.*, 2010, **217**, 76–82.
- 12 R. Emmerich and O. Löw, *Zeitschrift für Hyg. und Infekt.*, 1899, **31**, 1–65.
- 13 P. G. Caltrider, in *Antibiotics: Volume I Mechanism of Action*, eds. D. Gottlieb and P. D. Shaw, Springer Berlin Heidelberg, Berlin, Heidelberg, 1967, pp. 117–121.
- 14 K. Strebhardt and A. Ullrich, *Nat. Rev. Cancer*, 2008, **8**, 473–480.
- 15 K. J. Williams, *J. R. Soc. Med.*, 2009, **102**, 343–348.
- 16 N. C. Lloyd, H. W. Morgan, B. K. Nicholson and R. S. Ronimus, *Angew. Chem., Int. Ed.*, 2005, **44**, 941–944.
- 17 G. D. Wright, *Nat. Prod. Rep.*, 2017, **34**, 694–701.
- 18 H. Otten, *J. Antimicrob. Chemother.*, 1986, **17**, 689–690.
- 19 J. Davies, *Can. J. Infect. Dis. Med. Microbiol.*, 2006, **17**, 287–290.
- 20 T. P. Van Boeckel, S. Gandra, A. Ashok, Q. Caudron, B. T. Grenfell, S. A. Levin and R. Laxminarayan, *Lancet. Infect. Dis.*, 2014, **14**, 742–750.
- 21 G. L. Patrick, *An Introduction to Medicinal Chemistry*, Oxford



- University Press, Oxford, UK, 3rd edn., 2005.
- 22 H. Brockmann and W. Henkel, *Chem. Ber.*, 1951, **84**, 284–288.
- 23 G. P. Dinos, *Br. J. Pharmacol.*, 2017, **174**, 2967–2983.
- 24 J. M. McGuire, R. L. Bunch, R. C. Anderson, H. E. Boaz, E. H. Flynn, H. M. Powell and J. W. Smith, *Antibiot. Chemother.*, 1952, **2**, 281–283.
- 25 B. Weisblum, *Antimicrob. Agents Chemother.*, 1995, **39**, 577–585.
- 26 G. G. Zhanel, M. Dueck, D. J. Hoban, L. M. Vercaigne, J. M. Embil, A. S. Gin and J. A. Karlowsky, *Drugs*, 2001, **61**, 443–498.
- 27 D. T. Chu and P. B. Fernandes, *Antimicrob. Agents Chemother.*, 1989, **33**, 131–5.
- 28 L. A. Mitscher, *Chem. Rev.*, 2005, **105**, 559–592.
- 29 K. J. Aldred, R. J. Kerns and N. Osheroff, *Biochemistry*, 2014, **53**, 1565–1574.
- 30 T. D. M. Pham, Z. M. Ziora and M. A. T. Blaskovich, *MedChemComm*, 2019, **10**, 1719–1739.
- 31 D. C. Hooper and G. A. Jacoby, *Cold Spring Harb. Perspect. Med.*, 2016, **6**, a025320.
- 32 D. Karl, M. Muhammad, K. R. J. and Z. Xilin, *Antimicrob. Agents Chemother.*, 2008, **52**, 385–392.
- 33 M. L. Nelson and S. B. Levy, *Ann. N. Y. Acad. Sci.*, 2011, **1241**, 17–32.
- 34 A. Daemrlich, *Hist. Technol.*, 2009, **25**, 237–256.
- 35 E. Y. Klein, T. P. Van Boeckel, E. M. Martinez, S. Pant, S. Gandra, S. A. Levin, H. Goossens and R. Laxminarayan, *Proc. Natl. Acad. Sci.*, 2018, **115**, E3463–E3470.
- 36 *UK One Health Report - Joint Report on Antibiotic Use and Antibiotic Resistance, 2013-2017*, New Haw, Addlestone, UK, 2019.
- 37 S. R. Bushby and G. H. Hitchings, *Br. J. Pharmacol. Chemother.*, 1968, **33**, 72–90.
- 38 P. A. Masters, T. A. O’Bryan, J. Zurlo, D. Q. Miller and N. Joshi, *Arch. Intern. Med.*, 2003, **163**, 402–410.
- 39 G. H. Hitchings, *J. Infect. Dis.*, 1973, **128**, S433–S436.
- 40 R. N. Brogden, A. A. Carmine, R. C. Heel, T. M. Speight and G. S. Avery, *Drugs*, 1982, **23**, 405–430.
- 41 E. J. Begg and M. L. Barclay, *Br. J. Clin. Pharmacol.*, 1995, **39**, 597–603.

- 42 K. M. Krause, A. W. Serio, T. R. Kane and L. E. Connolly, *Cold Spring Harb. Perspect. Med.*, 2016, **6**, a027029.
- 43 N. Thamban Chandrika and S. Garneau-Tsodikova, *Chem. Soc. Rev.*, 2018, **47**, 1189–1249.
- 44 J. Poehlsgaard and S. Douthwaite, *Nat. Rev. Microbiol.*, 2005, **3**, 870–881.
- 45 M. S. Butler, K. A. Hansford, M. A. T. Blaskovich, R. Halai and M. A. Cooper, *J. Antibiot. (Tokyo)*, 2014, **67**, 631–644.
- 46 J. C. Barna and D. H. Williams, *Annu. Rev. Microbiol.*, 1984, **38**, 339–357.
- 47 P. M. Wright, I. B. Seiple and A. G. Myers, *Angew. Chem., Int. Ed.*, 2014, **53**, 8840–8869.
- 48 B. Ribeiro da Cunha, L. P. Fonseca and C. R. C. Calado, *Antibiot. (Basel, Switzerland)*, 2019, **8**, 45.
- 49 S. J. Brickner, M. R. Barbachyn, D. K. Hutchinson and P. R. Manninen, *J. Med. Chem.*, 2008, **51**, 1981–1990.
- 50 M. S. Butler and M. A. Cooper, *J. Antibiot. (Tokyo)*, 2011, **64**, 413–425.
- 51 M. S. Butler, M. A. Blaskovich and M. A. Cooper, *J. Antibiot. (Tokyo)*, 2013, **66**, 571–591.
- 52 M. R. Barbachyn and C. W. Ford, *Angew. Chem., Int. Ed.*, 2003, **42**, 2010–2023.
- 53 D. N. Wilson, *Nat. Rev. Microbiol.*, 2014, **12**, 35–48.
- 54 D. N. Wilson, F. Schluenzen, J. M. Harms, A. L. Starosta, S. R. Connell and P. Fucini, *Proc. Natl. Acad. Sci. U. S. A.*, 2008, **105**, 13339–13344.
- 55 M. S. Butler, M. A. T. Blaskovich and M. A. Cooper, *J. Antibiot. (Tokyo)*, 2017, **70**, 3–24.
- 56 M. S. Butler and D. L. Paterson, *J. Antibiot. (Tokyo)*, 2020, **73**, 329–364.
- 57 R. L. Nation and J. Li, *Curr. Opin. Infect. Dis.*, 2009, **22**, 535–543.
- 58 L. D. Högberg, A. Heddini and O. Cars, *Trends Pharmacol. Sci.*, 2010, **31**, 509–515.
- 59 C. L. Ventola, *P T.*, 2015, **40**, 277–83.
- 60 Y. Cetinkaya, P. Falk and C. G. Mayhall, *Clin. Microbiol. Rev.*, 2000, **13**,

- 686–707.
- 61 N. Gupta, B. M. Limbago, J. B. Patel and A. J. Kallen, *Clin. Infect. Dis.*, 2011, **53**, 60–67.
- 62 Y. Y. Liu, Y. Wang, T. R. Walsh, L. X. Yi, R. Zhang, J. Spencer, Y. Doi, G. Tian, B. Dong, X. Huang, L. F. Yu, D. Gu, H. Ren, X. Chen, L. Lv, D. He, H. Zhou, Z. Liang, J. H. Liu and J. Shen, *Lancet Infect. Dis.*, 2016, **16**, 161–168.
- 63 K. K. Kumarasamy, M. A. Toleman, T. R. Walsh, J. Bagaria, F. Butt, R. Balakrishnan, U. Chaudhary, M. Doumith, C. G. Giske, S. Irfan, P. Krishnan, A. V. Kumar, S. Maharjan, S. Mushtaq, T. Noorie, D. L. Paterson, A. Pearson, C. Perry, R. Pike, B. Rao, U. Ray, J. B. Sarma, M. Sharma, E. Sheridan, M. A. Thirunarayan, J. Turton, S. Upadhyay, M. Warner, W. Welfare, D. M. Livermore and N. Woodford, *Lancet Infect. Dis.*, 2010, **10**, 597–602.
- 64 K. Talkington, *Superbugs Don't Respect Borders*, 2017, <http://www.pewtrusts.org/en/research-and-analysis/articles/2017/10/10/superbugs-dont-respect-borders>, (accessed 19 July 2018).
- 65 H. K. Allen, J. Donato, H. H. Wang, K. A. Cloud-Hansen, J. Davies and J. Handelsman, *Nat. Rev. Microbiol.*, 2010, **8**, 251–259.
- 66 A. C. Pawlowski, W. Wang, K. Koteva, H. A. Barton, A. G. McArthur and G. D. Wright, *Nat. Commun.*, 2016, **7**, 1–10.
- 67 *Antibacterial Agents in Clinical Development*, Geneva, 2017.
- 68 F. M. Burnet, *Natural History of Infectious Disease*, University Press, 3rd edn., 1962.
- 69 B. Spellberg, *Clin. Infect. Dis.*, 2008, **47**, 294.
- 70 G. B. Pier, *Clin. Infect. Dis.*, 2008, **47**, 1113–1114.
- 71 B. Spellberg and B. Taylor-Blake, *Infect. Dis. Poverty*, 2013, **2**, 3.
- 72 R. Barrett and G. J. Armelagos, *An Unnatural History of Emerging Infections*, Oxford University Press, Oxford, 2013.
- 73 *Schatz's contribution to the discovery of streptomycin was not recognised by history for many years, with Waksman the sole recipient of the 1952 Nobel Prize for Medicine for the discovery.*
- 74 V. Mistiaen, *Time, and the great healer*, 2002,

[https://www.theguardian.com/education/2002/nov/02/research.hi  
ghereducation](https://www.theguardian.com/education/2002/nov/02/research.hi<br/>ghereducation) (accessed 18 April 2020).

- 75 D. M. Livermore, *J. Antimicrob. Chemother.*, 2011, **66**, 1941–1944.
- 76 A. Towse, C. K. Hoyle, J. Goodall, M. Hirsch, J. Mestre-Ferrandiz and J. H. Rex, *Health Policy (New York)*, 2017, **121**, 1025–1030.
- 77 A. R. M. Coates, G. Halls and Y. Hu, *Br. J. Pharmacol.*, 2011, **163**, 184–194.
- 78 *Pharm. J.*, 2017, **299**, 7906.
- 79 U. Möllmann, L. Heinisch, A. Bauernfeind, T. Köhler and D. Ankel-Fuchs, *BioMetals*, 2009, **22**, 615–624.
- 80 P. Klahn and M. Brönstrup, *Nat. Prod. Rep.*, 2017, **34**, 832–885.
- 81 T. Tsukihara, H. Aoyama, E. Yamashita, T. Tomizaki, H. Yamaguchi, K. Shinzawa-Itoh, R. Nakashima, R. Yaono and S. Yoshikawa, *Science*, 1995, **269**, 1069–1074.
- 82 J. L. Beard, *J. Nutr.*, 2001, **131**, 616–635.
- 83 B. M. Hoffman, D. Lukoyanov, Z. Y. Yang, D. R. Dean and L. C. Seefeldt, *Chem. Rev.*, 2014, **114**, 4041–4062.
- 84 M. Lou Guerinot, *Annu. Rev. Microbiol.*, 1994, **48**, 743–772.
- 85 S. C. Andrews, A. K. Robinson and F. Rodriguez-Quinones, *FEMS Microbiol. Rev.*, 2003, **27**, 215–237.
- 86 J. R. Chipperfield and C. Ratledge, *BioMetals*, 2000, **13**, 165–168.
- 87 C. A. Finch, K. Deubelbeiss, J. D. Cook, J. W. Eschbach, L. A. Harker, D. D. Funk, G. Marsaglia, R. S. Hillman, S. Slichter, J. W. Adamson, A. Ganzoni and E. R. Giblett, *Medicine (Baltimore)*, 1970, **49**, 17–53.
- 88 E. L. Mackenzie, K. Iwasaki and Y. Tsuji, *Antioxid. Redox Signal.*, 2008, **10**, 997–1030.
- 89 B. Halliwell and J. M. Gutteridge, *Biochem. J.*, 1984, **219**, 1–14.
- 90 Z. D. Liu and R. C. Hider, *Coord. Chem. Rev.*, 2002, **232**, 151–171.
- 91 S. T. Ong, J. Z. Shan Ho, B. Ho and J. L. Ding, *Immunobiology*, 2006, **211**, 295–314.
- 92 M. P. Soares and G. Weiss, *EMBO Rep.*, 2015, **16**, 1482–1500.
- 93 M. I. Hood and E. P. Skaar, *Nat. Rev. Microbiol.*, 2012, **10**, 525–537.
- 94 U. Bilitewski, J. A. V. Blodgett, A. K. Duhme-Klair, S. Dallavalle, S. Laschat, A. Routledge and R. Schobert, *Angew. Chem., Int. Ed.*, 2017,

- 56**, 14360–14382.
- 95 K. N. Raymond, E. A. Dertz and S. S. Kim, *Proc. Natl. Acad. Sci.*, 2003, **100**, 3584–3588.
- 96 R. C. Hider and X. Kong, *Nat. Prod. Rep.*, 2010, **27**, 637–657.
- 97 M. Miethke and M. A. Marahiel, *Microbiol. Mol. Biol. Rev.*, 2007, **71**, 413–451.
- 98 W. R. Harris, C. J. Carrano and K. N. Raymond, *J. Am. Chem. Soc.*, 1979, **101**, 2722–2727.
- 99 H. Boukhalfa and A. L. Crumbliss, *BioMetals*, 2002, **15**, 325–339.
- 100 K. N. Raymond, B. E. Allred and A. K. Sia, *Acc. Chem. Res.*, 2015, **48**, 2496–2505.
- 101 C. J. Carrano, H. Drechsel, D. Kaiser, G. Jung, B. Matzanke, G. Winkelmann, N. Rochel and A. M. Albrecht-Gary, *Inorg. Chem.*, 1996, **35**, 6429–6436.
- 102 M. Valdebenito, A. L. Crumbliss, G. Winkelmann and K. Hantke, *Int. J. Med. Microbiol.*, 2006, **296**, 513–520.
- 103 N. D. Hammer and E. P. Skaar, *Annu. Rev. Microbiol.*, 2011, **65**, 129–147.
- 104 N. P. Endicott, E. Lee and T. A. Wencewicz, *ACS Infect. Dis.*, 2017, **3**, 542–553.
- 105 V. Braun and M. Braun, *FEBS Lett.*, 2002, **529**, 78–85.
- 106 N. Noinaj, M. Guillier, T. J. Barnard, and S. K. Buchanan, *Annu. Rev. Microbiol.*, 2010, **64**, 43–60.
- 107 L. D. Jordan, Y. Zhou, C. R. Smallwood, Y. Lill, K. Ritchie, W. T. Yip, S. M. Newton and P. E. Klebba, *Proc. Natl. Acad. Sci.*, 2013, **110**, 11553–11558.
- 108 H. Celia, N. Noinaj, S. D. Zakharov, E. Bordignon, I. Botos, M. Santamaria, T. J. Barnard, W. A. Cramer, R. Lloubes and S. K. Buchanan, *Nature*, 2016, **538**, 60–65.
- 109 W. Köster, *Res. Microbiol.*, 2001, **152**, 291–301.
- 110 R. J. Abergel, A. M. Zawadzka, T. M. Hoette and K. N. Raymond, *J. Am. Chem. Soc.*, 2009, **131**, 12682–12692.
- 111 I. J. Schalk, *J. Inorg. Biochem.*, 2008, **102**, 1159–1169.
- 112 I. J. Schalk and L. Guillon, *Amino Acids*, 2013, **44**, 1267–1277.

- 113 J. S. Brown and D. W. Holden, *Microbes Infect.*, 2002, **4**, 1149–1156.
- 114 H. Contreras, N. Chim, A. Credali and C. W. Goulding, *Curr. Opin. Chem. Biol.*, 2014, **19**, 34–41.
- 115 N. Noinaj, S. K. Buchanan and C. N. Cornelissen, *Mol. Microbiol.*, 2012, **86**, 246–257.
- 116 C. J. Parker Siburt, T. A. Mietzner and A. L. Crumbliss, *Biochim. Biophys. Acta - Gen. Subj.*, 2012, **1820**, 379–392.
- 117 A. K. Pogoutse and T. F. Moraes, *Crit. Rev. Biochem. Mol. Biol.*, 2017, **52**, 314–326.
- 118 M. Ghosh, P. A. Miller, U. Möllmann, W. D. Claypool, V. A. Schroeder, W. R. Wolter, M. Suckow, H. Yu, S. Li, W. Huang, J. Zajicek and M. J. Miller, *J. Med. Chem.*, 2017, **60**, 4577–4583.
- 119 J. Roosenberg II, Y.-M. Lin, Y. Lu and M. Miller, *Curr. Med. Chem.*, 2000, **7**, 159–197.
- 120 G. P. H. Dietz and M. Bähr, *Mol. Cell. Neurosci.*, 2004, **27**, 85–131.
- 121 S. J. Milner, C. T. Carrick, K. G. Kerr, A. M. Snelling, G. H. Thomas, A. K. Duhme-Klair and A. Routledge, *ChemBioChem*, 2014, **15**, 466–471.
- 122 X. Wang, C. A. Borges, X. Ning, M. Rafi, J. Zhang, B. Park, K. Takemiya, C. Lo Sterzo, W. R. Taylor, L. Riley and N. Murthy, *Bioconjug. Chem.*, 2018, **29**, 1729–1735.
- 123 S. A. Dingsdag, B. C.-M. Yap, N. Hunter and M. J. Crossley, *Org. Biomol. Chem.*, 2015, **13**, 98–109.
- 124 J.-L. Gao, A. H. Kwan, A. Yammine, X. Zhou, J. Trehwella, B. M. Hugrass, D. A. T. Collins, J. Horne, P. Ye, D. Harty, K.-A. Nguyen, D. A. Gell and N. Hunter, *Nat. Commun.*, 2018, **9**, 4097.
- 125 L. Randaccio, S. Geremia, N. Demitri and J. Wuerges, *Molecules*, 2010, **15**, 3228–3259.
- 126 M. Giedyk, A. Jackowska, M. Równicki, M. Kolanowska, J. Trylska and D. Gryko, *Chem. Commun.*, 2019, **55**, 763–766.
- 127 J. Y. Wu, P. Srinivas and J. M. Pogue, *Infect. Dis. Ther.*, 2020, **9**, 17–40.
- 128 D. M. Reynolds, A. Schatz and S. A. Waksman, *Proc. Soc. Exp. Biol. Med.*, 1947, **64**, 50–54.
- 129 D. M. Reynolds and S. A. Waksman, *J. Bacteriol.*, 1948, **55**, 739–752.
- 130 H. Maehr, in *Antibiotics: Isolation, Separation and Purification*, eds.

- M. J. Weinstein and G. H. Wagman, Elsevier, Amsterdam, 1978, pp. 521–585.
- 131 F. A. Kuehl, M. N. Bishop, L. Chaiet and K. Folkers, *J. Am. Chem. Soc.*, 1951, **73**, 1770–1773.
- 132 G. F. Gause, *BMJ*, 1955, **2**, 1177–1179.
- 133 Y.-M. Lin, M. Ghosh, P. A. Miller, U. Möllmann and M. J. Miller, *BioMetals*, 2019, **32**, 425–451.
- 134 E. O. Stapley and R. E. Ormond, *Science*, 1957, **125**, 587–589.
- 135 J. Turková, O. Mikeš and F. Šorm, *Coll. Czech. Chem. Commun.*, 1966, **31**, 2444–2454.
- 136 G. Benz, T. Schröder, J. Kurz, C. Wünsche, W. Karl, G. Steffens, J. Pfitzner and D. Schmidt, *Angew. Chem., Int. Ed. Engl.*, 1982, **21**, 527–528.
- 137 A. L. Stefanska, M. Fulston, C. S. V. Hough-Frydrych, J. J. Jones and S. R. Warr, *J. Antibiot. (Tokyo)*, 2000, **53**, 1346–1353.
- 138 V. Braun, K. Günthner, K. Hantke and L. Zimmermann, *J. Bacteriol.*, 1983, **156**, 308–315.
- 139 V. Braun, A. Pramanik, T. Gwinner, M. Köberle and E. Bohn, *BioMetals*, 2009, **22**, 3–13.
- 140 T. C. Johnstone and E. M. Nolan, *Dalton Trans.*, 2015, **44**, 6320–6339.
- 141 Z. Lin, X. Xu, S. Zhao, X. Yang, J. Guo, Q. Zhang, C. Jing, S. Chen and Y. He, *Nat. Commun.*, 2018, **9**, 3445.
- 142 L. Vértesy, W. Aretz, H.-W. Fehlhaber and H. Kogler, *Helv. Chim. Acta*, 1995, **78**, 46–60.
- 143 T. A. Wencewicz, U. Möllmann, T. E. Long and M. J. Miller, *BioMetals*, 2009, **22**, 633–648.
- 144 P. Huber, H. Leuenberger and W. Keller-Schierlein, *Helv. Chim. Acta*, 1986, **69**, 236–245.
- 145 H. Bickel, E. Gäumann, G. Nussberger, P. Reusser, E. Vischer, W. Voser, A. Wettstein and H. Zähler, *Helv. Chim. Acta*, 1960, **43**, 2105–2118.
- 146 H. Bickel, P. Mertens, V. Prelog, J. Seibl and A. Walser, *Tetrahedron*, 1966, **22**, 171–179.
- 147 A. Urban, S. Eckermann, B. Fast, S. Metzger, M. Gehling, K. Ziegelbauer, H. Rübsamen-Waigmann and C. Freiberg, *Appl. Environ.*

- Microbiol.*, 2007, **73**, 6436–6443.
- 148 V. Braun, S. I. Patzer and K. Hantke, *Biochimie*, 2002, **84**, 365–380.
- 149 X. Thomas, D. Destoumieux-Garzón, J. Peduzzi, C. Afonso, A. Blond, N. Birlirakis, C. Goulard, L. Dubost, R. Thai, J.-C. Tabet and S. Rebuffat, *J. Biol. Chem.*, 2004, **279**, 28233–28242.
- 150 M. A. Fischbach, H. Lin, D. R. Liu and C. T. Walsh, *Nat. Chem. Biol.*, 2006, **2**, 132–138.
- 151 I. R. Shimi and A. Dewedar, *Arch. Mikrobiol.*, 1966, **54**, 246–252.
- 152 H.-J. Plattner, B. Stens, H. Diekmann and I. R. Shimi, *J. Antibiot. (Tokyo)*, 1980, **33**, 1208–1209.
- 153 A. Dewedar, N. M. Abdallah and F. E. Mourad, *Folia Microbiol. (Praha)*, 1982, **27**, 222–227.
- 154 I. R. Shimi, G. M. Imam and B. M. Haroun, *J. Antibiot. (Tokyo)*, 1969, **22**, 106–111.
- 155 E. Z. Khafagy and B. M. Haroun, *J. Antibiot. (Tokyo)*, 1974, **27**, 874–880.
- 156 I. R. Shimi and S. Shoukry, *J. Antibiot. (Tokyo)*, 1966, **19**, 110–114.
- 157 F. Knüsel and J. Nüesch, *Nature*, 1965, **206**, 674–676.
- 158 M. G. P. Page, *Clin. Infect. Dis.*, 2019, **69**, S529–S537.
- 159 K. H. Negash, J. K. S. Norris and J. T. Hodgkinson, *Molecules*, 2019, **24**, 3314.
- 160 H. Kong, W. Cheng, H. Wei, Y. Yuan, Z. Yang and X. Zhang, *Eur. J. Med. Chem.*, 2019, **182**, 111615.
- 161 M. J. Miller and R. Liu, *Acc. Chem. Res.*, 2021, **54**, 1646–1661.
- 162 A. Pandey and E. Boros, *Chem. – Eur. J.*, 2021, **27**, 7340–7350.
- 163 J. W. Southwell, C. M. Black and A.-K. Duhme-Klair, *ChemMedChem*, 2021, **16**, 1063–1076.
- 164 M. G. P. Page, *Ann. N. Y. Acad. Sci.*, 2013, **1277**, 115–126.
- 165 B. R. Wilson, A. R. Bogdan, M. Miyazawa, K. Hashimoto and Y. Tsuji, *Trends Mol. Med.*, 2016, **22**, 1077–1090.
- 166 H. Zahner, H. Diddens, W. Keller-Schierlein and H. Nageli, *Jpn. J. Antibiot.*, 1977, **30**, Supplement 201-206.
- 167 N. Ohi, B. Aoki, T. Kuroki, M. Matsumoto, K. Kojima and T. Nehashi, *J. Antibiot.*, 1987, **40**, 22–28.



- 168 T. Maejima, M. Inoue and S. Mitsuhashi, *Antimicrob. Agents Chemother.*, 1991, **35**, 104–110.
- 169 N. A. Watanabe, T. Nagasu, K. Katsu and K. Kitoh, *Antimicrob. Agents Chemother.*, 1987, **31**, 497–504.
- 170 C. Ji, P. A. Miller and M. J. Miller, *J. Am. Chem. Soc.*, 2012, **134**, 9898–9901.
- 171 T. Zheng and E. M. Nolan, *J. Am. Chem. Soc.*, 2014, **136**, 9677–9691.
- 172 T. Aoki, H. Yoshizawa, K. Yamawaki, K. Yokoo, J. Sato, S. Hisakawa, Y. Hasegawa, H. Kusano, M. Sano, H. Sugimoto, Y. Nishitani, T. Sato, M. Tsuji, R. Nakamura, T. Nishikawa and Y. Yamano, *Eur. J. Med. Chem.*, 2018, **155**, 847–868.
- 173 T. G. C. Bird, J. C. Arnould, A. Bertrandie and F. H. Jung, *J. Med. Chem.*, 1992, **35**, 2643–2651.
- 174 H. Nikaido and E. Y. Rosenberg, *J. Bacteriol.*, 1990, **172**, 1361–1367.
- 175 A. P. Tomaras, J. L. Crandon, C. J. McPherson, M. A. Banevicius, S. M. Finegan, R. L. Irvine, M. F. Brown, J. P. O'Donnell and D. P. Nicolau, *Antimicrob. Agents Chemother.*, 2013, **57**, 4197–4207.
- 176 I. Saikawa, S. Minami and Y. Watanabe, *J. Infect. Chemother.*, 1996, **2**, 53–64.
- 177 F. Paech, S. Messner, J. Spickermann, M. Wind, A.-H. Schmitt-Hoffmann, A. T. Witschi, B. A. Howell, R. J. Church, J. Woodhead, M. Engelhardt, S. Krähenbühl and M. Maurer, *Arch. Toxicol.*, 2017, **91**, 3647–3662.
- 178 R. B. Sykes, W. H. Koster and D. P. Bonner, *J. Clin. Pharmacol.*, 1988, **28**, 113–119.
- 179 L. J. Farrell, R. Lo, J. J. Wanford, A. Jenkins, A. Maxwell and L. J. V. Piddock, *J. Antimicrob. Chemother.*, 2018, **73**, 2284–2297.
- 180 A. Bryskier, *J. Antibiot. (Tokyo)*, 2000, **53**, 1028–1037.
- 181 G. R. G. Ruiz, H. H. Wyatt and J. F. Price, *Drugs for the Treatment of Respiratory Diseases*, Cambridge University Press, Cambridge, 2003.
- 182 M. E. Flanagan, S. J. Brickner, M. Lall, J. Casavant, L. Deschenes, S. M. Finegan, D. M. George, K. Granskog, J. R. Hardink, M. D. Huband, T. Hoang, L. Lamb, A. Marra, M. Mitton-Fry, J. P. Mueller, L. M. Mullins, M. C. Noe, J. P. O'Donnell, D. Pattavina, J. B. Penzien, B. P. Schuff, J.

- Sun, D. A. Whipple, J. Young and T. D. Gootz, *ACS Med. Chem. Lett.*, 2011, **2**, 385–390.
- 183 M. Ghosh and M. J. Miller, *Bioorg. Med. Chem.*, 1996, **4**, 43–48.
- 184 A. Zhou, T. M. Kang, J. Yuan, C. Beppler, C. Nguyen, Z. Mao, M. Q. Nguyen, P. Yeh and J. H. Miller, *Antimicrob. Agents Chemother.*, 2015, **59**, 276–281.
- 185 A. Tarapdar, J. K. S. Norris, O. Sampson, G. Mukamolova and J. T. Hodgkinson, *Beilstein J. Org. Chem.*, 2018, **14**, 2646–2650.
- 186 S. Alt, N. Burkard, A. Kulik, S. Grond and L. Heide, *Chem. Biol.*, 2011, **18**, 304–313.
- 187 A. Paulen, V. Gasser, F. Hoegy, Q. Perraud, B. Pesset, I. J. Schalk and G. L. A. Mislin, *Org. Biomol. Chem.*, 2015, **13**, 11567–11579.
- 188 M. Ghosh and M. J. Miller, *Bioorg. Med. Chem.*, 1995, **3**, 1519–1525.
- 189 C. Ji and M. J. Miller, *Bioorg. Med. Chem.*, 2012, **20**, 3828–3836.
- 190 S. R. Md-Saleh, E. C. Chilvers, K. G. Kerr, S. J. Milner, A. M. Snelling, J. P. Weber, G. H. Thomas, A. K. Duhme-Klair and A. Routledge, *Bioorg. Med. Chem. Lett.*, 2009, **19**, 1496–1498.
- 191 S. J. Milner, A. Seve, A. M. Snelling, G. H. Thomas, K. G. Kerr, A. Routledge and A.-K. Duhme-Klair, *Org. Biomol. Chem.*, 2013, **11**, 3461.
- 192 S. J. Milner, A. M. Snelling, K. G. Kerr, A. Abd-El-Aziz, G. H. Thomas, R. E. Hubbard, A. Routledge and A. K. Duhme-Klair, *Bioorg. Med. Chem.*, 2014, **22**, 4499–4505.
- 193 A. Pandey, C. Savino, S. H. Ahn, Z. Yang, S. G. Van Lanen and E. Boros, *J. Med. Chem.*, 2019, **62**, 9947–9960.
- 194 C. Hennard, Q. C. Truong, J. F. Desnottes, J. M. Paris, N. J. Moreau and M. A. Abdallah, *J. Med. Chem.*, 2001, **44**, 2139–2151.
- 195 T. A. Wencewicz, T. E. Long, U. Möllmann and M. J. Miller, *Bioconjug. Chem.*, 2013, **24**, 473–486.
- 196 G. L. A. Mislin and I. J. Schalk, *Metallomics*, 2014, **6**, 408–420.
- 197 J. Rautio, N. A. Meanwell, L. Di and M. J. Hageman, *Nat. Rev. Drug Discov.*, 2018, **17**, 559–587.
- 198 A. Alouane, R. Labruère, T. Le Saux, F. Schmidt and L. Jullien, *Angew. Chem., Int. Ed.*, 2015, **54**, 7492–7509.
- 199 M. Srinivasarao and P. S. Low, *Chem. Rev.*, 2017, **117**, 12133–12164.

- 200 J. D. Bargh, A. Isidro-Llobet, J. S. Parker and D. R. Spring, *Chem. Soc. Rev.*, 2019, **48**, 4361–4374.
- 201 K. C. Nicolaou and S. Rigol, *Angew. Chem., Int. Ed.*, 2019, **58**, 11206–11241.
- 202 E. Ragozin, B. Redko, E. Tuchinsky, A. Rozovsky, A. Albeck, F. Grynszpan and G. Gellerman, *Pept. Sci.*, 2016, **106**, 119–132.
- 203 F. Kratz, I. A. Müller, C. Ryppa and A. Warnecke, *ChemMedChem*, 2008, **3**, 20–53.
- 204 C. A. Blencowe, A. T. Russell, F. Greco, W. Hayes and D. W. Thornthwaite, *Polym. Chem.*, 2011, **2**, 773–790.
- 205 M. E. Roth, O. Green, S. Gnaim and D. Shabat, *Chem. Rev.*, 2016, **116**, 1309–1352.
- 206 R. Walther, J. Rautio and A. N. Zelikin, *Adv. Drug Deliv. Rev.*, 2017, **118**, 65–77.
- 207 P. L. Carl, P. K. Chakravarty and J. A. Katzenellenbogen, *J. Med. Chem.*, 1981, **24**, 479–480.
- 208 F. M. H. de Groot, W. J. Loos, R. Koekkoek, L. W. A. van Berkomp, G. F. Busscher, A. E. Seelen, C. Albrecht, P. de Bruijn and H. W. Scheeren, *J. Org. Chem.*, 2001, **66**, 8815–8830.
- 209 D. Gupta, S. V. Gupta, K.-D. Lee and G. L. Amidon, *Mol. Pharm.*, 2009, **6**, 1604–1611.
- 210 T. Zheng and E. M. Nolan, *Bioorg. Med. Chem. Lett.*, 2015, **25**, 4987–4991.
- 211 P. A. Trail, D. Willner, S. J. Lasch, A. J. Henderson, S. Hofstead, A. M. Casazza, R. A. Firestone, I. Hellstrom and K. E. Hellstrom, *Science*, 1993, **261**, 212–215.
- 212 P. R. Hamann, L. M. Hinman, I. Hollander, C. F. Beyer, D. Lindh, R. Holcomb, W. Hallett, H.-R. Tsou, J. Upešlacis, D. Shochat, A. Mountain, D. A. Flowers and I. Bernstein, *Bioconjug. Chem.*, 2002, **13**, 47–58.
- 213 P. D. Senter, *Curr. Opin. Chem. Biol.*, 2009, **13**, 235–244.
- 214 M. R. Junttila, W. Mao, X. Wang, B.-E. Wang, T. Pham, J. Flygare, S.-F. Yu, S. Yee, D. Goldenberg, C. Fields, J. Eastham-Anderson, M. Singh, R. Vij, J.-A. Hongo, R. Firestein, M. Schutten, K. Flagella, P. Polakis and A. G. Polson, *Sci. Transl. Med.*, 2015, **7**, 314ra186.

- 215 I. R. Vlahov and C. P. Leamon, *Bioconjug. Chem.*, 2012, **23**, 1357–1369.
- 216 N. K. Damle and P. Frost, *Curr. Opin. Pharmacol.*, 2003, **3**, 386–390.
- 217 V. H. J. van der Velden, J. G. te Marvelde, P. G. Hoogeveen, I. D. Bernstein, A. B. Houtsmuller, M. S. Berger and J. J. M. van Dongen, *Blood*, 2001, **97**, 3197–3204.
- 218 C. A. Blencowe, D. W. Thornthwaite, W. Hayes and A. T. Russell, *Org. Biomol. Chem.*, 2015, **13**, 8703–8707.
- 219 B. A. Kellogg, L. Garrett, Y. Kovtun, K. C. Lai, B. Leece, M. Miller, G. Payne, R. Steeves, K. R. Whiteman, W. Widdison, H. Xie, R. Singh, R. V. J. Chari, J. M. Lambert and R. J. Lutz, *Bioconjug. Chem.*, 2011, **22**, 717–727.
- 220 A. Kock, K. Zuwala, A. A. A. Smith, P. Ruiz-Sanchis, B. M. Wohl, M. Tolstrup and A. N. Zelikin, *Chem. Commun.*, 2014, **50**, 14498–14500.
- 221 M. C. Finniss, K. S. Chu, C. J. Bowerman, J. C. Luft, Z. A. Haroon and J. M. DeSimone, *Med. Chem. Commun.*, 2014, **5**, 1355–1358.
- 222 C. F. Riber, A. A. A. Smith and A. N. Zelikin, *Adv. Healthc. Mater.*, 2015, **4**, 1887–1890.
- 223 Z. Deng, J. Hu and S. Liu, *Macromol. Rapid Commun.*, 2020, **41**, 1900531.
- 224 A. K. Jain, M. G. Gund, D. C. Desai, N. Borhade, S. P. Senthilkumar, M. Dhiman, N. K. Mangu, S. V Mali, N. P. Dubash, S. Halder and A. Satyam, *Bioorg. Chem.*, 2013, **49**, 40–48.
- 225 D. W. Norbeck, W. Rosenbrook, J. B. Kramer, D. J. Grampovnik and P. A. Lartey, *J. Med. Chem.*, 1989, **32**, 625–629.
- 226 T. H. Pillow, M. Schutten, S.-F. Yu, R. Ohri, J. Sadowsky, K. A. Poon, W. Solis, F. Zhong, G. Del Rosario, M. A. T. Go, J. Lau, S. Yee, J. He, L. Liu, C. Ng, K. Xu, D. D. Leipold, A. V Kamath, D. Zhang, L. Masterson, S. J. Gregson, P. W. Howard, F. Fang, J. Chen, J. Gunzner-Toste, K. K. Kozak, S. Spencer, P. Polakis, A. G. Polson, J. A. Flygare and J. R. Junutula, *Mol. Cancer Ther.*, 2017, **16**, 871–878.
- 227 A. Brezden, M. F. Mohamed, M. Nepal, J. S. Harwood, J. Kuriakose, M. N. Seleem and J. Chmielewski, *J. Am. Chem. Soc.*, 2016, **138**, 10945–10949.
- 228 L. Brülisauer, M. A. Gauthier and J.-C. Leroux, *J. Control. Release*,

- 2014, **195**, 147–154.
- 229 M. Danial and A. Postma, *Ther. Deliv.*, 2017, **8**, 359–362.
- 230 M. Sengeee, J. J. Eksteen, S. L. Nergård, T. Vasskog and L. K. Sydnes, *Bioconjug. Chem.*, 2019, **30**, 1489–1499.
- 231 M. K. Joubert, M. Hokom, C. Eakin, L. Zhou, M. Deshpande, M. P. Baker, T. J. Goletz, B. A. Kerwin, N. Chirmule, L. O. Narhi and V. Jawa, *J. Biol. Chem.*, 2012, **287**, 25266–25279.
- 232 O. Koniev and A. Wagner, *Chem. Soc. Rev.*, 2015, **44**, 5495–5551.
- 233 A. D. Baldwin and K. L. Kiick, *Bioconjug. Chem.*, 2011, **22**, 1946–1953.
- 234 H. Wu, P. J. LeValley, T. Luo, A. M. Kloxin and K. L. Kiick, *Bioconjug. Chem.*, 2018, **29**, 3595–3605.
- 235 C. Bahou, R. J. Spears, A. E. Aliev, A. Maruani, M. Fernandez, F. Javaid, P. A. Szijj, J. R. Baker and V. Chudasama, *Chem. Commun.*, 2019, **55**, 14829–14832.
- 236 M. Fernández, A. Shamsabadi and V. Chudasama, *Chem. Commun.*, 2020, **56**, 1125–1128.
- 237 J. M. Atkinson, R. A. Falconer, D. R. Edwards, C. J. Pennington, C. S. Siller, S. D. Shnyder, M. C. Bibby, L. H. Patterson, P. M. Loadman and J. H. Gill, *Cancer Res.*, 2010, **70**, 6902–6912.
- 238 M. Poreba, *FEBS J.*, 2020, **287**, 1936–1969.
- 239 G. M. Dubowchik, R. A. Firestone, L. Padilla, D. Willner, S. J. Hofstead, K. Mosure, J. O. Knipe, S. J. Lasch and P. A. Trail, *Bioconjug. Chem.*, 2002, **13**, 855–869.
- 240 O. Redy and D. Shabat, *J. Control. Release*, 2012, **164**, 276–282.
- 241 A. Raposo Moreira Dias, A. Pina, A. Dean, H.-G. Lerchen, M. Caruso, F. Gasparri, I. Fraietta, S. Troiani, D. Arosio, L. Belvisi, L. Pignataro, A. Dal Corso and C. Gennari, *Chem. – Eur. J.*, 2019, **25**, 1696–1700.
- 242 I. F. Antunes, H. J. Haisma, P. H. Elsinga, R. A. Dierckx and E. F. J. de Vries, *Bioconjug. Chem.*, 2010, **21**, 911–920.
- 243 M. Grinda, J. Clarhaut, B. Renoux, I. Tranoy-Opalinski and S. Papot, *Med. Chem. Commun.*, 2012, **3**, 68–70.
- 244 T. Legigan, J. Clarhaut, I. Tranoy-Opalinski, A. Monvoisin, B. Renoux, M. Thomas, A. Le Pape, S. Lerondel and S. Papot, *Angew. Chem., Int. Ed.*, 2012, **51**, 11606–11610.

- 245 S. Kolodych, C. Michel, S. Delacroix, O. Koniev, A. Ehkirch, J. Eberova, S. Cianféroni, B. Renoux, W. Krezel, P. Poinot, C. D. Muller, S. Papot and A. Wagner, *Eur. J. Med. Chem.*, 2017, **142**, 376–382.
- 246 S. Park, S. Y. Kim, J. Cho, D. Jung, D. Seo, J. Lee, S. Lee, S. Yun, H. Lee, O. Park, B. Seo, S. H. Woo and T. K. Park, *Bioconjug. Chem.*, 2019, **30**, 1957–1968.
- 247 M. Roth-Konforti, O. Green, M. Hupfeld, L. Fieseler, N. Heinrich, J. Ihssen, R. Vorberg, L. Wick, U. Spitz and D. Shabat, *Angew. Chem., Int. Ed.*, 2019, **58**, 10361–10367.
- 248 P. Liu, J. Xu, D. Yan, P. Zhang, F. Zeng, B. Li and S. Wu, *Chem. Commun.*, 2015, **51**, 9567–9570.
- 249 W. S. Shin, J. Han, P. Verwilt, R. Kumar, J.-H. Kim and J. S. Kim, *Bioconjug. Chem.*, 2016, **27**, 1419–1426.
- 250 A. B. Mauger, P. J. Burke, H. H. Somani, F. Friedlos and R. J. Knox, *J. Med. Chem.*, 1994, **37**, 3452–3458.
- 251 L. Hu, C. Yu, Y. Jiang, J. Han, Z. Li, P. Browne, P. R. Race, R. J. Knox, P. F. Searle and E. I. Hyde, *J. Med. Chem.*, 2003, **46**, 4818–4821.
- 252 T. A. Shepherd, L. N. Jungheim, D. L. Meyer and J. J. Starling, *Bioorg. Med. Chem. Lett.*, 1991, **1**, 21–26.
- 253 L. N. Jungheim and T. A. Shepherd, *Chem. Rev.*, 1994, **94**, 1553–1566.
- 254 S. Maity, X. Wang, S. Das, M. He, L. W. Riley and N. Murthy, *Chem. Commun.*, 2020, **56**, 3516–3519.
- 255 J. D. Bargh, S. J. Walsh, A. Isidro-Llobet, S. Omarjee, J. S. Carroll and D. R. Spring, *Chem. Sci.*, 2020, **11**, 2375–2380.
- 256 H. Mutlu, C. M. Geiselhart and C. Barner-Kowollik, *Mater. Horiz.*, 2018, **5**, 162–183.
- 257 X. Ji, Z. Pan, B. Yu, L. K. De La Cruz, Y. Zheng, B. Ke and B. Wang, *Chem. Soc. Rev.*, 2019, **48**, 1077–1094.
- 258 A. Dal Corso, L. Pignataro, L. Belvisi and C. Gennari, *Chem. – Eur. J.*, 2019, **25**, 14740–14757.
- 259 R. Rossin, R. M. Versteegen, J. Wu, A. Khasanov, H. J. Wessels, E. J. Steenbergen, W. ten Hoeve, H. M. Janssen, A. H. A. M. van Onzen, P. J. Hudson and M. S. Robillard, *Nat. Commun.*, 2018, **9**, 1484.
- 260 R. M. Versteegen, W. ten Hoeve, R. Rossin, M. A. R. de Geus, H. M.

- Janssen and M. S. Robillard, *Angew. Chem., Int. Ed.*, 2018, **57**, 10494–10499.
- 261 F. Rivault, C. Liébert, A. Burger, F. Hoegy, M. A. Abdallah, I. J. Schalk and G. L. A. Mislin, *Bioorg. Med. Chem. Lett.*, 2007, **17**, 640–644.
- 262 S. Noël, V. Gasser, B. Pesset, F. Hoegy, D. Rognan, I. J. Schalk and G. L. A. Mislin, *Org. Biomol. Chem.*, 2011, **9**, 8288–8300.
- 263 C. Ji and M. J. Miller, *BioMetals*, 2015, **28**, 541–551.
- 264 W. Neumann, M. Sassone-Corsi, M. Raffatellu and E. M. Nolan, *J. Am. Chem. Soc.*, 2018, **140**, 5193–5201.
- 265 W. Neumann and E. M. Nolan, *J. Biol. Inorg. Chem.*, 2018, **23**, 1025–1036.
- 266 T. J. Sanderson, PhD Thesis, University of York, 2016.
- 267 R. Liu, P. A. Miller, S. B. Vakulenko, N. K. Stewart, W. C. Boggess and M. J. Miller, *J. Med. Chem.*, 2018, **61**, 3845–3854.
- 268 J. H. Boyce, B. Dang, B. Ary, Q. Edmondson, C. S. Craik, W. F. DeGrado and I. B. Seiple, *J. Am. Chem. Soc.*, 2020, **142**, 21310–21321.
- 269 I. J. Schalk, *J. Med. Chem.*, 2018, **61**, 3842–3844.
- 270 I. J. Schalk, *Clin. Microbiol. Infect.*, 2018, **24**, 801–802.
- 271 S. W. Ryter and L. E. Otterbein, *BioEssays*, 2004, **26**, 270–280.
- 272 B. Olas, *Chem. Biol. Interact.*, 2014, **222**, 37–43.
- 273 J. MacMicking, Q. Xie and C. Nathan, *Annu. Rev. Immunol.*, 1997, **15**, 323–350.
- 274 K. Incze, J. Farkas, V. Mihályi and E. Zukál, *Appl. Microbiol.*, 1974, **27**, 202–205.
- 275 D. O. Schairer, J. S. Chouake, J. D. Nosanchuk and A. J. Friedman, *Virulence*, 2012, **3**, 271–279.
- 276 Z. Sadrearhami, T.-K. Nguyen, R. Namivandi-Zangeneh, K. Jung, E. H. H. Wong and C. Boyer, *J. Mater. Chem. B*, 2018, **6**, 2945–2959.
- 277 O. Soren, A. Rineh, D. G. Silva, Y. Cai, R. P. Howlin, R. N. Allan, M. Feelisch, J. C. Davies, G. J. Connett, S. N. Faust, M. J. Kelso and J. S. Webb, *J. Antimicrob. Chemother.*, 2020, **75**, 117–125.
- 278 A. W. Carpenter and M. H. Schoenfisch, *Chem. Soc. Rev.*, 2012, **41**, 3742–3752.
- 279 K. Shatalin, I. Gusarov, E. Avetissova, Y. Shatalina, L. E. McQuade, S. J.

- Lippard and E. Nudler, *Proc. Natl. Acad. Sci.*, 2008, **105**, 1009–1013.
- 280 L. Luhachack and E. Nudler, *Curr. Opin. Microbiol.*, 2014, **21**, 13–17.
- 281 M.-C. Chung, A. Narayanan, T. G. Popova, F. Kashanchi, C. L. Bailey and S. G. Popov, *Biochem. Biophys. Res. Commun.*, 2013, **430**, 125–130.
- 282 R. Singh, U. Manjunatha, H. I. M. Boshoff, Y. H. Ha, P. Niyomrattanakit, R. Ledwidge, C. S. Dowd, I. Y. Lee, P. Kim, L. Zhang, S. Kang, T. H. Keller, J. Jiricek and C. E. Barry 3rd, *Science*, 2008, **322**, 1392–1395.
- 283 J. M. Lewis and D. J. Sloan, *Ther. Clin. Risk Manag.*, 2015, **11**, 779–791.
- 284 S. J. Keam, *Drugs*, 2019, **79**, 1797–1803.
- 285 L. S. Nobre, J. D. Seixas, C. C. Romão and L. M. Saraiva, *Antimicrob. Agents Chemother.*, 2007, **51**, 4303–4307.
- 286 X. Ji and B. Wang, *Acc. Chem. Res.*, 2018, **51**, 1377–1385.
- 287 K. Ling, F. Men, W.-C. Wang, Y.-Q. Zhou, H.-W. Zhang and D.-W. Ye, *J. Med. Chem.*, 2018, **61**, 2611–2635.
- 288 J. S. Ward, J. M. Lynam, J. Moir and I. J. S. Fairlamb, *Chem. – Eur. J.*, 2014, **20**, 15061–15068.
- 289 N. S. Sitnikov, Y. Li, D. Zhang, B. Yard and H. G. Schmalz, *Angew. Chem., Int. Ed.*, 2015, **54**, 12314–12318.
- 290 L. K. C. De La Cruz, S. L. Benoit, Z. Pan, B. Yu, R. J. Maier, X. Ji and B. Wang, *Org. Lett.*, 2018, **20**, 897–900.
- 291 A. F. N. Tavares, L. S. Nobre and L. M. Saraiva, *FEMS Microbiol. Lett.*, 2012, **336**, 1–10.
- 292 H. M. Southam, T. W. Smith, R. L. Lyon, C. Liao, C. R. Trevitt, L. A. Middlemiss, F. L. Cox, J. A. Chapman, S. F. El-Khamisy, M. Hippler, M. P. Williamson, P. J. F. Henderson and R. K. Poole, *Redox Biol.*, 2018, **18**, 114–123.
- 293 P. Güntzel, C. Nagel, J. Weigelt, J. W. Betts, C. A. Pattrick, H. M. Southam, R. M. La Ragione, R. K. Poole and U. Schatzschneider, *Metallomics*, 2019, **11**, 2033–2042.
- 294 N. Rana, H. E. Jesse, M. Tinajero-Trejo, J. A. Butler, J. D. Tarlit, M. L. von und zur Muhlen, C. Nagel, U. Schatzschneider and R. K. Poole, *Microbiology*, 2017, **163**, 1477–1489.
- 295 L. Flanagan, R. R. Steen, K. Saxby, M. Klatter, B. J. Aucott, C. Winstanley, I. J. S. Fairlamb, J. M. Lynam, A. Parkin and V.-P. Friman,



- Front. Microbiol.*, 2018, **9**, 195.
- 296 A. Liakopoulos, R. M. La Ragione, C. Nagel, U. Schatzschneider, D. E. Rozen and J. W. Betts, *J. Glob. Antimicrob. Resist.*, 2020, **22**, 594–597.
- 297 W. Wang, X. Ji, Z. Du and B. Wang, *Chem. Commun.*, 2017, **53**, 1370–1373.
- 298 P. Henderson, *Pract. Winer. Vineyard J.*, 2009, 1–6.
- 299 E. Lück and M. Jager, in *Antimicrobial Food Additives: Characteristics ·Uses ·Effects*, Springer Berlin Heidelberg, Berlin, Heidelberg, 1997, pp. 102–115.
- 300 W. Wang and B. Wang, *Front. Chem.*, 2018, **6**, 559.
- 301 S. R. Malwal, D. Sriram, P. Yogeewari, V. B. Konkimalla and H. Chakrapani, *J. Med. Chem.*, 2012, **55**, 553–557.
- 302 D. Crich and I. Sharma, *Angew. Chem., Int. Ed.*, 2009, **48**, 7591–7594.
- 303 S. R. Malwal, D. Sriram, P. Yogeewari and H. Chakrapani, *Bioorg. Med. Chem. Lett.*, 2012, **22**, 3603–3606.
- 304 K. A. Pardeshi, S. R. Malwal, A. Banerjee, S. Lahiri, R. Rangarajan and H. Chakrapani, *Bioorg. Med. Chem. Lett.*, 2015, **25**, 2694–2697.
- 305 K. Johansson, M. Ito, C. M. S. Schophuizen, S. Mathew Thengumtharayil, V. D. Heuser, J. Zhang, M. Shimoji, M. Vahter, W. H. Ang, P. J. Dyson, A. Shibata, S. Shuto, Y. Ito, H. Abe and R. Morgenstern, *Mol. Pharm.*, 2011, **8**, 1698–1708.
- 306 C.-H. Whang, E. Yoo, S. K. Hur, K. S. Kim, D. Kim and S. Jo, *Chem. Commun.*, 2018, **54**, 9031–9034.
- 307 B. Roy, M. Kundu, A. K. Singh, T. Singha, S. Bhattacharya, P. K. Datta, M. Mandal and N. D. P. Singh, *Chem. Commun.*, 2019, **55**, 13140–13143.
- 308 J. A. Malla, R. M. Umesh, S. Yousf, S. Mane, S. Sharma, M. Lahiri and P. Talukdar, *Angew. Chem., Int. Ed.*, 2020, **59**, 7944–7952.
- 309 S. R. Malwal, M. Gudem, A. Hazra and H. Chakrapani, *Org. Lett.*, 2013, **15**, 1116–1119.
- 310 S. R. Malwal and H. Chakrapani, *Org. Biomol. Chem.*, 2015, **13**, 2399–2406.
- 311 J. J. Day, Z. Yang, W. Chen, A. Pacheco and M. Xian, *ACS Chem. Biol.*, 2016, **11**, 1647–1651.

- 312 R. Kodama, K. Sumaru, K. Morishita, T. Kanamori, K. Hyodo, T. Kamitanaka, M. Morimoto, S. Yokojima, S. Nakamura and K. Uchida, *Chem. Commun.*, 2015, **51**, 1736–1738.
- 313 S. Li, R. Liu, X. Jiang, Y. Qiu, X. Song, G. Huang, N. Fu, L. Lin, J. Song, X. Chen and H. Yang, *ACS Nano*, 2019, **13**, 2103–2113.
- 314 Y. Venkatesh, K. S. Kiran, S. S. Shah, A. Chaudhuri, S. Dey and N. D. P. Singh, *Org. Biomol. Chem.*, 2019, **17**, 2640–2645.
- 315 K. A. Pardeshi, T. A. Kumar, G. Ravikumar, M. Shukla, G. Kaul, S. Chopra and H. Chakrapani, *Bioconjug. Chem.*, 2019, **30**, 751–759.
- 316 Y.-S. Kwon, A. Kobayashi, S.-I. Kajiyama, K. Kawazu, H. Kanzaki and C.-M. Kim, *Phytochemistry*, 1997, **44**, 887–889.
- 317 M. Gañan, A. J. Martínez-Rodríguez and A. V Carrascosa, *Food Control*, 2009, **20**, 739–742.
- 318 Y. Uruma, P. Y. M. Yen, K. Sawada and M. Doe, *J. Pharm. Chem. Biol. Sci.*, 2016, **4**, 39–47.
- 319 T. Fukuyama, M. Cheung, C. K. Jow, Y. Hidai and T. Kan, *Tetrahedron Lett.*, 1997, **38**, 5831–5834.
- 320 O. W. Griffith, *Free Radic. Biol. Med.*, 1999, **27**, 922–935.
- 321 V. I. Lushchak, *J. Amino Acids*, 2012, **2012**, 1–26.
- 322 L. B. Poole, *Free Radic. Biol. Med.*, 2015, **80**, 148–157.
- 323 D. P. Jones, in *Protein Sensors and Reactive Oxygen Species - Part B: Thiol Enzymes and Proteins*, eds. H. Sies and L. Packer, Academic Press, 2002, vol. 348, pp. 93–112.
- 324 M. A. Mansoor, A. M. Svardal and P. M. Ueland, *Anal. Biochem.*, 1992, **200**, 218–229.
- 325 D. P. Jones, J. L. Carlson, V. C. Mody, J. Cai, M. J. Lynn and P. Sternberg, *Free Radic. Biol. Med.*, 2000, **28**, 625–635.
- 326 W. A. Kleinman and J. P. Richie, *Biochem. Pharmacol.*, 2000, **60**, 19–29.
- 327 X. Fu, S. A. Cate, M. Dominguez, W. Osborn, T. Özpolat, B. A. Konkle, J. Chen and J. A. López, *Sci. Rep.*, 2019, **9**, 115.
- 328 V. Van Loi, M. Rossius and H. Antelmann, *Front. Microbiol.*, 2015, **6**, 187.
- 329 D. Ritz and J. Beckwith, *Annu. Rev. Microbiol.*, 2001, **55**, 21–48.

- 330 I. S. Arts, A. Gennaris and J.-F. Collet, *FEBS Lett.*, 2015, **589**, 1559–1568.
- 331 R. A. Owens and P. E. Hartman, *J. Bacteriol.*, 1986, **168**, 109–114.
- 332 M. Eser, L. Masip, H. Kadokura, G. Georgiou and J. Beckwith, *Proc. Natl. Acad. Sci.*, 2009, **106**, 1572–1577.
- 333 G. Smirnova, N. Muzyka and O. Oktyabrsky, *Microbiol. Res.*, 2012, **167**, 166–172.
- 334 Y. Xu, J. Chen, Y. Li, S. Peng, X. Gu, M. Sun, K. Gao and J. Fang, *Org. Biomol. Chem.*, 2015, **13**, 2634–2639.
- 335 Z. Wang, H. Wu, P. Liu, F. Zeng and S. Wu, *Biomaterials*, 2017, **139**, 139–150.
- 336 W. Shen, W. Liu, H. Yang, P. Zhang, C. Xiao and X. Chen, *Biomaterials*, 2018, **178**, 706–719.
- 337 W. Phetsang, S. Chaturongakul and C. Jiarpinitnun, *Monatshefte für Chemie - Chem. Mon.*, 2013, **144**, 461–471.
- 338 H. Nikaido, *Microbiol. Mol. Biol. Rev.*, 2003, **67**, 593–656.
- 339 D. H. Klaubert, J. M. Essery and J. F. Barrett, *Expert Opin. Investig. Drugs*, 1994, **3**, 133–144.
- 340 S.-H. Oh, H.-S. Park, H.-S. Kim, J.-Y. Yun, K. Oh, Y.-L. Cho and J.-H. Kwak, *Int. J. Antimicrob. Agents*, 2017, **50**, 700–706.
- 341 W. J. Page and M. Von Tigerstrom, *Microbiology*, 1988, **134**, 453–460.
- 342 A. Souto, M. A. Montaos, M. Balado, C. R. Osorio, J. Rodríguez, M. L. Lemos and C. Jiménez, *Bioorg. Med. Chem.*, 2013, **21**, 295–302.
- 343 P. W. West and G. C. Gaeke, *Anal. Chem.*, 1956, **28**, 1816–1819.
- 344 K. A. Pardeshi, G. Ravikumar and H. Chakrapani, *Org. Lett.*, 2018, **20**, 4–7.
- 345 Y.-Q. Sun, J. Liu, J. Zhang, T. Yang and W. Guo, *Chem. Commun.*, 2013, **49**, 2637.
- 346 I. Mancini, G. Guella, G. Chiasera and F. Pietra, *Tetrahedron Lett.*, 1998, **39**, 1611–1614.
- 347 M. S. Ning, S. E. Price, J. Ta and K. M. Davies, *J. Phys. Org. Chem.*, 2010, **23**, 220–226.
- 348 J. G. Santos, M. E. Aliaga, K. Alarcón, A. Torres, D. Céspedes and P. Pavez, *Org. Biomol. Chem.*, 2016, **14**, 6479–6486.

- 349 A.-K. Duhme, R. C. Hider and H. H. Khodr, *Chem. Ber. Recl.*, 1997, **130**, 969–973.
- 350 H. H. Khodr, R. C. Hider and A. K. Duhme-Klair, *J. Biol. Inorg. Chem.*, 2002, **7**, 891–896.
- 351 S. Lei, B. Jin, Q. Zhang, Z. Zhang, X. Wang, R. Peng and S. Chu, *Polyhedron*, 2016, **119**, 387–395.
- 352 A. D’Amato, P. Ghosh, C. Costabile, G. Della Sala, I. Izzo, G. Maayan and F. De Riccardis, *Dalton Trans.*, 2020, **49**, 6020–6029.
- 353 C. G. Pitt, Y. Bao, J. Thompson, M. C. Wani, H. Rosenkrantz and J. Metterville, *J. Med. Chem.*, 1986, **29**, 1231–1237.
- 354 K. Pappas, X. Zhang, W. Tang and S. Fang, *Tetrahedron Lett.*, 2009, **50**, 5741–5743.
- 355 W. Tang and S. Fang, *Tetrahedron Lett.*, 2008, **49**, 6003–6006.
- 356 K. G. Kleb, *Angew. Chemie*, 1968, 284–285.
- 357 W. R. Bowman and D. R. Coghlan, *Tetrahedron*, 1997, **53**, 15787–15798.
- 358 F. Ravalico, S. L. James and J. S. Vyle, *Green Chem.*, 2011, **13**, 1778.
- 359 D. D. Perrin, *Dissociation Constants of Organic Bases in Aqueous Solution*, Butterworths, London, 1965.
- 360 W. A. Loughlin, I. D. Jenkins and M. J. Petersson, *J. Org. Chem.*, 2013, **78**, 7356–7361.
- 361 W. Y. Kim, H. Shi, H. S. Jung, D. Cho, P. Verwilt, J. Y. Lee and J. S. Kim, *Chem. Commun.*, 2016, **52**, 8675–8678.
- 362 C. Y. Zamora, A. G. E. Madec, W. Neumann, E. M. Nolan and B. Imperiali, *Bioorg. Med. Chem.*, 2018, **26**, 5314–5321.
- 363 W. R. Harris, K. N. Raymond and F. L. Weigl, *J. Am. Chem. Soc.*, 1981, **103**, 2667–2675.
- 364 J. S. Renny, L. L. Tomasevich, E. H. Tallmadge and D. B. Collum, *Angew. Chem., Int. Ed.*, 2013, **52**, 11998–12013.
- 365 D. L. White, R. C. Scarrow and K. N. Raymond, *J. Am. Chem. Soc.*, 1985, **107**, 6540–6546.
- 366 T. B. Karpishin, M. S. Gebhard, E. I. Solomon and K. N. Raymond, *J. Am. Chem. Soc.*, 1991, **113**, 2977–2984.
- 367 Y. Murakami and K. Nakamura, *Bull. Chem. Soc. Jpn*, 1963, **36**, 1408–

- 1411.
- 368 A. Avdeef, S. R. Sofen, T. L. Bregante and K. N. Raymond, *J. Am. Chem. Soc.*, 1978, **100**, 5362–5370.
- 369 R. C. Scarrow, P. E. Riley, K. Abu-Dari, D. L. White and K. N. Raymond, *Inorg. Chem.*, 1985, **24**, 954–967.
- 370 D. J. Raines, PhD Thesis, University of York, 2014.
- 371 A. Ninh Pham, A. L. Rose, A. J. Feitz and T. D. Waite, *Geochim. Cosmochim. Acta*, 2006, **70**, 640–650.
- 372 R. J. Motekaitis and A. E. Martell, *J. Coord. Chem.*, 1994, **31**, 67–78.
- 373 R. C. Scarrow, D. J. Ecker, C. Ng, S. Liu and K. N. Raymond, *Inorg. Chem.*, 1991, **30**, 900–906.
- 374 Y. Ma, Y. Xie and R. C. Hider, *Analyst*, 2013, **138**, 96–99.
- 375 W. Przychodzeń and A. Chimiak, *Phosphorus. Sulfur. Silicon Relat. Elem.*, 1998, **143**, 77–83.
- 376 E. Pierri, D. Tsamouras and E. Dalas, *J. Cryst. Growth*, 2000, **213**, 93–98.
- 377 S. Scaccia, M. Carewska and P. P. Prosini, *Thermochim. Acta*, 2004, **413**, 81–86.
- 378 T. Roncal-Herrero, J. D. Rodríguez-Blanco, L. G. Benning and E. H. Oelkers, *Cryst. Growth Des.*, 2009, **9**, 5197–5205.
- 379 T. Zhang, Y. Lu and G. Luo, *Chinese J. Chem. Eng.*, 2017, **25**, 211–215.
- 380 C. M. H. Ferreira, I. S. S. Pinto, E. V Soares and H. M. V. M. Soares, *RSC Adv.*, 2015, **5**, 30989–31003.
- 381 H. Hondo, F. Moriuchi and J. Sunamoto, *J. Org. Chem.*, 1981, **46**, 1333–1336.
- 382 H. P. Burchfield, *Nature*, 1958, **181**, 49–50.
- 383 A. J. Cohen and J. N. Smith, *Biochem. J.*, 1964, **90**, 449–.
- 384 B. P. Howden, J. K. Davies, P. D. R. Johnson, T. P. Stinear and M. L. Grayson, *Clin. Microbiol. Rev.*, 2010, **23**, 99–139.
- 385 S. Y. C. Tong, J. S. Davis, E. Eichenberger, T. L. Holland and V. G. Fowler, *Clin. Microbiol. Rev.*, 2015, **28**, 603–661.
- 386 G. Ghssein, C. Brutesco, L. Ouerdane, S. Wang, C. Hajjar, R. Lobinski, D. Lemaire, P. Richaud, A. Espaillet, F. Cava, D. Pignol and P. Arnoux, *Science*, 2016, **352**, 1105–1109.

- 387 R. J. Courcol, D. Trivier, M. Bissinger, G. U. Y. R. Martin and M. R. W. Brown, *Infect. Immun.*, 1997, **65**, 1944–1948.
- 388 M. L. Reniere, G. Pishchany and E. P. Skaar, *Iron Uptake and Homeostasis in Microorganisms*, Caister Academic Press, Norfolk, UK, 2010.
- 389 F. C. Beasley, C. L. Marolda, J. Cheung, S. Buac and D. E. Heinrichs, *Infect. Immun.*, 2011, **79**, 2345–2355.
- 390 M. H. Zwietering, I. Jongenburger, F. M. Rombouts and K. van 't Riet, *Appl. Environ. Microbiol.*, 1990, **56**, 1875–1881.
- 391 D. Chu and D. J. Barnes, *Sci. Rep.*, 2016, **6**, 25191.
- 392 A. Brauner, O. Fridman, O. Gefen and N. Q. Balaban, *Nat. Rev. Microbiol.*, 2016, **14**, 320–330.
- 393 A.-A. D. Jones, D. Medina-Cruz, N. Y. Kim, G. Mi, C. Bartomeu-Garcia, L. Baranda-Pellejero, N. Bassous and T. J. Webster, *bioRxiv*, DOI:10.1101/2020.07.19.210930.
- 394 A. M. Earl, R. Losick and R. Kolter, *J. Bacteriol.*, 2007, **189**, 1163–1170.
- 395 E. A. Dertz, A. Stintzi and K. N. Raymond, *J. Biol. Inorg. Chem.*, 2006, **11**, 1087–1097.
- 396 J. Ollinger, K. Song, H. Antelmann, M. Hecker and J. D. Helmann, *J. Bacteriol.*, 2006, **188**, 3664–3673.
- 397 A. M. Zawadzka, Y. Kim, N. Maltseva, R. Nichiporuk, Y. Fan, A. Joachimiak and K. N. Raymond, *Proc. Natl. Acad. Sci.*, 2009, **106**, 21854–21859.
- 398 G. M. Grandchamp, L. Caro and E. A. Shank, *Appl. Environ. Microbiol.*, 2017, **83**, 1–17.
- 399 G. Sezonov, D. Joseleau-Petit and R. D'Ari, *J. Bacteriol.*, 2007, **189**, 8746–8749.
- 400 O. Tenaillon, D. Skurnik, B. Picard and E. Denamur, *Nat. Rev. Microbiol.*, 2010, **8**, 207–217.
- 401 D. W. Hilbert, in *E. coli Infections: Causes, Treatment and Prevention*, eds. M. C. Rogers and N. D. Peterson, Nova Science Publishers, 2011, pp. 1–66.
- 402 K. Hantke, *FEMS Microbiol. Lett.*, 1990, **67**, 5–8.
- 403 K. Hantke, G. Nicholson, W. Rabsch and G. Winkelmann, *Proc. Natl.*

- Acad. Sci. U. S. A.*, 2003, **100**, 3677–3682.
- 404 M. Zhu, M. Valdebenito, G. Winkelmann and K. Hantke, *Microbiology*, 2005, **151**, 2363–2372.
- 405 M. A. Fischbach, H. Lin, L. Zhou, Y. Yu, R. J. Abergel, D. R. Liu, K. N. Raymond, B. L. Wanner, R. K. Strong, C. T. Walsh, A. Aderem and K. D. Smith, *Proc. Natl. Acad. Sci. U. S. A.*, 2006, **103**, 16502–7.
- 406 Q. Gao, X. Wang, H. Xu, Y. Xu, J. Ling, D. Zhang, S. Gao and X. Liu, *BMC Microbiol.*, 2012, **12**, 143.
- 407 V. Braun and R. Burkhardt, *J. Bacteriol.*, 1982, **152**, 223–231.
- 408 A. G. Torres, P. Redford, R. A. Welch and S. M. Payne, *Infect. Immun.*, 2001, **69**, 6179–6185.
- 409 R. E. Watts, M. Totsika, V. L. Challinor, A. N. Mabbett, G. C. Ulett, J. J. D. Voss and M. A. Schembri, *Infect. Immun.*, 2012, **80**, 333–344.
- 410 L. J. Searle, G. Méric, I. Porcelli, S. K. Sheppard and S. Lucchini, *PLoS One*, 2015, **10**, 1–14.
- 411 J. Liu, K. Duncan and C. T. Walsh, *J. Bacteriol.*, 1989, 791–798.
- 412 M. Sakaitani, F. Rusnak, N. R. Quinn, C. Tu, T. B. Frigo, G. A. Berchtold and C. T. Walsh, *Biochemistry*, 1990, **29**, 6789–6798.
- 413 J. Clarke, PhD Thesis, University of York, 2017.
- 414 J. H. J. Mueller and E. R. E. Johnson, *J. Immunol.*, 1941, **40**, 33–38.
- 415 T. E. Clarke, V. Braun, G. Winkelmann, L. W. Tari and H. J. Vogel, *J. Biol. Chem.*, 2002, **277**, 13966–13972.
- 416 C. Hansch, A. Leo and R. W. Taft, *Chem. Rev.*, 1991, **91**, 165–195.
- 417 C. Kay, P. J. Murray, L. Sandow and A. B. Holmes, *Tetrahedron Lett.*, 1997, **38**, 6941–6944.
- 418 T. Fukuyama, C.-K. Jow and M. Cheung, *Tetrahedron Lett.*, 1995, **36**, 6373–6374.
- 419 G. M. Williams, R. A. E. Carr, M. S. Congreve, C. Kay, S. C. McKeown, P. J. Murray, J. J. Scicinski and S. P. Watson, *Angew. Chem., Int. Ed.*, 2000, **39**, 3293–3296.
- 420 M. S. Congreve, M. Ladlow, P. Marshall, N. Parr, J. J. Scicinski, T. Sheppard, E. Vickerstaffe and R. A. E. Carr, *Org. Lett.*, 2001, **3**, 507–510.
- 421 M. S. Congreve, S. V. Ley and J. J. Scicinski, *Chem. – Eur. J.*, 2002, **8**,

- 1768–1776.
- 422 M. S. Congreve, C. Kay, J. J. Scicinski, S. V Ley, G. Williams, P. J. Murray, S. C. McKeown and S. P. Watson, *Tetrahedron Lett.*, 2003, **44**, 4153–4156.
- 423 S. P. Andrews and M. Ladlow, *J. Org. Chem.*, 2003, **68**, 5525–5533.
- 424 M. Pattarawarapan and K. Burgess, *Angew. Chem., Int. Ed.*, 2000, **39**, 4299–4301.
- 425 M. Pattarawarapan, J. Chen, M. Steffensen and K. Burgess, *J. Comb. Chem.*, 2001, **3**, 102–116.
- 426 D. Xin, A. Jeffries and K. Burgess, *ACS Comb. Sci.*, 2017, **19**, 414–421.
- 427 S. Yokoshima, Y. Abe, N. Watanabe, Y. Kita, T. Kan, T. Iwatsubo, T. Tomita and T. Fukuyama, *Bioorg. Med. Chem. Lett.*, 2009, **19**, 6869–6871.
- 428 M. Ito, A. Shibata, J. Zhang, M. Hiroshima, Y. Sako, Y. Nakano, K. Kojima-Aikawa, B. Mannervik, S. Shuto, Y. Ito, R. Morgenstern and H. Abe, *ChemBioChem*, 2012, **13**, 1428–1432.
- 429 J. D. Hayes, J. U. Flanagan and I. R. Jowsey, *Annu. Rev. Pharmacol. Toxicol.*, 2004, **45**, 51–88.
- 430 N. Allocati, M. Masulli, C. Di Ilio and L. Federici, *Oncogenesis*, 2018, **7**, 8.
- 431 J.-J. Lee, S. Ha, H.-J. Kim, H. J. Ha, H.-Y. Lee and K.-J. Lee, *ACS Chem. Biol.*, 2014, **9**, 2883–2894.
- 432 M. W. Van Gisbergen, M. Cebula, J. Zhang, A. Ottosson-Wadlund, L. Dubois, P. Lambin, K. D. Tew, D. M. Townsend, G. R. M. M. Haenen, M. J. Driittij-Reijnders, H. Saneyoshi, M. Araki, Y. Shishido, Y. Ito, E. S. J. Arnér, H. Abe, R. Morgenstern and K. Johansson, *Mol. Pharm.*, 2016, **13**, 2010–2025.
- 433 R. E. Juárez-Hernández, P. A. Miller and M. J. Miller, *ACS Med. Chem. Lett.*, 2012, **3**, 799–803.
- 434 T. Zheng, J. L. Bullock and E. M. Nolan, *J. Am. Chem. Soc.*, 2012, **134**, 18388–18400.
- 435 S. Fardeau, A. Dassonville-Klimpt, N. Audic, A. Sasaki, M. Pillon, E. Baudrin, C. Mullié and P. Sonnet, *Bioorg. Med. Chem.*, 2014, **22**, 4049–4060.



- 436 T. J. Sanderson, C. M. Black, J. W. Southwell, E. J. Wilde, A. Pandey, R. Herman, G. H. Thomas, E. Boros, A.-K. Duhme-Klair and A. Routledge, *ACS Infect. Dis.*, 2020, **6**, 2532–2541.
- 437 G. S. Tillotson, *J. Med. Microbiol.*, 1996, **44**, 320–4.
- 438 S. Pal, V. Ramu, N. Taye, D. G. Mogare, A. M. Yeware, D. Sarkar, D. S. Reddy, S. Chattopadhyay and A. Das, *Bioconjug. Chem.*, 2016, **27**, 2062–2070.
- 439 S. Davies, L. Qiao, B. L. Oliveira, C. D. Navo, G. Jiménez-Osés and G. J. L. Bernardes, *ChemBioChem*, 2019, **20**, 1541–1546.
- 440 *Medical Expenditure Panel Survey*, Rockville, MD, 2018.
- 441 The Top 300 Drug List,  
<https://clincalc.com/DrugStats/Top300Drugs.aspx> (accessed 12 March 2021).
- 442 D. C. Hooper, *Emerg. Infect. Dis.*, 2001, **7**, 337–341.
- 443 C. Gagliotti, L. Nobilio and M. L. Moro, *Clin. Microbiol. Infect.*, 2007, **13**, 328–331.
- 444 S. M. Hamed, W. F. Elkhatib, H. A. El-Mahallawy, M. M. Helmy, M. S. Ashour and K. M. A. Aboshanab, *Sci. Rep.*, 2018, **8**, 12268.
- 445 OSIRIS Property Explorer,  
<https://openmolecules.org/propertyexplorer/> (accessed 21 August 2021).
- 446 J. L. Vázquez, S. Merino, O. Domenech, M. Berlanga, M. Viñas, M. T. Montero and J. Hernández-Borrell, *Int. J. Pharm.*, 2001, **220**, 53–62.
- 447 G.-M. Cárdenas-Youngs and J.-L. Beltrán, *J. Chem. Eng. Data*, 2015, **60**, 3327–3332.
- 448 T. E. Renau, J. P. Sanchez, M. A. Shapiro, J. A. Dever, S. J. Gracheck and J. M. Domagala, *J. Med. Chem.*, 1995, **38**, 2974–2977.
- 449 J. Sun, S. Sakai, Y. Tauchi, Y. Deguchi, J. Chen, R. Zhang and K. Morimoto, *Eur. J. Pharm. Biopharm.*, 2002, **54**, 51–58.
- 450 A. I. Caço, F. Varanda, M. J. Pratas de Melo, A. M. A. Dias, R. Dohrn and I. M. Marrucho, *Ind. Eng. Chem. Res.*, 2008, **47**, 8083–8089.
- 451 E. Banin, A. Lozinski, K. M. Brady, E. Berenshtein, P. W. Butterfield, M. Moshe, M. Chevion, E. P. Greenberg and E. Banin, *Proc. Natl. Acad. Sci.*, 2008, **105**, 16761–16766.

- 452 M. A. Llamas, F. Imperi, P. Visca and I. L. Lamont, *FEMS Microbiol. Rev.*, 2014, **38**, 569–597.
- 453 M. Petrik, E. Umlaufova, V. Raclavsky, A. Palyzova, V. Havlicek, J. Pfister, C. Mair, Z. Novy, M. Popper, M. Hajduch and C. Decristoforo, *Eur. J. Nucl. Med. Mol. Imaging*, 2021, **48**, 372–382.
- 454 P. L. Khimji and A. A. Miles, *Br. J. Exp. Pathol.*, 1978, **59**, 137–147.
- 455 M. K. Paczosa, R. J. Silver, A. L. McCabe, A. K. Tai, C. H. McLeish, D. W. Lazinski and J. Meccas, *Infect. Immun.*, 2020, **88**, e00034-20.
- 456 C. H. Huang, H. Takemoto, T. Nomoto, K. Tomoda, M. Matsui and N. Nishiyama, *ChemMedChem*, 2017, **12**, 19–22.
- 457 M. Jereb and L. Hribernik, *Green Chem.*, 2017, **19**, 2286–2295.
- 458 O. M. Mulina, A. I. Ilovaisky and A. O. Terent'ev, *Eur. J. Org. Chem.*, 2018, **2018**, 4648–4672.
- 459 Y. M. Pu, A. Christesen and Y. Y. Ku, *Tetrahedron Lett.*, 2010, **51**, 418–421.
- 460 S. M. F. Jamieson, D. G. Brooke, D. Heinrich, G. J. Atwell, S. Silva, E. J. Hamilton, A. P. Turnbull, L. J. M. Rigoreau, E. Trivier, C. Soudy, S. S. Samlal, P. J. Owen, E. Schroeder, T. Raynham, J. U. Flanagan and W. A. Denny, *J. Med. Chem.*, 2012, **55**, 7746–7758.
- 461 M. Wang, M. Gao, K. D. Miller, G. W. Sledge and Q. H. Zheng, *Bioorg. Med. Chem. Lett.*, 2012, **22**, 1569–1574.
- 462 W. Wei, S. Zhou, D. Cheng, Y. Li, J. Liu, Y. Xie, Y. Li and Z. Li, *Bioorg. Med. Chem. Lett.*, 2017, **27**, 3365–3369.
- 463 M. Patra, A. Bauman, C. Mari, C. A. Fischer, O. Blacque, D. Häussinger, G. Gasser and T. L. Mindt, *Chem. Commun.*, 2014, **50**, 11523–11525.
- 464 F. Gao, C. Ieritano, K. T. Chen, G. M. Dias, J. Rousseau, F. Bénard and Y. Seimbille, *Org. Biomol. Chem.*, 2018, **16**, 5102–5106.
- 465 P. J. Murray, C. Kay, J. J. Sciciński, S. C. McKeown, S. P. Watson and R. A. E. Carr, *Tetrahedron Lett.*, 1999, **40**, 5609–5612.
- 466 P. G. M. Wuts, Ed., in *Greene's Protective Groups in Organic Synthesis*, John Wiley & Sons, Ltd, 5th edn., 2014, pp. 533–646.
- 467 R. Erez and D. Shabat, *Org. Biomol. Chem.*, 2008, **6**, 2669–2672.
- 468 U. Tehler, J. H. Fagerberg, R. Svensson, M. Larhed, P. Artursson and C. A. S. Bergström, *J. Med. Chem.*, 2013, **56**, 2690–2694.

- 469 U. Schmidt, M. Zah and A. Lieberknecht, *J. Chem. Soc. Chem. Comm.*, 1991, 1002–1004.
- 470 S. Banala, P. Ensle and R. D. Süßmuth, *Angew. Chem., Int. Ed.*, 2013, **52**, 9518–9523.
- 471 C. F. Bender, C. L. Paradise, V. M. Lynch, F. K. Yoshimoto and J. K. De Brabander, *Tetrahedron*, 2018, **74**, 909–919.
- 472 J. Azéma, B. Guidetti, J. Dewelle, B. Le Calve, T. Mijatovic, A. Korolyov, J. Vaysse, M. Malet-Martino, R. Martino and R. Kiss, *Bioorg. Med. Chem.*, 2009, **17**, 5396–5407.
- 473 K. Zhu and J. S. Panek, *Org. Lett.*, 2011, **13**, 4652–4655.
- 474 D. J. Haydon, J. M. Bennett, D. Brown, I. Collins, G. Galbraith, P. Lancett, R. Macdonald, N. R. Stokes, P. K. Chauhan, J. K. Sutariya, N. Nayal, A. Srivastava, J. Beanland, R. Hall, V. Henstock, C. Noula, C. Rockley and L. Czaplewski, *J. Med. Chem.*, 2010, **53**, 3927–3936.
- 475 R. Skouta, S. J. Dixon, J. Wang, D. E. Dunn, M. Orman, K. Shimada, P. A. Rosenberg, D. C. Lo, J. M. Weinberg, A. Linkermann and B. R. Stockwell, *J. Am. Chem. Soc.*, 2014, **136**, 4551–4556.
- 476 J. Liu, D. Obando, L. G. Schipanski, L. K. Groebler, P. K. Witting, D. S. Kalinowski, D. R. Richardson and R. Codd, *J. Med. Chem.*, 2010, **53**, 1370–1382.
- 477 Q. Laurent, L. K. Batchelor and P. J. Dyson, *Organometallics*, 2018, **37**, 915–923.
- 478 A. G. Cosby, S. H. Ahn and E. Boros, *Angew. Chem., Int. Ed.*, 2018, **57**, 15496–15499.
- 479 S. H. Combe, A. Hosseini, A. Parra and P. R. Schreiner, *J. Org. Chem.*, 2017, **82**, 2407–2413.
- 480 P. La Manna, C. Talotta, G. Floresta, M. De Rosa, A. Soriente, A. Rescifina, C. Gaeta and P. Neri, *Angew. Chem., Int. Ed.*, 2018, **57**, 5423–5428.
- 481 J. M. Álvarez-Calero, Z. D. Jorge and G. M. Massanet, *Org. Lett.*, 2016, **18**, 6344–6347.
- 482 D. Koszelewski, A. Brodzka, A. Madej, D. Trzepizur and R. Ostaszewski, *J. Org. Chem.*, 2021, **86**, 6331–6342.
- 483 M. S. Beevers, S. Bratt, A. W. P. Jarvie and M. C. Perry, *J. Chem. Soc.*

- Perkin Trans. 2*, 1993, 1569–1573.
- 484 K. D. Mjos, J. F. Cawthray, E. Polishchuk, M. J. Abrams and C. Orvig, *Dalton Trans.*, 2016, **45**, 13146–13160.
- 485 P. Jones, B. Villeneuve, C. Fei, J. Demarte, A. J. Haggarty, K. T. Nwe, D. A. Martin, A.-M. Lebuis, J. M. Finkelstein, B. J. Gour-Salin, T. H. Chan and B. R. Leyland-Jones, *J. Med. Chem.*, 1998, **41**, 3062–3077.
- 486 T. G. Back and J. E. Wulff, *Angew. Chem., Int. Ed.*, 2004, **43**, 6493–6496.
- 487 P. Patel, C. N. Reddy, V. Gore, S. Chourey and Q. Ye, *ACS Med. Chem. Lett.*, 2014, **5**, 815–819.
- 488 C. Nagendra, Q. Ye, S. Chourey, S. Gravel, W. S. Powell and J. Rokach, *Tetrahedron Lett.*, 2015, **56**, 6896–6899.
- 489 N. Rajabi, M. Auth, K. R. Troelsen, M. Pannek, D. P. Bhatt, M. Fontenas, M. D. Hirschey, C. Steegborn, A. S. Madsen and C. A. Olsen, *Angew. Chem., Int. Ed.*, 2017, **56**, 14836–14841.
- 490 R. Leung-Toung, T. F. Tam, Y. Zhao, C. D. Simpson, W. Li, D. Desilets and K. Karimian, *J. Org. Chem.*, 2005, **70**, 6230–6241.
- 491 A. Evers, R. D. Hancock, A. E. Martell and R. J. Motekaitis, *Inorg. Chem.*, 1989, **28**, 2189–2195.
- 492 T. Schmiederer, S. Rausch, M. Valdebenito, Y. Mantri, E. Mösker, T. Baramov, K. Stelmaszyk, P. Schmieder, D. Butz, S. I. Müller, K. Schneider, M.-H. Baik, K. Hantke and R. D. Süßmuth, *Angew. Chem., Int. Ed.*, 2011, **50**, 4230–4233.
- 493 T. Richardson-Sanchez, W. Tieu, M. P. Gotsbacher, T. J. Telfer and R. Codd, *Org. Biomol. Chem.*, 2017, **15**, 5719–5730.
- 494 C.-H. Chiu, T.-C. Jheng, B.-C. Peng, W.-S. Chung and K.-K. T. Mong, *Eur. J. Org. Chem.*, 2020, **2020**, 3650–3659.
- 495 L. M. Koeth, A. King, H. Knight, J. May, L. A. Miller, I. Phillips and J. A. Poupard, *J. Antimicrob. Chemother.*, 2000, **46**, 369–376.
- 496 M. A. Wikler, *CLSI*, 2006, **26**, M7-A7.
- 497 M. A. Hackel, M. Tsuji, Y. Yamano, R. Echols, J. A. Karlowsky and D. F. Sahm, *Diagn. Microbiol. Infect. Dis.*, 2019, **94**, 321–325.
- 498 International Organization for Standardization, *ISO 20776-1: 2019*, 2019.

- 499 M. Loose, K. G. Naber, A. Coates, F. M. E. Wagenlehner and Y. Hu, *Front. Microbiol.*, 2020, **11**, 54.
- 500 M. Birus, Z. Bradic, N. Kujundzic and M. Pribanic, *Inorg. Chem.*, 1984, **23**, 2170–2175.
- 501 P. V. Bernhardt, *Dalton Trans.*, 2007, 3214–3220.
- 502 A. C. Leney and A. J. R. Heck, *J. Am. Soc. Mass Spectrom.*, 2017, **28**, 5–13.
- 503 A. Aron, D. Petras, R. Schmid, J. M. Gauglitz, I. Büttel, L. Antelo, H. Zhi, C. C. Saak, K. P. Malarney, E. Thines, R. J. Dutton, M. Raffatellu and P. C. Dorrestein, *bioRxiv*, DOI:10.1101/824888.
- 504 R. Schmid, D. Petras, L.-F. Nothias, M. Wang, A. T. Aron, A. Jagels, H. Tsugawa, J. Rainer, M. Garcia-Aloy, K. Dührkop, A. Korf, T. Pluskal, Z. Kameník, A. K. Jarmusch, A. M. Caraballo-Rodríguez, K. C. Weldon, M. Nothias-Esposito, A. A. Aksenov, A. Bauermeister, A. Albarracin Orio, C. O. Grundmann, F. Vargas, I. Koester, J. M. Gauglitz, E. C. Gentry, Y. Hövelmann, S. A. Kalinina, M. A. Pendergraft, M. Panitchpakdi, R. Tehan, A. Le Gouellec, G. Aleti, H. Mannocho Russo, B. Arndt, F. Hübner, H. Hayen, H. Zhi, M. Raffatellu, K. A. Prather, L. I. Aluwihare, S. Böcker, K. L. McPhail, H.-U. Humpf, U. Karst and P. C. Dorrestein, *Nat. Commun.*, 2021, **12**, 3832.
- 505 L. Konermann, *J. Am. Soc. Mass Spectrom.*, 2017, **28**, 1827–1835.
- 506 E. M. van der Aar, M. J. de Groot, T. Bouwman, G. J. Bijloo, J. N. Commandeur and N. P. Vermeulen, *Chem. Res. Toxicol.*, 1997, **10**, 439–449.
- 507 A. E. Voelker and R. Viswanathan, *J. Org. Chem.*, 2013, **78**, 9647–9658.
- 508 A. E. Voelker and R. Viswanathan, *Bioconjug. Chem.*, 2013, **24**, 1295–1301.
- 509 Y. Nomi, H. Alzawa, T. Kurata, K. Shindo and C. Van Nguyen, *Biosci. Biotechnol. Biochem.*, 2009, **73**, 2408–2411.
- 510 E. Petruzzella, A. Curci, N. Margiotta, G. Natile and J. D. Hoeschele, *Inorg. Chim. Acta*, 2016, **452**, 130–136.
- 511 L. B. Rice, *J. Infect. Dis.*, 2008, **197**, 1079–1081.
- 512 S. Santajit and N. Indrawattana, *Biomed Res. Int.*, 2016, **2016**, 2475067.

- 513 G. Funke, D. Monnet, C. deBernardis, A. von Graevenitz and J. Freney, *J. Clin. Microbiol.*, 1998, **36**, 1948–1952.
- 514 M. Ligozzi, C. Bernini, M. G. Bonora, M. De Fatima, J. Zuliani and R. Fontana, *J. Clin. Microbiol.*, 2002, **40**, 1681–1686.
- 515 T. K. W. Ling, Z. K. Liu and A. F. B. Cheng, *J. Clin. Microbiol.*, 2003, **41**, 4705–4707.
- 516 *The European Committee on Antimicrobial Susceptibility Testing. Breakpoint Tables for Interpretation of MICs and Zone Diameters. Version 11.0*, 2021.
- 517 M. T. Sebulsky, D. Hohnstein, M. D. Hunter and D. E. Heinrichs, *J. Bacteriol.*, 2000, **182**, 4394–4400.
- 518 T. Funahashi, T. Tanabe, K. Mihara, K. Miyamoto, H. Tsujibo and S. Yamamoto, *Biol. Pharm. Bull.*, 2012, **35**, 753–760.
- 519 T. M. G., C. B. W., S. Yuanzheng, C. D. W. and Z. D. V., *Antimicrob. Agents Chemother.*, 2012, **56**, 5419–5421.
- 520 J. A. Lindsay and T. V. Riley, *J. Med. Microbiol.*, 1991, **35**, 45–48.
- 521 D. Heuck, W. Witte, C. Bräulke and R. Reissbrodt, *Zentralblatt für Bakteriologie*, 1994, **280**, 304–311.
- 522 C.-M. Kim and S.-H. Shin, *J. Korean Med. Sci.*, 2009, **24**, 289–295.
- 523 K. Hantke, *Mol. Gen. Genet. MGG*, 1983, **191**, 301–306.
- 524 M. Nelson, C. J. Carrano and P. J. Szaniszlo, *BioMetals*, 1992, **5**, 37–46.
- 525 W. Rabsch and G. Winkelmann, *Biol. Met.*, 1991, **4**, 244–250.
- 526 K. Hirai, H. Aoyama, S. Suzue, T. Irikura, S. Iyobe and S. Mitsunashi, *Antimicrob. Agents Chemother.*, 1986, **30**, 248–253.
- 527 H. Nikaido, *J. Biol. Chem.*, 1994, **269**, 3905–3908.
- 528 P. Neves, E. Berkane, P. Gameiro, M. Winterhalter and B. de Castro, *Biophys. Chem.*, 2005, **113**, 123–128.
- 529 L. Vinué, M. A. Corcoran, D. C. Hooper and G. A. Jacoby, *Antimicrob. Agents Chemother.*, 2016, **60**, 1537–1545.
- 530 L. E. Bryan and J. Bedard, *Eur. J. Clin. Microbiol. Infect. Dis.*, 1991, **10**, 232–239.
- 531 A. H. Delcour, *Biochim. Biophys. Acta - Proteins Proteomics*, 2009, **1794**, 808–816.
- 532 P. B. Savage, *Ann. Med.*, 2001, **33**, 167–171.

- 533 J. M. Andrews, *J. Antimicrob. Chemother.*, 2001, **48 Suppl 1**, 5–16.
- 534 E. L. Henly, J. A. R. Dowling, J. B. Maingay, M. M. Lacey, T. J. Smith and S. Forbes, *Antimicrob. Agents Chemother.*, 2021, **63**, e01892-18.
- 535 M. Liveris and J. Miller, *J. Chem. Soc.*, 1963, 3486–3492.
- 536 J. Miller and W. Kai-Yan, *J. Chem. Soc.*, 1963, 3492–3495.
- 537 J. A. Joule and K. Mills, *Heterocyclic Chemistry*, John Wiley & Sons, Ltd, Chichester, 5th edn., 2010.
- 538 K. Nepali, H.-Y. Lee and J.-P. Liou, *J. Med. Chem.*, 2019, **62**, 2851–2893.
- 539 D. I. Edwards, *J. Antimicrob. Chemother.*, 1993, **31**, 9–20.
- 540 S. Patterson and S. Wyllie, *Trends Parasitol.*, 2014, **30**, 289–298.
- 541 C. T. A. Evelo, A. A. M. G. Spooren, R. A. G. Bisschops, L. G. M. Baars and J. M. Neis, *Blood Cells, Mol. Dis.*, 1998, **24**, 280–295.
- 542 M. D. Roldán, E. Pérez-Reinado, F. Castillo and C. Moreno-Vivián, *FEMS Microbiol. Rev.*, 2008, **32**, 474–500.
- 543 Z.-Z. Yang, S.-F. Qi, D.-X. Zhao and L.-D. Gong, *J. Phys. Chem. B*, 2009, **113**, 254–259.
- 544 T. J. Ritchie, S. J. F. Macdonald, S. Peace, S. D. Pickett and C. N. Luscombe, *Med. Chem. Commun.*, 2012, **3**, 1062–1069.
- 545 T. J. Ritchie and S. J. F. Macdonald, *Eur. J. Med. Chem.*, 2016, **124**, 1057–1068.
- 546 J. R. Cooper, *Cancer Res.*, 1958, **18**, 1084–1088.
- 547 K. A. Koeplinger, Z. Zhao, T. Peterson, J. W. Leone, F. S. Schwende, R. L. Heinrikson and A. G. Tomasselli, *Drug Metab. Dispos.*, 1999, **27**, 986–991.
- 548 Z. Zhao, K. A. Koeplinger, T. Peterson, R. A. Conradi, P. S. Burton, A. Suarato, R. L. Heinrikson and A. G. Tomasselli, *Drug Metab. Dispos.*, 1999, **27**, 992–998.
- 549 J. Bornholdt, J. Felding, R. P. Clausen and J. L. Kristensen, *Chem. – Eur. J.*, 2010, **16**, 12474–12480.
- 550 J. W. Clapp, *J. Biol. Chem.*, 1956, **223**, 207–214.
- 551 D. F. Colucci and D. A. Buyske, *Biochem. Pharmacol.*, 1965, **14**, 457–466.
- 552 A. S. Kalgutkar, R. Jones and A. Sawant, in *Metabolism, Pharmacokinetics and Toxicity of Functional Groups: Impact of*

*Chemical Building Blocks on ADMET*, The Royal Society of Chemistry, 2010, pp. 210–274.

- 553 S. L. Graham, K. L. Shepard, P. S. Anderson, J. J. Baldwin, D. B. Best, M. E. Christy, M. B. Freedman, P. Gautheron and C. N. Habecker, *J. Med. Chem.*, 1989, **32**, 2548–2554.
- 554 S. L. Graham, J. M. Hoffman, P. Gautheron, S. R. Michelson, T. H. Scholz, H. Schwam, K. L. Shepard, A. M. Smith and R. L. Smith, *J. Med. Chem.*, 1990, **33**, 749–754.
- 555 O. W. J. Woltersdorf, H. Schwam, J. B. Bicking, S. L. Brown, S. J. deSolms, D. R. Fishman, S. L. Graham, P. D. Gautheron, J. M. Hoffman and R. D. Larson, *J. Med. Chem.*, 1989, **32**, 2486–2492.
- 556 Y.-Z. Xu, *Tetrahedron*, 1998, **54**, 187–196.
- 557 J. Li, J.-J. Deng, Z. Yin, Q.-L. Hu, Y. Ge, Z. Song, Y. Zhang, A. S. C. Chan, H. Li and X.-F. Xiong, *Chem. Sci.*, 2021, **12**, 5209–5215.
- 558 H. F. Motiwala, Y.-H. Kuo, B. L. Stinger, B. A. Palfey and B. R. Martin, *J. Am. Chem. Soc.*, 2020, **142**, 1801–1810.
- 559 J. A. Pfefferkorn, J. Lou, M. L. Minich, K. J. Filipski, M. He, R. Zhou, S. Ahmed, J. Benbow, A. Perez, M. Tu, J. Litchfield, R. Sharma, K. Metzler, F. Bourbonais, C. Huang, D. A. Beebe and P. J. Oates, *Bioorg. Med. Chem. Lett.*, 2009, **19**, 3247–3252.
- 560 J. Litchfield, R. Sharma, K. Atkinson, K. J. Filipski, S. W. Wright, J. A. Pfefferkorn, B. Tan, R. E. Kosa, B. Stevens, M. Tu and A. S. Kalgutkar, *Bioorg. Med. Chem. Lett.*, 2010, **20**, 6262–6267.
- 561 N. Toda, S. Asano and C. F. Barbas III, *Angew. Chem., Int. Ed.*, 2013, **52**, 12592–12596.
- 562 A. Chiotellis, F. Sladojevich, L. Mu, A. Müller Herde, I. E. Valverde, V. Tolmachev, R. Schibli, S. M. Ametamey and T. L. Mindt, *Chem. Commun.*, 2016, **52**, 6083–6086.
- 563 Q. Zhang, S. Dall'Angelo, I. N. Fleming, L. F. Schweiger, M. Zanda and D. O'Hagan, *Chem. – Eur. J.*, 2016, **22**, 10998–11004.
- 564 C. Zhang, E. V. Vinogradova, A. M. Spokoyny, S. L. Buchwald and B. L. Pentelute, *Angew. Chem., Int. Ed.*, 2019, **58**, 4810–4839.
- 565 M. R. Bauer, A. C. Joerger and A. R. Fersht, *Proc. Natl. Acad. Sci.*, 2016, **113**, E5271–E5280.



- 566 L. Li, X. Jiang, S. Huang, Z. Ying, Z. Zhang, C. Pan, S. Li, X. Wang and Z. Zhang, *ACS Med. Chem. Lett.*, 2017, **8**, 407–412.
- 567 T. Förster, E. Shang, K. Shimizu, E. Sanada, B. Schölermann, M. Huebecker, G. Hahne, M. P. López-Alberca, P. Janning, N. Watanabe, S. Sievers, F. Giordanetto, T. Shimizu, S. Ziegler, H. Osada and H. Waldmann, *Eur. J. Org. Chem.*, 2019, **2019**, 5486–5496.
- 568 A. E.-H. El-Kadiry, J. Abusarah, Y. E. Cui, N. El-Hachem, I. Hammond-Martel, H. Wurtele, S. Thomas, M. Ahmadi, M. Balood, S. Talbot and M. Rafei, *Front. Pharmacol.*, 2020, **11**, 237.
- 569 C. Zambaldo, E. V Vinogradova, X. Qi, J. Iaconelli, R. M. Suciu, M. Koh, K. Senkane, S. R. Chadwick, B. B. Sanchez, J. S. Chen, A. K. Chatterjee, P. Liu, P. G. Schultz, B. F. Cravatt and M. J. Bollong, *J. Am. Chem. Soc.*, 2020, **142**, 8972–8979.
- 570 R. O. Roblin Jr and J. W. Clapp, *J. Am. Chem. Soc.*, 1950, **72**, 4890–4892.
- 571 S. W. Wright and K. N. Hallstrom, *J. Org. Chem.*, 2006, **71**, 1080–1084.
- 572 K. Bahrami, M. M. Khodaei and M. Soheilzad, *Synlett*, 2009, 2773–2776.
- 573 H. Kwart and L. J. Miller, *J. Am. Chem. Soc.*, 1958, **80**, 884–887.
- 574 H. Kwart and B. R. William, *J. Org. Chem.*, 1965, **30**, 1188–1195.
- 575 J. Bornholdt, K. W. Fjære, J. Felding and J. L. Kristensen, *Tetrahedron*, 2009, **65**, 9280–9284.
- 576 US 2010/0256092 A1, 2010.
- 577 I. E. Marx, T. A. Dineen, J. Able, C. Bode, H. Bregman, M. Chu-Moyer, E. F. DiMauro, B. Du, R. S. Foti, R. T. Fremeau, H. Gao, H. Gunaydin, B. E. Hall, L. Huang, T. Kornecook, C. R. Kreiman, D. S. La, J. Ligutti, M.-H. J. Lin, D. Liu, J. S. McDermott, B. D. Moyer, E. A. Peterson, J. T. Roberts, P. Rose, J. Wang, B. D. Youngblood, V. Yu and M. M. Weiss, *ACS Med. Chem. Lett.*, 2016, **7**, 1062–1067.
- 578 M. B. van Niel, B. P. Fauber, M. Cartwright, S. Gaines, J. C. Killen, O. René, S. I. Ward, G. de Leon Boenig, Y. Deng, C. Eidenschenk, C. Everett, E. Gancia, A. Ganguli, A. Gobbi, J. Hawkins, A. R. Johnson, J. R. Kiefer, H. La, P. Lockey, M. Norman, W. Ouyang, A. Qin, N. Wakes, B. Waszkowycz and H. Wong, *Bioorg. Med. Chem. Lett.*, 2014, **24**,

- 5769–5776.
- 579 C. Doebelin, R. Patouret, R. D. Garcia-Ordonez, M. R. Chang, V. Dharmarajan, D. S. Kuruvilla, S. J. Novick, L. Lin, M. D. Cameron, P. R. Griffin and T. M. Kamenecka, *ChemMedChem*, 2016, **11**, 2607–2620.
- 580 H. Nishida, I. Fujimori, Y. Arikawa, K. Hirase, K. Ono, K. Nakai, N. Inatomi, Y. Hori, J. Matsukawa, Y. Fujioka, A. Imanishi, H. Fukui and F. Itoh, *Bioorg. Med. Chem.*, 2017, **25**, 3447–3460.
- 581 WO 2019/008025, 2019.
- 582 WO 2004/074283, 2004.
- 583 WO 2014/049047, 2014.
- 584 M. Zhu, W. Wei, D. Yang, H. Cui, L. Wang, G. Meng and H. Wang, *Org. Biomol. Chem.*, 2017, **15**, 4789–4793.
- 585 G. R. Revankar, N. B. Hanna, N. Imamura, A. F. Lewis, S. B. Larson, R. A. Finch, T. L. Avery and R. K. Robins, *J. Med. Chem.*, 1990, **33**, 121–128.
- 586 A. Kowalska, M. Latocha and K. Pluta, *Med. Chem. Res.*, 2015, **24**, 3107–3116.
- 587 I. M. Yonova, C. A. Osborne, N. S. Morrisette and E. R. Jarvo, *J. Org. Chem.*, 2014, **79**, 1947–1953.
- 588 G. Wastensson and K. Eriksson, *Crit. Rev. Toxicol.*, 2020, **50**, 219–271.
- 589 S. Liu, X. Zeng and B. Xu, *Org. Chem. Front.*, 2020, **7**, 1690–1695.
- 590 B. Nguyen, E. J. Emmett and M. C. Willis, *J. Am. Chem. Soc.*, 2010, **132**, 16372–16373.
- 591 J. R. DeBergh, N. Niljianskul and S. L. Buchwald, *J. Am. Chem. Soc.*, 2013, **135**, 10638–10641.
- 592 W. Li, H. Li, P. Langer, M. Beller and X.-F. Wu, *Eur. J. Org. Chem.*, 2014, **2014**, 3101–3103.
- 593 J. Aziz, S. Messaoudi, M. Alami and A. Hamze, *Org. Biomol. Chem.*, 2014, **12**, 9743–9759.
- 594 S. Ye, G. Qiu and J. Wu, *Chem. Commun.*, 2019, **55**, 1013–1019.
- 595 A. Shavnya, S. B. Coffey, A. C. Smith and V. Mascitti, *Org. Lett.*, 2013, **15**, 6226–6229.
- 596 Y. Chen, P. R. D. Murray, A. T. Davies and M. C. Willis, *J. Am. Chem. Soc.*, 2018, **140**, 8781–8787.

- 597 V. Vedovato, E. P. A. Talbot and M. C. Willis, *Org. Lett.*, 2018, **20**, 5493–5496.
- 598 T. Q. Davies, M. J. Tilby, D. Skolc, A. Hall and M. C. Willis, *Org. Lett.*, 2020, **22**, 9495–9499.
- 599 J. R. Colombe, J. R. Debergh and S. L. Buchwald, *Org. Lett.*, 2015, **17**, 3170–3173.
- 600 G. Laudadio, E. Barmpoutsis, C. Schotten, L. Struik, S. Govaerts, D. L. Browne and T. Noël, *J. Am. Chem. Soc.*, 2019, **141**, 5664–5668.
- 601 N. Youseflouei, S. Alizadeh, M. Masoudi-Khoram, D. Nematollahi and H. Alizadeh, *Electrochim. Acta*, 2020, **353**, 136451.
- 602 P. K. Chinthakindi and P. I. Arvidsson, *Eur. J. Org. Chem.*, 2018, **2018**, 3648–3666.
- 603 J. Dong, L. Krasnova, M. G. Finn and K. B. Sharpless, *Angew. Chem., Int. Ed.*, 2014, **53**, 9430–9448.
- 604 E. Ciuffarin, L. Senatore and M. Isola, *J. Chem. Soc. Perkin Trans. 2*, 1972, 468–471.
- 605 J. L. Kice and E. A. Lunney, *J. Org. Chem.*, 1975, **40**, 2125–2127.
- 606 J. A. McKee, S. K. Sharma and M. J. Miller, *Bioconjug. Chem.*, 1991, **2**, 281–291.
- 607 M. S. Diarra, M. C. Lavoie, M. Jacques, I. Darwish, E. K. Dolence, J. A. Dolence, A. Ghosh, M. Ghosh, M. J. Miller and F. Malouin, *Antimicrob. Agents Chemother.*, 1996, **40**, 2610–2617.
- 608 U. Möllmann, A. Ghosh, E. K. Dolence, J. A. Dolence, M. Ghosh, M. J. Miller and R. Reissbrodt, *BioMetals*, 1998, **11**, 1–12.
- 609 A. Stintzi, C. Barnes, J. Xu and K. N. Raymond, *Proc. Natl. Acad. Sci.*, 2000, **97**, 10691–10696.
- 610 H. Naikare, J. Butcher, A. Flint, J. Xu, K. N. Raymond and A. Stintzi, *Metallomics*, 2013, **5**, 988–996.
- 611 D. J. Raines, J. E. Clarke, E. V. Blagova, E. J. Dodson, K. S. Wilson and A.-K. Duhme-Klair, *Nat. Catal.*, 2018, **1**, 680–688.
- 612 V. Gasser, E. Baco, O. Cunrath, P. Saint August, Q. Perraud, N. Zill, C. Schleberger, A. Schmidt, A. Paulen, D. Bumann, G. L. A. Mislin and I. J. Schalk, *Environ. Microbiol.*, 2016, **18**, 819–832.
- 613 L. Moynié, S. Milenkovic, G. L. A. Mislin, V. Gasser, G. Mallocci, E. Baco,

- R. P. McCaughan, M. G. P. Page, I. J. Schalk, M. Ceccarelli and J. H. Naismith, *Nat. Commun.*, 2019, **10**, 3673.
- 614 WO2008124450 A1, 2008, 226–227.
- 615 US201/0214803 A1, 2012, 170.
- 616 WO 2019/043139 A1, 2019.
- 617 A. K. Ghosh, W. J. Thompson, M. K. Holloway, S. P. McKee, T. T. Duong, H. Y. Lee, P. M. Munson, A. M. Smith, J. M. Wai, P. L. Darke, J. A. Zugay, E. A. Emini, W. A. Schleif, J. R. Huff and P. S. Anderson, *J. Med. Chem.*, 1993, **36**, 2300–2310.
- 618 A. P. Massey, W. R. Harley, N. Pasupuleti, F. A. Gorin and M. H. Nantz, *Bioorg. Med. Chem. Lett.*, 2012, **22**, 2635–2639.
- 619 R. M. Morley, H.-W. Tse, B. Feng, J. C. Miller, D. T. Monaghan and D. E. Jane, *J. Med. Chem.*, 2005, **48**, 2627–2637.
- 620 E. Eichhorn, J.-P. Roduit, N. Shaw, K. Heinzmann and A. Kiener, *Tetrahedron: Asymmetry*, 1997, **8**, 2533–2536.
- 621 S. R. Md-Saleh, PhD Thesis, University of York, 2009.
- 622 S. A. C. Carabineiro, T. Thavorn-Amornsri, M. F. R. Pereira and J. L. Figueiredo, *Water Res.*, 2011, **45**, 4583–4591.
- 623 J. Cornish, K. E. Callon, C. Q. Lin, C. L. Xiao, T. B. Mulvey, G. J. Cooper and I. R. Reid, *Am. J. Physiol.*, 1999, **277**, E779–83.
- 624 A. Pini, L. Lozzi, A. Bernini, J. Brunetti, C. Falciani, S. Scali, S. Bindi, T. Di Maggio, G. M. Rossolini, N. Niccolai and L. Bracci, *Amino Acids*, 2012, **43**, 467–473.
- 625 D. Marcovici-Mizrahi, H. E. Gottlieb, V. Marks and A. Nudelman, *J. Org. Chem.*, 1996, **61**, 8402–8406.
- 626 A. K. Ghosh and M. Brindisi, *J. Med. Chem.*, 2015, **58**, 2895–2940.
- 627 X. Xiong and Y.-Y. Yeung, *Angew. Chem., Int. Ed.*, 2016, **55**, 16101–16105.
- 628 L. N. S. Crespín, A. Greb, D. C. Blakemore and S. V. Ley, *J. Org. Chem.*, 2017, **82**, 13093–13108.
- 629 D. R. Appleton, A. N. Pearce and B. R. Copp, *Tetrahedron*, 2010, **66**, 4977–4986.
- 630 J. W. Southwell, Unpublished Results, 2020.
- 631 M. E. Jung, E. C. Yang, B. T. Vu, M. Kiankarimi, E. Spyrou and J. Kaunitz,

- J. Med. Chem.*, 1999, **42**, 3899–3909.
- 632 G. Zhao, M. J. Miller, S. Franzblau, B. Wan and U. Möllmann, *Bioorg. Med. Chem. Lett.*, 2006, **16**, 5534–5537.
- 633 W. H. Perkin and F. W. Stoye, *J. Chem. Soc., Trans.*, 1923, **123**, 3171–3176.
- 634 F. M. Dean, J. Goodchild, L. E. Houghton, J. A. Martin, R. B. Morton, B. Parton, A. W. Price and N. Somvichien, *Tetrahedron Lett.*, 1966, **7**, 4153–4159.
- 635 S. R. Aristegui, M. D. El-Murr, B. T. Golding, R. J. Griffin and I. R. Hardcastle, *Org. Lett.*, 2006, **8**, 5927–5929.
- 636 J. I. Lee, *Bull. Korean Chem. Soc.*, 2016, **37**, 1132–1135.
- 637 M. M. C. Lam, K. L. Wyres, L. M. Judd, R. R. Wick, A. Jenney, S. Brisse and K. E. Holt, *Genome Med.*, 2018, **10**, 77.
- 638 L. Moynié, A. Luscher, D. Rolo, D. Pletzer, A. Tortajada, H. Weingart, Y. Braun, M. G. P. Page, J. H. Naismith and T. Köhler, *Antimicrob. Agents Chemother.*, 2017, **61**, e02531-16.
- 639 M. Ghosh, P. A. Miller and M. J. Miller, *J. Antibiot. (Tokyo)*, 2020, **73**, 152–157.
- 640 C. P. Neal, P. P. E. Freestone, A. F. Maggs, R. D. Haigh, P. H. Williams and M. Lyte, *FEMS Microbiol. Lett.*, 2001, **194**, 163–169.
- 641 M. Lyte, P. P. E. Freestone, C. P. Neal, B. A. Olson, R. D. Haigh, R. Bayston and P. H. Williams, *Lancet*, 2003, **361**, 130–135.
- 642 M. F. Richter, B. S. Drown, A. P. Riley, A. Garcia, T. Shirai, R. L. Svec and P. J. Hergenrother, *Nature*, 2017, **545**, 299–304.
- 643 J. Hudzicki, in *Kirby-Bauer Disk Diffusion Susceptibility Test Protocol*, 2009.
- 644 B. Bonev, J. Hooper and J. Parisot, *J. Antimicrob. Chemother.*, 2008, **61**, 1295–1301.
- 645 J. Alsenz and M. Kansy, *Adv. Drug Deliv. Rev.*, 2007, **59**, 546–567.
- 646 P. M. Nowak, F. Sagan and M. P. Mitoraj, *J. Phys. Chem. B*, 2017, **121**, 4554–4561.
- 647 E. Wilde, PhD Thesis, University of York, 2017.
- 648 D. J. Raines, O. V Moroz, K. S. Wilson and A.-K. Duhme-Klair, *Angew. Chem., Int. Ed.*, 2013, **52**, 4595–4598.

- 649 G. Trojandt, U. Herr, K. Polborn and W. Steglich, *Chem. – A Eur. J.*, 1997, **3**, 1254–1268.
- 650 A. S. Shawali, A. Harhash, M. M. Sidky, H. M. Hassaneen and S. S. Elkaabi, *J. Org. Chem.*, 1986, **51**, 3498–3501.
- 651 G. Siano, S. Crespi, M. Mella and S. M. Bonesi, *J. Org. Chem.*, 2019, **84**, 4338–4352.
- 652 US 2014/0121211, 2014.
- 653 L. Váradi, M. Wang, R. R. Mamidi, J. L. Luo, J. D. Perry, D. E. Hibbs and P. W. Groundwater, *Bioorg. Med. Chem.*, 2018, **26**, 4745–4750.
- 654 J. Ordóñez-Hernández, A. Jiménez-Sánchez, H. García-Ortega, N. Sánchez-Puig, M. Flores-Álamo, R. Santillan and N. Farfán, *Dye. Pigment.*, 2018, **157**, 305–313.
- 655 A. R. Tyler, A. O. Okoh, C. L. Lawrence, V. C. Jones, C. Moffatt and R. B. Smith, *Eur. J. Med. Chem.*, 2013, **64**, 222–227.
- 656 L. Biesen, N. Nirmalanathan-Budau, K. Hoffmann, U. Resch-Genger and T. J. J. Müller, *Angew. Chem., Int. Ed.*, 2020, **59**, 10037–10041.
- 657 A. M. Porto, L. Altieri, A. J. Castro and J. A. Brioux, *J. Chem. Soc. B*, 1966, 963–972.
- 658 M. Tercel and W. A. Denny, *J. Chem. Soc., Perkin Trans. 1*, 1998, 509–520.
- 659 A. G. Ross, B. M. Benton, D. Chin, G. De Pascale, J. Fuller, J. A. Leeds, F. Reck, D. L. Richie, J. Vo and M. J. LaMarche, *Bioorg. Med. Chem. Lett.*, 2015, **25**, 3468–3475.
- 660 P. Loupias, I. Dechamps-Olivier, L. Dupont, P. Vanlemmens, C. Mullié, N. Taudon, A. Bouchut, A. Dassonville-Klimpt and P. Sonnet, *Pharmaceuticals (Basel)*, 2019, **12**, 160.